Gas Phase Chemical Physics Program

DOE Principal Investigators'
Abstracts

June 1 – 3, 2022

Chemical Sciences, Geosciences, and Biosciences Division
Office of Basic Energy Sciences
Office of Science
U.S. Department of Energy

The research grants and contracts described in this document are supported by the U.S. DOE Office of Science, Office of Basic Energy Sciences, Chemical Sciences, Geosciences and Biosciences Division.

Foreword

This volume summarizes the 41st annual Research Meeting of the Gas Phase Chemical Physics (GPCP) Program sponsored by the U. S. Department of Energy (DOE), Office of Basic Energy Sciences (BES). The participants of this meeting include the DOE laboratory and university principal investigators (PIs) within the BES GPCP Program, and this volume includes descriptions of the current GPCP portfolio of research projects. The purpose of the annual meeting is to facilitate scientific interchange among the PIs and to promote a sense of program identity.

The GPCP program advances fundamental understanding of chemical reactivity, kinetics, and dynamics at the level of electrons, atoms, molecules, and nanoparticles. A continuing goal of this program is to understand energy flow and reaction mechanisms in complex, nonequilibrium, gas-phase environments. The foundational knowledge produced by this research portfolio constitutes crucial contributions in support of the missions of the Chemical Sciences, Geosciences, and Biosciences (CSGB) division and BES.

The CSGB division has seen a number of changes during the past year, including the retirements of the Division Director, Bruce Garrett, and the Fundamental Interactions (FI)Team Lead, Jeff Krause. Gail Mclean is serving as acting Division Director, and Tom Settersten is the new FI Team Lead. We thank Bruce and Jeff for their outstanding leadership of the CSGB division and FI team and look forward to working with Gail and Tom.

In addition to the outstanding work of the GPCP PIs in delivering the exciting science described in this volume, we would also like to acknowledge their tireless efforts in submitting progress reports, reviewing proposals, and submitting research highlights. We also extend a special thanks to Teresa Crockett, Kerry Hochberger, and Mary Beth Luther of BES Operations and Linda Severs of the Oak Ridge Institute for Science and Education (ORISE) for working behind-the-scenes to ensure smooth operation of the GPCP program.

Wade Sisk
Tom Settersten

Table of Contents

Nanoparticle Surface Kinetics and Dynamics by Single Nanoparticle Mass Spectrometry

Scott L. Anderson, Chemistry Department, University of Utah
315 S. 1400 E. Salt Lake City, UT 84112 anderson@chem.utah.edu

Program Scope

This project is focused on developing and using single nanoparticle mass spectrometry (NPMS) to measure reaction kinetics and emission spectroscopy for individual nanoparticles (NPs) at high temperatures (T_{NP}). The focus in the past year has been on high T_{NP} oxidation of different types of carbon NPs, and on the high temperature chemistry of silicon and silica NPs under inert and oxidizing atmospheres. SiO_x chemistry was chosen to test the ability of the method to probe surface chemistry of high temperature materials with more complex behavior than carbon. Si and silica NPs are also interesting because we can study surface chemistry at temperatures ranging well above the bulk melting temperature, T_{melt}, which should dramatically vary the kinetics for diffusion of atoms between the surface layer and NP core. Because NPMS is a new tool for measuring surface reaction kinetics at high and ultra-high temperatures, significant effort continues in method development.

In addition to providing temperature-dependent reaction kinetics of interest for modeling purposes, we are probing the effects of two different kinds of heterogeneity on NP kinetics and optical properties: 1. NPs are inherently heterogeneous, with significant NP-to-NP variation in size, shape, and structure, all of which can affect reaction kinetics and spectroscopy. 2. *Individual NPs* also have distributions of surface sites that react differently, and the site distributions and resulting reaction kinetics change as the NP *evolves* at high temperatures. For carbon NPs, evolution includes large-scale structural transformations that result in dramatic changes in etching rates for all types of carbon NPs, albeit with transformation rates that vary by orders of magnitude for different carbon materials.[1] We also showed that the transformation is catalyzed by the presence of O_2, presumably because defects created by CO/CO_2 loss facilitate isomerization. For Si and silica, the initial sublimation and etching kinetics vary substantially from one NP to the next, but once the NP has been heated above T_{melt}, the differences are much smaller. For $T_{NP} \leq$ ~1600 K the SiO_x NPs also eventually passivate due to formation of a stable oxide layer, but at higher T_{NP} the oxide is unstable and etching continues indefinitely.

Methodology

The instrument used in the experiments,[2, 3] and the optical system needed to record emission spectra for T_{NP} determination,[4, 5] have been described previously. Details of the operating procedures are in reports of graphite and graphene sublimation[2] and oxidation kinetics.[1, 3] In essence, a single NP of the material of interest is trapped in the gas phase, laser heated with T_{NP} determined by fitting the blackbody-like emission spectrum, and the NP mass is measured as a function of time as the NP sublimes or reacts with gaseous reactants like O_2 or C_2H_2. The mass change vs. time can be analyzed to extract kinetics and evolution of the kinetics over time. In addition to the main instrument, we have a "test" instrument with identical NP inlet and trap, but with simpler optical system. This is used to try new techniques without interfering with the main experiments.

The single NP approach avoids ensemble averaging, thus providing unique insights into heterogeneity and structure-reactivity relationships, but it is a slow method. To enable study of larger numbers of NPs we have devoted considerable effort to automating the experiment, aiming at eventually at 24/7 unattended operation. Currently, most aspects of the experiment are automated, and the major effort in this area is currently on automating analysis of the large data sets generated in each experiment.

Results in the past year

Carbon NPs:

During the past year we focused on studies of the O_2 etching chemistry for carbon NPs from graphite, graphene oxide, carbon black, nanodiamond, and carbon nano-onion feedstocks.[1] The work was motivated by the previous observation that long-term O_2 oxidation of graphite and graphene NPs, resulted in the NPs eventually become inert to O_2,[3] signaling a major transformation in the structure of at least the surface layer of the NPs. Thus, we wanted to examine the effects of carbon feedstock structure on this transformation. In addition, comparing graphite and graphene oxide (which loses CO to generate a large

number of basal plane defects), allowed the effects of graphitic defects vs. edge sites to be compared. Reaction rates were measured as a function of T_{NP}, time, and P_{O2} in a variety of reaction protocols.

Typical raw results are shown in Fig. 1. The top shows how the NP mass and integrated emission intensity varied as a diamond aggregate NP (i.e., an aggregate of much smaller primary nanodiamonds) was heated, alternating between inert atmosphere (white background), and 4.3 x 10^{-5} Torr of O_2 (aqua background). The lower frame shows the baseline mass loss rates (R_{base} – right axis), along with the R_{base}-subtracted oxidative etching rate (R_{oxid} - outer left axis). R_{base} results from etch reaction with residual O_2 in the chamber background, plus sublimation for T > 1500 K. Raw rates are given in Da/sec/nm^2 of estimated surface area. To allow comparison of NPs with different sizes and at different P_{O2}, R_{oxid} was converted to an etching efficiency (EE_{O2} – inner left axis) given in terms of Da of mass lost *per* O_2 collision. It can be seen that EE_{O2} at 1200 K was initially ~3x10^{-3} Da/collision, but that it fell rapidly with increasing time/T_{NP}. During the 2nd ramp the NP was essentially inert to O_2 at all T_{NP}, and the sublimation rate at high T_{NP} was also much slower than in the 1st ramp. The dramatically increased chemical and physical stability is attributed to transformation of the NP to have nano-onion (fullerene-like) structure. This process is known to occur rapidly for diamond. Indeed, for diamond, even brief heating above ~1400 K is sufficient to render the NP inert.

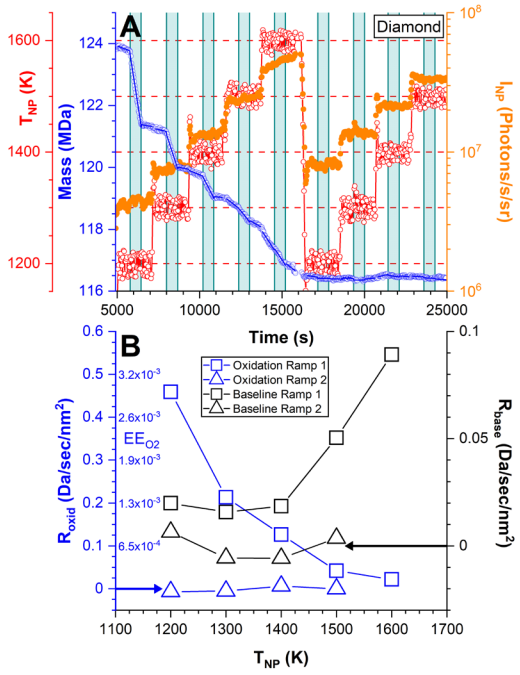

Fig. 1. A. Stepped T_{NP} ramp for a diamond NP, showing mass and integrated emission intensity (I_{NP}) vs. T_{NP}. B. Mass loss rates in both inert (R_{base}) and oxidizing conditions (R_{oxid} and EE_{O2})

Fig. 2 shows the much more complicated transformation typical of graphitic carbon. In this experiment, the mass of a graphite NP was monitored for ~20 hours in 4.3 x 10^{-5} Torr of O_2. When $O_2$was first introduced (aqua) EE_{O2} was initially ~10^{-3} Da/collision, but as shown in both frames, the mass loss rate and EE_{O2} varied dramatically over time, with waves of rapid etching punctuated by extended periods when the NP was nearly inert. Note that the second wave of etching (cyan - inset) was actually a series of very fast waves that each removed 1 – 1.5 MDa (~1 MLs-worth) of material. Finally, when the NP became inert at the end of the 3rd etching wave (white), it remained inert for >10 hours. At that point, we tried repeatedly doubling P_{O2} to see if reactivity could be restored. A small amount of mass loss was observed (expanded vertical scale in A), but EE_{O2} remained two orders of magnitude smaller than the initial EE_{O2}.

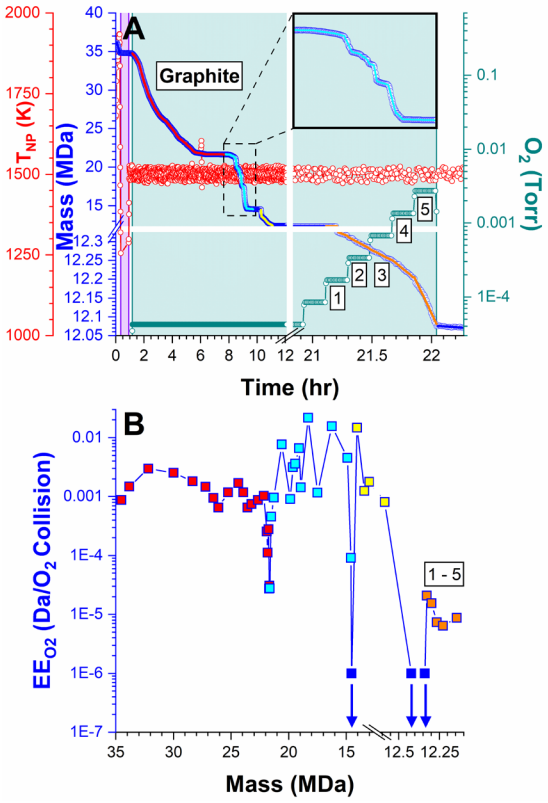

Fig. 2. Oxidative etching of a graphite NP as a function of time at 1500 K. B. EE_{O2} as function of the declining NP mass.

An interesting observation for graphite NPs was that the final transitions to inertness were always preceded by periods when EE_{O2} oscillated, reaching values up to an order of magnitude higher than the initial EE_{O2}. This indicates that the NP surface structure went through periods when the number of reactive surface sites was much higher than that of the initial graphite NP. This behavior is only seen for graphite NPs.

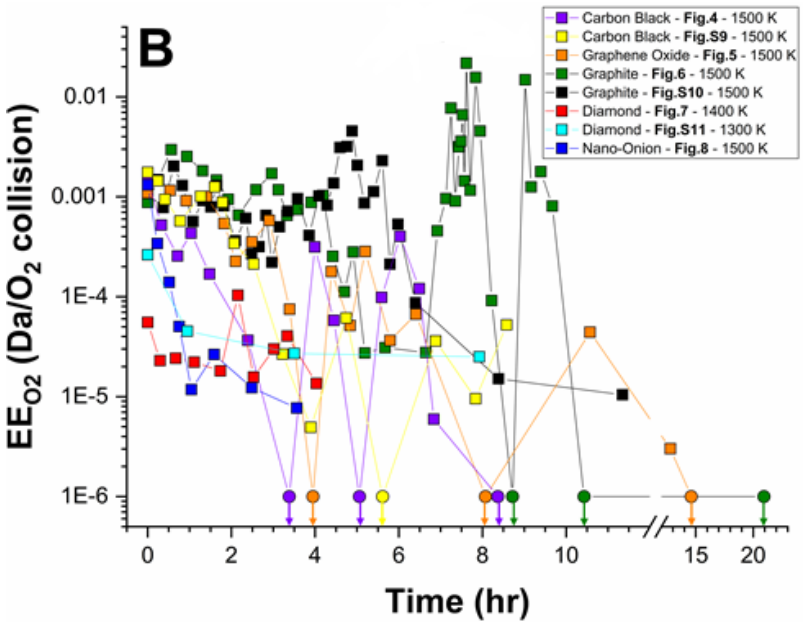

Fig. 3. Evolution of EE_{O2} for carbon NPs under oxidizing conditions.

Fig. 3 compares the evolution behavior for typical NPs of each of the carbon feedstocks. It can be seen that the speed at which NPs evolve to low O_2 reactivity varies as follows: Diamond ≈ Nano-onion > Carbon Back > Graphene Oxide > Graphite. Note also that while some oscillation of EE_{O2} over time is observed for all carbon NPs, only the graphitic NPs maintain high reactivity right up to the point where they rapidly transition to inertness. As a result, they lose the most mass in the process of onionizing.

Silicon/silica NPs

We have studied sublimation, oxidative etching, and the transition between active and passive oxidation for both Si and SiO_2 NPs. Silica NPs are, of course, initially inert to oxidative etching, but if they are briefly heated to T>2000 K, they become reactive, and also their emissivity increases dramatically. Both effects are attributed to decomposition of the oxide at high T_{NP}, leaving behind a reduced Si-rich NP, with *initial* O_2 etching reactivity quite similar to that of Si NPs.

A simple example of etching behavior for an Si NP is shown in Fig. 4. The NP was pre-heated to 1900 K to melt it and clean the surface, then T_{NP} was set to 1350 K and the mass loss and optical properties were measured in both inert (white) and oxidizing (aqua) atmospheres. It can be seen that the initial EEO_2 was ~4.8 x 10^{-3} Da/O_2 collision, and that the etching rate was roughly constant for several hours, during which the NP lost half its initial mass. Then at the ~4 hour point, EE_{O2} quickly dropped by more than two orders of magnitude, signaling growth of a passivating surface layer. High reactivity followed by abrupt passivation was observed for all NPs for T_{NP} up to 1500 K. At 1750 K, the NPs are initially somewhat less reactive, and while EE_{O2} declines gradually over time, the NPs never become completely passivated, presumably because the silica surface is unstable.

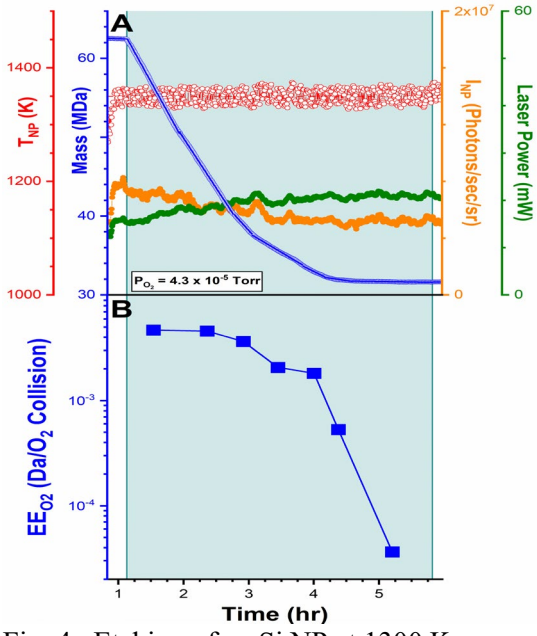

Fig. 4. Etching of an Si NP at 1300 K.

There is a substantial Si oxidation literature, albeit mostly at lower temperatures. The basic mechanism includes: O_2 dissociative adsorption, SiO desorption, SiO_2 island nucleation, passivation by formation of a stable SiO_2 surface layer, oxide

destabilization at very high T. The interesting point is that our T_{NP}/P_{O2} conditions are ***all*** in the range where passivation is not seen for bulk Si surfaces, whereas we clearly see passivation at long etching times for $T_{NP} \leq 1500K$. Several other observations relating to this behavior are: 1. If an Si NP is oxidized to the point of passivation, then briefly heated above 2500 K, high etching reactivity is restored, but only briefly. 2. If the same experiment is done with a reduced silica NP (i.e., with an Si-rich surface), the initial reactivity is similar to Si, but the NP passivates rapidly. Tentatively, we suggest that diffusion of O between the surface layer and layers deeper in the NP core can account for these observations. The Si NP initially has a pure Si core, and during the initial fast etching, in addition to losing O as SiO desorption, we hypothesize that there is some diffusion of O into the surface, gradually building up the O:Si ratio. At some point, the concentration of sub-surface O is sufficient to nucleate formation of SiO_2, which is substantially more stable with respect to desorption than isolated SiO groups. As the silica layer grows, it passivates the NP surface. When the passivated NP is briefly flashed >2500 K, the silica surface decomposes, creating a reactive Si-rich surface layer, but this passivates again rapidly because there is still significant O in the sub-surface region. Similarly, silica NPs that have been activated by heating to high T_{NP} also have substantial O in the sub-surface region, and therefore passivate rapidly. If this scenario is correct, the failure to observe passivation of bulk Si at high T may result from the sample bulk acting as a sink for O, whereas for an NP, the core would tend to saturate with O more rapidly.

In addition to the publications noted below, three additional papers on Si and SiO_x sublimation and etching, and on growth reactions of different carbon NP in collisions with C_2H_2 are in preparation. The lead student on the project, Daniel Rodriguez, received his Ph.D., and is currently a postdoc at Los Alamos. Daniel's thesis won the department's Cheves Walling thesis award in 2021-2022.

Plans for the coming year:

I plan to focus on two areas: 1. The main focus will be on reactions of carbon NPs with other oxidizers, including water, N_2O, and radical species (O, OH) created in a discharge source. 2. Our method potentially could become the go-to method for studying surface chemistry at ultra-high temperatures (to >4,000 K). Given the interest in ultra-high temperature materials for a variety of applications, we will do a pilot study of HfC (T_{melt} ~4200 K) oxidation. The challenge will be to distinguish processes that add mass (HfO_2 formation) and that remove mass (CO, CO_2 loss, O or O_2 loss from HfO_2), however, I expect that these will occur over different T_{NP} ranges, allowing them to be at least partly disentangled. It should also be possible to obtain insight into O/C diffusion in the hot NP. For example, once a passivating HfO_2 layer has formed, we may see continuing slow mass loss that indicating that some CO loss continues, which would imply that C is diffusing through the oxide layer.

References (All acknowledge support from DOE GPCP program)

1. Rodriguez, D. J.; Lau, C. Y.; Friese, A. M.; Magasinski, A.; Yushin, G.; Anderson, S. L., High-Temperature Oxidation of Single Carbon Nanoparticles: Dependence on the Surface Structure and Probing Real-Time Structural Evolution via Kinetics. *Journal of the American Chemical Society* **2022,** *144* (11), 4897-4912.
2. Long, B. A.; Lau, C. Y.; Rodriguez, D. J.; Tang, S. A.; Anderson, S. L., Sublimation Kinetics for Individual Graphite and Graphene Nano-particles (NPs): NP-to-NP Variations and Evolving Structure-Kinetics and Structure-Emissivity Relationships. *J. Am. Chem. Soc.* **2020,** *(on line 7/22/2020)*.
3. Rodriguez, D. J.; Lau, C. Y.; Long, B. A.; Tang, S. A.; Friese, A. M.; Anderson, S. L., O_2-oxidation of individual graphite and graphene nanoparticles in the 1200–2200 K range: Particle-to-particle variations and the evolution of the reaction rates and optical properties. *Carbon* **2021,** *173*, 286-300.
4. Long, B. A.; Rodriguez, D. J.; Lau, C. Y.; Anderson, S. L., Thermal emission spectroscopy for single nanoparticle temperature measurement: optical system design and calibration. *Appl. Opt.* **2019,** *58* (3), 642-649.
5. Long, B. A.; Rodriguez, D. J.; Lau, C. Y.; Schultz, M.; Anderson, S. L., Thermal Emission Spectroscopy of Single, Isolated Carbon Nanoparticles: Effects of Particle Size, Material, Charge, Excitation Wavelength, and Thermal History. *J. Phys. Chem. C* **2020,** *124*, 1704-1716.

Chemical Dynamics in the Gas Phase at Argonne: Chemical Kinetics

Rebecca L. Caravan, Stephen J. Klippenstein, Robert S. Tranter
Chemical Sciences and Engineering Division, Argonne National Laboratory, Lemont, IL, 60439

caravarl@anl.gov, sjk@anl.gov, tranter@anl.gov

Program Scope

The goal of this program is to explore foundational problems in gas phase chemical kinetics through a combination of experimental studies and *ab initio* chemical kinetics calculations. We use these methods to explore reactions on complex potential energy surfaces (PESs), which includes assessments of the reaction rates, the role of incomplete thermalization in kinetics, the potential importance of novel classes of reactions, and the role of all aspects of the global PES. The close linkage of experimental and theoretical studies of prototypical reactions allows us to deeply explore key kinetic questions, while generating kinetic data of relevance to a variety of complex, chemically reactive, non-equilibrium systems such as combustion, atmospheric chemistry, and atomic layer deposition. Our efforts to address these key science questions will benefit from continued development of unique experimental and theoretical methods. The experimental approach spans a wide range of reaction conditions using a combination of shock tube and flow reactor methods. A suite of optical and mass spectrometric diagnostics allow in-depth interrogation of reactions. Extensive use of synchrotron (VUV and x-ray) techniques enhance the laboratory capabilities.

Recent Progress

Broad band UV-Visible time resolved absorption: We are finalizing construction of a new flow reactor equipped for laser photolysis and broad band UV-Visible absorption. This apparatus will facilitate kinetics and mechanistic studies using multiplexed species detection over a broad range of T and P, with sub-millisecond time-resolution. This technique has been demonstrated to be a versatile and powerful approach for kinetics studies of reactive intermediates and incorporates design elements from Sheps (Sandia) and others.

Aromatics: We have completed an experimental and theoretical study of the multichannel dissociation of styrene. The study combined laser schlieren densitometry (LS) experiments in the diaphragmless shock tube (DFST) with time-of-flight mass spectrometry (TOFMS) studies in the DFST and the high repetition rate shock tube (HRRST). The DFST/TOFMS used electron impact ionization whereas the HRRST/TOFMS work was conducted at the Advanced Light Source (ALS) with tunable VUV photoionization. The experimental literature on styrene dissociation is sparse and suggests that styrene dissociates to benzene and vinylidene. However, this is not consistent with the LS experiments or the mass spectra that show phenylacetylene as a major early product at the lower temperatures of the studies and polyacetylenes up to C_8H_2 at the higher. Theoretical work by Sivaramakrishnan showed that dissociation of styrene is actually a multichannel process with seven active channels. The dominant channel at all conditions forms H + ∝-styryl radical that rapidly yields H + phenylacetylene. A chemical kinetic model that reproduces the LS studies very well has been developed and solid understanding of the initial dissociation of styrene obtained. It is likely that the prior experimental studies were observing benzene and acetylene formed in secondary processes rather than primary ones and routes to these products were identified in the modeling studies. Currently, the work is being expanded in collaboration with Comandini (CNRS) to examine the formation of polyaromatic hydrocarbons (PAH) and understand the transition in product distributions from aromatic at low temperatures to polyacetylenes at high temperatures.

Fluorinated species: A study of the pyrolysis of difluoromethane, a common refrigerant, was started in collaboration with Sivaramakrishnan and Jasper. Recently, Matsugi and Lynch separately studied the dissociation using similar techniques. They agreed on the initial rate of dissociation by HF elimination but had some disagreement concerning late HF production via reactions of CHF radicals. DFST/LS studies were performed over a broad range of conditions to examine the initial dissociation of CH_2F_2. Models built

from the work of Matsugi and an earlier study by Cobos and co-workers failed to reproduce the LS experiments. Furthermore, DFST and HRRST TOFMS studies showed that HCCH and FCCH were formed in roughly equal amounts at reaction conditions relevant to all the experimental studies. The observation of HCCH was not expected based on the literature, which predicted only FCCH. Theoretical work by Sivaramakrishnan and Jasper identified a number of previously overlooked channels for CHF recombination that lead to both HCCH and HCCF. Inclusion of the revised chemistry for CHF resulted in satisfactory simulation of the LS experiments.

X-ray fluorescence: Measurements of temperature fields in sooting diffusion flames with McEnally (Yale) and Xuan (Penn State) using x-ray fluorescence of Kr-atoms (7-BM beamline, APS) continued. The experimental results provided a solid set of data for developing accurate 2D CFD models of the flames that allow for more accurate interpretation of experiments within the flames. A study on methane/air flames is in press. In this work both the oxidizer and fuel streams were doped with Kr giving a uniform number density of Kr across the flame. While relatively easy to interpret, these experiments consumed a significant amount of Kr. Consequently, in a later study (C_2H_4/air) Kr was doped only into the fuel stream. This resulted in much less Kr being used and allowed temperature fields in the fuel jet and flame boundaries to be obtained. However, radial diffusion of Kr becomes significant and the Kr mole fraction has to be estimated by modeling of the flame. The model results are sensitive to the boundary conditions, particularly the burner surface temperature and the sensitivity increases for richer flames. A detailed error analysis has been conducted that allows the influence of various parameters to be determined at different flame positions.

Experiments were also performed in a lean, pre-mixed ethylene flame to determine the perturbation of the flame by a thermocouple (125 micron, type R) inserted into it. The lead wires tended to distort in the flame and the distortion varied depending on the location in the flame resulting in the thermocouple bead moving away from the target location. However, this was relatively easily accounted for by centering the x-ray beam on the bead at each observation point. An extensive set of data were collected and are being analyzed with a goal of testing models for temperature corrections to in-flame thermocouple measurements.

Criegee intermediate reactivity: Investigations of Criegee intermediate (CI) reactivity continued with Lester (Penn), Osborn, Taatjes (Sandia), and our collaborators outside the program including Carl Percival (NASA JPL) and Dudley Shallcross (University of Bristol). One example of our work together is provided below; we also refer to the Lester and Sandia abstracts for discussions of our projects together.

Acetaldehyde oxide (CH_3CHOO) is a two-carbon CI comprising two distinct conformers (*syn* and *anti*) that have a large barrier (~38.6 kcal mol^{-1}) to interconversion. Taatjes *et al.* previously found evidence for a remarkable conformer-dependent reactivity of CH_3CHOO towards water vapor.[1] Further experimental and theoretical studies of other CH_3CHOO bimolecular reactions (e.g., by Chao *et al.*[2] and Mull *et al.*[3]) have revealed an apparent commonality of stark conformer-dependent reactivity in systems involving 1,2-insertion mechanisms, which lead to the formation of functionalized hydroperoxide type reaction products: in these systems, the transition state energies for reactions of *syn* conformers are ~5-7 kcal mol^{-1} higher than for *anti* conformers. We investigated the reaction of CH_3CHOO with dimethylamine (DMA), which we find operates via a 1,2-insertion mechanism. Theory predicts a submerged barrier on the reaction coordinate for the *syn* conformer, whereas the *anti* reaction is completely barrierless.[4] These differences are predicted to result in very dramatic conformer-dependent reactivity: despite both reactions being energetically downhill, the reaction of *anti*-CH_3CHOO with DMA is ~34,000 times faster, suggesting that the submerged barrier on the *syn* PES acts as a significant bottleneck for reaction. Our conformer-specific experimental studies support this theoretically predicted conformer dependence as well as the 1,2-insertion process.

We also performed theoretical calculations to explore the unimolecular dissociation of two additional CIs in collaboration with Lester. First, the doubly substituted methyl-ethyl Criegee intermediate (MECI) was studied to explore the effect of multiple hindered rotors on the kinetics. The theoretical analyses illustrated the variation between single- and multi-structure harmonic, 1- and multi-dimensional hindered rotor

treatments, with and without vibrationally adiabatic corrections for the latter method. Comparison with other previously studied CI systems provided insight into substituent effects on unimolecular decay under both energy-dependent and thermal conditions. In a second study, we examined the kinetics for passage through a 1,6-H-atom transfer pathway in 2-butenal-oxide. The reaction through this pathway, which required a preliminary conformational change, was found to proceed much more rapidly than the traditional 1,4-H-atom transfers in smaller CIs.

•*QOOH Dissociation Kinetics:* Our collaboration with Lester's group to examine the kinetics of a hydroperoxyalkyl radical (•QOOH) dissociation [•$CH_2(CH_3)_2COOH$] continued, as discussed in more detail in Lester's abstract. The dissociation kinetics measurements were extended to a partially deuterated •QOOD analog [•$CH_2(CH_3)_2COOD$] and the infrared spectroscopic signature of •QOOH was examined (also with McCoy). The •QOOD study further validated the importance of heavy-atom tunnelling.

Tunneling Corrections: Our theoretical efforts to analyze the kinetics of CIs and of •QOOH sparked our interest in quantitatively modelling the chemical reactivity at the low temperatures of relevance to atmospheric chemistry. This led to our development of a closed-form expression for the tunneling rate constant in non-separable systems. Interestingly, this expression introduces a novel "entanglement factor" that modulates the reaction rate. Notably, an extended form of this expression properly accounts for the conservation of angular momentum. In contrast, other approaches have considered only transverse vibrational modes, which correlates with employing a decoupled rotational partition function for the orientational modes. This new tunneling formalism allows one to predict thermal and energy-resolved rate constants over broad ranges of temperatures and energies from simple considerations of the anharmonic force field at the saddle point, quantitatively explains in simple terms the so-called "quantum bobsled" effect, and has interesting similarities to the semiclassical TST approach of Miller and coworkers.

Kinetic Phenomenology: Phenomenological rate laws are most useful when they are valid over the full range of temperature, pressure, and conditions sampled in a chemically reactive environment. Although, the eigensolutions to the master equation provide a direct correspondence between the microscopic dynamics and the macroscopic kinetics (i.e., the phenomenological rate laws) the functional form of these relations varies with condition. This variance arises from the fact that the number of kinetically stable chemical species generally varies with temperature T and pressure P. For example, hydroperoxyalkyl radicals (QOOH), which are of central importance to low temperature chain branching, typically become unstable at precisely the temperatures and pressures of interest to kinetic modeling (e.g., 600 K at 1 atm). Well merging procedures provide the appropriate description of the rate constants for the set of well-defined species at any given T, P. But how should one express the rates across the full range of T, P?

We have now derived and implemented in MESS a "well extension" procedure that resolves this problem by providing meaningful extrapolations of the rate constants beyond their range of physical validity. This approach satisfies the following important set of conditions: First, the rate constants effectively coincide with the actual rate constants in their region of existence. Second, when species merge at higher temperatures and/or lower pressures, the extended rate constants are large enough to guarantee thermal equilibrium within the combined species group. Last, but not least, the extended rate constants satisfy detailed balance. We have also implemented an alternative solution that involves an extended well reduction approach, where one simply presumes that given sets of wells are lumped together into a single chemical species at all temperatures. Such approximate lumping procedures find utility in controlling the numbers of species to be modeled; particularly in PAH modeling, for example.

Future Work

Broad band UV-Visible time resolved absorption: The final components of the new broadband UV-Visible time-resolved absorption experiment are being ordered and awaiting delivery. Once construction and testing are completed, we will commence kinetic and spectroscopic studies of reactive intermediates. Initial work will focus on CIs and peroxy radicals, complementing ALS experiments and theoretical efforts.

Fluorinated alkanes: The CH_2F_2 experiments indicate significant incubation delays at lower pressures, which suggests that vibrational relaxation is slow. Preliminary experiments generated strong LS signals at temperatures too low for dissociation of CH_2F_2 that are symptomatic of slow relaxation. Initial efforts will focus on completing a study of vibrational relaxation in CH_2F_2, which will result in more accurate modeling of the dissociation of CH_2F_2 at low pressures. These studies will complement work on partially fluorinated ethanes where anomalous relaxation behavior was observed.

Aromatics: We will continue our efforts on PAH formation and reactions of aromatic and resonantly stabilized radicals. Initially, we will build on the styrene work with experimental and theoretical studies of of alkyl benzenes, of which styrene is a key product. We also propose to further studies of the mechanisms of PAH formation by developing new thermal sources for aromatic and resonantly stabilized radicals mainly based on our experience with organic nitrites. Of particular interest, is re-examining the recombination and disproportionation branching ratios of phenyl radicals and benzyl radicals utilizing the same photoionization mass spectrometry methods that we applied to alkyl radicals where we found that contrary to common assumptions the branching ratios are not necessarily independent of temperature.

Criegee intermediate reactivity: Investigations of CI reactivity will continue with our core team of collaborators, including Osborn, Taatjes, and Lester of this program. This ongoing work will be strengthened and complemented by new insights using the Argonne broadband UV-Visible time-resolved absorption experiment once construction and characterization are complete.

We will undertake experimental and theoretical studies on the unimolecular and bimolecular reactivity of MECI (see Lester abstract also). Our initial investigations suggest the presence of a variety of roaming radical channels, which will be explored and verified through a combination of experiment, theory, and modeling. Interestingly, theory suggests that a two-step sequence of independent roaming reactions can occur from the initial reactants. We will also interrogate the influence of conjugation versus structure on the reactivity of CIs by comparison of the bimolecular reactivity of MECI with that of its unsaturated, resonance-stabilized analogue, methyl vinyl ketone oxide. This work will build on our previous investigations of four-carbon, resonance stabilized Criegee intermediates (sCIs): methyl vinyl ketone oxide and methacrolein oxide.

One particularly challenging project we will undertake is investigating the impact of resonance-stabilization of CIs on their oligomerization reactions, e.g., via initial reactions with organic acids and hydroperoxides. This research will build on our previous work on the oligomerization reactions of the simplest sCI, outlined in our 2021 abstract.

Peroxy radical-Criegee intermediate interconversion: With Wilson (LBNL), we are initiating direct gas-phase studies to interrogate the mechanisms operating in the apparent facile interconversion of hydroxy-functionalized RO_2 to sCIs. Recently, the Beauchamp[5] and Wilson[6] groups found compelling evidence for the interconversion of β-hydroxyfunctionalized RO_2 (HO-RO_2) to CIs in heterogeneous environments. The Wilson group observed signatures of CI-specific reaction products in experimental studies of HO-RO_2, despite no known sources of sCIs. Because of the vastly different reactivity of RO_2 and CIs, interconversion pathways would result in substantial changes to our current understanding of complex oxygenated environments. Unambiguous identification and elucidation of the reaction mechanism that interconnects these two classes of intermediates would transform our understanding of their relative importance across a variety of environments, such as Earth's lower atmosphere, and in the low-temperature combustion of fuels. We will undertake a combined experimental and theoretical effort to investigate the mechanisms responsible for this interconversion. Our studies will initially focus on the simplest HO-RO_2 (HO-C_2H_4OO), and will extend in complexity to branched HO-RO_2 and to isoprene-derived HO-RO_2. Initial experimental work will be conducted via MPIMS investigations at the ALS in collaboration with Osborn and Taatjes and will be complemented by high-level theoretical calculations.

DOE Supported Publications 2019 - present

1. **Small Ester Combustion Chemistry: Computational Kinetics and Experimental Study of Methyl Acetate and Ethyl Acetate,** A. Ahmed, W. J. Pitz, C. Cavallotti, M. Mehl, N. Lokachari, E. J. K. Nilsson, J.-Y. Wang, A. A. Konnov, S. W. Wagnon, B. Chen, Z. Wang, H. J. Curran, S. J. Klippenstein, W. J. Roberts, S. M. Sarathy, *Proc. Combust. Inst.* **37**, 419-428 (2019).
2. **Simulating the Density of Organic Species in the Atmosphere of Titan with a Coupled Ion-Neutral Photochemical Model,** V. Vuitton, R. V. Yelle, S. J. Klippenstein, P. Lavvas, S. M. Horst, *Icarus* **324**, 120-197 (2019).
3. **EStokTP: Electronic Structure to Temperature- and Pressure-Dependent Rate Constants – A code for Automatically Predicting the Thermal Kinetics of Reactions,** C. Cavallotti, M. Pelucchi, Y. Georgievskii, S. J. Klippenstein, *J. Chem. Theory Comp*. **15**, 1122-1145 (2019).
4. **Ab Initio Kinetics for Pyrolysis and Combustion Systems,** S. J. Klippenstein, C. Cavallotti; in: Mathematical Modeling of Complex Reaction Systems: Pyrolysis and Combustion, T. Faravelli, F. Manenti, and E. M. Ranzi, Eds. Computer Aided Chemical Engineering Series, Elsevier: New York, (2019).
5. **Propane Clusters in Titan's Lower Atmosphere: Insights from a Combined Theory/Laboratory Study,** J. Bourgalais, O. Durif, S. D. Le Picard, P. Lavvas, F. Calvo, S. J. Klippenstein, L. Biennier, *Mon. Not. Roy. Ast. Soc*. **488**, 676-684 (2019).
6. **A Modular, Multi Diagnostic, Automated Shock Tube for Gas-Phase Chemistry,** M. E. Fuller, M. Skowron., R. S. Tranter, C. F. Goldsmith, *Rev. Sci. Instrum.*, 90, 064104 (2019)
7. **Thermal Dissociation Of Alkyl Nitrites And Recombination Of Alkyl Radicals,** J. B. Randazzo, M. E. Fuller, C. F. Goldsmith, R. S. Tranter, *Proc. Combust. Inst.*, 37,703-710 (2019).
8. **Investigation of Sampling-Probe Distorted Temperature Fields with X-Ray Fluorescence Spectroscopy,** N. Hansen, R. S. Tranter, J. B. Randazzo, J. P. A. Lockhart, A. L. Kastengren, *Proc. Combust. Inst.*, 37, 1401-1408 (2019).
9. **Synthesis, Electronic Spectroscopy, and Photochemistry of Methacrolein Oxide: A Four-Carbon Unsaturated Criegee Intermediate from Isoprene Ozonolysis,** M. F. Vansco, B. Marchetti, N. Tronsiriwat, T. Bhagde, G. Wang, P. J. Walsh, S. J. Klippenstein, M. I. Lester, *J. Am. Chem. Soc.* **141,** 15058-15069 (2019).
10. **Photodissociation Transition States Characterized by Chirped Pulse Millimeter Wave Spectroscopy,** K. Prozument, J. H. Baraban, P. B. Changala, G. B. Park, R. G. Shaver, J. S. Muenter, S. J. Klippenstein, V. Y. Chernyak, R. W. Field, *Proc. Nat. Acad. Sci*. **117**, 146-151 (2020).
11. **Reaction Profiles and Kinetics for Radical-Radical Hydrogen Abstraction via Multireference Coupled Cluster Theory,** C.-H. Wu, D. B. Magers, L. B. Harding, S. J. Klippenstein, W. D. Allen, *J. Chem. Theory Comp.* **16***,* 1511-1525 (2020).
12. **Experimental and Theoretical Studies of the Doubly-Substituted Methyl-Ethyl Criegee Intermediate: Infrared Action Spectroscopy and Unimolecuar Decay to OH Radical Products,** V. P. Barber, A. S. Hansen, S. J. Klippenstein, M. I. Lester**,** *J. Chem. Phys.* **152***, 094301* (2020).
13. **Direct Kinetic Measurements and Theoretical Predictions of an Isoprene-Derived Criegee Intermediate,** R. L. Caravan, M. F. Vansco, K. Au, M. A. H. Khan, Y.-L. Li, F. A. F. Winiberg, K. Zuraski, Y.-H. Lin, W. Chao, N. Trongsiriwat, P. J. Walsh, D. L. Osborn, C. J. Percival, J. Jr-M. Lin, D. E. Shallcross, L. Sheps, S. J. Klippenstein, C. A. Taatjes, M. I. Lester**,** *Proc. Nat. Acad. Sci.* **117**, 9733-9740 (2020).
14. **Formic Acid Catalyzed Isomerization and Adduct Formation of an Isoprene-Derived Criegee Intermediate: Experiment and Theory,** M. F. Vansco, R. L. Caravan, S. Pandit, K. Zuraski, F. A. F. Winiberg, K. Au, T. Bhagde, N. Trongsiriwat, P. J. Walsh, D. L. Osborn, C. J. Percival, S. J. Klippenstein, C. A. Taatjes, M. I. Lester**,** *Phys. Chem. Chem. Phys*. **22***,* 26796-26805 (2020).
15. **An Experimental and Theoretical Study of the High Temperature Reactions of All Four Butyl Radical Isomers,** J. B. Randazzo, R. Sivaramakrishnan., A. W. Jasper, T. Sikes, P. T. Lynch, R. S. Tranter, *Phys. Chem. Chem. Phys*, 22, 18304 -18319 (2020).
16. **Automated Theoretical Chemical Kinetics: Exploring the Initial Stages of Pyrolysis,** S. N. Elliott, K. B. Moore, A. V. Copan, M. Keceli, C. Cavallotti, Y. Georgievskii, H. F. Schaefer III, S. J. Klippenstein**,** *Proc. Combust. Inst.* **38**, 375-384 (2021).
17. **Functionalized Hydroperoxide Formation from the Reaction of Methacrolein-Oxide, an Isoprene-Derived Criegee Intermediate, with Formic Acid: Experiment and Theory** M. F. Vansco, K. Zuraski, F. A. F. Winiberg, K. Au, N. Trongsiriwat, P. J. Walsh, D. L. Osborn, C. J. Percival, S. J. Klippenstein, C. A. Taatjes, M. I. Lester, R. L. Caravan, *Molecules*, **26**, 3058 (2021).

18. **Entanglement Effect and Angular Momentum Conservation in a Non-separable Tunneling Treatment**, Y. Georgievskii, S. J. Klippenstein, *J. Chem. Theo. Comp*. **17**, 3863-3885 (2021).
19. **Watching a Hydroperoxyalkyl Radical (•QOOH) Dissociate**, A. S. Hansen, T. Bhagde, K. B. Moore III, Daniel R. Moberg, A. W. Jasper, Y. Georgievskii, M. F. Vansco, S. J. Klippenstein, M. I. Lester, *Science*, **373**, 679-682 (2021).
20. **Initiation Reactions in the High Temperature Decomposition of Styrene,** T. Sikes, C. B. Banyon, R. A. Schwind, P. T Lynch., A. Comandini, R. Sivaramakrishnan, R. S. Tranter, *Phys. Chem. Chem. Phys*, 23, 18432-18448 (2021).
21. **Editorial Joe V. Michael Memorial Issue** R. S. Tranter, N. Chaumeix, M. S. Wooldridge, *Int. J. Chem. Kinet.,* https://doi.org/10.1002/kin.21481 (2021).
22. **Ring Opening in Cycloheptane and Dissociation of 1-Heptene at High Temperatures,** T. Sikes, K. Bell Burdett., R. L. Speth, C. F. Goldsmith, R. Sivaramakrishnan, R. S. Tranter, *Proc. Combust. Inst.*, 38, 929-937 (2021).
23. **Theoretical Kinetics Predictions for $NH_2 + HO_2$,** S. J. Klippenstein, P. Glarborg, *Combust. Flame*, **236**, 111787 (2022).
24. **Dramatic Conformer-Dependent Reactivity of Acetaldehyde Oxide Criegee Intermediate with Dimethylamine via a 1,2-Insertion Mechanism,** M. F. Vansco, M. Zou, I. O. Antonov, K. Ramasesha, B. Rotavera, D. L. Osborn, Y. Georgievskii, C. J. Percival, S. J. Klippenstein, C. A. Taatjes, M. I. Lester, R. L. Caravan, *J. Phys. Chem. A*, 126, 710-719 (2022).
25. **Infrared Spectroscopic Signature of a Hydroperoxyalkyl Radical (•QOOH),** A. S. Hansen, T. Bhagde, Y. Qian, A. Cavazos, R. M. Huchmala, M. A. Boyer, C. F. Gavin-Hanner, S. J. Klippenstein, A. B. McCoy, M. I. Lester**,** *J. Chem. Phys*., 156, 014301 (2022).
26. **Rapid Allylic 1,6 H-Atom Transfer in an Unsaturated Criegee Intermediate,** A. S. Hansen, Y. Qian, C. A. Sojdak, M. Kozlowski, V. J. Esposito, J. S. Francisco, S. J. Klippenstein, M. I. Lester, *J. Am. Chem. Soc*., 144, 5945-5955 (2022).
27. **Energy-Resolved and Time-Dependent Unimolecular Dissociation of Hydroperoxyalkyl Radicals (•QOOH),** T. Bhagde, A. S. Hansen, S. Chen, P. J. Walsh, S. J. Klippenstein, M. I. Lester**,** *Faraday Disc*., accepted (2022).
28. **In Situ Temperature Measurements in Sooting Methane/Air Flames Using Synchrotron X-Ray Fluorescence of Seeded Krypton Atoms,** M. J. Montgomery, H. Kwon, A. L. Kastengren, L. D. Pfefferle, T. Sikes, R. S. Tranter ,Y. Xuan, C. S. McEnally, *Sci. Adv.,* https://doi.org/10.1126/sciadv.abm7947 (2022).
29. **Open Questions on the Reactivity of Criegee Intermediates** R. L. Caravan, M. F. Vansco, M. I. Lester, *Comm. Chem.*4, 44 (2021)
30. **Experimental Evidence of Dioxole Unimolecular Decay Pathway for Isoprene-Derived Criegee Intermediates** M.F. Vansco, R.L. Caravan, K. Zuraski, F.A.F. Winiberg, K. Au, N. Trongsiriwat, P.J. Walsh, D.L. Osborn, C.J. Percival, M.A.H. Khan, D.E. Shallcross, C.A. Taatjes and M.I. Lester, *J. Phys. Chem. A* 124, 3542-3554 (2020).
31. **Insertion Products in the Reaction of Carbonyl Oxide Criegee Intermediates with Acids: Chloro(Hydroperoxyl)Methane Formation from Reaction of CH_2OO with HCl and DCl**. C. A. Taatjes, R. L. Caravan. F. A. F. Winiberg, K. Zuraski, K. Au, L. Sheps, D. L. Osborn, L. Vereecken, C. J. Percival*. Mol. Phys*. e1975199 (2021).
32. **Absolute Photoionization Cross Section of the Simplest Enol, Vinyl Alcohol,** D. Rösch, R. L. Caravan, C. A. Taatjes, K. Au, R. Almeida and D. L. Osborn, *J. Phys. Chem. A* 125, 7920-7928 (2021).

References

[1] C. A. Taatjes, O. Welz, A. J. Eskola, J. D. Savee, A. M. Scheer, D. E. Shallcross, B. Rotavera, E. P. F. Lee, J. M. Dyke and D. K. W. Mok, Science **340**, 177-180 (2013).
[2] W. Chao, Y.-H. Lin, C. T. Yin, W. H. Lin, K. Takahashi and J. J. M. Lin, Phys. Chem. Chem. Phys. **21**, 13633-13640 (2019).
[3] H. F. Mull, G. J. R. Aroeira, J. M. Turney and H. F. Schaefer Phys. Chem. Chem. Phys. **22**, 22555-22566 (2020).
[4] M. F. Vansco, M. Zou, I. O. Antonov, K. Ramasesha, B. Rotavera, D. L. Osborn, Y. Georgievskii, C. J. Percival, S. J. Klippenstein, C. A. Taatjes, M. I. Lester and R. L. Caravan, J. Phys. Chem. A, **126**, 710-719 (2021).
[5] X. Zhang, K. M. Barraza and J. L. Beauchamp, Proc. Nat. Acad. Sci. **115**, 3255-3260 (2018).
[6] M. Zeng, N. Heine and K. R. Wilson, Proc. Nat. Acad. Sci. **117**, 4486-4490 (2020).

Chemical Dynamics in the Gas Phase at Argonne: Chemical Dynamics

Ahren W. Jasper, Stephen T. Pratt, and Kirill Prozument
Chemical Sciences and Engineering Division, Argonne National Laboratory, Lemont, IL 60439
ajasper@anl.gov, stpratt@anl.gov, and prozument@anl.gov

Program Scope

Complementary experimental and theoretical studies of gas phase dynamics are performed to explore unimolecular and bimolecular reactivity, energy flow within molecules and between collision partners, and the detailed mechanisms through which chemistry takes place. The studies produce improved theoretical methods and new fundamental descriptions of chemical dynamics at the molecular scale. The theoretical component is supplied by Jasper who emphasizes methods development and applications for collisional energy transfer, rovibrational anharmonicity, and electronically nonadiabatic chemistry, with recent studies taking advantage of high-performance computing. The experimental component is supplied by Pratt and Prozument. Pratt uses photoionization and photodissociation experiments to elucidate the spectroscopy and dynamics of highly excited molecules and radicals and to characterize the photoionization cross sections of reactive species, with future work focusing on inner- and outer-valence shell processes as well as new experiments using ultrafast free-electron laser sources. Prozument develops and applies chirped-pulse millimeter-wave spectroscopy to probe chemical dynamics and kinetics as well as artificial intelligence methods to assign rotational spectra. His future work involves a multi-experiment approach to understanding dynamical phenomena at different energy scales and in varied environments through the quantification of time- and vibrational-state-dependent branching ratios. Solving the inverse problem in rotational spectroscopy using artificial intelligence methods will also be pursued.

Recent Progress

Theory. A major goal of this work is to develop, apply, and demonstrate the accuracy of a priori predictions of collisional energy transfer (CET) and pressure dependent kinetics. In a recent study, low-pressure-limit microcanonical (collisional activation) and thermal rate constants were predicted using a combination of ab initio potential energy surfaces, classical trajectories, transition state theory, and a detailed kinetic model for systems where experimental information was available for validation. The a priori approach involved no adjustable parameters and employed a detailed "two-dimensional" (in both E, the total energy of the reactant, and J, its total angular momentum) description of CET. The predicted rate constants were found to be in excellent agreement with experiment (to better than ~25%) and performed equally well for atomic, diatomic, and polyatomic baths. Figure 1 shows a comparison for $H+O_2+M$.

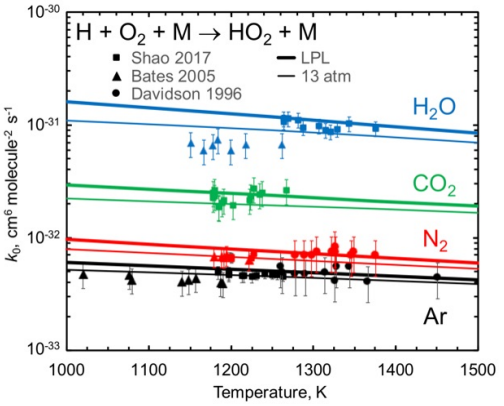

Fig 1. Low-pressure-limit (LPL) thermal rate constants k_0 for $H+O_2+M$ in four baths. The thicker lines show the calculated LPLs, and the thinner lines show the calculated rate constants at 13 atm. The predictions are compared with results from three experimental studies from Hanson's group.

Lower-level theories for CET were developed to provide the collision parameters α, σ, and ε required by less accurate but widely used kinetic models. We characterized more than 300 alkanes, alcohols, and hydroperoxides for common bath gases and including branched and multifunctional species with up to 16 nonhydrogen atoms N. From the data set, class-dependent formulas for the LJ parameters σ and ε were obtained as a function of N, and an "effective rotor" method was developed that mapped the expected value of α for a branched or multifunctional species onto a corresponding normal (linear) reference series.

We carried out several CET applications in collaboration with modelers and experimentalists, including $O_3(+M)$, $NH_3(+M)$, and $N_2H_4(+M)$ with Glarborg and co-workers, $N_3H_5(+M)$ and $N_4H_6(+M)$ with Green and co-workers, QOOH(+M) with Lester and co-workers, and several studies with Tranter and

Sivaramakrishnan. As an example, to support a modeling study from Glarborg we extended Macdonald's measured collision efficiencies for NH_3(+M) and N2H4(+M) to more baths and temperatures.

With Davis, the automation and validation of potential energy surface generation strategies was studied. Supported by an ASCR Leadership Computing Challenge (ALCC) computer time award, a strategy for symmetrizing permutationally invariant polynomial (PIP) expansions for systems of any stoichiometry was presented. Systems with up to 15 atoms and 39 degrees of freedom were considered, and permutational invariance was enforced in expansions with 30 million terms and 13 atom types. Later, we demonstrated a reduction in the number of terms needed for accurate PIP expansions using multi-pass greedy subset selection, a strategy borrowed from the statistics and signal processing literature, which is a kind of machine learning. The size of the reduced basis sets scaled ~linearly with dimensionality.

Experimental Photoionization and Photodissociation. Pratt is performing photoabsorption and photoionization experiments to highlight and elucidate specific intramolecular energy conversion processes among the rotational, vibrational, and electronic degrees of freedom in small molecules. New work includes time-resolved studies using free electron laser (FEL) facilities to complement and extend the frequency domain work performed in the laboratory and at synchrotron facilities.

Our experimental effort in photoionization and photodissociation dynamics focuses on both stable and reactive species, and it relies on laboratory-based techniques using lasers as well as facilities-based experiments using synchrotrons and FELs. Most of the synchrotron work is performed at the SOLEIL Synchrotron, which has several beamlines providing extremely high-resolution vacuum-ultraviolet light. This work requires a team of researchers, and we have been fortunate to work with an international group including Nahon, Garcia, and de Oliveira (SOLEIL), Gans and Boyé-Péronne (ISMO), Loison (Bordeaux), Holland (STFC, UK), and Powis (Nottingham).

In the past few years, we expanded our studies of electronic interactions to include inner-valence and inner-shell photoionization. This work characterizes how "molecular" effects might modify the "atomic" behavior of the inner-shell electrons. New high-resolution photoelectron spectroscopy measurements were performed near the Xe 3d and 4d edges in XeF_2 and were compared to measurements on atomic Xe and new theoretical predictions. While measurements of the Auger-Meitner electrons provided insight into the relaxation processes of the photoions, perhaps more interesting were the electrons from resonant neutral states excited just below the corresponding inner-shell ionization thresholds. These states correspond to shape resonances and Rydberg states that tend to decay by resonant Auger-Meitner processes (autoionization) into a large number of final states. Future synchrotron-based work will include systematic studies of these resonant processes below the I 4d and Xe 4d thresholds of CH_3I and XeF_2, respectively. This work will also be extended to iodobenzene and related methyl halides.

Recently, we participated in two collaborations and led a third collaboration to develop the potential of ultrafast VUV light sources for photoionization and photodissociation. The first two collaborations involved NH_3 and N_2 and were led by Stolow (Ottawa) and Ueda (Tohoku), respectively. An ultrafast VUV pulse was used to prepare coherent superpositions of rovibronic states, and a probe pulse was used to ionize the superpositions. Photoelectron distributions were recorded as a function of the time delay of probe pulse. These data showed how to disentangle different contributions (electronic coherences vs. population dynamics) to the time-dependent angular distribution parameters.**Error! Bookmark not defined.**

Last year, we led a large collaboration at the FERMI FEL to perform time-resolved photoelectron spectroscopy experiments on acetylene in which the (ν_1,ν_2,ν_3) = (0,1,7) and (1,0,5) vibronic levels of the $A\ ^1A_u$ state were populated by a 200-nm pump pulse, and the intermediate state was ionized by a VUV pulse from the FEL. The experiments follow the time evolution of the selected levels as revealed by photoelectron spectroscopy. Several decay channels are available at this pump energy, including internal conversion to high vibrational levels of the ground state, intersystem crossing to three different triplet states, dissociation to H + C_2H and H_2 + C_2, as well as isomerization to the vinylidene structure. The ongoing analysis of the data is complicated by the large signal from unpumped acetylene, but our preliminary analysis shows clear time-dependent behavior occurring on the ~100 fs timescale.

Chirped-Pulse Rotational Spectroscopy: Substitution reactions and tautomerization in acetone pyrolysis. In this project, collaboration within the Gas-Phase Chemical Physics Group at Argonne led to a comprehensive understanding of acetone pyrolysis. Notably, a new reaction involving H-atom substitution of the CH_3 group in acetone was demonstrated using the Modeling (Sivaramakrishnan), Experiment (Prozument), Theory (Klippenstein, Ruscic, Harding)—MET—paradigm, as outlined in Fig.

2. Following the initial Experimental discovery of the acetaldehyde product, the Modeling and Theory components suggested the substitution (addition/elimination) pathway in addition to the major H-atom abstraction pathway to ketene. The predicted branching ratio for [CH_3CHO]/[CH_2CO] of ~0.03 agreed with the experimental value. These often-neglected substitution reactions may be important in other thermally activated gas-phase reactions. Furthermore, using accurate thermochemistry, the importance of keto-enol tautomerization of acetone in this pyrolysis reaction was demonstrated. This insight guided additional experiments that confirmed the presence of the related products water, propene, and propyne.

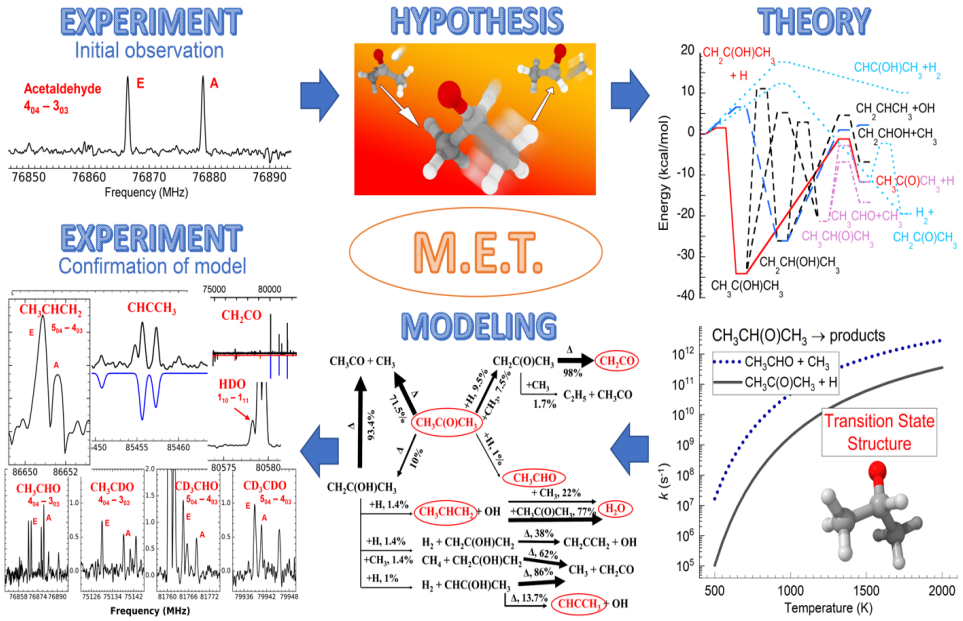

Fig. 2. The Modeling, Experiment, Theory (MET) paradigm applied to acetone

Future Work

Theory. We propose to develop models for predicting microcanonical low-pressure-limit rate constants using transition state theories (TST) instead of trajectories, with TST generalized to include energy- (momentum-) dependent dividing surfaces. Although described in foundational TST papers from Wigner and Keck, generalizations of the usual coordinate-only dividing surfaces have not found widespread use. When reactants and products are distinguished from one another by their internal energies, as in CET, TST dividing surfaces can be defined as a constraint on this energy. Such a simple constraint provides a valid dividing surface but surely features significant recrossing, and more accurate dividing surfaces likely involve more complex constraints on the momenta. Trajectories will be analyzed to develop useful momentum-dependent dividing surfaces that minimize recrossing with the goal of exploring whether or not transition state dividing surfaces for CET that are simple enough to be useful can be identified. Closely related to CET applications are intramolecular vibrational energy redistribution (IVR) applications, where one wishes to follow the flow of energy within a molecule to test statistical assumptions central to conventional TST, and IVR applications will also be pursued.

Another area where TST generalizations will be pursued is the characterization of nonthermal and nonequilibrium kinetics. The TST rate constant expression can be written $k = \frac{1}{2}\int dxdpf^{\ddagger}v/\Pi_R\int dxdpf_R$, i.e., as ½ the ratio of a phase space integral of the flux through the transition state dividing surface to a product of phase space integrals for the reactants. To evaluate this expression, one must *choose* the functions $f^{\ddagger}$ and f_R that describe the population distributions at the transition state and the reactants. When microcanonical or thermal equilibration choices are consistently made, the familiar TST expressions result. We will consider alternate choices appropriate for nonthermal reactions of recent interest like $H_2O^* + H \rightarrow H_2 + O_2$. In this example, we would employ mixed equilibration assumptions for f_R, with f_{H2O^*} described microcanonically with an internal energy E close to its dissociation threshold and f_{rel} for the relative H_2O + H translational coordinates described thermally by a temperature T. The corresponding choice for $f^{\ddagger}$ is not obvious (other than it should depend on E and T), as unambiguous 1-to-1 relationships between the degrees of freedom at the transition state and the reactants do not exist. Full-dimensional quasiclassical trajectories will be used to test and improve the accuracy of competing choices for $f^{\ddagger}$.

Experimental Photoionization and Photodissociation. We will continue to analyze time-resolved data for acetylene and double-resonance ionization and photoabsorption data for N_2. As this work progresses, we will record additional double-resonance spectra as necessary. We will continue to determine absolute cross sections for small free radicals using ion imaging spectroscopy. Radical precursors with a C-I bond are particularly attractive because they can generally be photodissociated near 266 nm and because the ionization energy of the I atom is low, minimizing the possibility of dissociative photoionization of the radical. We are hoping that the analysis of our recent experiments at SOLEIL will provide an improved cross section for I and thus result in better determinations for the radical species.

We will continue to study shake-up processes in the valence shell of N_2 and our inner-shell studies of CH_3I and XeF_2. Configuration interaction can become very large in inner-valence states, where the single-electron ionization energy can be close to the double ionization energy of outer valence orbitals. In this case, two-hole, one-particle states can have energies close to those of the one-hole states, and configuration interaction can be so strong that the molecular orbital picture breaks down. Even with highly specific detection methods, single-photon techniques are limited in how they can address such situations, and the interpretation of experiments rests largely on theory. Pratt is the lead on a collaborative beamtime proposal that was awarded at the FERMI FEL to use two-photon excitation to access the doubly excited configurations directly, and thus provide an additional window into these states.

The photoelectron spectrum of Xe above the 4p edge is a classic example of this phenomenon. In this case, the spectrum does not show the expected $^2P_{3/2}$ and $^2P_{1/2}$ peaks, but rather shows a single strong, structured peak with additional weaker features to higher energy. This observation results from strong mixing of $4d^{-2}nf$ and $4d^{-2}np$ states at the same energy as the $4p^{-1}$ states. We propose to record photoelectron spectra using two-photon excitation by the FEL to enhance the observation of the doubly excited configurations and thus provide a better experimental characterization of the 4p threshold. We will explore the corresponding processes in XeF_2, which will allow the observation of the "4p"σ_u* resonance and how it breaks up due to configuration interaction in its core. (Transitions to the "4p"σ_u* resonance are forbidden in single-photon excitation.) More generally, two-photon spectroscopy enabled by intense FEL sources will provide more direct access to two-hole, one-particle states formed by the resonant Auger-Meitner processes many different species.

We will soon purchase an intense, high-repetition-rate, ultrafast, line-tunable VUV laser system that will be delivered in the coming year. This system will allow UV-pump, VUV-probe experiments at selected VUV energies. Velocity-map ion imaging experiments would then allow detailed exploratory measurements for future FEL work. Longer term developments will include the extension to time-dependent photodissociation and photoionization studies with photoion and photoelectron detection.

Chirped-Pulse Rotational Spectroscopy. The inverse problem for rotational spectroscopy is formulated as the need to predict the molecular geometry from a rotational spectrum. We hypothesize that training an artificial neural network[a] on molecular spectra and geometries may be a fruitful direction to address that challenge. Prozument and Davis have established a collaboration with Prof. Eric Jonas and his graduate student Marcus Schwarting from the Department of Computer Science, University of Chicago to address that task. The forward problem (calculated geometries → rotational spectra) is now mostly solved and is being used to create a molecular data set suitable for the task. We plan to choose the optimal DFT method for geometry optimization and for calculating the magnitude and the direction of dipole moments. We will explore how the accuracy of the DFT calculations affects whether our prediction of the molecular identity from a spectrum is unique or if, at least, a set of predicted candidate molecules is possible. We anticipate the optimal transport metric for comparing rotational spectra developed by Davis to be essential for evaluating the accuracy of the simulated spectra in this work.

We plan additional studies of oxidation chemistry using our newly designed heated microreactor. For instance, we are interested in determining a pathway to formaldehyde from $C_2H_4 + O_2$. Naturally, a network of reactions initiated by the H-atom abstraction to form $HO_2 + C_2H_3$ is the major contributor. We are also interested in exploring whether singlet oxygen molecules may play a role by inserting themselves into the C=C double bond: $O_2(^1\Delta_g) + CH_2CH_2 \rightarrow 2\ CH_2O$.[b] Time-resolved photodissociation experiments[c] are planned with nitrogen-containing species such as formamide (NH_2CHO), methyl carbamate ($CH_3OC(O)NH_2$), urethane ($CH_3CH_2OC(O)NH_2$), and benzamide ($C_6H_5C(O)NH_2$). Competition between

these processes in highly energized molecules will be investigated: H-atom scrambling; H-atom transfer; HCN, HNC, and HNCO elimination via tight transition states; H-N and H-C simple bond fissions.
[a]D. P. Zaleski and K. Prozument, *J. Chem. Phys.* 149, 104106 (2018). [b]R. Sun, K. Park, W. A. de Jong, H. Lischka, T. L. Windus, and W. L. Hase, *J. Chem. Phys.* 137, 044305 (2012). [c]D. P. Zaleski, L. B. Harding, S. J. Klippenstein, B. Ruscic, and K. Prozument, *J. Phys. Chem. Lett.* 8, 6180 (2017).

Publications supported by this project since 2019

1. D. E. Couch, G. Kukkadapu, A. J. Zhang, A. W. Jasper, C. A. Taatjes, and Nils Hansen, The role of radical-radical chain propagating pathways in the phenyl + propargyl reaction. *Proc. Combust. Inst.*, accepted (2022).
2. J. Cho, Y. Tao, Y. Georgievskii, S. J. Klippenstein, A. W. Jasper, and R. Sivaramakrishnan, The role of collisional energy transfer on the thermal and prompt dissociation of 1-methyl allyl. *Proc. Combust. Inst.*, accepted (2022).
3. Z. Wang, H. Zhao, C. Yan, Y. Lin, A. D. Lele, W. Xu, B. Rotavera, A. W. Jasper, S. J. Klippenstein, and Yiguang Ju, Methanol oxidation up to 100 atm in a supercritical pressure jet-stirred reactor. *Proc. Combust. Inst.*, accepted (2022).
4. J. Jian, H. Hashemi, H. Wu, A. W. Jasper, and P. Glarborg, A reaction mechanism for ozone dissociation and reaction with hydrogen at elevated temperature. *Fuel* 322, 124138 (2022).
5. A. W. Jasper, Predicting third-body collision efficiencies for water and other polyatomic baths. *Faraday Discuss.,* online (2022). DOI: 10.1039/D2FD00038E
6. C. Yan, H. Zhao, Z. Wang, G. Song, Y. Lin, C. R. Mulvihill, A. W. Jasper, S. J. Klippenstein, and Y. Ju, Low- and intermediate-temperature oxidation of dimethyl ether up to 100 atm in a supercritical pressure jet-stirred reactor. *Combust. Flame,* online (2022). DOI: 10.1016/j.combustflame.2022.112059
7. R. Forbes, P. Hockett, I. Powis, J. D. Bozek, S. T. Pratt, and D. M. P. Holland, Auger electron angular distributions following excitation or ionization from the Xe 3d and F 1s levels in xenon difluoride, *Phys. Chem. Chem. Phys.*, **24**, 1367-1379 (2022).
8. I. Fischer and S. T. Pratt, Photoelectron spectroscopy in molecular physical chemistry, *Phys. Chem. Chem. Phys.* **24**, 1944-1959 (2022).
9. D. R. Moberg, A. W. Jasper, and M. J. Davis, Parsimonious potential energy surface expansions using dictionary learning with multi-pass greedy selection. *J. Phys. Chem. Lett.* **12**, 9169–9174 (2021).
10. A. R. Conrad, N. Hansen, A. W. Jasper, N. K. Thomason, L. Hidaldo-Rodrigues, S. Treshock, and D. M. Popolan-Vaida, Identification of the acetaldehyde oxide Criegee intermediate reaction network in the ozone-assisted low-temperature oxidation of trans-2-butene. *Phys. Chem. Chem. Phys.* **23**, 23554–23566 (2021).
11. D. R. Moberg and A. W. Jasper, Permutationally invariant polynomial expansions with unrestricted complexity, *J. Chem. Theory Comput.* **17**, 5440–5455 (2021).
12. A. S. Hansen, T. Bhagde, K. B. Moore III, D. R. Moberg, A. W. Jasper, Y. Georgievskii, M. F. Vansco, S. J. Klippenstein, and M. I. Lester, Watching a hydroperoxyalkyl radical (•QOOH) dissociate. *Science* **373**, 679–682 (2021).
13. P. Glarborg, H. Hashemi, S. Cheskis, and A. W. Jasper, On the rate constant for NH_2 + HO_2 and third body collision efficiencies for NH_2 + H (+M) and NH_2 + NH_2 (+M). *J. Phys. Chem. A* **125**, 1505–1516 (2021).
14. J. A. Miller, R. Sivaramakrishnan, C. F. Goldsmith, M. P. Burke, A. W. Jasper, J. Zádor, N. Hansen, N. J. Labbe, and P. Glarborg, Combustion chemistry in the twenty-first century: Developing theory-informed chemical kinetics models. *Prog. Energy Combust. Sci.* **83**, 100886 (2021).
15. Y. Tao, A. W. Jasper, Y. Georgievskii, S. J. Klippenstein, and R. Sivaramakrishnan, Termolecular chemistry facilitated by radical-radical recombinations and its impact on flame speed predictions. *Proc. Combust. Inst*. **31**, 515–522 (2021).
16. N. Hansen, G. Kukkadapu, B. Chen, S. Dong, H. J. Curran, C. A. Taatjes, A. J. Eskola, D. L. Osborn, L. Sheps, W. J. Pitz, K. Moshammer, A. W. Jasper, W. Chen, J. Yang, and Z. Wang, The impact of the third O_2 addition reaction network on ignition delay times of neo-pentane. *Proc. Combust. Inst*. **31**, 299–307 (2021).
17. M. Fushitani, S. T. Pratt, D. You, S. Saito, Y. Luo, K. Ueda, H. Fujise, A. Hishikawa, H. Ibrahim, F. Légaré, P. Johnsson, J. Peschel, E. R. Simpson, A. Olofsson, J. Mauritsson, P. A. Carpeggiani, Praveen K. Maroju, M. Moioli, D. Ertel, R. Shah, G. Sansone, T. Csizmadia, M. Dumergue, N. G. Harshitha, S.Kühn, C. Callegari, O. Plekan, M. Di Fraia, M. Danailov, Luca Giannessi, L. Raimondi, M. Zangrando, G. De Ninno, P. Rebernik Ribic, and K. C. Prince, Time-resolved photoelectron imaging of complex resonances in molecular nitrogen, *J. Chem. Phys.* **154**, 144305 (2021).
18. R. Forbes, P. Hockett, I. Powis, J. D. Bozek, D. M. P. Holland, and S. T. Pratt, Photoionization from the Xe 4d orbitals of XeF_2, *J. Chem. Phys.* **155**, 194301 (2021).
19. M. Patanen, A. R. Abid, S. T. Pratt, A. Kivimäki, A. B. Trofimov, A. D. Skitnevskay, E. K. Grigoricheva, E. V. Gromov, I. Powis, and D. M. P. Holland, Valence shell photoelectron angular distributions and vibrationally resolved spectra of imidazole: A combined experimental-theoretical study, *J. Chem. Phys.* 155, 054304 (2021).
20. R. Lambo, C. -Y. Xu, S. T. Pratt, H. Xu, J. C. Zappala, K. G. Bailey, Z. -T. Lu, P. Mueller, T. P. O'Connor, B. B. Kamorzin, D. S. Bezrukov, Y. Xie, A. A. Buchachenko, and J. T. Singh, High resolution spectroscopy of neutral Yb atoms in a solid Ne matrix, *Phys. Rev. A*, **104**, 062809 (2021).
21. D. P. Zaleski, R. Sivaramakrishnan, H. R. Weller, N. A. Seifert, D. H. Bross, B. Ruscic, K. B. Moore III, S. N. Elliott, A. V. Copan, L. B. Harding, S. J. Klippenstein, R. W. Field, and K. Prozument, Substitution reactions in the pyrolysis of acetone revealed through a modeling, experiment, theory paradigm, *J. Am. Chem. Soc.* **143**, 3124–3142 (2021).
22. N. A. Seifert, K. Prozument, and M. J. Davis, Computational optimal transport for molecular spectra: The fully discrete

case, *J. Chem. Phys.* **155**, 184101 (2021).
23. A. C. Rousso, A. W. Jasper, Y. Ju, and N. Hansen, Extreme low temperature combustion chemistry: Ozone-initiated oxidation of methyl hexanoate, *J. Phys. Chem. A* **124**, 9897–9914 (2020).
24. J. B. Randazzo, A. W. Jasper, R. Sivaramakrishnan, T. Sikes, P. T. Lynch, and R. S. Tranter, An experimental and theoretical study of the high temperature reactions of four butyl radical isomers, *Phys. Chem. Chem. Phys.* **22**, 18304–18319 (2020).
25. Z. Wang, N. Hansen, A. W. Jasper, B. Chen, S. M. Popolan-Vaida, K. K. Yalamanchi, A. Najjar, P. Dagaut, and S. M. Sarathy, Cool flame chemistry of diesel surrogate compounds: n-decane, 2-methylnonane, 2,7-dimethyloctane, and n-butylcyclohexane. *Combust. Flame* **219**, 384–392 (2020).
26. A. W. Jasper, "Third-body" collision parameters for hydrocarbons, alcohols, and peroxides and an effective internal rotor approach for estimating them. *Int. J. Chem. Kinet.* **52**, 387–402 (2020).
27. A. W. Jasper, Microcanonical rate constants for unimolecular reactions in the low-pressure limit. *J. Phys. Chem. A* **124**, 1205–1226 (2020).
28. R. Forbes, S. T. Pratt, A. De Fanis, A. R. Milosavljević, C. Nicolas, J. D. Bozek, N. A. Besley, and D. M. P. Holland, Photoabsorption, photoionization, and auger processes at the carbon K-edge in CH_3I, *Phys. Rev.* A **101**, 023408 (2020).
29. R. Forbes, A. De Fanis, D. Rolles, S. T. Pratt, I. Powis, N. A. Besley, A. R. Milosavljević, C. Nicolas, J. D. Bozek, and D. M. P. Holland, Photoionization of the I 4d and valence orbitals of methyl iodide, *J. Phys.* B **53**, 155101 (2020).
30. S. Hartweg, J. -C. Loison, S. Boyé-Péronne, B. Gans, D. M. P. Holland, G. A. Garcia, L. Nahon, and S. T. Pratt, Photoionization of the C_4H_5 isomers, *J. Phys. Chem.* A **124**, 6050-6060 (2020).
31. H. R. Hrodmarsson, B. Gans, S. Boyé-Péronne, G. A. Garcia, L. Nahon, S. T. Pratt, D. M. P. Holland, The effect of autoionization on the HBr^+ $^2\Pi_{3/2,1/2}$ state photoelectron angular distributions *Chem. Phys.* 539, 110961 (2020).
32. V. Makhija, K. Véyrinas, A. E. Boguslavskiy, R. Forbes, I. Wilkinson, R. Lausten, S. P. Neville, S. T. Pratt, M. S. Schuurman, and A. Stolow, Ultrafast molecular frame electronic coherences from lab frame scattering anisotropies, *J. Phys. B* **53**, 114001 (2020).
33. K. Prozument, J. H. Baraban, P. B. Changala, G. B. Park, R. G. Shaver, J. S. Muenter, S. J. Klippenstein, V. Y. Chernyak, and R. W. Field, Photodissociation transition states characterized by chirped pulse millimeter wave spectroscopy, *Proc. Nat. Acad. Sci.* **117**, 146–151(2020).
34. K. Prozument, B. G. Sartakov, and A. F. Vilesov, Mixed ortho-H_2 and para- H_2 clusters studied by vibrational coherent anti-Stokes Raman spectroscopy, *Phys. Rev. B* **101**, 184507 (2020).
35. O. J. Harper, M. Hassenfratz, J.-C. Loison, G. A. Garcia, N. de Oliveira, H.R. Hrodmarsson, S. T. Pratt, S. Boyé-Péronne, and B. Gans, Quantifying the photoionization cross section of the hydroxyl radical, J. Chem. Phys. **150**, 141103 (2019); *J. Chem. Phys.* **152**, 189903 (2020).
36. N. Hansen, K. Moshammer, and A. W. Jasper, Isomer-selective detection of keto-hydroperoxides in the low-temperature oxidation of tetrahydrofuran. *J. Phys. Chem. A* **123**, 8274–8284 (2019).
37. A. W. Jasper, L. B. Harding, C. Knight, and Y. Georgievskii, Anharmonic rovibrational partition functions at high temperatures: Tests of reduced-dimensional models for systems with up to three fluxional modes. *J. Phys. Chem. A* **123**, 6210–6228 (2019).
38. A. Grinberg Dana, K. B. Moore, A. W. Jasper, and W. H. Green, Large Intermediates in hydrazine decomposition: A theoretical study of the N_3H_5 and N_4H_6 potential energy surfaces. *J. Phys. Chem. A* **123,** 4679–4692 (2019).
39. A. W. Jasper and M. J. Davis, Parameterization strategies for intermolecular potentials for predicting trajectory-based collision parameters. *J. Phys. Chem. A* **123**, 3464–3480 (2019).
40. A. C. Rousso, N. Hansen, A. W. Jasper, and Y. Ju, Identification of the Criegee intermediate reaction network in ethylene ozonolysis: Impact on energy conversion strategies and atmospheric chemistry. *Phys. Chem. Chem. Phys.* **21**, 7341–7357 (2019).
41. A. W. Jasper, R. Sivaramakrishnan, and S. J. Klippenstein, Nonthermal rate constants for $CH_4^* + X \rightarrow CH_3 + HX$, X = H, O, OH, and O_2. *J. Chem. Phys.* **150**, 114112 (2019).
42. M. Keçeli, S. Elliott, Y.-P. Li, M. S. Johnson, C. Cavallotti, Y. Georgievskii, W. H. Green M. Pelucchi, J. M. Wozkiak, A. W. Jasper, and S. J. Klippenstein, Automated computational thermochemistry for butane oxidation: A prelude to predictive automated combustion kinetics. *Proc. Combust. Inst.* **37**, 363–371 (2019).
43. D. H. Bross, A. W. Jasper, B. Ruscic, and A. F. Wagner, Toward accurate high temperature anharmonic partition functions. *Proc. Combust. Inst.* **37**, 315–322 (2019).
44. A. Sen and S. T. Pratt, Double-resonance studies of electronically autoionizing states of molecular nitrogen, *Mol. Phys.* **117**, 2930-2940 (2019).
45. H. R. Hrodmarsson, J.-C. Loison, U. Jacovella, D. M. P. Holland, S. Boyé-Péronne, B. Gans, G. A. Garcia, L. Nahon, and S. T. Pratt, Valence-shell photoionization of the C_4H_5 radical, *J. Phys. Chem. A* **123**, 1521-1528 (2019).
46. A. B. Trofimov, A. M. Belogolova, S. A. Serebrennikova, R. Forbes, S. T. Pratt, and D. M. P. Holland, An experimental and theoretical study of the C 1s ionization satellites in CH_3I, *J. Chem. Phys.* **150**, 224303 (2019).
47. B. Gans, G. A. Garcia, S. Boyé-Péronne, S. T. Pratt, J.-C. Guillemin, A. Aguado, O. Roncero, and J. C. Loison, Origin band of the first photoionizing transition of hydrogen isocyanide, *Phys. Chem. Chem. Phys.* **21**, 2337-2344 (2019).

Chemical Dynamics in the Gas Phase at Argonnne: Thermochemistry

Branko Ruscic and Stephen J. Klippenstein
Chemical Sciences and Engineering Division, Argonne National Laboratory,
9700 South Cass Avenue, Lemont, IL 60439
ruscic@anl.gov, sjk@anl.gov

Program Scope

The *spiritus movens* of this program is the need to provide the scientific community with accurate and reliable thermochemical information on chemical species that are relevant in energy-generating chemical processes or play prominent roles in subsequent environmental chemistry. Detailed knowledge of thermodynamic parameters for a broad array of stable and ephemeral chemical species is pivotal to chemistry and essential in many industries. In particular, the availability of accurate, reliable, and internally consistent thermochemical values is a *conditio sine qua non* in kinetics, reaction dynamics, formulation of plausible reaction mechanisms, and construction of predictive models of complex chemical environments. In addition, the availability of accurate thermochemical values has historically been the prime driver for steady advancements of increasingly sophisticated electronic structure theories.

The focus of this program is on bringing substantial innovations to the thermochemical field through development of new methodologies, and utilizing them to systematically improve both the quality and quantity of available thermochemical data relevant to energy–producing processes. In order to achieve the stated goals, this program has developed a novel approach that is centered on analyzing and optimally utilizing the information content of *all available* thermochemically relevant determinations. The aim is not only to dynamically produce the best currently possible thermochemical parameters for the targeted chemical species, but also to allow efficient updates with new knowledge, properly propagating its consequences through all affected chemical species, as well as to provide critical tests of new experimental or theoretical data, and generate pointers to new determinations that are most likely to efficiently improve the overall thermochemical knowledge base. In order to provide a broad perspective of this area of science, the effort of this Subtask is synergistically coordinated with related experimental and theoretical efforts within other Subtasks of the Chemical Dynamics in the Gas Phase Group at Argonne.

Recent Progress

Over the past year we have continued the development of Active Thermochemical Tables (ATcT). Briefly, ATcT - the centerpiece of the Thermochemistry Subtask of the Chemical Dynamics in the Gas Phase Program at Argonne - are a new paradigm for developing accurate and reliable thermochemical values for stable and reactive chemical species. Thermochemical determinations (reaction enthalpies, equilibrium constants, bond dissociation energies, etc.) by definition involve several chemical species, and thus define the enthalpy of formation of the target chemical species *relative* to other species. Consequently, enthalpies of formation generally do not correspond to directly measured quantities; rather, they are indirectly defined via complex manifolds of thermochemical dependencies. Historically, extracting the enthalpies of formation from intertwined (and frequently inconsistent) dependencies was an intractable proposition, resulting in a simplified *sequential* approach of inferring the enthalpies of formation one at the time (A begets B, B begets C, etc.), delivering static sets of values that contain hidden progenitor-progeny relationships and cannot be updated with new knowledge without introducing inconsistencies. The success of ATcT is rooted in treating the intertwined determinations as a network of simultaneous dependences that is amenable to mathematical and statistical manipulation, converting the originally intractable problem to an information-rich environment that produces a quantum leap in the quality and reliability of the resulting thermochemistry. The Thermochemical Network (TN) corresponds to a system of qualified constrains that must be simultaneously satisfied in order to produce enthalpies of formation that correctly reflect the epistemic content of the TN. Because of the unavoidable presence of

determinations with 'optimistic' uncertainties (a.k.a. erroneous determinations), ATcT first performs an iterative statistical analysis, which isolates them and brings the TN to self-consistency. Once self-consistency is achieved, ATcT proceeds to solve the TN simultaneously for all included species.

The most significant vehicle for disseminating the ATcT results is the ATcT website, ATcT.anl.gov, which continues to grow in popularity, and is generally hyped in the literature as the most reliable source of accurate enthalpies of formation for species relevant in combustion and atmospheric chemistry, as well as other areas. The website is attracting 20,000 – 30,000 visitors each month. Though it is not straightforward to exactly quantify the website traffic (e. g. distinguishing between a lengthier single visit with multiple queries and repeat visits), a scrutiny of the cumulative Apache server logs indicates that during the previous 12 months the website has been visited by approximately a quarter million *different* IP addresses (i.e. not counting repeat visits from the same IP address).

During the last year, we have publicly released two versions of ATcT results, 1.122q and 1.122r.[1,2] Of note is that ATcT results are strictly versioned, and - once published - remain indefinitely available on the website. ATcT TN ver. 1.122q played an important role in our revision[3] (by 2 kcal/mol) of the ostensibly very accurate experimental enthalpy of formation of oxalic acid, conducted in collaboration with D. Feller (WSU), and in our careful evaluation of alternative high-level theoretical approaches suitable for oxygen-rich radicals (using methyl and ethyl peroxy radicals as tests), conducted in collaboration with R. Dawes (MST).[4] That version contains 1790 chemical species, interconnected by >23,000 determinations. The latest web version, ATcT TN 1.122r, contains >25,500 active thermochemically-relevant determinations and incorporates 2032 chemical species, thus formally surpassing JANAF's volume of 1816 species (albeit JANAF has a significantly broader diversity of species, involving 47 chemical elements, compared to 14 elements in ATcT TN ver. 1.122r). This version of ATcT results was employed in our pilot study that explored the effects of anharmonicity on thermophysical quantities, using CH_2OH as a test case.[5]

The current developmental version of the TN (1.126, the ontogenesis of which is still in progress) has grown to ~2970 chemical species, interconnected by >31,000 active thermochemically-relevant determinations (both from experiment and high-level theory), as well as several thousands of inactive determinations that have been rendered obsolescent during earlier ATcT TN analyses and rounds of improvements.

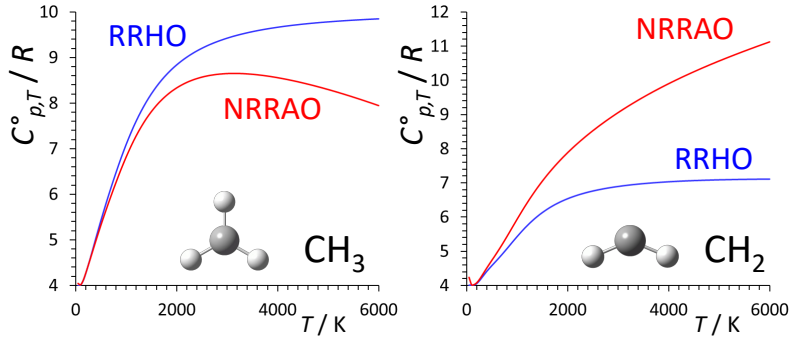

Figure 1. Illustration of significant differences in thermophysical properties for methyl and methylene radicals, obtained by NRRAO (red) and RRHO (blue) approaches, using heat capacity as an example.

Our earlier study of NRRAO (non-rigid rotor anharmonic oscillator) thermophysical properties of CH_2OH has been complemented last year by a study involving the use of our NRRAO approach to further improve and finalize the thermophysical properties of CH_3 and CH_2,[6] two key radicals. The spectroscopic constants needed for estimating NRRAO thermophysical properties were obtained by complementing the best available experimental constants with higher–order constants obtained via VPT2 at the CCSD(T)/ANO1 level of theory. The results demonstrate that in both of these radicals, the standard RRHO (rigid rotor harmonic oscillator) thermophysical properties are clearly inadequate at combustion temperatures (see Figure 1, where for simplicity only the behavior of the heat capacity is displayed, noting that, since it depends both on the first and the second derivative of the partition function, it usually corresponds to the most sensitive thermophysical property). Methylene exhibits the more usual departure of NRRAO properties from RRHO properties, typical of species where most of the anharmonicities are negative, producing densities of states that are larger than those predicted by harmonic behavior. On the

other hand, methyl displays the opposite behavior, largely governed by the positive anharmonicity of the CH_3 inversion.

Another study that should be mentioned here is that of the pyrolysis of acetone,[7] which is discussed in more detail in the Dynamics Subtask of this Program. This collaborative study, involving the MET (modelling, experiment, theory) paradigm, includes many members of the Gas Phase Chemical Dynamics Program, and vividly demonstrates the synergistic interaction across multiple Subtasks of our program.

We have also continued a broad range of collaborations outside the Gas Phase Chemical Dynamics Group at ANL. In particular, the ATcT Task Force One (J. Stanton and T. L. Nguyen and their groups at UF, B. Ellison, UColorado, B. Changala, Harvard-Smithsonian, J. Baraban and his group at Ben-Gurion, and D. H. Bross, ANL) continues to be very active, maintaining weekly teleconference meeting. We have several ongoing projects, and would like to highlight here the current expansion of ATcT coverage with sulfur compounds. The study combines existing experimental determinations with state-of-the-art HEAT computations performed at UF, which will result in the establishment of accurate thermochemistry for key sulfur-containing species such as SO, SO_2, SO_3, H_2SO_4, etc., and will force a revision of the CODATA enthalpy of formation of S atom (a key quantity for electronic structure methods that utilize the route of total atomization energy to derive enthalpies of formation). A different project within this Task Force focused on exploring the limit of what can be achieved with current computational capabilities.[8] A select benchmark of 4 molecules (HF, CO, N_2, H_2O) for which the relevant components could be computed using very large basis sets (including aug–cc–pV7Z and aug–cc–pV8Z, which were newly constructed for the purpose of this study), and for which ATcT can provide total atomization enthalpies with uncertainties under ± 5 cm^{-1}, has led to the inference that the current computational accuracy limit is the order of ± 8–15 cm^{-1}. This study also enabled us to perform a careful re–examination of the standard HEAT family of computations, developed some time ago using ATcT benchmarks.[9]

A second Task Force (collab. with K. Peterson, WSU and his group, and D. H. Bross, ANL) is aiming to expand ATcT into actinides. Historically, the thermochemistry of actinides relied on difficult and inconsistent experimental determinations, which can be now either corroborated or challenged with highly improved computational methods developed at WSU, synergistically combining theory and experiment.

In collaboration with the ECC project (led by J. Zador, Sandia CRF), we have started enabling ATcT to describe the thermochemistry of adsorbates that occur on the gas phase/solid phase interfaces. We have now developed the core systematics for these species, which parallels in a number of ways the ATcT systematics for aqueous thermochemistry (albeit with an inherently higher complexity).

Through DOE-ASCR funding we have developed software (AutoMech) for generating thermochemical properties from automated sequences of electronic structure calculations.[10-12] Currently, this software allows us to implement arbitrary composite electronic structure methods, with full torsional sampling, multidimensional torsional treatments including vibrationally adiabatic analyses along the torsions, a variety of approximate one-dimensional torsional schemes, and vibrational perturbation theory based anharmonic corrections. The availability of this software affords us with many exciting new opportunities for large scale studies of chemical effects on thermochemistry, which we have begun to explore as part of this program. In particular, in collaboration with the Curran group, we used the AutoMech software to explore the ab initio thermochemical properties of large sets of species of relevance to C1-C8 alkane oxidation. As part of these studies, we explored the accuracy of various assumptions, applied the methodology to large sets of species, produced new group values for use in kinetic modeling, and studied the effect of employing ab initio properties on ignition delay simulations. Four manuscripts describing this work are in various stages of preparation.

An important feature of our AutoMech code is its fully automated implementation of the connectivity-based hierarchy (CBH) scheme of Raghavachari and coworkers,[13] up to CBH-2, building from an ANL0 based database for the reference species. Notably, the set of species mapped in our recent ANL0 study[14] captures almost the full set of CBH-2 references. Of course, the ANL0 database itself relies on the ATcT

values for the smallest reference species (i.e., H_2, CH_4, and H_2O for C/O/H species). This implementation allows for the automated prediction of high accuracy ($2\sigma \sim \pm 0.5$ kcal/mol) 0 K heats of formation for arbitrarily large acyclic C/O/H species at DFT level costs starting from just the SMILEs or InChI representation for the molecule of interest.

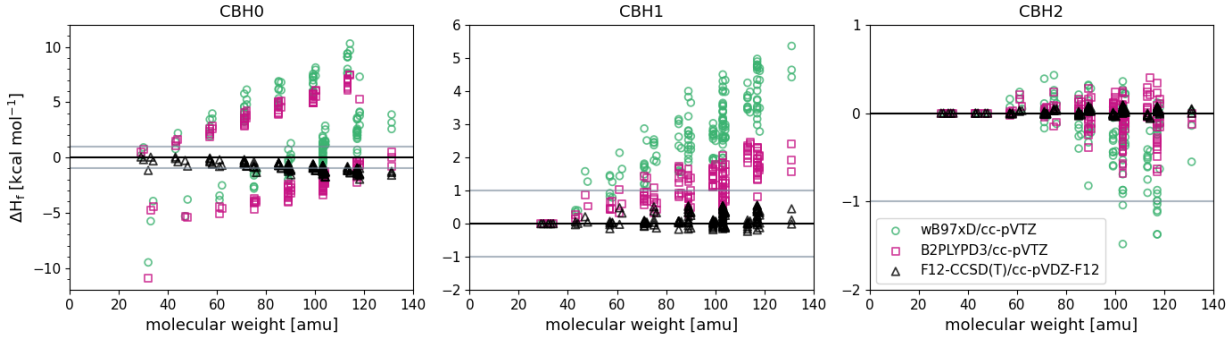

Figure 2. This plot shows the differences in the heat of formations [ΔH^0_f (0 K)] for 158 species calculated using various electronic structure methods (see inset) relative to those calculated with the CBH-2 scheme for F12-CCSD(T)/cc-pVTZ-F12//B2PLYPD3/cc-pVTZ.

For example, with this approach, we have recently evaluated the 0 K heat of formation for a representative set of 210 alkane (RH), alkyl (R), peroxy (RO_2), and alkylhdyroxperoxy (QOOH) species containing up to 8 carbon atoms at the ωb97-xD/cc-pVTZ, B2PLYPD3-cc-pVTZ, CCSD(T)-F12/cc-pVDZ-F12//B2PLYP-D3/cc-pVTZ, and CCSD(T)-F12/cc-pVTZ-F12//B2PLYP-D3/cc-pVTZ levels and for CBH-0, CBH-1, and CBH-2 reference reactions. As illustrated in Fig. 2, the CBH-2 scheme yields remarkably small variations in the predicted 0 K heat of formation for the various methods relative to the CCSD(T)-F12/cc-pVTZ-F12 based CBH-2 values. Indeed, for the CBH-2 B2PLYPD3/cc-pVTZ results, the mean error is only -0.04 kcal/mol, while the square root of the variance from this value is only 0.19 kcal/mol. Notably, the final accuracy of the predictions also depends on the accuracy of the values for the underlying reference species, thus motivating continued efforts at determining high accuracy values for the core chemical species.

Future Plans

Future plans of this program pivot around further development and expansion of the Active Thermochemical Tables approach, continuing to provide accurate thermochemistry to the scientific community, and driving targeted thermochemically-relevant theoretical and experimental investigations of radicals and transient species that are intimately related to combustion and post-combustion atmospheric processes. A significant part of the effort will be focused on continued ‘finalization’ and dissemination of the resulting ATcT thermochemistry, typically involving groups of related chemical species. One important component of this process, focused on their enthalpies of formation, consists of testing and analyzing the TN dependencies, using tools such as the variance/covariance decomposition approach and analyses of the influence of relevant determinations via the hat-matrix, followed by improving the connectivity within the TN and adding new high-quality results (either virtual, i.e. computational, or actual, i.e. experimental) to coerce the resulting thermochemistry toward stable, ‘release quality’ values. This iterative process unavoidably results in an expansion of the TN with new related chemical species, which is an added benefit. Another equally important component focuses on enhancing the accuracy of the partition functions, typically by upgrading RRHO partition functions to NRRAO partition functions, which is also a currently ongoing effort. Future plans also incorporate the expansion of the per-species data presented on our website, as well as expansion of ATcT coverage to other interesting areas of chemistry (catalysis, batteries, etc.)

Our proposed theoretical thermochemistry work will continue with further developments and applications of the AutoMech code. This work will involve the expanded application of the CBH-2 schemes to additional sets of molecules. As part of these applications, we will extend the code and the

thermochemical data for the reference species to handle other elements and molecular structures. We will also dig more deeply into the role of low frequency motions for the partition functions of large molecules such as large alkanes and bioesters. Finally, we will explore the utility of the databases we generate for machine learning based representations of the properties.

This work is supported by the U.S. Department of Energy, Office of Basic Energy Sciences, Division of Chemical Sciences, Geosciences, and Biosciences, under Contract No. DE–AC02–06CH11357.

References

[1] B. Ruscic and D. H. Bross, Active Thermochemical Tables (ATcT) Values Based on Ver. 1.122q of the Thermochemical Network, Argonne National Laboratory, Lemont, Ill. (2021), available at *https://atct.anl.gov/Thermochemical%20Data/version%201.122q/index.php*; DOI: 10.17038/CSE/1822363
[2] B. Ruscic and D. H. Bross, Active Thermochemical Tables (ATcT) Values Based on Ver. 1.122q of the Thermochemical Network, Argonne National Laboratory, Lemont, Ill. (2021), available at *https://atct.anl.gov/Thermochemical%20Data/version%201.122q/index.php*; DOI: 10.17038/CSE/1822363
[3] D. Feller, D. H. Bross, and B. Ruscic, *J. Phys. Chem. A* **123**, 3481–3496 (2019).
[4] B. K. Welch, R. Dawes, D. H. Bross, and B. Ruscic, *J. Phys. Chem. A* **123**, 5673–5682 (2019).
[5] D. H. Bross, H.–G. Yu, L. B. Harding, and B. Ruscic, *J. Phys. Chem. A* **123**, 4212–4231 (2019).
[6] B. Ruscic and D. H. Bross, *Mol. Phys.* **119**, e1969046 (2021).
[7] D. P. Zaleski, R. Sivaramakrishnan, H. R. Weller, N. A. Seifert, D. H. Bross, B. Ruscic, K. B. Moore III, S. N. Elliott, A. V. Copan, L. B. Harding, S. J. Klippenstein, R. W. Field, and K. Prozument, *J. Am. Chem. Soc.* **143**, 3124–3142 (2021).
[8] J. H. Thorpe, J. L. Kilburn, D. Feller, P. B. Changala, D. H. Bross, B. Ruscic, and J. F. Stanton, *J. Chem. Phys.* **155**, 184109 (2021).
[9] M. E. Harding, J. Vázquez, B. Ruscic, A. K. Wilson, J. Gauss, and J. F. Stanton, *J. Chem. Phys.* **128**, 114111 (2008).
[10] M. Keceli, S. N. Elliott, Y.-P. Li, M. S. Johnson, C. Cavallotti, Y. Georgievskii, W. H. Green, M. Pelucchi, J. M. Wozniak, A. W. Jasper, and S. J. Klippenstein, *Proc. Combust. Inst.* **37,** 363-371 (2019).
[11] S.N. Elliott, K. B. Moore III, A. V. Copan, M. Keceli, C. Cavallotti, Y. Georgievskii, H. F. Schaefer III, S. J. Klippenstein**,** *Proc. Combust. Inst.* **38**, 375-384 (2021).
[12] A Software Package for Automatically Computing and Storing Electronic Structure, Thermochemical, Kinetic, and Transport Properties for Gas Phase Chemical Mechanisms, *https://github.com/Auto-Mech*
[13] R. O. Ramabhadran, K. Raghavachari, *J. Chem. Theory Comput.* **7**, 2094–2103 (2011).
[14] S. J. Klippenstein, L. B. Harding, B. Ruscic**,** *J. Phys. Chem. A* **121,** 6580-6602 (2017).

Publications resulting from DOE sponsored research (2019 – present)

- *Mechanism, Thermochemistry, and Kinetics of the Reversible Reactions: $C_2H_3 + H_2 \rightleftharpoons C_2H_4 + H \rightleftharpoons C_2H_5$*, T. L. Nguyen, D. H. Bross, B. Ruscic, G. B. Ellison, and J. F. Stanton, *Faraday Discuss.* (accepted) (2022); DOI: 10.1039/D1FD00124H
- *Influence of Thermochemistry on the Reactivity of Propane, the Pentane Isomers, and n-Heptane in the Low Temperature Regime*, M. K. Ghosh, S. Panigraphy, S. Dong, S. N. Elliott, S. J. Klippenstein, and H. J. Curran, *Proc. Combust. Inst.* (accepted) (2022).
- *Elaborated Thermochemical Treatment of HF, CO, N_2, and H_2O: Insight into HEAT and Its Extensions*, J. H. Thorpe, J. L. Kilburn, D. Feller, P. B. Changala, D. H. Bross, B. Ruscic, and J. F. Stanton, *J. Chem. Phys.* **155**, 184109/1-13 (2021); DOI: 10.1063/5.0069322
- *Active Thermochemical Tables: The Thermophysical and Thermochemical Properties of Methyl, CH_3, and Methylene, CH_2, Corrected for Nonrigid Rotor and Anharmonic Oscillator Effects*, B. Ruscic and D. H. Bross, *Mol. Phys.* **119**, e1969046/1-17 (2021) (*J. F. Stanton Festschrift*); DOI: 10.1080/00268976.2021.1969046
- *Active Thermochemical Tables (ATcT) Enthalpies of Formation Based on Version 1.122q of the Thermochemical Network*, B. Ruscic and D. H. Bross, Argonne National Laboratory, Lemont, Ill. (2021), https://atct.anl.gov/Thermochemical%20Data/version%201.122q/index.php; DOI: 10.17038/1821118
- *Active Thermochemical Tables (ATcT) Enthalpies of Formation Based on Version 1.122r of the Thermochemical Network*, B. Ruscic and D. H. Bross, Argonne National Laboratory, Lemont, Ill. (2021), https://atct.anl.gov/Thermochemical%20Data/version%201.122r/index.php; DOI: 10.17038/CSE/1822363
- *Reactions of NO_3 with Aromatic Aldehydes: Gas Phase Kinetics and Insights into the Mechanism of the Reaction*, Y. Ren, L. Zhou, A. Mellouki, V. Daële, M. Idir, S. S. Brown, B. Ruscic, R. S. Paton, M. R. McGillen, and A. R. Ravishankara, *Atmos. Chem. Phys.* **21**, 13537-13551 (2021); DOI: 10.5194/acp-21-

13537-2021

- *Adsorbate Partition Functions via Phase Space Integration: Quantifying the Effect of Translational Anharmonicity on Thermodynamic Properties*, K. Blöndal, K. Sargsyan, D. H. Bross, B. Ruscic, and C. F. Goldsmith, *J. Phys. Chem. C* **125**, 20249-20260 (2021); DOI: 10.1021/acs.jpcc.1c04009
- *Substitution Reactions in the Pyrolysis of Acetone Revealed through a Modeling, Experiment, Theory Paradigm*, D. P. Zaleski, R. Sivaramakrishnan, H. R. Weller, N. A. Seifert, D. H. Bross, B. Ruscic, K. B. Moore III, S. N. Elliott, A. V. Copan, L. B. Harding, S. J. Klippenstein, R. W. Field, and K. Prozument, *J. Am. Chem. Soc.* **143**, 3124-3142 (2021); DOI: 10.1021/jacs.0c11677
- *Automated theoretical chemical kinetics: Predicting the kinetics for the initial stages of pyrolysis*, S.N. Elliott, K. B. Moore III, A. V. Copan, M. Keçeli, C. Cavallotti, Y. Georgievskii, H. F. Schaefer III, and S. J. Klippenstein, *Proc. Combust. Inst.* **38**, 375-384 (2021); DOI: 10.1016/j.proci.2020.06.019
- *Active Thermochemical Tables (ATcT) Enthalpies of Formation Based on Version 1.122p of the Thermochemical Network*, B. Ruscic and D. H. Bross, Argonne National Laboratory, Argonne, Ill. (2020); URL: https://atct.anl.gov/Thermochemical%20Data/version%201.112p/
- *Active Thermochemical Tables (ATcT) Enthalpies of Formation Based on Version 1.122o of the Thermochemical Network*, B. Ruscic and D. H. Bross, Argonne National Laboratory, Argonne, Ill. (2020); URL: https://atct.anl.gov/Thermochemical%20Data/version%201.112o/
- *Active Thermochemical Tables (ATcT) Enthalpies of Formation Based on Version 1.122n of the Thermochemical Network*, B. Ruscic and D. H. Bross, Argonne National Laboratory, Argonne, Ill. (2020); URL: https://atct.anl.gov/Thermochemical%20Data/version%201.112n/
- *Active Thermochemical Tables (ATcT) Enthalpies of Formation Based on Version 1.122h of the Thermochemical Network*, B. Ruscic and D. H. Bross, Argonne National Laboratory, Argonne, Ill. (2020); URL: https://atct.anl.gov/Thermochemical%20Data/version%201.112h/
- *High-Accuracy Extrapolated ab initio Thermochemistry. IV. A Modified Recipe for Computational Efficiency*, J. H. Thorpe, C. A. Lopez, T. L. Nguyen, J. H. Baraban, D. H. Bross, B. Ruscic, and J. F. Stanton, *J. Chem. Phys.* **150***,* 224102/1-16 (2019); DOI: 10.1063/1.5095937
- *An Automated Thermochemistry Protocol Based on Explicitly Correlated Coupled-Cluster Theory: The Methyl and Ethyl Peroxy Families*, B. K. Welch, R. Dawes, D. H. Bross, and B. Ruscic, *J. Phys. Chem. A* **123**, 5673-5682 (2019); DOI: 10.1021/acs.jpca.9b04381
- *Active Thermochemical Tables (ATcT) Enthalpies of Formation Based on Version 1.122g of the Thermochemical Network*, B. Ruscic and D. H. Bross, Argonne National Laboratory, Argonne, Ill. (2019); URL: https://atct.anl.gov/Thermochemical%20Data/version%201.112g/
- *Active Thermochemical Tables: The Partition Function of Hydroxymethyl (CH_2OH) Revisited*, D. H. Bross, H.-G. Yu, L. B. Harding, and B. Ruscic, *J. Phys. Chem. A* **123**, 4212-4231 (2019) (*Hanna Reisler Festschrift*); DOI: 10.1021/acs.jpca.9b02295
- *Thermochemistry*, B. Ruscic and D. H. Bross, *Comp. Aided Chem. Eng.* **45**, 3-114 (2019); DOI: 10.1016/B978-0-444-64087-1.00001-2 (Ch. 1 in *Mathematical Modelling of Gas-Phase Complex Reaction Systems: Pyrolysis and Combustion*, T. Faravelli, F. Manenti, and E. Ranzi, Eds., Elsevier: Amsterdam 2019)
- *Active Thermochemical Tables (ATcT) Enthalpies of Formation Based on Version 1.122e of the Thermochemical Network*, B. Ruscic and D. H. Bross, Argonne National Laboratory, Argonne, Ill. (2019); https://atct.anl.gov/Thermochemical%20Data/version%201.112e/
- *Enthalpy of Formation of $C_2H_2O_4$ (Oxalic Acid) from High-Level Calculations and the Active Thermochemical Tables Approach*, D. Feller, D. H. Bross, and B. Ruscic, *J. Phys. Chem. A* **123**, 3481-3496 (2019); DOI: 10.1021/acs.jpca.8b12329
- *A Master Equation Simulation for the •OH + CH_3OH Reaction*, T. L. Nguyen, B. Ruscic, and J. F. Stanton, *J. Chem. Phys.* **150**, 084105/1-8 (2019); DOI: 10.1063/1.5081827
- *Automated Computational Thermochemistry for Butane Oxidation: A Prelude to Predictive Automated Combustion Kinetics*, M. Keceli, S. N. Elliott, Y.-P. Li, M. S. Johnson, C. Cavallotti, Y. Georgievskii, W. H. Green, M. Pelucchi, J. M. Wozniak, A. W. Jasper, and S. J. Klippenstein*, Proc. Combust. Inst.* **37**, 363-371 (2019); DOI: 10.1016/j.proci.2018.07.113
- *Toward Accurate High Temperature Anharmonic Partition Functions*, D. H. Bross, A. W. Jasper, B. Ruscic, and A. F. Wagner, *Proc. Combust. Inst.* **37**, 315-322 (2019); DOI: 10.1016/j.proci.2018.05.028

Chemical Dynamics in the Gas Phase at Argonne: Theory, Modeling, and Methods

Ron L. Shepard, Raghu Sivaramakrishnan, and Michael J. Davis
Chemical Sciences and Engineering Division, Argonne National Laboratory, Lemont, IL 60439

shepard@tcg.anl.gov, raghu@anl.gov, davis@tcg.anl.gov

The Theory, Modeling, and Methods Subtask focuses on the development of three research areas corresponding to: electronic structure methods; the generation and analysis of chemical kinetic mechanisms for simulating complex systems; and the exploration of chemically reactive systems, including isolated chemical reactions, complex chemical kinetic mechanisms, and spectroscopy, through the methods of novel numerical analysis. These efforts are closely connected to the goals of the other three subtasks and result in substantial cross-fertilization.

Theoretical Studies of Potential Energy Surfaces and Computational Methods: Ron Shepard
This project involves the development, implementation, and application of theoretical methods for the calculation and characterization of potential energy surfaces (PES) involving molecular species that occur in combustion, atmospheric, and general gas-phase chemistry. An accurate and balanced treatment of reactants, intermediates, and products for both ground and excited electronic states is required. This difficult challenge is met with general multiconfiguration self-consistent field (MCSCF) and multireference configuration interaction (MRCI) methods [see *Chem. Rev.* **112**, 108 (2012) and *J. Chem. Phys.* **152**, 134110 (2020)]. More recently, the *graphically contracted function* (GCF) method has been developed to address some of the practical limitations of the traditional MCSCF and MRCI approaches, including the number of active electrons that may be accommodated and the overall expense associated with the study of larger molecular systems [see *J. Chem. Phys.* **141**, 064105 (2014) and references therein]. These methods are developed and maintained within the COLUMBUS Program System.

Recent Progress
The capability to compute the spin-density matrix is now available for MCSCF wave functions within COLUMBUS. The spin-density matrix is defined with the elements

$$D_{qp}^{(1,0;M)} = \left\langle \psi;S,M \middle| \sqrt{2}\hat{T}_{pq}^{1,0} \middle| \psi;S,M \right\rangle = \left\langle \psi;S,M \middle| \hat{a}_{p\alpha}^{\dagger}\hat{a}_{q\alpha} - \hat{a}_{p\beta}^{\dagger}\hat{a}_{q\beta} \middle| \psi;S,M \right\rangle .$$

The $\hat{T}_{pq}^{1,0}$ operator in this equation is a single-excitation, triplet, spin-tensor. In a determinant-based formulation, this is relatively simple to compute as the difference of the spin-orbital reduced density matrices, $D_{qp}^{[\sigma;M]} = \left\langle \psi;S,M \middle| \hat{a}_{p\sigma}^{\dagger}\hat{a}_{q\sigma} \middle| \psi;S,M \right\rangle$ with $\sigma \in \{\alpha,\beta\}$. In the graphical unitary group approach (GUGA) used in COLUMBUS, this spin-orbital occupation information is not available. Instead, the maximal $M{=}S$ member of the spin multiplet is computed as,

$$D_{qp}^{(1,0;S)} = \frac{\left(2-\frac{1}{2}N\right)}{S+1} D_{qp}^{(0,0)} - \frac{1}{S+1}\sum_{k} d_{qkkp} ,$$

where $D_{qp}^{(0,0)}$ and d_{qkkp} are the normal 1- and 2-RDM elements that are available within the MCSCF procedure and where N is the total number of electrons. The other $M{\neq}S$ multiplet members are then given by the Wigner-Eckart relation, $\mathbf{D}^{(1,0;M)} = \frac{M}{S}\mathbf{D}^{(1,0;S)}$. A feature of this formulation is that the spin-density matrix for a singlet wave function is seen to be zero, $D_{qp}^{(1,0;0)} = \left\langle \psi;0,0 \middle| \sqrt{2}\hat{T}_{pq}^{1,0} \middle| \psi;0,0 \right\rangle = 0$, because the triangle inequality is violated for the spin triple (0,1,0). It also follows that the spin-density matrix for any $\left|\psi;S,0\right\rangle$ wave function is zero. This might be surprising because spin-contaminated $M{=}0$ wave functions, for example computed with

the unrestricted Hartree-Fock (UHF) method, typically have nonzero spin-densities. Such spin-density matrices have been extensively studied [R. Pauncz, *Alternant Molecular Orbital Method*, (Saunders Philadelphia, 1967)] using semiemperical Hamiltonian operators. This apparent paradox is resolved by considering the formal expansion of the spin-contaminated wave function within a spin-eigenfunction basis,

$$\left|\psi;*,M\right\rangle = \sum_{S=|M|}^{S_{\max}} x_S \left|\psi;S,M\right\rangle,$$

with $S_{\max}$=min(½N,n-½N). A spin-density matrix element is then given by

$$\left\langle \psi;*,M\left|\hat{D}^{1,0}_{qp}\right|\psi;*,M\right\rangle = \sum_{S,S'} x_S x_{S'} \left\langle \psi;S,M\left|\hat{D}^{1,0}_{qp}\right|\psi;S',M\right\rangle$$

$$= \sum_{S=|M|}^{S_{\max}} x_S^2 \left\langle \psi;S,M\left|\hat{D}^{1,0}_{qp}\right|\psi;S,M\right\rangle + \sum_{S=|M|}^{S_{\max}-1} x_S x_{S+1} \left\langle \psi;S,M\left|\hat{D}^{1,0}_{qp}+\hat{D}^{1,0}_{pq}\right|\psi;S+1,M\right\rangle.$$

This summation index simplification occurs because of the triangle inequality constraints on the spin triple (S,1,S'). Every nonzero $S\neq|M|$ contribution in the first summation and the entire second summation is the result of spin-contamination. For M=0, the first summation vanishes entirely, but the second summation remains; thus the entire M=0 spin-density is due to spin-contamination. The spatial spin-distribution is

$$\rho^{[-;M]}(\mathbf{r}) = \sum_{pq} \varphi_q(\mathbf{r}) D^{(1,0;M)}_{qp} \varphi_p(\mathbf{r})^* = \boldsymbol{\varphi}(\mathbf{r})\mathbf{D}^{(1,0;M)}\boldsymbol{\varphi}(\mathbf{r})^\dagger.$$

This quantity determines, for example, splittings in ESR spectra. An M=0 wave function that is a spin-eigenfunction has a spin-distribution that vanishes at every point in space, whereas an M=0 spin-contaminated wave function has positive and negative regions of spin-density which, when integrated over all space, results in the M=0 expectation value. Our future spin-density efforts will include extending this capability to the MRCI and MR-AQCC methods within COLUMBUS.

Mechanisms and Models for Simulating Gas Phase Chemical Reactivity: Raghu Sivaramakrishnan

The scope of this program involves the development and analysis of detailed chemical kinetics mechanisms and models used for predictive simulations of gas phase reactivity in complex systems. Kinetics modeling has been used predominantly as an engineering tool for making predictions for practical applications in combustion and chemical conversions. However, within the context of the chemical physics BES program we have utilized a concerted Modeling-Experiment-Theory (MET) approach in collaboration with colleagues in the group and externally to further our understanding of the chemical kinetics of gas phase reactions.

Recent Progress

Initiation Reactions in Styrene Dissociation at High Temperatures

This work on styrene dissociation was initiated in collaboration with Tranter and co-workers with a view to understanding the degradation chemistry of aromatics. Additionally, thermal decomposition is a dominant route for recycling polystyrene, and therefore the degradation chemistry of its monomer, styrene, also assumes significance for reactor design considerations and for understanding the product distribution. Lastly, literature studies on the gas-phase pyrolysis of styrene are sparse and these studies do not agree on the mechanistic routes for initiation, let alone the kinetics of the concerned processes. The present shock-tube laser-schlieren results indicate onset of reaction at T > 1800 K. The PES for styrene decomposition was characterized at the CCSD(T)/cc-pV∞Z//M06-2X/cc-pVTZ and G4 levels of theory. The lowest energy process is a molecular channel forming vinylidene and benzene. A ring-walk mechanism, similar to one identified on the C_7H_8 PES, leading to the formation of ortho-iso-styrene, was also shown to be energetically accessible albeit with a slightly higher barrier than the lowest energy molecular

process. Unlike the C_7H_8 case though, there is a lower-energy exit channel from ortho-iso-styrene leading to the formation of H_2 and phenylacetylene. C-H bond-fission leading to H + $C_6H_5CCH_2$ is only 6.5 kcal/mol endothermic to the lowest energy molecular process, indicating that bond fissions may have a role to play at the high-T relevant to the present shock-tube experiments. This is confirmed by the master equation calculations using the present ab-initio results that indicate that H + $C_6H_5CCH_2$ and C_2H_3 + C_6H_5 are the two dominant channels at high-T with the other C-H fissions cumulatively assuming significance at higher-T. The lowest energy H_2CC: + C_6H_6 channel accounts for no more than 5% of the reaction flux at the present conditions. The present theoretical analysis on the initiation reactions was also used to assemble an updated sub-mechanism that will also be used in subsequent studies in collaboration with Tranter and collaborators to interpret the formation of products from styrene pyrolysis and oxidation. This work [17] was highlighted as a *PCCP 2021 hot article* by the editors.

Initiation and Secondary Reactions in the Thermal Dissociation of CH_2F_2

In collaboration with Tranter and Jasper we have initiated experiment, theory, and modeling studies on the initiation and secondary reactions involved in the dissociation of difluoromethane, a widely used hydrofluorocarbon (HFC) refrigerant. Apart from the practical implications, our recent interest stems from our prior studies on HFC's with a view to using these as chemical thermometers in shock tubes, and the potential for observing and characterizing non-RRKM effects in such molecules. Additionally, there have been recent studies by Troe et al and Matsugi et al. on CH_2F_2 dissociation that agree that the initiation step is predominantly HF loss but are at odds with the subsequent secondary steps. Our present initial analysis also agrees with the prior studies in that HF elimination is the only initiation step in CH_2F_2 dissociation. However, the mechanism assembled for CH_2F_2 dissociation using literature results for the initiation and secondary reactions is unable to simulate our laser schlieren (LS) shock tube results, and preliminary analysis reveals fast radical reactions not considered in these recent studies. For example, self-reaction of CHF radicals was considered in literature studies to form only HF + HCCF (Fig 1. PES, black lines taken as is from Matsugi and Shiina. However, a reanalysis of the PES of this reaction reveals energetically accessible radical pathways that are exothermic to the CHF + CHF entrance channel (red lines indicate C-H and C-F fissions and blue lines indicate potential direct abstraction pathways) and not considered by Matsugi and Shiina. With theoretically predicted VRC-TSTS capture rates for CHF + CHF from Jasper, our preliminary master equation analysis reveals ~20% flux towards H- and F-atom channels at high-T (>1500 K). With more facile production of H- and F-atoms, subsequent chain-propagation reactions of CH_2F_2 are now more rapid and can now resolve the unexplained formation of CF_2 from the studies of Cobos et al. Additionally, the facile production of H-atoms serves to rapidly convert the HCCF product to HCCH (also observed in the present shock tube studies with TOFMS). We propose to continue our analysis of secondary reactions of the CHF/CF_2 diradicals with a view to build a complete and updated model for CH_2F_2 pyrolysis. Additionally, initial LS experiments at low temperatures show strong vibrational relaxation. This will be further investigated and extend our knowledge of relaxation in fluorinated alkanes. The updated sub-mechanism for CH_2F_2 is expected to be used to also interpret flame studies performed to characterize the flammability properties of this important refrigerant.

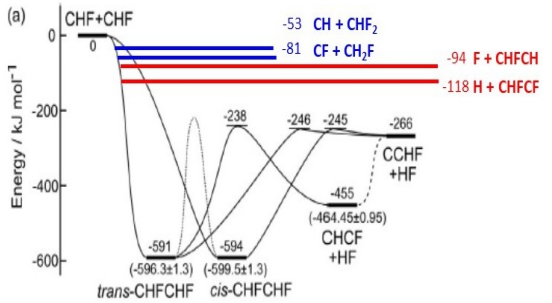

Fig. 1: CHF + CHF PES.

Exploration of chemical reactivity and spectroscopy using novel numerical analysis: Michael J. Davis

This work involves the exploration of chemically reactive systems, including isolated chemical reactions and complex chemical-kinetics mechanisms, as well as molecular spectroscopy. The work relies on modern-day numerical analysis. The analysis is generally applicable, and we have been able to use it in work with other subtasks, as well as for projects outside our group.

Recent Progress

Work on fitting potential energy surfaces has continued. It is a collaboration with Jasper. We developed methods for fitting potential energy surfaces based on dictionary learning which scaled well with basis-set order and with the size of the molecular system [18]. Dictionary learning chooses basis functions from a dictionary which consists of one or more basis sets. We used a single basis set for our dictionary, permutationally invariant polynomials (PIPS). We fit three reactive and three non-reactive potential energy surfaces, as pictured in Fig. 2. Because the potential energy surfaces are to be used for chemical dynamics, non-essential basis functions are unwanted and dictionary learning with multipass greedy selection reduces the size of the basis set by at least a factor of 10, as shown in Fig. 2, leading to chemical dynamics calculations 50 to 100 times faster [18].

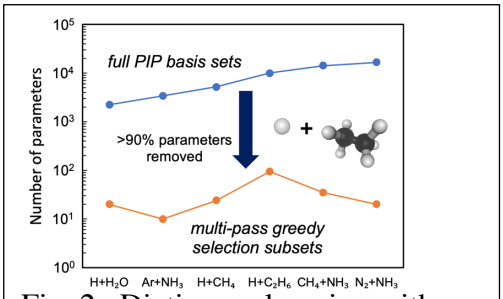

Fig. 2. Dictionary learning with multipass greedy selection reduces basis set size by over a factor of 10.

We have continued our application of computational optimal transport to molecular spectra with Prozument and Seifert (University of New Haven). Computational optimal transport is a way to quantitatively compare spectra and is part of our program to generate molecular structural information from molecular spectra in an automatic fashion. It is an essential comparator of molecular spectra when both spectra are discrete [19] or when one spectrum is discrete and the other continuous [21], cases where comparators are difficult to define using both line positions and intensities. It can be used to compare spectra even when the number and positions of lines/features differ, using the transport distance (t_d). Figure 2 shows comparisons of theoretical and experimental rotational spectra of the 12 conformers of 1-hexanal [19].

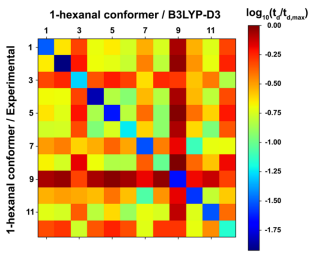

Fig. 3. Demonstrates how the transport distance matches the correct theoretical and experimental spectra of 1-hexanal (see diagonal and color bar)

Here t_d matches the correct experimental and theoretical spectra [the smallest distances are along the diagonal (color bar)]. Figure 4 shows a comparison between a theoretical stick spectrum and a continuous experimental absorption spectrum of SO_2 [21]. The top plot in Fig. 4 shows the cumulative distributions functions (cdfs) for the experimental spectrum (black) and theoretical spectrum (red), which are shown in the plot below. The difference in the cdfs define the transport distance (71.9 cm^{-1}), which includes a shift of -110 cm^{-1} between the theoretical spectrum and the observed band origin, defining a value of the theoretical band origin. This demonstrates how the

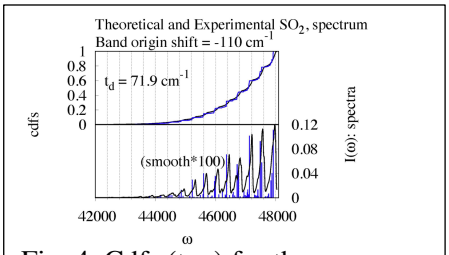

Fig. 4. Cdfs (top) for the theoretical and experimental SO_2 spectra which are compared in the bottom (theoretical is red).

transport distance can be used to compare theoretical stick spectrum to their experimental counterparts and how the theoretical spectrum can be adjusted.

Future Plans

The work on fitting potential energy surfaces will continue. The multi-pass greedy algorithms will be tested with dictionaries that include multiple basis sets, combining ones optimal for wells and others for steeper or flatter portions of the potentials. We will implement unsupervised learning methods which will reduce the number of quantum chemistry calculations. Figure 5 shows a slice of a potential surface for He + HO_2. In this calculation only 21 fitting points were used to fit a basis set with 20 terms because the sampling was tailored to the basis set and further refined using optimal experimental design, an unsupervised learning technique.

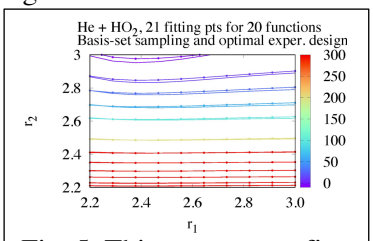

Fig. 5. This compares a fit to an exact potential energy surface (lines with dots).

The work on computational optimal transport will continue. We are completing a project using it to compare two continuous spectra. Cdfs are shown in Fig. 6 comparing a continuous experimental spectrum and a theoretical continuous spectrum (red), both provided to us by Hua Guo (B. Jiang *et al*, JCP, 2017). This plot shows how the cdfs are displaced, suggesting the type of adjustment made in Fig. 4 is warranted. We also plan to use optimal transport to design basis sets for variational calculations and the analysis of complicated point clouds generated in molecular simulations.

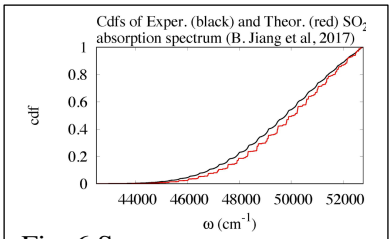

Fig. 6 See text.

Publications (2019-2022)

1. R. Shepard, and S. R. Brozell, "The All Configuration Mean Energy Multiconfiguration Self-Consistent-Field Method I. Equal Configuration Weights", Mol. Phys. **117**, 2374-2390 (2019). DOI: 10.1080/00268976.2019.1635275.

2. R. Shepard, S. R. Brozell, and G. Gidofalvi, "The All Configuration Mean Energy (ACME) MCSCF Method", 7th Annual OpenMolcas Developers' Workshop Book of Abstracts, 27 (2019).

3. R. Shepard, S. R. Brozell, and G. Gidofalvi, "On the All Configuration Mean Energy Condition", 59th Sanibel Symposium Proceedings (2019).

4. R. Shepard, S. R. Brozell, and G. Gidofalvi, "Some Recent Applications of the Graphical Unitary Group Approach", The Utah Workshop on Quantum Methods in Molecular and Solid-State Theory Abstracts, (2019).

5. S. Bai, M. J. Davis, R. Sivaramakrishnan, R. T. Skodje, "A Chemical Pathway Perspective on the Kinetics of Low-Temperature Ignition of Propane", Comb. and Flame **202** (2019) 154-178.

6. A. W. Jasper and M. J. Davis, "Parameterization Strategies for Intermolecular Potentials for Trajectory-Based Collision Parameters", J. Phys. Chem. A **123** (2019) 3464-3480.

7. H. Lischka, R. Shepard, T. Müller, P. G. Szalay, R. M. Pitzer, A. J. A. Aquino, M. M. A. do Nascimento, M. Barbatti, L. T. Belcher, J.-P. Blaudeau, I. Borges Jr., S. R. Brozell, E. A. Carter, A. Das, G. Gidofalvi, L. Gonzalez, W. L. Hase, G. Kedziora, M. Kertesz, F. Kossoski, F. B. C. Machado, S. Matsika, S. A. do Monte, D. Nachtigallova, R. Nieman, M. Oppel, C. A. Parish, F. Plasser, R. F. K. Spada, E. A. Stahlberg, E. Ventura, D. R. Yarkony, and Z. Zhang, "The Generality of the GUGA MRCI Approach in COLUMBUS for Treating Complex Quantum Chemistry", J. Chem. Phys. **152**, 134110 (2020). DOI: 10.1063/1.5144267.

8. R. Shepard, S. R. Brozell, J. Larson, P. Hovland, and S. Leyffer, "An Arc Density Maximum Flow Algorithm", 60th Sanibel Symposium Abstracts (2020).

9. R. Shepard, S. R. Brozell, and G. Gidofalvi, "Representations of Shavitt Graphs Within the Graphical Unitary Group Approach", J. Computational Chem. **41**, 129-135 (2020). DOI: 10.1002/jcc.26080.
10. J. B. Randazzo, R. Sivaramakrishnan, A. W. Jasper, T. Sikes, P. T. Lynch, R. S. Tranter, "An Experimental and Theoretical Study of the High Temperature Reactions of the Four Butyl Radical Isomers", Phys. Chem. Chem. Phys. **22** (2020) 18304-18319.
11. A. Mannodi-Kanakkithodi, M. Y. Toriyama, F. G. Sen, M. J. Davis, R. F. Klie, and M. K. Y. Chan, "Machine-Learned Impurity Level Prediction for Semiconductors: The Example of Cd-Based Chalcogenides", NPJ Comput. Mater. **6** (2020) Article No. 39, 14 pages.
12. R. Shepard, S. R. Brozell, J. Larson, P. Hovland, and S. Leyffer, "Wave Function Analysis with a Maximum Flow Algorithm", Mol. Phys. **119**, e1861351 (2021). DOI: 10.1080/00268976.2020.1861351.
13. S. R. Brozell and R. Shepard, "Edge Counts for the Auxiliary Pair Graph Within the Graphical Unitary Group Approach", Mol. Phys. **119**, e1950858 (2021). DOI: 10.1080/00268976.2021.1950858.
14. R. Sivaramakrishnan, J. R. Barker, "A Pioneer of Direct Measurements to Advance Modern Gas-Phase Chemical Kinetics", Editorial, Int. J. Chem. Kin. **53** (2021) 3-6.
15. T. Sikes, K. B. Burdett, R. L. Speth, C. F. Goldsmith, R. Sivaramakrishnan, R. S. Tranter, "Ring Opening in Cycloheptane and Dissociation of 1-heptene at High Temperatures", Proc. Combust. Inst. **38** (2021) 929-937.
16. D. P. Zaleski, R. Sivaramakrishnan, H. R. Weller, N. A. Seifert, D. H. Bross, B. Ruscic, K. B. Moore III, S. N. Elliott, A. V. Copan, L. B. Harding, S. J. Klippenstein, R. W. Field, K. Prozument, "Substitution Reactions in the Pyrolysis of Acetone Revealed through a Modeling, Experiment, Theory Paradigm", J. Am. Chem. Soc. **143** (2021) 3124-3142.
17. T. Sikes, R. Sivaramakrishnan, C. Banyon, R. A. Schwind, P. T. Lynch, A. Comandini, R. S. Tranter, "Initiation Reactions in the High Temperature Decomposition of Styrene", Phys. Chem. Chem. Phys. **23** (2021) 18432-18448.
18. D. R. Moberg, A. W. Jasper, and M. J. Davis. "Parsimonious Potential Energy Surface Using Dictionary Learning with Multipass Greedy Selection", J. Phys. Chem Lett. **12** (2021) 969-974.
19. N. A. Seifert, K. Prozument, and M. J. Davis, "Computational Optimal Transport for Molecular Spectra: The Fully Discrete Case", J. Chem. Phys. **155** (2021) 184101, 18 pages.
20. C. L. Cortes, P. Lefebvre, N. Lauk, M. J. Davis, S. K. Gray, N. Sinclair, and D. Oblak, "Adaptive Calibration of Photon Indistinguishability in Quantum Networks Using Bayesian Optimization", Phys. Rev. Appl. **17** (2022) 034067, 17 pages.
21. N. A. Seifert, K. Prozument, and M. J. Davis "Computational Optimal Transport for Molecular Spectra: The Semi-Discrete Case", J. Chem. Phys. **156** (2022) 134117, 16 pages.
22. R. Shepard, "The Cosine-Sine Decomposition with Different-Orbitals-for-Different-Spins Determinants", Mol. Phys. (submitted, 2022).
23. R. F. K. Spada, M. P. Franco, R. Nieman, A. J. A. Aquino, R. Shepard, F. Plasser, and H. Lischka, "Spin-Density Calculation via the Graphical Unitary Group Approach", Mol. Phys. (submitted, 2022).
24. R. Sivaramakrishnan, A. W. Jasper, P. T. Lynch, and R. S. Tranter, "Radical Chain Propagation Induced by Secondary Reactions in the Thermal Dissociation of CH_2F_2", In Preparation, J. Phys. Chem. Lett. (2022).
25. R. Sivaramakrishnan, N. J. Labbe, S. J. Klippenstein, "Molecular and Radical Channels in the High Temperature Decomposition of Methylformate", In Preparation, J. Phys. Chem. A (2022).
26. N. A. Seifert, K. Prozument, and M. J. Davis "Computational Optimal Transport for Molecular Spectra: The Fully Continuous Case" preprint (2022).

ARGONNE-SANDIA CONSORTIUM ON HIGH-PRESSURE COMBUSTION CHEMISTRY

Stephen J. Klippenstein, Ahren W. Jasper, Raghu Sivaramakrishnan, Robert S. Tranter
*Chemical Sciences and Engineering Division, Argonne National Laboratory, Lemont, IL, 60439

Leonid Sheps, Nils Hansen, Craig A. Taatjes
#Combustion Research Facility, MS 9055, Sandia National Laboratories Livermore, CA 94551-0969
sjk@anl.gov; cataatj@sandia.gov

Program Scope

The goal of this project is to explore the fundamental effects of pressure on chemical kinetics and to employ that knowledge in the development of accurate models for combustion chemistry at the high pressures of current and future combustion devices. We design and implement novel experiments, theory, and modeling to probe high-pressure combustion kinetics from elementary reactions, to submechanisms, and ultimately to flames. We continue to invest in the development of sensitive time-resolved experimental probes of reaction intermediates, which enable direct pressure-dependent studies of chemical systems of interest to high-pressure combustion chemistry and other DOE energy missions. We are applying novel master equation and stochastic simulation methods to accurately predict the kinetics of key processes. The theoretical predictions and experimental observations are employed in non-empirical modeling that provides high fidelity chemical models for combustion processes, and, more importantly, identifies departures from standard chemical kinetics assumptions. Recently, we have been pursuing detailed understandings of non-equilibrium effects and of radical oxidation chemistry. We are currently integrating modeling, experiment, and theory (MET) through feedback loops at all levels of chemical complexity for small alkanes, alcohols, and ethers (including cyclic variants) as key prototype fuels. The consortium expands and enhances collaborations between Argonne's Chemical Dynamics in the Gas Phase Group and the Combustion Chemistry Group in Sandia's Combustion Research Facility.

Recent Progress

***HRRST*:** In collaboration with Comandini and Chaumeix (CNRS-Orleans), we have continued investigations of PAH (polyaromatic hydrocarbon) by HRRST/i^{2}PEPICO experiments at the SOLEIL synchrotron. Toluene (0.1% in Ar) was pyrolyzed (T_5=1488 ±18 K and P_5=7.6±0.1 bar). Data were acquired in two modes: in the pulsed mode, Fig. 1, ~110,000 experiments were averaged and time dependencies of all species were obtained; in the 'continuous' mode time dependencies were sacrificed to obtain better signal/noise in a shorter duration and only ~46,000 shocks were averaged. PAH up to around m/z 360 were observed and reliable photoelectron spectra were obtained for species up to ~ m/z 220. The combination of acquisition modes is promising for future campaigns. Very recently, (April 2022) similar experiments were performed at the Swiss Light Source allowing a comparison of data acquired with different spectrometers and very different photon sources.

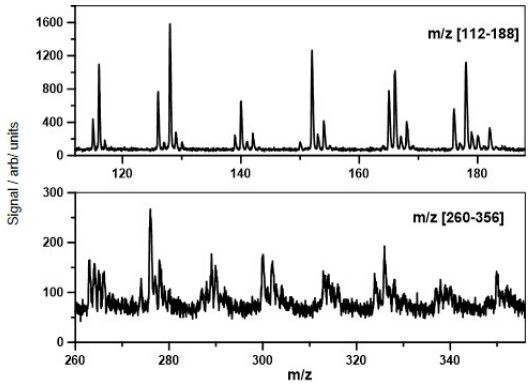

Figure 1: Post shock mass spectra from HRRST/i^{2}PEPICO experiments with toluene. MS acquired in pulsed mode and correspond to formation of PAH up to several rings.

A significant advance has been made to HRRST/PIMS experiments at the Advanced Light Source (ALS), which was motivated in part by the SOLEIL work. In December 2021 experiments were performed at the T4 endstation of 9.0.2 and utilized a monochromator. This resulted in a large reduction in the photon flux relative to prior experiments at T2 but the light was 'clean' i.e. not contaminated with high harmonics. The mass spectra obtained were weaker than from T2 but the S/N was very good and the intensity was easily improved by averaging 500 shocks instead 100-200.

HRRST/PIMS studies on cyclohexane yielded the unexpected observation of ethylene and 1,3-butadiene as the dominant reaction products. Based on the generally accepted mechanism for dissociation of cyclohexane by ring opening yielding 1-hexene and rapid dissociation of 1-hexene these would be expected to be minor products. However, modeling indicates that the fast production of H-atoms from 1-hexene dissociation products leads to the rapid attack of H on cyclohexane to give cyclohexyl radicals at the elevated pressures of these experiments. The dissociation products of cyclohexyl are largely responsible for the observed product distributions. However, a number of open questions remain not least of which is that literature models do not reproduce the observed product concentrations. The key part appears to be an inadequate description of the dissociation of cyclohexyl radicals. Furthermore, there is little information on the high pressure pyrolysis of 1-hexene especially at short reaction times or with time dependencies. Thus, in Dec 2021, experiments were performed with cycloheptane, cyclopentane, 1-pentene, 1-hexene and 1-heptene to elucidate their reaction chemistries at high pressures and form the basis for solid models.

Master-equation modeling of cyclopentane oxidation. Last year we reported on a detailed experimental study of cyclopentane oxidation at P up to 10 bar and T = 400 – 700 K, where we quantified key radical intermediates cy-C_5H_9OO (ROO) and HOO-cy-C_5H_8OO (OOQOOH), along with the main product cy-C_5H_8 (cyclopentene) and the products of second O_2 addition, by time-resolved synchrotron photoionization mass spectrometry (PIMS). In the last year, we used these data to benchmark a new approach to modeling complex reactions. We optimized a theory-based primary sub-mechanism, comprised of the first and second O_2 addition pathways (cy-C_5H_9 + O_2 and HOO-cy-C_5H_8 + O_2, respectively), embedded in a full-scale cyclopentane combustion simulation. We generated hundreds of model realizations by Monte Carlo sampling of calculated quantum chemical parameters (energies and molecular frequencies) of key species in the primary sub-mechanism and performing master equation (ME)-based kinetic simulations. Sensitivity analyses identified a small subset of ~ 15 important ME parameters, which we then optimized *via* a genetic algorithm. The main results of this work are summarized in Fig. 2. Our time-resolved experimental data constrained the rate coefficients of two key competing reactions, ROO ⟶ QOOH and ROO ⟶ HO_2 + cy-C_5H_8, bringing the predicted and measured time profiles into quantitative agreement. Notably, the optimized rate coefficients improve the modeling of previous jet-stirred reactor experiments (Al Rashidi *et al.,* Proc. Comb. Inst., 36 (2017), 469), demonstrating the value of time-resolved detection of chemical intermediates in constraining complex reaction mechanisms

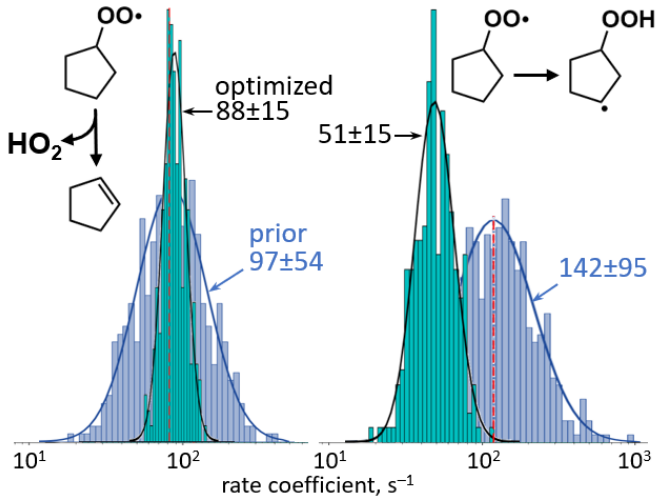

Figure 2. Prior (blue) and optimized (gray) probability distributions of the rate coefficients of the two central elementary reactions in cyclopentane oxidation at P = 10 bar, T = 575 K.

Detailed probing of autoignition reactions of dimethyl ether (DME): We also applied our method of measuring absolute concentrations of short-lived intermediates to detect all relevant chemical species in the autoignition of DME at T = 400 – 650 K. These species include stable products (CH_2O and methyl formate), along with three reactive intermediates that have never been experimentally quantified before: peroxy radicals CH_3OCH_2OO (ROO), $HOOCH_2OCH_2OO$ (OOQOOH), and hydroperoxymethyl formate $HOOCH_2OCHO$ (HPMF). The five detected species have distinct temperature-dependent formation and decay timescales, enabling us to determine their concentrations from a global kinetic fit, constrained to the total C atom balance. Comparison of our results to three DME oxidation models revealed that the models

underestimated the ROO and OOQOOH decay rates and failed to predict the branching ratios to the closed shell species. Increasing the rate coefficient of ROO ⟶ QOOH isomerization and introducing a new reaction, OH + ROO, brought the model predictions into better agreement with experiments. This points the way to future improvement in DME oxidation models and suggests that OH + peroxy reactions, which were found to be rapid in the atmosphere, may also be important at combustion conditions.

Non-Boltzmann Effects in Diethyl Ether Oxidation from a MET analysis: A combined modeling experimental theory analysis was used to demonstrate an important role for non-Boltzmann effects in the low temperature oxidation of diethyl ether. The analysis explored the sequence of non-Boltzmann effects starting from the QOOH, proceeding to the O_2QOOH, KHP, and ultimately to the OQ'O. The latter dissociation indicates important non-Boltzmann effects on both product branching and rate constants. Detailed comparisons were made with both time-dependent flow reactor measurements performed through the HPCC and with literature jet stirred reactor data.

Experimental development: We continued to invest in new experimental capabilities for high-pressure chemistry. We concluded a calibration study of a high-pressure time-resolved Fluorescence Assay for Gas Expansion (FAGE) apparatus and a high-pressure rapid-mixing laminar flow reactor (HPFR), both of which were initially constructed using LDRD funding. We calibrated the sensitivity and time resolution of these experiments. The HPFR is scheduled for use in an upcoming ALS campaign. The HPFR enables thermal (rather than photolytic) reaction initiation, expanding the range of useful radical generation schemes and complementing our existing reactors. The FAGE will enable critical, quantitative measurements of OH and HO_2 at pressures up to 10s of bar, which are practically impossible by other detection methods.

Role of Collisional Energy Transfer in the Thermal and Prompt Dissociation of 1-methylallyl: We quantified the effect of the uncertainty in energy transfer parameters on the thermal and prompt dissociation kinetics of a resonance stabilized radical, 1-methyl allyl (1MA), of relevance to the combustion of 1- and 2-butene isomers. Simulations using literature kinetics models were performed to assess the impact of these uncertainties on flame propagation and speciation data in laminar flames of 1-butene and 2-butene. Analyses of the uncertainty propagated by the energy transfer parameters for 1MA dissociation to the laminar flame speed indicate an intricate coupling between the kinetics of 1MA dissociation (chain propagation) and its reaction with H-atoms (chain-termination) (cf. Fig 3). Ab-initio kinetics calculations were performed for the pressure-dependent reaction of 1MA with H-atoms. Lastly, theoretically calculated energy transfer parameters were used to best characterize the kinetics and branching between these chain propagating and chain-terminating channels.

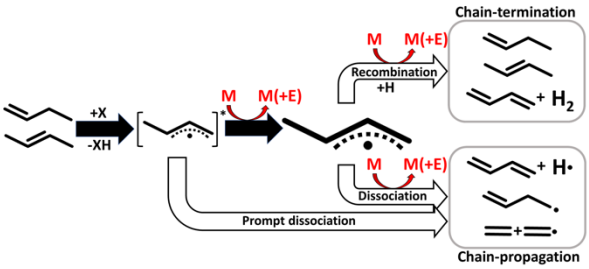

Figure 3. Impact of collisional energy transfer on chemical pathways in butene flames

Modeling-Experiment-Theory (MET) Analysis of Reactions Initiated from Cl + Methylformate: Excimer laser photolysis of Cl_2 was used as a source of Cl-atoms to initiate reactions with methylformate (MF) in the gas phase to generate CH_3OCO and CH_2OCHO radicals and characterize their decomposition kinetics. Experiments were performed in a low-pressure quartz flow tube at 10 torr and over the temperature range from 400-750 K. Time-resolved concentration profiles of numerous species (MF, CH_3, Cl_2, HCl, CO_2, CH_3Cl, CH_2O, and $CH_2ClOCHO$) originating from the title reaction were measured using multiplexed photoionization mass spectrometry (MPIMS). Simulations of the experimental data using a kinetics model, supported by quantum chemical calculations, were used to constrain the total rate constants for the title reaction. Branching ratios to the two primary radical channels (CH_3OCO + HCl, CH_2OCHO + HCl) were shown to be in good agreement with our ab-initio based theoretical kinetics predictions. Simulations also indicated that the present theoretical predictions for CH_2OCHO dissociation and secondary reaction with

Cl atoms provided the best fit to the CH_2O and $CH_2ClOCHO$ species profiles. Theoretical predictions indicate that well-skipping to CO + HCl + CH_2O is the dominant channel in Cl + CH_2OCHO.

Future Plans

***HRRST**:* The chemistry of aromatic species continues to be an area of considerable interest. Building on our studies of styrene we will investigate the high temperature and high pressure chemistry of alkylbenzenes. Styrene is an important intermediate in pyrolysis of alkylbenzenes and our recent mechanism for styrene decomposition will form a core part of an alkylbenzene mechanism. As part of an extensive study by the HPCC on tetrahydrofuran (THF) pyrolysis and oxidation we have conducted initial experiments at the ALS on THF pyrolysis. These experiments will be expanded in future runs and complement flow reactor and theoretical studies as part of the HPCC MET approach. The preliminary investigations of THF revealed the need for a thorough examination of the gas mixture preparation apparatus for material compatibility with THF. We will also begin a comprehensive study of benzyne isomers as part of an effort to explore the isomerization, addition, and self-reactions of benzyne isomers utilizing the complete suite of experimental tools in the HPCC.

Autoignition chemistry of propane, neopentane and tetrahydrofuran (THF): We began experimental studies of propane, neopentane, and tetrahydrofuran oxidation to broaden our exploration of molecular structure effects on fundamental reaction kinetics. Propane is the smallest prototypical alkane fuel, for which the HPCC has developed theory-based reaction mechanisms, and for which we have studies at low pressures. Recently, our improved experimental sensitivity enabled the detection of ROO, OOQOOH, and KHP in propane oxidation, allowing for quantitative exploration of its radical chain-branching pathways. Neo-pentane is a reactive branched alkane, which proceeds through a single ROO, OOQOOH, and KHP isomer, due to its high molecular symmetry. This simplification reduces the uncertainties in experimental species assignments and enables further rigorous MET analyses. THF is a prototypical cyclic ether, which we have studies previously. However, it has competing OH- and HO_2-elimination pathways from OOQOOH, which could not be quantified by mass spectrometry because the PI cross-section of OH and HO_2 co-products are not known. We now intend to use the new, recently-built high-P FAGE instrument to quantify these pathways and develop a detailed oxidation sub-mechanism for THF. Complementary theoretical analyses are underway or planned.

Absolute Photoionization (PI) Spectra of Combustion Radicals: We will conclude our study of the PI spectra of 1- and 2-propyl, 1-, 2-, sec-, and *tert*-butyl radicals, formed by H abstraction from partially deuterated alkanes. Furthermore, we will complete our measurements of the PI spectra of ethyl and 1- and 2-propyl peroxy radicals. Knowledge of isomer-specific cross-sections of these species will be critical to quantitative probing of radical self-reactions, in which *T*- and *P*-dependent competition between disproportionation and stabilization channels is predicted.

Optimal experimental design (OED): We collaborated with Najm (Sandia) to develop a physics-based instrument response model for PIMS (cf. Sandia's Advanced Diagnostics abstract). We plan to combine this instrument model with detailed kinetics mechanisms of representative hydrocarbons of HPCC interest to design future experiments for optimal information gain. We envision an approach that uses Bayesian inference to identify the most sensitive chemical model parameters and propose experiments to constrain their uncertainties in an iterative feedback loop, culminating with practically fully-determined mechanisms.

Prompt Dissociations of Resonance Stabilized Free Radicals: Our recent analyses of the uncertainty propagated by the energy transfer parameters for 1-methylallyl (1MA) thermal and prompt dissociation to the laminar flame speed, indicate an intricate coupling between the kinetics of 1MA dissociation (chain propagation) and its reaction with H-atoms (chain-termination). We have initiated studies to extend such analyses of this competition between the unimolecular dissociation reactions and bimolecular reactions with H-atoms to other model allylic RSR's (allyl, 2-methylallyl, 1,1-dimethylallyl, 1,2-dimethylallyl, and 1,3-dimethylallyl). These studies will help to quantify the role of prompt dissociations in generic RSR's.

Nonthermal Reactions in Hydrogen Oxidation: Recent theoretical studies have shown that in a typical third-body reaction A + B (+ M) → AB (+M), the ephemeral rovibrationally excited AB* complexes formed from the association reaction, A + B ↔ AB*, can undergo nonthermal reactions AB* + X → AB + X in the presence of large concentrations (0.5-21%) of reactive colliders. Reactions of HO_2* (from H + O_2) are of relevance because of their prominent role in H_2-oxidation. HO_2* + H involves multiple product channels that are energetically accessible (direct abstraction, addition eliminations, roaming, etc.). The two major channels relevant in the reaction of thermal HO_2 + H are: (R5) HO_2 + H → OH + OH and (R6) HO_2 + H → H_2 + O_2.At room-temperature (R5) is the exclusive product channel from H + HO_2. At combustion relevant temperatures, branching between (R5) and (R6) is central to characterizing the second explosion limit in hydrogen oxidation. Among the two reactions, (R5) is an addition-elimination reaction that has very little T-dependence. On the other hand, (R6) is a direct abstraction that has noticeable T-dependence. At energy distributions relevant to HO_2* (from H + O_2), which corresponds to effective temperatures of ~ 5000 K, extrapolations of the Arrhenius fits for (R5) and (R6) result in channel-switching with the termination reaction (R6) now being the dominant channel. Other channels involving the formation of O-atoms (singlet and triplet) and $^1O_2$ have been ignored and preliminary dynamics studies have been performed to characterize branching in this complex multi-channel system. Flame simulations will be performed using these dynamics results to quantify the impact of including nonthermal reactions of HO_2*.

N_2O Dissociation and Nonadiabatic Statistical Theory: The thermal dissociation of N_2O has long served as a prototypical nonadiabatic singlet-triplet crossing, in part due to its key role in NO_x formation. Nevertheless, we find there is much room for improvement in the current efforts to predict and model the kinetics of this dissociation. Preliminary investigations indicate that anharmonic effects and tunneling effects are of key importance. We intend to improve the treatment of these effects as well as incorporate first principles modeling of the pressure dependence through the coupling of the 2DME with trajectory analyses of the energy transfer rates. We are also developing a novel quantized version of NAST.

Stochastic Dynamics: We propose to use stochastic sampling enabled by Argonne's high-performance computing resources to study nonthermal systems, quantify and improve our 2DME collision kernel, characterize the influence of collisions on threshold reactivity of multi-channel systems, and study the reactivity of transient van der Waals complexes at high pressures.

Publications acknowledging support from this program, 2019-Present

1. **Direct Measurements of Channel Specific Rate Constants in OH + C_3H_8 Illuminates Prompt Dissociations of Propyl Radicals,** R. Sivaramakrishnan, C. F. Goldsmith, S. L. Peukert, J. V. Michael, *Proc. Combust. Inst.* 37**,** 231-238 (2019).
2. **High-Pressure Oxidation of Propane**, H. Hashemi, J. M. Christensen, L. B. Harding, S. J. Klippenstein, P. Glarborg, *Proc. Combust. Inst*. 37, 461-468 (2019).
3. **Influence of Ether Functional Group on Ketohydroperoxide Formation in Cyclic Hydrocarbons: Tetrahydropyran and Cyclohexane,** J. C. Davis, A. L. Koritzke, R. L. Caravan, I. O. Antonov, M. G. Christianson, A. C. Doner, D. L. Osborn, L. Sheps, C. A. Taatjes, B. Rotavera, *J. Phys. Chem. A* 123, 3634-3646 (2019).
4. **Kinetics of 1-Butyl and 2-Butyl Radical Reactions with Molecular Oxygen: Experiment and Theory**, A. J. Eskola, T. T. Pekkanen, S. P. Joshi, R. S. Timonen, S. J. Klippenstein, *Proc. Combust. Inst*. 37, 291-298 (2019).
5. **Nonthermal Rate Constants for CH_4* + X → CH_3 + HX, X = H, O, OH, and O_2**, A. W. Jasper, R. Sivaramakrishnan, S. J. Klippenstein, *J. Chem. Phys.* 150, 114112 (2019).
6. **Reference Natural Gas Flames at Nominally Autoignitive Engine-Relevant Conditions**, A. Krisman, C. Mounaim-Rouselle, R. Sivaramakrishnan, J. A. Miller, J. H. Chen, *Proc. Combust. Inst.* 37, 1631-1638 (2019).
7. **Sensitive Mass Spectrometer for Time-Resolved Gas-Phase Studies at High Pressures**, L. Sheps, I. Antonov, K. Au, *J. Phys. Chem. A* 123, 10804-10814 (2019).
8. **Comment on "Influence of Multiple Conformations and Paths on Rate Constants and Product Branching Ratios. Thermal Decomposition of 1-Propanol Radicals"**, J. Zador, J. A. Miller, *J. Phys. Chem. A*, 123, 1129-1130 (2019).
9. **An Experimental and Theoretical Study of the High Temperature Reactions of Four Butyl Radical Isomers**, J. B. Randazzo, A. W. Jasper, R. Sivaramakrishnan, T. Sikes, P. T. Lynch, R. S. Tranter, *Phys. Chem. Chem. Phys.* **22**, 18304-18319 (2020).
10. **Direct Time-Resolved Detection and Quantification of Key Reactive Intermediates in Diethyl Ether Oxidation at T = 450 – 600 K**, M. Demireva, K. Au, L. Sheps, *Phys. Chem. Chem. Phys.* 22, 24649-24661 (2020).
11. **Isomer-Dependent Reaction Mechanisms of Cyclic Ether Intermediates: Cis-2,3-Dimethyloxirane and Trans-2,3-Dimethyloxirane.** A. C. Doner, M. M. Davis, A. L. Koritzke, M. G. Christianson, J. M. Turney, H. F. Schaefer III, L. Sheps, D. L. Osborn, C. A. Taatjes, B. Rotavera, *Int. J. Chem. Kinet.* (2020).

12. **Low Temperature Oxidation of Diethyl Ether: Reactions of Hot Radicals Across Coupled Potential Energy Surfaces**, A. D. Danilack, S. J. Klippenstein, Y. Georgievskii, C. F. Goldsmith, *Proc. Combust. Inst.* 38, 671-679 (2020).
13. **Solenoid Actuated Driver Valve for High Repetition Rate Shock Tubes**, R. S. Tranter, T. Sikes, *Rev. Sci. Instrum.* 91, 056101 (2020).
14. **Temporally and Spatially Resolved X-Ray Densitometry in a Shock Tube**, R. A. Shaik, A. L. Kastengren, R. S. Tranter, P. T. Lynch, *Combust. Flame* 224, 136-149 (2020).
15. **Termolecular Chemistry Facilitated by Radical-Radical Recombinations and Its Impact on Flame Speed Predictions**, Y. Tao, A. W. Jasper, Y. Georgievskii, S. J. Klippenstein, R. Sivaramakrishnan, *Proc. Combust. Inst.* 38, 515-522 (2021).
16. **"Third-Body" Collision Parameters for Hydrocarbons, Alcohols, and Peroxides and an Effective Internal Rotor Approach for Estimating Them**, A. W. Jasper, *Int. J. Chem. Kinet.* **52**, 387-402 (2020).
17. **Combustion Chemistry in the Twenty-First Century: Developing Theory-Informed Chemical Kinetics Models**, J. A. Miller, R. Sivaramakrishnan, Y. Tao, C. F. Goldsmith, M. P. Burke, A. W. Jasper, N. Hansen, N. J. Labbe, P. Glarborg, J. Zádor, *Prog. Energy Combust. Sci.* **83**, 100886 (2021).
18. **Reaction Mechanisms of a Cyclic Ether Intermediate: Ethyloxirane**. M. G. Christianson, A. C. Doner, M. M. Davis, A. L. Koritzke, J. M. Turney, H. F. Schaefer III, L. Sheps, D. L. Osborn, C. A. Taatjes, B. Rotavera, *Int. J. Chem. Kinet.* 53, 127-145 (2021).
19. **Reactions of Propyl Radicals: A Shock Tube–VUV Photoionization Mass Spectrometry Study** C. K. Banyon, T. Sikes, R. S. Tranter, *Combust. Flame*, 224, 14-23 (2021).
20. **Pyrolysis of Ethanol Studied in a New High-Repetition-Rate Shock Tube Coupled to Synchrotron-Based Double Imaging Photoelectron/Photoion Coincidence Spectroscopy**, S. Nagaraju, R. S. Tranter, F. E. Cano Ardila, S. Abida, P. T. Lynch, G. A. Garcia, J. F. Gil, L. Nahon, N. Chaumeix, A. Comandini, *Combust. Flame* 226, 53-68 (2021).
21. **Substitution Reactions in the Pyrolysis of Acetone Revealed through a Modeling, Experiment, Theory Paradigm,** D. P. Zaleski, R. Sivaramakrishnan, H. R. Weller, N. A. Seifert, D. H. Bross, B. Ruscic, K. B. Moore III, S. N. Elliott, A. V. Copan, L. B. Harding, S. J. Klippenstein, R. W. Field, K. Prozument, *J. Am. Chem. Soc.* 143, 3124-3142 (2021).
22. **Entanglement Effect and Angular Momentum Conservation in a Non-separable Tunneling Treatment**, Y. Georgievskii, S. J. Klippenstein, *J. Chem. Theo. Comp.* **17**, 3863-3885 (2021).
23. **Diastereomers and Low-Temperature Oxidation**, A. D. Danilack, C. R. Mulvihill, S. J. Klippenstein, C. F. Goldsmith, *J. Phys. Chem. A*, 125, 8064-8073 (2021).
24. **Non-Boltzmann Effects in Chain Branching and Pathway Branching for Diethyl Ether Oxidation**, C. R. Mulvihill, A. D. Danilack, C. F. Goldsmith, M. Demireva, L. Sheps, Y. Georgievskii, S. N. Elliott, S. J. Klippenstein, *Energy Fuels,* **35**, 17890-17908 (2021).
25. **Initation Reactions in the High Temperature Decomposition of Styrene,** T. Sikes, C. Banyon. R. A. Schwind, P. T. Lynch, A. Comandini, R. Sivaramakrishnan, R. S. Tranter, *Phys. Chem. Chem. Phys*. 23, 18432-18448 (2021).
26. **The Impact of the Third O_2 Addition Reaction Network on Ignition Delay Times of Neo-Pentane.** N. Hansen, G.Kukkadapu, B. Chen, S. Dong, H. Curran, C. A. Taatjes, A. Eskola, D. Osborn, L. Sheps, W. Pitz, *Proc. Comb. Inst.* 38, 299-307 (2021).
27. **Quantitative Detection of Products and Radical Intermediates in Low-Temperature Oxidation of Cyclopentane.** L. Sheps, A. L. Dewyer, M. Demireva, J. Zádor, *J. Phys. Chem. A 125*, 4467-4479 (2021).
28. **High Pressure, High Flow Rate Batch Mixing Apparatus for High Throughput Experiments,** A. Dalmiya, J. M. Mehta, R. S. Tranter, P. T. Lynch, *Rev. Sci. Instrum.* 92, 114104 (2021).
29. **Parsimonious Potential Energy Surface Expansions using Dictionary Learning with Multi-Pass Greedy Selection**, D. R. Moberg, A. W. Jasper, and M. J. Davis, *J. Phys. Chem. Lett*. 12, 9169–9174 (2021).
30. **Watching a Hydroperoxyalkyl Radical (•QOOH) Dissociate**, A. S. Hansen, T. Bhagde, K. B. Moore III, D. R. Moberg, A. W. Jasper, Y. Georgievskii, M. F. Vansco, S. J. Klippenstein, and M. I. Lester, *Science* 373, 679-682 (2021).
31. **Permutationally Invariant Polynomial Expansions with Unrestricted Complexity**, D. R. Moberg and A. W. Jasper, *J. Chem. Theory Comput*. 17, 5440–5455 (2021).
32. **HO_2 + HO_2: High Level Theory and the Role of Singlet Channels**, S. J. Klippenstein, R. Sivaramakrishnan, U. Burke, K. P. Somers, H. J. Curran, L. Cai, H. Pitsch, M. Pelucchi, T. Faravelli, P. Glarborg, *Comb. Flame* 111975 (2022).
33. **Low- and Intermediate-Temperature Oxidation of Dimethyl Ether up to 100 atm in a Supercritical Pressure Jet-Stirred Reactor,** C. Yan, H. Zhao, Z. Wang, G. Song, Y. Lin, C. R. Mulvihill, A. W. Jasper, S. J. Klippenstein, Y. Ju**,** *Combust. Flame*, 236, 112059 (2022).
34. **Bayesian Model Calibration for Vacuum-Ultraviolet Photoionisation Mass Spectrometry**, J. Oreluk, L. Sheps, H. Najm, *Comb. Theo. Mod.* 1-28 (2022).
35. **Methanol Oxidation up to 100 Atm in a Supercritical Pressure Jet-Stirred Reactor,** Z. Wang, H. Zhao, C. Yan, Y. Lin, A. D. Lele, W. Xu, B. Rotavera, A. W. Jasper, S. J. Klippenstein, Y. Ju, *Proc. Combust. Inst.* 39, accepted for presentation (2022).
36. **Exploring Cyclohexane Pyrolysis Through Shock Tube PIMS Experiments,** C. K. Banyon, R. E. Hawtoff, T. Sikes, R. S. Tranter, *Proc. Combust. Inst.* 39, accepted for presentation (2022).
37. **The Role of Collisional Energy Transfer on the Thermal and Prompt Dissociation of 1-methylallyl**, J. Cho, Y. Tao, Y. Georgievskii, S. J. Klippenstein, A. W. Jasper, R. Sivaramakrishnan, *Proc. Combust. Inst.* 39, accepted for presentation (2022).

Chemical Kinetic Data of Benchmark Accuracy through Multi-Scale Informatics Strategies

Michael P. Burke

Department of Mechanical Engineering, Department of Chemical Engineering, & Data Science Institute
Columbia University, New York, NY 10027
mpburke@columbia.edu

Program Scope

The reliability of predictive simulations for advanced energy conversion devices depends on the availability of accurate data for thermochemistry, chemical kinetics, and transport. In that regard, accurate data are critically important for both their direct use in predictive simulations and for benchmarking improved theoretical methodologies that can similarly produce accurate data for predictive simulations. The use of informatics-based strategies for the determination of accurate thermochemical data with well-defined uncertainties, i.e. the Active Thermochemical Tables (ATcT),[1] has revolutionized the field of thermochemistry – ATcT provides thermochemical data of unprecedented accuracy for direct use in predictive simulation and has served as a key enabler of *ab initio* electronic structure methodologies of equally impressive accuracy. In this program, we are developing an analogous active database for *chemical kinetics* to establish high-accuracy kinetic data for predictive simulation and to evaluate emerging *ab initio*-based theoretical kinetics methods, using novel multiscale informatics strategies we are developing. Particular emphasis is placed on reaction systems for which non-thermal kinetic sequences arise and for which combining theoretical and experimental data is necessary to unravel complex reaction data into chemical information, where this program advances the state of the art in computational methodologies for those purposes.

Recent Progress

There are several significant challenges in deriving high-accuracy kinetic data of relevance to the complex reactions encountered in combustion, planetary atmospheres, and interstellar environments. First, even the most "direct" experimental rate constant determinations are often influenced by uncertainties in secondary reactions – leading to a complex web of interdependences among kinetic parameters for many reactions (and an opportunity to gain more information than has been attained previously, since uncertainties are seldom at the noise floor of the measurements). Second, there is rarely enough experimental data to constrain the full temperature, pressure, and composition (*T/P/*$\underline{X}$) dependence of many rate constants – rendering usual rate-parameter-based uncertainty quantification approaches ineffective. Third, many reactions of interest to various application domains and gas-phase theoretical chemistry involve non-thermal kinetic sequences[2-3,iii] – posing an additional problem for rate-parameter-based approaches.

During the past several years, we have been developing a multi-scale uncertainty quantification approach, MultiScale Informatics (MSI),[4-6,i,ii,iv] to address the challenges involved in 1) unraveling the complex web of interdependences among reactions in complex systems data (by reinterpreting the raw data from multi-reaction systems used to determine rate constants experimentally), 2) sufficiently constraining the *T/P/*$\underline{X}$ dependence of rate constants (by incorporating theoretical calculations to extrapolate constraints imposed by limited data), and 3) analyzing data from reaction systems involving non-thermal kinetic sequences (by leveraging the physics-based framework to account for such processes). In this program, we are applying and expanding MSI to develop a high-accuracy kinetics database through carefully chosen reaction systems that serve to both anchor the database and grow it in ways leveraging its anchored foundations – while addressing outstanding scientific questions and identifying new ones.

HO_2 + HO_2 = products. We have completed our analysis of the HO_2 + HO_2 reaction, for which recent theoretical calculations and experimental determinations appeared inconsistent. For example, while recent theory calculations[7-8] revealed consistent values at lower intermediate temperatures as the experimental determinations of Hong et al.,[9] the calculations showed a milder temperature dependence – with significant implications for the extrapolation to higher temperatures. Furthermore, calculations of Klippenstein et al.[8] indicated a previously unknown channel $HO_2 + HO_2 = OH + OH + O_2$ (R2), which may confound all earlier analyses, and likewise revealed additional theory uncertainties of relevance.

Our present MSI results indicate that the theoretical calculations for R2 and R3 near their nominal values exhibit no systematic inconsistencies with the *raw* experimental data, including at the lowest and highest experimental temperatures of Hong et al.[9], despite the apparent disagreement among reported rate constants. That is, our analysis identified an alternative interpretation of the *raw* experimental data that are consistent with all other data, including the theoretical calculations and other experimental data spanning low to high temperature. We are nearly finished writing up this analysis for journal publication.

$H + O_2 = OH + O$, $OH + H_2 = H_2O + H$, $O + H_2 = OH + O$, $H + HO_2$ = products, TBHP fragment kinetics, CH_2O kinetics, and other reaction systems. We have incorporated a large variety of data spanning several important reaction systems as part of an ongoing simultaneous analysis of all of them – aiming to both properly anchor the active network and determine refined values for their rate constants and uncertainties (including for the first three reactions listed above, whose rate constants are generally well known but still hindered by uncertainties in the other reactions listed above). For example, our uncertainty-weighted sensitivity analysis for data used to determine rate constants for OH + H_2 indicate strong influences from several reactions involving the decomposition fragments from the common OH-precusor tert-butylhydroperoxide (TBHP) including $CH_3 + CH_3$, CH_3 + OH, and OH + CH_3COCH_3; and our uncertainty-weighted sensitivity analysis for data used to determine rate constants for H + O_2 indicate strong influences of the H + HO_2 reactions and CH_2O kinetic systems (and vice versa).

CH_2O (+M) and CH_2O + O_2. Not only is the CH_2O decomposition system (Fig. 1) tightly entangled with many other rate constant determinations, but also its decomposition mechanism is important to both combustion and atmospheric chemistry. Along with CH_2O + O_2 (to which some thermal rate constant determinations are coupled), CH_2O (+M) poses a number of interesting scientific questions in the quest for resolution of inconsistencies among theoretical calculations and experimental determinations under pyrolytic and photolytic conditions. To this end, we are assembling a description of CH_2O decomposition under pyrolytic and photolytic initiation, leveraging very recent high-level *ab initio*-TST calculations[10] for the theoretical treatment.

Here we report on two interesting insights that have emerged from these efforts. The first is related to the recent experimental measurements of CH_2O photochemistry in air from the Kable group[11] that indicate radical formation for photon energies significantly below the energetic threshold for H + HCO dissociation. They suggested that this radical formation is due to bimolecular reactions of rovibrationally excited CH_2O* with O_2 present in air.[11] We performed master equation calculations of the CH_2O photochemical system to provide an independent *a priori* theoretical assessment of the proposed mechanism (and to serve as a theoretical treatment in our combined analysis of data from pyrolysis and photolysis). Our calculations, which employ the recent high-level theoretical characterization of unimolecular CH_2O kinetics[10]

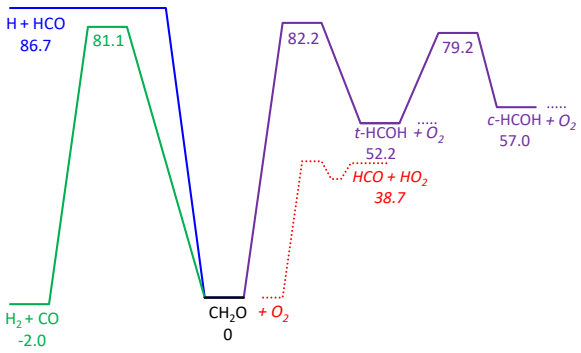

Fig. 1. Potential energy surface for the CH_2O/*t*-HCOH/*c*-HCOH system[10] and bimolecular reactions with O_2.

and our statistical estimates for the excitation-enhanced rate constants of $CH_2O + O_2$ (and HCOH + O_2), support the notion that rovibrationally excited CH_2O^* with O_2 can result in significant radical formation below the H + HCO dissociation threshold (Fig. 2). Our calculations also indicate the possibility of radical formation due to another (photoisomerization-assisted) mechanism involving HCOH + O_2.

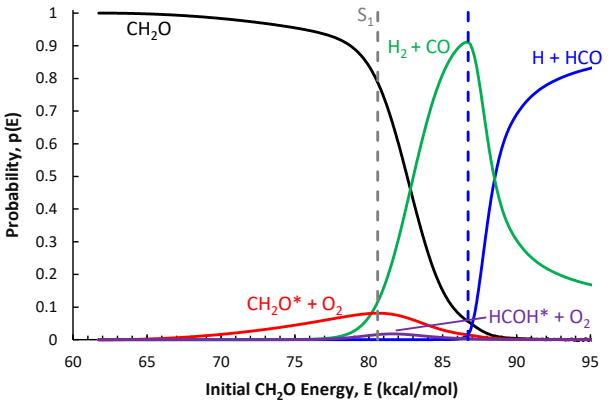

Fig. 2. Probability that CH_2O formed with initial energy, E, forms various products after the relaxational period. For reference, the minimum energy of the first electronically excited singlet state, S_1, through which low-photon-energy CH_2O photochemistry proceeds, is also shown.

The second relates to the $CH_2O + O_2$ reaction under thermal – or, more precisely, *nearly* thermal – conditions (Fig. 3). Specifically, we have found that even non-associative bimolecular reactions, whose rate constants are usually considered pressure-independent, can in fact depend on pressure at pressures below the high-pressure limit for unimolecular dissociation of at least one of the reactants. For context, reactant molecules at sufficiently high energies are known to dissociate more quickly than collisions can reestablish the Boltzmann distribution of the internal energies of the molecule during its dissociation – resulting in the well-known pressure dependence in rate constants for unimolecular reactions due to the preferential depletion of the high energy states capable of dissociation. However, we note that the same high energy states depleted due to dissociation would often be among those that would contribute the most to bimolecular reactions with an energy barrier – which may result in pressure-dependent rate constants for even non-associative bimolecular reactions, whose rate constants are usually thought to be pressure-independent. In our recent submission for the upcoming Faraday Discussions meeting, we presented results from a case study for CH_2O dissociation, isomerization, and bimolecular reaction with O_2 to explore this notion. Notably, our calculations indicate that the effect of dissociation-induced non-equilibrium distributions on bimolecular reactions can be substantial – even when the chemical timescales are well separated from internal energy relaxational timescales (as for CH_2O). These effects are considerably more pronounced for reactions involving HCOH, which cease to exist as chemical species at intermediate temperatures, and our calculations reveal significant problems with some treatments of species merging in phenomenological kinetics that assume rapid equilibration among isomers.

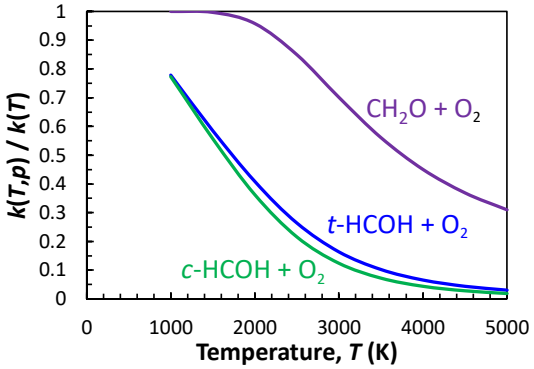

Fig. 3. Deviations of ME-calculated T-P dependent rate constants (at 1 atm) from the thermal rate constants for $CH_2O + O_2$ and from treatments for HCOH + O_2 that assume t-HCOH and c-HCOH are in thermal equilibrium and chemical equilibrium with CH_2O.

Methodological improvements: We have rewritten our MSI code as a modular Python package[iv] to facilitate expansions in the size of the systems and datasets and in the ranges of data types, kinetics theories, and sources of uncertainty. To this end, we have added many new functionalities for experimental data types and active parameter types. This code also automates active parameter selection and dictionary assembly and contains other features that enable analysis of large complex systems with large datasets.

Now that we have completed our AutoNonBoltzmann code[v] (presented last year), we are now in the process of integrating it with the rest of the MSI package to enable interpretation of non-equilibrium systems data,

inclusion of new sources of uncertainty, and incorporation of new data types. For reference, AutoNonBoltzmann is general-purpose wrapper for the Argonne MESS code[12] for automated calculations of non-Boltzmann sequences spanning multiple potential energy surfaces, which require coupling together multiple master equations to track the evolution of rovibrational energy distributions across them.[iii,v]

Both our modular MSI package and our AutoNonBoltzmann code are available now on github. [iv-v]

Future Plans

We plan to complete our simultaneous analyses of the inextricably entangled reactions involving $H + O_2 = OH + O$, $OH + H_2 = H + H_2O$, $O + H_2 = H + OH$, $H + HO_2$ = products, and TBHP fragments ($CH_3 + CH_3$, $CH_3 + OH$, and $OH + CH_3COCH_3$) discussed above and continue venturing into less characterized and difficult-to-isolate subsystems, such as those involving CH_2O and HCO, where the anchored database can be leveraged for the analysis and associated non-equilibrium kinetic sequences. Along the way, we plan to continue methodological improvements to the MSI approach that broaden the datatypes that can be used as targets (including the abovementioned CH_2O photochemical experiments[11]), enable a greater degree of data redundancy, and allow more rigorous evaluations of theoretical methodologies, particularly those for calculating non-equilibrium kinetic sequences.

References

1. B. Ruscic, et al. *J Phys Chem A* 108 (2004) 9979–9997.
2. M.P. Burke, S.J. Klippenstein. *Nature Chemistry* 9 (2017) 1078-1082.
3. N.J. Labbe, R. Sivaramakrishnan, C.F. Goldsmith, Y. Georgievskii, J.A. Miller, S.J. Klippenstein. *J. Phys. Chem. Lett.* 7 (2015) 85–89.
4. M.P. Burke, S.J. Klippenstein, and L.B. Harding. *Proc Combust Inst* 34 (2013) 547–555.
5. M.P. Burke, et al. *J Phys Chem A* 119 (2015) 7095–7115.
6. M.P. Burke. *International Journal of Chemical Kinetics* 48 (2016) 212–235.
7. D. D. Zhou, K. Han, P. Zhang, L. B. Harding, M. J. Davis, R. T. Skodje. *J Phys Chem A* 116 (2012) 2089–2100.
8. S. J. Klippenstein, et al. 11th U.S. National Combustion Meeting (2019).
9. Z. Hong, K.-Y. Lam, R. Sur, S. Wang, D.F. Davidson, R.K. Hanson. *Proc Combust Inst* 34 (2013) 565–571.
10. S. J. Klippenstein, unpublished.
11. B. Welsh, M. Corrigan, Assaf, M. Jordan, C.M. Fittschen, S. Kable. A181-0022. AGU Fall Meeting 2020.
12. Y. Georgievskii, J.A. Miller, M.P. Burke, S.J. Klippenstein *J Phys Chem A* 117 (2013) 12146–12154.

BES-supported products (2019-present)

i. C.E. LaGrotta, M.C. Barbet, L. Lei, M.P. Burke, "Towards a High-Accuracy Kinetic Database Informed by Theoretical and Experimental Data: $CH_3 + HO_2$ as a Case Study," *Proceedings of the Combustion Institute* 38 (2021) 1043-1051.

ii. C.E. LaGrotta, L. Lei, M.C. Barbet, Z. Hong, D.F. Davidson, R.K. Hanson, M.P. Burke, "Towards Resolution of Lingering Discrepancies in the H_2O_2 Decomposition System: $HO_2 + HO_2$," 12th U.S. National Combustion Meeting, College Station, Texas, May 2021.

iii. L. Lei, M.P. Burke, "An Extended Methodology for Automated Calculations of Non-Boltzmann Kinetic Sequences: $H + C_2H_2 + X$ and Combustion Impact," *Proceedings of the Combustion Institute* 38 (2021) 661-669.

iv. C.E. LaGrotta, M.C. Barbet, L. Lei, M.P. Burke. MSI: A Package for MultiScale Informatics. https://github.com/TheBurkeLab/MSI.

v. L. Lei, M.P. Burke. AutoNonBoltzmann: A Code for Automated Calculations of Non-Boltzmann Kinetic Sequences.

vi. M.P. Burke, "Master Equation Calculations to Assess the Role of Non-Thermal Bimolecular Reactions in Formaldehyde Photochemistry," American Geophysical Union 2021 Fall Meeting, New Orleans, Louisiana, December 2021.

vii. M.P. Burke, Q. Meng, C. Sabaitis. submitted to Faraday Discussions (2022).

Dynamics and Energetics of Elementary Combustion Reactions and Transient Species
Grant DE-FG03-98ER14879

Robert E. Continetti (rcontinetti@ucsd.edu)
Department of Chemistry and Biochemistry, University of California San Diego
9500 Gilman Drive, La Jolla, CA 92093-0340

I. Program Scope

This research program continues to focus on experimental studies of fundamental chemical reactions that provide benchmarks for advancing our theoretical understanding of chemical reactions, in particular the potential energy surfaces (PESs) that govern the reactions, and computational studies of the reaction dynamics. The focus of our efforts has been on the bimolecular reactions of the hydroxyl radical,[1] the fluorine atom,[2] and oxygenated carbon radicals.[3, 4] These experiments have provided benchmark information on the potential energy surfaces and dynamics of important combustion systems (HOCO) and elementary reactions ($F+H_2O$), as well as insights into the photochemistry of negative ions, anion resonances and vibrational Feshbach resonances in neutral reactions. Notably in a number of cases these efforts have involved collaboration with leading theoretical groups.[2,5,6,7] The experiments employ a photoelectron-photofragment coincidence (PPC) spectrometer equipped with a cryogenic octopole accumulator trap (COAT) for the preparation of anions thermalized below 20K.[8] These cold anions are used to load an electrostatic ion beam trap (EIBT),[9] allowing the PPC measurement to be carried out on 7 keV ions, with the fast beam enabling detection in coincidence of photoelectrons, stable photoneutrals, and photofragments. The PPC experiment yields a kinematically complete measurement of energy partitioning in reactions induced by photodetachment of precursor anions. During the last year, we have published studies on two systems where the photodetachment of a precursor anion complex can be used to probe the dynamics on the potential energy surface of hydroxyl radical reactions: $OH^-(C_2H_4)$, probing the entrance channel for the $OH + C_2H_4 \rightarrow H_2O + C_2H_3$ reaction and $CH_3O^-(H_2O)$, probing the exit channel of the $OH + CH_3OH \rightarrow H_2O + CH_3O$ reaction. While we had hoped that the experiment would be back online early in this project period, rebuilding the EIBT has been more challenging than expected, coupled with challenges in bringing the laser system back online following the COVID-19 pandemic interruption, but it is now functioning, and in the last months of the present no-cost-extension grant period we will work on resolving an outstanding question with anion internal excitation in a study of the propiolate anion $CH_3CCCO_2^-$ that can be resolved now with COAT before returning to studies of fluoride complexes and preparing for a return to IR excitation experiments[10, 11] on excitation and isomerization of HOCO.

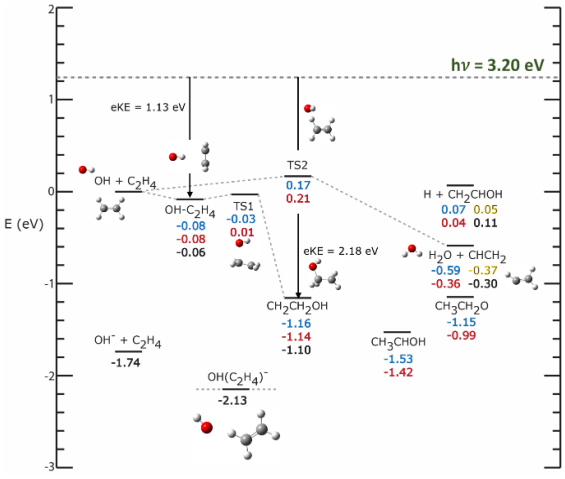

Figure 1. Energetics for the C_2H_5O system. All energies are in eV relative to the reactant asymptote $OH + C_2H_4$ with zero-point energy corrections. The energetics in blue and red correspond to previously reported theoretical values.[9,10] The values in yellow are from the Active Thermochemical Tables.[11] The energetics in black were computed in this study at the CCSD(T)/aug-cc-pVTZ level using MP2/aug-cc-pVDZ optimized geometries.

II. Recent Progress

Photodetachment of $OH^-(C_2H_4)$ - the Entrance Channel for $OH + C_2H_4 \rightarrow H_2O + C_2H_3$

Given the central role the hydroxyl radical plays in the low-temperature oxidation processes in the atmosphere and combustion, reactions between OH and simple alkanes, alkenes, and alcohols have been of particular interest. A recent PPC spectroscopy study revealed key aspects of the dissociation dynamics of the $OH-CH_4$ system (DOE pub.3), and in this project period we have published our findings on the $OH-C_2H_4$ system. The results are in many ways similar to the observations for the $OH-CH_4$ system in spite of the substitution of the simple alkene for methane in the anion complex. As a system with 21 degrees of freedom, we have no potential energy surface or dynamics calculations to compare with, but the calculated stationary points on the surface, extended by our own calculations, are shown in **Figure 1**.[12-14]

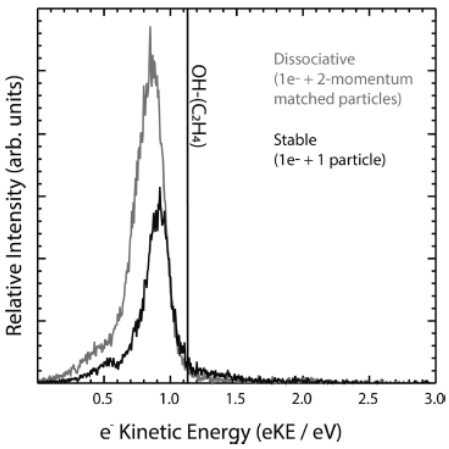

Figure 2. Overlaid photoelectron spectra of stable and dissociative channels for $OH^-(C_2H_4)$ at E_{hv} = 3.20 eV. The stable contribution is shown in black, and the dissociative channel in gray. The vertical line at eKE = 1.13 eV corresponds to an adiabatic electron affinity of 2.07 eV for the entrance van der Waals complex, (see energetics in **Figure 1**).

PPC measurements carried out on $OH^-(C_2H_4)$ at E_{hv} = 3.20 eV found stable complexes $OH\text{-}C_2H_4 + e^-$ as well as dissociative $OH + C_2H_4 + e^-$ reactants. The dominant channel was dissociation to the reactant channel accompanied by minor excitation in C-H stretching modes of C_2H_4. Similar to the $OH\text{-}CH_4$ system, weak repulsion between $OH\text{-}C_2H_4$ led to relatively low kinetic energy release (KER < 0.2 eV) between the dissociating reactants in the entrance channel. The PPC spectrum showing the correlation of electron kinetic energy (eKE) and kinetic energy release (KER), as well as the total kinetic energy spectrum have been published, and both provide insights into the energy partitioning in this system, with dissociative events characterized by a low KER. The photoelectron spectrum is consistent primarily with production of $OH + C_2H_4$ without significant internal excitation, however there is a small feature indicative of the production of vibrationally excited products, most likely in stretch excitation of the C_2H_4 reactant.

It was also found that there is a significant channel (1/3) producing $OH\text{-}C_2H_4$ complexes that are stable over the 8 μs flight time from laser-ion-beam interaction region to the detector. **Figure 2** compares the stable and dissociative photoelectron spectra, and shows that the photoelectron spectrum for stable complexes is narrower than the dissociative spectrum, and peaks 0.07 eV higher in energy. Both spectra show evidence for C-H stretch excitation far exceeding the dissociation energy of the neutral entrance channel complex. This indicates that vibrational Feshbach resonances built on the weak H-bond in the entrance channel complex play a role in this system, as previously observed in $F + H_2O$ and $F + CH_3OH$ systems.[2,5] This OH + alkene system with 21 degrees of freedom still represents a challenge even for quasiclassical trajectory calculations given that an accurate full-dimensional potential energy surface is not available for the neutral surface, or the anion. This remains a great challenge, but we hope that benchmark results like the ones presented here will provide motivation for future developments in the understanding of high dimensionality systems.

Photodetachment of $CH_3O^-(H_2O)$: Probing the Exit Channel of $OH + CH_3OH \rightarrow H_2O + CH_3O$

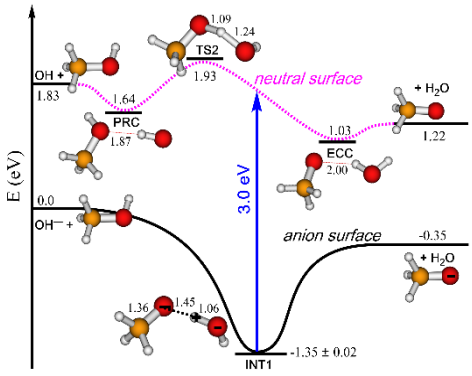

Figure 3. Relevant reaction coordinate diagram for the anion and neutral potential energy surfaces calculated using the mHEAT-345(Q) method.[7]

During this project period we also published a study of the photodetachment of $CH_3O^-(H_2O)$ as a probe of the exit channel of the $OH + CH_3OH \rightarrow H_2O + CH_3O$ reaction, in collaboration with Nguyen and Stanton.[7] In an effort to expand our studies to increasingly oxidized systems, we initially aimed to study the $OH + CH_3OH$ reaction by preparing the $OH^-(CH_3OH)$ anion at m/z = 49 amu. However, owing to the difference in proton affinities of hydroxide versus methoxide, the $CH_3O^-(H_2O)$ anion is the more stable complex, as confirmed in a collaboration with Nguyen and Stanton. They showed via high-level m-HEAT calculations that the initial precursor anion is $CH_3O^-(H_2O)$, and that photodetachment of this system has Franck-Condon overlap with the exit channel for the exothermic $OH + CH_3OH \rightarrow H_2O + CH_3O$ reaction in a manner reminiscent of the $F + H_2O$ and $F + CH_3OH$ systems previously studied.[2, 5] The energetics are shown in the reaction coordinate diagram in **Figure 3**. The anion complex, INT1, has a structure intermediate between TS2 and the exit channel complex (ECC), as can be seen in the $H_3CO\text{-}HOH$ bond length increase from 1.09 Å at TS2, to 1.45 Å in INT1 and 2.00 Å in ECC. The energetics calculated using the mHEAT

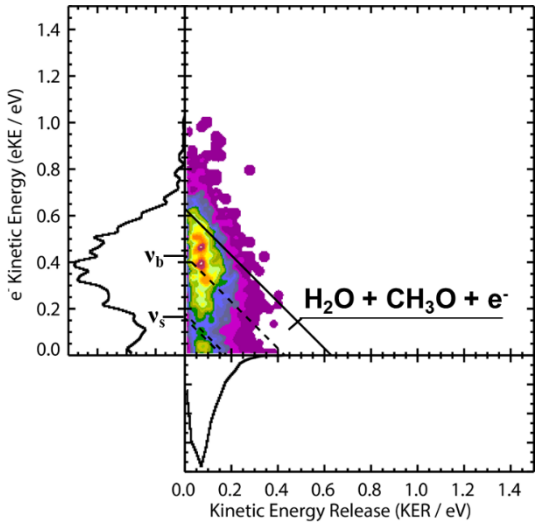

Figure 4. PPC spectrum of $CH_3O^-(H_2O)$ at E_{hv} = 3.20 eV, showing the maximum kinetic energies for dissociative photodetachment, including limits for excitation of bend (ν_b) and stretch (ν_s) quanta in the products as annotated.

method match the experimental results well, as shown in the PPC spectrum in **Figure 4**, where the solid diagonal line corresponds to the formation of $CH_3O + H_2O + e^-$ in the ground vibrational levels, and the dashed line limits corresponding to bending (ν_b) and stretch excitation (ν_s) in the H_2O product. The PPC spectrum provides a measure of the internal state distribution of the $CH_3O + H_2O$ products and shows that most are produced with limited internal excitation. However there is a feature peaking at the limit for excitation of the water bend, as well as evidence for some stretch excitation below the double dashed diagonal lines corresponding to one quantum in either the symmetric or asymmetric water stretch.

Notably in these experiments we found ~30% of the complexes are stable over the 7.8 μs flight time to the neutral particle detector. A comparison of the stable and dissociative photoelectron spectra is shown in **Figure 5**. Here the energetics are referenced to the zero-point level in the exit channel complex, and the peak shifts from 0.35 to 0.45 eV between dissociative and stable spectra, respectively. As noted by the dashed line at 0.62 eV, the peak in the stable spectrum is consistant with one quantum in the H_2O bend, if we assume the CH_3O group is essentially a spectator, as expected in this H-atom transfer reaction. Comparison with the PPC spectrum in **Figure 4** shows that the majority of the stable events lie above the energetic limit for DPD to $CH_3O + H_2O + e^-$ products. This shows that this system also exhibits vibrational Feshbach resonances built on the H-bonded exit channel complex, as discussed for $OH(C_2H_4)$.[6]

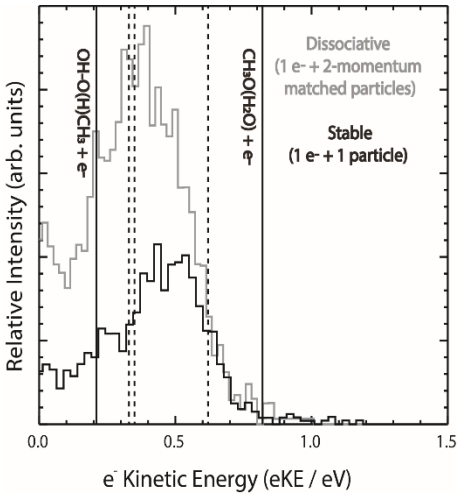

Figure 5. Photoelectron spectra for stable and dissociative events. Here annotation is relative to excitation in the ECC ($CH_3O(H_2O)$) as noted by the solid vertical line at 0.82 eV. The pre-reactive complex (PRC) is also shown, but there is no expected Franck-Condon overlap.

II. Future Work – Impacts of COVID-19

Progress in the laboratory over the past year continued to be impacted by the follow-on effects of the COVID-19, with the lab entirely shutdown from mid-March to mid-June 2020, and only usable under strict social distancing limits through March 2021. In addition, during this period, in October 2020, the cryopump and cold head system for the EIBT failed and required major maintenance that was only completed by the vendor and returned to the laboratory in March 2021. Challenges in reassembling the EIBT, efforts to improve the charge-sensitive pickup used to monitor ions trapped in the EIBT, as well as warranty-related service issues with the Ti:Sa have delayed new experiments. However, the apparatus is now online again. Over the next six months of the project we are going to focus on resolving the question of internal excitation in the propiolate anion $CH_3CCO_2^-$ that was the outstanding question in an earlier joint theory-experiment study undertaken in collaboration with Stanton and co-workers. Now, using the COAT we will be able to cool the anions to less than 20K, and definitively rule out the presence of unrelaxed high-frequency vibrations in the anion and experimentally define the energetics in this system that represents a notable challenge for quantum chemistry given the interaction of the carbon-carbon triple bond with the carboxyl group in the neutral propiolyl radical. With that data in hand, we intend to move to studies of the effect of solvation by examining the $F^-(H_2O)_2$ system, other halide complexes, and oxidized carbon species, including CO_3^-, CO_4^- and HCO_3^-. Finally, we intend to resume the to expand on our earlier studies of the effects of IR excitation in the $F^-(H_2O)$ system.[11] Initial experiments using IR excitation will be to promote the *cis*-$HOCO^-$/*trans*-$HOCO^-$ and HCO_2^-/$HOCO^-$ isomerizations, and then to pursue examination of mode-specific effects on the dissociation dynamics of

HOCO by the DPD of vibrationally excited $HOCO^-$ anions. We look forward to continuing to produce state-of-the-art benchmark experimental results to guide the future development of quantum chemistry and dynamics theory in increasingly complex systems relevant to combustion and atmospheric processes and our fundamental understanding of chemistry.

III. DOE-supported publications by this project 2019-2022

1. Y. Albeck, K. G. Lunny, Y. Benitez, A. J. Shin, D. Strasser and R. E. Continetti, *Resonance-Mediated Below-Threshold Delayed Photoemission and Non-Franck-Condon Photodissociation of Cold Oxyallyl Anions* Angew. Chem. Int. Ed. **58**, 5312-5315 (2019). https://doi.org/10.1002/anie.201900386
2. B. Shen, K. G. Lunny, Y. Benitez, R. E. Continetti, *Photoelectron-Photofragment Coincidence Spectroscopy with Ions Prepared in a Cryogenic Octopole Accumulation Trap: Collisional Excitation and Buffer Gas Cooling,* Front. Chem. **7**, 295 (2019). https://doi.org/10.3389/fchem.2019.00295
3. Y. Benitez, D. Lu, K. G. Lunny, J. Li, H. Guo, R. E. Continetti, *Photoelectron-Photofragment Coincidence Studies on the Dissociation Dynamics of the OH-CH_4 Complex*, J. Phys. Chem. A. **123**, 4825-4833 (2019). https://doi.org/10.1021/acs.jpca.9b02441
4. Y. Benitez, A.J. Parsons, K.G. Lunny and R.E. Continetti, *Dissociative photodetachment dynamics of the $OH^-(C_2H_4)$ anion complex*, J. Phys. Chem. A. **125**, 4540-4547 (2021). doi: 10.1021/acs.jpca.1c01835
5. Y. Benitez, T.L. Nguyen, A.J. Parsons, J.F. Stanton and R.E. Continetti, *Probing the exit channel of the OH + $CH_3OH \rightarrow H_2O + CH_3O$ reaction by photodetachment of $CH_3O^-(H_2O)$*, J. Phys. Chem. Lett. **13**, 142-148 (2021). doi: 10.1021/acs.jpclett.1c03568

References

1. C. J. Johnson, R. Otto and R. E. Continetti, Physical Chemistry Chemical Physics **16**, 19091-19105 (2014).
2. R. Otto, J. Ma, A. W. Ray, J. S. Daluz, J. Li, H. Guo and R. E. Continetti, Science **343**, 396-399 (2014).
3. A. W. Ray, B. B. Shen, B. L. J. Poad and R. E. Continetti, Chemical Physics Letters **592**, 30-35 (2014).
4. B. L. J. Poad, A. W. Ray and R. E. Continetti, Journal of Physical Chemistry A **117**, 12035-12041 (2013).
5. A. W. Ray, J. Agarwal, B. B. Shen, H. F. Schaefer and R. E. Continetti, Phys. Chem. Chem. Phys. **18**, 30612-30621 (2016).
6. Y. Benitez, D. Lu, K. G. Lunny, J. Li, H. Guo and R. E. Continetti, J. Phys. Chem. A **123**, 4825-4833 (2019).
7. Y. Benitez, T. L. Nguyen, A. J. Parsons, J. F. Stanton and R. E. Continetti, J. Phys. Chem. Lett. **13**, 142-148 (2021).
8. B. B. Shen, K. G. Lunny, Y. Benitez and R. E. Continetti, Front. Chem. **7**, 295 (2019).
9. C. Johnson, B. Shen, B. Poad and R. Continetti, Review of Scientific Instruments **82**, 105105 (2011).
10. R. Otto, A. W. Ray, J. S. Daluz and R. E. Continetti, EPJ Techniques and Instrumentation **1**(1), 3 (2014).
11. A. W. Ray, J. Ma, R. Otto, J. Li, H. Guo and R. E. Continetti, Chem. Sci. **8**, 7821-7833 (2017).
12. E. Kamarchik, L. Koziol, H. Reisler, J. M. Bowman and A. I. Krylov, J. Phys. Chem. Lett. **1**, 3058-3065 (2010).
13. J. P. Senosiain, S. J. Klippenstein and J. A. Miller, J. Phys. Chem. A **110**, 6960-6970 (2006).
14. B. Ruscic and D. H. Bross, (ATcT.anl.gov, 2021).

Reaction Dynamics of Organic Radicals and Carbenes

H. Floyd Davis
Dept. of Chem. & Chem. Biology, Cornell University, Ithaca, NY 14853-1301
hfd1@cornell.edu

I. Program Scope:

Bimolecular or photochemical reactions of organic radicals can yield high-energy isomers of stable molecules. Notable examples include methylcarbene (ethylidene-CH_3CH), dimethylcarbene (CH_3CCH_3) and its isomer ethylcarbene (CH_3CH_2CH). These carbenes lie about 300 kJ/mol (3 eV) above the stable ethene and propene isomers. We have prepared these carbenes by photolysis of stable molecular precursors and free radicals, and measured product kinetic energy and angular distributions. These studies provide insight into the topography of the potential energy surfaces for unimolecular and bimolecular reactions of radicals and carbenes.

II. Recent Progress:

Our DOE-supported research employs Endstation 1 (ES1), a rotatable source crossed molecular beams apparatus originally utilizing synchrotron radiation for photoionization detection. At Cornell University, it has been combined with a high intensity VUV beamline in the 8.8-11.9 eV range employing tabletop pulsed lasers.[1,2]

a) Production of Ethylidene (CH_3CH) by Photolysis of Methylketene and Propenal [3,4]

Among the most elusive organic molecules is ethylidene (CH_3CH).[3,4] In 2020, we reported that ethylidene can be produced in the triplet ground state at energies below threshold for intersystem crossing through photolysis of methylketene or propenal (acrolein). Our observations were consistent with a high potential energy barrier for isomerization on the triplet surface.[5] Electronically excited singlet ethylidene is also produced, rapidly undergoing isomerization by a 1,2-hydrogen atom shift *after departure of the CO*, producing highly vibrationally excited ethylene. The product translational energy distributions, measured at m/e = 28 and 26, verify the theoretically calculated enthalpy of formation of triplet ethylidene, and are consistent with a singlet-triplet energy gap of about 12.5 kJ/mol.

During the current funding period, we have studied the photodissociation of propenal at nine wavelengths between 320 and 387 nm, corresponding to local absorption peaks in the known jet-cooled UV-spectrum.[6] For comparison, we have also studied the photodissociation of methylketene, prepared by flash pyrolysis of propionic anhydride at corresponding wavelengths. Due to dimerization of liquid methylketene, which occurs on timescales of minutes even at -60°C, we developed a new method for production of methylketene involving continuous in-situ pyrolysis of propionic anhydride.[4] This facilitates production of stable molecular beams containing highly reactive monoalkyl ketenes such as methylketene and ethylketene.

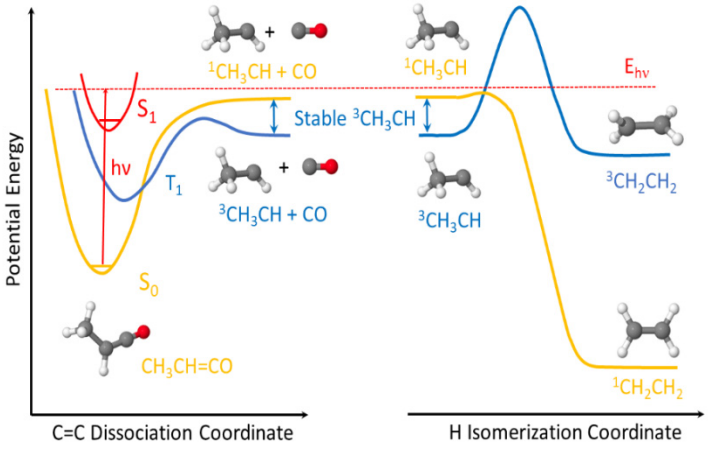

Fig. 1. *Methylketene photodissociation produces ethylidene + carbon monoxide. Triplet ethylidene ($^3CH_3CH$) is stable to intersystem crossing and isomerization if produced with internal energies below the singlet electronically excited state ($^1CH_3CH$).*

At wavelengths longer than 320 nm, the only products from single photon excitation of methylketene and propenal involve CO elimination producing singlet or triplet ethylidene. In the case of propenal photolysis, a 1,3-H atom shift

produces the methylketene intermediate after electronic excitation. The singlet-triplet ethylidene branching ratio is strongly wavelength dependent, with production of ground state triplet ethylidene becoming dominant at wavelengths longer than 360 nm for both propenal and methylketene. Upon tuning the excitation laser to wavelengths *longer* than 370 nm for both parent molecules, the photodissociation signals from both molecules become very weak, with the products formed with very low translational energies. A careful analysis of the data indicates that a significant potential energy barrier on the triplet methylketene PES, analogous to that for ketene photodissociation, is responsible for these observations. Thus the weak signals observed in our experiments at long wavelengths primarily result from 2-photon excitation (e.g., at the propenal origin band at 386 nm) yielding H atoms and methylketenyl radicals, analogous to that seen in the 193 nm photodissociation of propenal.[7]

b) Dimethylcarbene vs. Direct Propene Formation in Dimethylketene Photodissociation[8]

Carbenes are usually produced by photolysis of stable precursors such as diazoalkanes, alkyldiazirines, or ketenes. *Sequential* kinetic pathways for deactivation of nascent carbenes usually involve bimolecular reactions in competition with isomerization producing stable products such as alkenes. However, the *direct* photolytic production of stable products, effectively bypassing formation of free carbenes, has been postulated for over 50 years, but remains very poorly understood. Often termed "reaction in excited state", *RIES*, examples include 1,2-hydrogen migration within photoexcited carbene precursors yielding alkenes, and the Wolff rearrangement in photogenerated carbonyl-substituted carbenes producing ketenes.[9]

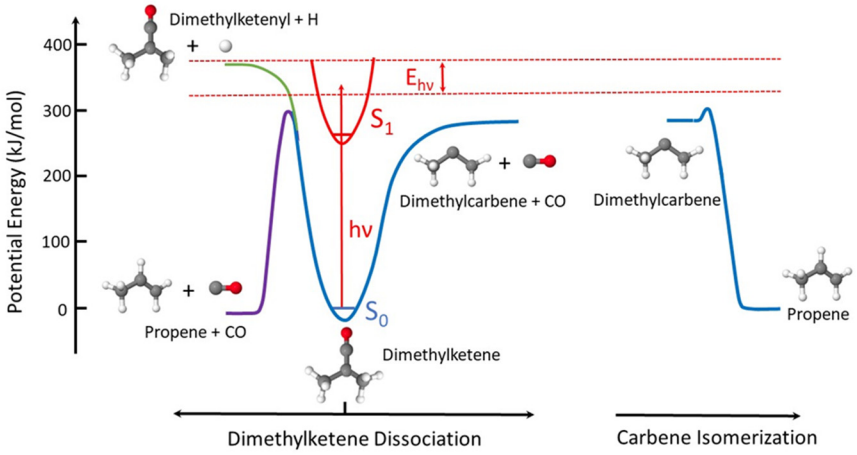

Fig. 2: *Dimethylketene photodissociation produces dimethylcarbene + carbon monoxide. Alternatively, propene + carbon monoxide can be produced via a direct reaction mechanism effectively bypassing formation of free dimethylcarbene (RIES).*

In this study, the two competing CO elimination channels from photoexcited gaseous dimethylketene, producing dimethylcarbene and propene, were studied as a function of electronic excitation energy. A significant fraction of the dimethylcarbene → propene isomerization exothermicity (~300 kJ/mol) was released as propene + CO translational energy, indicating that *propene is formed prior to, or concurrent with, CO elimination*. An increase in the propene yield with increasing excitation energy suggests that the effective potential energy barrier for this channel lies ~ 24 kJ/mol *above* the energetic threshold for dimethylcarbene formation via C=C bond fission. Possible mechanisms for propene elimination via *RIES* are discussed in light of the observed energy dependence for the competing pathways.

c) Isomer-Specific C-C Bond Fission in the 248 nm Photodissociation of Propyl Radicals[10]

Studies of the UV photodissociation of alkyl radicals provide insight into the nonadiabatic behavior governing the C-H and C-C bond fission in prototypical open shell species. Although the chemical kinetics and thermodynamics of alkyl radicals on their ground potential energy surfaces are relatively well understood, many questions remain unanswered regarding the dynamics of the electronically excited Rydberg states of alkyl radicals accessed by near-UV excitation.

Over the past decades, numerous experimental studies of the photodissociation of alkyl radicals, ranging from the simplest, methyl (CH_3), to larger branched and cyclic C_6 species, have been carried out using complimentary methods. With the exception of one study,[11] only the C-H bond fission channels have been characterized. The lack of knowledge pertaining to C-C bond fission is remarkable because it is energetically open for UV excitation of *all* C_2 and larger alkyl radicals, including ethyl radicals (C_2H_5) excited near their lowest lying absorption maximum near 245 nm.

In this work, the C-C bond fission channels in 1- and 2-propyl radicals following electronic excitation at 248 nm were studied with single photon ionization of nascent products. The radicals were produced in a molecular beam by flash pyrolysis of azo-1-propane and azo-2-propane. For comparison, the photolysis of 1-nitropropane and 2-nitropropane at 213 nm was also employed for generation of the radicals.

For 1-propyl radicals, C-C bond fission led primarily to formation of methylene (CH_2) and ethyl radicals (C_2H_5). In contrast, C-C bond fission in 2-propyl radicals produced methyl radicals (CH_3) plus ethylidene ($CHCH_3$). This study confirms that C-C bond fission plays an important role in alkyl radical photodissociation. The observation of *isomer-specific* dissociation dynamics in a system where isomerization is expected to proceed readily on the ground state PES demonstrates that C-C bond fission is likely dominated by *direct* dissociation from the excited state, rather than from ground state dynamics following internal conversion.

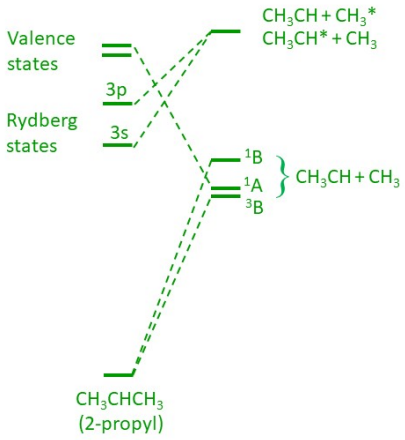

Fig. 3: *Simplified correlation diagram for C-C bond fission in electronically excited 2-propyl.*

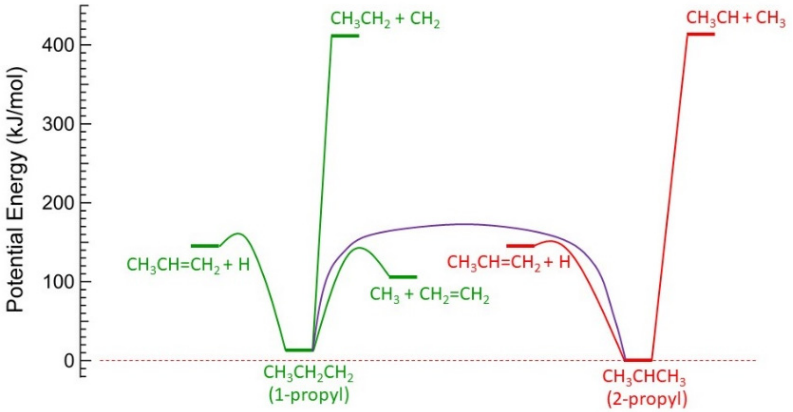

Fig. 4: *Energetics of dissociation and isomerization of 1- and 2-propyl radicals.*

III. Future Plans:

We plan to continue our experimental studies of the production and unimolecular reactions of alkyl-substituted carbenes. As noted above, methylcarbene (CH_3CH) and dimethylcarbene (CH_3CCH_3) represent prototypical alkylcarbenes with triplet and singlet ground electronic states, respectively. Ethylcarbene (CH_3CH_2CH), an isomer of dimethylcarbene and propene, represents an interesting case where the ground electronic state is expected to be triplet. This species can be produced by photodissociation of ethylketene, which can be produced by pyrolysis of butyric anhydride, which is commercially available. In preliminary studies, we clearly observe formation of ethylcarbene upon photodissociation of ethylketene at 355 nm. The translational energy distributions are consistent with the considerably higher enthalpy of formation of triplet ethylcarbene relative to dimethylcarbene. In addition, we observe a second primary C-C bond

fission channel producing CH_3 + $CH_2CH{=}CO$. The occurrence of this second C-C bond fission channel is not surprising due to the relatively weak C-C bond in the ethyl moiety, and suggests that dissociation is likely proceeding on the lowest singlet or triplet ethylketene potential energy surfaces.

We plan to carry out a series of pump-probe experiments using an existing single beam molecular beam apparatus with a linear Wiley-McLaren TOF spectrometer employing single photon ionization using tunable light in the 8-10 eV range. Several different systems will be studied. First, we plan to study the photodissociation of methylketene and propenal near 370 nm in the vicinity of the potential energy barrier on the triplet methylketene PES. In this energy range, the exclusive products are ground state triplet ethylidene and CO, with dissociation likely occurring on the *nanosecond timescales* close to the barrier. By varying the pump-probe delay, we will attempt to map out the dissociation timescales directly for triplet ethylidene formation as a function of excitation energy. We also plan to use the same apparatus to characterize the internal energies of pulsed beams containing 1- and 2-propyl radicals produced using different techniques, including pyrolysis of azoalkanes, as well as photolysis and electrical discharge of haloalkanes. In these photoionization studies, the VUV laser will be tuned near the ionization thresholds of the alkyl radicals. In addition, we will attempt to prepare molecular beams of simple alkylcarbenes for use in reactive scattering experiments. We anticipate that production of beams containing triplet ethylidene via near-threshold photodissociation of methylketene or propenal should be feasible.

IV. References (* denotes publications supported by this DOE grant since 2019):

1. D.R. Albert and H.F. Davis "Experimental Studies of Bimolecular Reaction Dynamics Using Pulsed Tabletop VUV Photoionization Detection", *Phys. Chem. Chem. Phys.* **15**, 14566-14580 (2013).
2.* M. A. Todt, S. Datta, A. Rose, K. Leung, and H. F. Davis, "Subpicosecond HI Elimination in the 266 nm Photodissociation of Branched Iodoalkanes", *Phys. Chem. Chem. Phys.,* **22**, 27338-27347 (2020).
3*.S. Datta and H.F. Davis, "Direct observation of ethylidene, the elusive high-energy isomer of ethylene", *J. Phys. Chem. Lett.*, 11, 10476-10481 (2020).
4.* S. Datta and H.F. Davis, "Dynamics of Ethylidene Production by Photolysis of Methylketene and Propenal", *manuscript in preparation.*
5. M. T. Nguyen, M.H. Matus, W.A. Lester, and D.A. Dixon, "Heats of Formation of Triplet Ethylene, Ethylidene, and Acetylene", *J. Phys. Chem. A*. **112**, 2082-2087 (2008).
6. K.W. Paulisse, T.O. Friday , M.L. Graske, and W.F. Polik, Vibronic spectroscopy and lifetime of S1 acrolein", *J. Chem. Phys.* **113**, 184 (2000).
7. B.F. Parsons, D.E. Szpunar and L.J. Butler, H. atom high-n Rydberg TOF spectroscopy of C-H bond fission in acrolein dissociated at 193 nm, J. Chem. Phys. 117, 7889 (2002).
8*.S. Datta and H.F. Davis, "Dimethylcarbene vs. Direct Propene Formation in Dimethylketene Photodissociation", *J. Phys. Chem. A. **2021**, 125, 6940-6948.*
9. M.S. Platz, "A Perspective on Physical Organic Chemistry", *J. Org. Chem.* **79**, 2341-2353 (2014).
10*.S. Datta, M.A. Todt, and H. F. Davis, "Isomer-Specific C-C Bond Fission in Photoexcited Propyl Radicals Leads to Isomer-Selective Carbene and Radical Products", *J. Phys. Chem. Lett.* **2021**, 12, 11926-11930.
11. B. Negru, G.M.P. Just, D. Park, and D.M. Neumark, "Photodissociation dynamics of the t-butyl radical via photofragment translational energy spectroscopy at 248 nm.", *Phys. Chem. Chem. Phys.,* **13**, 8180 (2011).

Electronic structure methods and protocols with application to dynamics, kinetics and thermochemistry

Richard Dawes, dawesr@mst.edu
Missouri University of Science and Technology
400 W. 11th street, Rolla, MO 65409

I. Program Scope:

(NOTE – this project is supported jointly through the CTC and GPCP programs and this report will be submitted to both programs)

Hydrocarbon combustion involves the reaction dynamics of a tremendous number of species beginning with many-component fuel mixtures and proceeding via a complex system of intermediates to form primary and secondary products. Combustion conditions corresponding to new advanced engines and/or alternative fuels rely increasingly on autoignition and low-temperature-combustion chemistry. In these regimes various transient radical species such as HO_2, ROO·, ·QOOH, HCO, NO_2, HOCO, and Criegee intermediates play important roles in determining the detailed as well as more general dynamics. A clear understanding and accurate representation of these processes is needed for effective modeling. Given the difficulties associated with making reliable experimental measurements of these systems, computation can play an important role in developing these energy technologies.

Accurate calculations have their own challenges since even within the simplest dynamical approximations such as transition state theory, the rates depend exponentially on critical barrier heights and these may be sensitive to the level of quantum chemistry. Moreover, it is well-known that in many cases it is necessary to go beyond statistical theories and consider the dynamics. Quantum tunneling, resonances, radiative transitions, and non-adiabatic effects governed by spin-orbit or derivative coupling can be determining factors in those dynamics.

Building upon progress made during a period of prior support through the *DOE Early Career Program*, this project combines developments in the areas of potential energy surface (PES) fitting and multistate multireference quantum chemistry to allow spectroscopically and dynamically/kinetically accurate investigations of key molecular systems (such as those mentioned above), many of which are radicals with strong multireference character and have the possibility of multiple electronic states contributing to the observed dynamics.

An ongoing area of investigation is to develop general strategies for robustly convergent electronic structure theory for global multichannel reactive surfaces including diabatization of energy and other relevant surfaces such as dipole transition. Combining advances in *ab initio* methods with automated interpolative PES fitting allows the construction of high-quality PESs (incorporating thousands of high-level data) to be done rapidly through parallel processing on high-performance computing (HPC) clusters.

In addition, new methods and approaches to electronic structure theory will be developed and tested through applications. This project will explore limitations in traditional multireference calculations (*e.g.*, MRCI) such as those imposed by internal contraction, lack of high-order correlation treatment and poor scaling. Methods such as DMRG-based extended active-space CASSCF and various Quantum Monte Carlo (QMC) methods will be applied (including VMC/DMC and FCIQMC). Insight into the relative significance of different orbital spaces and the robustness of application of these approaches on leadership class computing architectures will be gained. A computational thermochemistry project recently conducted through support by the DOE SCGSR student fellowship program and collaboration with Branko Ruscic (Argonne National Labs) will be extended. A workflow framework that allows community driven expansion of the ATcT thermochemical database will be further developed. Synergy with other components of this research program such as automated PES fitting and multireference quantum chemistry will be used to address challenges encountered by the standard approaches to computational thermochemistry (those being single-reference quantum chemistry and perturbative treatments of the anharmonic vibrational

energy, which break down for some cases of electronic structure or floppy strongly coupled vibrational modes).

Recent Progress: This section describes recent progress achieved along various directions of the project occurring over the past 12 months since the last abstract was provided in May 2021 (start date of this project was 03-01-2019).

Fourteen articles citing DOE support have appeared so far since 2021[1-14] including one in *Faraday Discussions*,[3] one featured with cover art in *JPC A*,[8] and one in *Ann. Rev. Phys. Chem.*[10] Several other papers are in prep, mostly related to further developments and application of our code to automatically generate PESs suitable for quantum dynamics or spectroscopic studies.

A main thrust mentioned above has been on robust calculation and fitting of energy and property surfaces for strongly coupled and intersecting excited electronic states. Last year we reported fitting 22 energies, couplings, and components of properties for NO_2 in the Franck-Condon region.[8] We have since greatly extended the coordinate and energy ranges of the fits (globally out to NO + O), generating and processing new data sets. Due to the increased complexity of the data, we developed a visual-based tool for processing and diabatizing data.

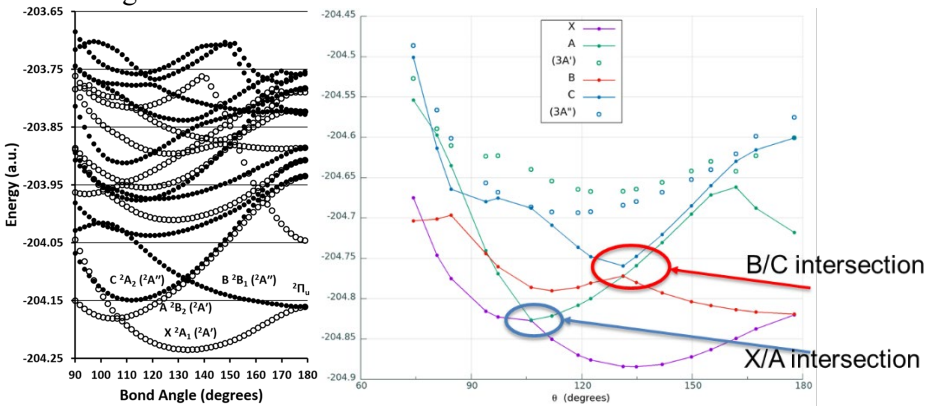

Figure 1: (at left) Bend cut through PESs of NO_2 at CASSCF level showing rich complexity of electronic states. (at right) Raw data at the MRCI-F12 level showing two intersection regions to be treated by diabatization, but also other crossings at higher energy.

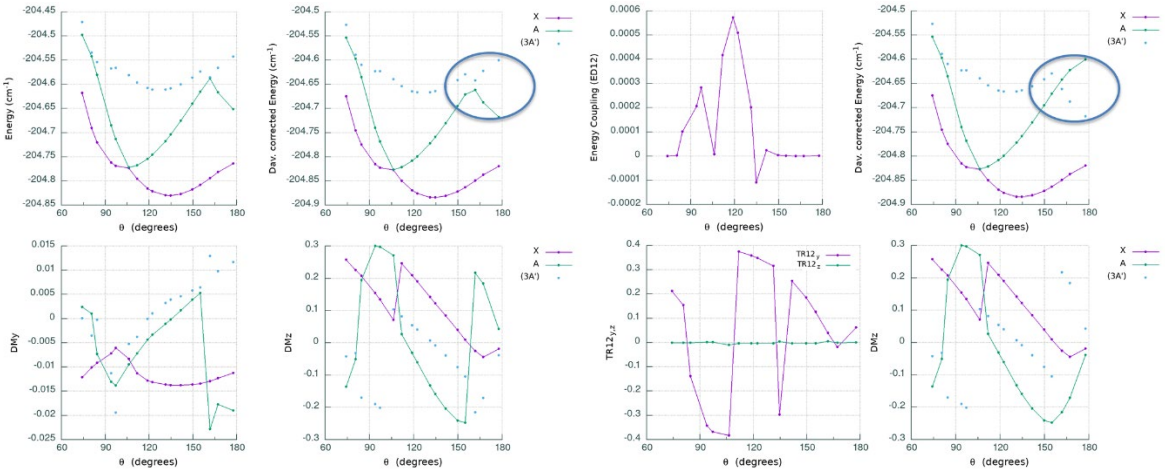

Figure 2: The new tool renders plots of various energies, couplings, and properties. Data can be selected to be swapped or removed. Notice how the last three data points for the A-state (circled) have been swapped with those of the 3A' state to extend the A-state diabat, despite that higher crossing not being included in the diabatization. At this stage, the phase is still arbitrary as seen in the coupling and TR12 plots at right.

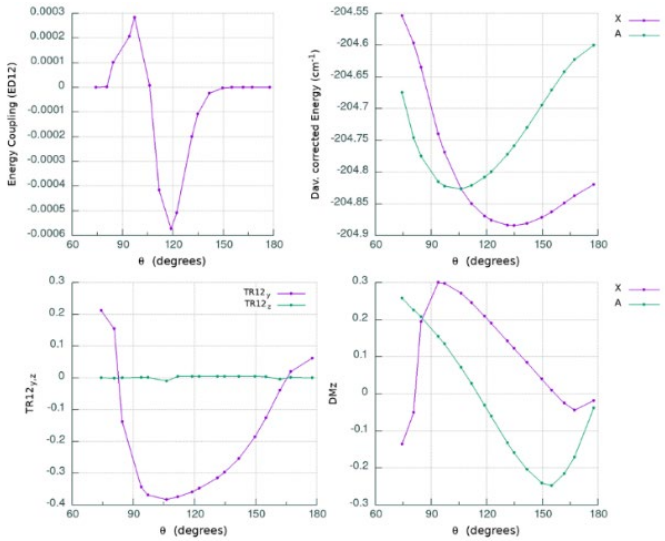

Figure 3: Once a choice of phase convention is specified, each quantity can be verified to be behaving smoothly and accordingly, ready for fitting.

We have developed a flexible Fortran based master code that performs neural network fitting. The parallel code runs hundreds of Matlab processes simultaneously to efficiently explore the effectiveness of various possible network architectures, as well as to assemble the best committee of fits. Permutation symmetry and anti-symmetry are imposed as appropriate (e.g., the two coupling surfaces in NO_2 discussed above are anti-symmetric upon exchange of O-atoms). Fitting couplings is considerably more challenging than the related energy diabats, since their topography, phase and dependence on geometry is much more complex. We have found that the region of significant coupling, and even its phase in this system, are often well predicted by the size of the diabatic energy gap and the sign of difference. Adding this quantity to the set of NN inputs dramatically improves the accuracy of fit for the coupling.

$$F_1=(p_{13}+p_{23})$$
$$F_2=(p_{13})^2+(p_{23})^2$$
$$F_3=p_{12}$$
$$F_4=(V_{22}-V_{11})$$

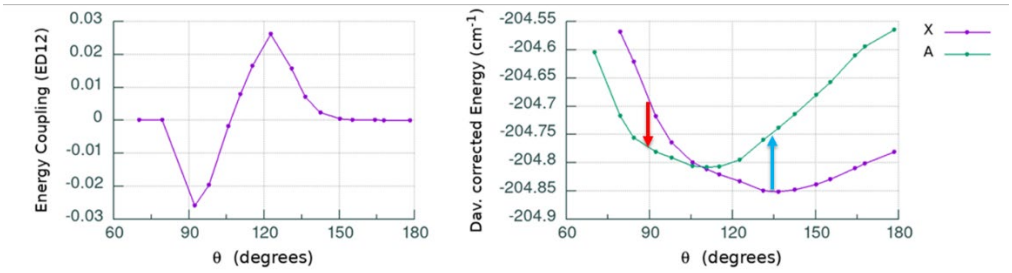

Figure 4: The 4 NN inputs used to fit the off-diagonal coupling surface. The first three are Fundamental Invariants (FI) related to the geometry, and used to impose symmetry (anti-symmetry in this case), while the 4th is the energy gap between diabats, the inclusion of which greatly improves the fit since it predicts the location and phase of the coupling.

Grant Number and Title: Grant No. DE-SC0019740; Electronic structure methods and protocols with application to dynamics, kinetics and thermochemistry.

[1] Denis-Alpizar, Otoniel, Ernesto Quintas-Sánchez, and Richard Dawes. "State-to-state rate coefficients for HCS+ in rotationally inelastic collisions with H2 at low temperatures." *Monthly Notices of the Royal Astronomical Society* 512, no. 4 (2022): 5546-5551.

[2] Dzenis, Karlis, Alexandre Faure, B. A. Mcguire, A. J. Remijan, P. J. Dagdigian, C. Rist, Richard Dawes, Ernesto Quintas-Sánchez, François Lique, and M. Hochlaf. "Collisional Excitation and Non-LTE Modeling of Interstellar Chiral Propylene Oxide." *The Astrophysical Journal* 926, no. 1 (2022): 3.

[3] Sun, Ge, Shanyu Han, Xianfeng Zheng, Yu Song, Yuan Qin, Richard Dawes, Daiqian Xie, Jingsong Zhang, and Hua Guo. "Unimolecular Dissociation Dynamics of Electronically Excited HCO (): Rotational Control of Nonadiabatic Decay." *Faraday Discussions* (2022).

[4] Quintas-Sánchez, Ernesto, Richard Dawes, and Otoniel Denis-Alpizar. "Theoretical study of the HCS+–H2 van der Waals complex: potential energy surface, rovibrational bound states, and rotationally inelastic collisional cross sections." *Molecular Physics* 119, no. 21-22 (2021): e1980234.

[5] Balança, Christian, Ernesto Quintas-Sánchez, Richard Dawes, Fabien Dumouchel, François Lique, and Nicole Feautrier. "Inelastic rate coefficients for collisions of C4H− with H2." *Monthly Notices of the Royal Astronomical Society* 508, no. 1 (2021): 1148-1155.

[6] Gancewski, Maciej, Hubert Jóźwiak, Ernesto Quintas-Sánchez, Richard Dawes, Franck Thibault, and Piotr Wcisło. "Fully quantum calculations of O2–N2 scattering using a new potential energy surface: Collisional perturbations of the oxygen 118 GHz fine structure line." *The Journal of Chemical Physics* 155, no. 12 (2021): 124307.

[7] Han, Shanyu, Ge Sun, Xianfeng Zheng, Yu Song, Richard Dawes, Daiqian Xie, Jingsong Zhang, and Hua Guo. "Rotational Modulation of Ã 2 A ″-State Photodissociation of HCO via Renner–Teller Nonadiabatic Transitions." *The Journal of Physical Chemistry Letters* 12, no. 28 (2021): 6582-6588.

[8] Ndengué, Steve, Ernesto Quintas-Sánchez, Richard Dawes, and David Osborn. "The Low-Lying Electronic States of NO2: Potential Energy and Dipole Surfaces, Bound States, and Electronic Absorption Spectrum." *The Journal of Physical Chemistry A* 125, no. 25 (2021): 5519-5533.

[9] Endres, Eric S., Steve Ndengué, Olga Lakhmanskaya, Seunghyun Lee, Francesco A. Gianturco, Richard Dawes, and Roland Wester. "Temperature-dependent rotationally inelastic collisions of OH− and He." *Physical Review A* 103, no. 5 (2021): 052807.

[10] Quintas-Sánchez, Ernesto, and Richard Dawes. "Spectroscopy and Scattering Studies Using Interpolated Ab Initio Potentials." *Annual review of physical chemistry* 72 (2021): 399-421.

[11] Bop, Cheikh T., François Lique, Alexandre Faure, Ernesto Quintas-Sánchez, and Richard Dawes. "Non-LTE modelling of cyanoacetylene: evidence for isomer-specific excitation." *Monthly Notices of the Royal Astronomical Society* 501, no. 2 (2021): 1911-1919.

[12] Desrousseaux, Benjamin, Ernesto Quintas-Sánchez, Richard Dawes, Sarantos Marinakis, and François Lique. "Collisional excitation of interstellar PN by H2: New interaction potential and scattering calculations." *The Journal of Chemical Physics* 154, no. 3 (2021): 034304.

[13] Bop, Cheikh T., Ernesto Quintas-Sánchez, Sangeeta Sur, Mathurin Robin, François Lique, and Richard Dawes. "Inelastic scattering in isotopologues of O 2–Ar: the effects of mass, symmetry, and density of states." *Physical Chemistry Chemical Physics* 23, no. 10 (2021): 5945-5955.

[14] Desrousseaux, Benjamin, François Lique, Javier R. Goicoechea, Ernesto Quintas-Sánchez, and Richard Dawes. "CF+ excitation in the interstellar medium." *Astronomy & Astrophysics* 645 (2021): A8.

Theoretical and Experimental Studies of Elementary Hydrocarbon Species and Their Reactions (DE-SC0018412)

Gary E. Douberly and Henry F. Schaefer III
University of Georgia, Center for Computational Quantum Chemistry and Department of Chemistry, 1004 Cedar St., Athens, GA 30602-1546
douberly@uga.edu

Program Scope

New theoretical and experimental methods in chemical physics being developed by the PIs provide great opportunities for the study of molecular species and chemical reactions of fundamental importance in combustion processes. In this research, high level quantum mechanical formalisms are a significant source of critical predictions concerning molecular systems that may be challenging for experiments. Moreover, our helium droplet experiments have opened whole new vistas for the spectroscopic study of molecular species relevant to combustion environments. Theoretical developments proposed herein include a focus on obtaining highly accurate energetics for species pertinent to combustion reactions. Experimental developments focus on strategies to characterize transient combustion intermediates associated with low-temperature hydrocarbon oxidation processes, which have been difficult to probe with other methodologies. The combination of theory and experiment to solve problems inaccessible to either alone is a hallmark of this research.

Nearly all of the proposed non-methodological experimental research will benefit from state-of-the-art molecular electronic structure theory. In some cases, the experimental group needs theoretical predictions prior to beginning a new set of experiments. In other cases, experimental findings are puzzling and need theory for interpretation. We have an abundance of experiences with both sets of problems, and the PIs have already collaborated in several such situations. Some situations where theory-experiment interaction will be particularly important include: (i) the C_nH_m + O(^3P) reactions, where predictions of structures, energetics, and spectroscopic properties of complexes and adducts on both singlet and triplet potential energy surfaces will be required; (ii) the spectroscopic studies of $(NH_2)_2$, NH-(NH_2), and other pre-reactive radical-radical complexes, where an interpretation will require computations of structures, energetics, and intersystem crossing rates; (iii) the near-IR and mid-IR studies of HOO-alkene complexes and related QOOH species, where computations of the excited state potential energy surface in the vicinity of the exit-channel complex will be essential; and (iv) the mid-IR studies of $\cdot C_nH_{2n+1}$ radicals, where the spectra are complicated by anharmonic and Coriolis resonances to an extent that the interpretation of these spectra will only be achievable through comparisons to effective Hamiltonian computations that employ highly accurate quartic force fields and Coriolis parameters.

Recent Projects

Infrared Spectroscopy of Alkyl and Alkyl Peroxy Radicals in Solid para-Hydrogen and Helium Droplets (Experiment/Theory Collaboration)

We have continued our collaboration with Yuan-Pern Lee's group at the National Chiao Tung University in Taiwan. We continue to analyze spectra of alkyl radicals and alkyl peroxy radicals isolated in solid *para*-H_2, and we have recently published a paper in the *Journal of Molecular Spectroscopy* that reports the comprehensive assignment of the mid-IR spectra of *n*- and *i*-propyl radicals. In these studies, we are employing both normal mode and local mode effective Hamiltonian models to help assign spectra. We are studying the transferability of local mode Hamiltonian coupling parameters over a range of alkyl radical systems. We have recently recorded spectra of all four butyl radicals in helium droplets. These spectra are compared directly to those recorded for the solid-para hydrogen matrix environment. We are finding that the local mode anharmonic vibrational model is working for the more complicated butyl radical systems. An example comparison of experimental helium droplet and computed local-mode spectra is shown below for the tert-butyl radical. Papers describing the butyl radical spectra are in preparation with an anticipated submission date this summer.

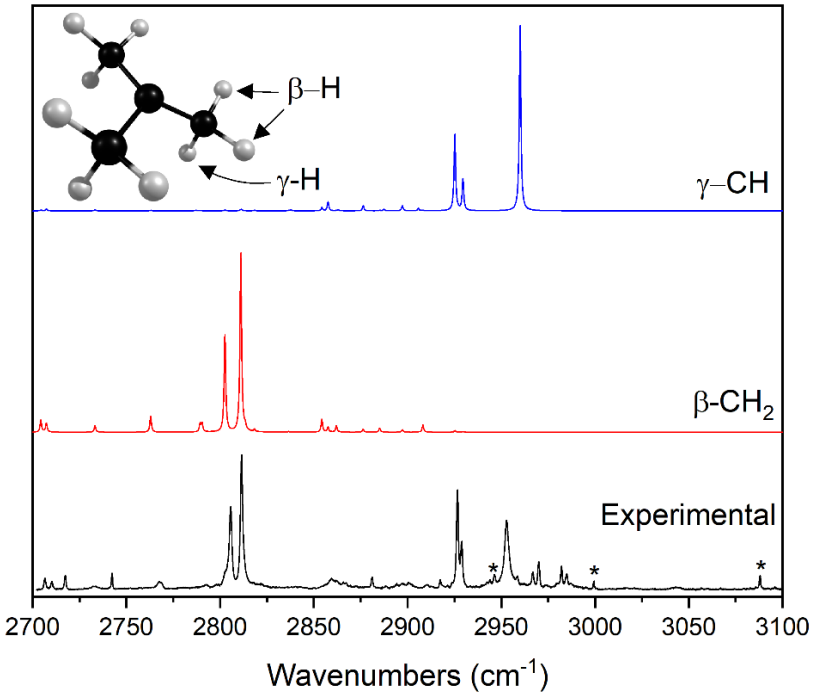

We have published a lengthy, invited review article on the theoretical methods and associated comparisons to experiment for the novel computational anharmonic vibrational spectroscopy models employed in this work.

Peter R. Franke, John F. Stanton, Gary E. Douberly, "How to VPT2: Accurate and Intuitive Simulations of CH Stretching Infrared Spectra Using VPT2+K with Large Effective Hamiltonian Resonance Treatments" *Journal of Physical Chemistry A* (Invited Review), **125**, 1301-1324 (2021).

Selection of Theory Projects (no experimental contribution to the work).

H. F. Mull, P. R. Franke, C. Sargent, G. E. Douberly, J. M. Turney, and H. F. Schaefer, "Four Isomers of In_2H_2: A Careful Comparison Between Theory and Experiment," *Special Issue of Molecular Physics in Honor of John F. Stanton*, (2021), 119, 21-22. DOI: 10.1080/00268976.2021.1979675

Four constitutional isomers of diindium dihydride were studied utilizing rigorous quantum mechanical methods. Geometries were optimized with the CCSD(T) method using the aug-cc-pwCVTZ basis set and a small-core pseudopotential for the indium atoms. Relative energetics were determined at the CCSD(T)/CBS level of theory, and the higher order δT(Q) contributions are also computed. The monobridged and vinylidene-like isomers lie 10.8 and 13.6 kcal mol^{-1} above the planar dibridged isomer, respectively. At 0 K, the trans isomer is the least favored energetically, differing from the dibridged isomer by 16.6 kcal mol^{-1}. Anharmonic vibrational frequencies were predicted to provide theoretical insight into future experimental studies. Very detailed comparisons are made to matrix isolation experiments from the group of Downs and the group of Andrews. Numerous agreements and disagreements were found.

A. K. Bralick, B. Z. Abbott, G. E. Douberly, and H. F. Schaefer, "The Isomerization of H_2XY to HXYH (X, Y = O, S, and Se)," *Special Issue of Molecular Physics in Honor of Professor Juergen Troe,* (2021), 119, 17-18. DOI: 10.1080/00268976.2021.1976429

Oxywater (H_2OO) is an intermediate in the oxidation of hydrogen peroxide (HOOH), and along with its relatives H_2SS and H_2SeSe, plays an important role in atmospheric and biochemical processes. In this research, we studied the isomerization of H_2XY species to HXYH (X, Y = O, S, Se) using *ab initio* methods. Geometries and harmonic frequencies were obtained using both a scalar relativistic X2C-1e-CCSD(T) approach and non-relativistic CCSD(T) using an effective core potential on Se. A focal point approach was used to extrapolate electronic energies at CCSD(T)/aug-cc-pVTZ geometries to a CCSDT(Q)/CBS level of theory. The isomerization reactions of H_2XX to HXXH have barriers of 6.6, 20.6, and 14.1 kcal mol^{-1} and exothermicities of 45.8, 27.2, and 28.3 kcal mol^{-1} for X=O, S, and Se, respectively. The isomerization reactions of H_2OS and H_2SO to HOSH have barriers of 15.4 and 44.2 kcal mol^{-1} and exothermicities of 36.2 and 17.7 kcal mol^{-1}. The isomerization reactions of H_2OSe and H_2SeO to HOSeH have barriers of 10.1 and 36.2 kcal mol^{-1} and exothermicities of 33.5 and 31.7 kcal mol^{-1}. The isomerization reactions of H_2SSe and H_2SeS to HSSeH have barriers of 16.2 and 18.1 kcal mol^{-1} and exothermicities of 23.3 and 32.1 kcal mol^{-1}.

Ongoing Experimental Work and Future Plans

Sequential Capture of $O(^3P)$ and Alkenes by Helium Nanodroplets: Infrared Spectroscopy and Ab Initio Computations of the Triplet Biradical Intermediates

According to Smith *et al*. [Smith, I. W. M.; Sage, A. M.; Donahue, N. M.; Herbst, E.; Quan, D. *Faraday Discuss.* **2006**, 133, 137.], for molecule + radical reactions, the energetic difference between the molecule's ionization energy (IE) and the radical's electron affinity (EA) can provide insight into the nature of the reaction barrier, either *above* or *below* the reactant

asymptote. They propose that a difference (IE − EA) greater than 8.75 eV indicates a real barrier above the asymptotic limit, whereas a value below 8.75 eV indicates a submerged barrier. Indeed, this difference for the O(^{3}P) + HCN system is 12.2 eV. Accordingly, the barrier to oxygen insertion into the CN π system is ~10 kcal/mol above the reactant asymptote, and a van der Waals complex is observed when these species are brought together in a 0.4 K helium nanodroplet. However, O(^{3}P) reactions with *alkenes* are predicted to cross the postulated 8.75 eV threshold as the alkene substitution pattern evolves from ethene (no substitution) to propene (methyl group substitution) to butene (dimethyl substitution, of which there are four different isomers), and this trend was tested by Sabbah *et al.* [Sabbah, H.; Biennier, L.; Sims, I.R.; Georgievskii, Y.; Klippenstein, S.J.; Smith, I. W. *Science* **2007**, 317, 102.]. Their findings corroborated the behavior predicted by Smith *et al.* The HCN + O(^{3}P) results presented recently by us demonstrate the feasibility for analogous alkene + O(^{3}P) spectroscopic studies, in which O(^{3}P) and alkenes of varying substitution are combined in helium droplets *via* the sequential capture scheme. As the *real* reaction barrier (*i.e.* for the ethene and propene reactions) evolves to being *submerged* below the asymptotic limit (*i.e.* for the butene reactions), one might expect that strongly bound reaction intermediates, such as triplet biradicals, will be observed in helium droplets, rather than van der Waals complexes. Given the fact that a 10,000 atom helium droplet can dissipate 140 kcal/mol, it should be possible to quench the internal energy of these reaction intermediates and probe them for the first time spectroscopically.

Joseph T. Brice, Peter R. Franke, Gary E. Douberly "Sequential Capture of O(^{3}P) and HCN by Helium Nanodroplets: Infrared Spectroscopy and Ab Initio Computations of the $^3\mathbf{\Sigma}$ O-HCN Complex" *Journal of Physical Chemistry A,* **121**, 9466-9473 (2017). Published: November 2017.

Selected Publications acknowledging DOE support (2019-2022):

1. Peter R. Franke, Joseph T. Brice, Christopher P. Moradi, Henry F. Schaefer, Gary E. Douberly, "Ethyl + O_2 in Helium Nanodroplets: Infrared Spectroscopy of the Ethylperoxy Radical" *Journal of Physical Chemistry A*, **123**, 3558-3568 (2019). DOI: 10.1039/c9cp01476d. Published: April 2019.

2. Alaina R. Brown, Joseph T. Brice, Peter R. Franke, Gary E. Douberly, "Infrared Spectrum of Fulvenallene and Fulvenallenyl in Helium Droplets" *Journal of Physical Chemistry A*, **123**, 3782-3792 (2019). DOI: 10.1021/acs.jpca.9b01661. Published: April 2019.

3. Peter R. Franke, Kevin B. Moore, Henry F. Schaefer, Gary E. Douberly, "*tert*-Butyl Peroxy Radical: Ground and First Excited State Energetics and Fundamental Frequencies" *Physical Chemistry Chemical Physics*, **21**, 9747-9758 (2019). DOI: 10.1039/C9CP01476D. Published: April 2019.

4. Michael C. Bowman, Gary E. Douberly, Henry F. Schaefer, "Convergent Energies and Anharmonic Vibrational Spectra of Ca_2H_2 and Ca_2H_4 Constitutional Isomers" *Physical Chemistry Chemical Physics*, **21**, 10914-10922 (2019). DOI: 10.1039/c9cp01643k. Published: May 2019.

5. Gregory T. Pullen, Peter R. Franke, Karolina A. Haupa, Yuan-Pern Lee, Gary E. Douberly, "Infrared Spectroscopy of *n*-Propyl and *i*-Propyl Radicals in Solid *para*-Hydrogen" *Journal of Molecular Spectroscop*y, **363**, 111170 (2019). DOI: 10.1016/j.jms.2019.07.001. Published September 2019.

6. Mathew M. Davis, Jared D. Weidman, Adam S. Abbott, Gary E. Douberly, Justin M. Turney, Henry F. Schaefer, "Characterization of the 2-Methylvinoxy Radical + O_2 Reaction: A Focal Point Analysis and Composite Multireference Study" *Journal of Chemical Physics*, (2019), 151, 124302. DOI: 10.1063/1.5113800. Published: September 2019.

7. Jonathon P. Misiewicz, Kevin B. Moore, Peter R. Franke, W. James Morgan, Justin M. Turney, Gary E. Douberly, and Henry F. Schaefer, "Sulfurous and Sulfonic Acids: Predicting the Infrared Spectrum and Setting the Surface Straight" *Journal of Chemical Physics*, **152**, 024302 (2020). DOI: 10.1063/1.5133954. Published January 2020.

8. Jared D. Weidman, Justin M. Turney, Henry F. Schaefer, "Energetics and Mechanisms for the Acetonyl + O_2 Reaction: An Important System for Atmospheric and Combustion Chemistry" Journal of Chemical Physics, 152, 114301 (2020). DOI: 10.1063/1.514859. Published: March 2020.

9. Michael C. Bowman, Alexandra D. Burke, Justin M. Turney, Henry F. Schaefer, "Conclusive Determination of Ethynyl Radical Hydrogen Abstraction Energetics and Kinetics" Molecular Physics, 118 (2020). DOI: 10.1080/00268976.2020.1769214. Published: June 2020.

10. Peter R. Franke, John F. Stanton, Gary E. Douberly, "How to VPT2: Accurate and Intuitive Simulations of CH Stretching Infrared Spectra Using VPT2+K with Large Effective Hamiltonian Resonance Treatments" *Journal of Physical Chemistry A* (Invited Review), **125**, 1301-1324 (2021). DOI: 10.1021/acs.jpca.0c09526. Published January 2021.

11. Matthew G. Christianson, Anna C. Doner, Matthew M. Davis, Alanna L. Koritzke, Justin M. Turney, Henry F. Schaefer, Leonid Sheps, David L. Osborn, Craig A. Taatjes, and Brandon Rotavera. "Reaction Mechanisms of a Cyclic Ether Intermediate: Ethyloxirane" *Int. J. Chem. Kinet.* **53**, 43-59 (2021). DOI: 10.1002/kin.21423. Published: January 2021.

12. Anna C. Doner, Matthew M. Davis, Alanna L. Koritzke, Matthew G. Christianson, Justin M. Turney, Henry F. Schaefer, Leonid Sheps, David L. Osborn, Craig A. Taatjes, Brandon Rotavera, "Isomer-Dependent Reaction Mechanisms of Cyclic Ether Intermediates: cis-2,3-dimethyloxirane and trans-2,3-dimethyloxirane" *Int. J. Chem. Kinet.* **53**, 127-145 (2021). DOI: 10.1002/kin.21429. Published: January 2021.

13. A. D. Burke, M. C. Bowman, J. M. Turney, and H. F. Schaefer, "Energetics and Kinetics of Various Cyano Radical Hydrogen Abstractions," *Phys. Chem. Chem. Phys.* **23**, 3389-3400 (2021). DOI: 10.1039/D0CP06228F. Published January 2021.

14. Adam S. Abbott, Boyi Z. Abbott, Justin M. Turney, Henry F. Schaefer, "Arbitrary-Order Derivatives of Quantum Chemical Methods via Automatic Differentiation" *J. Phys. Chem. Lett.* **12**, 3232-3239 (2021). DOI: 10.1021/acs.jpclett.1c00607. Published: March 2021.

15. Mull, H.F.; Franke, P.R.; Sargent, C.; Douberly, G.E.; Turney, J.M.; Schaefer, H.F. "Four isomers of In_2H_2: a careful comparison between theory and experiment" *Molecular Physics*, **119**, 21-22 (2021). DOI: 10.1080/00268976.2021.1979675. Published: September 2021.

16. Bralick, A.K.; Abbott, B.Z.; Douberly, G.E.; Schaefer, H.F. "The isomerisation of H_2XY to HXYH (X, Y = O, S, and Se)*" *Molecular Physics*, **119**, 17-18 (2021). DOI: 10.1080/00268976.2021.1976429. Published: September 2021.

17. Mull, H.F.; Turney, J.M.; Douberly, G.E.; Schaefer, H.F. "Kinetic stability of pentazole" *Journal of Physical Chemistry A,* **121**, 9092-9098 (2021). DOI: 10.1021/acs.jpca.1c06252. Published: October 2021.

18. Li, G.; Yao, Y.; Lü, S.; Xie, Y.; Douberly, G.E.; Schaefer, H.F. "Potential energy profile for the Cl + $(H_2O)_3$ → HCl + $(H_2O)_2$OH reaction. A CCSD(T) study" *Physical Chemistry Chemical Physics*, **23**, 26837-26842 (2021). DOI: 10.1039/D1CP04309A. Published: November 2021.

Coordination and Solvation of Actinide Cations

DOE Award No. DE-SC0018835

Michael A. Duncan
Department of Chemistry, University of Georgia, Athens, Georgia 30602

maduncan@uga.edu

Program Scope

Actinide metal and metal oxide cation-molecular complexes are studied in the gas phase to investigate their bonding, ligand coordination and solvation. Cation-molecular complexes of the form $M^{n+}(L)_y$, where M = U or Th in singly- or doubly-charged states, and L = small molecules such as H_2O, CO, N_2, CO_2 or CH_3CN, are produced in a molecular beam by pulsed laser vaporization of solid metal targets. Similar methods are used to produce metal oxide complexes. Complexes containing a metal or oxide core ion with a specific number of ligand or solvent molecules are cooled by a supersonic expansion, size-selected in a mass spectrometer, and studied with infrared or UV-visible laser photodissociation spectroscopy. Vibrational spectra reveal the shifts that occur for ligand/solvent vibrations upon binding to these metals and how these vary with the charge state, the number of ligands or solvent molecules present, the geometric and electronic structures of complexes, and the possible occurrence of ligand reactions mediated by the metal center. UV-visible spectra reveal the excited states of the same kinds of complexes. Additional experiments employ photofragment imaging technology to further investigate cation-molecular bond energies. The experimental work is complemented by computational chemistry, with careful attention to relativistic and spin-orbit effects. The goal of these studies is an increased understanding of the fundamental interactions and electronic structure involved in actinide bonding, coordination and solvation.

Recent Progress

In recent work, we used laser vaporization to produce ion-molecule complexes of uranium-acetone, and both uranium and thorium cation complexes with cyclo-octatetraene (C_8H_8, known as "COT"). These systems were investigated with mass spectrometry and ion photodissociation to investigate coordination behavior and possible photochemical reactions that might occur upon ultraviolet excitation. In the dissociation of these complexes, intact ligand elimination was detected, but also the loss of C_2H_2 (acetylene) via a photochemical reaction (Figure 1a). A similar reaction was seen previously for transition-metal or lanthanide cation-COT complexes. $U^+(C_5H_5)$ and $U^+(C_3H_3)$ fragment ions were also detected. These unexpected reaction products were missing for thorium ions. As part of this study, we also made and photodissociated Th^+(benzene) and U^+(benzene). The products of photodissociation for U^+(benzene) did not include the $U^+(C_3H_3)$ and $U^+(C_5H_5)$ ions. This established that these fragment ions are formed directly from U^+(COT) and not from a sequence involving a U^+(benzene) intermediate.

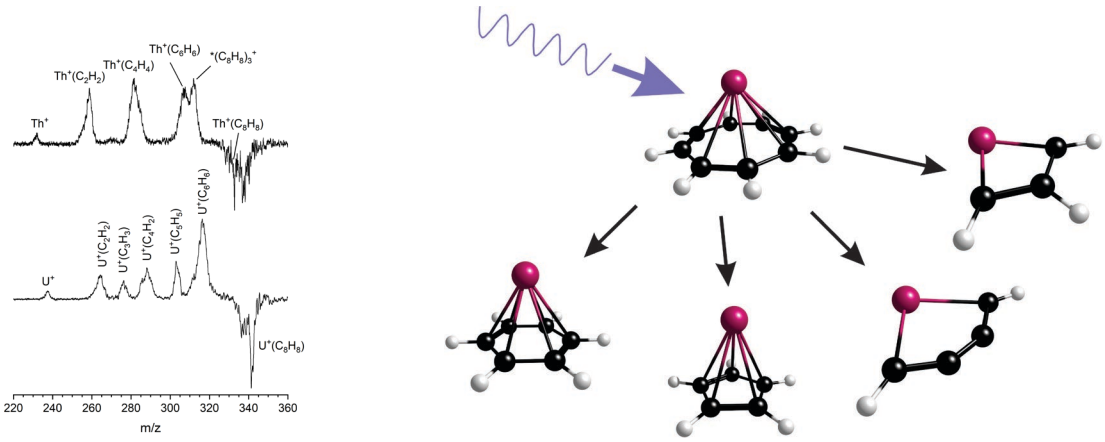

Figure 1. a) Photodissociation mass spectra of M^+(COT) complexes, showing different ligand fragmentation processes for uranium vs thorium complexes. b) The most stable structures of the fragment ions formed from U^+(COT) photochemistry.

We continued our studies on the infrared spectroscopy of $U^+(L)_x$ and $UO_n(L)_x^+$ complexes. In the past, we examined the carbonyl complexes of uranium and uranium oxide cations. In more recent work, we have extended these studies to complexes with L = CO_2, N_2, and water. Our work on $U^+(N_2)_n$, which was recently published, established that the nitrogen molecules bind end-on to the U^+ ion, with a coordination number of eight. The $U^+(N_2)_8$ complex had a cubic structure with a single IR band. More recent studies focused on $U^+(CO_2)_n$ complexes in the region of the CO_2 asymmetric stretch vibration. Computational work indicated the possibility of both metal-CO_2 electrostatic complexes and the formation of O-U^+-CO or U^+-oxalate (C_2O_4) reaction products. The spectra for singly charged $U^+(CO_2)_n$ complexes were inconclusive (Figure 2a), with no clear evidence for the predicted reaction products, but the bands for these structures were predicted to appear at or below the low energy threshold where the laser operates. Future studies will use a different laser configuration to access lower frequencies. The spectra of doubly charged $UO^{2+}(CO_2)_n$ complexes were more interesting, providing clear evidence for a filled coordination at eight ligands. The interesting structure has five CO_2 molecules binding on the same side of the uranium atom as the oxygen that forms the oxide, and three CO_2 molecules opposite this, as shown in Figure 2b. A significant aspect of these infrared studies was to ascertain the best computational method with which to reproduce infrared spectra. Many computational studies have focused on the *energies* produced by different methods, but we have found that reproducing infrared *spectra* is more challenging. We used our data on $UO_2^+(CO)_5$ complexes as a test case. Our previous computational work was done in a collaboration with Prof. Laura Gagliardi and used DFT with the PBE functional and the VTZP(C,O) SDD(U) basis set. This method predicted that the CO stretch frequency of this complex would be shifted to a lower frequency than the free-CO vibration (i.e., a "red" shift), whereas the experiment measured a blue shift. In newer theory work, we use the B3LYP functional and the cc-pVTZ-PP basis set, which has been optimized for uranium chemistry. This method reproduces the measured blue shift for the CO stretch in this complex.

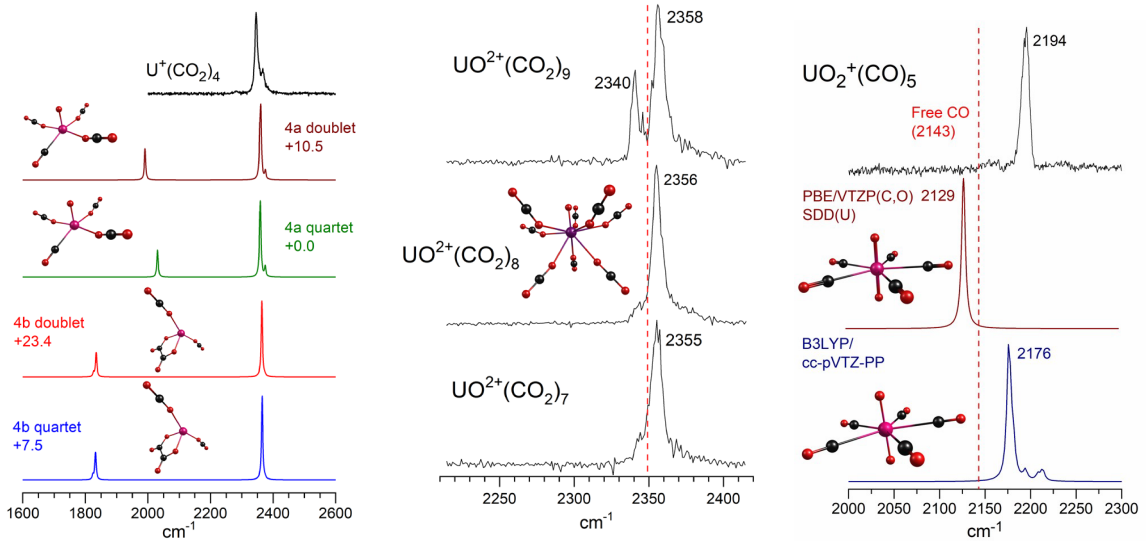

Figure 2. a) IR spectra for $U^+(CO_2)_4$ complexes compared to the predictions of theory for oxide-carbonyl $UO^+(CO)(CO_2)_3$ versus oxalate $U^+(C_2O_4)(CO_2)_2$ reaction product complexes. b) IR-PD spectra of $UO^{2+}(CO_2)_{7,8,9}$ showing the appearance of an un-shifted CO_2 vibration at n = 9 after the coordination is filled at n = 8. c) The spectrum of $UO_2^+(CO)_5$ versus the predictions of theory using two different methods.

We have continued to develop our experiment on the photofragment imaging of mass-selected ions, which probes their energetics and dissociation dynamics. We have recently used this instrument for photofragment imaging of carbon cluster cations. Multiphoton absorption is necessary to initiate dissociation, but the surprising result is that linear-chain structures (e.g., C_6^+) have lower kinetic energy release (KER) than cyclic structures (e.g., C_{20}^+), which have explosive release of high KER, believed to result from the release of ring strain (Figure 3).

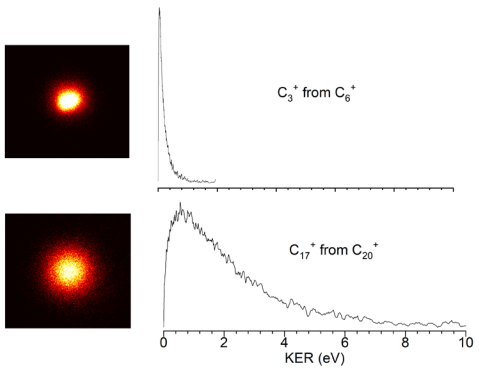

Figure 3. The photofragment images and KER spectra measured for C_6^+ and C_{20}^+ for multiphoton excitation at 355 nm. Although the C_{17}^+ fragment ion from C_{20}^+ is much heavier than the C_3^+ ion from C_6^+, its off-axis velocity is greater, producing a much greater KER.

Future Plans

We will continue the infrared spectroscopy experiments by examining uranium-acetylene and uranium-benzene complexes. Uranium cations have been suggested previously to catalyze the cyclo-trimerization reaction to form benzene, but there is no spectroscopic evidence to confirm

this. We will also examine smaller uranium and thorium carbonyls with unfilled coordination to continue to test the capability of theory in describing vibrational spectra.

BES Supported Publications (2019 – 2022)

1. M. A. Duncan, "Metal Cation Coordination and Solvation Studied with Infrared Spectroscopy in the Gas Phase," in *Physical Chemistry of Cold Gas Phase Functional Molecules and Clusters*, T. Ebata and M. Fujii, eds., Springer, Berlin, 2019, p. 157.

2. J. H. Marks, T. B. Ward, A. D. Brathwaite, *S. Ferguson*, M. A. Duncan, "Cyclotrimerization of Acetylene in Gas Phase $V^+(C_2H_2)_n$ Complexes: Detection of Intermediates and Products with Infrared Spectroscopy," *J. Phys. Chem. A* **123**, 6733−6743 (2019). DOI: 10.1021/acs.jpca.9b04962.

3. P. D. Carnegie, J. H. Marks, A. D. Brathwaite, T. B. Ward, M. A. Duncan, "Microsolvation in $V^+(H_2O)_n$ Clusters Studied with Selected-Ion Infrared Spectroscopy," *J. Phys. Chem. A* **124**, 1093−1103 (2020). DOI: 10.1021/acs.jpca.9b11275.

4. J. H. Marks, P. Kahn, M. Vasiliu, D. A. Dixon, M. A. Duncan, "Photodissociation and Theory to Investigate Uranium Oxide Cluster Cations," *J. Phys. Chem. A* **124**, 1940−1953 (2020). DOI: 10.1021/acs.jpca.0c00453.

5. J. H. Marks, T. B. Ward, A. D. Brathwaite, M. A. Duncan, "Infrared Spectroscopy of $Zn(Acetylene)_n^+$ Complexes: Ligand Activation and Nascent Polymerization," *J. Phys. Chem. A* **124**, 4764−4776 (2020). DOI: 10.1021/acs.jpca.0c03358.

6. A. D. Brathwaite, T. B. Ward, J. H. Marks, M. A. Duncan, "Coordination and Solvation in Gas Phase $Ag^+(C_2H_2)_n$ Complexes Studied with Selected-Ion Infrared Spectroscopy," *J. Phys. Chem. A* **124**, 8562−8573 (2020). DOI: 10.1021/acs.jpca.0c08081.

7. B. M. Rittgers, D. Leicht, M. A. Duncan, "Cation-π Complexes of Silver Studied with Photodissociation and Velocity-Map Imaging," *J. Phys. Chem. A* **124**, 9166−9176 (2020). DOI: 10.1021/acs.jpca.0c08498.

8. J. H. Marks, E. Miliordos, M. A. Duncan, "Infrared Spectroscopy of RG-$Co^+(H_2O)$ Complexes (RG = Ar, Ne, He): The Role of Rare Gas "Tag" Atoms," *J. Chem. Phys.* **154**, 064306 (2021). DOI: 10.1063/5.0041069.

9. J. H. Marks, B. M. Rittgers, M. J. van Stipdonk, M. A. Duncan, "Photodissociation and Infrared Spectroscopy of Uranium-Nitrogen Cation Complexes," *J. Phys. Chem. A* **125**, 7278−7288 (2021). (Dan Neumark Festschrift). DOI: 10.1021/acs.jpca.1c05823.

10. N. J. Dynak, B. M. Rittgers, J. E. Colley, D. J. Kellar, M. A. Duncan, "Photofragment Imaging of Carbon Cluster Cations: Explosive Ring Rupture," *J. Phys. Chem. Lett*., in press.

11. J. H. Marks, A. G. Batchelor, J. R. C. Blais, M. A. Duncan, "Cationic Complexes of Uranium and Thorium with Cyclooctatetraene: Photochemistry and Decomposition Products. *J. Phys. Chem. A*, submitted.

Signatures of Reaction Mechanisms in the Vibrational Level Population Distribution of Reaction Products

Robert W. Field
Massachusetts Institute of Technology
Cambridge, MA 02139
rwfield@mit.edu

I. Significance. The **transition state** and **reaction pathway** are core concepts of Chemistry, but direct experimental characterization of transition states is exceptionally difficult. The reason for this difficulty is that chemical systems spend a very short time, on the order of one half of a vibrational period (for vibrational frequency ω_e=1000 cm^{-1}, the half-period is 17 femtoseconds), to pass through the transition state structure.

II. Methods. Recent developments in molecular spectroscopy and in schemes for producing and stabilizing highly energized molecular species offer new classes of experimental information about transition states and reaction pathways. Chirped Pulse Fourier Transform Micro-Wave (CP-FTMW) and millimeter-Wave (mmW) rotational spectroscopies can capture the isotopologue-specific vibrational population distributions (VPDs) of the polar-molecule products of unimolecular and bimolecular reactions. A molecular fragment, born at a transition state, carries rich and detailed information about the structure of its birthplace. An example of such detail, which is a central part of this project, is the vibrational angular momentum, ℓ, of linear triatomic molecules, such as HCN, which can carry information about the planarity of the transition state. The Even-Lavie (E-L) type pulsed valve and the Cryogenic Buffer Gas Beam (CBGB) are two intense, clustering-free sources of beams that produce translationally and rotationally cold molecules. Although the final translational and rotational temperatures achieved in the molecular beams exiting an E-L valve and the CBGB are similar, the two sources start from quite different initial pressure and temperature conditions: 20 bar and 300K for the E-L valve, 10^{-5} bar and 20 K for the CBGB.

III. Objectives. Two types of cold-molecule sources, the E-L valve and the CBGB, serve as complementary bases for experiments using CP-FTmmW spectroscopy to measure the VPD of small-molecule products of unimolecular photodissociation reactions. Vibrational mode-specific relaxation dynamics in both E-L valve and CBGB sources will be studied prior to the photolysis experiments. The VPD is encoded in the relative intensities of the close-lying set of "vibrational satellites" of a single $J \leftarrow J+1$ rotational transition. VPDs are a class of internal-structure information that is complementary to the external-consequence momentum-release and mass-resolved vector-velocity distribution studies that have been the gold standard of modern studies of chemical kinetics. This rotational and vibrationally resolved information, along with the multiplexed detection nature of CP-FTmmW spectroscopy is qualitatively different from methods used in traditional molecular dynamics studies. The CBGB is a more versatile apparatus, capable of sampling the VPD of the products of cold (20 K) bimolecular reactions, including "stopped kinetics." A molecule, initially formed in an exoergic reaction, is rapidly cooled by collisions with the Ne@20K buffer gas. This molecule can be trapped, awaiting instructions from its spectroscopist/kineticist masters, behind >20 K high barriers on its potential energy surface. In order for us to understand and interpret the VPD data borne out of the transition state, it is necessary to characterize the collisional environment of the molecular beam sources. We describe these experiments in the next section.

III. Foundational studies. The original plan was to use laser excitation of a selected vibration-rotation level of an electronically excited state or either H_2CO or SO_2 and to use the accurately calculated Franck-Condon factors to provide the initial population distribution of vibrational levels in the electronic ground state. Our measurements of the relative intensities of vibrational satellites in the CP-FTmmW spectrum of a ground state rotational transition would display the effects of collisional relaxation of vibrational levels. Initial experiments showed that neither H_2CO nor SO_2 is suitable for our planned experiments. For H_2CO, the $\tilde{A} - \tilde{X}$ electronic transition moment turned out to be too small for the use of laser induced fluorescence to produce sufficiently large populations of excited vibrational levels of the electronic ground state. The populations were a factor of ~10 too small to use CP-FTmmW rotational spectra to measure the collisionally-relaxed Vibrational Population Distribution (VPD). Although the SO_2 $\tilde{C} - \tilde{X}$ electronic transition moment is more than a factor of 10 larger than that for the H_2CO $\tilde{A} - \tilde{X}$ transition, the Franck-Condon VPD in the SO_2 $\tilde{X}$ state is spread over a factor of 10 more vibrational levels than in H_2CO. We have temporarily put the laser induced fluorescence method of creating an *a priori* known VPD on hold.

An alternative method to create an *a priori* known VPD is based on the Boltzmann population distribution law. The pulsed supersonic nozzle was maintained at a fixed temperature to ensure that the initial conditions were described by a Boltzmann distribution. The vibrational temperature (T_{vib}) in the collision-free region of the molecular beam was calculated using the intensities of the vibrational satellites with relative to that of the ground vibrational state pure-rotational transition. We mapped all the commonly varied supersonic expansion conditions across two different valve systems: General valve and the E-L valve. A set of small and medium sized molecules (SO_2, CHF_3, CH_3CN, and CH_2CHCN) were chosen to study the vibrational relaxation (VR) of analyte molecules in a pulsed seeded supersonic expansion. The following parameters were systematically varied:

- Type of the valve: an Even-Lavie type valve (E-L valve) vs. the widely used General valve. The stagnation pressure of the EL-valve was 20 bar and that of the General valve was 2 bar.
- Nozzle temperature (T_{noz}) of the EL-valve at 325 K and 450 K.
- Orifice diameters of the conical opening of the General valve at 0.50 mm and 1.00 mm.
- Stagnation pressure of the General valve at 2 bar and 4 bar.
- Concentration of the gaseous analyte molecules (SO_2, CHF_3) were varied from 0.1% to 100 %, which apart from changing the number of collisions, also changes the collision partner.
- Collision partner of the molecules under study was varied by virtue of the choice of carrier gas: He, Ne, Ar, H_2, and N_2.

From our study of VR in a supersonic environment, we observed the following:

- For collision of the analyte molecules with He carrier gas, we observed a uniform near-linear relationship of the extent of VR (T_{vib}/T_{noz}) with respect to the fundamental frequency (ν) of the vibrational mode in its v=1 level. This linearity was consistent throughout all the experiments where the chemical composition was maintained at high dilution (≤1% by volume of the analyte molecules).
- At higher concentrations of analyte molecules (SO_2 and CHF_3) in He carrier gas, Van der Waals (VdW) effects and velocity slip along the expansion axis was observed. The onset of clustering occurred within 3% of SO_2 concentration, which was detected using independent but complementary laser-based techniques (Laser induced fluorescence and Millimeter wave optical double resonance). Enhanced VR occurred due to predissociation of vibrationally excited VdW complexes in the beam.
- As the carrier gas was changed, deviations from linearity of VR vs mode frequency, ν, was observed. Although the near-linearity relationship was maintained, these deviations were mode-specific. Systematic variation and comparison of the collision partner (mass, polarizability,

vibrational and rotational modes) showed the following trend in the efficiency of VR: He ~ H_2 < Ne ~ Ar < N_2.

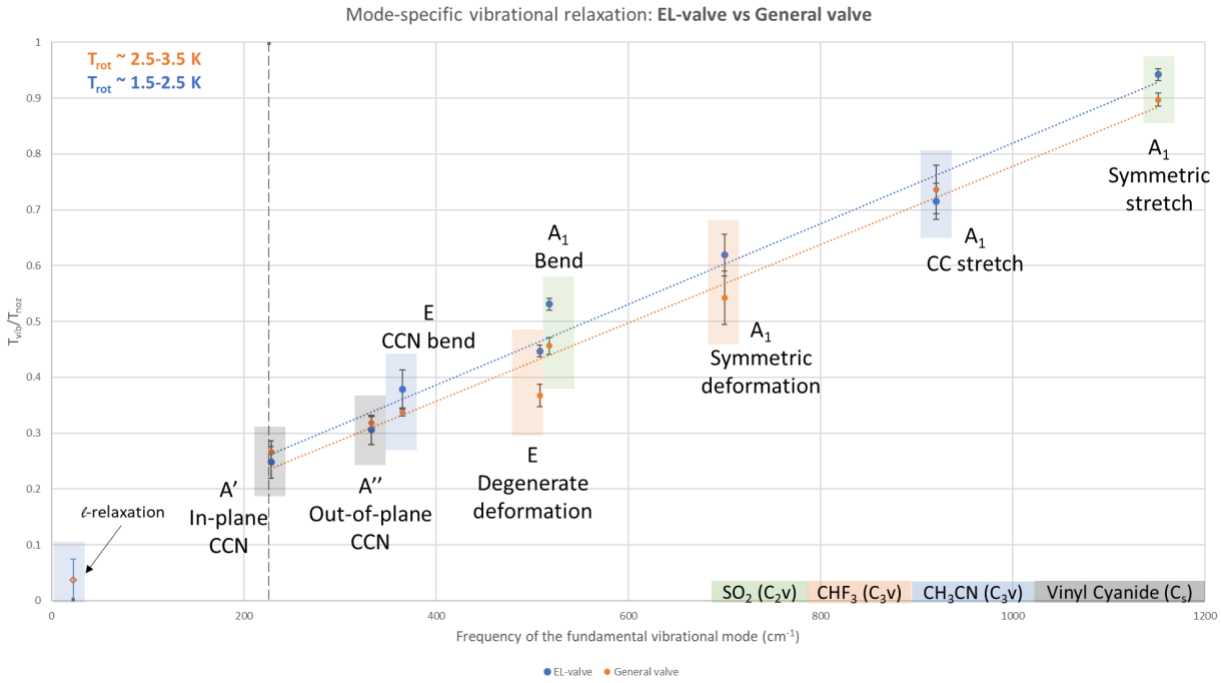

Figure: Vibrational relaxation (T_{vib}/T_{noz}) data v=1 levels of low frequency modes in an E-L valve (blue points) and the General valve (orange points) are shown with their standard deviations (legend: bottom center). A linear trendline is plotted for both experiment data sets. The kT_{noz} at 325 K (226 cm^{-1}, grey) is shown as vertical dashed lines. The ℓ-type relaxation for the General valve (open point) is shown without error bars due to our ability to collect only one data point. The ℓ-type relaxation for the E-L valve is shown only as an upper limit due to non-observation. The rotational temperature (T_{rot}) at both values of T_{noz} are shown at the top left corner. The vibrational mode shadings are color-coded with respect to molecule (legend: bottom right). The mode symmetry and the type of mode is shown beside each datapoint.

T_{vib} deviation of v=2 levels. We observe a slightly higher T_{vib} (slightly larger population than expected) for v=2 states of the lowest lying vibrational modes for SO_2, CHF_3, and CH_3CN. This was observed in some of the temperature plots by Sanz et al [Sanz M. E., McCarthy M. C., Thaddeus P., "Vibrational excitation and relaxation of five polyatomic molecules in an electrical discharge," *J. Chem. Phys.* **122**, 194319 (2005)].

ℓ-relaxation in CH_3CN. The vibrational levels of molecules with a doubly degenerate bending mode are labeled by v and ℓ quantum numbers, where ℓ is the vibrational angular momentum. The possible values of ℓ are $\ell = v, v-2, \ldots 0$ (even-v) or 1 (odd-v). The energy level spacing between the ℓ =2 and ℓ =0 components of v=2 is usually much smaller than the v, v-1 energy difference. One expects collisional ℓ -relaxation to be much faster than v-relaxation, but, owing to the usually small energy differences between ℓ = 0 and 2 levels, there have been few measurements of ℓ-relaxation. CH_3CN is a convenient small molecule to study ℓ-relaxation because the difference between the ℓ = 0 and ℓ = ±2 components of in the $2\nu_8$ vibrational level is 22.4 cm^{-1}, larger than in most small molecules [Müller et al, "Rotational spectroscopy as a tool to investigate interactions between vibrational polyads in symmetric top molecules: Low-lying states $\nu_8 \leq 2$ of methyl cyanide, CH_3CN," *J. Mol. Spec.* **312**, 22-37 (2015)]. This implies that small changes in the relative intensities of the ℓ components of the $2\nu_8$ vibrational satellite will not significantly affect the calculated T_ℓ (ℓ -temperature). T_ℓ was found to be <20K for both valves.

IV. Future direction. We are setting up the experiment to perform photolysis of s-Triazine using the 4th harmonic (266 nm) of the pulsed Nd:YAG laser. The photolysis will occur within 0.5 cm downstream of

the nozzle orifice. Downstream collisions will rotationally (but only minimally vibrationally) cool the HCN photodissociation product. The CPmmW spectrum will sample the Vibrational Population Distribution of both HCN and HNC photofragments. We also plan to perform photolysis using an excimer laser at 193 nm.

We also plan experiments using a Ne@20K and Ar@100K Cryogenic Buffer Gas Beam (CBGB). The operating conditions in these molecule sources are quite different: E-L valve at 10 or 20 bar, General valve at 2-4 bar, and CBGB at 10^{-5} bar.

V. Publications.

R. W. Field and A. G. Suits, "Modern Techniques, Modern Concepts, and Molecules Doing Stuff," ACS Book Chapter in Emerging Trends in Chemical Applications of Lasers, H.-L. Dai, M. Berman, and L. Young (editors) (in press).

J. Jiang, Z. Du, J. Liévin and R. W. Field, "One-Color (~220 nm) Resonance-Enhanced (S_1–S_0) Multi-Photon Dissociation of Acetylene: Probe of the C_2 $A^1\prod_u$ — $X^1\sum^+_g$ band by Frequency Modulation Spectroscopy," *Mol. Phys* .**361**, 24-33(2019). https://doi.org/10.1080/00268976.2020.1724340.

K. Prozument, J. H. Baraban, P. B. Changala, G. B. Park, R. G. Shaver, J. S. Muenter, S. J. Klippenstein, V. Y. Chernyak and R. W. Field, "Vinyl Cyanide Photodissociation: Transition States Characterized by Chirped-Pulse Millimeter-Wave Measurement of HCN and DCN Vibrational Population Distributions," *Proc. Nat. Acad .Sci.* **117**(1), 146-151(2020) . http://dx.doi.org/10.1073/pnas.1911326116.

J. Jiang, Z. Du, and R. W. Field, "Determination of the Sign of the Population Difference in a Two-Level System by Frequency-Modulation Spectroscopy," *Mol. Phys.* **118**(7), e660007/1-10(2020). http://dx.doi.org/10.1080/00268976.2019.1660007.

J. Jiang, A. K. Muthike, T. J. Erickson, and R. W. Field, "One-color (212-220 nm) Resonantly-Enhanced (S_1-S_0) Multi-Photon Dissociation of Acetylene," *J. Mol. Spectrosc*. **361**, 24-33 (2019). http://dx.doi.org/10.1016/j.jms.2019.05.006

Daniel P. Zaleski, Raghu Sivaramakrishnan, Hailey R. Weller, Nathan A. Seifert, David H. Bross, Branko Ruscic, Kevin B. Moore III, Sarah N. Elliott, Andreas V. Copan, Lawrence B. Harding, Stephen J. Klippenstein, Robert W. Field, Kirill Prozument**, "**Substitution Reactions in the Pyrolysis of Acetone Revealed through a Modeling, Experiment, Theory Paradigm," *J. Am. Chem. Soc.* **143**(8), 3124–3142 (2021).

Piyush Mishra, Alexander W. Hull, Timothy J. Barnum, Brett A. McGuire, Robert W. Field, "Chirped-Pulse Fourier-Transform Millimeter-wave Rotational Spectroscopy of Furan in its ν_{10} and ν_{13} Excited Vibrational States", Submitted to *J. Mol Spectrosc*.

TOWARDS MACHINE LEARNING MOLECULAR DYNAMICS: EFFECT OF DATA PARTITIONING ON MODEL RESULTS

C. Franklin Goldsmith, PI
Brown University

Program Scope

One of the grand challenges for the Department of Energy is the ability to simulate the complex interactions between fluid mechanics and chemical kinetics for gases at high pressures (e.g. 100 bar). Under these conditions, the ideal gas equation of state is not valid. Although considerable advances have been made regarding real-gas equations of state for thermodynamic properties, the same cannot be said of chemical kinetics under extreme pressures. The standard approach in computational kinetics assumes that reactions occur under isolated conditions. Real-gas behavior can have a profound effect on the chemical source terms in reactive flow simulations. These many-body interactions can change both the rate constants and the product branching fractions.

In this project, we are investigating different methodologies to quantify many-body effects on transition states and thence high-pressure effects on rate constants. The specific aims are: (i) develop chemically accurate surrogate potential energy surfaces for computational kinetics with explicit solvent molecules, and use this surrogate model within molecular dynamics simulations; (ii) quantify the effects of high pressures on rate constants for different reaction families; (iii) determine the pressure at which solvent cage effects will cause the branching fractions in bond-fission reactions to favor molecular elimination products; and (iv) analyze the results for possible trends that can be applied heuristically.

Additionally, we have begun to develop a purely theory-based mechanism for fluorinated compounds to understand the incineration of per- and poly-fluorinated alkyl substances (PFAS).

Recent Progress

The past year has continued to focus on the development of a machine learning molecular dynamics (MLMD) methodology. The goal is to develop a platform, as close to black box as possible, that will enable us to go from electronic structure calculations to a full-dimensional force-field model for use in molecular dynamics for arbitrary systems.

In order to develop a potential model suitable for MD, we need to provide sufficient sampling in both intramolecular and intermolecular interactions. Our current work uses density functional theory (DFT) to provide the required training data. Preliminary work focused on random sampling within internal-coordinate space as a way of exploring in intramolecular interactions. This approach, while computationally advantageous, did a poor job of covering the regions of phase space that were explored during the MD simulations. Instead, we used ab initio molecular dynamics (AIMD) to generate the training data.

Our prior work focused exclusively on methane. More recently, we have expanded our approach to include water as well, since reaction kinetics in supercritical water are an important application area. In addition to working on MLMD for these two pure-component systems, a major area of development is uncertainty quantification. Specifically, we are interested in how the standard procedure of dividing the original data into a training set and a test set impacts the model performance.

Broadly speaking, machine learning is most useful when the training data is abundant and/or easy to generate. For example, if we're using machine learning to identify cats, we can download millions of images of cats, practically for free. For ab initio systems, in contrast, that is not necessarily true. The cost of generating newer, larger, and/or better training data is substantial, and a key goal in using machine learning for molecular dynamics is minimizing the size of the training set, so as to minimize this computational cost.

A standard approach in machine learning is to divide the original training data into two sets: a training set and a test set. Typically, 90% of the original data is used for training, and the remaining 10% of data are set aside to test the model prediction. The 90/10 portioning is determined using a random seed. We have investigated how sensitive the model predictions are to the random seed.

Training data were generated using AIMD simulations in Orca. For methane, we used ωB97M-D3/def2-TZVP(-f) functional/basis set. For water, we used M062X-D3/ def2-TZVP(-f). A repulsive wall was used to confine the molecules to a fixed volume, which allows us to maintain a fixed density while still being able to use gaussian-type basis functions (instead of planewave basis functions with periodic boundary conditions). The methane simulations consisted of 12 CH_4 molecules, and the water simulations consisted of 32 H_2O. 80 unique AIMD simulations were performed, resulting in 80,000 timesteps for training data.

Next, we generated 100 unique MLMD models using random seeds determined by a Sobol sequence between 1 and 10,000. For each seed, a new neural network potential was obtained from the training data. The training was done with the N2P2 package so that we could directly use the pre-established LAMMPS wrapper for N2P2. To evaluate the 100 distinct NN models, we considered how well they could predict the mass density. 512 CH_4/H_2O molecules were simulated with periodic boundary conditions using the LAMMPS/ N2P2 interface. The initial configurations were generated using the VMD TopoTools plugin. The system was first equilibrated for 25 ps in the *NPH* ensemble coupled to a Langevin thermostat to keep the temperature constant. The equilibrated system was then used for a 0.5 ns production run in the *NPT* ensemble. Preliminary studies confirmed that 0.5 ns is enough for obtaining the equilibrated mass density. The timestep of 0.5 fs was applied to all simulations and the configurations were collected every 100 fs. The resulting dataset was sufficient to predict the mass density as a function of time. The average mass density (after the initial equilibration) was then recorded.

For CH_4 we considered four different conditions: 100K/1 bar, 100K/1000 bar, 300K/500bar, and 300K/1000 bar; for H_2O, the conditions were: 300K/1 bar, 300K/1000 bar, 1000K/5000bar, and 1000K/10000 bar. These conditions range from liquid to vapor to supercritical. For each random seed, the resulting ML potential was used in an MD simulation to predict the mass density. The resulting $\rho(T,p)$ was compared against a literature equation of state, taken from Cantera. The error for these conditions is plotted below.

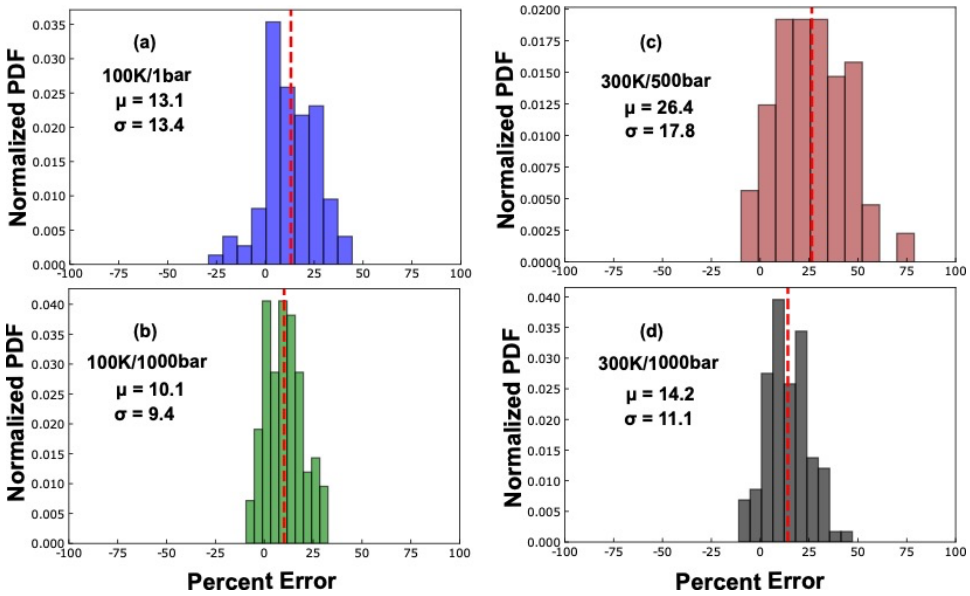

Figure 2: histogram of error in predicted mass density for methane at four conditions.

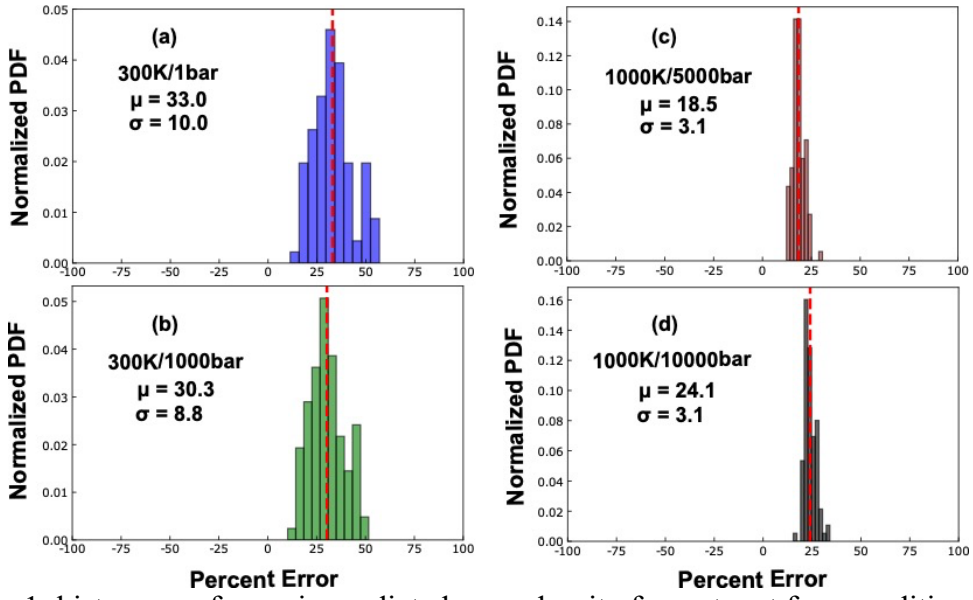

Figure 1: histogram of error in predicted mass density for water at four conditions

The results in Figures 1 and 2 suggest that there is considerable uncertainty in the MLMD predictions due simply to how the training data is proportioned. Although more data would help to alleviate this problem, that approach might not be practical. For systems where the "correct" answer is available from an equation of state, such as for CH_4 and H_2O, we can simply choose the ML potential that minimizes the error. This approach allows us to correctly predict the mass density for both liquids and dense gases using a single potential model. For other cases, where the density is not available, we can instead choose the potential closest to the mean. As demonstrated by Figures 1-2, this approach is likely to be off by a fixed amount, on the order of 10-20%.

Future Plans for MLMD

More recently, we have extended this work to consider transition states. Our goal is to compute the change in volume of activation, $\mathbf{\Delta}V^{\ddagger}$, as a function of temperature and pressure. This $\mathbf{\Delta}V^{\ddagger}(T, p)$ will enable us to compute real-gas corrections for rate constants. Our trial reaction is $OH + C_3H_8 \rightarrow H_2O + n\text{-}C_3H_7$. The basic procedure we developed for the equation of state modeling is replicated. The only difference is that we place a "solute" molecule (in this case, OH, C_3H_8, and the first-order saddle point for the H-abstraction reaction). The internal degrees of freedom of the solute are frozen. As with the EoS results, we first compute the $V(T, p)$ using the *NPT* ensemble. The change in volume of activation is then given by $\mathbf{\Delta}V^{\ddagger}(T, p) = V_{TS}(T, p) - V_{OH}(T, p) - V_{C3H8}(T, p)$.

PFAS

Finally, we have begun work on a theory-based mechanism for PFAS incineration. Our initial step is to extend the ANL0 methodology to include F-containing species. In order to do so, we must first decide what the appropriate reference species is. We considered F_2, HF, and CF_4. The predicted heats of formation are compared against the available data in the ATcT. Fortunately, the results are nearly identical. We have selected CF_4, based upon the fact that the C-F bond is our primary goal in PFAS modeling.

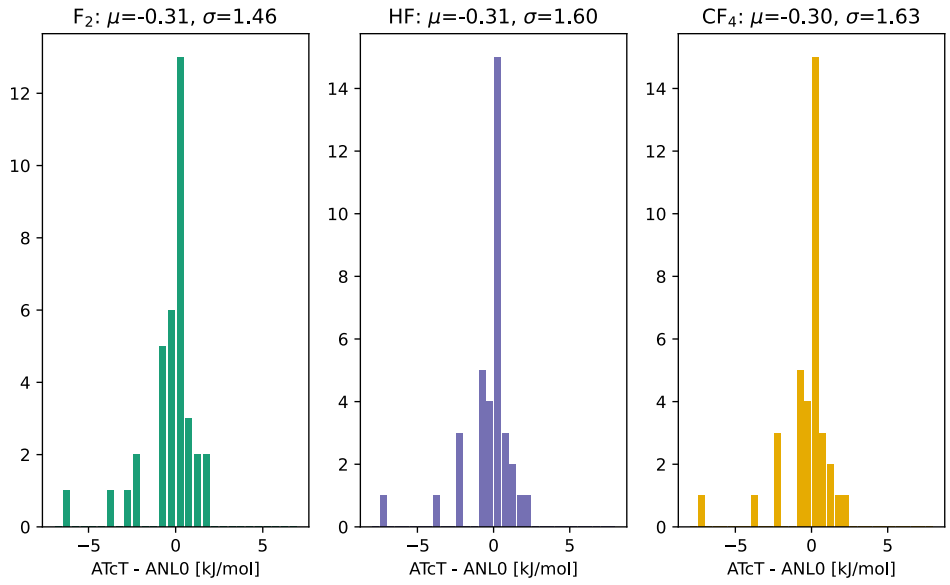

Figure 3: error using three different reference species for F.

DE-SC0021206: Langevin Dynamics modeling of gas-phase ion-ion recombination

Principal Investigator: Ranganathan Gopalakrishnan, Ph. D., rgplkrsh@memphis.edu
Mailing Address: 310D Engineering Science, University of Memphis, Memphis, TN 38152.

Program Scope: The recombination of ions in the gas-phase plays a significant role in the chemical composition, energy, and charge balance of partially ionized gas environments such as flames, plasmas, inter-planetary gas clouds and ultra-cold (~few K) systems like cryogenics and quantum computers. Motivated by the lack of robust theoretical models of gas-phase ion-ion recombination, a data-driven approach to modeling the recombination rate constant β_r by analyzing trajectories calculated using Langevin Dynamics (LD) simulations considering the ion-ion electrostatic interactions, ion number concentration, and ion-neutral gas interactions is pursued in this project. At gas pressures $> 100\ Pa$, the effect of ion-neutral gas molecule collisions is captured implicitly through the drag and diffusion terms in the Langevin formulation, allowing the calculation of the recombination rate considering the motion of the cation(s) and anion(s) only. The recombination rate constant β_r will be parameterized by calculating the average collision time between cation and anion in the presence of neutral gas molecules for a wide range of gas pressure p and temperature T of interest to previously mentioned applications ($p > 10^2 Pa, T > 100\ K$). In this framework, various chemical physics that include the effect of ionic structure, molecular rotation, ion number concentration, electron transfer kinetics will be systematically explored to develop regression expressions. An exhaustive set of experimental data for β_r obtained using FALP-VENDAMS method (mostly from Albert Viggiano's group at AFRL, Smith's group at University of Birmingham, and a few other groups) is used to evaluate the accuracy of the developed expressions and the % difference between prediction and measurement will be used as feedback to revise the modeling assumptions. To provide accurate inputs to the Langevin Dynamics calculation of β_r, the ionic structures will be determined using the Gaussian16® package. The ion mobility or diffusion coefficient will be obtained from published experimental data or calculated using the IMoS ion mobility calculation package[1].

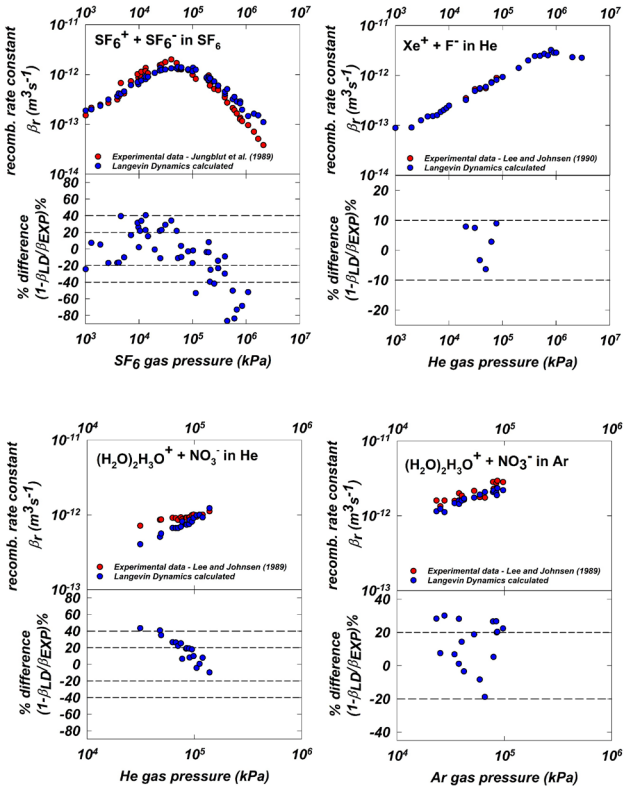

Figure 1: Comparison of experimentally measured and Langevin Dynamics computed values of the recombination rate constant β_r as a function of gas pressure at 300 K.

Ion recombination or mutual neutralization is modeled within the framework of classical physics and thus does not explicitly model the quantum nature of electron transfer kinetics from the anion to the cation (proton exchange reactions are not considered). This requires a precise, universal definition of what constitutes collisional recombination that may be thought of to happen in two steps: transport driven by ion-ion potential interaction φ_{i-i} and ion thermal energy $k_B T$, followed by electron transfer when the ions are "sufficiently" close.

$$\varphi_{i-i}(\vec{r}_{\pm}) = \sum_{i=1}^{N_+}\sum_{j=1}^{N_-}\left(4\varepsilon_{ij}\left[\left(\frac{\sigma_{ij}}{r_{ij}}\right)^{12} - \left(\frac{\sigma_{ij}}{r_{ij}}\right)^{6}\right] + \frac{\delta_i \delta_j e^2}{4\pi\varepsilon_o r_{ij}}\right) \ldots (1)$$

Here, r_{ij} is the distance between atom i in the cation (that has a total number of atoms N_+) and atom j in the anion (consisting of N_- atoms) and σ_{ij} can be understood as the distance between two atoms at which the potential energy (due to van der Waals or polarization interaction) between the ions is zero. Two atoms, as they get closer, feel a strong repulsion $\sim r^{-12}$ due to electron degeneracy pressure. For low energy ions, overcoming this repulsion is not feasible and so the ions scatter off of each other at a distance of closest approach that is of the same order of magnitude as σ_{ij}.

Summary of progress: We have been investigating recombination on two fronts:

1) *The calculation of β_r for recombination under dilute conditions by simulating the motion of a single cation and single anion using Langevin Dynamics.* Herein, we investigate the dependence of β_r on the gas pressure and temperature. The key focus here is to model electron transfer without resorting to quantum mechanics. Specifically, a length scale that appears in the ion-ion potential (eq. 1) and can be unambiguously evaluated for any ion pair of known chemical composition without free parameters is hypothesized and used to detect a successful recombination event in the simulation. The β_r calculations using this length scale is compared against experimental data. It is seen that this approximation does reasonably well for instances of recombination at pressures > 1 kPa for both poly- and monoatomic ions. It also explains the experimental data well for instances where one of the ions is polyatomic and the other is monoatomic at pressures as low as ~1 torr (133 Pa). Based on the comparison with data for instances where both the cation and anion are monoatomic, two questions arise, and current work focuses on answering those questions as described here.

Cation	Anion	300K	400K	500K	550K
Ar^+	Br_2^-	1.19	1.44	1.44	
Kr^+	Br_2^-	0.78	0.83		
Ar^+	Cl_2^-	1.12	1.13		1.20
Ar^+	CN^-	1.33			
Ar^+	FCl^-	1.16	1.19	1.60	
Ar^+	NO_2^-	0.65		0.65	
Ar^+	$PSCl^-$	0.68	0.68		0.64
Ar^+	$COCl_2^-$	0.74	0.70		
Ar^+	NO_3^-	0.76			
Ar^+	$POCl_2^-$	0.79	0.81	0.86	
Kr^+	$POCl_2^-$	0.80	0.78	1.17	
Ar^+	$PSCl_2^-$	0.83	0.90		0.94
Ar^+	CF_3O^-	0.74	0.90	0.88	0.95
Ar^+	$POCl_3^-$	0.69	0.69	0.64	
Kr^+	$POCl_3^-$	0.68	0.68	0.80	
Ar^+	SF_4^-	0.90	0.88	0.83	
Kr^+	SF_4^-	0.78			
Ar^+	SF_5^-	1.01	0.98	0.97	
Kr^+	SF_5^-	1.08			
Ar^+	SF_6^-	0.72	0.78	0.71	
Kr^+	SF_6^-	0.75			

Table 1: Ratio of Langevin Dynamics computed and experimentally measured values of the recombination rate constant β_r as a function of temperature at ~1 torr for monoatomic cations and polyatomic anions.

Details of this effort: We started with the hypothesis that electron transfer takes place with 100% probability when two atoms i and j approach each other with a distance less than or equal to σ_{ij}: $r_{ij} \leq \sigma_{ij}$. To evaluate this hypothesis, we carried out Langevin Dynamics simulations of the cation and anion in a periodic domain and used the mean collision time to compute β_r and subsequently compared the same with experimental data. The % the difference, calculated as $\left(1 - \frac{\beta_r^{LD}}{\beta_r^{exp}}\right)$%, is used to assess the accuracy of the modeling assumptions by systematically comparing the simulation-derived rate constant β_r^{LD} and experimentally measured β_r^{exp}. **Figure 1** panels A – D present, respectively, comparisons for $SF_6^+ + SF_6^-$ reaction in SF_6 (Experimental data from Jungblut *et al.*[2]), $Xe^+ + F^-$ in He (data from Lee and Johnsen[3]), $(H_2O)_2H_3O^+ + NO_3^-$ in He and Ar (data from Lee and Johnsen[4]). The agreement is unbiased and within $\sim \pm 30\%$ across the board with only a few outliers. The presented LD calculations reveal reasonable agreement to support the hypothesis that σ_{ij} is an excellent approximation for the distance at which electron tunneling takes place with near certainty for the modeled ion recombination reactions. Most importantly, the presented comparisons are at pressures $\geq 1\ kPa$.

	Cl^-	Br^-	I^-
Ne^+	1.44	1.01	0.70
Ar^+	9.37	6.15	1.41
Kr^+	18.27	14.80	2.88
Xe^+	34.15	7.99	11.35
O^+	2.25	0.75	1.84
N^+	4.23	2.43	2.25

Table 2: Ratio of Langevin Dynamics computed and experimentally measured values of the recombination rate constant β_r as a function of temperature at ~1 torr for monoatomic cations and monoatomic anions.

To further explore whether σ_{ij} holds up as the length scale of electron transfer for recombination reactions at pressures lower than 1 kPa, we simulated several ion recombination reactions experimentally studied at ~1 torr gas pressure. **Table 1** shows the % difference for a series of reactions involving monoatomic cations (Ar^+, Kr^+) and polyatomic anions in He buffer gas published by Miller *et al.*[5]. The gas temperature in this dataset was varied from $300 - 500\ K$. The presented comparison between LD simulation predictions and measurements reveals agreement within $\pm 30\%$ with few outliers. Likewise, we are currently working on calculating β_r for reactions between polyatomic cations and monoatomic anions (Br^-, Cl^-, I^-) in He buffer gas reported by Shuman *et al.*[6] and Sawyer *et al.*[7]. For this dataset, gas temperature was $300\ K$ and pressure was 1.5 torr. It remains to be seen how the comparison will turn out. There is good reason to believe that reactions between monoatomic and polyatomic ions reveals reasonable agreement that is unbiased. Lastly, the combination of monoatomic anions and monoatomic cation was explored as summarized in **Table 2**. Here, for convenience in interpretation, the ratio of $\frac{\beta_r^{LD}}{\beta_r^{exp}}$ is tabulated instead of the % difference. It can be readily seen that the simulations exceed the experiment by a factor of 2 – 20 for reactions between monoatomic ions. This clearly shows that the LD simulations (done using $r_{ij} \leq \sigma_{ij}$ as the condition for electron transfer) predict that electron transfer takes place more often than it does in reality and necessitates a more sophisticated treatment of the electron transfer kinetics.

Future Plans: To summarize, the simple criterion of $r_{ij} \leq \sigma_{ij}$ to denote electron transfer from anion to a cation when they are close enough reasonably explains the recombination rate constant in cases of one or both of the ions being polyatomic at pressures >1 kPa. It also explains the observed rate constants for monoatomic cation-anion at pressures >~133 Pa. It, however, overpredicts the rate constant by 2 – 20 times at the same pressure.

This presents us with two questions to answer:

1. How to accurately calculate the recombination rate constant at low pressures?
2. Why does the criterion $r_{ij} \leq \sigma_{ij}$ work at high pressures and for polyatomic ions?

We plan to answer both of these questions using a semi-classical Landau-Zener curve crossing approach integrated with trajectory simulations. In this approach, the intersection of the potential energy curves of the incoming ions and outgoing neutrals are used to estimate the separation r_{ij} at which the electron transfer takes place. The probability of electron transfer is coupled to the trajectory simulations (classical MD or LD) to calculate both β_r and the product branching ratio (proportion of neutrals formed in ground state and various excited states). Current work includes modeling the recombination of monoatomic ions to address #1 and extracting the average distance where electron transfer is seen to take place to answer #2.

2) *Parameterizing the interplay of gas pressure p_g, temperature T_g and ion-pair number density n_i on β_r by simulating the motion of N cation-anion pairs interacting simultaneously Langevin Dynamics (LD).* Herein, we investigate how β_r varies primarily with ion-pair number density. For $n_i \leq 10^{14} m^{-3}$, it is taken for granted that ion recombination is a dilute process wherein the cation and anion interact with each other without a significant number of charges being present in their vicinity. As n_i increases, it is conceivable that the chance of two ions interacting with each other in isolation decreases and the encounters between a group of ions becomes more probable. To systematically probe this effect, we varied n_i between $10^{14} - 10^{22} m^{-3}$. We generalized our LD calculation of β_r by including N cation-anion pairs that lead to a desired ion-pair number density at a specified p_g, T_g. Following validation of our LD code against data for the ion pairs discussed previously under dilute conditions (n_i~$10^{14} m^{-3}$), we used the $2N$-body LD code to also predict β_r under dilute conditions for consistency check. The LD code that successfully predicts β_r in the dilute limit was then used to carry out parametric studies in which p_g~$10^3 - 10^6 Pa, T_g$~$> 100\ K, n_i$~$10^{14} - 10^{20} m^{-3}$ for two ion pairs SF_6^+, SF_6^- and Xe^+, F^-. The simulation results reveal several interesting trends and set the stage up for a complete set of β_r models developed by fitting LD simulation data that holistically capture the effect of n_i, p_g, T_g for specific ion pairs.

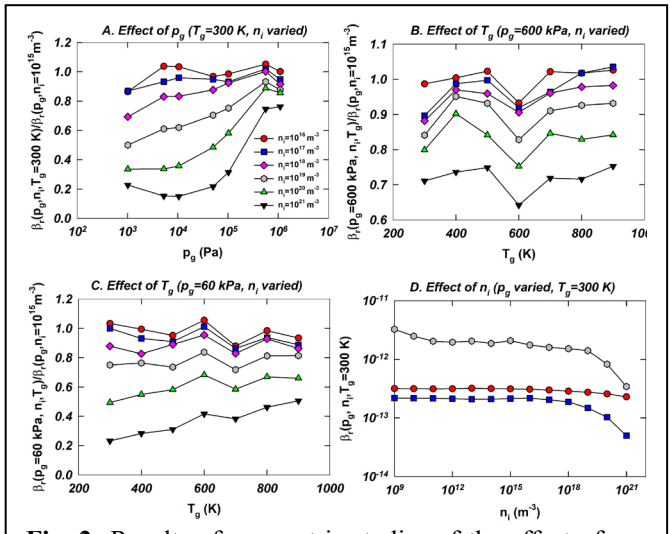

Fig. 2: Results of parametric studies of the effect of gas pressure p_g, temperature T_g and ion-pair number density n_i for SF_6^+ cation recombining with SF_6^- anion in SF_6 gas.

Details of this effort: With the LD simulations using one ion pair (one cation and one anion) in the dilute limit agreeing well with experimental data, we chose two specific ions pairs to probe the effect of ion-pair number density. While every ion pair is chemically different, but they do share common physics as well. For instance, the ion motion is driven by electrostatic interactions as well as interactions with the gas molecules. Thus, we aim to develop expressions for β_r for numerous ion pairs for which we can find experimental data for validation at least in the dilute limit. The first step in that effort was to ensure that the $2N$-body LD simulations yield predictions that are independent of the choice of N and domain volume (the simulation timestep was also chosen sufficiently small to ensure that the results do not depend on the same). It is first established that the calculation method for β_r is insensitive to our subjective choices $\left(\frac{\partial}{\partial N}\left(\frac{\beta_r(p_g,T_g,n_i)}{\beta_r(p_g,T_g,n_i\to 0)}\right)\approx 0\right)$ for $n_i = 10^{14}-10^{22}m^{-3}, p_g = 10^3-10^6 Pa$ by varying N for SF_6^+, SF_6^- and Xe^+, F^- ion pairs (These results are not shown here for brevity). We also, computed β_r at dilute conditions $n_i \to 0$ to check if values match with the (2-body) dilute limit simulation and experimental data (also not displayed here). Subsequently, **Figure 2** and **3**, respectively, present $\frac{\beta_r(p_g,T_g,n_i)}{\beta_r(p_g,T_g,n_i\to 0)}$, a ratio of the recombination rate constant for SF_6^+, SF_6^- and Xe^+, F^-. Herein, we varied all three parameters (p_g, T_g, n_i).

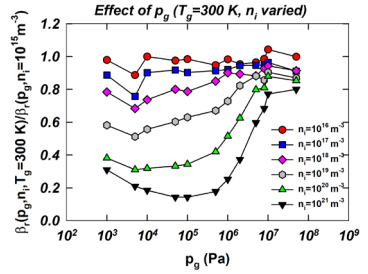

Fig 3: Results of parametric studies of the effect of p_g, T_g, n_i for Xe^+ cation recombining with F^- anion in He gas.

Future Plans: Current work includes parametric studies using LD simulations to understand the dependence of β_r on n_i for the ion pairs covered in Figure 1, and Tables 1, 2. Work is underway to include rotational Langevin equations to track the ion orientation using quaternions. The combined translation and rotation of the ions will allow a comprehensive model of β_r. Classical MD is used to compute the rotational diffusion coefficients of ions.

Publications of DOE sponsored research:

1. Suresh[#], V., Li[#], L., Redmond Go Felipe, J. and Gopalakrishnan, R., Modeling nanoparticle charge distribution in the afterglow of non-thermal plasmas and comparison with measurements. *Journal of Physics D: Applied Physics* 54(27): 275205. https://iopscience.iop.org/article/10.1088/1361-6463/abf70c
2. Suresh*, V. and Gopalakrishnan, R. (***invited*** methods article), Tutorial: Langevin Dynamics methods for aerosol particle trajectory simulations and collision rate constant modeling. *Journal of Aerosol Science* 155: 105476. https://doi.org/10.1016/j.jaerosci.2021.105746

Manuscripts in preparation of DOE sponsored research:

1. Li[#], L., Roy[#], M., Liu, Z., and Gopalakrishnan, R., Langevin Dynamics modeling of the gas-phase ion recombination rate constant to delineate the effect of gas pressure, temperature and ion number density and comparisons against experimental data.
2. Liu, Z., and Gopalakrishnan, R., Coupling Landau-Zener curve crossing with trajectory simulations to calculate the rate constant for gas-phase ion recombination reactions.

References

1. Larriba-Andaluz, C. and Prell, J.S., *Fundamentals of ion mobility in the free molecular regime. Interlacing the past, present and future of ion mobility calculations.* International Reviews in Physical Chemistry, 2020. **39**(4): p. 569-623.
2. Jungblut, H., Hansen, D., and Schmidt, W.F., *Ion-ion recombination in electronegative gases.* Ieee Transactions on Electrical Insulation, 1989. **24**(2): p. 343-348.
3. Lee, H.S. and Johnsen, R., *Recombination of Xe+ with F− ions in ambient helium.* The Journal of Chemical Physics, 1990. **93**(7): p. 4868-4873.
4. Lee, H.S. and Johnsen, R., *Ion–ion recombination studies in ambient helium and argon at atmospheric densities.* The Journal of Chemical Physics, 1989. **90**(11): p. 6328-6334.
5. Miller, T.M., Shuman, N.S., and Viggiano, A.A., *Behavior of rate coefficients for ion-ion mutual neutralization, 300–550 K.* The Journal of Chemical Physics, 2012. **136**(20): p. 204306.
6. Shuman, N.S., Wiens, J.P., Miller, T.M., and Viggiano, A.A., *Kinetics of ion-ion mutual neutralization: Halide anions with polyatomic cations.* Journal of Chemical Physics, 2014. **140**(22).
7. Sawyer, J.C., Hedvall, P., Miller, T.M., Engeling, K.W., Larson, Å., Orel, A.E., Viggiano, A.A., and Shuman, N.S., *Reactions of C+ + Cl−, Br−, and I−—A comparison of theory and experiment.* The Journal of Chemical Physics, 2019. **151**(24): p. 244301.

Computer-Aided Construction of Chemical Kinetic Models

William H. Green
Department of Chemical Engineering
Massachusetts Institute of Technology
Cambridge, MA 02139
whgreen@mit.edu

I. Program Scope

Our goal is to make it possible to quantitatively predict chemical kinetics, even for systems with hundreds of important reactions. Predictive kinetics is exactly what is needed for computer-aided design of new chemical reaction systems.[10] We have used our new method to predict yields of new reactor designs, performance of proposed alternative fuels, and other energy storage systems, pyrolysis of fuels, plastics, and biomass, and the stability and fate of man-made materials exposed to the atmosphere [32,33]. The ability to make quantitative predictions is critical for fundamental scientific studies: e.g. for designing and correctly interpreting kinetics experiments involving more than a handful of reactions, and for correctly assessing if a new observation is 'expected' or instead reveals new science.

However, making quantitatively accurate predictions is challenging [1,3-5,8-11], particularly for the complicated systems where computer predictions are most helpful for supplementing human intuition. Sometimes an error in a single rate or molecular parameter, or the omission of a single important reaction from the kinetic model, can lead to serious mis-predictions.

To deal with the complexity of reacting chemistry, we use the computer to both construct and solve kinetic models. Because these large models contain so many parameters (e.g. k's, K_{eq}'s) one never has sufficient data to determine each parameter experimentally. Instead we use theoretical values for many of the numbers in the model, and refine the most sensitive numbers through experiments or higher level calculations.[4,10] Typically there are several numerical values for each rate parameter: estimates (including those derived using machine-learning methods), numbers from detailed quantum chemistry calculations, and values derived from experiments. Since there are multiple values, with various uncertainties, for hundreds of reactions, this line of research connects fundamental studies of individual reactions with data science [14-16,24,25,34] and uncertainty quantification.[8,15]

We continue to develop improved methods for modeling gas phase systems, including better methods for building reaction networks [3-5,10-11] and for predicting the pressure-dependence of rate coefficients.[12] Recently we have also developed efficient methods for computing solvent effects[16], and we have demonstrated coupling between gas phase and catalytic reactions [17]. We also develop methods for quantifying uncertainties,[8,15] and for model-reduction. The models are tested with experimental data measured in our lab [18-20] or measured by collaborators [22,23,26,31].

II. Recent Results

A. Chemistry of Cyclics & Polycyclics, esp. Polycyclic Aromatics

The formation of aromatics, particularly polycyclic aromatics, is a major problem in many systems, leading to particulate air pollution, fouling of equipment and engines, and emissions of carcinogens. This chemistry is likely to continue to be important even in the far future, in systems using biofuels and biomass, in methane pyrolysis to produce hydrogen, and in systems which convert waste plastic.

While cyclization chemistry has been heavily studied, many basic issues are still unresolved and we are still far from having models which are simultaneously consistent with experimental observations, rate theory, and the laws of thermodynamics. The chemistry is surprisingly complicated, with several quite different mechanisms of molecular weight growth running simultaneously, and a large number of distinct polycyclic radicals, many of them with multiple resonance forms.[3] Also, the properties of these fused-

ring species and transition states are not as systematic as the acyclic and monocyclic molecules, leading to larger errors in estimates of thermochemistry and reaction rates.

To try to fill in the gaps in existing knowledge, my group has directly measured several different ring-forming reactions [18-20], and resolved an important discrepancy about the formation of 3-ring PAH from naphthalene [18,21]. We have also computed many rate and thermochemical parameters using quantum chemistry[1,13,21] and developed improved estimators [11,14,24,25], allowing us to create accurate detailed kinetic models for formation of 2- and 3-ring PAH.[21,26-28]

B. Tracking isotopes, correcting symmetry factors in TST calculations

RMG can now very reliably predict the relative yields of isotopomers in the reaction products, or vice-versa infer the original site-specific isotope enrichment from those measured in the final products.[23] This avoids the need to synthesize authentic standards of specific isotopomers. In the course of this work we discovered a factor of 2 error in published formulae for TST k's for X+X reactions. This small absolute error is often much larger than the small differences in reactivity of different isotopomers, so it is crucial to get it right. We have carefully explained the issue in recent papers.[6,7]

C. Improvements to the Overall Mechanism Construction Process

We have developed an improved overall workflow, where we iterate between adding additional reactions to the mechanism (e.g. using the RMG software package) and improving the values of uncertain rate and thermo parmeters in the existing model (e.g. by automatically spawning quantum chemistry calculations and using the results to improve thermo estimates [1,22]). Adding reactions reduces the mechanism truncation error [4], i.e. it improves the structure of the model, while the second step reduces the error in the model parameters. We recently published a Perspective [10] discussing the overall kinetic model construction procedure at a high level, and a book chapter giving more technical detail.[4]

We are collaborating with Stephen Klippenstein and Judit Zador to automate the whole process of building a kinetic model including all the needed quantum chemistry calculations. We have made advances in speeding these calculations [5,31] and in quantifying the uncertainties in the final kinetic model predictions, accounting for the often highly-correlated errors in the parameters.[8] Many of the advances reported here have been incorporated into the open-source RMG software as version 3.0 [11]. The individual rate and thermochemical parameter estimates are also available in human-friendly form on our popular (~1,000 unique visitors per month) website (rmg.mit.edu).

D. Fast methods for estimating TS geometries and Reaction Barriers.

A key challenge for this field has been the difficulty of computing reaction rates, largely due to the difficulty of (i) identifying which reactions have low enough barriers that they are worth computing and (ii) providing a good enough guess at the transition state geometry so that the computation will converge. We would like to automate the steps, to allow us to build models with thousands of reactions and also to make it practical for non-experts to make good kinetic models for their systems of interest. We developed a machine learning model to provide high quality initial guess geometries for transition states [24], and very recently we computed the transition states of more than 10,000 reactions at high level (CCSD(T)) [13]. For many reactions the CCSD(T) and DFT barrier heights agree within 5 kcal/mole as one might expect, but for hundreds of the reactions the two methods give barriers that differ by more than 10 kcal/mole, and some by more than 20 kcal/mole. We are investigating the origin of these big discrepancies. We trained a Machine Learning model using the CCSD(T) barriers, providing a fast estimate of Ea that is apparently more reliably accurate than a DFT calculation.[14]

III. Future Plans

Upgrading Estimators and Automating Quantum Chemistry. As discussed above, we have recently developed much better ways to estimate reaction barriers, thermochemistry, solvent effects, etc., and ways to automatically spawn quantum chemistry calculations to improve the numerical values. These

improved values significantly change the kinetic model predictions compared with models made using Benson-type functional group estimates. We are using Machine Learning techniques to create fast estimators that emulate the slow quantum chemistry, with confidence intervals. Next step is to integrate all this into RMG to make it possible to rapidly and automatically improve the kinetic models as they are being constructed. It appears it may be possible to predict kinetics in solvents and in mixed gas-liquid systems about as well as we can predict it in gas phase; if true this would greatly increase the impact of this line of research.

Benzyne-driven formation of polycyclics. We hypothesize benzyne-mediated pathways explain several of the unexpected products observed in pyrolysis experiments.[29] We are currently experimentally studying the chemically-activated reaction of ortho-benzyne (C_6H_4) with benzene to form naphthalene: $C_6H_4 + C_6H_6 \rightarrow C_{10}H_8 + C_2H_2$. Comandini and Brezinsky [30] computed that this reaction would be fast in the combustion-relevant T,P range, but no one has studied it directly, and it is not included in existing soot-formation models. In our initial flash photolysis VUV PIMS experiments, we observe a strong m/z=128 ($C_{10}H_8$) signal, suggesting this reaction does indeed run as predicted by Comandini and Brezinsky. We also see m/z=142 ($C_{11}H_{10}$), probably methylnaphthalene, from the analogous reaction of benzyne with toluene. After measuring the rate coefficient, we will include this reaction family in RMG so it will automatically be included in future kinetic models.

Publications and submitted journal articles supported by DOE BES 2019-2022

1. M. Keceli et al. Automated Computational Thermochemistry for Butane Oxidation: A Prelude to Predictive Automated Combustion Kinetics. *Proc. Combust. Inst.* **37**, 363-371 (2019).
2. A. Grinberg Dana et al. Large Intermediates in Hydrazine Decomposition: A Theoretical Study of the N_3H_5 and N_4H_6 Potential Energy Surfaces. *J. Phys. Chem. A* **123**, 4679-4692 (2019).
3. A. Grinberg Dana, M.Liu, W.H. Green. Automated Chemical Resonance Generation and Structure Filtration for Kinetic Modeling. *Int. J. Chem. Kinet.* **51**, 760–776 (2019).
4. W.H. Green. Automatic Generation of Reaction Mechanisms. *Computer-Aided Chemical Engineering* **45**, 259-294 (2019).
5. A. Jocher *et al.* Scalability strategies for automated reaction mechanism generation. *Computers & Chemical Engineering* **131**, 106578 (2019).
6. M.J. Goldman, S. Ono, W.H. Green. Accepted method for computing X+X rates is incorrect, causes large errors in isotope analysis. *J. Phys. Chem. A* **123,** 2320–2324 (2019).
7. M.J. Goldman, S. Ono, W.H. Green. Addition to 'Accepted method for computing X+X rates is incorrect, causes large errors in isotope analysis'. *J. Phys. Chem. A* **124,** 257 (2020).
8. C.W. Gao, M. Liu, W.H. Green. Uncertainty Analysis of Correlated Parameters in Automated Reaction Mechanism Generation. *Int. J. Chem. Kinet.* **52**, 266-282 (2020).
9. R.J. Gillis, W.H. Green. Thermochemistry Prediction and Automatic Mechanism Generation for Oxygenated Sulfur Systems: A Case Study of Dimethyl Sulfide Oxidation. *ChemSystemsChem* **2**, e1900051 (2020). http://dx.doi.org/10.1002/syst.201900051
10. W.H. Green. Moving from Postdictive to Predictive Kinetics in Reaction Engineering. *AIChE J.* **66**, e17059 (2020). https://doi.org/10.1002/aic.17059
11. M. Liu, *et al.* RMG 3.0: Advances in Automatic Mechanism Generation. *J. Chem. Inf. Model* **61**, 2686-26969 (2021). https://doi.org/10.1021/acs.jcim.0c01480
12. M. S. Johnson, W.H. Green. Examining the Accuracy of Methods for Obtaining Pressure Dependent Rate Coefficients. *Faraday Discussions* (2022). https://doi.org/10.1039/D2FD00040G
13. K. Spiekermann, L. Pattanaik, W.H. Green. High Accuracy Barrier Heights, Enthalpies, and Rate Coefficients for Chemical Reactions. *Scientific Data* (submitted).
14. K. Spiekermann, L. Pattanaik, W.H. Green. Fast Predictions of Reaction Barrier Heights: Towards Coupled-Cluster Accuracy. *J. Phys. Chem. A* (submitted).

Other Literature Cited

15. G. Scalia, C.M. Grambow, B.Pernici, Y.-P. Li, W.H. Green. Evaluating Scalable Uncertainty Estimation Methods for DNN-Based Molecular Property Prediction. *J. Chem. Inf. Model.* **60**, 2697–2717 (2020).
16. Y. Chung *et al.* Group Contribution and Machine Learning Approaches to Predict Abraham Solute Parameters, Solvation Free Energy, and Solvation Enthalpy. *J. Chem. Inf. Model.* **62**, 433-446 (2022).
17. Y. Liu, C.J. McGill, W.H. Green, P. Deshlara. Effects of Surface Species and Homogeneous Reactions on Rates and Selectivity in Ethane Oxidation on Oxide Catalysts. *AIChE J.* **67,** e17483 (2021).
18. J. Yang, M.C. Smith, M.B. Prendergast, T.-C. Chu, W.H. Green. $C_{14}H_{10}$ Polycyclic Aromatic Hydrocarbons Formation by Acetylene Addition to Naphthalenyl Radicals Observed. *Physical Chemistry Chemical Physics* **23**, 14325-14339 (2021).
19. M.C. Smith *et al.* Direct Measurement of Radical-Catalyzed C_6H_6 Formation from Acetylene. *J. Phys. Chem. A* **124**, 2871-2884 (2020).
20. T.-C. Chu *et al.* From Benzene to Naphthalene, Direct Measurement of Reactions and Intermediates of Phenyl Radical and Acetylene. *Physical Chemistry Chemical Physics* **21**, 22248 (2019).
21. Te-Chun Chu *et al.* Theoretical Study on the HACA Chemistry of Naphthalenyl Radicals and Acetylene: the formation of $C_{12}H_8$, $C_{14}H_8$, and $C_{14}H_{10}$ species. *Int. J. Chem. Kinet.* **52**, 752 (2020).
22. G. Pio, X. Dong, E. Bolzano, W.H. Green. Automatically Generated Model for Light Alkene Combustion. *Combustion & Flame* **241,** 112080 (2022).
23. M.J. Goldman *et al.* Computer Generated Isotope Model Achieves Experiment-Level Accuracy of Fidelity for Position-Specific Isotope Analysis. *Chem. Geo.* **514**, 1-9 (2019).
24. Lagnajit Pattanaik, John B. Ingraham, Colin A. Grambow, William H. Green. Generating Transition States with Deep Learning. *Phys. Chem. Chem. Phys.* **22**, 23618-23626 (2020).
25. C.M. Grambow, Y.-P. Li, W. H. Green. Accurate Thermochemistry with Small Datasets: A Bond Additivity Correction and Transfer Learning Approach. *J. Phys. Chem. A* **123**, 5826 (2019).
26. T.-C. Chu et al. Modeling of aromatics formation in fuel-rich methane oxy-combustion with an automatically generated pressure-dependent mechanism. *Phys. Chem. Chem. Phys.* **21**, 813 (2019).
27. L. Lai, H.-W. Pang, W.H. Green. Formation of Two-Ring Aromatics in Hexylbenzene Pyrolysis. *Energy & Fuels* **34**, 1365-1377 (2020).
28. M. Liu et al. Predicting polycyclic aromatic hydrocarbon formation with an automatically generated mechanism for acetylene pyrolysis. *Int. J. Chem. Kinet.* **53**, 27-42 (2021).
29. B. Shukla, A. Susa, A. Miyoshi, M. Koshi. Role of phenyl radicals in the growth of polycyclic aromatic hydrocarbons. *J. Phys. Chem. A*, 112:2362–2369 (2008).
30. A. Comandini, K. Brezinsky. Theoretical study of the formation of naphthalene from the radical/π-bond addition between single-ring aromatic hydrocarbons. *J. Phys. Chem. A* **115,** 5547–5559 (2011).
31. F.H. Vermeire *et al.* Detailed Kinetic Modeling for the Pyrolysis of a Jet A Surrogate. *Energy & Fuels* **36**, 1304–1315 (2022).
32. M.J. Goldman, W.H. Green, J.H. Kroll. Chemistry of simple organic peroxy radicals under atmospheric through combustion conditions: Role of temperature, pressure, and NOx level. *J. Phys. Chem. A* **125***,* 10303 -10314 (2021).
33. V.P. Barber, W.H. Green, J.H. Kroll. Screening for New Pathways in Atmospheric Oxidation Chemistry with Automated Mechanism Generation, *J.Phys. Chem. A* **125**, 6772-6788 (2021).
34. E. Heid, W.H. Green. Machine learning of reaction properties via learned representations of the condensed graph of reaction (CGR). *J. Chem. Inf. Model.* (accepted). https://doi.org/10.1021/acs.jcim.1c00975

Nonadiabatic Photochemistry

DE-SC0015997

Hua Guo[1], Donald G. Truhlar,[2] and David R. Yarkony[3]

[1]*Department of Chemistry and Chemical Biology, University of New Mexico, Albuquerque, New Mexico 87131.*[2]*Department of Chemistry, University of Minnesota, Minneapolis, Minnesota 55455.* [3]*Department of Chemistry, Johns Hopkins University, Baltimore, Maryland 21218*

e-mail: hguo@unm.edu; truhlar@umn.edu; yarkony@jhu.edu

PROGRAM SCOPE

This project involves the development and application of methods for treating electronically nonadiabatic processes both with fitted diabatic potential energy matrices (DPEMs) and by direct dynamics in the adiabatic representation. The project includes both electronic structure theory and dynamics, and the dynamics involves both fully quantal and semiclassical theoretical method development and calculations.

PROGRESS IN THE LAST YEAR

Hua Guo

Fitting of diabatic potential energy matrices. In collaboration with Yarkony, we have explored various machine learning approaches to constructing high accuracy diabatic potential energy matrices and property matrices for H_2CO.[1] These global analytical expressions open the door to accurate dynamics calculations of both internal conversion and intersystem crossing, as well as spectroscopy.[2] In addition, a definitive review of the advances in this direction by Guo and Yarkony was recently published.[3]

Nonadiabatic photodissociation of HCO. HCO has provided a proving ground for understanding the nonadiabatic Renner-Teller coupling and its impact on the dynamics. In collaboration with Zhang at UC Riverside and Dawes at MUST, we have recently investigated the photodissociation of HCO in the first band using full-dimensional PESs.[4] Our results indicated strong modulation of the parent rotational angular momentum.

Nonadiabatic collision dynamics. The quenching of OH(A) by H_2 is a prototypic nonadiabatic process, facilitated by two conical intersection (CI) seams among three electronic states. In collaboration with Yarkony, we have recently elucidated the nonadiabatic dynamics using a full-dimensional quantum method on an accurate DPEM.[5] We found that the adiabatic channel dominates, while the reactive and non-reactive quenching channels have roughly the same branching ratios. The large adiabatic channel is attributed to stereodynamics, in which the OH-H_2 approach has no access to the CI seams, which is located in the HO-H_2 orientation. The quantum dynamics results are reconciled with available experimental data, which led to new understanding of this reaction. More recently, we have collaborated with Truhlar and carried out semiclassical surface hopping calculations on an improved DPEM from his group and the results are consistent with those obtained using the Yarkony DPEM.[6]

We have devised a wave packet based method for cold nonadiabatic reactions and applied it to the Li + HF reaction.[7]

With our collaborators, we have been continuing our investigations of dynamics of bimolecular scattering and reactions. These studies include the ring-polymer molecular dynamics determination of the rate coefficient for the H + O_3 reaction[8] and its dynamics leading to the OH vibrational population inversion,[9] the mode specificity of the Cl + C_2H_6 reaction,[10]

In addition, we have collaborated with Truhlar to construct lowest doublet, quartet, and sextet PESs for the NO + O ⇔ N + O_2 system.[11]

Donald G. Truhlar

We developed a way to include invariance of the adiabatic potential energy surfaces to permutation of identical nuclei as a restraint in the direct diabatization by neural network (DDNN) method.[12]

We showed that decoherence changes the nature of the intersystem crossing dynamics in thioformaldehyde not just quantitatively but qualitatively.[13]

We developed the methods of curvature-driven trajectory surface hopping and curvature-driven coherent switching with decay of mixing that allow one to calculate electronically nonadiabatic direct dynamics without evaluating either wave function overlaps or nonadiabatic coupling vectors (NACs).[14] This may be used to speed up calculations as compared to using electronic structure NACs. Such speedup may enable longer-time trajectories and/or better ensemble averaging. Even more promising is that curvature-driven couplings can be used for direct dynamics calculations of electronically nonadiabatic processes with electronic structure methods for which NACs or time derivatives are not available.

We wrote a comprehensive perspective on diabatic states (326 references).[15]

With Guo, we compared new OH* + H_2 dynamics calculations with an improved DPEM to earlier OH* + H_2 calculations published jointly by Guo and Yarkony.[5] The various theoretical results all agree that nonreactive quenching dominates reactive quenching.[6]

David R. Yarkony

Inclusion of Degenerate irreducible representations in NN-Surfgen. Incorporation of CNPI degeneracy can greatly reduce the effort required to fit a DPEM. However since we do least squares fitting [using DoE funded NN-Surfgen], using a complete set of permutationally equivalent data does not guarantee a DPEM with that symmetry. One way to incorporate the correct symmetry is to use standard point group symmetry tools to build a skeletal DPEM. Then replace what would normally be a constant coefficient, with the output of a NN, built from permutationally invariant polynomials (PIP)s. We have applied this idea to the benchmark system H_3^+, whose lowest three states carry A_1 and E irreducible representations, obtaining a good fit. But the real challenge is H_3O, which we will address.

Spin-Orbit Interaction in NN-Surfgen. Spin conserving (internal conversion) and spin non-conserving (intersystem crossing) are two classes of competing nonadiabatic processes. The introduction of NN representations of DPEMs based on fit-and-diabatize (FaD) algorithms made it clear that NNs could be used to include any smooth function, including the spin-orbit interaction, in those same DPEMs. This would allow internal conversion and intersystem crossing to "compete" evenhandedly, with ALL relevant quantities fit by NNs. This approach, along with other aspects of FaD, is reviewed recently by us.[3] Below we sketch the procedures some of which were developed with NSF funding, that enable the capability.

The derivative coupling operator is independent of electron spin. Therefore functions with different values of the total electron spin angular momentum quantum number *S* (for all geometries) are diabatic, hence spin-diabatic. In order to treat intersystem crossing, we add the spin-orbit interaction H^{so} in the Breit-Pauli approximation to the nonrelativistic Hamiltonian H^0 (giving $H=H^0+H^{so}$) and work in a diabatized spin-diabatic basis with the diabatization determined by the relevant DPEMs. The relevant DPEMs, one for each value of *S*, are the standard diabats derived from H^0 which is singular in the adiabatic representation at conical

intersections. However, all quantities are smooth in the diabatized spin-diabatic representation and so can be fit by NNs using NN-Surfgen/H^{so}. Yarkony has incorporated this novel technology into his formaldehyde DPEM.[1] He is extending that work to treat thioformaldehyde, which has been treated by Truhlar using on the fly techniques providing an opportunity for comparison.

FUTURE PLANS

Hua Guo

We will be focusing on the nonadiabatic dynamics for the OH(A) + H_2 reaction, which includes the reactive and nonreactive quenching channels, using the newly developed DPEMs from both the Yarkony and Truhlar groups. We will use semiclassical methods to describe the nonadiabatic dynamics in the reactive quenching channel, with product state resolution. The comparison of the two DPEMs will shed light on the differences in the electronic structure methods and fitting algorithms. We plan to further investigate the nonadiabatic predissociation of the H_2-HO(A) complex in the entrance channel and determine the energies and lifetimes. The mode specificity of the predissociation lifetimes sheds insight into the effect of the conical intersection on nonadiabatic transitions.

In addition, we will explore the internal conversion and intersystem crossing in H_2CO. This is an interesting system because of the two possible nonadiabatic routes, via internal conversion to the S_0 state and intersystem crossing to the T_1 state. The calculated energies and lifetimes can be compared with a large set of experimental data. These nonadiabatic processes are also at the center of the roaming dynamics on the S_0 state. An accurate DPEM including all three electronic states has been developed by Yarkony.[1]

Finally, we plan to implement the multi-configuration time-dependent Hartree (MCTDH) approach to high-dimensional nonadiabatic photodissociation dynamics, using the DPEMs developed by the Truhlar and Yarkony groups. This is necessary because of the limitations of grid-based methods which scales exponentially with the size. We hope to address first the 6-dimensional ammonia photodissociation and 9-dimensional photodissociation of hydroxymethyl radical. The key difficulty is the re-expression of the DPEM in the sum-of-product form, with proper CNPI symmetry.

Donald G. Truhlar

We will combine the recently developed compressed multi-state pair-density functional theory with curvature-driven coherent switching with decay of mixing to study several systems more efficiently than was possible with previously available methods. Systems under current study include photoisomerization of ethylene and 1,3-cyclohexadiene, photodissociation of methyl radical, *o*-fluorothiophenol, bromoacetyl chloride, and CH_2ClBr, and two-spin-state reactivity of $FeO^+ + H_2 \rightarrow Fe^+ + H_2O$.

David R. Yarkony

Branching fractions are a parameter used to quantify nonadiabatic reactions. They are challenging to calculate but reveal much about the nonadiabatic process. We will determine the branching fractions for CH_2OH, CH_3NH_2 and the particularly challenging collisional quenching $OH(A^2\Sigma^+) + H_2 \rightarrow OH(X^2\Pi) + H_2$; H_2O + H, whose DPEM as noted above is scheduled to be refit. Yarkony will work with Guo and Truhlar on branching fractions for these nonadiabatic processes.

As part of a planned research effort to juxtapose internal conversion and intersystem crossing, Yarkony will use NN-Surfgen/H^{so} to treat thioformaldehyde a benchmark system already studied by Truhlar.

CITED PUBLICATIONS

(1) Guan, Y.; Xie, C.; Guo, H.; Yarkony, D. R. Enabling a unified description of both internal conversion and intersystem crossing in formaldehyde: A global coupled quasi-diabatic Hamiltonian for its S_0, S_1, and T_1 states. *J. Chem. Theo. Comput.* **2021**, *17*, 4157-4168.

(2) Xie, C.; Guan, Y.; Yarkony, D. R.; Guo, H. Vibrational energy levels of the S_0 and S_1 states of formaldehyde using an accurate ab initio based global diabatic potential energy matrix. *Mole. Phys.* **2021**, *119*, e1918775.

(3) Guan, Y.; Xie, C.; Yarkony, D. R.; Guo, H. High-fidelity first principles nonadiabaticity: Diabatization, analytic representation of global diabatic potential energy matrices, and quantum dynamics. *Phys. Chem. Chem. Phys.* **2021**, *23*, 24962-24983.

(4) Han, S.; Sun, G.; Zheng, X.; Song, Y.; Dawes, R.; Xie, D.; Zhang, J.; Guo, H. Rotational modulation of $\tilde{A}^2A''$ -state photodissociation of HCO via Renner–Teller nonadiabatic transitions. *J. Phys. Chem. Lett.* **2021**, *12*, 6582-6588.

(5) Zhao, B.; Han, S.; Malbon, C. L.; Manthe, U.; Yarkony, D. R.; Guo, H. Full-dimensional quantum stereodynamics of the non-adiabatic quenching of $OH(A^2\Sigma^+)$ by H_2. *Nat. Chem.* **2021**, *13*, 909-915.

(6) Han, S.; de Oliveira-Filho, A. G. S.; Shu, Y.; Truhlar, D. G.; Guo, H. Semiclassical trajectory studies of reactive and nonreactive scattering of $OH(A\ ^2\Sigma^+)$ by H_2 based on an improved full-dimensional ab initio diabatic potential energy matrix. *ChemPhysChem* **2022**, *n/a*, e202200039.

(7) Buren, B.; Chen, M.; Sun, Z.; Guo, H. Quantum wave packet treatment of cold nonadiabatic reactive scattering at the state-to-state level. *J. Phys. Chem. A* **2021**, *125*, 10111-10120.

(8) Chen, Q.; Hu, X.; Guo, H.; Xie, D. Theoretical H + O_3 rate coefficients from ring polymer molecular dynamics on an accurate global potential energy surface: assessing experimental uncertainties. *Phys. Chem. Chem. Phys.* **2021**, *23*, 3300-3310.

(9) Chen, Q.; Hu, X.; Guo, H.; Xie, D. Insights into the formation of hydroxyl radicals with nonthermal vibrational excitation in the Meinel airglow. *J. Phys. Chem. Lett.* **2021**, *12*, 1822-1828.

(10) Papp, D.; Li, J.; Guo, H.; Czakó, G. Vibrational mode-specificity in the dynamics of the Cl + $C_2H_6 \rightarrow$ HCl + C_2H_5 reaction. *J. Chem. Phys.* **2021**, *155*, 114303.

(11) Varga, Z.; Liu, Y.; Li, J.; Paukku, Y.; Guo, H.; Truhlar, D. G. Potential energy surfaces for high-energy N + O_2 collisions. *J. Chem. Phys.* **2021**, *154*, 084304.

(12) Shu, Y.; Varga, Z.; Sampaio de Oliveira-Filho, A. G.; Truhlar, D. G. Permutationally restrained diabatization by machine intelligence. *J. Chem. Theo. Comput.* **2021**, *17*, 1106-1116.

(13) Zhang, L.; Shu, Y.; Sun, S.; Truhlar, D. G. Direct coherent switching with decay of mixing for intersystem crossing dynamics of thioformaldehyde: The effect of decoherence. *J. Chem. Phys.* **2021**, *154*, 094310.

(14) Shu, Y.; Zhang, L.; Chen, X.; Sun, S.; Huang, Y.; Truhlar, D. G. Nonadiabatic dynamics algorithms with only potential energies and gradients: Curvature-driven coherent switching with decay of mixing and curvature-driven trajectory surface hopping. *J. Chem. Theo. Comput.* **2022**, *18*, 1320-1328.

(15) Shu, Y.; Varga, Z.; Kanchanakungwankul, S.; Zhang, L.; Truhlar, D. G. Diabatic states of molecules. *J. Phys. Chem. A* **2022**, *126*, 992–1018.

Publications 2019-2022

(1) Xie, C.; Malbon, C. L.; Guo, H.; Yarkony, D. R. Up to a sign. The insidious effects of energetically inaccessible conical intersections on unimolecular reactions. *Acc. Chem. Res.* **2019**, *52*, 501-509.

(2) Yarkony, D. R.; Xie, C.; Zhu, X.; Wang, Y.; Malbon, C. L.; Guo, H. Diabatic and adiabatic representations: Electronic structure caveats. *Comput. Theo. Chem.* **2019**, *1152*, 41-52.

(3) Han, S.; Zheng, X.; Ndengué, S.; Song, Y.; Dawes, R.; Xie, D.; Zhang, J.; Guo, H. Dynamical interference in the vibronic bond breaking reaction of HCO. *Sci. Adv.* **2019**, *5*, eaau0582.

(4) An, F.; Han, S.; Hu, X.; Xie, D.; Guo, H. First-principles dynamics of collisional intersystem crossing: resonance enhanced quenching of C(^{1}D) by N_2. *Phys. Chem. Chem. Phys.* **2019**, *21*, 8645-8653.

(5) Lu, D.-d.; Xie, C.-j.; Li, J.; Guo, H. Rate coefficients and branching ratio for multi-channel hydrogen abstractions from CH_3OH by F. *Chin. J. Chem. Phys.* **2019**, *32*, 84-88.

(6) Lu, D.; Li, J.; Guo, H. Stereodynamical control of product branching in multi-channel barrierless hydrogen abstraction of CH_3OH by F. *Chem. Sci.* **2019**, *10*, 7994-8001.

(7) Xie, C.; Malbon, C. L.; Xie, D.; Yarkony, D. R.; Guo, H. Nonadiabatic dynamics in photodissociation of hydroxymethyl in the $3^2A(3p_x)$ Rydberg state: A nine-dimensional quantum study. *J. Phys. Chem. A* **2019**, *123*, 1937-1944.

(8) Guan, Y.; Guo, H.; Yarkony, D. R. Neural network based quasi-diabatic Hamiltonians with symmetry adaptation and a correct description of conical intersections. *J. Chem. Phys.* **2019**, *150*, 214101.

(9) Guan, Y.; Zhang, D. H.; Guo, H.; Yarkony, D. R. Representation of coupled adiabatic potential energy surfaces using neural network based quasi-diabatic Hamiltonians: 1,2 $^2A'$ states of LiFH. *Phys. Chem. Chem. Phys.* **2019**, *21*, 14205-14213.

(10) Wang, Y.; Xie, C.; Guo, H.; Yarkony, D. R. A quasi-diabatic representation of the 1,2^{1}A states of methylamine. *J. Phys. Chem. A* **2019**, *123*, 5231-5241.

(11) Zuo, J.; Chen, Q.; Hu, X.; Guo, H.; Xie, D. Dissection of the multichannel reaction of acetylene with atomic oxygen: from the global potential energy surface to rate coefficients and branching dynamics. *Phys. Chem. Chem. Phys.* **2019**, *21*, 1408-1416.

(12) Chang, J.; Guo, L.; Wang, R.; Mou, J.; Ren, H.; Ma, J.; Guo, H. Absorption spectra of acetylene, vinylidene, and their deuterated isotopologues on ab initio potential energy and dipole moment surfaces. *J. Phys. Chem. A* **2019**, *123*, 4232-4240.

(13) Amarasinghe, C.; Li, H.; Perera, C. A.; Besemer, M.; van der Avoird, A.; Groenenboom, G. C.; Xie, C.; Guo, H.; Suits, A. G. Differential cross sections for state-to-state collisions of NO(v = 10) in near-copropagating beams. *J. Phys. Chem. Lett.* **2019**, *10*, 2422-2427.

(14) Hu, X.; Zuo, J.; Xie, C.; Dawes, R.; Guo, H.; Xie, D. An ab initio based full-dimensional potential energy surface for OH + O_2 ⇄ HO_3 and low-lying vibrational levels of HO_3. *Phys. Chem. Chem. Phys.* **2019**, *21*, 13766-13775.

(15) Long, B.; Bao, J. L.; Truhlar, D. G. Kinetics of the strongly correlated CH_3O + O_2 reaction: The importance of quadruple excitations in atmospheric and combustion chemistry. *J. Am. Chem. Soc.* **2019**, *141*, 611-617.

(16) Zhang, R. M.; Truhlar, D. G.; Xu, X. Kinetics of the toluene reaction with OH radical. *Research* **2019**, *2019*, 19.

(17) Long, B.; Bao, J. L.; Truhlar, D. G. Rapid unimolecular reaction of stabilized Criegee intermediates and implications for atmospheric chemistry. *Nat. Commun.* **2019**, *10*, 2003.

(18) Truhlar, D. G.; Hiberty, P. C.; Shaik, S.; Gordon, M. S.; Danovich, D. Orbitals and the Interpretation of Photoelectron Spectroscopy and (e,2e) Ionization Experiments. *Angew. Chem. Int. Ed.* **2019**, *58*, 12332-12338.
(19) Shu, Y.; Kryven, J.; Sampaio de Oliveira-Filho, A. G.; Zhang, L.; Song, G.-L.; Li, S. L.; Meana-Pañeda, R.; Fu, B.; Bowman, J. M.; Truhlar, D. G. Direct diabatization and analytic representation of coupled potential energy surfaces and couplings for the reactive quenching of the excited $^2\Sigma^+$ state of OH by molecular hydrogen. *J. Chem. Phys.* **2019**, *151*, 104311.
(20) Zhang, L.; Truhlar, D. G.; Sun, S. Full-dimensional three-state potential energy surfaces and state couplings for photodissociation of thiophenol. *J. Chem. Phys.* **2019**, *151*, 154306.
(21) Xing, L.; Wang, Z.; Truhlar, D. G. Multistructural anharmonicity controls the radical generation process in biofuel combustion. *J. Am. Chem. Soc.* **2019**, *141*, 18531-18543.
(22) Zhang, L.; Truhlar, D. G.; Sun, S. Association of Cl with C_2H_2 by unified variable-reaction-coordinate and reaction-path variational transition-state theory. *Proc. Natl. Acad. Sci. U. S. A.* **2020**, *117*, 5610-5616.
(23) Xie, C.; Zhao, B.; Malbon, C. L.; Yarkony, D. R.; Xie, D.; Guo, H. Insights into the mechanism of nonadiabatic photodissociation from product vibrational distributions. The remarkable case of phenol. *J. Phys. Chem. Lett.* **2020**, *11*, 191-198.
(24) Malbon, C. L.; Zhao, B.; Guo, H.; Yarkony, D. R. On the nonadiabatic collisional quenching of OH(A) by H_2: a four coupled quasi-diabatic state description. *Phys. Chem. Chem. Phys.* **2020**, *22*, 13516-13527.
(25) Guan, Y.; Xie, C.; Guo, H.; Yarkony, D. R. Neural network based quasi-diabatic representation for S_0 and S_1 states of formaldehyde. *J. Phys. Chem. A* **2020**, *124*, 10132-10142.
(26) Han, S.; Gunthardt, C. E.; Dawes, R.; Xie, D.; North, S. W.; Guo, H. Origin of the "odd" behavior in the ultraviolet photochemistry of ozone. *Proc. Natl. Acad. Sci. U. S. A.* **2020**, *117*, 21065-21069.
(27) Han, S.; Wang, Y.; Guan, Y.; Yarkony, D. R.; Guo, H. Impact of diabolical singular points on nonadiabatic dynamics and a remedy: Photodissociation of ammonia in the first band. *J. Chem. Theo. Comput.* **2020**, *16*, 6776–6784.
(28) Guan, Y.; Guo, H.; Yarkony, D. R. Extending the representation of multistate coupled potential energy surfaces to include properties operators using neural networks: Application to the 1,2^{1}A states of ammonia. *J. Chem. Theo. Comput.* **2020**, *16*, 302-313.
(29) An, F.; Chen, J.; Hu, X.; Guo, H.; Xie, D. Nonadiabatic electronic energy transfer in the chemical oxygen–iodine laser: Powered by derivative coupling or spin–orbit coupling? *J. Phys. Chem. Lett.* **2020**, *11*, 4768-4773.
(30) Liu, Y.; Song, H.; Xie, D.; Li, J.; Guo, H. Mode specificity in the OH + $HO_2 \rightarrow H_2O + O_2$ reaction: Enhancement of reactivity by exciting a spectator mode. *J. Am. Chem. Soc.* **2020**, *142*, 3331-3335.
(31) Zuo, J.; Chen, Q.; Hu, X.; Guo, H.; Xie, D. Theoretical investigations of rate coefficients for H + O_3 and HO_2 + O reactions on a full-dimensional potential energy surface. *J. Phys. Chem. A* **2020**, *124*, 6427-6437.
(32) Li, J.; Varga, Z.; Truhlar, D. G.; Guo, H. Many-body permutationally invariant polynomial neural network potential energy surface for N_4. *J. Chem. Theo. Comput.* **2020**, *16*, 4822-4832.
(33) Lu, D.; Li, J.; Guo, H. Comprehensive dynamical investigations on the Cl + $CH_3OH \rightarrow$ HCl + CH_3O/CH_2OH reaction: Validation of experiment and dynamical insights. *CCS Chem.* **2020**, *2*, 882-894.

(34) Jiang, B.; Li, J.; Guo, H. High-fidelity potential energy surfaces for gas phase and gas-surface scattering processes from machine learning. *J. Phys. Chem. Lett.* **2020**, *11*, 5120-5131.
(35) Li, J.; Zhao, B.; Xie, D.; Guo, H. Advances and new challenges to bimolecular reaction dynamics theory. *J. Phys. Chem. Lett.* **2020**, *11*, 8844-8860.
(36) Wu, J.; Gao, L. G.; Ning, H.; Ren, W.; Truhlar, D. G. Direct dynamics of a large complex hydrocarbon reaction system: The reaction of OH with exo-tricyclodecane (the main component of Jet Propellant-10). *Combus. Flame* **2020**, *216*, 82-91.
(37) Wu, J.; Gao, L. G.; Ren, W.; Truhlar, D. G. Anharmonic kinetics of the cyclopentane reaction with hydroxyl radical. *Chem. Sci.* **2020**, *11*, 2511-2523.
(38) Shu, Y.; Zhang, L.; Varga, Z.; Parker, K. A.; Kanchanakungwankul, S.; Sun, S.; Truhlar, D. G. Conservation of angular momentum in direct nonadiabatic dynamics. *J. Phys. Chem. Lett.* **2020**, *11*, 1135-1140.
(39) Wu, J.; Gao, L. G.; Varga, Z.; Xu, X.; Ren, W.; Truhlar, D. G. Water catalysis of the reaction of methanol with OH radical in the atmosphere is negligible. *Angew. Chem. Int. Ed.* **2020**, *59*, 10826-10830.
(40) Shu, Y.; Zhang, L.; Mai, S.; Sun, S.; González, L.; Truhlar, D. G. Implementation of coherent switching with decay of mixing into the SHARC program. *J. Chem. Theo. Comput.* **2020**, *16*, 3464-3475.
(41) Shu, Y.; Zhang, L.; Sun, S.; Truhlar, D. G. Time-derivative couplings for self-consistent electronically nonadiabatic dynamics. *J. Chem. Theo. Comput.* **2020**, *16*, 4098-4106.
(42) Ferro-Costas, D.; Truhlar, D. G.; Fernández-Ramos, A. Pilgrim: A thermal rate constant calculator and a chemical kinetics simulator. *Comput. Phys. Commun.* **2020**, *256*, 107457.
(43) Parker, K. A.; Truhlar, D. G. Semiglobal diabatic potential energy matrix for the N–H photodissociation of methylamine. *J. Chem. Phys.* **2020**, *152*, 244309.
(44) Zhang, R. M.; Xu, X.; Truhlar, D. G. Low-pressure limit of competitive unimolecular reactions. *J. Am. Chem. Soc.* **2020**, *142*, 16064-16071.
(45) Shu, Y.; Truhlar, D. G. Diabatization by machine intelligence. *J. Chem. Theo. Comput.* **2020**, *16*, 6456-6464.
(46) Truhlar, D. G. Semiclassical Multidimensional Tunneling Calculations. In *Tunnelling in Molecules: Nuclear Quantum Effects from Bio to Physical Chemistry*, Kaestner, J., Kozuch, S. Eds.; RSC Publishing, 2021; pp 261-282.
(47) Shu, Y.; Varga, Z.; Sampaio de Oliveira-Filho, A. G.; Truhlar, D. G. Permutationally restrained diabatization by machine intelligence. *J. Chem. Theo. Comput.* **2021**, *17*, 1106-1116.
(48) Varga, Z.; Liu, Y.; Li, J.; Paukku, Y.; Guo, H.; Truhlar, D. G. Potential energy surfaces for high-energy N + O_2 collisions. *J. Chem. Phys.* **2021**, *154*, 084304.
(49) Zhang, L.; Shu, Y.; Sun, S.; Truhlar, D. G. Direct coherent switching with decay of mixing for intersystem crossing dynamics of thioformaldehyde: The effect of decoherence. *J. Chem. Phys.* **2021**, *154*, 094310.
(50) Gao, L. G.; Fleming, D. G.; Truhlar, D. G.; Xu, X. Large anharmonic effects on tunneling and kinetics: Reaction of propane with muonium. *J. Phys. Chem. Lett.* **2021**, *12*, 4154-4159.
(51) Long, B.; Wang, Y.; Xia, Y.; He, X.; Bao, J. L.; Truhlar, D. G. Atmospheric kinetics: Bimolecular reactions of carbonyl oxide by a triple-level strategy. *J. Am. Chem. Soc.* **2021**, *143*, 8402-8413.

(52) Zhang, R. M.; Xu, X.; Truhlar, D. G. Energy dependence of ensemble-averaged energy transfer moments and its effect on competing decomposition reactions. *J. Phys. Chem. A* **2021**, *125*, 6303-6313.
(53) Xia, Y.; Long, B.; Lin, S.; Teng, C.; Bao, J. L.; Truhlar, D. G. Large pressure effects caused by internal rotation in the s-cis-syn-acrolein stabilized Criegee intermediate at tropospheric temperature and pressure. *J. Am. Chem. Soc.* **2022**, *144*, 4828-4838.
(54) Xie, C.; Guan, Y.; Yarkony, D. R.; Guo, H. Vibrational energy levels of the S_0 and S_1 states of formaldehyde using an accurate ab initio based global diabatic potential energy matrix. *Mole. Phys.* **2021**, *119*, e1918775.
(55) Han, S.; Sun, G.; Zheng, X.; Song, Y.; Dawes, R.; Xie, D.; Zhang, J.; Guo, H. Rotational modulation of $\tilde{A}^2A''$ -state photodissociation of HCO via Renner–Teller nonadiabatic transitions. *J. Phys. Chem. Lett.* **2021**, *12*, 6582-6588.
(56) Guan, Y.; Xie, C.; Yarkony, D. R.; Guo, H. High-fidelity first principles nonadiabaticity: Diabatization, analytic representation of global diabatic potential energy matrices, and quantum dynamics. *Phys. Chem. Chem. Phys.* **2021**, *23*, 24962-24983.
(57) Guan, Y.; Xie, C.; Guo, H.; Yarkony, D. R. Enabling a unified description of both internal conversion and intersystem crossing in formaldehyde: A global coupled quasi-diabatic Hamiltonian for its S_0, S_1, and T_1 states. *J. Chem. Theo. Comput.* **2021**, *17*, 4157-4168.
(58) Chen, Q.; Hu, X.; Guo, H.; Xie, D. Theoretical H + O_3 rate coefficients from ring polymer molecular dynamics on an accurate global potential energy surface: assessing experimental uncertainties. *Phys. Chem. Chem. Phys.* **2021**, *23*, 3300-3310.
(59) Chen, Q.; Hu, X.; Guo, H.; Xie, D. Insights into the formation of hydroxyl radicals with nonthermal vibrational excitation in the Meinel airglow. *J. Phys. Chem. Lett.* **2021**, *12*, 1822-1828.
(60) Papp, D.; Li, J.; Guo, H.; Czakó, G. Vibrational mode-specificity in the dynamics of the Cl + $C_2H_6 \rightarrow$ HCl + C_2H_5 reaction. *J. Chem. Phys.* **2021**, *155*, 114303.
(61) Zhao, B.; Han, S.; Malbon, C. L.; Manthe, U.; Yarkony, D. R.; Guo, H. Full-dimensional quantum stereodynamics of the non-adiabatic quenching of OH($A^2\Sigma^+$) by H_2. *Nat. Chem.* **2021**, *13*, 909-915.
(62) Shu, Y.; Zhang, L.; Chen, X.; Sun, S.; Huang, Y.; Truhlar, D. G. Nonadiabatic dynamics algorithms with only potential energies and gradients: Curvature-driven coherent switching with decay of mixing and curvature-driven trajectory surface hopping. *J. Chem. Theo. Comput.* **2022**, *18*, 1320-1328.
(63) Zhang, R. M.; Xu, X.; Truhlar, D. G. TUMME: Tsinghua University Minnesota Master Equation program. *Comput. Phys. Commun.* **2022**, *270*, 108140.
(64) Shu, Y.; Varga, Z.; Kanchanakungwankul, S.; Zhang, L.; Truhlar, D. G. Diabatic states of molecules. *J. Phys. Chem. A* **2022**, *126*, 992–1018.

Integrated Data-driven Methods for Scientific Discovery of Non-equilibrium Thermochemical Processes in Complex Environments from Ultrafast X-ray Measurements at LCLS

Matthias Ihme, Stanford University (Principal Investigator) mihme@stanford.edu
Eric Darve, Stanford University (Co-Investigator)
Stefano Ermon, Stanford University (Co-Investigator)
Dimosthenis Sokaras, SLAC National Accelerator Laboratory (Co-Investigator)
Jana Thayer, SLAC National Accelerator Laboratory (Co-Investigator)
Adrianus van Duin, Penn State University (Co-Investigator)
Diling Zhu, SLAC National Accelerator Laboratory (Co-Investigator)

1 Program Scope

Recent advances achieved with the ultrafast coherent X-ray-Free Electron Laser at the Linac Coherent Light Source (LCLS) and the anticipated LCLS-II upgrade empower us to probe non-equilibrium processes at atomistic scales with femtosecond (fs) temporal resolution. However, despite unprecedented LCLS capabilities, the enormous complexity, data volume (current acquisition rate, 1 GB/s; projected as 200 GB/s with the LCLS-II upgrade), and experimental access constitute major challenges for scientific discovery. The proposed research will directly tackle this urgent issue by developing novel and advanced data-science methods, machine-learning (ML) approaches, and uncertainty-quantification (UQ) techniques to enable ultrafast X-ray Photon Correlation Spectroscopy (XPCS) measurements that are closely supported through tightly coupled atomistic-scale simulations to discover non-equilibrium processes and chemical reactions of fluids at supercritical conditions.

To enable the rapid experimental screening of the complex thermochemical state-space and the efficient exploration of non-equilibrium reaction pathways in systems at supercritical conditions, innovative Bayesian optimization techniques will be developed that combine highly adaptive search strategies and probabilistic models for balancing the exploration of highly uncertain areas and the exploitation of promising ones. To accelerate scientific discovery, novel data-driven assimilation techniques will be developed that integrate XPCS measurements into molecular dynamics (MD) simulations, taking into consideration experimental uncertainties and incomplete models. Novel ML approaches will be developed for directly training MD force-fields from ultrafast XPCS measurements that evolve on comparable spatiotemporal scales, offering powerful new opportunities for improving the predictive accuracy of MD simulations.

These highly complementary data-science methods will be employed for scientific discovery of non-equilibrium processes in mixtures of supercritical fluids that are associated with intermolecular cluster transfer, cage effects, and chemical reactivity. To this end, we seek to examine multicomponent mixtures of relevance to environmental, chemical, and industrial applications. Of particular interest is examining how non-equilibrium cluster transfer, molecular caging, and diffusive transport at ultrafast timescales can be manipulated to affect reaction pathways and thermochemical responses at the macroscopic level.

2 Research Progress

2.1 Bayesian optimization for rapid state-space exploration

Bayesian optimization (BO) is a popular method for black-box global optimization, in which the goal is to efficiently optimize an unknown function through a sequence of pointwise queries. A variety of problems in science and engineering can be viewed as examples of this problem, including tasks in materials discovery, cosmological estimation, particle accelerator tuning, and hyperparameter optimization. In these, each query is typically expensive, and the goal is thus to perform optimization

using as few queries as possible. In BO, a probabilistic model of the unknown function is used to judiciously select a sequence of queries in order to perform optimization efficiently.

In many real situations, we have a black-box function with a non-uniform and dynamic cost, where querying different inputs can have different costs, and this cost function may change over time. For example, when each query is associated with accessing thermodynamic states that are separated in state-space; making queries in a state space of environmental conditions such as pressure and temperature; querying hyperparameter accuracies at different fidelities (e.g. numbers of epochs); traversing synthesis paths of molecules; and querying for emittance in particle accelerators under hysteresis conditions. In these settings, we show that typical methods for BO, which rely on myopic (one-step-ahead) acquisition functions, perform suboptimally and may fail to converge, getting stuck in local optima and becoming unable to sufficiently explore. To mitigate these issues, we develop a non-myopic acquisition function that allows forward planning behavior which can outperform its myopic counterparts, especially in the non-uniform dynamic cost setting. Through variational inference and amortization, we can perform efficient gradient based optimization of this acquisition function. Our method has intimate connections with other classes of decision making algorithms, such as reinforcement learning.

2.2 Analysis of reaction trajectories

An untapped potential of experimental XPCS measurements is the ability to resolve the dynamics of molecular systems at the ultrafast timescales. Traditionally, this has been done using: (a) analytical estimates from theoretical chemistry, or (b) *ab-initio molecular dynamics* (AIMD). On its own, either option is limited by the lack of theory for non-equilibrium reaction dynamics and the infeasibility to simulate large timescales using strictly molecular dynamics, respectively. However, by supplementing the methods with results obtained from XPCS measurements, a direct pathway for delineating the chemical dynamics can be forged. An example of such a process can be seen below, where HCFC-133a ($C_2H_2F_3Cl$) and Thiophene (C_4H_4S) are simulated using NewtonX [Barbatti et al., 2014] using the time-dependent density functional theory (TDDFT) framework.

In this framework, the molecule is excited with a user-specified photon pulse at t_0 and the molecular response is studied using AIMD --- by advancing the quantum and classical equations of motion in time. Then, by probing the molecular geometry at various timesteps, one can assemble the dynamics of the system. This is shown in Fig. 1(a)-(b), where the molecules undergo distinct changes in their geometry (and concomitantly in their thermophysical properties) within the ultrafast time regime. While the exact molecular structure can only be accessed via AIMD, the radial distribution function (RDF) can be readily computed from XPCS measurements. The RDF, in turn, contains the molecular imprint and embeds the molecular geometry, as seen in Fig. 1(c)-(d). Therefore, XPCS measurements can directly lead to the understanding of chemical dynamics of mixtures in ultrafast timescales. Yet, setting up experimental measurements and performing complete molecular simulations that span the entire phase space remains a costly, time consuming, and labor-intensive process. As a result, a key scientific question underlies the selection of optimal parameters to run the experiments and simulations at. (In this context, optimal parameters refer to the physical conditions that will maximize the amount of physics extracted from the data.)

Efforts are currently underway to couple the Perturbed Chain-Statistical Associating Fluid Theory (PC-SAFT) [Gross et al., 2001] equation of state with BO (see Sec. 2.1) to guide this investigation. A working implementation of PC-SAFT, applicable to both associating and non-associating mixtures, has already been developed, and it was shown that PC-SAFT outperforms classical cubic equations of state in predicting the thermophysical properties of mixtures near the critical point. This is because PC-SAFT accounts for complex molecular interactions through hard chain contributions (analogous to hard spheres), dispersion, and agglomeration of molecules into long chains (association). Adding BO in the loop is the immediate next step in this regard.

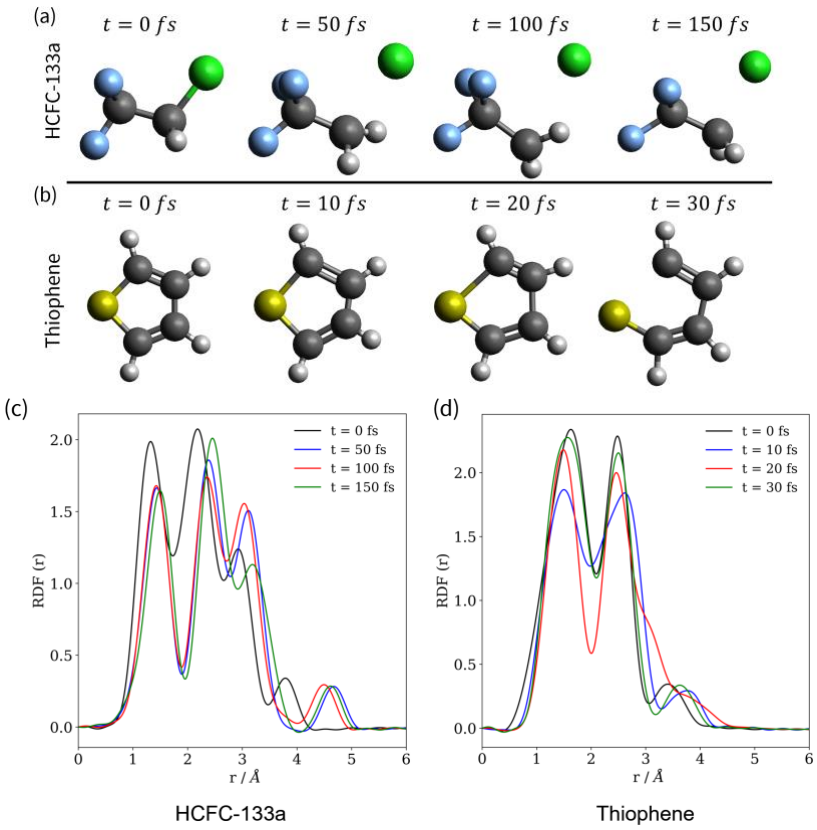

Figure 1: Results from NewtonX for (a) HCFC-133a and (b) Thiophene; HCFC-133a undergoes rapid bond dissociation in the C-Cl bond, whereas Thiophene goes through a ring opening. Panels (c) and (d) show the corresponding the RDFs of the geometries, computed using the Independent Atom Model [Thomas Wolf: https://github.com/ThomasJAWolf/Diffraction_simulation]. The changes in the RDF can be directly linked to changes in the molecular geometry.

2.3 MD force-field training and validation

In order to enable molecular dynamics simulations on iodine/Xenon systems – including the exothermic recombination of iodine radicals to the I_2 molecule – we develop a ReaxFF parameter set for I/Xe systems. The Xe initial parameters were taken from the parameter set used by Yoon et al. (2017) to study noble gas impact on graphene surfaces. The I/Xe and I/I interactions were trained by quantum mechanical (QM). For the I/I interactions the CASSCF was used, while for the I/Xe interactions the more approximate DFT method was used – since the CASSCF could not be converged for the Xe-atoms. The van Duin group used these data to train ReaxFF parameters – obtaining very good agreement with both the CASSCF and the DFT data, in particular for the I-I dissociation energy (-38.05 kcal/mol for ReaxFF; -37.94 kcal/mol for CASSCF) and the I-I bond radius (2.7399 Angstrom ReaxFF; 2.690 Angstrom CASSCF). For the I/Xe interactions we included data for for I/Xe and I_2/Xe interactions. The ReaxFF reproduction of the I/Xe data is very good – including the weak van der Waals attraction (-1.94 kcal/mol for ReaxFF; -2.08 kcal/mol for CASSCF), but for the I_2/Xe interactions – were we used both a colinear and a perpendicular approach – we found minor differences between ReaxFF and QM – indicating that the 2-body Morse function used in ReaxFF may not be fully accurate to capture these interactions. For the Xe-Xe pair, ReaxFF predicts a -0.34 kcal/mol van der Waals minimum, which is not reproduced by the DFT data used in the training – but the ReaxFF results agrees well with Xe-crystal cohesive energies. The repulsive part of the Xe-Xe interaction curve from DFT is well reproduced by ReaxFF.

Using this I/Xe ReaxFF parameter set we performed a series of molecular dynamics simulations starting from a 2I-radical/18 Xe system. Using the NVE microcanonical ensemble we saw that the initial temperature of this system (300K) rose to around 950K due to the exothermic I_2 formation. The I_2 was stable in this system – since it transferred some of its excess kinetic energy directly to the Xe-atoms and remained in a highly excited vibrational state.

2.3 Analysis of Binary Mixing systems

Due to the presence of two Widom lines as well as different levels of inhomogeneity, analysis of binary mixtures under supercritical conditions is very challenging. For this study, we chose xenon and carbon dioxide as our system, since these two gases have critical point close to each other, making them miscible. We performed MD simulation of Xe/CO2 mixture at 303K and 85bar (close to the critical point of CO2) for different mixture composition. For CO2 we used the TraPPE force field while Lennard Jones 12-6 potential for xenon. To understand the system dynamics, we evaluated the intermediate scattering function, $F(Q,\tau)$, for the different mixtures at Q = 0.12Å^{-1} (Fig. 1a). At this Q value, the decay in $F(Q,\tau)$ corresponds to long range density fluctuations. Upon fitting $F(Q,\tau)$ with the

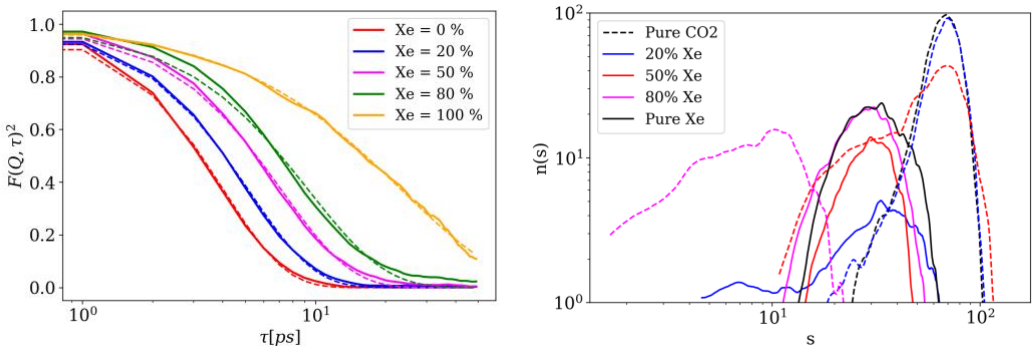

Figure 2: (a) Intermediate scattering function for different Xe/CO2 mixtures at Q = 0.12Å^{-1}. The dotted lines are Kohlrausch–Williams–Watts fit. (b) Cluster size distribution of Xe and CO2 obtained using DBSCAN. The solid lines show the Xe clusters while the dotted lines are the CO2 clusters

Kohlrausch-Williams-Watt (KWW) expression, we found that pure CO2 shows hyperdiffusivity (KWW exponent $\gamma > 1$). Upon adding xenon to the system, the hyperdiffusive behavior gets attenuated and the mixture shifts towards simple exponential dynamics.

To analyze this phenomenon further, we computed the cluster size distribution of CO2 and Xe in the mixture using DBSCAN (Fig. 2b). We can see that CO2 forms much larger clusters (dotted lines) compared to xenon (solid lines), since the operating conditions are near the critical point of CO2. The faster decay of $F(Q,\tau)$ for pure CO2 (red curve in Fig 2a) suggests that these large CO2 clusters are not very stable. Thus, the large and unstable clusters of CO2 cause inhomogeneity in the system and results in hyperdiffusivity. On the other hand, for pure xenon, we see pure diffusive decay in $F(Q,\tau)$ (KWW exponent $\gamma = 1$). The Xe clusters are small and stable due to the higher mass of xenon. As such, adding more xenon reduces the density fluctuations and increases the decay time of $F(Q,\tau)$.

Here we observe hyperdiffusivity in supercritical gases, a phenomenon which has been reported previously for complex fluids such as colloids and aerogels. Next step in this study would be looking into temperature and pressure condition near critical point of xenon to test whether we observe similar dynamics.

3 Future Plans

The next step in our research as follows:

- Perform XPCS measurement on binary mixtures (a beamline proposal has been submitted, awaiting approval)
- Integration of BO algorithm with thermodynamic state-space evaluation to enable optimal state-space exploration; demonstrate this capability at SSRL SAXS beamline
- Develop data-assimilation method to integrate XPCS measurements with atomistic-scale simulations
- Generate XPCS data for data analytics and force-field training

Publications and visibility from this research

1. Ihme, M., **Chung, W. T.**, and Mishra, A. A., "Combustion machine learning: Principles, progress and prospects." *Progress in Energy and Combustion Science*, 91, 101010, 2022.
2. Ihme, M. "Machine learning methods for reacting flows at macro and micro-scales." Telluride workshop "Machine Learning and Informatics for Chemistry and Materials" September 2021.

References

J. Gross and G. Sadowski, Perturbed-Chain SAFT: An Equation of State Based on a Perturbation Theory for Chain Molecules, Ind. Eng. Chem. Res., 40, 1244-1260 (2001).

M. Barbatti, et al., NEWTON-X: a surface-hopping program for nonadiabatic molecular dynamics; WIREs: Comp. Mol. Sci., 4, 26 (2014)

K. Yoon, et al. Atomistic-scale simulations of the defect formation in graphene under noble gas irradiation. ACS Nano 10, 8376-8384 (2016).

Probing Supercritical Phase Transition using Ultrafast X-ray Diagnostics

Principal Investigator: Matthias Ihme
Department of Mechanical Engineering
Stanford University,
488 Escondido Mall, Stanford, CA 94305
email: mihme@stanford.edu

Co-Investigator Dimosthenis Sokaras
SLAC National Accelerator Laboratory,
2575 Sand Hill Road, Menlo Park, California 94025

Program Scope

The objective of this research is to probe dynamical processes within supercritical fluids that are associated with the thermal motion, molecular diffusion, and intermolecular cluster transition at supercritical conditions. Of particular interest is hereby to examine the ultrafast timescales of the cluster transfer and intermolecular cluster-exchange processes across the structural transition line. To this end, X-ray Photon Correlation Spectroscopy (XPCS) at the Linac Coherent Light Source (LCLS) will be utilized to measure equilibrium and non-equilibrium processes by continuously scanning the delay range of two X-ray pulses up to few picoseconds with better than 20 femtosecond temporal resolution.

Over recent years, several hypotheses have been put forward to elucidate supercritical transition states. Despite significant progress on the fundamental understanding of fluids at these supercritical conditions, important questions concerning the microstructure and dynamical processes remain [1-5]. A particular research issue is hereby the fundamental understanding of the morphology of the molecular microstructure and its effect on the macroscopic behaviour and thermodynamic response functions. It is widely believed that the supercritical state is homogeneous without structural and dynamic observables to distinguish between a liquid and a vapor. However, recent investigations have identified regions of distinct liquid-like or vapor-like properties even under supercritical conditions [1,5]. Specifically, it was shown that the transition between liquid-like and vapor-like states occurs across an extension to the coexistence line, marked by almost discontinuous changes in fluid properties. This transition was first identified experimentally by Nishikawa and Tanaka [6] and stands in contrast to the classical presentation of the supercritical state space as a featureless, homogeneous domain.

Structurally, the most important properties of supercritical fluids are the dynamic heterogeneities and local density fluctuations that are present within the fluid state at the microscopic level. These inhomogeneities are associated with the formation of molecular clusters of various sizes with liquid-like properties separated by voids of unbound gas-phase molecules which continuously restructure itself at picosecond timescales.

By utilizing ultrafast X-ray Photon Correlation Spectroscopy (XPCS) at the Linac Coherent Light Source (LCLS) as an experimental probe of these structural changes at the molecular level we seek to elucidate the higher-order phase transition from a liquid-like to a vapor-like state in the region extending the critical point. Open questions we seek to address particularly with XPCS are: (i) the underlying mechanisms responsible for the density fluctuations at supercritical conditions and how these dynamical processes at the molecular level affect the thermodynamic response functions and (ii) on what timescales do dynamical processes evolve that are associated with thermalization, molecular diffusion, and intermolecular cluster transfer.

Research Progress

Experimental apparatus

We designed, built, and tested a high-pressure, high-temperature cell, shown in Figure 1, to study the dynamics of supercritical fluids such as carbon dioxide and water. This cell will be used in X-ray Photon

Correlation Spectroscopy (XPCS) and Wide/Small Angle X-ray Scattering (WAXS/SAXS) experiments to characterize the molecular movement, interactions, and formation of clusters in fluids at supercritical conditions.

The pressure cell was based on a previous design from Dr. John Fulton at the Pacific Northwest National Laboratory (PNNL) [6,7]. With his advice, we were able to choose the proper equipment for our high pressure system and resolve technical issues we encountered during testing. The cell is constructed from a corrosion-resistant titanium alloy and comprises three components: the main body, a window cone, and a retaining nut. The fluid is contained between two 100 μm-thick single-crystal diamond windows, which allow optical access to the X-ray beam with minimal attenuation of the scattering signal. A cross section of the cell is illustrated in Figure 1. The diamond windows seal against highly polished titanium surfaces with a shallow taper, forming an unsupported-area type seal that improves the yield strength of the windows [8]. The windows are initially held in place using a thin layer of a curable silicone resin (Vacseal, SPI supplies). The seal between the cell body and the window cone is a metal-to-metal conical design commonly used in high pressure experiments [8]. The window cone has a 59° angle, while the cell body has a female cone with a 60° angle. The thickness of the sample fluid can be varied between 150 μm and 1 mm by using different window cones. The maximum design pressure of the cell is 450 bar, and its maximum design temperature is 725 K. This was determined using finite element analysis (thermal and mechanical) and design guidelines laid out in [8,9]. A Teledyne ISCO 100DM syringe pump is used to deliver the fluid and pressurize the system, with an uncertainty in sample pressure better than 3.5 bar. The cell is heated with eight cartridge heaters, and the sample temperature is continuously monitored using an RTD sensor. A Cryo-Con PID temperature controller is used to set and maintain the temperature of the cell.

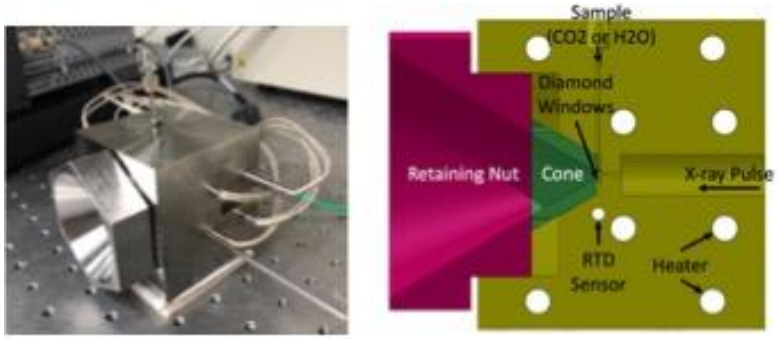

Figure 1: High-pressure cell with cartridge heaters and temperature sensor (left) and cross section through pressure cell (right).

Figure 2 summarizes the results of a supercritical water test with the high-pressure cell. The sample was maintained at 230 bar, 380 °C initially, and the pressure was raised to 250 bar after 2 hours. We were able to maintain these operating conditions with a leakage rate of less than 0.4 $ml.h^{-1}$. The cell reached the operating temperature within 30 minutes and maintained this temperature with fluctuations less than ±0.01 °C during the experiment. These results demonstrate that the pressure cell can be used to perform long-duration, continuous measurements at light-sources with a relatively short setup time and without the need for interruption to refill the pump.

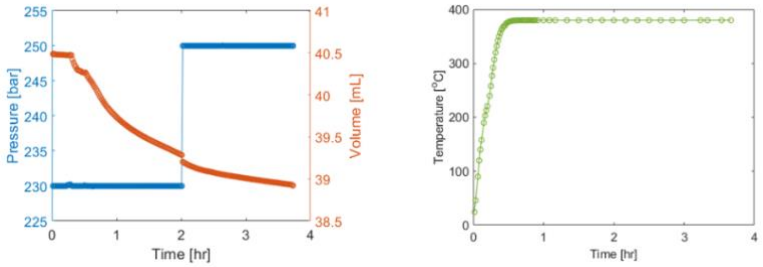

Figure 2: Experimental demonstration of the pressure cell operational capabilities using supercritical water. (left) Pressure and volume as a function of time. (right) Sample temperature as a function of time

Small Angle X-ray Scattering Experiment

We performed Small Angle X-ray Scattering (SAXS) measurements of supercritical carbon dioxide (critical point 78 bar, 31 °C) at the SSRL Beamline 4-2 at SLAC National Accelerator Laboratory. The objective of these measurements was to demonstrate the performance of our high-pressure cell at supercritical conditions and collect preliminary data on supercritical mixtures for the XPCS measurements. The X-ray energy in the experiment was 15 keV, and a Pilatus detector was placed 2.5 m from the sample. Data was recorded with 5 seconds exposure time, and the computed SAXS curves

were averaged over 50 frames after background subtraction of the empty pressure cell. In this setup, the pressurized fluid (CO_2, 99.999% purity) is supplied by a syringe pump (Teledyne ISCO 100DM, maximum pressure 690 bar), and confined between two 100 µm-thick diamond windows in the cell. The sample temperature was controlled with cartridge heaters and maintained with an RTD sensor and PID control; deviations in the temperature and pressure during a measurement were within $\Delta T = \pm 0.1$ °C and $\Delta P = \pm 0.1$ bar, respectively.

The scattering intensity obtained between momentum transfer (Q) of 0.03-0.08 $Å^{-1}$ for supercritical carbon dioxide at T = 31.5 °C is plotted in Figure 3. Local density fluctuations in supercritical fluids lead to an increase in the SAXS scattering intensity near the critical point. We performed Ornstein-Zernike analysis [10] on the SAXS scattering intensities to obtain the density fluctuations of carbon dioxide at four reduced temperatures T_r ($T_r = T/T_c$), shown in Figure 3. These data are in good agreement with previous studies, which have identified a ridge in the *P-T* phase diagram along the curve that extends from the liquid-gas coexistence curve into the supercritical region, where the density fluctuations are maximized when the isothermal or isobar line crosses this curve [10]. The peak in maximum density fluctuation at $T_r = 1.0013$ agrees with this observation demonstrates the high accuracy and stability of our system.

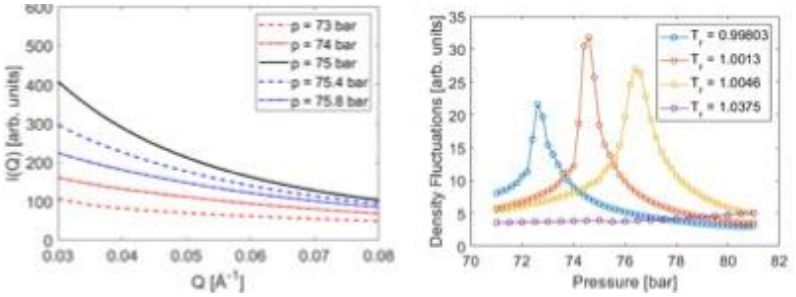

Figure 3: SAXS intensity measurements for supercritical CO2 at T=31.1°C (left) and density fluctuations near critical point as a function of pressure and reduced temperature.

X-ray Photon Correlation Spectroscopy

XPCS measurements were conducted at the XPP hutch at LCLS in beamtime XPPLW3319 during Run 19. The measurements were done with a photon energy of 9.5 keV. The hard X-ray pulse pairs required for the ultrafast XPCS measurement was delivered by the split-delay unit located at the XPP hutch. Downstream of the split-delay unit, and pulse energy of 2 μJ was expected to be delivered to the CO2 sample.

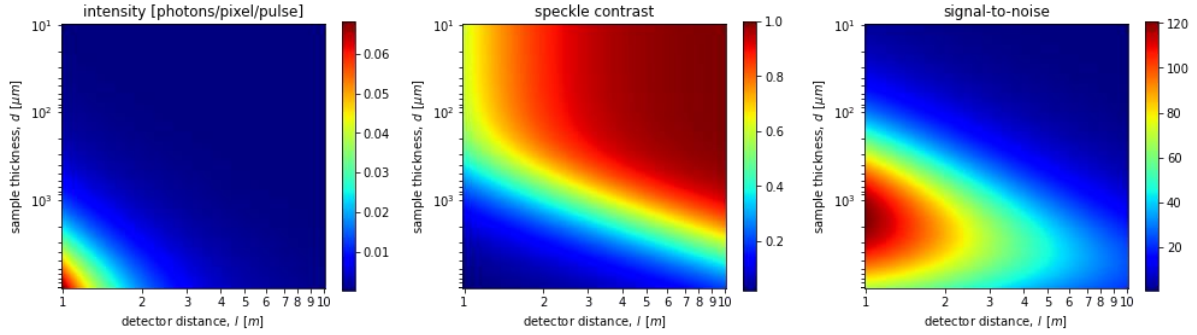

Figure 4: The estimated scattering intensity (left), speckle contrast (middle) and signal-to-noise ratio (right) of the XPCS measurement for different sample thickness and detector distance.

To design the experiment, we performed comprehensive analysis to design experimental setting, using XPCS theory presented in Ref. [11-13]. Theoretical results for the estimated signal level of the XPCS measurement is shown in Figure 4 for different sample thickness and detector distance.

Combining the information presented in Figure 4 and constrains of the hardware at LCLS, we optimized the XPCS measurement, resulting in the following setup: Downstream the CO2 sample, a total of 4 ePix detectors were used to collect the speckle patterns. Each ePix detector has 768×704 pixels, with a pixel size of 50 μm. According to Figure 4 the detector is placed 5m downstream of the CO2 sample. Therefore, we measured a Q range of 0.01-0.1 A. over the detector.

In this experiment, three different time delays (4ps, 8ps and 13ps) were measured. The ePix detectors were divided into regions with constant momentum transfer (with 10% variation) and the

speckle contrasts of the photonized detector images were obtained with a maximum likelihood algorithm. An example of the detector image and the contrast curve is presented in Figure 5.

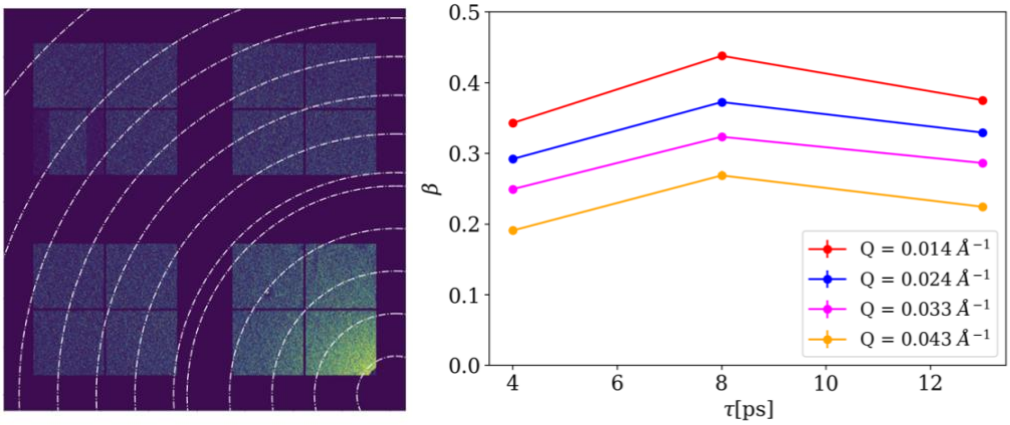

Figure 5: Image of the 4 ePix detectors. The regions between white circles denotes constant Q value. The plot on the right corresponds to the speckle contrast β vs pulse delay τ obtained for the smallest Q values for three different delays – 4ps, 8ps and 13ps.

In Figure 6, we present the intensity distribution across the detectors (static structure factor of supercritical CO2) using the mean photon density. We also show the signal-to-noise ratio at the detectors for different Q values. The smallest signal-to-noise ratio is for the ePix 1 detector (the upper left tile shown in the left plot of Figure 5) which is placed farthest from the beamline (highest momentum transfer). Within the uncertainty of the experiment result, no contrast change is observed within the measured delay time range and Q range.

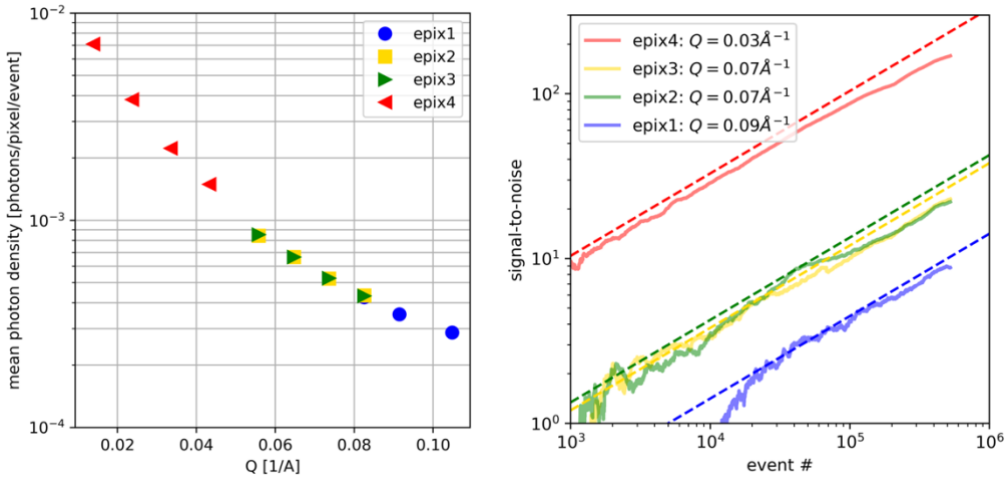

Figure 6: Mean photon density and signal-to-noise of the 4 detectors. The dashed line in the signal-to-noise ratio plot corresponds to analytical estimation given by $SNR \propto \beta \bar{k} \sqrt{N_{frames}}$ *where* $\bar{k}$ *is the mean photon count per shot and* N_{frames} *is the number of frames or shots*

Main Findings and Next Steps

The results from these XPCS-measurments have multiple implications and guide our next research steps:

- We demonstrated first XPCS measurements on supercritical fluids; from the theoretical perspective of MD simulation, the discrepancy between simulations and measurements indicates the necessity of a more systematic investigation of the sample system. A larger sample system may be required to fully recover the experiment observations. Furthermore, the unexpected results of the lack of short-time-scale dynamics indicates a profound discrepancy in the theory and force-field dynamics. Addressing this issue is subject of ongoing research.
- On the experiment side, we will continue our investigation of supercritical CO2 at a longer delay time. Limited by the experiment hardware, we were not able to probe longer delay times during

the LW3319 beamtime. Going to longer delay time and eventually observing the decay of the contrast can provide essential knowledge to understand the microscopic dynamics.

- During the analysis of our data, the low count rate at relatively large Q values made the data interpretation susceptible to detector defects. We are currently developing new and more robust algorithms to facilitate the analysis and interpretation of the observed data. We anticipate that this new algorithm can help with future XPCS data analysis in general.
- Our measurements showed that the split-delay device in the XPP hutch is very stable. This makes it possible to collect data over an extended period. Our measurement indicated the need for extending the delay-time measurements to > 20ps. To address this, we consider replacing the existing crystals with larger ones or adding a new pair of channel-cut crystals to further elongate the delay time to about 100 ps. Extending this capability will be of great utility to researchers interested in the microscopic dynamics of fluids in general.
- Beyond the investigation of CO2, we are extending our measurement to examine supercritical H2O, which has substantially shorter time dynamics than CO2. These experiments are scheduled as part of an upcoming LCLS Run 20.

Publication and Visibility from this research

Lin, M.-F., Singh, N., Liang, S., Mo, M., Nunes, P. Ledbetter, K., Yang, J., Kozina, M. Weathersby, S., Shen, X., Cordones-Hahn, A., Wolf, T., Gaffney, K., Pemmaraju, D., Ihme, M., and Wang, X., "Imaging the short-lived hydroxyl-hydronium pair in ionized liquid water." *Science*, 374, 6563, 92-95, 2021.

References

[1] G. G. Simeoni, et al. The Widom line as the crossover between liquid-like and gas-like behaviour in supercritical fluids. Nat. Phys. 6.7 (2010): 503-507

[2] P. F. McMillan and H. E. Stanley. Going supercritical. Nat. Phys. 6.7 (2010): 479-480.

[3] J. Frenkel. Kinetic Theory of Liquids. Dover, 1955.

[4] H. E. Stanley. Introduction to Phase Transitions and Critical Phenomena. International Series of Monographs on Physics. Oxford University Press, 1971.

[5] F. Gorelli, M. Santoro, T. Scopigno, M. Krisch, and G. Ruocco. Liquidlike behavior of supercritical fluids. Phys. Rev. Lett., 97(24):245702, 2006.

[6] L. B. Skinner, M. Galib, J. L. Fulton, C. J. Mundy, J. B. Parise, V.-T. Pham, G. K. Schenter, and C. J. Benmore, "The structure of liquid water up to 360 MPa from x-ray diffraction measurements using a high Q-range and from molecular simulation", J. Chem. Phys. 144, 134504 (2016).

[7] J.L. Fulton, Y. Chen, S.M. Heald, M. Balasubramanian, "High-pressure, high-temperature x-ray absorption fine structure transmission cell for the study of aqueous ions with low absorption-edge energies", Review of Scientific Instruments 75, 5228-5231 (2004).

[8] W. F. Sherman and A. A. Stadtmuller, Experimental Techniques in High-Pressure Research. (John Wiley and Sons, Inc., New York, 1987).

[9] N.J. Brooks, B. E. Gauthe, N.J. Terrill, S.E. Rogers, R. H. Templer, O. Ces, and J.M. Seddon, "Automated high pressure cell for pressure jump x-ray diffraction", Review of Scientific Instruments 81, 064103 (2010).

[10] K. Nishikawa and I. Tanaka. Correlation lengths and density fluctuations in supercritical states of carbon dioxide. Chem. Phys. Lett. 244.1-2 (1995): 149-152

[11] Y. Sun, et al. Compact hard X-ray split-delay system based on variable- gap channel-cut crystals. Opt. Lett., 44(10):2582–2585, 2019.

[12] G. Grübel, A. Madsen, and A. Robert, X-ray Photon Correlation Spectroscopy (XPCS) in Soft Matter Characterization in X-ray and Neutron Techniques for Nanomaterials Characterization, edited by R. Borsali and B. Pecora, pp. 54–195, 2008.

[13] Möller, Johannes, et al. "X-ray photon correlation spectroscopy of protein dynamics at nearly diffraction-limited storage rings." IUCrJ 6.5 (2019): 794-803.

Tracking the Mechanisms of Catalytic Reactions on Ligand-Protected Gold Nanoclusters

Christopher J. Johnson
Department of Chemistry
Stony Brook University
100 Nicolls Rd., Stony Brook, NY 11794-3400
chris.johnson@stonybrook.edu

Program Scope

This research program focuses on catalytic transformations leveraging atomically-precise nanoclusters as potential designer electrocatalysts. Atomically-precise nanoclusters typically feature a metal or metalloid core of tens to hundreds of atoms surrounded by a stabilizing and solubilizing layer of organic ligands with a total diameter of 1-2 nm. They merge desirable qualities of molecular and nanoscale catalysts: they can, in principle, be produced or isolated with exactly specified structures and formulae like molecules, but feature densities of states and compositions more consistent with nanoscale objects. Nanoclusters have been extensively pursued as catalysts, showing promise in a number of reactions.[4] We are focusing on the electroreduction of CO_2, for which two prototypical nanoclusters have shown enhanced activity that depends on specific aspects of their composition.[1, 5] The goals of this project are:

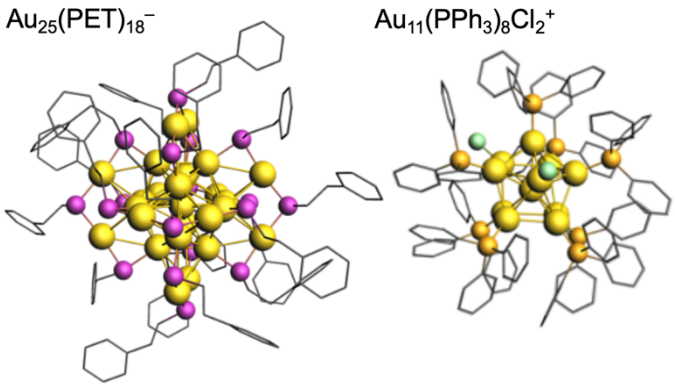

Figure 1: X-ray crystal structures of $Au_{25}(PET)_{18}^-$ (PET = phenylethanthetiol) and $Au_{11}(PPh_3)_8Cl_2^+$ (PPh_3 = triphenylphosphine). Here gold = Au, pink = S, orange = P, and green = Cl.[1-2]

1. to determine the active site for electrochemical CO_2 reduction by the ubiquitous $Au_{25}(SR)_{18}$ nanocluster,
2. to determine the mechanism of CO_2 reduction by Au_{11} nanoclusters,
3. to synthesize nanoclusters with improved catalytic activity by tailoring active sites and optimizing ligand and metal dopant chemistry.

The $Au_{25}(SR)_{18}$ nanocluster, shown in Figure 1, has been shown to be catalytically active towards CO_2 and the mechanism has been investigated computationally. Quantum chemical calculations suggest that a ligand dissociates, leaving an undercoordinated Au atom that can take CO_2 as a ligand.[7] However, experimentally probing this mechanism directly is made challenging by the inability to isolate the ligand-off species. We are using mass spectrometry to produce and isolate this species and compare its activity towards CO_2 with that of the intact nanocluster. We will also track this activity as a function of metal doping, as this has been shown to increase activity. Recent reports have shown that the Au_{11} nanocluster (Figure 1) shows activity towards CO_2 that can be manipulated by exchange of a single triphenylphosphine (PPh_3) ligand for an N-heterocyclic carbene (NHCs).[1] Key questions remain about the charge state of the active species, the nature of the active site, and the source of ligand-based enhancement of activity. We will probe the activated complex and track the degree of CO_2 activation as a function of ligand composition to isolate the effects of ligand steric hindrance and electronic stabilization. Finally, we will develop a prototype nanocluster platform that features several potential active sites and manipulate the ligand chemistry to selectively expose each active site. We will then evaluate the changes in the degree of activation of each modification to develop an intuitive framework for optimizing nanocluster catalysts for CO_2 reduction.

Recent Progress

In the initial phases of this project, we have synthesized and characterized the $Au_{25}(SR)_{18}$ nanocluster and its silver-doped and ligand-exchanged analogues as well as the precursor to the Au_{11} nanocluster. Despite its clear position as the most well-studied nanocluster, the electronic structure of Au_{25} has only been qualitatively understood,[8] and quantum chemical calculations have not yet reached predictive accuracy. This is even more apparent for doped variants, which are typically not able to be isolated with the purity required to make unambiguous measurements.[9] Using the gas-phase cryogenic ion trap approach that we developed in our laboratory, we recorded high-resolution electronic absorption spectra of Au_{25} and $Au_{24}Ag$, the latter of which was the first spectrum of the unambiguously isolated doped nanocluster. Figure 2 compares the spectral resolution possible with room temperature solution-phase measurements, low-temperature solution phase measurements, and gas phase measurements. Despite the seemingly small differences between the low-temperature and gas phase results, key details emerge in the gas phase spectrum that enable spectral decomposition and the extraction of high-precision fitting parameters. As shown in Figure 3, we were able to clearly resolve the changes to the electronic spectrum upon doping, which showed that most transitions blue shift as expected, but the key HOMO-LUMO transition actually red shifts.

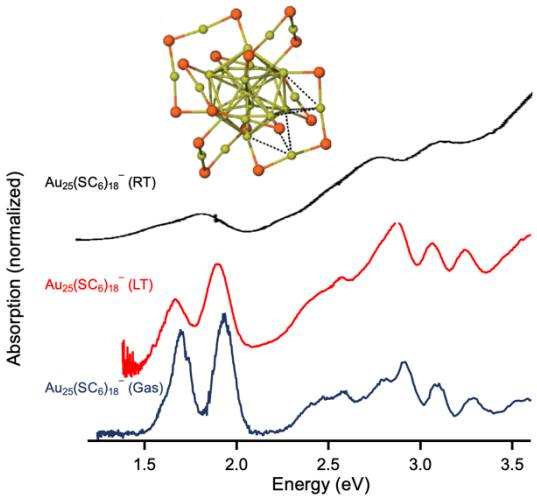

Figure 2: Comparison of the spectra of $Au_{25}(PET)_{18}^-$ recorded using a conventional UV/vis spectrometer at room temperature (top),[3] a UV/vis spectrometer with a cryogenic sample holder at 78 K (middle),[6] and the gas phase technique developed in our laboratory (bottom).

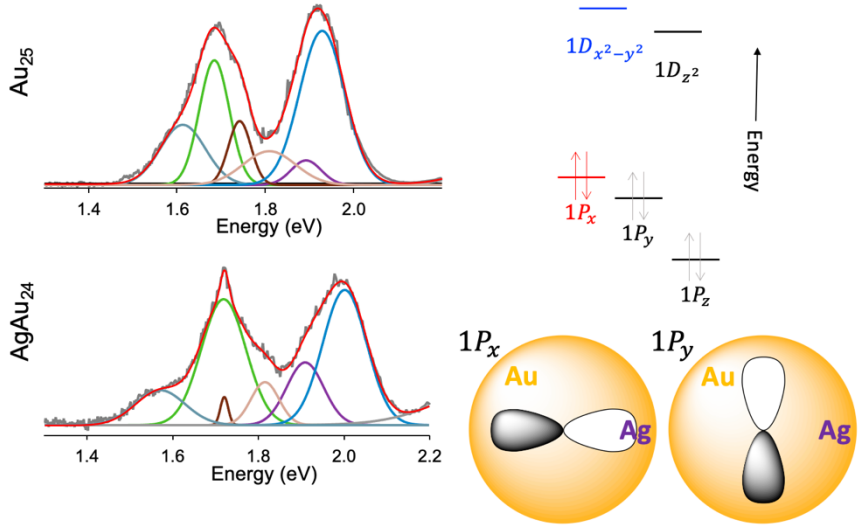

Figure 3: Decomposition of the spectra of Au_{25} and $Au_{24}Ag$ (left) allowed us to develop a molecular orbital-based description of the electronic impact of Ag doping on the cluster. This understanding derives from a simple particle-in-a-box treatment of the gold core, in which the silver atom appears as a bump in the square well potential. Solution of the 3D Schrodinger equation for this potential shows that the HOMO, which has P_x symmetry, is destabilized by this perturbation because it features significant electron density on the dopant atom, while P_y and P_z have nodal planes along the dopant atom and are thus minimally shifted. The PIB calculation nearly quantitatively reproduces the shift observed in the HOMO-LUMO transition in the experimental spectrum.

We developed an intuitive explanation for this observation based on a simple particle-in-a-box model, showing that it could be explained simply by in induced asymmetry in the potential of the gold core of the cluster by the dopant with a slightly lower ionization energy. In a nutshell, the HOMO, which has Px symmetry, appears to align such that one lobe shows significant overlap with the Ag dopant, while the Py and Pz orbitals align such that the dopant is located along their nodal plane where they have minima in their electron densities. Thus, the dopant will destabilize the HOMO,

while minimally perturbing HOMO-1 and HOMO-2. Similar arguments can be made for the LUMO and LUMO+1, which have the symmetry of D orbitals. This minimal MO model is enough to account for the shifts seen in the spectra upon Ag doping. Furthermore, explicit particle-in-a-box calculations evaluating this model also produce energetic shifts in near quantitative agreement for these transitions despite omitting important electronic interactions like exchange, correlation, and relativistic effects. These high resolution spectra and their interpretation will be key to identifying and understanding the electronic orbitals responsible for binding CO_2 and transferring charge to it, as the orbitals most strongly interacting with the CO_2 MOs in bonding interactions are the ones most likely to be perturbed. The precision of these experiments ensures that this perturbation will be detected for any interaction strong enough to be catalytically relevant.

We prepared the Au_{11} precursor Au_9H. Beyond its synthetic utility, the Au_9H nanocluster also serves as a prototype H-containing cluster. These cluster-bound H atoms are important for the hydrogenation of CO_2 but are extremely difficult to observe in typical chemical analyses. The identification of the cluster-H stretching vibration in Au9H adds important data to the existing evidence on the nature of cluster-bound H atoms, a topic of a recent surge in interest. H atoms my act as anionic ligands, they may donate their electrons to the cluster core and participate in delocalized orbitals, or somewhere in between. This stretching frequency is a key benchmark that must be reproduced by any theoretical accounting of this cluster, and is a spectroscopic marker for determining if cluster-bound H atoms are active in the catalytic mechanism for a variety of reactions.

We recorded the infrared spectra of Au_9H, Au_9D, and Au_9 as shown in Figure 4 and identified the cluster-H(D) stretching band as a broad, weak feature around 1500 (1150) cm^{-1}. The shift upon deuteration suggests that this vibrational mode corresponds to a reduction in reduced mass of a factor of 1.3, somewhat less than the limit of 1.41 for a hypothetical cluster-H diatomic but large enough to suggest that the relevant normal mode is dominated by H(D) motion. We then successfully bound CO_2 to this cluster and noted a complete disappearance of the H-atom stretching transition, suggesting that the CO_2 molecule interacts with the H atom in a stronger fashion than mere physisorption. We confirmed this by binding N_2 and NH_3 to the same cluster, in which N_2 recovered the H atom stretching feature and NH_3 similarly eliminated it. While this alone does not give direct insight into the potential for CO_2 hydrogenation on this cluster, it is an intriguing first hint that this H atom may be particularly reactive.

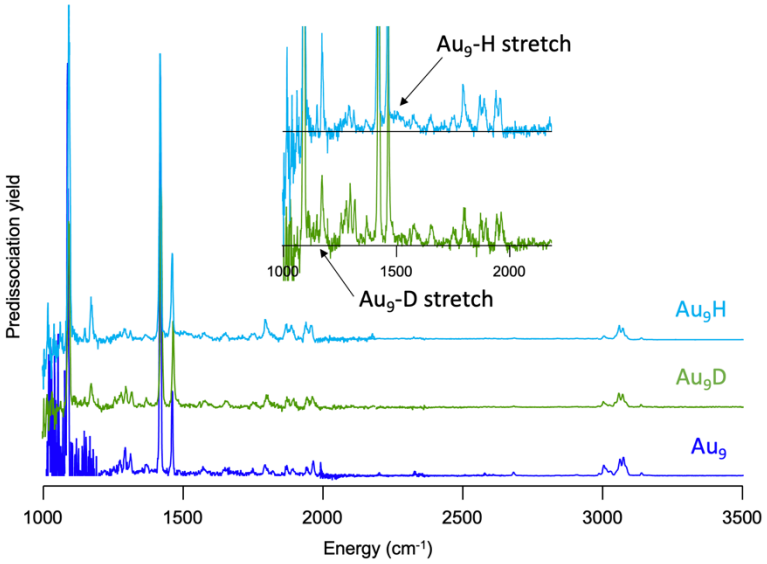

Figure 4: Comparison of the vibrational spectra of Au_9, Au_9H, and Au_9D, recorded at ~4 K. Inset is a blow up of the cluster-H(D) stretching region, showing a weak, broad band at 1500 for the H-cluster that shifts to1150 cm^{-1} in the D-cluster. The H/D shift of this band is consistent with a normal mode primarily characterized by H(D) motion.

Future Plans

With these initial studies successfully completed, we now turn our attention to producing ligand-dissociated Au_{25} nanoclusters. We will take two approaches in parallel: we will construct an electrochemical interface

to the electrospray ionization source of our mass spectrometer to electrochemically reduce the cluster, and we will use a high-temperature ion trap to thermally dissociate ligands. The electrochemical interface is based on a successful implementation for similar mass-spectrometer-based spectroscopy experiments,[10] in which an electrochemical flow cell is inserted just before the electrospray emitter. The high-temperature ion trap approach leverages an ion trap that currently exists in our laboratory but which has not yet been implemented. If either approach is successful, we will then use variable-temperature ion trap experiments to evaluate the binding enthalpy and entropy of CO_2 to these clusters and infrared spectroscopy to evaluate the degree of activation of CO_2. In parallel, we will finish the synthesis of the Au_{11} nanoclusters and proceed with similar experiments to establish the mechanism of CO_2 reduction catalyzed by this cluster. Finally, will investigate the fate of the CO_2-bound hydrogen in Au_9H, which will provide critical first steps in tracking more complex mechanisms that involve both CO_2 activation and proton or H-atom transfer. These efforts will be substantially improved by the upgrad of our infrared laser sources with improved nonlinear crystals (ZGP, replacing $AgGaSe_2$) that deliver a 3-5x increase in laser power between 2400 and 800 cm-1, the critical fingerprint region for activated CO_2 and product vibrations. The 10x improvement in signal-to-noise enabled by this development will improve our ability to detect weak transitions from baseline noise and more faithfully decompose congested spectral regions to track shifts in fingerprint bands.

References

1. Narouz, M. R., et al., N-heterocyclic carbene-functionalized magic-number gold nanoclusters. *Nat. Chem.* **2019**, *11*, 419-425.
2. Heaven, M. W.; Dass, A.; White, P. S.; Holt, K. M.; Murray, R. W., Crystal Structure of the Gold Nanoparticle $[N(C_8H_{17})_4][Au_{25}(SCH_2CH_2Ph)_{18}]$. *J. Am. Chem. Soc.* **2008**, *130*, 3754-3755.
3. Zhu, M.; Aikens, C. M.; Hollander, F. J.; Schatz, G. C.; Jin, R., Correlating the Crystal Structure of A Thiol-Protected Au_{25} Cluster and Optical Properties. *J. Am. Chem. Soc.* **2008**, *130*, 5883-5885.
4. Zhao, S.; Jin, R.; Jin, R., Opportunities and Challenges in CO_2 Reduction by Gold- and Silver-Based Electrocatalysts: From Bulk Metals to Nanoparticles and Atomically Precise Nanoclusters. *ACS Energy Lett.* **2018**, *3*, 452-462.
5. Alfonso, D. R.; Kauffman, D.; Matranga, C., Active sites of ligand-protected Au_{25} nanoparticle catalysts for CO_2 electroreduction to CO. *J. Chem. Phys.* **2016**, *144*, 184705.
6. Devadas, M. S.; Bairu, S.; Qian, H.; Sinn, E.; Jin, R.; Ramakrishna, G., Temperature-Dependent Optical Absorption Properties of Monolayer-Protected Au25 and Au38 Clusters. *J. Phys. Chem. Lett.* **2011**, *2*, 2752-2758.
7. Kauffman, D. R.; Alfonso, D.; Matranga, C.; Qian, H.; Jin, R., Experimental and Computational Investigation of Au_{25} Clusters and CO_2: A Unique Interaction and Enhanced Electrocatalytic Activity. *J. Am. Chem. Soc.* **2012**, *134*, 10237-10243.
8. Kang, X.; Chong, H.; Zhu, M., $Au_{25}(SR)_{18}$: the captain of the great nanocluster ship. *Nanoscale* **2018**, *10*, 10758-10834.
9. Fei, W.; Antonello, S.; Dainese, T.; Dolmella, A.; Lahtinen, M.; Rissanen, K.; Venzo, A.; Maran, F., Metal Doping of $Au_{25}(SR)_{18}^-$ Clusters: Insights and Hindsights. *J. Am. Chem. Soc.* **2019**, *141*, 16033-16045.
10. Fournier, J. A.; Wolk, A. B.; Johnson, M. A., Integration of Cryogenic Ion Vibrational Predissociation Spectroscopy with a Mass Spectrometric Interface to an Electrochemical Cell. *Anal. Chem.* **2013**, *85*, 7339-7344.

Studies of non-equilibrium high pressure kinetics at supercritical H2O/CO2 conditions using a new supercritical jet stirred reactor

PI: Yiguang Ju
Department of Mechanical and Aerospace Engineering, Princeton University, Princeton, NJ 08540
Email: yju@princeton.edu

Proposal scope: CO_2 emission from burning fossil fuels has caused increasing concerns about climate change. High pressure and low temperature advanced compression ignition engines using biofuels and supercritical CO_2 (S-CO_2) power cycles have a great potential for higher efficiency and lower carbon emissions. The objectives of this proposal is to develop a new, supercritical pressure jet stirred reactor (SP-JSR) operating up to 300 atm and to advance fundamental understanding of non-equilibrium chemical kinetics via the effects of strong intermolecular force, reactive multi-body reactions, non-equilibrium vibrational energy distribution, and the uncertainty of energy distribution due to collisional broadening on low temperature combustion and HO_2 chemistry with CO_2 and H_2O dilutions. Non-equilibrium effects via real gas intermolecular force, reactive termolecular reactions involving HO_2 and OH, vibrational non-equilibrium energy distribution, and collisional energy broadening at high pressure will be examined. Key HO_2 reactions with fuels and radicals will be studied by using microsecond time-resolved mid-IR Faraday rotation spectroscopy (FRS) and high-level quantum chemistry calculations. The obtained high pressure data and the newly measured and computed reaction rates will be used to develop and validate new high pressure combustion models by including non-equilibrium chemical kinetic effects. The present studies will advance the fundamental understanding of non-equilibrium chemical kinetics and HO_2 chemistry at extreme pressures.

What was accomplished under these goals?

1. **A supercritical pressure jet stirred reactor development**: A supercritical pressure jet stirred reactor (SP-JSR) was developed for high pressure kinetic studies up to 200 atm. SP-JSR is successfully used to examine the high pressure kinetics of small alkanes and oxygenated fuels.
2. **Low- and intermediate-temperature oxidation of dimethyl ether up to 100 atm:** The supercritical pressure jet-stirred reactor (SP-JSR) recently developed at Princeton provides a new platform for conducting kinetic studies at low and intermediate temperatures at extremely high pressures with a uniform temperature distribution and a short flow residence time. This paper uses the SP-JSR to investigate DME oxidation at equivalence ratios of 0.175, 1.0, and 1.72, for pressures of 10 and 100 atm, and temperatures ranging from 400 to 900 K. The results demonstrate weakened NTC behavior at 100 atm relative to 10 atm due to increased flux through $QOOH + O_2 = O_2QOOH$ relative to $QOOH = 2\ CH_2O + OH$ at 100 atm. Furthermore, the intermediate-temperature oxidation window is shifted to lower temperatures at 100 atm. The experimental data are compared with several chemical kinetic models from the literature. The existing models are seen to agree quite well with the experimental data at 10 atm. However, the models fail to properly capture the NTC behavior at 100 atm. Reaction pathway analyses indicate that both the low- and intermediate-temperature chemistries are controlled by RO_2 consumption pathways. The reaction rates for several of the important reactions, such as $DME + OH = CH_3OCH_2 + H_2O$, $H_2O_2\ (+M) = 2\ OH\ (+M)$, and $2\ HO_2 = 2\ OH + O_2$ are updated in this work. The updated model improves the predictability for all key species.
3. **Methanol oxidation up to 100 atm in a supercritical pressure jet-stirred reactor:** Methanol oxidation was studied by using the recently developed supercritical pressure jet-stirred reactor

(SP-JSR) at pressures of 10 and 100 atm, temperatures from 550 to 950 K, and equivalence ratios of 0.1, 1.0, and 9.0 in experiments and numerical simulations. The experimental results (Fig. 1) show that the onset temperature of CH_3OH oxidation at 100 atm is around 700 K, which is more than 100 K lower than the onset at 10 atm and this trend cannot be predicted by the existing kinetic models. Furthermore, negative temperature coefficient (NTC) behavior was clearly observed at 100 atm under fuel rich conditions. To understand the observed temperature shift in the reactivity and the NTC effect, we updated some key elementary reaction rates of relevance to high pressure CH_3OH oxidation from the literature and added some new low-temperature reaction pathways such as $CH_2O + HO_2 = HOCH_2O_2$ (RO_2), $RO_2 + RO_2 = HOCH_2O$ (RO) + $HOCH_2O$ (RO) + O_2, and $CH_3OH + RO_2 = CH_2OH + HOCH_2O_2H$ (ROOH). Although the model with these updates improves the prediction somewhat for the experimental data at 100 atm and reproduces well high-temperature ignition delay times and laminar flame speed data in the literature, discrepancies still exist for some aspects of the 100 atm low-temperature oxidation data. In addition, it was found that the pressure-dependent HO_2 chemistry shifts to lower temperature as the pressure increases such that the NTC effect at fuel-lean conditions is suppressed. Therefore, as shown in the experiments, the NTC phenomenon was only observed at the fuel-rich condition where the fuel radicals are abundant and the HO_2 chemistry at high pressure is weakened by the lack of oxygen and thus comparatively little HO_2 formation.

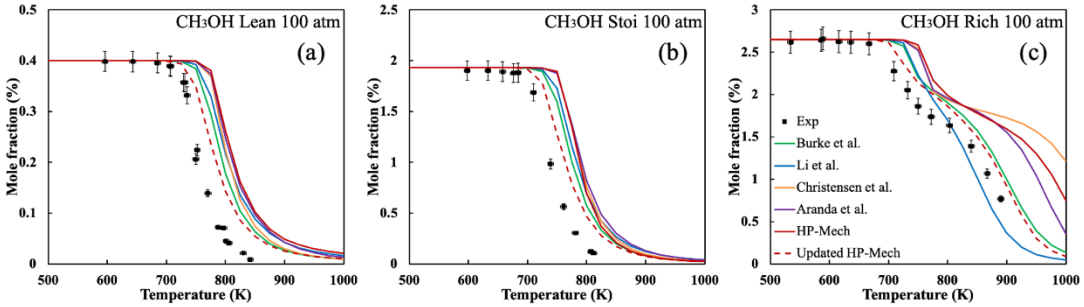

Fig. 1 Comparisons between predicted and measured temperature evolutions of CH_3OH oxidation at equivalence ratio of: (a) 0.1, (b) 1.0, and (c) 9.0 at 100 atm.

4. **Studies of low and intermediate temperature oxidation of propane up to 100 atm:** The low and intermediate temperature oxidation of propane has been investigated by using a novel supercritical pressure jet stirred reactor (SP-JSR) with and without 20% CO_2 additions at fuel lean and rich conditions at 10 and 100 atm and 500-1000 K. The mole fractions of C_3H_8, O_2, CO, CO_2, CH_2O, C_2H_4, CH_3CHO, and C_3H_6 are quantified by using a micro-gas chromatograph (μ-GC). The experiment shows that different from that of 10 atm, at 100 atm only a weak NTC behavior is observed because of the significant shift of the intermediate temperature HO_2 chemistry to lower temperature. In addition, at 100 atm, existing models in literatures can successfully capture the onset temperatures of the low and intermediate chemistry, while under-predict the fuel oxidation quantitatively and fail to capture the NTC behavior between 650-780 K at both fuel lean and rich conditions. Similar discrepancy was observed in studies of n-butane and DME oxidations in literatures, which implying that there exists a large uncertainty in hierarchy model development of fuels with low temperature chemistries at high pressures. Reaction pathways and sensitivity analyses show that RO_2 competing reactions through (P1) $RO_2 = QOOH$, (P2) $RO_2 = C_3H_6$

+ HO_2, (P3) RO_2 + CH_2O / HO_2 = RO_2H + HCO / O_2 dominate the low and intermediate temperature chemistries at 100 atm, which differ from the dominant pathway through QOOH consumption reactions at lower pressures. Especially, P3 is a new pathway of RO_2 consumption at high pressures, while is not observed in importance at low pressures. Special attention should be paid to the accurate computations of n-$C_3H_7O_2$ / i-$C_3H_7O_2$ + CH_2O and n-$C_3H_7O_2$ / i-$C_3H_7O_2$ + in the P3 pathway and n-$C_3H_7O_2$ / i-$C_3H_7O_2$ decomposition reactions in the P2 pathway at high pressures.

5. **Kinetics and Extinction of Non-premixed Cool and Warm Flames of Dimethyl Ether at Elevated Pressure**: Cool flame transition and extinction limits as well as oxygen concentration dependence at elevated pressures provide insights of the low-temperature and high-pressure fuel reactivity. A new experimental high-pressure counterflow burner platform was designed and developed to achieve the studies of high-pressure cool flames. Dimethyl ether (DME) was chosen to study its non-premixed cool flame in high-pressure counterflow burner at pressure up to 5 atm, perhaps for the first time. This paper investigates the effects of pressure on cool flame structure, extinction and transition limits, and oxygen concentration dependence as well as ozone assisted warm flames of DME in experiments and numerical simulations. The results show that the reignition transition from cool flame to hot flame occurs either with the decrease of the strain rate at a given fuel concentration and pressure or with the increase of fuel mole fraction or pressure at a given strain rate. Furthermore, it is shown that the higher pressure shifts the cool flame to higher strain rates and results in higher cool flame extinction strain rates. However, the existing kinetic model of DME fails in predicting the cool flame extinction limit at elevated pressures. Besides, the cool flame extinction limits are proportional to *n*th power of the oxygen concentration, $[O_2]^n$, and the increase of pressure leads to stronger extinction limit dependence (larger *n*) on oxygen concentration. The present experiment and detailed kinetic analysis show clearly that increasing pressure promotes the low-temperature chemistry including the oxygen addition reactions. In addition, stable warm flame was first experimentally observed by using DME at elevated pressure with ozone sensitization.

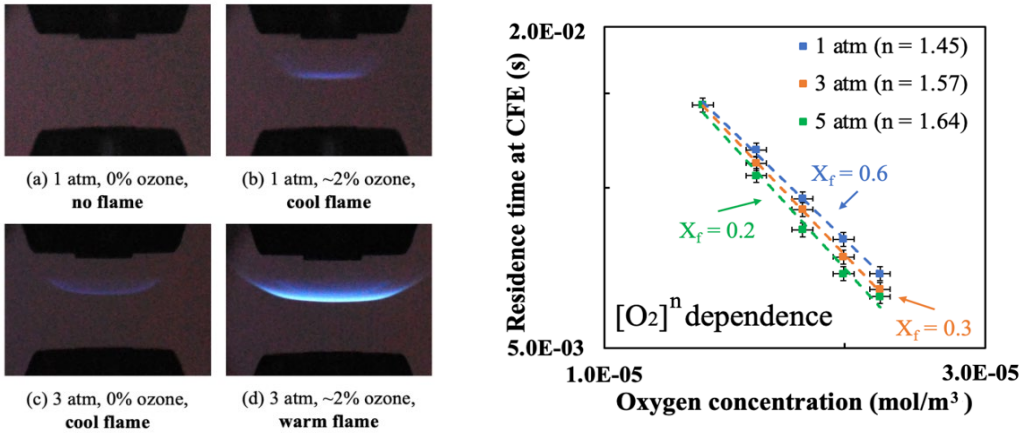

Fig. 2. Left: Non-premixed DME cool and warm flame images with fuel mole fraction of 0.3 and at 1 and 3 atm. The images were taken using a f/2.8 lens aperture with 2 s exposure time. Right: Measured non-premixed DME cool flame residence time at extinction versus oxygen concentration for different pressures

Training opportunities

The research provides opportunities for career training of two graduate students and two postdocs to conduct high pressure low temperature combustion and kinetic studies. In addition, it gives an opportunity for them to have a join mentoring in collaboration with two top chemistry theorists, Drs. Ahren Jasper and Stephen Klippenstein, at Argonne National Laboratory.

Publications:

[1] H. Zhao, C. Yan, T. Zhang, G. Ma, M.J. Souza, C.-W. Zhou, Y. Ju, Studies of high-pressure n-butane oxidation with CO2 dilution up to 100 atm using a supercritical-pressure jet-stirred reactor, **Proceedings of Combustion Insittute** 38 (2021) 279–287.

[2] Mengni Zhou, Omar R. Yehia, Wenbin Xu, Christopher B. Reuter, Ziyu Wang, Chao Yan, Bo Jiang, Yiguang Ju, The radical index and the effect of oxygen concentration on non-premixed cool flame extinction of large n-alkanes, **Combustion and Flame**, 231 (2021) 111471.

[3] Ju, Y., 2021. Understanding cool flames and warm flames. Proceedings of the Combustion Institute, 38(1), pp.83-119.

[4] Chao Yan, Hao Zhao, Ziyu Wang, Guohui Song, Ying Lin, Clayton R. Mulvihill, Ahren W. Jasper, Stephen J. Klippenstein, Yiguang Ju, Low- and intermediate-temperature oxidation of dimethyl ether up to 100 atm in a supercritical pressure jet-stirred reactor, **Combustion and Flame**, 2022, 112059. https://doi.org/10.1016/j.combustflame.2022.112059

[5] Ziyu Wang, Chao Yan, Ying Lin, Mengni Zhou, Bo Jiang, Ning Liu, Hongtao Zhong, Yiguang Ju, Kinetics and Extinction of Non-premixed Cool and Warm Flames of Dimethyl Ether at Elevated Pressure, **39th Intenational Combustion Symposium**, accepted, 2022

[6] Ziyu Wang, Hao Zhao, Chao Yan, Ying Lin, Aditya D. Lele, Wenbin Xu, Brandon Rotavera, Ahren W. Jasper, Stephen J. Klippenstein, Yiguang Ju, Methanol oxidation up to 100 atm in a supercritical pressure jet-stirred reactor, **39th Intenational Combustion Symposium**, accepted, 2022.

[7] Hao Zhao, Chao Yan, Guohui Song, Ziyu Wang, Yiguang Ju, Studies of low and intermediate temperature oxidation of propane up to 100 atm in a supercritical-pressure jet-stirred reactor, **39th Intenational Combustion Symposium**, accepted, 2022.

Future work

1. Publish the work of high pressure low temperature oxidation of H2 and CH4.
2. Conduct the high pressure oxidation of higher ethers.
3. Study the effect of real gas in kinetic modeling of liquid fuels

Technical Impacts

1. extended the JSR studies to 100 atm or higher and created a new platform for kinetic studies at extreme pressure.
2. demonstrated that the competition of HO2 chemistry and with low temperature chemistry suppressed the negative temperature coefficient effect.
3. demonstrate for the first time that methanol has low temperature chemistry at 100 atm.

DoE Impacts

1. Understanding the low temperature fuel oxidation under engine conditions.
2. Helped to design advanced engines with low carbon emissions.
3. Contributed to the development of biofuels

Probing the Reaction Dynamics of Hydrogen-Deficient Hydrocarbon Molecules and Radical Intermediates via Crossed Molecular Beams

Ralf I. Kaiser
Department of Chemistry, University of Hawai'i at Manoa, Honolulu, HI 96822
ralfk@hawaii.edu

1. Program Scope

The major goals of this project are to explore experimentally by exploiting molecular beams to study the fundamental reaction dynamics and underlying potential energy surfaces (PESs) of hydrocarbon molecules and their corresponding (resonantly free stabilized and aromatic) radical precursors, which are relevant to the formation and molecular growth of polycyclic aromatic hydrocarbons (PAHs). *First*, reactions are initiated in a crossed molecular beams machine under single collision conditions by crossing two supersonic reactant beams containing radicals and/or closed shell species under a well-defined collision energy and intersection angle. By recording angular-resolved time of flight (TOF) spectra, we obtain information on the reaction products, intermediates involved, branching ratios of competing reaction channels, reaction energetics, and on the underlying reaction mechanisms. *Second*, in collaboration with Dr. Musahid Ahmed (Chemical Sciences Division, Lawrence Berkeley Laboratory), reactions are carried out in a chemical reactor at well characterized pressure and temperature distributions with reaction products interrogated isomer-selectively by tunable vacuum ultraviolet light (VUV) via photoionization (PI) coupled with a reflectron time of flight mass spectrometer (ReTOFMS). Merged with electronic structure calculations (Prof. Alexander M. Mebel, Florida International University), these data are of fundamental importance to comprehend the underlying formation mechanisms of two key classes of molecules involved in molecular mass-growth processes leading to carbonaceous nanostructures from the bottom up: resonantly stabilized free radicals (RSFRs) and polycyclic aromatic hydrocarbons.

2. Recent Progress

First, we elucidated fundamental molecular mass growth processes leading to the formation of (polycyclic) aromatic hydrocarbons carrying up to three six-membered rings: benzene (1), naphthalene (2), phenanthrene (3), and anthracene (4) (Figure 1) via recombination of resonantly stabilized free radicals (RSFR): propargyl (C_3H_3), cyclopentadienyl (C_5H_5), benzyl (C_7H_7), 1-indenyl (C_9H_7)) [**P25, 26, P30, P31**]. A key finding is the elucidation of an isomer-selective synthesis driven by discrete, spin-dictated mechanisms. The formation of phenanthrene ($C_{14}H_{10}$ (3)) is initiated through a classical barrierless radical-radical recombination of two benzyl radicals with radical centers at the exocyclic methylene (CH_2) moiety on the singlet ground state surface. However, formation of anthracene ($C_{14}H_{10}$ (4)) commences unconventionally on the excited state triplet surface (a^3A) through [3+3] cycloaddition involving a transition state with a cyclic arrangement of the atoms in a six-membered ring along with a reorganization of σ and π bonds via excited-state dynamics initiated by a single collision. The excited-state dynamics leading eventually to anthracene ($C_{14}H_{10}$ (4)) defy conventional wisdom that PAH formation via radical-radical reactions solely takes place on electronic ground state (singlet) surfaces via initial recombination of the doublet reactants at their radical centers. The facile formation of anthracene via excited-state dynamics on the triplet surface through cycloaddition as showcased here presents a fundamental shift in currently "accepted" views and opens up the door for a more "rapid" synthesis of aromatic, multi-ringed structures such as three-ring PAHs from mono-ringed radical precursors at high-temperature conditions relevant to combustion and deep space. It further delivers a strategy to explore chemical reactions of aromatic and resonantly stabilized free radicals under high temperature environments of relevance to synthetic and materials chemistry leading eventually to carbonaceous nanostructures like fullerenes, nanocages, and nanotubes. *Second*, we provided testimony on a facile formation of discrete acyclic isomers of cyclopentadiene (C_5H_6) – a fundamental molecular building block required to 'bend' PAHs such as corannulene ($C_{20}H_{10}$, **P24**) out of plane - via crossed molecular beam studies of methylidyne (CH) and ethynyl (C_2H) radicals; in combustion systems, these isomers can be converted to the thermodynamically most stable cyclopentadiene (C_5H_6) isomer through hydrogen assisted isomerization pathways [**P23, P28, P29, P32**].

3. Future Plans

First, we are expanding our radical- radical reactions (RRR) exploiting C3-C9 radical reactants to discover new pathways leading to PAHs carrying up to five rings. *Second*, we will work toward a better understanding of reaction mechanisms leading eventually to coronene ($C_{24}H_{12}$) – a fundamental molecular building block of two-dimensional PAHS and graphene nanosheets – involving Hydrogen Abstraction – C_2H_2 (acetylene) Addition (HACA), Hydrogen Abstraction – Vinylacetylene Addition (HAVA), and Phenyl Addition – DehydroCyclization (PAC). *Finally*, crossed molecular beam experiments will be carried out to explore the energetics, dynamics, and potential energy surfaces (PESs) of reactions of key resonantly stabilized free radicals (RSFR) with closed shell hydrocarbons to form three prototype aromatic molecules in the gas phase under single collision conditions: monocyclic aromatics (benzene, C_6H_6), bicyclic aromatics carrying two six-membered rings (naphthalene; $C_{10}H_8$), and bicyclic aromatics carrying one six- and one five-membered ring (indene; C_9H_8).

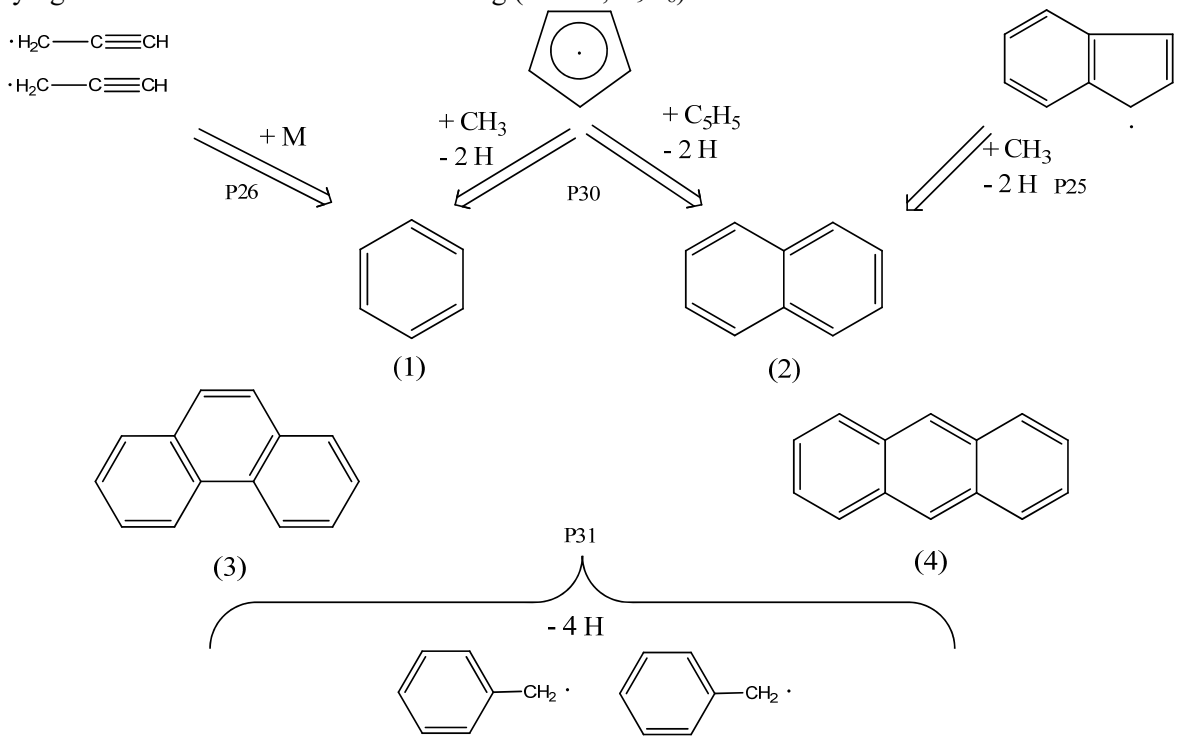

Fig. 1: Elucidated pathways to aromatic hydrocarbons carrying one, two, and three six-membered rings (benzene (1), naphthalene (2), phenanthrene (3), anthracene (4)) via radical – radical reactions of resonantly stabilized free radicals (RSFRs) (propargyl (C_3H_3), cyclopentadienyl (C_5H_5), benzyl (C_7H_7), 1-indenyl (C_9H_7)) exploiting molecular beams [**P25, 26, P30, P31**].

4. Acknowledgements

This work is supported by US Department of Energy (Basic Energy Sciences; DE-FG02-03-ER15411).

5. Publications Acknowledging DE-FG02-03ER15411 (6/2019 – now)

1 L. Zhao, R. I. Kaiser, B. Xu, U. Ablikim, W. Lu, M. Ahmed, M. M. Evseev, E. K. Bashkirov, V. N. Azyazov, A. H. Howlader, S. F. Wnuk, A. M. Mebel, Gas-Phase Synthesis of Triphenylene ($C_{18}H_{12}$), ChemPhysChem 20, 791-797 (2019).

2 L. Zhao, R. I. Kaiser, B. Xu, U. Ablikim, W. Lu, M. Ahmed, M. M. Evseev, E. K. Bashkirov, V. N. Azyazov, M. V. Zagidullin, A. N. Morozov, A. H. Howlader, S. F. Wnuk, A. M. Mebel, D. Joshi, G. Veber, F. R. Fischer, Gas Phase Synthesis of [4]-Helicene, Nat. Commun. 10, 1510 (2019).

3 A. M. Thomas, C. He, L. Zhao, G. R. Galimova, A. M. Mebel, R. I. Kaiser, Combined Experimental and Computational Study on the Reaction Dynamics of the 1-Propynyl (CH_3CC)-1,3-Butadiene

($CH_2CHCHCH_2$) System and the Formation of Toluene under Single Collision Conditions, J. Phys. Chem. A (H. Reisler Special Issue) 123, 4104-4118 (2019).

4 L. Zhao, M. B. Prendergast, R. I. Kaiser, B. Xu, W. Lu, U. Ablikim, M. Ahmed, A. D. Oleinikov, V. N. Azyazov, A. M. Mebel, A. H. Howlader, S. F. Wnuk, Reactivity of the Indenyl Radical (C_9H_7) with Acetylene (C_2H_2) and Vinylacetylene (C_4H_4), ChemPhysChem 20, 1437-1447 (2019).

5 C. He, L. Zhao, A. M. Thomas, A. N. Morozov, A. M. Mebel, R. I. Kaiser, Elucidating the Chemical Dynamics of the Elementary Reactions of the 1-Propynyl Radical (CH_3CC; X^2A_1) with Methylacetylene (H_3CCCH; X^1A_1) and Allene (H_2CCCH_2; X^1A_1), J. Phys. Chem. A. 123, 5446-5462 (2019).

6 L. Zhao, M. Prendergast, R. I. Kaiser, B. Xu, U. Ablikim, W. Lu, M. Ahmed, A. D. Oleinikov, V. N. Azyazov, A. H. Howlader, S. F. Wnuk, A. M. Mebel, How to Add a Five-Membered Ring to Polycyclic Aromatic Hydrocarbons (PAHs) – Molecular Mass Growth of the 2-Naphthyl Radical ($C_{10}H_7$) to Benzindenes ($C_{13}H_{10}$) as a Case Study, Phys. Chem. Chem. Phys. 21**,** 16737-16750 (2019).

7 C. He, A. M. Thomas, G. R. Galimova, A. M. Mebel, R. I. Kaiser, Gas Phase Formation of the Interstellar Molecule Methyltriacetylene, ChemPhysChem 20, 1912-1917 (2019).

8 L. Zhao, R. I. Kaiser, W. Lu, B. Xu, M. Ahmed, A. N. Morozov, A. M. Mebel, A. H. Howlader, S. F. Wnuk, Molecular Mass Growth through Ring Expansion in Polycyclic Aromatic Hydrocarbons via Radical-Radical Reactions, Nat. Commun. 10, 3689 (2019).

9 A. M. Thomas, L. Zhao, C. He, G. R. Galimova, A. M. Mebel, Directed Gas-Phase Synthesis of Triafulvene under Single-Collision Conditions, Angew. Chem. Int. Ed. 58, 15488 (2019).

10 C. He, L. Zhao, A. M. Thomas, G. R. Galimova, A. M. Mebel, R. I. Kaiser, A Combined Experimental and Computational Study on the Reaction Dynamics of the 1-Propynyl Radical (CH_3CC; X^2A_1) with Ethylene (H_2CCH_2; X^1A_{1g}) and the Formation of 1-Penten-3-yne ($CH_2CHCCCH_3$; X^1A'), Phys. Chem. Chem. Phys. 21, 22308 (2019).

11 L. Zhao, M. Prendergast, R. I. Kaiser, B. Xu, U. Ablikim, M. Ahmed, B.-J. Sun, Y.-L. Chen, A. H. H. Chang, R. K Mohamed, F. R. Fischer, Synthesis of Polycyclic Aromatic Hydrocarbons by Phenyl Addition–Dehydrocyclization: The Third Way, Angew. Chem. Int. Ed. 58, 17442 (2019).

12 A. M. Thomas, S. Doddipatla, R. I. Kaiser, G. R. Galimova, A. M. Mebel, A Barrierless Pathway Accessing the C_9H_9 and C_9H_8 Potential Energy Surfaces via the Elementary Reaction of Benzene with 1-Propynyl, Sci. Rep. (Special Issue Molecular Reaction Dynamics) 9, 17595 (2019).

13 C. He, A. M. Thomas, G. R. Galimova, A. M. Mebel, R. I. Kaiser, Gas-Phase Formation of 1-Methylcyclopropene and 3-Methylcyclopropene via the Reaction of the Methylidyne Radical (CH; $X^2\Pi$) with Propylene (CH_3CHCH_2; X^1A'), J. Phys. Chem. A 123, 10543-10555 (2019).

14 C. He, A. M. Thomas, G. R. Galimova, A. N. Morozov, A. M. Mebel, R. I. Kaiser, Gas-Phase Formation of Fulvenallene (C_7H_6) via the Jahn-Teller Distorted Tropyl (C_7H_7) Radical Intermediate under Single-Collision Conditions, J. Am. Chem. Soc. 142, 3205-3213 (2020).

15 L. Zhao, R. I. Kaiser, B. Xu, U. Ablikim, M. Ahmed, M. M. Evseev, E. K. Bashkirov, V. N. Azyazov, A. M. Mebel, A Unified Mechanism on the Formation of Acenes, Helicenes, and Phenacenes in the Gas Phase, Angew. Chem. Int. Ed. 59, 4051-4058 (2020).

16 C. He, L. Zhao, S. Doddipatla, A. M. Thomas, A. A. Nikolayev, G. R. Galimova, V. N. Azyazov, A. M. Mebel, R. I. Kaiser, Gas-Phase Synthesis of 3-Vinylcyclopropene via the Crossed Beam Reaction of the Methylidyne Radical (CH; $X^2\Pi$) with 1,3-Butadiene ($CH_2CHCHCH_2$; X^1A_g), ChemPhysChem 21, 1295-1309 (2020).

17 L. Zhao, R. I. Kaiser, W. Lu, M. Ahmed, M. M. Evseev, E. K. Bashkirov, V. N. Azyazov, C. Tönshoff, F. Reicherter, H. F. Bettinger, A. M. Mebel, A Free Radical Prompted Barrierless Gas-Phase Synthesis of Pentacene, Angew. Chem. Int. Ed. 59, 11334-11338 (2020).

18 L. Zhao, R. I. Kaiser, W. Lu, M. Ahmed, A. D. Oleinikov, V. N. Azyazov, A. M. Mebel, A. H. Howlader, S. F. Wnuk, Gas Phase Formation of Phenalene via 10π-Aromatic, Resonantly Stabilized Free Radical Intermediates, Phys. Chem. Chem. Phys. 22, 15381-15388 (2020).

19 L. Zhao, R. I. Kaiser, W. Lu, O. Kostko, M. Ahmed, M. M. Evseev, E. K. Bashikirov, A. D. Oleinikov, V. N. Azyazov, A. M. Mebel, A. H. Howlader, S. F. Wnuk, Gas Phase Formation of Cyclopentanaphthalene (Benzindene) Isomers via Reactions of 5- and 6-Indenyl Radicals with Vinylacetylene, Phys. Chem. Chem. Phys. 22, 22493-22500 (2020).

20 A. H. Howlader, K. Diaz, A. M. Mebel, R. I. Kaiser, S. F. Wnuk, Iodoindenes: Synthesis and Application to Cross-Coupling, Tetrahedron Lett., 61, 152427 (2020).

21 C. He, G. R. Galimova, Y. Luo, L. Zhao, A. K. Eckhardt, R. Sun, A. M. Mebel, R. I. Kaiser, A Chemical Dynamics Study on the Gas-Phase Formation of Triplet and Singlet C_5H_2 Carbenes, Proc. Natl. Acad. Sci. U.S.A. 117, 30142-30150 (2020).

22 S. Doddipatla, G. R. Galimova, H. Wei, A. M. Thomas, C. He, Z. Yang, A. N. Morozov, C. N. Shingledecker, A. M. Mebel, R. I. Kaiser, Low-Temperature Gas-Phase Formation of Indene in the Interstellar Medium, Sci. Adv. 7, eabd4044 (2021).

23 C. He, A. A. Nikolayev, L. Zhao, A. M. Thomas, S. Doddipatla, G. R. Galimova, V. N. Azyazov, A. M. Mebel, R. I. Kaiser, Gas-Phase Formation of C_5H_6 Isomers via the Crossed Molecular Beam Reaction of the Methylidyne Radical (CH; $X^2\Pi$) with 1,2-Butadiene (CH_3CHCCH_2; X^1A'), J. Phys. Chem. A 125, 126-138 (2021).

24 L. Zhao, S. Doddipatla, R. I. Kaiser, W. Lu, O. Kostko, M. Ahmed, L. B. Tuli, A. N. Morozov, A. H. Howlader, S. F. Wnuk, A. M. Mebel, V. N. Azyazov, R. K. Mohamed, F. R. Fischer, Gas-Phase Synthesis of Corannulene - A Molecular Building Block of Fullerenes, Phys. Chem. Chem. Phys. 23, 5740-5749 (2021).

25 R. I. Kaiser, N. Hansen, An Aromatic Universe–A Physical Chemistry Perspective, J. Phys. Chem. A Invited Perspective 125, 3826-3840 (2021).

26 L. Zhao, W. Lu, M. Ahmed, M. V. Zagidullin, V. N. Azyazov, A. N. Morozov, A. M. Mebel, R. I. Kaiser, Gas-Phase Synthesis of Benzene via the Propargyl Radical Self-Reaction, Sci. Adv. 7, eabf0360 (2021).

27 L. Zhao, M. Prendergast, R. I. Kaiser, B. Xu, W. Lu, M. Ahmed, A. H. Howlader, S. F. Wnuk, A. S. Korotchenko, M. M. Evseev, E. K. Bashkirov, V. N. Azyazovde, A. M. Mebel, A Molecular Beam and Computational Study on the Barrierless Gas Phase Formation of (Iso)quinoline in Low Temperature Extraterrestrial Environments, Phys. Chem. Chem. Phys. 23, 18495 (2021).

28 A. A. Nikolayev, V. N. Azyazov, R. I. Kaiser, A. M. Mebel, Theoretical Study of the Reaction of the Methylidyne Radical (CH; $X^2\Pi$) with 1-Butyne (CH_3CH_2CCH; X^1A'), J. Phys. Chem. A 125, 9536-9547 (2021).

29 C. He, K. Fujioka, A. A. Nikolayev, L. Zhao, S. Doddipatla, V. N. Azyazov, A. M. Mebel, R. Sun, R. I. Kaiser, A Chemical Dynamics Study of the Reaction of the Methylidyne Radicals (CH, $X^2\Pi$) with Dimethylacetylene (CH_3CCCH_3, X^1A_{1g}), Phys. Chem. Chem. Phys. 24, 578-593 (2022).

30 R. I. Kaiser, L. Zhao, W. Lu, M. Ahmed, M. V. Zagidullin, V. N. Azyazov, A. M. Mebel, Formation of Benzene and Naphthalene through Cyclopentadienyl-Mediated Radical−Radical Reactions, J. Phys. Chem. Lett. 13, 208–213 (2022).

31 R. I. Kaiser, L. Zhao, W. Lu, M. Ahmed, V. S. Krasnoukhov, V. N. Azyazov, A. M. Mebel, Unconventional Excited-State Dynamics in the Concerted Benzyl (C_7H_7) Radical Self-Reaction to Anthracene ($C_{14}H_{10}$), Nat. Commun. 13, 786 (2022).

32 S. J. Goettl, C. He, D. Paul, A. A. Nikolavev, V. N. Azyazov, A. M. Mebel, R. I. Kaiser, Gas-Phase Study of the Elementary Reaction of the D1-Ethynyl Radical (C_2D; $X^2\Sigma^+$) with Propylene (C_3H_6; X^1A') Under Single-Collision Conditions, J. Phys. Chem. A 126, 1889–1898 (2022).

MECHANISTIC INVESTIGATIONS OF GAS-PHASE AND SURFACE-MEDIATED OXIDATIVE COUPLING REACTIONS

Coleman Kronawitter and Ambarish Kulkarni

Department of Chemical Engineering, University of California, Davis

One Shields Ave, Davis, CA 95616

ckrona@ucdavis.edu, arkulkarni@ucdavis.edu

PROGRAM SCOPE

In heterogeneous catalytic systems for chemical synthesis and energy conversion, the solid surface plays an essential role in controlling reaction kinetics, and as a result, the vast majority of mechanistic investigation in this field is dedicated to the characterization of surface events. However, it is known that for many reaction classes and system conditions, gas phase events critically influence reaction outcomes, as well as dictate the nature of events occurring on surfaces through gas-surface species exchange.

A core objective of this project is to develop and implement an integrated experiment-theory approach to provide new insights into the interconnected roles of the surface and the near-surface gas phase in heterogeneous catalytic oxidative coupling reactions. This work is enabled by use of:

(1) New research technologies, originally developed for the field of combustion science, which through recent adaptation now facilitate interrogation of the local, near-surface gas phase above catalyst surfaces in *operando* conditions.

(2) Site-isolated supported metal catalysts (often atomically dispersed), comprehensively characterized to define active sites and minimize site heterogeneity over length scales of experimental interrogation.

(3) DFT models to understand the site-isolated catalysts of (2) and microkinetic models to interpret reaction results from (1) and (2), deriving relationships between specific active site structures and local reaction outcomes.

Efforts focus on two reactions: (i) the oxidative coupling of methane (OCM), a high-temperature reaction, which, for the most-studied catalysts relies heavily on the gas-phase coupling of radicals for ethylene production; and (ii) the oxidative coupling of methanol-derived oxygenates (sometimes referred to as methanol coupling for brevity), which involves critical transformations for production of valuable commodity chemicals.

This project strives to bring clarity to the relationship between active site structures on surfaces and the composition of species in the near-surface gas phase during these reactions. Catalysts with low levels of site heterogeneity are critical to connect specific sites with product/intermediate distributions. For this reason, we develop new atomically-dispersed supported metal catalysts, which are comprehensively characterized through spectroscopy, microscopy, and computational modeling.

RECENT PROGRESS

Characterization of the near-surface gas-phase during oxidative methanol conversion

Through collaboration with Sandia National Laboratories' Combustion Research Facility (SNL-CRF), this project utilizes, among others, near-surface time-of-flight molecular beam mass spectrometry (near-surface MBMS) as a primary tool for interrogation of gas phase composition above working catalysts.

Investigation of methanol oxidation with Pd-based catalysts and the identification and study of the elusive intermediate methoxymethanol

We have used near-surface MBMS to examine the oxidative conversion of methanol for a number of catalyst material systems. Our initial work, in collaboration with SNL-CRF [*ACS Catalysis*, **2021**, 11, 155−168], focused on Ag – a common catalyst for formaldehyde production by oxidative dehydrogenation of methanol. Next, we used Pd-based catalysts, which are commonly studied for production of C_{2+} building-

block chemicals, including methyl formate and dimethoxymethane. In these extensive efforts, we measured the near-surface gas phase composition as a function of temperature and reactant feed ratio during methanol oxidation for Pd, Au, AuPd, Au_2Pd, and $AuPd_2$ catalysts.

One of the most notable outcomes of this work with Pd-based catalysts has been the identification and study of methoxymethanol as an elusive near-surface gas-phase intermediate during methanol oxidation; this work has recently resulted in a publication [*J. Phys. Chem. Lett.*, **2021**, 12, 11252–11258.]. Representative mass spectrometry data that led to the discovery that methoxymethanol is a near-surface gas-phase intermediate is provided in Figure 1.

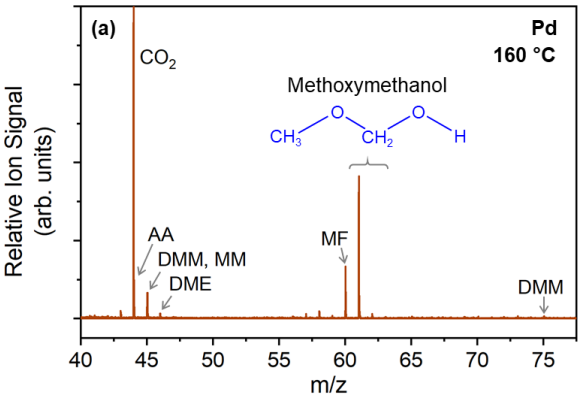

Figure 1. Near-surface molecular beam mass spectrometry results associated with methanol oxidation over polycrystalline Pd. Representative mass spectrum (m/z = 40−77.5) and corresponding neutral species recorded during catalysis at 160 °C. P = 600 Torr. From *J. Phys. Chem. Lett.*, **2021**, 12, 11252–11258.

We analyzed the integrated intensity of the peak at m/z = 61 – a fragment ion ($C_2H_5O_2^+$) from dissociative ionization of methoxymethanol – which is proportional to concentration, in various conditions (temperatures and reactant feed ratios). This facilitated interpretation of the reaction system in the context of concurrently generated products. Figure 2 provides the temperature dependence of the integrated signals for methoxymethanol, carbon dioxide, methyl formate, and dimethoxymethane for three different methanol/oxygen feed ratios. In analyzing this data, we also sought to make our methodology more quantitative. To this end, we calibrated the system's detection sensitivity for each species for which one can obtain a pure reference sample (CO_2, methyl formate, and dimethoxymethane). These calibrated species are in quantitative ratio to one another – i.e., ratios represent product mole fraction ratios. Unfortunately, no reference sample of methoxymethanol is available, and therefore methoxymethanol signals cannot be calibrated in this way. However, relative changes of methoxymethanol signals with temperature and feed ratio are meaningful.

The top of Figure 3 provides an overview of the chemical species observed in the near-surface region, placed in the context of the primary chemical steps likely applicable to this catalytic system. In supplementary efforts to understand this reaction system and the role of methoxymethanol, we performed calculations using density functional theory to examine the energetic feasibility of key steps (those highlighted in yellow) on Pd(111) surfaces.

The bottom of Figure 3 depicts the change in Gibbs free energy over the reaction coordinate for key steps from the initial state of a Pd(111) surface with adsorbed HCHO* and CH_3O*. Surface coupling occurs through interaction of the

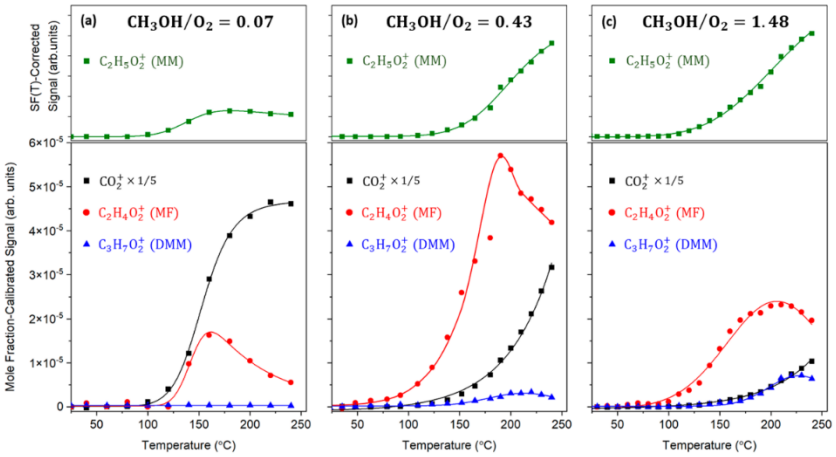

Figure 2. Temperature dependences of signals for methoxymethanol, CO_2, MF, and DMM during oxidative conversion of methanol over Pd. P = 600 Torr; sampling nozzle located 500 μm above the surface. Results for three reactant feed ratios (CH_3OH/O_2) are provided: (a) 0.07, (b) 0.43, and (c) 1.48. From *J. Phys. Chem. Lett.*, **2021**, 12, 11252–11258.

electron-dense oxygen in CH_3O* and the electron-deficient carbon in HCHO*, which results in CH_3OCH_2O*. Dehydrogenation of both CH_3OCH_2O* and methoxymethanol has been invoked for the production of MF. Dehydrogenation of CH_3OCH_2O* to MF is presumed to occur here oxidatively through abstraction by O* because it has been shown that chemisorbed oxygen plays a crucial role in MF generation over supported and unsupported Pd. We presume the formation of methoxymethanol from CH_3OCH_2O* originates from hydrogenation by nearby H* species; other hydrogenation pathways may be possible but were not considered in this study. Overall, these results imply that desorption of methoxymethanol is feasible in the experimental conditions.

We also continue to develop DFT-derived microkinetic models, with the goal of modeling reactions with combined surface-mediated and gas-phase steps. Through these efforts, we aim to analyze reaction networks based on the universal detection of species afforded by MBMS.

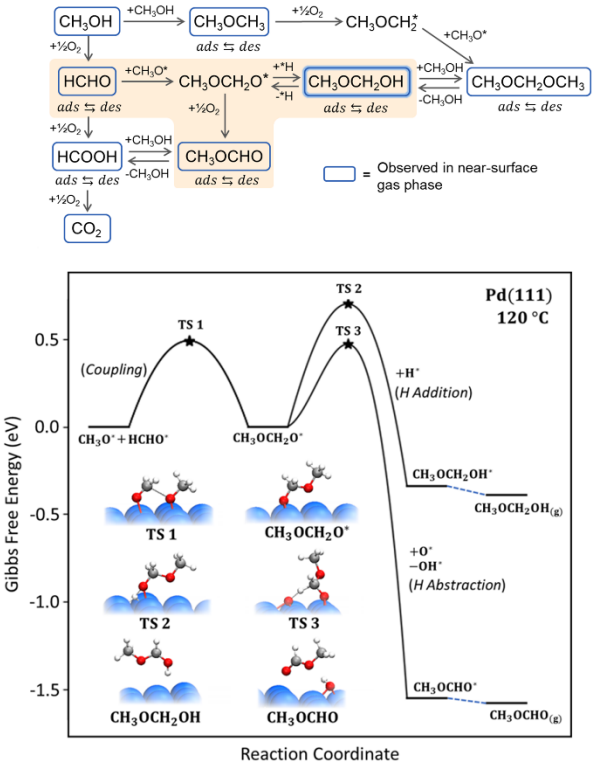

Figure 3. Top: Overview of species observed in the near-surface gas phase over Pd catalysts Bottom: DFT-calculated Gibbs free energy change over the reaction coordinate for formation of methoxymethanol and methyl formate through coupling of adsorbed methoxy and formaldehyde. From *J. Phys. Chem. Lett.*, **2021**, 12, 11252–11258.

<u>*Operando* detection of surface-bound species</u>

We use *operando* diffuse reflectance FTIR (DRIFTS) to probe the steady-state composition of surface-bound species during reaction. We have so far recorded measurements of adsorbates associated with methanol oxidation over Pd supported on MgO, in both a highly oxidized state (containing Pd(II), identified to be PdO) and a reduced state (containing both Pd(II) and Pd(0)). The goal here is to correlate surface-bound species with the near-surface gas phase composition measured by MBMS. This is accomplished by pressing the catalyst powder into a dense wafer, which is then used in a stagnation flow configuration. Analysis of these data sets is ongoing, and so far we have made a number of new insights into the connections between the surface and near-surface gas phase compositions during methanol oxidation with this prototypical catalyst.

Atomically dispersed catalysts and their characterization using DFT-based interpretation of X-ray absorption spectroscopy data

To develop new structure-function relationships for coupling reactions that directly connect the near-surface gas phase composition to specific reaction centers, we aim to use oxide-supported transition metal (TM) catalysts with highly dispersed (often atomically dispersed), active sites. We use MgO as a support – its simple cubic structure, irreducibility, and characterizable surface hydroxylation make it valuable for both synthesis and fundamental studies.

In work for this project, we have developed and use a systematic, theory-led workflow for characterization of atomically dispersed catalysts. Our approach combines state-of-the-art characterization techniques (e.g., microscopy – high-angle annular dark field scanning transmission electron microscopy (HAADF-STEM) and X-ray absorption spectroscopy – extended X-ray absorption fine structure (EXAFS) and high-energy resolution fluorescence detection (HERFD-XANES) with large-scale DFT calculations and automated analyses to positively identify the local environment for atomically dispersed catalysts. The work in this

aspect of the project has been conducted in collaboration with Bruce Gates (UC Davis) and Simon Bare (SLAC National Accelerator Lab). We focused initially on atomically dispersed Pt cations supported by MgO. To the best of our knowledge, these studies represent the first examples of a well-characterized sub-surface platinum cation stabilized within an MgO lattice.

The first impactful outcome of this work involved the synthesis of a material consisting of atomically dispersed cationic Pt in the subsurface of MgO. The atomic-scale structure of the site catalytically active for CO oxidation was characterized extensively; this resulted in a publication [*J. Am. Chem. Soc.*, **2021**, 143, 20144–20156]. An essential aspect of this work was the DFT-based fitting procedure to interpret X-ray absorption data (especially extended X-ray absorption fine structure (EXAFS)), which involves

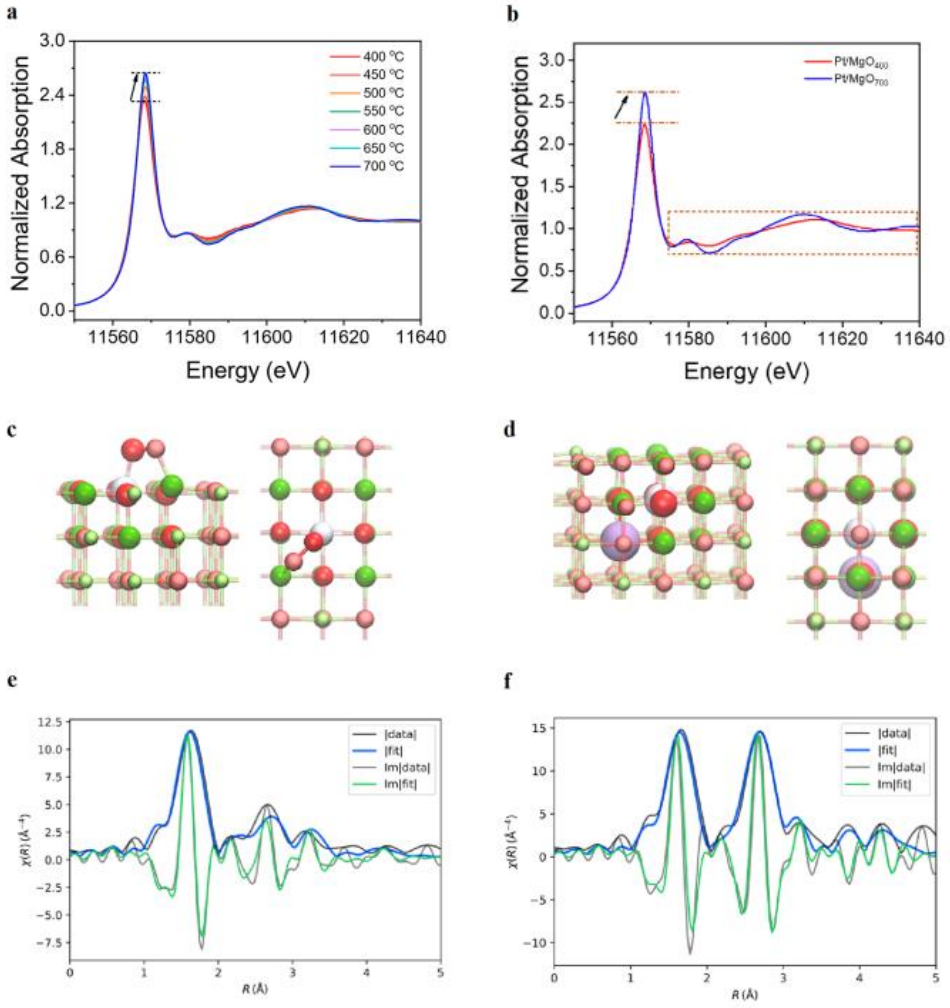

Figure 4. (a) Conventional XANES spectra characterizing Pt/MgO at various temperatures, representing structural changes taking place during calcination. (b) XANES spectra characterizing Pt/MgO_{400} and Pt/MgO_{700}, each in helium flowing at 20 mL(NTP)/min at room temperature. The DFT-optimized geometries of the most stable (c) surface structure: [100]/sub0/*O_2 side view and top view and (d) subsurface structure $[100]^{Mg\text{-}vac}$/sub1 side view and top view. EXAFS spectra characterizing (e) Pt/MgO_{400} and (f) Pt/MgO_{700} in helium flowing at 20 mL (NTP)/min at room temperature in R-space (k^3-weighted) with the corresponding EXAFS fits based on [100]/sub0/*O_2 and $[100]^{Mg\text{-}vac}$/sub1 structures, respectively, showing the magnitude (fit: blue; experiment: black) and imaginary portions (fit: green; experiment: black) of Fourier transforms of the data. From *J. Phys. Chem. Lett.*, **2022**, 13, 3896–3903.

development of a library of DFT-optimized structures and use of these structures to fit the governing EXAFS equations (see details in *J. Am. Chem. Soc.*, **2021**, 143, 20144–20156; this developed fitting procedure is referred to as *QuantEXAFS*). This study combined EXAFS, high energy resolution fluorescence detection X-ray absorption near edge structure ((HERFD)-XANES), atomic-resolution STEM imaging, and CO oxidation catalysis studies to characterize the active site with unprecedented clarity.

Another recent study of the Pt/MgO system involved contrasting the structure and catalytic activity of atomically dispersed cationic Pt in two different sites on the MgO support; this work resulted in a publication (*J. Phys. Chem. Lett.*, **2022**, 13, 3896–3903). Specifically, cationic Pt located on the surface was contrasted with the Pt located in the subsurface, as in the article referenced above. In addition, the DFT-based fitting procedure described above (QuantEXAFS) was successfully applied to develop an understanding of the contrasting atomic-scale structure of these Pt-MgO sites.

Representative data from this study is provided in Figure 4. Figure 4a,b provides conventional Pt L-edge XANES spectra as a function of sample calcination temperature, which provide a means to evaluate the changing oxidation state of Pt in the sample. The samples were also studied using EXAFS (Figure 4e,f). Through the DFT-based fitting and evaluation procedure, the 700 °C-calcined sample (Pt/MgO_{700}) was known to contain the subsurface cationic Pt noted above. Furthermore, this procedure facilitated the conclusion that the 400 °C-calcined sample (Pt/MgO_{400}) contained Pt in the surface layer. The Pt/MgO_{400} sample with surface-located Pt is capable of adsorbing CO at room temperature, consistent with its reduced oxygen coordination number. The DFT-optimized structure of the active sites associated with the best fits and determined to be most energetically feasible are shown in Figure 4c,d.

This study also contrasted the catalytic activity for CO oxidation between the samples. It was found that the Pt in Pt/MgO_{400} rapidly migrates on the surface at elevated temperatures in the presence of CO and O_2, causing sintering and formation of Pt nanoparticles. In contrast, the Pt/MgO_{700} showed much greater stability (but lower activity than the Pt/MgO_{400} sample – whose activity was due to the Pt nanoparticles that formed in situ). The detailed characterization in this study provided valuable information on the relationship between the structural properties of supported cationic Pt and stability in reaction conditions.

FUTURE WOK

Integrate atomically dispersed catalysts into workflow for combining surface and near-surface gas phase characterization during catalysis

We will apply our integrated experiment-theory approach for studying coupling reactions with gas- and surface-mediated steps with the use of highly characterized catalysts with well-defined active sites.

We are specifically interested in correlating catalytic activity for oxidative methanol and methane conversion with the speciation of intermediates in the gas phase and with the atomic-scale structure of supported transition metal active sites. The goal of this work is to derive relationships between local composition/structure of (uniform) active sites and the local gas-phase universal speciation during reaction.

Our initial efforts establish that careful efforts are required to tune reaction conditions that facilitate measurements in the near-surface gas phase while maintaining stabilities of the well-characterized active sites of atomically dispersed catalysts. Our first work has involved the study of atomically dispersed Pd in the subsurface of MgO, given our experience with Pd films and nanoparticles for methanol oxidation, described above.

We also continue to work with SNL-CRF on optimization of experimental setups to facilitate study of the oxidative coupling of methane. We synthesize catalysts and characterize them in reactor studies and using conventional materials science tools. Our near-term experimental goals involve optimization of the conditions to track methyl radicals using electron-impact ionization at Sandia.

Publications from September 2019 - Present

1. **Supported Metal Pair-Site Catalysts**

   E. Guan, J. Ciston, S.R. Bare, R.C. Runnebaum, A. Katz, A.R. Kulkarni, C.X. Kronawitter, B.C. Gates

   ACS Catalysis, **2020**, 10, 9065–9085.

2. **Near-Surface Imaging of the Multi-Component Gas Phase above a Silver Catalyst During Partial Oxidation of Methanol**

   B. Zhou, E. Huang, R. Almeida, S. Gurses, A. Ungar, J. Zetterberg, A.R. Kulkarni, C.X. Kronawitter, D.L. Osborn, N. Hansen, J. Frank

   ACS Catalysis, **2021**, 11, 155−168.

3. **A Theory-Guided X-Ray Absorption Spectroscopy Approach for Identifying Active Sites in Atomically-Dispersed Transition Metal Catalysts**

   Y. Chen, R. Rana, T. Sours, F.D. Vila, S. Cao, T. Blum, A.S. Hoffman, C.-Y. Fang, Z. Huang, C. Shang, C. Wang, J. Zeng, M. Chi, C.X. Kronawitter, S.R. Bare, B.C. Gates, A.R. Kulkarni

   J. Am. Chem. Soc., **2021**, 143, 20144–20156.

4. **Near-Surface Gas-Phase Methoxymethanol Is Generated by Methanol Oxidation over Pd-Based Catalysts**

   S.M. Gurses, T. Price, A. Zhang, J.H. Frank, N. Hansen, D.L. Osborn, A.R. Kulkarni, C.X. Kronawitter

   J. Phys. Chem. Lett., **2021**, 12, 11252–11258.

5. **Atomically Dispersed Platinum in Surface and Subsurface Sites on MgO Have Contrasting Catalytic Properties for CO Oxidation**

   Y. Chen, R. Rana, Z. Huang, F.D. Vila, T. Sours, J.E. Perez-Aguilar, X. Zhao, J. Hong, A.S. Hoffman, X. Li, C. Shang, T. Blum, J. Zeng, M. Chi, M. Salmeron, C.X. Kronawitter, S.R. Bare, A.R. Kulkarni, B.C. Gates

   J. Phys. Chem. Lett., **2022**, 13, 3896–3903.

Novel Micro-Reactor Development for Fundamental Gas Phase Chemical Kinetics Applications

Nicole J. Labbe,[1] G. Barney Ellison,[2] John W. Daily[1]
[1]Department of Mechanical Engineering
[2]Department of Chemistry
University of Colorado Boulder
UCB 427, 1111 Engineering Drive, Boulder, CO 80301-0427
Nicole.Labbe@colorado.edu, John.Daily@colorado.edu, Barney@jila.colorado.edu

Program Scope

The Labbe Lab at the University of Colorado Boulder has recently made significant advances in the manufacturing of high aspect ratio, silicon carbide (SiC) reactors for gas phase chemical physics applications. Leveraging these recent advances, this project seeks to reinvent the Chen Nozzle, [1,2] a radical generating micro-reactor, for modern gas phase chemical physics fundamental experiments. In this work, we seek to answer questions regarding the Chen Nozzle, and use that information to create a new suite of reactors for our community's use. In particular, questions we seek to answer are:

- How do reactor material properties such as surface finish, compaction, and thermal conductivity affect the performance of the reactor?
- By adding a nozzle constriction in the reactor, are we able to control pressure within the reactor main body as predicted, and can we leverage that for fall-off regime kinetics studies?
- Can new materials or surface finishes be leveraged to change the reactivity of the reactor itself for oxidation studies or to reduce potential kinetic wall interactions?

Ultimately, the goal of this research project is to understand the influence of materials on reactor design for these small, short-residence time radical sources, and identify how to manipulate materials for targeted kinetics work.

Recent Progress

Development of Novel Microreactors for Gas Phase Kinetics Experiments: Recently, the Labbe Lab has developed a new method for manufacturing silicon carbide tubes with custom internal geometries using a hybrid traditional and additive manufacturing approach. The result is a new reactor with comparable ceramic properties to the silicon carbide tubes used previously in our research group and others based on the Chen Nozzle. [1,2] However, two critical differences exist: 1) the reactors are constructed in a way to improve material properties of the reactors themselves, and 2) custom geometries can now be created such as the inclusion of a tapered nozzle at the end, which effectively chokes flow and stabilizes pressure throughout the reactor body. Furthermore, this process has been refined for further reactor customization including

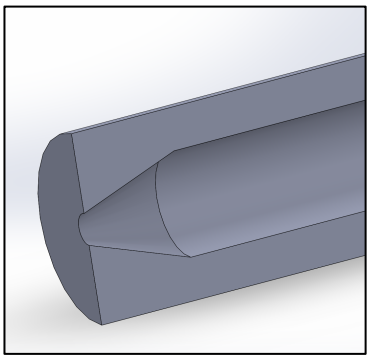

Figure 1: Cross section of the taper tip in our redesigned micro-reactors

versatility in internal geometry design and compatibility with alternative ceramics to silicon carbide.

Material Property Improvements: Last spring, final iterations on our design process for our nozzle reactors were completed, and we began a study to compare the new reactors created with our process to the Chen Nozzles as sourced from Saint Gobain SiC tubes. We explored several material characterization methods including modulus of rupture evaluations, X-Ray Detraction measurements, Micro0-CT and SEM imaging, and optical imaging. We will refer to our new ceramic reactor material as "Calix High Strength 2" and the Saint Gobain stock as "Hexoloy."

Modulus of rupture evaluations indicated the superior performance of the Calix High Strength 2 material as compared to the Hexoloy grade of SiC. A higher modulus of rupture translates to better resistive heating characteristics combined with a longer experimental life cycle. Currently used Hexoloy reactors are discarded after approximately 20 cycles of use due to reduced thermal response and fracturing at points of electrical contact. With the higher component density achieved using this composition and compaction process, it is expected to double the usable life cycle of these new reactors. A higher strength also confirms that this material system can approach the theoretical density limit, producing parts with fewer pores reducing the chance of failure during operation.

X-ray Diffraction results validated that the processing method described in this work does not introduce any material inconsistencies as compared to currently used components. The data obtained confirm the fundamental composition of the nozzle reactor is identical in comparison to the tube reactor. This ensures that the new reactor will not require any modifications for integration with the application. Existing protocols for reactor handling and heating can be continued with this ratification of the nozzle reactor composition.

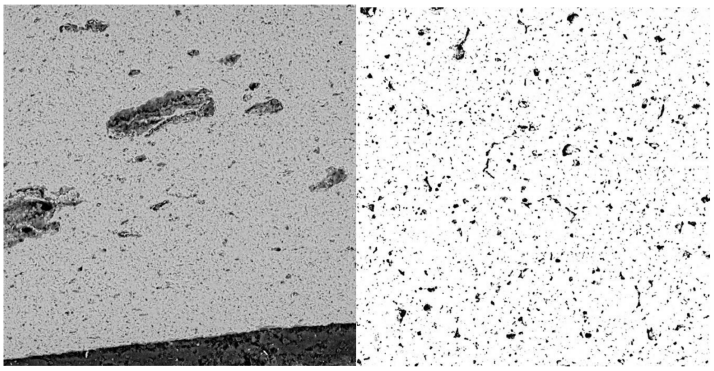

Figure 2: Scanning Electron Microscope (SEM) images at 1000 X magnification showing internal defects in the Saint Gobain sourced Chen reactor (left) as compared to our new nozzle reactor (right) produced using the technique described in this work.

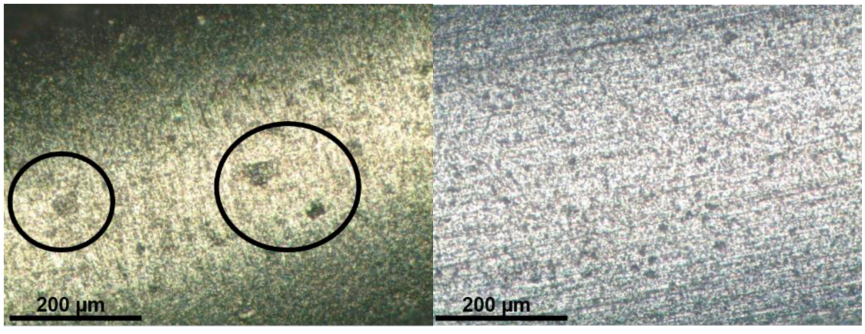

Figure 3: Optical microscope images at 50 X zoom showing the Saint Gobain sourced Chen reactor (left) and the new nozzle reactor produced using the process (right) described in this work.

Micro-CT and SEM imaging enabled a non-destructive method to observe the taper inside the new nozzle reactors and to verify the linearity of the cavity inside the reactor. Concentricity of the cavity within the reactor was another parameter that was studied and feedback from initial images was used to

Parameter	Saint Gobain Hexoloy	Calix High Strength 2	Notes
Max Use Temperature	1900°C	2100°C*	*Measured in the lab at 10^{-7} vacuum
Flexural Strength (Mpa)			Measured using the standard 4 point ASTM 1161 test using the B-bar configuration
@ Room Temp	280	450	
@ 1450°C	270	400	
@ 1600°C	300	480	
Density (g/cc)	3.05	2.15	Measured using ASTM density test
Apparent Porosity (%)	5-10	< 2	Optical Micrography
Modulus of Elasticity (Gpa)			ASTM acoustic measurement test
@ 20°C	420	435	
@ 1300°C	363	390	
Thermal Conductivity (W/mK) @ 1200°C	34.8	75	
Coefficient of Thermal Expansion (1/°C)	4.02 x 10^{-6}	4.02 x 10^{-6}	Dialatometry test (LVDT Measurement)

Table 1: Comparison of properties between the two reactor materials.

inform the tooling design of both processes and the anchoring methods used to center the mandrel. Both imaging techniques resulted in a clean, straight cavity devoid of any tool indentations and internal voids for the new nozzle reactor produced using our new manufacturing process. This is in direct contrast to the Chen Nozzle reactors from Saint Gobain stock, where the cavity was not concentric with the outer diameter. The images show significant pitting inside the cavity of the Saint Gobain Chen reactors along with flow lines consistent with tooling age on the extrusion dies. Also, clear from the images is the irregularity of the interior walls of the reactor coupled with large voids of the order size of 40 microns. This has also been previously confirmed in a study using X-ray fluorescence and absorbance [3] and has been identified as a factor affecting flow characteristics.

Optical imaging highlighted the exterior surface features of the reactors. Using this technique, the presence of superficial flaws (which can result in regions of low strength, localized around these defects) is observed on the Saint Gobain sourced Chen reactors. This is in direct contrast to the smooth surface of the nozzle reactor with almost no pores visible even at maximum magnification. The effect of these flaws on the tube reactor extends beyond lowered density and can also affect the maximum temperature to which the reactor can be heated resistively (1800 K for the Saint Gobain sourced Chen reactor as compared to 2100 K with the nozzle reactor) limiting experimental applicability.

Additional Ceramic Compatibility: In addition to being able to produce high aspect ratio silicon carbide geometries the application of this technique has been expanded to include additional engineering ceramic materials as well. The same process flow has been applied to produce components with the reactor geometry using alumina and Yttria Stabilized Zirconia (YSZ). Standard RTP powders with minor modifications have been used to successfully produce components with wall thicknesses lower than 500 μm and feature sizes as small as 300 μm. Compositional changes to the raw material include reducing grain sizes of the major component ceramic to less than 40 microns. All other processing parameters and sequences are kept common across materials. This capability allows for multiple materials to be fabricated simultaneously highlighting the versatility of the processing methodology.

Figure 4: YSZ (top) and alumina (bottom) nozzle reactors created with our ceramic micro-reactor manufacturing process.

Advanced Geometry Designs: In addition to producing the micro-reactor for use with different diagnostic techniques to study pyrolysis and potentially oxidation reactions, other high aspect ratio configurations have also been produced using this method. One such geometry involves creating a spiral helix in the interior of the reactor aperture. This modification is possible by redesigning the central stainless-steel mandrel to contain features that would allow the helical geometry to be formed inside the tube. The baseline design of this tooling component is kept in common with the other tools used to produce the micro-reactor with changes made to only the central major diameter. This component can then be rapidly fabricated using additive manufacturing methods like Direct Metal Laser Sintering (DMLS). An example of this new design is shown in Figure 5 along with the post compaction silicon carbide green component mounted on the tooling. Modifications such as these are easily achieved thanks to the modular design approach used in the tooling as well the flexibility of the raw material composition to produce high-density compacts through multiple compaction routes.

Figure 5: (Left) Image of the stainless-steel mandrel produced using DMLS. (Right) Image of the silicon carbide compact post isostatic pressing

Future Plans

Our future work centers around testing the new reactors for use in gas-phase kinetic studies. Our first goal is to determine whether adding a nozzle constriction in the reactor can control pressure within the reactor main body as predicted, and if we can leverage that for fall-off regime kinetics studies. The central mandrel in the reactor tooling is what dictates the geometry of the end constriction. By redesigning the mandrel and 3-D printing it to have alternative exit diameters, new reactors with variable exit diameters may be produced with the same manufacturing techniques discussed previously. We have identified three potential test systems:

1) $CH_3 + CH_3$: methyl-methyl recombination has a pressure and temperature dependent swing between recombination and dissociative recombination.
2) $CH_3 + HCCCH_2$: methyl + propargyl reactions can also undergo a competition between addition to form 1,3-butadiene versus addition-elimination to form $H + CH_3CHCCH$, which ultimately β-scissions to CH_2CHCCH.
3) Cyclopentadienyl recombination: Cyclopentadienyl radicals recombine to form fulvenes, which ultimately isomerize to naphthalene. The overall reaction rates are highly pressure sensitive and would indicate pressure dependence within the reactor.

Additionally, we aim to study how material improvements in the reactor ceramic production may reduce potential secondary wall interactions. In particular, deuterated anisole studies in our lab have suggested wall-assisted H-atom reactions may be occurring using the Saint Gobain sourced Nozzle reactors. With the new materials reducing wall cavities significantly, radical trapping may be reduced enough to prevent significant wall reactions. We will repeat these experiments as part of a study to understand material properties and wall reactions.

References

[1] P. Chen, S.D. Colson, W.A. Chupka, J.A. Berson, *Flash pyrolytic production of rotationally cold free radicals in a super sonic jet. Resonant multiphoton spectrum of the $3p^2A_2'' \leftarrow X^2A_2''$ origin band of CH_3,* J. Phys. Chem. 90 (1986) 2319-2321

[2] D.W. Kohn, H. Clauberg, P. Chen, *Flash pyrolysis nozzle for generation of radicals in a supersonic jet expansion*, Review of Scientific Instruments 63 (1992)

[3] R.S. Tranter, A.L. Kastengren, J.P. Porterfield, J.B. Randazzo, J.P.A. Lockhart, J.H. Baraban, G.B. Ellison, *Measuring flow profiles in heated miniature reactors with X-ray fluorescence spectroscopy,* Proc. Combust. Inst. 36 (2017) 4603-4610

Publications, Presentations, and Submitted Articles Acknowledging This Grant (2019-present)

1. D. E. Couch, Q. L. Nguyen, D. D. Hickstein, H. C. Kapteyn, M. M. Murnane, and N. J. Labbe, "*Detection of the Keto- Enol Tautomerization in Acetaldehyde, Acetone, Cyclohexanone, and Methyl Vinyl Ketone with a Novel VUV Light Source*". Proc. Combust. Inst. (2020), 1737-1744.
2. C. O. Rogers, K. S. Lockwood, Q. L. Nguyen, and N. J. Labbe*, "Diol Isomer Revealed as the Source of Methyl Ketene from Propionic Acid". Int. J. Chem. Kinetics 53 (2021) 12712-1284.*
3. C. O. Rogers, D. Kaczmarek, T. Kasper, and N. J. Labbe, "*Probing the Low-Temperature Chemistry of Methyl Hexanoate: Insights from Oxygenate Intermediates*". Proc. Combust. Inst. 38 (2020), 621-629.
4. K. Lockwood, N. J. Labbe*, "Insights on Keto-Hydroperoxide Formation from O2 Addition to the Beta-Tetrahydrofuran Radical"* Proc. Combust. Inst. (2020), 533-541.
5. C. Rogers, K. Cummins, J. Porterfield, J. W. Daily, G. B. Ellison, N. J. Labbe, *"The Pyrolysis Chemistry of Propionic Acid and Ethyl Propionate in a Microreactor"* Oral Presentation at the US National Combustion Meeting, Pasadena, CA, March 2019
6. C. Rogers, K. Cummins, J. Porterfield, J.W. Daily, G.B. Ellison, N.J. Labbe *"The Pyrolysis Chemistry of Propionic Acid and Ethyl Propionate Revealed,"* International Conference on Chemical Kinetics, Orleans, France, June 2019. [Invited Talk]
7. C. Rogers, J.P. Porterfield, J.W. Daily, G.B. Ellison, N.J. Labbe. *"Pyrolysis of Ethyl Esters in a Micro-Reactor*," International Symposium on Molecular Spectroscopy, Champaign-Urbana, Illinois, June 2019.
8. N.J. Labbe. "*Next Generation Microreactors for Rapid Reaction Speciation Data*," Western States Section of the Combustion Institute Spring Technical Meeting, Stanford, California, March 2022. [Plenary Talk]

Molecular Reactivity in Complex Systems

Musahid Ahmed (mahmed@lbl.gov), (Daniel Neumark (dneumark@berkeley.edu), Kevin Wilson (krwilson@lbl.gov)

MS 6R 2100, Chemical Sciences Division, LBNL, Berkeley, CA-94720

Background and Significance

Our effort in molecular reactivity in complex systems targets complex multistep and multiphase chemical transformations built from isolated elementary bimolecular reactions to gas-surface reaction dynamics. The gas phase is central for controlling the multiphase chemistry with additional kinetic processes, playing a key role in governing the overall reactive outcome. Cross-cutting themes of *Chemistry at Complex Interfaces* and *Reaction Pathways in Diverse Environments* are explored, providing valuable insight into microscopic processes relevant to energy generation, storage, and thermal science. Activities in this Subtask drive new theory and simulation, to enrich the molecular level interpretation of experiments. The Gas Phase Chemical Physics program at Berkeley Lab is uniquely placed to conduct this research, with theory and experiment coupled with extensive use of DOE national user facilities such as the Advanced Light Source and NERSC.

Recent Progress:

Photoionization Dynamics and Hydrogen Bonding in Clusters:[1-6] Polyol-water clusters provide a template to probe ionization and solvation processes of paramount interest in atmospheric and interstellar chemistry. We generate glycerol water clusters in a continuous supersonic jet expansion and interrogate the neutral species with synchrotron-based tunable vacuum ultraviolet photoionization mass spectrometry. A judicious combination of backing pressure, nozzle temperature, and water vapor pressure allows for tuning the mol % of glycerol. Theoretical calculations (Head-Gordon, subtask 3) on neutral and ionized clusters visualize the hydrogen bond network in these clusters and provide an assessment of the number of glycerol-glycerol, glycerol-water, and water-water hydrogen bonds in the cluster, as well as their interaction energies. This method of bond counting and interaction energy assessment explains the changes in the mass spectrum as a function of mol % and offers a glimpse of the disruption of the hydrogen bond network in glycerol-water clusters. The calculations also reveal interesting barrier-less chemical processes in photoionized glycerol water clusters that are either activated or do not occur without the presence of water.[1] We have extended our studies using alcohol-water clusters, from which we learned about ionic hydrogen bonds, towards deep eutectic solvents. These "designer solvents" have many applications and the task-specific nature of these solvents requires a molecular-level understanding. We have experimentally collected data on ethylene glycol and propylene glycol. Contrary to ethylene glycol and glycerol, propylene glycol has been controversial for its non-colligative behavior. Its two isomers, 1,2- and 1,3-propylene glycol, give an additional dimension where one can study the effects of adjoining hydroxyl groups *vs*. non-adjoining hydroxyl groups in cluster formation and hydrogen bonding.

Small neutral molecules and ions can act as nucleating species, which typically play key roles in molecular growth. We have recently developed an experimental strategy for characterizing neutral *vs*. ion-induced growth using in-source ionization of molecular beams with VUV synchrotron radiation. This method allowed us to probe systems that are relevant to atmospheric chemistry and to develop a framework in which to understand novel hydrogen bonding and non-covalent interactions. We have completed a study of growth processes in pure water clusters to act as a bridge from the gas phase to condensed phase dynamics. Time-of-flight mass spectrometry reveal enhanced population of various water clusters based upon ionization energy and photoionization distance from source, suggesting there are "magic" numbers below the traditional 21 that predominates in the literature. The spectral distributions are representative of a non-equilibrium frozen state and theory (Head-Gordon, subtask 3) is used to assign structure and energetics for these new magic numbers.

Molecular Beam Experiments on Flat Liquid Jets: The gas-liquid interface is a ubiquitous chemical environment in nature. It plays a major role in industrial processes, atmospheric chemistry, and environmental science. Examples include air-fuel mixing in internal combustion engines, acid rain formation, and the uptake of CO_2 at the ocean-air interface, where about one third of anthropogenically generated CO_2 is absorbed. It is thus desirable to develop a molecular-scale understanding of chemistry at the gas-liquid interface. To this end, an experimental setup for molecular beam scattering from flat liquid sheets has been developed, with the goal of studying reactions at gas-liquid interfaces for volatile liquids. Specifically, a crossed-molecular beam instrument that can measure angular and translational energy distributions of scattered products has been adapted for liquid jet scattering. A microfluidic chip creates a stable flat liquid sheet inside vacuum from which scattering occurs, and both evaporation and scattering from this sheet are characterized by a rotatable mass spectrometer that can measure product time-of-flight distributions. A manuscript has recently been submitted that describes the instrument and reports on first measurements of evaporation of dodecane and Ne from a Ne-doped dodecane flat jet, as well as scattering of Ne from a flat jet of pure dodecane.

Two types of experiments have been carried out: evaporation and scattering. The evaporation of Ne-doped dodecane solutions is explored in order to isolate the trapping-desorption (TD) process, which is one of the major channels encountered in scattering experiments, and a detailed understanding of evaporation from a flat jet is key to successfully interpreting scattering experiments. Additionally, evaporation provides the opportunity to explore the performance of our instrument as liquid evaporation from cylindrical jets has been extensively considered. Molecular beam scattering experiments of Ne from a dodecane flat jet have also been carried out using fast and slow Ne beams. Measurement of the scattered Ne velocity and angular distributions enables elucidation of the impulsive scattering (IS) and TD mechanisms. Results as a function of incident and scattering angle are satisfactorily fit to a "soft sphere" model.

Radical reactions lead to molecular growth.[7-20] The growth of polycyclic aromatic hydrocarbons (PAHs) has been explored by Ahmed in collaboration with Ralf Kaiser (Hawaii), and Alex Mebel (FIU). Radical-radical reactions under high pressure and temperature conditions prevalent in the microreactor provides a rich tapestry to understand the underlying reaction dynamics that drive molecular growth in carbonaceous systems. We report a mechanism on how naphthalene can be formed via a rapid 1-indenyl radical-methyl radical reaction.[20] In the case of the propargyl + propargyl self-recombination reaction, experiment coupled to theory reveal, benzene, and three other structural isomers (1,5-hexadiyne, fulvene, and 2-ethynyl-1,3-butadiene) and o-benzyne are detected, and their branching ratios are quantified experimentally and verified with the aid of computational fluid dynamics and kinetic simulations.[9] The formation of benzene via the cyclopentadienyl-methyl reaction and of naphthalene through the cyclopentadienyl self-reaction, is revealed.[7] These systems offer benchmarks for the conversion of a five-membered ring to the 6π-aromatic (benzene) and the generation of the simplest 10π-PAH (naphthalene) at elevated temperatures. We report on a combined computational and experimental study of the benzyl radical self-reaction to phenanthrene and anthracene through unconventional, isomer-selective excited state dynamics.[8] Whereas phenanthrene formation is initiated via a barrier-less recombination of two benzyl radicals on the singlet ground state surface, formation of anthracene commences through an exotic transition state on the excited state triplet surface through cycloaddition.

Non-covalent Interaction and Heterogeneous Reaction Probabilities: It is well-known that in the field of enzyme catalysis that weak interactions (e.g. hydrogen and halogen bonds) can play an important role in altering the energetics of a reaction. Less well known is how these weak interactions can enhance reactivity at gas-liquid interfaces. For example, we are interested in understanding how weak interactions alter key non-reactive pathways that govern trace gas uptake and reaction at a liquid interface. These non-reactive kinetic steps include gas adsorption/desorption and

solvation/desolvation. In recently published work,[21] we have used a model reaction, the electrophilic addition of Cl_2 to an alkene, to understand how these non-reactive pathways govern heterogeneous reaction probabilities. Our results indicate that the Cl_2 reaction with aerosol alkenes, although slow, is sequential; adding two Cl functional groups per C=C site. When the particle is doped with species (an additive) that contain alcohol or carbonyl functional groups (which are inert towards Cl_2) the apparent reaction rate is accelerated by ~10-20X. Doping the aerosol with alkanes or esters groups either does not change the reactivity or decreases it by a factor of ~3. Adding small gas phase oxygenated molecules (such as ethanol, acetic acid), which adsorb to the aerosol interface, are observed to play similar catalytic roles during heterogeneous chlorination. These results suggest that these oxygenated spectator molecules act as gas-liquid phase transfer catalysts either by enhancing the accommodation of Cl_2 by the aerosol or by catalyzing the electrophilic addition reaction directly. Both of these mechanisms are being explored in future plans.

Future Plans:

Gas Phase Dynamics in Confined Spaces: Gas phase molecules in confined environments encounter unique forces and dynamics which completely transform their reaction outcomes and have profound and deep implications for the future of energy supply and climate change. For instance, a fundamental molecular understanding of atmospheric CO_2 uptake, storage and transformation in metal organic frameworks is a grand challenge. Another example is the complex chemical and structural properties of the solid liquid vapor interface under non-equilibrium conditions, for instance evaporation, condensation, transport and chemistry of water in nanoscale architectures. The generally fast diffusion of gases in porous materials leads to rapid exchange of surface, interface, and bulk species and therefore simultaneous measurement of their properties is crucial. Recently, we have incorporated a microfluidic device, System for Analysis of Liquid Interfaces (SALVI) to mass spectrometry to probe phase transitions, electrochemistry,[4] and photochemistry[2] on environmental and energy-related processes. Liquids are sealed in between Si_3N_4 membranes in a microchannel with 2 – 3 μm apertures and surface tension across the aperture holds the liquid in high vacuum. The molecules evaporating from the liquid surface are interrogated by VUV photons and then detected by mass spectrometry. We propose to physically chop the emanating vapor to measure its time-of-flight to obtain velocities and hence translational dynamics. The novelty in our instrumentation is the multimodal nature of the spectroscopies and the temporal analysis of gas uptake and transformations under ambient conditions to probe chemical bonding and structure. Using the SALVI device, we have demonstrated the capability of probing phase changes in an ionic liquid with uptake of CO_2 gas. (10.1039/c7cp03754f) We will design a similar system, but now will provide temporal pulses of gas using a piezo valve (operating at kHz rep rates). We will interrogate the dynamics of the gas phase molecules inside the MOF cavity using Raman spectroscopy (50-4000 cm^{-1}) allowing access to the lattice dynamics of the MOF cage in the THz regime, and the gas-organic linker functional group information via Infrared spectroscopy. The emanating gas phase molecules will be probed via mass spectrometry. Preliminary results on a Co MOF-74 synthesized within a quartz capillary allowed us to track both the adsorption and desorption kinetics of ambient air upon temperature cycling with our home-made Raman laser system. A particularly exciting direction, is that Jin Qian (subtask 3) is developing methods to calculate X-Ray, THz, IR and Raman spectra that will guide interpretation of the experimental results.

Two color spectroscopies to probe gas phase dynamics: The experimental program in subtask 2 relies heavily on the use of VUV and soft X-Ray photons available at the ALS. Plans are underway to upgrade the ALS to a diffraction limited storage ring (ALS-U). This upgrade will enable the production of highly focused and coherent X-ray beams that are 100-1000 times brighter than is produced by the current machine. However, this will lead to substantial reduction in beamtime in the coming years, and the ALS will go dark for about a year in the fall of 2025. To prepare for this, we have embarked on a

new program which will utilize a powerful MHz rep rate laser to generate tunable light between 300 nm to 20 microns, and simultaneously allow for four-wave mixing to generate VUV light at 10.8 eV. Access to VUV allows us to continue our mass spectrometry program on a second instrument which will have access to aerosol and molecular beams with also incorporation of the SALVI device. Indeed, the modularity of our design, allows sources to be transitioned effortlessly between the instruments located on the ALS floor and the ancillary chemical dynamics laser lab. While tunable VUV will not be available, we do believe access to 2 color spectroscopies spanning the ultraviolet to the Far Infrared will allow a seamless continuation of the experimental program. An added advantage of the high power and repetition rate source is that non-linear forms of spectroscopy also become accessible which will allow the interrogation of interfaces and aerosols.

Molecular Beam Experiments on Flat Liquid Jets: The immediate goal of this project is to perform scattering experiments off more volatile solvents, with water as the primary target. Our current approach is to make solutions of water with ethylene glycol so that the liquid temperature can be lowered beyond the freezing point of water in order to reduce the water vapor pressure as much as possible. Preliminary scattering experiments using rare gas atoms show strong evidence that the scattering is dominated by gas-liquid interactions (as opposed to the vapor cloud around the flat jet). We are also working with Acrea 3D to carry out 3D printing of new designs for our microfludic flat jets in order to optimize their performance in scattering experiments.

Multiphase Chemistry of Criegee Intermediates (CI): Motivated by our prior experimental work,[22-24] we are continuing studies with Martin Head-Gordon (Subtask 3), to develop a robust theoretical understanding of the reaction pathways that connect CI and β-hydroxy peroxy radicals (β-RO_2). We are also exploring a number of other candidate bimolecular/unimolecular mechanisms to assess mechanistic viability. These pathways are in addition to two mechanisms already proposed in the literature to explain β-RO_2 conversion to CIs: the Beauchamp group (*Proc. Nat. Acad. Sci.* **115**, 3255-3260 (2018) postulated a unimolecular decomposition mechanism, whereas Wagner (*J. Phys. Chem. A,* 2021, 125, 1, 406–410) suggested that CIs could be formed in bimolecular peroxy radical self-reactions. In addition, we are working with Rebecca Caravan's group (ANL) to use small gas phase alkenes to further understand these interconversion pathways. This will be done using the multiplexed photoionization mass spectrometer (D. Osborn, Sandia) coupled to the tunable VUV output of the Chemical Dynamics Beamline at the ALS. Once we have obtained a robust theoretical description of the coupling of CIs and β-RO_2, we will revise our existing multiphase kinetic models accordingly to test theoretical predictions against our previous experimental results.

Non-covalent Interaction and Heterogeneous Reaction Probabilities: We are continuing our work to understand how spectator molecules catalyze heterogeneous reactions. This includes planned experimental studies examining how molecules in the gas phase can adsorb to the aerosol interface to promote or inhibit the electrophilic addition of Cl_2 to alkenes. We will be conducting a systematic investigation of a series of gas phase alcohols and alkanes, which differ in their chain length and structure, in order to understand their partitioning to the aerosol interface and their relative catalytic activity. In collaboration with Jin Qian's group (subtask 3), we will be examining the role that alcohols might play in directly catalyzing Cl_2 addition to alkenes. New collaborations are being initiated to understand how alcohol additives might alter the interfacial solvation energies of Cl_2, which is another viable catalytic mechanism.

In new work examining the heterogeneous reaction of chlorine atoms with alkenes, in the presence of Cl_2, we have observed an unexpectedly large enhancement of reactivity and the predominance of chlorinated reaction products even under high O_2 conditions, where Cl atom recycling is expected to be minimal. These preliminary observations cannot be explained by known free radical oxidation or cycling mechanisms, but rather we find evidence for the multiphase catalytic coupling of free radical oxidation with electrophilic Cl_2 addition. This mechanism builds on previous work (see

recent progress),[21] which showed that oxygenated molecules act as gas-liquid phase transfer catalysts by promoting the accommodation of gas phase Cl_2 by the aerosol; thereby enhancing electrophilic addition. We anticipate that this maybe novel example of catalytic coupling of free radical oxidation and electrophilic addition at an aerosol interface.

Subtask 2 publications (2019-present)[25-30]

1. Lu, W.; Mackie, C. J.; Xu, B.; Head-Gordon, M.; Ahmed, M., A Computational and Experimental View of Hydrogen Bonding in Glycerol Water Clusters. *J Phys Chem A* **2022,** *126* (10), 1701-1710.

2. Sui, X.; Xu, B.; Yao, J.; Kostko, O.; Ahmed, M.; Yu, X. Y., New Insights into Secondary Organic Aerosol Formation at the Air-Liquid Interface. *J Phys Chem Lett* **2021,** *12* (1), 324-329.

3. Lu, W.; Metz, R. B.; Troy, T. P.; Kostko, O.; Ahmed, M., Exciton energy transfer reveals spectral signatures of excited states in clusters. *PCCP* **2020,** *22* (25), 14284-14292.

4. Komorek, R.; Xu, B.; Yao, J.; Kostko, O.; Ahmed, M.; Yu, X. Y., Probing sulphur clusters in a microfluidic electrochemical cell with synchrotron-based photoionization mass spectrometry. *PCCP* **2020,** *22* (26), 14449-14453.

5. Ahmed, M.; Kostko, O., From atoms to aerosols: probing clusters and nanoparticles with synchrotron based mass spectrometry and X-ray spectroscopy. *Phys Chem Chem Phys* **2020,** *22* (5), 2713-2737.

6. Xu, B.; Stein, T.; Ablikim, U.; Jiang, L.; Hendrix, J.; Head-Gordon, M.; Ahmed, M., Probing solvation and reactivity in ionized polycyclic aromatic hydrocarbon-water clusters with photoionization mass spectrometry and electronic structure calculations. *Faraday Discussions* **2019,** *217*, 414-433.

7. Kaiser, R. I.; Zhao, L.; Lu, W.; Ahmed, M.; Zagidullin, M. V.; Azyazov, V. N.; Mebel, A. M., Formation of Benzene and Naphthalene through Cyclopentadienyl-Mediated Radical-Radical Reactions. *J Phys Chem Lett* **2022,** *13* (1), 208-213.

8. Kaiser, R. I.; Zhao, L.; Lu, W.; Ahmed, M.; Krasnoukhov, V. S.; Azyazov, V. N.; Mebel, A. M., Unconventional excited-state dynamics in the concerted benzyl (C7H7) radical self-reaction to anthracene (C14H10). *Nat Commun* **2022,** *13* (1), 786.

9. Zhao, L.; Lu, W.; Ahmed, M.; Zagidullin, M. V.; Azyazov, V. N.; Morozov, A. N.; Mebel, A. M.; Kaiser, R. I., Gas-phase synthesis of benzene via the propargyl radical self-reaction. *Sci Adv* **2021,** *7* (21).

10. Zhao, L.; Doddipatla, S.; Kaiser, R. I.; Lu, W.; Kostko, O.; Ahmed, M.; Tuli, L. B.; Morozov, A. N.; Howlader, A. H.; Wnuk, S. F.; Mebel, A. M.; Azyazov, V. N.; Mohamed, R. K.; Fischer, F. R., Gas-phase synthesis of corannulene - a molecular building block of fullerenes. *Phys Chem Chem Phys* **2021,** *23* (10), 5740-5749.

11. Zhao, L.; Kaiser, R. I.; Xu, B.; Ablikim, U.; Ahmed, M.; Evseev, M. M.; Bashkirov, E. K.; Azyazov, V. N.; Mebel, A. M., A Unified Mechanism on the Formation of Acenes, Helicenes, and Phenacenes in the Gas Phase. *Angew. Chem.* **2020,** *59* (10), 4051-4058.

12. Zhao, L.; Kaiser, R. I.; Lu, W.; Kostko, O.; Ahmed, M.; Evseev, M. M.; Bashkirov, E. K.; Oleinikov, A. D.; Azyazov, V. N.; Mebel, A. M.; Howlader, A. H.; Wnuk, S. F., Gas phase formation of cyclopentanaphthalene (benzindene) isomers via reactions of 5- and 6-indenyl radicals with vinylacetylene. *PCCP* **2020,** *22* (39), 22493-22500.

13. Zhao, L.; Kaiser, R. I.; Lu, W.; Ahmed, M.; Oleinikov, A. D.; Azyazov, V. N.; Mebel, A. M.; Howlader, A. H.; Wnuk, S. F., Gas phase formation of phenalene via 10π-aromatic, resonantly stabilized free radical intermediates. *PCCP* **2020,** *22* (27), 15381-15388.

14. Zhao, L.; Kaiser, R. I.; Lu, W.; Ahmed, M.; Evseev, M. M.; Bashkirov, E. K.; Azyazov, V. N.; Tönshoff, C.; Reicherter, F.; Bettinger, H. F.; Mebel, A. M., A Free-Radical Prompted Barrierless Gas-Phase Synthesis of Pentacene. *Angew. Chem.* **2020,** *59* (28), 11334-11338.

15. Zhao, L.; Xu, B.; Ablikim, U.; Lu, W.; Ahmed, M.; Evseev, M. M.; Bashkirov, E. K.; Azyazov, V. N.; Howlader, A. H.; Wnuk, S. F.; Mebel, A. M.; Kaiser, R. I., Gas-Phase Synthesis of Triphenylene (C18H12). *ChemPhysChem* **2019,** *20* (6), 791-797.

16. Zhao, L.; Prendergast, M. B.; Kaiser, R. I.; Xu, B.; Lu, W.; Ablikim, U.; Ahmed, M.; Oleinikov, A. D.; Azyazov, V. N.; Mebel, A. M.; Howlader, A. H.; Wnuk, S. F., Reactivity of the Indenyl Radical (C9H7) with Acetylene (C2H2) and Vinylacetylene (C4H4). *ChemPhysChem* **2019,** *20* (11), 1437-1447.

17. Zhao, L.; Prendergast, M. B.; Kaiser, R. I.; Xu, B.; Ablikim, U.; Ahmed, M.; Sun, B.-J.; Chen, Y.-L.; Chang, A. H. H.; Mohamed, R. K.; Fischer, F. R., Synthesis of Polycyclic Aromatic Hydrocarbons by Phenyl Addition–Dehydrocyclization: The Third Way. *Angew. Chem.* **2019,** *58* (48), 17442-17450.

18. Zhao, L.; Prendergast, M.; Kaiser, R. I.; Xu, B.; Ablikim, U.; Lu, W.; Ahmed, M.; Oleinikov, A. D.; Azyazov, V. N.; Howlader, A. H.; Wnuk, S. F.; Mebel, A. M., How to add a five-membered ring to polycyclic aromatic hydrocarbons (PAHs) – molecular mass growth of the 2-naphthyl radical (C10H7) to benzindenes (C13H10) as a case study. *PCCP* **2019,** *21* (30), 16737-16750.

19. Zhao, L.; Kaiser, R. I.; Xu, B.; Ablikim, U.; Lu, W.; Ahmed, M.; Evseev, M. M.; Bashkirov, E. K.; Azyazov, V. N.; Zagidullin, M. V.; Morozov, A. N.; Howlader, A. H.; Wnuk, S. F.; Mebel, A. M.; Joshi, D.; Veber, G.; Fischer, F. R., Gas phase synthesis of [4]-helicene. *Nature Comm.* **2019,** *10* (1), 1510.

20. Zhao, L.; Kaiser, R. I.; Lu, W.; Xu, B.; Ahmed, M.; Morozov, A. N.; Mebel, A. M.; Howlader, A. H.; Wnuk, S. F., Molecular mass growth through ring expansion in polycyclic aromatic hydrocarbons via radical–radical reactions. *Nature Comm.* **2019,** *10* (1), 3689.

21. Zeng, M.; Wilson, K. R., Experimental evidence that halogen bonding catalyzes the heterogeneous chlorination of alkenes in submicron liquid droplets. *Chemical Science* **2021,** *12* (31), 10455-10466.

22. Zeng, M.; Heine, N.; Wilson, K. R., Evidence that Criegee intermediates drive autoxidation in unsaturated lipids. *Proceedings of the National Academy of Sciences* **2020,** *117* (9), 4486-4490.

23. Zeng, M.; Wilson, K. R., Efficient Coupling of Reaction Pathways of Criegee Intermediates and Free Radicals in the Heterogeneous Ozonolysis of Alkenes. *The Journal of Physical Chemistry Letters* **2020,** *11* (16), 6580-6585.

24. Arata, C.; Heine, N.; Wang, N.; Misztal, P. K.; Wargocki, P.; Bekö, G.; Williams, J.; Nazaroff, W. W.; Wilson, K. R.; Goldstein, A. H., Heterogeneous Ozonolysis of Squalene: Gas-Phase Products Depend on Water Vapor Concentration. *Envr. Sci. Tech.* **2019,** *53* (24), 14441-14448.

25. Jacobs, M. I.; Xu, B.; Kostko, O.; Wiegel, A. A.; Houle, F. A.; Ahmed, M.; Wilson, K. R., Using Nanoparticle X-ray Spectroscopy to Probe the Formation of Reactive Chemical Gradients in Diffusion-Limited Aerosols. *J. Phys. Chem. A* **2019**.

26. Barrozo, A.; Xu, B.; Gunina, A. O.; Jacobs, M. I.; Wilson, K.; Kostko, O.; Ahmed, M.; Krylov, A. I., To Be or Not To Be a Molecular Ion: The Role of the Solvent in Photoionization of Arginine. *J Phys Chem Lett* **2019,** *10* (8), 1860-1865.

27. Pohl, M. N.; Malerz, S.; Trinter, F.; Lee, C.; Kolbeck, C.; Wilkinson, I.; Thürmer, S.; Neumark, D. M.; Nahon, L.; Powis, I.; Meijer, G.; Winter, B.; Hergenhahn, U., Photoelectron circular dichroism in angle-resolved photoemission from liquid fenchone. *PCCP* **2022,** *24* (14), 8081-8092.

28. Thürmer, S.; Malerz, S.; Trinter, F.; Hergenhahn, U.; Lee, C.; Neumark, D. M.; Meijer, G.; Winter, B.; Wilkinson, I., Accurate vertical ionization energy and work function determinations of liquid water and aqueous solutions. *Chemical Science* **2021,** *12* (31), 10558-10582.

29. Mason, P. E.; Schewe, H. C.; Buttersack, T.; Kostal, V.; Vitek, M.; McMullen, R. S.; Ali, H.; Trinter, F.; Lee, C.; Neumark, D. M.; Thürmer, S.; Seidel, R.; Winter, B.; Bradforth, S. E.; Jungwirth, P., Spectroscopic evidence for a gold-coloured metallic water solution. *Nature* **2021,** *595* (7869), 673-676.

30. Malerz, S.; Trinter, F.; Hergenhahn, U.; Ghrist, A.; Ali, H.; Nicolas, C.; Saak, C.-M.; Richter, C.; Hartweg, S.; Nahon, L.; Lee, C.; Goy, C.; Neumark, D. M.; Meijer, G.; Wilkinson, I.; Winter, B.; Thürmer, S., Low-energy constraints on photoelectron spectra measured from liquid water and aqueous solutions. *PCCP* **2021,** *23* (14), 8246-8260.

Theory of Electronic Structure and Chemical Dynamics

Martin Head-Gordon, Jin Qian, Eric Neuscamman
Chemical Sciences Division, Lawrence Berkeley National Laboratory, Berkeley, California 94720.
mhead-gordon@lbl.gov, jqian2@lbl.gov, eneuscamman@lbl.gov

Scope of the Project: To expand knowledge of transient species such as radicals relevant to combustion chemistry, atmospheric photochemistry, and other areas including catalysis, new theoretical methods are needed for reliable computer-based prediction of their properties. In electronic structure theory, focus centers on the development of new density functional theory methods and new wave function theories. Newly developed theoretical methods, as well as existing approaches, are employed to study prototype radical reactions, often in collaboration with experimental efforts in the related subtasks (see separate LBNL abstracts). These studies help to deepen understanding of the role of reactive intermediates in diverse areas of chemistry. They also sometimes reveal frontiers where new theoretical developments are needed in order to permit better calculations in the future.

Recent Progress

Due to length limitations, only a selection of projects can be summarized here.

High Accuracy Excited States and Monte Carlo Optimization. Neuscamman and co-workers have continued to develop excited-state-specific methodologies in both quantum chemistry and quantum Monte Carlo (QMC) and to improve QMC wave function optimization techniques. (Blunt et al, 2019; Otis et al, 2019; Pineda Flores et al, 2019) Our most exciting recent developments have been to extend our state-specific work into core excited states. One interesting finding here is that, despite straightforwardly neglecting electron correlation, excited state mean field theory predicts oxygen, nitrogen, and carbon K-edges with an accuracy against experiment better than 1 eV. Upon adding second order perturbation theory (much as MP2 improves Hartree-Fock), the mean unsigned error for these K-edges drops to 0.3 eV, which is competitive with the best density functionals (and better than most!) used in ROKS. (Garner et al, 2020b) This finding shows us that the similarities in accuracy between MP2 and DFT extend into core states. We have also extended our excited-state-specific variational Monte Carlo (VMC) methodology in order to handle core states and found that it offers accuracies for K-edges in water, ammonia, and methane of about 0.2 eV, and peak separations within 0.07 eV. (Garner et al, 2020a) Although this is a preliminary test set, when we compare to experiment, we find that VMC peak separations are more accurate than other available methods, and that the K-edge accuracies are on par with the best available methods.

Electron correlation methods: Head-Gordon and co-workers are developing wavefunction-based electron correlation methods for problems where DFT suffers from self-interaction and/or strong correlation errors. Their recent regularized MP2 approach (Shee et al, 2021) provides a well-defined way to modify MP2, this simplest of electron correlation methods, to remove its divergence in the zero gap limit, and to substantially correct its known limitations for dispersion-dominated interactions and transition metal systems. As one highlight, the RMS errors for non-covalent interactions involving either small and medium-sized molecules (the S22 dataset), or large molecules (the L7 dataset) are reduced by a factor of approximately 5 using a suitable regularization parameter.

Orbital optimization and diagnosing strong correlations: Coupled with orbital optimization (OO), regularized MP2 provides a direct path to orbitals free of the delocalization error of DFT, and the over-localization and artificial symmetry-breaking errors of mean-field Hartree-Fock. This has proven useful for diagnosing the presence of strong correlation in organic systems (Lee et al, 2019) as well as transition metals (Shee et al, JCP, 2021). The resulting orbitals have also enabled dramatic improvements in the accuracy of MP3, relative to the use of mean field orbitals. These advantages can also be achieved with use of DFT orbitals (Rettig et al, JCTC, 2020). Even vibrational frequencies from CCSD(T) for open shell molecules can be significantly improved in this way (Bertels et al, JCTC, 2021).

Excited-state nonadiabatic dynamics: In collaboration with Steve Cotton and Bill Miller, the Head-Gordon group is assessing the performance of symmetric quasi-classical Meyer-Miller (SQC-

MM) theory for simulating non-adiabatic transitions in molecular photophysics and photochemistry. A benchmark assessment of branching ratios in photoexcited NaH comparing exact quantum dynamics, Ehrenfest and SQC-MM yielded very encouraging results (Talbot et al, PCCP 2022), with virtually quantitative agreement between SQC-MM and exact dynamics.

Chemical Applications: A rich variety of chemical applications have been completed, including a direct collaboration between the Head-Gordon group and Musa Ahmed (LBNL) on glycerol-water complexes, pre- and post-ionization (Lu et al, JPCA 2022), and interactions between the Head-Gordon group and members of the Berkeley catalysis group on mechanistic steps associated with CO2 to CO reduction (Wuttig et al, JACS 2021), as well as novel chemistry related to alkyne cyclotrimerization (Witzke et al, 2020) novel iron-I complexes involving N2 (Witzke et al, 2021).

Future Plans:

Multi-configurational core excitations and accelerated optimization: Current efforts focus on further improving wave function optimization and on extending our success with core excitations into radical, diradical, and other systems whose core states can be multi-configurational. Towards this end, we are developing a strongly correlated core excitation method based on state-specific CASSCF and selected configuration interaction, which will connect naturally to our existing VMC capabilities. This approach will allow us to study to what degree multi-reference mixing beyond spin recoupling impacts core states and their peak positions. In our ongoing work on VMC optimization, we have deciphered the primary cause of optimization instabilities in difficult excited state scenarios and have shown that our approach of hybridizing the best features of the linear method and accelerated descent methods neatly resolves the issue. Combined with our observations that state-specific orbital optimization at the quantum chemistry level (e.g. with our excited-state-specific CASSCF code) is equally effective as trying to re-optimize orbitals within VMC, this increased optimization efficiency positions us to apply VMC across a much wider range of excited state classes, including double excitations and charge transfer excitations in which preliminary data is extremely promising.

OO-MP2 analytical gradient theory: A full implementation of the regularized OO-MP2 gradient is nearly complete in the Head-Gordon group, and will enable assessment of the performance of this method across a range of structure-related properties. There is reason to be optimistic that some of the significant failures of MP2 structural properties related to orbital symmetry breaking will be greatly reduced by regularized OOMP2. Additional tests of how transferable the regularization parameter is from one class of systems to another will also be performed.

On-the-fly quasi-classical nonadiabatic dynamics: An improved implementation is being developed in the Head-Gordon group that much more efficiently evaluates nonadiabatic couplings between excited states and nuclear forces associated with that same set of excited states via single excitation configuration interaction (CIS), and time-dependent density functional theory (TDDFT) in the Tamm-Dancoff approximation. This will be combined with SQC-MM semiclassical non-adiabatic dynamics to enable direct simulations of nonadiabatic photochemistry and photophysics in polyatomic molecules.

Efficient real-space KS-DFT development: Key distinctions persist among the dominant practitioners of Kohn Sham-DFT (KS-DFT). On the one hand, quantum chemists favor orbital-like basis sets (usually gaussian type orbitals) and tend to focus their efforts on isolated molecular systems. In contrast, solid-state physicists leverage plane-wave basis sets (usually coupled with periodic boundary conditions) and tend to focus on descriptions of (quasi-) continuous solids and interfacial systems. Qian group is going to explore and develop a different, physically sound, and robust theoretical methodology that bridges the knowledge gap between molecular and continuum systems. Specifically, our recent development and implementation of Ab-initio Real-space Electronic Structure code (ARES) based on real-space projection and flexible boundary conditions open up new possibilities to investigate states of missing, additional, or displaced (core and valence) charges. The potential applications for this development involve core excitation predictions for finite systems from small (a few atoms) to large

(>10,000 atoms), as well as free energy predictions for gas in confined space (Subtask 2 with Musa Ahmed, LBNL).

Collaborative chemical applications: Collaborative applications to photoionized water clusters are underway (with Musa Ahmed, LBNL). Here the computational focus is identifying features that underpin stability of hydronium-water networks, to connect to experimental photoionization data. An additional on-going project is modelling oxidative chemistry in aerosols of long-chain hydrocarbons (with Kevin Wilson, LBNL), where the computational objective is comparing pathways that proceed by radical addition versus abstraction by radicals, as informed by experimental information on kinetics and product distributions. A third current project is computational modelling of combustion related reactions involving the reactive growth of unsaturated radicals (with Hope Michelson, Colorado), with particular focus on the range of C-H bond strengths in relevant intermediates on the pathway to soot inception, and how unimolecular hydrogen ejection processes may compete with abstraction processes. The new core excited tools developed by Neuscamman will be applied to problems of interest in the Leone and Neumark groups, to complement the ROKS-based approaches developed by the Head-Gordon group.

Recent Publications Citing DOE Support (2019-2022)

- Bertels, L.W.; J. Lee, and M. Head-Gordon, "Polishing the Gold Standard: The Role of Orbital Choice in CCSD(T) Vibrational Frequency Prediction", J. Chem. Theory Comput. 17, 742-755 (2021); doi: 10.1021/acs.jctc.0c00746
- Blunt, N. S.; Neuscamman, E., Excited-state diffusion Monte Carlo calculations: a simple and efficient two-determinant ansatz. *J. Chem. Theory Comput.* **2019**, 15, 178. DOI: 10.1021/acs.jctc.8b00879
- Chang, K.F.; M. Reduzzi, H. Wang, S.M. Poullain, Y. Kobayashi, L. Barreau, D. Prendergast, D.M. Neumark, and S.R. Leone, "Revealing electronic state-switching at conical intersections in alkyl iodides by ultrafast XUV transient absorption spectroscopy", Nat. Commun. 11, 4042 (2020); doi: 10.1038/s41467-020-17745-w
- Epifanovsky, E.; A.T.B. Gilbert, X. Feng, J. Lee, Y. Mao, N. Mardirossian, P. Pokhilko, A.F. White et al, "Software for the frontiers of quantum chemistry: An overview of developments in the Q-Chem 5 package", J. Chem. Phys. 155, 084801 (2021); doi: 10.1063/5.0055522.
- Eriksen, J.; T.A. Anderson, J.E. Deustua, K. Ghanem, D. Hait, M.R. Hoffmann, S. Lee, D. Levine, I. Magoulas, J. Shen, N. Tubman, K.B. Whaley, E. Xu, Y. Yao, N. Zhang, A. Alavi, G. Chan, M. Head-Gordon, W. Liu, P. Piecuch, S. Sharma, S. Ten-no, C. Umrigar, J. Gauss, "The Ground State Electronic Energy of Benzene", J. Phys. Chem. Lett. 11, 8922−8929 (2020); doi: 10.1021/acs.jpclett.0c02621
- Fang, J.; D. Hait, M. Head-Gordon, and M.C.Y. Chang, "Chemoenzymatic Platform for Synthesis of Chiral Organofluorines Based on Type II Aldolases", Ang. Chem. 131, 11967 –11971 (2019); doi: 10.1002/ange.201906805
- Garner, S. M.; Neuscamman, E., A variational Monte Carlo approach for core excitations, *J. Chem. Phys.*, **2020**, 153, 144108; doi: 10.1063/5.0020310
- Garner, S. M.; Neuscamman, E., Core Excitations with Excited State Mean Field and Perturbation Theory. *J. Chem. Phys.* **2020**, 153, 154102; doi: 10.1063/5.0020595
- Gobi, S.; Z. Lin, C. Zhu, M. Head-Gordon and R.I. Kaiser, "Oxygen Isotope Exchange Between Carbon Dioxide and Iron Oxides on Mars' Surface", J. Phys. Chem. Lett. 13, 2600−2606 (2022); doi: 10.1021/acs.jpclett.2c00289
- Hait, D.; A. Rettig, and M. Head-Gordon, "Well-behaved versus ill-behaved density functionals for single bond dissociation: Separating success from disaster functional by functional for stretched H_2", *J. Chem. Phys.* 150, 094115 (2019); doi: 10.1063/1.5080122
- Hait, D.; N.M. Tubman, D.S. Levine, K.B. Whaley, and M. Head-Gordon, "What levels of coupled cluster theory are appropriate for transition metal systems? A study using near exact quantum chemical values for 3d transition metal binary compounds" J. Chem. Theory Comput. 15, 5370−5385 (2019); doi: 10.1021/acs.jctc.9b00674
- Hait, D.; Y.H. Liang, and M. Head-Gordon, "Too big, too small or just right? A benchmark assessment of density functional theory for predicting the spatial extent of the electron density of small chemical systems", J. Chem. Phys. 154, 074109 (2021); doi: 10.1063/5.0038694
- Lee, J.; W. Huggins, M. Head-Gordon, and K.B. Whaley, "Generalized unitary coupled cluster wavefunctions for quantum computation", *J. Chem. Theory Comput.* 15, 311-324 (2019); doi: 10.1021/acs.jctc.8b01004

- Lee, J. and M. Head-Gordon, “Distinguishing Artificial and Essential Symmetry Breaking in a Single Determinant: Approach and Application to the C60, C36, and C20 Fullerenes”, *Phys. Chem. Chem. Phys.* 21, 4763-4778 (2019); doi: 10.1039/c8cp07613h
- Lee, J. and M. Head-Gordon, “Two Single-Reference Approaches to Singlet Biradicaloid Problems: Complex, Restricted Orbitals and Approximate Spin-Projection Combined With Regularized Orbital-Optimized Møller-Plesset Perturbation Theory”, J. Chem. Phys. 150, 244106 (2019); doi: 10.1063/1.5097613
- Lee, J.; L.W. Bertels, D.W. Small, and M. Head-Gordon, “Kohn-Sham density functional theory with complex, spin-restricted orbitals: Accessing a new class of densities without the symmetry dilemma”, Phys. Rev. Lett. 123, 113001 (2019); doi: 10.1103/PhysRevLett.123.113001
- Loipersberger, M.; L.W. Bertels, J. Lee, and M. Head-Gordon, “Exploring the Limits of Second- and Third-Order Møller-Plesset Perturbation Theory for Non-Covalent Interactions: Revisiting MP2.5 and Assessing the Importance of Regularization and Reference Orbitals”, J. Chem. Theory Comput. 17, 5582–5599 (2021); doi: 10.1021/acs.jctc.1c00469
- Lu, W.; C.J. Mackie, B. Xu, M. Head-Gordon and M. Ahmed, “A computational and experimental view of hydrogen bonding in glycerol water clusters”, J. Phys. Chem. A 126, 1701−1710 (2022); doi: 10.1021/acs.jpca.2c00659
- Otis, L.; Neuscamman, E., “Complementary First and Second Derivative Methods for Ansatz Optimization in Variational Monte Carlo” *Phys. Chem. Chem. Phys.* **2019**, 21, 14491; doi: 10.1039/C9CP02269D
- Pineda Flores, S. D. and E. Neuscamman, Excited State Specific Multi-Slater Jastrow Wave Functions. *J. Phys. Chem. A* **2019**, 123, 1487. DOI: 10.1021/acs.jpca.8b10671
- Rettig, A.; D. Hait, and M. Head-Gordon, "Third order Moller-Plesset theory made more useful? The role of density functional theory orbitals", J. Chem. Theory Comput. 16, 7473-7489 (2020); doi: 10.1021/acs.jctc.0c00986
- Shee, J.; M. Loipersberger, D. Hait, J. Lee and M. Head-Gordon, “Revealing the nature of electron correlation in transition metal complexes with symmetry-breaking and chemical intuition”, J. Chem. Phys. 154, 194109 (2021); doi: 10.1063/5.0047386
- Shee, J.; M. Loipersberger, A. Rettig, J. Lee, M. Head-Gordon, “Regularized Second-Order Møller−Plesset Theory: A More Accurate Alternative to Conventional MP2 for Noncovalent Interactions and Transition Metal Thermochemistry for the Same Computational Cost”, J. Phys. Chem. Lett. 12, 12084-12097 (2021); doi: 10.1021/acs.jpclett.1c03468
- Talbot, J.J.; M. Head-Gordon, W.H. Miller and S.J. Cotton, “Dynamic signatures of electronically nonadiabatic coupling in sodium hydride: a rigorous test for the symmetric quasi-classical model applied to realistic, ab initio electronic states in the adiabatic representation”, Phys. Chem. Chem. Phys. 24, 4820–4831 (2022); doi: 10.1039/d1cp04090a
- Toulson, B. W.; Borgwardt, M.; Wang, H.; Lackner, F.; Chatterley, A. S.; Pemmaraju, C. D.; Neumark, D. M.; Leone, S. R.; Prendergast, D.; Gessner, O.; Probing ultrafast C–Br bond fission in the UV photochemistry of bromoform with core-to-valence transient absorption spectroscopy, *Structural Dynamics* **2019**, 6, 054304; doi: 10.1063/1.5113798
- Tubman, N.M., C.D. Freeman, D.S. Levine, D. Hait, M. Head-Gordon, K.B. Whaley, “Modern Approaches to Exact Diagonalization and Selected Configuration Interaction with the Adaptive Sampling CI Method”, J. Chem. Theory Comput. 16, 2139-2159 (2020); doi: 10.1021/acs.jctc.8b00536
- Wang, H.; Odelius, M.; Prendergast, D., A combined multi-reference pump-probe simulation method with application to XUV signatures of ultrafast methyl iodide photodissociation, *J. Chem. Phys.* **2019**, 151, 124106-; doi: 10.1063/1.5116816
- Witzke, R.; D. Hait, K. Chakarawet, M. Head-Gordon, and T. D. Tilley, “Bimetallic Mechanism for Alkyne Cyclotrimerization with a Two-Coordinate Fe Precatalyst”, ACS Catal. 10, 7800−7807 (2020); doi: 10.1021/acscatal.0c01828
- Witzke, R.; D. Hait, M. Head-Gordon, T.D. Tilley, “Two-Coordinate Iron(I) Complexes on the Edge of Stability: Influence of Dispersion and Steric Effects”, Organometallics 40, 1758–1764 (2021); doi: 10.1021/acs.organomet.1c00218
- Wuttig, A.; J. Derrick, M. Loipersberger, A. Snider, M. Head-Gordon, C.J. Chang, and F.D. Toste, “Controlled Single Electron Transfer via Metal-Ligand Cooperativity Drives Divergent Nickel Electrocatalyzed Radical Pathways”, J. Am. Chem. Soc. 143, 6990-7001 (2021); doi: 10.1021/jacs.1c01487
- Xu, B.; T. Stein, U. Ablikim, L. Jiang, J. Hendrix, M. Head-Gordon, and M. Ahmed, “Probing solvation and reactivity in ionized polycyclic aromatic hydrocarbon-water clusters with photoionization mass spectrometry and electronic structure calculations”, Faraday Disc. 217, 414-433 (2019); doi: 10.1039/c8fd00229k

Fundamental Molecular Spectroscopy and Chemical Dynamics

Stephen R. Leone and Daniel M. Neumark
Lawrence Berkeley National Laboratory and Department of Chemistry,
University of California, Berkeley, California 94720
(510) 643-5467, srl@berkeley,edu
(510)-642-3502 dneumark@berkeley,edu

Scope of the Project: Decades of research into molecular dynamics, including branching fractions, dissociation dynamics, and energetics, have vastly improved our fundamental understanding of chemical processes. Measurements of radical spectroscopy, ions and excited state dynamics comprise key future goals of these efforts, especially the development of new ways to probe excited-state dynamics and photoproducts by the program of Leone and Neumark. The Leone group has pioneered ultrafast time-resolved table-top x-ray spectroscopic investigations of chemical dynamics at sufficiently high photon energies to access the carbon K-edge. Ultrafast x-ray transient absorption spectroscopy based on this methodology investigates transition states and products. Together, Leone and Neumark have developed a few-femtosecond x-ray capability based on attosecond pulse technology in the soft x-ray regime up to the carbon K edge. The Neumark program uses a methodology of slow electron velocity-map imaging of cryogenically cooled anions (cryo-SEVI), a high-resolution variant of photoelectron spectroscopy.

Recent Progress:

Ultrafast Soft X-ray Transient Absorption Experiments

Carbon K-edge spectroscopy was used to study pentamethylcyclopentadiene that sheds light on new photodynamics, which is in contrast to other ring systems such as cyclohexadiene. Previous work suggested that rather than undergoing ring opening, a relaxation to the ground electronic state would occur. This mechanism corresponds to the passage through two conical intersections from the initially populated $1B_2$ state and the dark $2A_1$ state and then subsequently to the $1A_1$ state. Probing from the core level has provided unique insights not observed in photoelectron spectroscopy, due to the general ability to selectively probe different atoms within the molecule. It was determined that a dissociation channel corresponding to loss of a hydrogen atom occurs on the timescale of 1 ps. The results mark a clear demonstration of the ability of transient x-ray spectroscopy to resolve radical species to a degree not attainable in traditional experiments such as photoelectron spectroscopy. Aiding in the assignment of this channel are calculations of the x-ray absorption spectra conducted by Martin Head-Gordon's group using density functional theory with the standard spin-unrestricted Kohn-Sham formalism. Based on the experimental and theorical results it is theoretically determined that the photo-induced dynamics following excitation may primarily pass through the $1B_2$ state with a barrier to form the radical.

Benzaldehyde under photoexcitation can dissociate into fragments, including CO and HCO. With 266 nm excitation, electronic ground state benzaldehyde is promoted to the S_2 ($\pi\pi^*$) state. The dynamics of this state has been studied by time-of-flight mass spectroscopy, multi-mass ion imaging spectroscopy, and ultrafast electron diffraction spectroscopy. Through internal conversion and intersystem crossing the molecule will relax to the S_1 ($n\pi^*$) and triplet states and eventually lead to the dissociated fragments. We used ultrafast time-resolved x-ray absorption spectroscopy at the carbon K-edge to distinguish the singlet and triplet states with

core-level probing. The transitions from carbon 1s to π are strongly blue shifted in the S_1 state. And the transitions from carbon 1s to π* are red shifted in the triplet states. Without requiring information on the oxygen K-edge, we are the able to distinguish singlet and triplet states by the carbon core-level absorption spectroscopy's sensitivity to molecular geometry and specific carbon atom chemical environments.

Additional work with the ultrafast soft x-ray-probe apparatus has been initiated with an extension to a 200 nm pump excitation arm, facilitating the study of a wider range of molecular systems previously inaccessible by x-ray transient absorption techniques. The increased absorption of many organic molecules at 200 nm, compared to 266 nm, and the ability to probe new types of orbitals coupled with the selectivity of x-ray spectroscopy will allow for powerful experiments to be performed. Significant amounts of 200 nm light were generated, corresponding to a maximum energy of 10 μJ with a pulse duration of approximately 150-200 fs and a bandwidth of 1 nm.

Preliminary work has been conducted on 1,3-butadiene, a prototypical polyene molecule, corresponding to the first transient x-ray measurements at the carbon K-edge with a 200 nm pump excitation, to our knowledge. Here excitation into the S_2 (^1B_u) bright state was initiated, following which relaxation through a conical intersection to the multireference S_1 (^1A_g) dark state occurs before passage through a subsequent conical intersection to the ground electronic state. The exact character of the S_1 to S_0 relaxation mechanism is still under consideration by researchers, with the primary pathway being either an ionic-like mechanism much like ethylene or a covalent-like mechanism reminiscent of longer polyenes. The sensitivity of x-ray absorption can distinguish these pathways from one another and it was observed that the covalent/polyene mechanism is responsible for the relaxation on a similar timescale ascribed to the S_1 state lifetime from previous studies in the literature.

Few-Femtosecond/Attosecond Soft X-ray Transient Absorption Experiments

For the newly built attosecond, few-femtosecond soft-x-ray apparatus, carbon tetrachloride (CCl_4) was excited via a broadband few-femtosecond 800 nm pulse, similar to experiments on sulfur hexafluoride (SF_6) and carbon dioxide (CO_2) discussed previously. Such a strong field process would correspond to excitation via impulsive stimulated Raman scattering and strong field ionization and the results provided valuable new information on both the neutral and ionized molecule. For CCl_4, the simultaneous observation of both the carbon K-edge (~280-300 eV) and chlorine $L_{2,3}$-edge (~195-220 eV) provides new information that clearly demarcates the location and potential surfaces of different atoms within the molecule, providing an new view of the excited state dynamics.

Regarding excitation via impulsive stimulated Raman scattering, the same vibrational superposition is observed through different core-excited states. Here the symmetric v_1 mode with a frequency of 456 cm^{-1} was observed at both the chlorine and carbon edges. X-ray absorption spectroscopy proves extremely sensitive to changes in the internuclear distance and was able to show that the various core-excited states respond differently to the same vibrational wavepacket, resulting in shifts in the energy of the x-ray absorption transitions. Calculations of the curvature of these core level potential energy surfaces were conducted by the Martin Head Gordon group and it was found that the relative slopes of the 3 core level states agree with the experimental results extremely well. From the combination of experimental and theoretical results it was determined that the terminal chlorine atoms show a much larger change along the normal coordinate than the central carbon atom.

In addition to the information gleaned from neutral CCl_4, the excitation with higher-energy few-femtosecond 800 nm pulses also resulted in strong field ionization, producing CCl_4^+. Calculations performed through the collaboration with the Martin Head-Gordon group were carried out with orbital-optimized density functional theory with the SCAN functional, which has been shown to be accurate to within 0.3 eV rms for both closed-shell and open shell species. The combination of calculations and experiments produced the overall results summarized below.

It was observed that CCl_4^+ undergoes symmetry breaking corresponding to a Jahn-teller driven distortion causing the initial tetrahedral T_d structure to become a symmetry broken C_{2v} type structure in 6 ± 2 fs. Further dynamics were observed corresponding to a further symmetry breaking with molecular rearrangement to a non-covalently bonded complex corresponding to a central C_{3v} geometry in 90 ± 10 fs. Here it was expected that the fourth chlorine atom is weakly coupled with the central carbon atom at roughly 3.38 Angstroms. It was observed that this chlorine slowly dissociates to CCl_3^+ and Cl in approximately 800 fs resulting in the final photoproducts. Additional higher-energy photochannels corresponding to CCl_3 and Cl^+ were also observed with a delay of 37 ± 6 fs and a growth rate of 85 ± 10 fs. It was observed that this high energy channel is much more efficient when produced with strong field ionization compared to techniques such as electron impact and single-photon ionization, leading to information regarding the efficiency of ion production with pulse duration.

Free radical spectroscopy

Using a newly acquired tunable infrared laser, the Neumark group can now obtain cryo-SEVI spectra for anions with low electron binding energy. Cryo-SEVI yields precise electron affinities and vibrational frequencies for free radicals, and the capability to explore hydrocarbon and related radicals with low electron affinities will complement the time-resolved experiments carried out with femtosecond and attosecond x-ray sources as described above. Specifically, cryo-SEVI was used to obtain the high-resolution photoelectron spectrum of the acetyl anion, CH_3CO^-, a less stable isomer of the more extensively studied vinoxide anion (CH_2CHO^-). The CH_3CO radical is formed from the dissociation of acetone and other ketones. It is an important intermediate in tropospheric hydrocarbon oxidation. Nonetheless, its spectroscopic characterization has been elusive. The cryo-SEVI spectrum yields a precise electron affinity for the acetyl radical, 0.435 eV, and well-resolved progressions are observed in three vibrational modes of the radical. Franck-Condon analysis indicates a significant change in geometry upon photodetachment primarily in the C-C-O bend angle.

Future Plans:

The UV-pump and soft x-ray-probe apparatus will continue to be used to spectroscopically investigate fundamental photochemical processes. Topics such as the decomposition of ketones and the production of diradicals, ring puckering and ring opening dynamics, in addition to the study of cycloaddition reactions, will continue to be a focus for research in the future. Additional investigations, including methyl vinyl ketone, furanone and norbornadiene, remain exciting possibilities to study such fundamental photochemical processes. To aid in the study of these molecules, compression of the 200 nm pump pulse will be implemented to greatly improve the temporal resolution of the experiment to approach the transform limited duration of 60 fs corresponding to the FWHM of 1 nm of the successfully produced pulse. Extending the cut-off energy of the soft x-ray probe to reach the nitrogen K-edge (410eV) will be undertaken through tuning the wavelength of the pulse driving the high harmonic generation process. The attosecond soft x-ray beamline will make use of the excellent temporal resolution

corresponding to the few femtosecond 800 nm pulses to study the Jahn-Teller distortion in strong field ionized methane. The improved temporal resolution of the setup will also be used for the study of charge migration dynamics on molecules such as uracil. Here an oscillating charge distribution in the π orbitals will allow for XAS to probe the hole density on each carbon molecule during such a migration. The attosecond beamline will also be combined with a 267 nm UV pump to provide the necessary temporal resolution to directly observe Jahn-Teller distortion in the abrupt formation of benzene cation and the excited state dynamics corresponding to the passage through a conical intersection, such as in acetylacetone and cyclohexadiene.

Cryo-SEVI experiments will be carried out on several peroxy radicals of interest, in particular two acyl peroxy species: peroxyformyl $HC(O)CO_2$ and peroxyacetyl $CH_3C(O)CO_2$. These species represent the next level of chemical complexity with respect to the alkyl peroxy radicals previously studied by the Neumark group, which complement planned carbon K-edge femtosecond transient absorption work on ketones. Moreover, both radicals play a key role as reactive intermediates in combustion and atmospheric chemistry. In a new research direction, cryo-SEVI experiments will be performed on anions that have been pre-excited with an infrared laser; this experiment, which will be carried out on the allyl anion, represents a novel means to measure infrared spectra of cold, gas phase anions and to simultaneously explore neutral vibrational energy levels and regions of the neutral potential energy surface that are inaccessible via detachment from the anion ground vibrational state.

Recent Publications Acknowledging DOE GPCP Support (2019-2022):

- Chang, K. F.; Wang, H.; Poullain, S. M.; Gonzalez-Vazquez, J.; Banares, L.; Prendergast, D.; Neumark, D. M.; Leone, S.R., "Conical intersection and coherent vibrational drnamics in alkyl iodides captured by attosecond transient absorption spectroscopy". J. Chem. Phys. 156, 114304 (**2022**). DOI: 10.1063/5.0086775
- Chambreau, S. D.; Popolan-Vaida, D. M.; Kostko, O.; Lee, J. K.; Zhou, Z.; Brown, T. A.; Jones, P.; Shao, K.; Zhang, J.; Vaghjiani, G.L.; Zare, R. N.; Leone, S.R., "Thermal and Catalytic Decomposition of 2-Hydroxyethylhydrazine and 2-Hydroxyethylhydrazinium Nitrate Ionic Liquid". J. Phys. Chem. A. 126, 373-394 (**2022**). DOI: 10.1021/acs.jpca.1c07408
- Scutelnic, V.; Tsuru, S.; Papai, M.; Yang, Z/; Epshtein, M.; Xue, T.; Haugen, E.; Kobayashi, Y.; Krylov, A. I.; Coriani, S.; Leone, S.R., "X-ray transient absorption reveals the ^1A_u ($n\pi^*$) state of pyrazine in electronic relaxation". Nat. Commun. 12, 5003 (**2021**). DOI: 10.1038/s41467-021-25045-0
- Rebholz, M.; Ding, T.; Despre, V.; Aufleger, L.; Hartmann, M.; Meyer, K.; StooB, V.; Magunia, A.; Wachs, D.; Birk, P.; Mi, Y.; Borisova, G. D.; Castanheira, C. C.; Rupprecht, P.; Schmid, G.; Schnorr, K.; Scgriter. C. D.; Moshammer, R.; Loh, Z.; Attar, A. R.; Leone, S.R.; Gaummitz, T.; Worner, H. J.; Roling, S.; Butz, M.; Zacharias, H.; Dusterer. S.; Treush, R.; Brenner, G.; Vester, J.; Kuleff, A. I.; Ott, C.; Pfeifer. T., "All-XUV Pump-Probe Transient Absorption Sepctroscopy of the Structural Molecular Dynamics of Di-iodomethane". Phys. Rev. X. 11, 031001 (**2021**). DOI: 10.1103/PhysRevX.11.031001
- Chang, K. F.; Wang, H.; Poullain, S. M.; Prendergast, D.; Neumark, D. M.; Leone, S.R., "Mapping wave packet difurcation at ta conical intersection in CH_3I by attosecond XUV transient absorption spectroscopy". J. Chem. Phys. 154, 234301 (**2021**). DOI: 10.1063/5.0056299

- Scutelnic, V.; Leone, S.R., "Elucidation of Molecular Dynamics by Extreme Ultraviolet and Soft X-ray Transient-Absorption Spectroscopy". ACS Symposium Series, Emerging Trends in Chemical Applications of Lasers, 1398, 1-14 **(2021)**. DOI: 10.1021/bk-2021-1398.ch001
- Chang, K. F.; Reduzzi, M.; Wang, H.; M.-Poullain, S.; Kobayashi, Y.; Barreau, L.; Prendergast, D.; Neumark, D. M.; Leone, S. R., "Revealing Electronic State-Switching at Conical Intersections in Alkyl Iodides by Ultrafast XUV Transient Absorption Spectroscopy". Nat. Commun. 11, 4042 **(2020).** DOI: 10.1038/s41467-020-17745-w.
- Epshtein, M.; Scutelnic, V.; Yang, Z.; Xue, T.; Vidal, M. L.; Krylov, A. I.; Coriani, S.; Leone, S. R. "Table-Top X-Ray Spectroscopy of Benzene Radical Cation". J. Phys. Chem. A, 124, 9524–9531 **(2020)**. DOI: 10.1021/acs.jpca.0c08736.
- Nichols, B.; Sullivan, E. N.; Neumark, D. M., "Photodissociation Dynamics of the tert-butyl perthiyl Radical". J. Chem. Phys. 152, 244301 **(2020).** DOI: 10.1063/5.0006913.
- Sullivan, E. N.; Saric, S.; Neumark, D. M., "Photodissociation of iso-Propoxy (i-C3H7O) Radical at 248 nm". Phys. Chem. Chem. Phys. 22, 17738-17748 **(2020)**. DOI: 10.1039/d0cp02493g.
- Vidal, M. L.; Epshtein, M.; Scutelnic, V.; Yang, Z.; Xue, T.; Leone, S. R.; Krylov, A. I.; Coriani, S. "Interplay of Open-Shell Spin-Coupling and Jahn–Teller Distortion in Benzene Radical Cation Probed by X-Ray Spectroscopy". J. Phys. Chem. A 124, 9532–9541 **(2020)**. DOI: 10.1021/acs.jpca.0c08732.
- Hait, D.; Haugen, E.; Yang, Z.; Oosterbaan, K.; Leone, S. R.; Head-Gordon, M., "Accurate Prediction of Core-Level Spectra of Radicals at Density Functional Theory Cost via Square Gradient Minimization and Recoupling of Mixed Configurations". J. Chem. Phys. 153, 134108 **(2020)**. DOI: 10.1063/5.0018833.
- Barreau, L.; Ross, A. D.; Garg, S.; Kraus, P. M.; Neumark, D. M.; Leone, S. R. "Efficient Table-Top Dual-Wavelength Beamline for Ultrafast Transient Absorption Spectroscopy in the Soft X-ray Region". Sci. Rep. 10, 5773 **(2020)**. DOI: 10.1038/s41598-020-62461-6
- Sullivan, E. N.; Nichols, B.; Neumark, D. M.; "Fast Beam Photofragment Translational Spectroscopy of the Phenoxy Radical at 225 nm, 290 nm, and 533 nm". Phys. Chem. Chem. Phys. 21, 14270-14277 (**2019**). DOI: 10.1039/c8cp06818f
- Ramphal, I.; Lee, C.; Neumark, D. M., "Photodissociation Dynamics of the Methylsulfinyl Radical at 248 nm". Molec. Phys. 117, 3043-3055 (**2019**). DOI: 10.1080/00268976.2019.1580781
- Schnorr, K.; Bhattacheriee, A.; Oosterbaan, K. J.; Delcey, M. G.; Yang, Z.; Xue, T.; Attar, A. R.; Chatterley, A. S.; Head-Gordon, M.; Leone, S. R., Gessner, O.; "Tracing the 267 nm-Induced Radical Formation in Dimethyl Disulfide Using Time-Resolved X-ray Absorption Spectroscopy". J. Phys. Chem. Lett. 10, 1382−1387 (**2019**). DOI: 10.1021/acs.jpclett.9b00159
- Sullivan, E. N.; Nichols, B.; Kugelgen, S. v.; Silva, G. d.; Neumark, D. M., "Multiphoton Dissociation Dynamics of the Indenyl Radical at 248 nm and 193 nm". J. Chem. Phys. 151, 174303 (**2019**). DOI: 10.1063/1.5121294.
- DeVine, J. A.; Babin, M. C.; Blackford, K.; Neumark, D. M., "High-Resolution Photoelectron Spectroscopy of the Pyridinide Isomers". J. Chem. Phys. 151, 064302 (**2019**). DOI: 10.1063/1.5115413.
- Geneaux, R.; Marroux, H. J. B.; Guggenmos, A.; Neumark, D. M.; Leone, S. R., "Transient Absorption Spectroscopy Using High Harmonic Generation: A Review of Ultrafast X-ray Dynamics in Molecules and Solids". Phil. Trans. R. Soc. A 377, 20170463 (**2019**). DOI: 10.1098/rsta.2017.0463

SPECTROSCOPY AND DYNAMICS OF REACTION INTERMEDIATES IN COMBUSTION CHEMISTRY

Marsha I. Lester
Department of Chemistry
University of Pennsylvania
Philadelphia, PA 19104-6323
milester@sas.upenn.edu

I. Program Scope

Our research aims to characterize important, yet often elusive, reaction intermediates in combustion chemistry using novel spectroscopic and dynamical methods. A new thrust is focused on characterizing hydroperoxyalkyl radical intermediates (•QOOH) containing a carbon radical center (•Q), which are important intermediates in low temperature combustion of hydrocarbon fuels and atmospheric oxidation of volatile organic compounds. In addition, our research continues to focus on carbonyl oxides (Criegee intermediates, $R_1R_2C{=}O^+O^-$) with novel zwitterionic character, which are important intermediates in tropospheric hydrocarbon oxidation and some combustion reactions.

II. Recent Progress

A. Infrared spectroscopy and unimolecular dissociation dynamics of •QOOH

A new thrust of our research is centered on the infrared (IR) spectroscopy and unimolecular dissociation dynamics of a prototypical hydroperoxyalkyl radical (•QOOH) intermediate, specifically the carbon-centered •QOOH radical transiently formed in isobutane oxidation or other branched hydrocarbons. This prototypical •QOOH radical is generated in the laboratory by H-atom abstraction from *tert*-butyl hydroperoxide (TBHP) in a quartz capillary reactor tube, where it is collisionally stabilized, then rapidly cooled in a pulsed supersonic expansion, and directly observed through its infrared fingerprint and energy-dependent unimolecular decay to hydroxyl (OH) and cyclic ether products. Prior experimental studies of this system under thermal conditions had observed only its products, in particular the rate of formation of OH radicals and •OOQOOH radicals formed upon addition of O_2.[1, 2]

This laboratory conducted IR pump – UV probe measurements to obtain IR action spectra and time-resolved unimolecular decay rates for the •QOOH radical.[3, 4] The experiments utilized IR pump excitation to vibrationally activate •QOOH at energies in the vicinity of the transition state (TS) barrier leading to OH products. A UV probe laser then detected the OH radical products resulting from unimolecular decay by UV laser-induced fluorescence (LIF). Scanning the IR pump laser provided a distinctive spectral fingerprint of the •QOOH radical from 2950 to 7050 cm^{-1}.[4] The observed transitions are associated with overtone OH and CH stretch transitions, combination bands involving OH or CH stretch and a lower frequency mode, and fundamental OH and CH stretch transitions. The •QOOH transitions observed in the IR action spectra are identified by comparison with anharmonic vibrational frequency calculations[4] and, in most cases, are readily distinguished from the TBHP precursor.[5]

The IR activation provides sufficient energy for the jet-cooled •QOOH radicals to surmount or tunnel through the TS barrier leading to OH and cyclic ether products. As a result, the energy-resolved and time-dependent evolution of the •QOOH radicals to OH (v=0, N) products yield microcanonical energy-dependent unimolecular decay rates $k(E)$ for •QOOH in the vicinity of the TS barrier. These direct time-domain measurements revealed unimolecular decay rates ranging from $3.2 \pm 1.0 \times 10^6$ s^{-1} (and corresponding lifetime, $\tau = 309 \pm 96$ ns) at 3579.5 cm^{-1} to $\geq 2.6 \pm 0.5 \times 10^8$ s^{-1} ($\tau \leq 3.8 \pm 0.8$ ns; laser limited) at 6971.5 cm^{-1}.[3] A subsequent study on •QOOD with partial deuteration (–OOH/D) and OD detection provided an additional window for probing the energy-dependent unimolecular dissociation rate at 5198 cm^{-1} of $1.0 \pm 0.3 \times 10^8$ s^{-1} ($\tau = 9.8 \pm 3.0$ ns).[6]

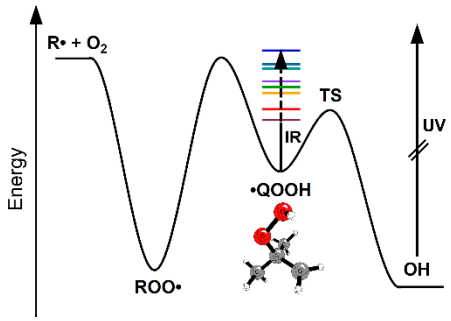

Figure 1. Schematic reaction pathway illustrating IR activation of a prototypical carbon-centered hydroperoxyalkyl radical (•QOOH) at energies above and below the transition state (TS) barrier to unimolecular reaction with direct time-resolved detection of OH products.

Energy-dependent microcanonical rates $k(E)$ are exquisitely sensitive to the properties of the TS barrier that leads to unimolecular reaction. For •QOOH, the experimental rates $k(E)$ are both more rapid and extend to lower energy than anticipated based on a prior exploration of the TS barrier involving a high-level focal point analysis that yielded a zero-point corrected dissociation barrier of 12.0 kcal mol^{-1}.[7] Rather, substantially higher-level electronic structure methods were required to obtain a more reliable barrier of 10.3 kcal mol^{-1} and imaginary frequency (763i cm^{-1}) at the TS, along with associated rovibrational properties at stationary points along the reaction coordinate.[3] The theoretical analysis revealed that the minimum energy pathway is composed of the simultaneous elongation of the O-O bond and contraction of the C-C-O angle, leading to OH radical and cyclic ether products. Subsequent statistical RRKM rate calculations that utilized the combined reduction in the TS barrier height and imaginary frequency resulted in excellent agreement with experimental rate measurements over a wide range of energies from 10 to 20 kcal mol^{-1}, and demonstrated that heavy atom tunneling significantly enhances (two-fold) the unimolecular decay rates.[3] Further validation was provided by the very good agreement between the experimental and computed rates for •QOOD, after accounting for small changes in zero point energy upon partial deuteration.[6]

The experimentally measured and theoretically validated microcanonical rates $k(E)$ also enabled reliable extension using a fully *a priori* method[8] to obtain the pressure-dependent thermal unimolecular rate constants $k(T,P)$ for a prototypical •QOOH,[3] which are in excellent accord with prior kinetic studies of $k(T,P)$ based on the of appearance of OH products.[1, 2] The thermal unimolecular rate constants $k(T,P)$ are generally used in global chemical models of oxidation in atmospheric and combustion environments.

B. Electronic spectroscopy and photoinitiated dynamics

We continued our investigation of the photodissociation dynamics of two Criegee intermediates derived from isoprene ozonolysis: formaldehyde oxide (CH_2OO) and methyl vinyl ketone oxide [$(CH_2{=}CH)(CH_3)COO$, MVK-oxide]. In MVK-oxide, we characterized the second $\pi^* \leftarrow \pi$ transition at $\lambda \leq 300$ nm, primarily associated with the vinyl group, by a UV-induced ground state depletion method with photoionization detection on the parent mass (m/z 86).[9] In both systems, velocity map imaging experiments revealed an onset of bimodal total kinetic energy release (TKER) distributions for the O (^{1}D) + H_2CO (X $^1A_1$) products at $\lambda \leq 350$ nm or O (^{1}D) + MVK (X $^1A'$) products at $\lambda \leq 300$ nm. In both cases, the product distributions exhibited a distinctive low TKER component associated with highly internally excited H_2CO or methyl vinyl ketone (MVK) co-products. For CH_2OO, complementary trajectory calculations indicated that the bimodal TKER distribution originates from multiple dissociation pathways through two regions of strong coupling that control the branching and energy distributions of the products.[10] For MVK-oxide, an isotropic angular distribution for the low TKER component suggested that the second pathway involves internal conversion to the ground electronic state and statistical dissociation.[9]

C. Photoionization mass spectrometry studies of bimolecular chemistry

In the past year, we extended our collaboration with Caravan, Klippenstein, and Taatjes on the bimolecular chemistry of Criegee intermediates. We examined functionalized hydroperoxide formation in the reaction of methacrolein oxide [$(CH_2=C)(CH_3)CHOO$, MACR-oxide], an isoprene derived Criegee intermediate, with formic acid.[11] We also characterized the dramatic conformer-dependent reactivity of *anti*-CH_3CHOO vs. *syn*-CH_3CHOO with dimethyl amine.[12] The key results of these studies are presented in Caravan's DOE abstract.

III. Ongoing and Future Work

Current and future experiments are exploring the impact of resonance stabilization on the unimolecular and bimolecular reactions of Criegee intermediates (CIs). Experiments at Penn are focused on electronic spectroscopy and photoinitiated dynamics. We are also continuing our collaboration with Caravan and Taatjes on experiments using the Sandia Multiplexed Photoionization Mass Spectrometer (MPIMS) at the Advanced Light Source. These studies compare the reactions of isoprene-derived CIs, MVK-oxide and MACR-oxide, which have extended conjugation across the vinyl (C=C) and carbonyl oxide ($C=O^+-O^-$) groups, with structurally similar four-carbon CIs having unconjugated functional groups. Ongoing analysis of unimolecular decay of four-carbon CIs via 1,4 H-atom transfer, generally followed by O-O bond fission that releases OH radicals,[13, 14] appears to also result in roaming-induced isomerization to hydroxycarbonyl products. Current experiments are examining the rates and products of bimolecular reactions of CIs – with and without extended conjugation – involving key atmospheric species (water vapor, SO_2, formic acid, NO_2). These bimolecular reactions involve remarkably different types of mechanisms, 1,2 addition, 1,4 addition, and secondary ozonide (SOZ) formation, which form more highly oxygenated products with greater mass.

IV. References

1. J. Zádor, H. Huang, O. Welz, J. Zetterberg, D. L. Osborn and C. A. Taatjes, Phys. Chem. Chem. Phys. **15**, 10753 (2013).
2. C. A. Whelan, M. A. Blitz, R. Shannon, L. Onel, J. P. Lockhart, P. W. Seakins and D. Stone, J. Phys. Chem. A **123**, 10254 (2019).
3. A. S. Hansen, T. Bhagde, K. B. Moore, D. R. Moberg, A. W. Jasper, Y. Georgievskii, M. F. Vansco, S. J. Klippenstein and M. I. Lester, Science **373**, 679 (2021).
4. A. S. Hansen, T. Bhagde, Y. Qian, A. Cavazos, R. M. Huchmala, M. A. Boyer, C. F. Gavin-Hanner, S. J. Klippenstein, A. B. McCoy and M. I. Lester, J. Chem. Phys. **156**, 014301 (2022).
5. A. S. Hansen, R. M. Huchmala, E. Vogt, M. A. Boyer, T. Bhagde, M. F. Vansco, C. V. Jensen, A. Kjærsgaard, H. G. Kjaergaard, A. B. McCoy and M. I. Lester, J. Chem. Phys. **154**, 164306 (2021).
6. T. Bhagde, A. S. Hansen, S. Chen, P. J. Walsh, S. J. Klippenstein and M. I. Lester, Faraday Discuss. (2022).
7. K. B. Moore, J. M. Turney and H. F. Schaefer, J. Chem. Phys. **146**, 194304 (2017).
8. A. W. Jasper, K. M. Pelzer, J. A. Miller, E. Kamarchik, L. B. Harding and S. J. Klippenstein, Science **346**, 1212 (2014).
9. G. Wang, T. Liu, A. Caracciolo, M. F. Vansco, N. Trongsiriwat, P. J. Walsh, B. Marchetti, T. N. V. Karsili and M. I. Lester, J. Chem. Phys **155**, 174305 (2021).
10. V. J. Esposito, T. Liu, G. Wang, A. Caracciolo, M. F. Vansco, B. Marchetti, T. N. V. Karsili and M. I. Lester, J. Phys. Chem. A **125**, 6571 (2021).
11. M. F. Vansco, K. Zuraski, F. A. F. Winiberg, K. Au, N. Trongsiriwat, P. J. Walsh, D. L. Osborn, C. J. Percival, S. J. Klippenstein, C. A. Taatjes, M. I. Lester and R. L. Caravan, Molecules **26**, 3058 (2021).
12. M. F. Vansco, M. Zou, I. O. Antonov, K. Ramasesha, B. Rotavera, D. L. Osborn, Y. Georgievskii, C. J. Percival, S. J. Klippenstein, C. A. Taatjes, M. I. Lester and R. L. Caravan, J. Phys. Chem A **126**, 710 (2022).

13. V. P. Barber, S. Pandit, A. M. Green, N. Trongsiriwat, P. J. Walsh, S. J. Klippenstein and M. I. Lester, J. Am. Chem. Soc. **140**, 10866 (2018).
14. V. P. Barber, A. S. Hansen, Y. Georgievskii, S. J. Klippenstein and M. I. Lester, J. Chem. Phys. **152**, 094301 (2020).

V. Publications supported by this DOE project (2020-present)

1. R. L. Caravan, M. F. Vansco, K. Au, M. A. H. Khan, Y.-L. Li, F. A. F. Winiberg, K. Zuraski, Y.-H. Lin, W. Chao, N. Trongsiriwat, P. J. Walsh, D. L. Osborn, C. J. Percival, J. Jr-M. Lin, D. E. Shallcross, L. Sheps, S. J. Klippenstein, C. A. Taatjes, and M. I. Lester, "Direct kinetic measurements and theoretical predictions of an isoprene-derived Criegee intermediate", *Proc. Natl. Acad. Sci.* **117**, 9733-9740 (2020). https://doi.org/10.1073/pnas.1916711117
2. M. F. Vansco, R. L. Caravan, K. Zuraski, F. A. F. Winiberg, K. Au, N. Trongsiriwat, P. J. Walsh, D. L. Osborn, C. J. Percival, M. A. H. Khan, D. E. Shallcross, C. A. Taatjes, and M. I. Lester, "Experimental evidence of dioxole unimolecular decay pathway for isoprene-derived Criegee intermediates", *J. Phys. Chem. A* **124**, 3542-3554 (2020). https://doi.org/10.1021/acs.jpca.0c02138
3. M. F. Vansco, R. L. Caravan, S. Pandit, K. Zuraski, F. A. F. Winiberg, K. Au, T. Bhagde, N. Trongsiriwat, P. J. Walsh, D. L. Osborn, C. J. Percival, S. J. Klippenstein, C. A. Taatjes, and M. I. Lester, "Formic Acid Catalyzed Isomerization and Adduct Formation of an Isoprene-Derived Criegee Intermediate: Experiment and Theory", *Phys. Chem. Chem. Phys* **22,** 26796-26805 (2020). https://doi.org/10.1039/D0CP05018K
4. R. L. Caravan, M. F. Vansco, and M. I. Lester, "Open questions on the reactivity of Criegee intermediates", *Commun. Chem*. **4**, 44 (2021). https://rdcu.be/chswf
5. V. J. Esposito, T. Liu, G. Wang, A. Caracciolo, M. F. Vansco, B. Marchetti, T. Karsili, and M. I. Lester, "Photodissociation Dynamics of CH_2OO on Multiple Potential Energy Surfaces: Experiment and Theory", *J. Phys. Chem. A* **125**, 6571-6579 (2021). https://doi.org/10.1021/acs.jpca.1c03643
6. A. S. Hansen, T. Bhagde, K. B. Moore III, D. R. Moberg, A. W. Jasper, Y. Georgievskii, M. F. Vansco, S. J. Klippenstein, and M. I. Lester, "Watching a Hydroperoxyalkyl Radical (•QOOH) Dissociate", *Science* **373**, 679-682 (2021).
7. M. F. Vansco, K. Zuraski, F. A. F. Winiberg, K. Au, N. Trongsiriwat, P. J. Walsh, D. L. Osborn, C. J. Percival, S. J. Klippenstein, C. A. Taatjes, M. I. Lester, and R. L. Caravan, "Functionalized Hydroperoxide Formation from the Reaction of Methacrolein-oxide, an Isoprene-Derived Criegee Intermediate, with Formic Acid: Experiment and Theory", *Molecules* **26**, 3058 (2021). https://doi.org/10.3390/molecules26103058
8. G. Wang, T. Liu, A. Caracciolo, M. F. Vansco, N. Trongsiriwat, P. J. Walsh, B. Marchetti, T. Karsili, and M. I. Lester, "Photodissociation Dynamics of Methyl Vinyl Ketone Oxide: A four-carbon unsaturated Criegee intermediate from isoprene ozonolysis", *J. Chem. Phys.* **155**, 174305 (2021). https://doi.org/10.1063/5.0068664
9. M. F. Vansco, M. Zou, I. O. Antonov, K. Ramasesha, B. Rotavera, D. L. Osborn, Y. Georgievski, C. J. Percival, S. J. Klippenstein, C. A. Taatjes, M. I. Lester, and R. L. Caravan, "Dramatic conformer-dependent reactivity of the acetaldehyde oxide Criegee intermediate with dimethylamine via a 1,2-insertion mechanism", *J. Phys. Chem. A* **126**, 710–719 (2022). https://doi.org/10.1021/acs.jpca.1c08941
10. T. Bhagde, A. S. Hansen, S. Chen, P. J. Walsh, S. J. Klippenstein, and M. I. Lester, "Energy-resolved and time-dependent unimolecular dissociation of hydroperoxyalkyl radicals (•QOOH)", *Faraday Discuss.* (2022), accepted manuscript. https://doi.org/10.1039/D2FD00008C

Chemistry of Ammonia-Based Fuels

Paul Marshall
Department of Chemistry and Center for Advanced Scientific Computing and Modeling
University of North Texas, 1155 Union Circle #305070, Denton, TX 76203
E-mail marshall@unt.edu

Program Scope

Ammonia can serve as a carbon-free energy transfer fuel when it is synthesized from green sources of energy such as wind, solar or hydroelectric. Liquid ammonia is relatively easily transported (by comparison to liquid hydrogen) and can be catalytically decomposed to release hydrogen for use in fuel cells, or directly burned for energy release, for example, as a substitute for diesel fuel. There are indications that ammonia's ignition and engine properties are improved by mixing with conventional fuel. This study is aimed at understanding the combustion chemistry of ammonia alone and in conjunction with hydrocarbons, so that with a reliable chemical mechanism, engines can be modified or designed intelligently.

Species to be considered are ammonia (NH_3) and the primary product of radical attack, amino radicals (NH_2). Recombination of a pair of NH_2 radicals leads to hydrazine (N_2H_4). Oxidation of NH_2 leads to nitrogen oxide intermediates and species such as NH_2O and NH_3O. Cross reactions with hydrocarbons, such as recombination of NH_2 and CH_3, will form amines (and perhaps unsaturated imines) and subsequent chemistry of the exemplar methylamine (CH_3NH_2) and related species will be investigated. Key radicals in high-temperature combustion are H and OH, where the rapid diffusion of atomic hydrogen in particular influences flame speed. In the ignition regime, below 1000 K, hydroperoxy (HO_2) radicals have important roles in determining ignition delay. Reactions with O_2 allow for initial attack on fuel molecules and radical formation, and can provide chain-branching at high temperatures. These systems will be studied both by theory and experiments, in the context of isolated elementary reactions and in multireaction systems, to gain fundamental insight into nitrogen chemistry, to permit detailed comparisons with theory, and to create a quantitative mechanism for combustion of ammonia/hydrocarbon mixtures.

Recent progress

Laser-photolysis laser-induced fluorescence is applied to measure radical kinetics under conditions (low concentration and short time) where single elementary reactions dominate the measured species profiles. Exploration of NH_2 chemistry is the first experimental target, and the rate constant k_1 for

$$NH_2 + N_2H_4 \rightarrow \text{products} \quad (1)$$

was measured at room temperature. We obtained the temperature dependence via Multistructural Improved Canonical Variational Transition State Theory with Small Curvature Tunneling, with geometries and scaled frequencies obtained with M06-2X/6-311+G(2df,2p) theory, and single-point energies from CCSD(T)-F12b/cc-pVTZ-F12 theory, plus a term to correct approximately for electron correlation through CCSDT(Q). Theory and experiment matched with a -2.8 kJ mol^{-1} correction to the calculated barrier height. This work has been submitted to the Proceedings of the Combustion Institute and is accepted for presentation.

Figure 1 shows good accord with the empirical estimate of Dean and Bozzelli, but our k_1 is much larger than the only other quantum chemistry work, by Li and Zhang, and much smaller than that measured by Gehring et al. Modeling their reaction conditions indicates low sensitivity to reaction 1. Modeling of hydrazine decomposition experiments in shock tubes by Michel and Wagner showed

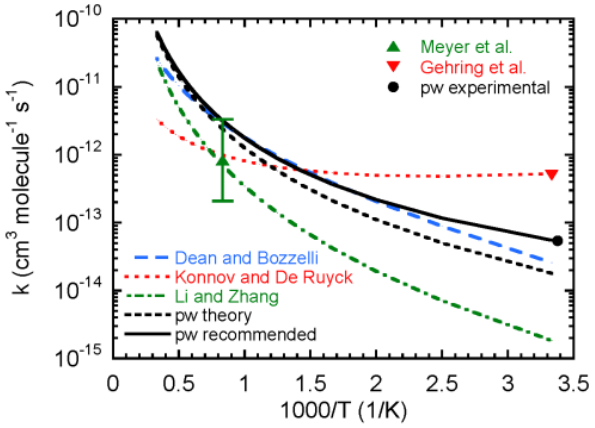

Figure 1. LP-LIF measurement and calculation for $NH_2 + N_2H_4$ and literature data.

sensitivity to reaction 1, behind N-N bond dissociation, although the half-life was underpredicted by up to a factor of 3. Further analysis of N_2H_4 dissociation continues with Glarborg and Troe.

A similar strategy of measurements combined with calculations and analysis has been applied to

$$NH_2 + H_2O_2 \rightarrow NH_3 + HO_2 \quad (2)$$

and the results are shown in Fig. 2. There are no other experiments for comparison, but we note that for the reverse reaction (relevant to HO_2 chemistry connected to ignition delay) our results agree well with the 1000 K value obtained by Cavalotti et al. with EStokTP. This work has been submitted to the Journal of Chemical Physics.

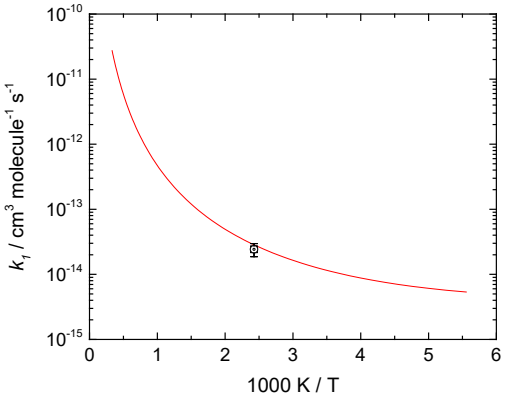

Figure 2. LP-LIF measurement (point) and calculation (line) for $NH_2 + H_2O_2$ and literature data.

Our measurements for

$$NH_2 + H_2CO \rightarrow \text{products} \quad (3)$$

indicate an activation energy of ca. 19 kJ mol^{-1}, by contrast to computed predictions by Barone and coworkers of a barrierless path to $H + HCONH_2$. Our own calculations are underway.

Further chemistry of NH_2 has been explored computationally, again based on M06-2X density functional and the 6-311++G(2df,2p) basis set for geometries and, after scaling, for zero-point vibrational energy and for fundamental frequencies used in partition functions. Relative enthalpies are obtained via direct extrapolation of coupled cluster CCSD(T) energies to the complete basis set limit, and the CBS-APNO approximation. A contribution was made to mechanistic interpretation of dimethyl ether (DME, CH_3OCH_3) co-combustion with NH_3, probed via ignition delays measured in a rapid Compression Machine at the University of Groningen. Kinetics for

$$NH_2 + CH_3OCH_3 \rightarrow NH_3 + CH_2OCH_3 \quad (4)$$

and the thermochemistry and bond strengths in $CH_3OCH_2NH_2$ were computed.

Mechanistic interpretation of rapid compression experiments at Technical University of Braunschweig on ammonia/methanol mixtures was assisted by evaluation of k_{5a} and k_{5b} for

$$NH_2 + CH_3OH \rightarrow NH_3 + CH_2OH \quad (5a)$$
$$\rightarrow NH_3 + CH_3O \quad (5b)$$

based on Canonical Variational Transition State Theory with internal torsions treated as uncoupled 1-D rotors. Tunneling was assessed from the curvature at the top of the vibrationally adiabatic barrier and the Eckart model. It is planned to return to these processes using MS-CVT at a later date. Modeling indicated that addition of methanol to ammonia fuel speeds ignition through increased [HO_2] and [OH] while recycling NH_2 back to NH_3 via reaction 5.

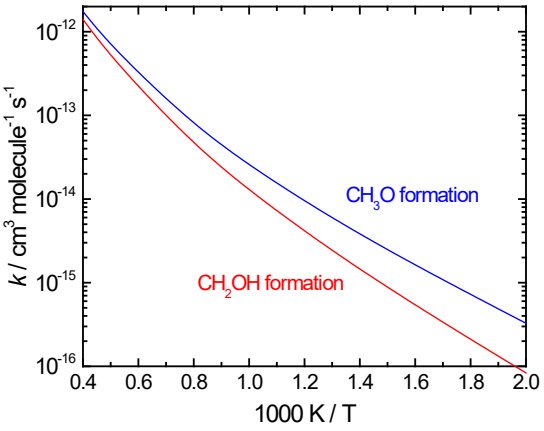

Figure 3. Computed rate constants for NH_2 reactions with CH_3OH.

There has been some question about the high-pressure limit for

$$NH_3 + M \rightleftarrows NH_2 + H + M \quad (6)$$

with shock-tube experiments interpreted to yield $k_{-6,\infty}$ values for $NH_2 + H$ recombination of 2×10^{12} to 2×10^{14} cm^3 mol^{-1} s^{-1}. Searches with multireference CASSCF-MP2 theory revealed no tight transition state and classical capture theory based on long-range dispersion interactions yielded $k_{-6,\infty} \approx 6.5 \times 10^{14}$ cm^3 mol^{-1} s^{-1} at 298 K and proportional to $T^{1/6}$. This result supports the idea that most experiments are at the low-pressure limit for reaction 6 and a mechanism for ammonia pyrolysis that incorporates a recommended $k_{-6,\infty} = (4 \pm 2) \times 10^{14}$ cm^3 mol^{-1} s^{-1} has been published.

Potential energy surfaces for the reaction of CH_3NH_3, and its subsequent products, with molecular O_2 have been investigated. Derived reaction enthalpies showed a rms error below 2 kJ mol^{-1} when compared to data from the Active Thermochemical Tables. Rate constants were derived with simple Canonical Transition State Theory for the following processes:

$$CH_3NH_2 + O_2 \rightarrow HO_2 + CH_2NH_2 \text{ and } CH_3NH \quad (7)$$
$$CH_2NH_2 \text{ and } CH_3NH + O_2 \rightarrow HO_2 + CH_2NH \quad (8)$$
$$CH_2NH + O_2 \rightarrow HO_2 + HCNH \text{ and } H_2CN \quad (9)$$

The associated process

$$CH_2NH_2 \rightleftarrows CH_3NH \quad \text{(high-pressure limit)} \quad (10)$$

was also characterized. Some of these reactions have been investigated before in the context of atmospheric chemistry. Thermochemistry and kinetics were derived for high-temperatures, and incorporated into a mechanism that successfully rationalized explosion limits for CH_3NH_2 and its oxidation in a fast flow reactor. Work remains to reach quantitative agreement with flame speeds and oxidation in the presence of high NO concentrations.

The high pressures and high NH_3 concentrations that arise with use of NH_3 as a fuel, rather than as a model for a fuel-nitrogen source of NO_x, mean that diamine formation may be important. Our published study focused on diazene (HNNH), emphasizing reactions of the Z (*cis*) isomer, as well as the

more usually studied and more stable E (*trans*) isomer. There is also the higher energy *ipso* H_2NN isomer. Pathways that interconvert the isomers, and formation and consumption reactions, were addressed, and low-pressure, falloff and high-pressure behaviors were quantified. One observation is that Z HNNH dissociation to H + NNH is almost two orders of magnitude faster than for the E isomer at atmospheric pressure. There are substantial barriers to E ⇄ Z for both bending and twisting pathways, so at low, ignition temperatures they may need to be treated as distinct species, while at high temperatures interconversion is fast and partial equilibrium may be attained.

Current computational studies of HNNH chemistry with molecular flame species are focused on NH_3, C_2H_4, C_2H_2, H_2 and the self-reaction. Preliminary results indicate intriguing pathways with hydrogen, where attack by H_2 at one end of Z HNNH leads to an $HNNH_2$ structure followed by migration of the second H atom towards the other N atom, to make hydrazine, while broadside attack proceeds to N_2 plus two new H_2 molecules as the original H_2 molecule dissociates.

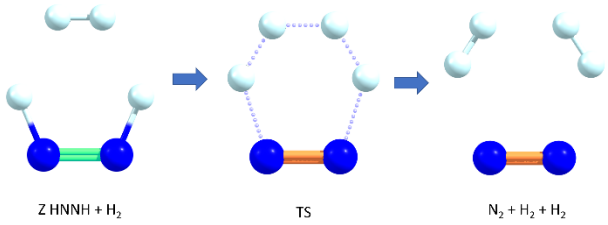

Figure 4. Reaction path for Z diazene plus hydrogen

Future Plans

Computationally, the unimolecular reactions of methylamine and ethylamine will be examined because the reverse of C-N bond breaking couples regular hydrocarbon chemistry and ammonia chemistry. Diazene work is on-going. Mechanism development in collaboration with Glarborg will continue, and species for further evaluation include NH_2O.

Experiments will continue, with resonance fluorescence detection of H atoms applied to the kinetics of H + CH_3NH_2. Theory will help assess H-abstraction from C-H vs N-H, and possible pathways to CH_4 + NH_2 and CH_3 + NH_3.

Our photolysis cell with FT-IR detection will be modified for high-temperature photochemistry, to investigate the relative reactivity and product formation for NH_3 and CH_3NH_2 reactions, initially with O atoms.

DOE Sponsored Publications 2020-2022

1. "Oxidation of Methylamine" P. Glarborg, C.S. Andreasen, H. Hashemi, R. Qian and P. Marshall, Int. J. Chem. Kinet., 52, 893-906 (2020).
2. "Ignition Delay Times of NH_3/DME Blends at High Pressure and Low DME fraction: RCM Experiments and Simulations" L. Dai, H. Hashemi, P. Glarborg, S. Gersen, P. Marshall, A. Mokhov and H. Levinsky, Combust. Flame, 227, 120-134 (2021).
3. "New Reactions of Diazene and Related Species for Modeling Combustion of Amine Fuels" P. Marshall, G. Rawling and P. Glarborg, Mol. Phys., 119, e1979674 (2021).
4. "Challenges in Kinetic Modeling of Ammonia Pyrolysis" P. Glarborg, H. Hamid and P. Marshall, Fuel Commun., 10, 100049 (2022).
5. "An Experimental and Modeling Study on Auto-Ignition Kinetics of Ammonia/Methanol Mixtures at Intermediate Temperature and High Pressure" M. Li, X. He, H. Hashemi, P. Glarborg, V.M. Lowe, P. Marshall, R. Fernandes and B. Shu, Combust. Flame, 242, 112160 (2022).

Thermal Decomposition of Cyclic, Oxygenated Hydrocarbons

Laura R. McCunn-Jordan
Chemistry Department, Marshall University
1 John Marshall Dr.
Huntington, WV 25755
mccunn@marshall.edu

Program Scope

The objective of this project is to investigate how chemical structure affects the thermal decomposition mechanisms of cyclic, oxygenated hydrocarbons that are relevant to biofuels and combustion. The primary specific aim of the proposed experiments is to identify the thermal decomposition products of dihydro-2-furanone, dihydro-3-furanone, 2-cyclopentenone, 3-cyclopentenone, 2-pyrone, and 4-pyrone. (Figure 1) A pulsed hyperthermal nozzle will be used to induce gas-phase pyrolysis at temperatures up to 1600 K. Product detection will be accomplished with a matrix-isolation FTIR spectrophotometer. A second specific aim of the project is to construct a mass spectrometer with tunable low-energy electron-impact ionization that can be used with the same hyperthermal nozzle. The introduction of a new detection technique will complement the FTIR experiments and provide a more complete characterization of the pyrolysis products, which is essential to the development of accurate thermal decomposition mechanisms.

The experiments are designed to probe the early steps in the pyrolysis mechanism, with the possibility of capturing radical intermediates. Two goals can be accomplished by this approach. First, the results will augment the existing body of knowledge created by shock-tube and static pyrolysis experiments, which typically probe the ultimate products of thermal decomposition on relatively long timescales. Adding to the variety of techniques in the literature will clarify pyrolysis mechanisms, which can include dozens of elementary steps. Second, identifying pyrolysis products of compounds that are intermediates or by-products in the production or combustion of new fuels will enable the prediction of pollutants from these fuels. The experimental results will contribute to the elucidation of pyrolysis mechanisms and enable the assessment of the environmental impact of various fuels. The completed research will build a foundation of knowledge for overcoming challenges to the nation's energy supply and environmental quality.

Recent Progress

Matrix-isolation FTIR experiments have been completed on all of the cyclic, oxygenated hydrocarbons targeted for study in this project: dihydro-2-furanone; dihydro-3-furanone; 2-cyclopentenone; 3-cyclopentenone, 2-pyrone and 4-pyrone. (Figure 1) Each molecule was mixed with argon at various dilute concentrations (0.02-0.4%) and subject to pyrolysis at a range of temperatures (800-1500 K). Products were identified with FTIR spectroscopy following matrix isolation.

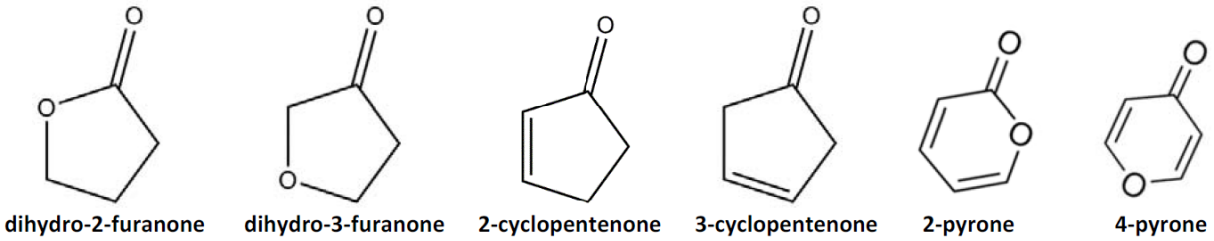

Figure 1. Cyclic, oxygenated hydrocarbons for pyrolysis studies

Pyrolysis reactions of dihydrofuranones

Dihydro-3-furanone, also known as oxolan-3-one, thermally decomposes to formaldehyde, carbon monoxide, ethylene, ketene, water, acetylene, and propyne over the employed pyrolysis temperature range of 800 to 1400 K and at concentrations of 0.1-0.4% in argon. (Figure 2) These products are consistent with four unimolecular reaction pathways predicted by CBS-QB3 calculations performed by collaborators Xinli Song (Wuhan Inst. for Math and Phys.) and Carol Parish (U. Richmond). The dominant pathway, based on calculated transition state energies, yields carbon monoxide, formaldehyde, and ethylene.

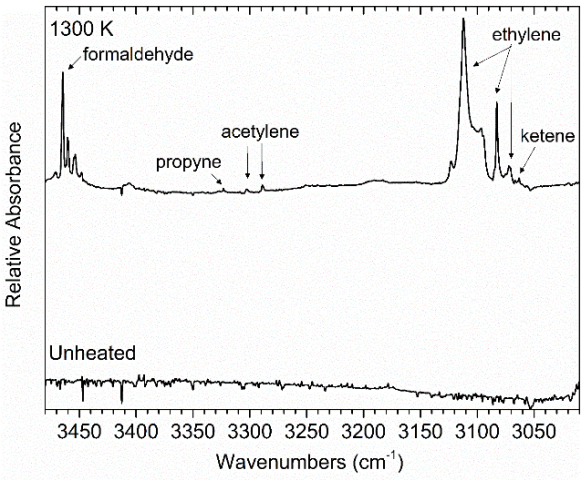

Figure 2. FTIR spectrum of pyrolysis products of dihydro-3-furanone isolated in an argon matrix, compared an unheated sample isolated in argon.

A small number of unassigned bands in the FTIR spectra suggest the presence of a substituted ketene, believed to be hydroxyketene. Optimization and frequency calculations of hydroxyketene at the B3LYP/6-311++G(d,p) level suggest that the experimentally observed bands at 2130 cm^{-1} and 3610 cm^{-1} belong to the C=C=O asymmetric stretch and OH stretch, respectively, of hydroxyketene. Hydroxyketene and ethylene are the products of a predicted minor pathway of unimolecular decomposition of dihydro-3-furanone, with a CBS-QB3 transition state energy 33 kcal/mol higher than that of the carbon monoxide + formaldehyde + ethylene pathway.

Pyrolysis of dihydro-2-furanone, more commonly known as gamma-butyrolactone, produces carbon dioxide, carbon monoxide, formaldehyde, ethylene, and ketene. Formaldehyde is noteworthy as it has not been observed in pyrolysis experiments performed with other techniques in the literature. Preliminary work has been undertaken to model the unimolecular reaction pathways of dihydro-2-furanone at the B3LYP/6-31G(d) level of theory.

Pyrolysis reactions of cyclopentenones

The cyclic ketone 2-cyclopentenone thermally decomposes to propene, acrolein, acetylene, ethylene, vinylacetylene, propargyl, and carbon monoxide over the employed pyrolysis temperatures of 1000 to 1400 K and at a concentration of 0.4% in argon. (Figure 3) The presence of propargyl radicals in these experiments is particularly interesting because it indicates that 2-

cyclopentenone could be a precursor to soot formation in certain high-temperature environments.

Bands at 2129 and 2123 cm^{-1} in the FTIR spectra following pyrolysis of 2-cyclopentenone suggest the presence of substituted ketenes. Preliminary calculations at the B3LYP/6-31G(d) level of theory have optimized transition states leading from 2-cyclopentenone to prop-2-enylketene and prop-1-enylketene. The lowest energy transition state at 332 kJ/mol leads to prop-2-enylketene with a hydrogen migration across the ring from carbon 5 to carbon 2. An alternate pathway with a higher barrier (477 kJ/mol) involves a H-migration from carbon 4 to carbon 3. Prop-1-enylketene is produced by H-migration from carbon 4 to carbon 5 with a barrier of 387 kJ/mol.

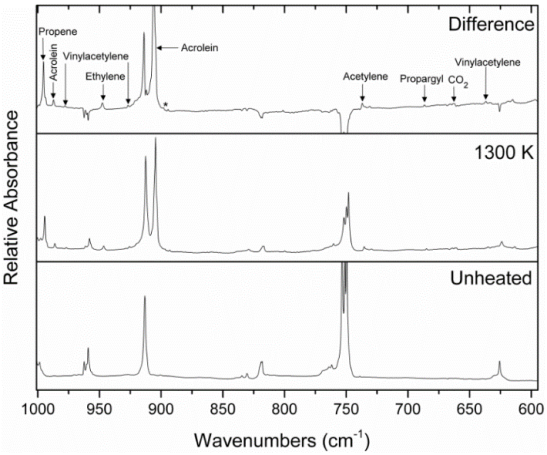

Figure 3. Ar-matrix FTIR spectrum of pyrolysis (1300 K) products of 2-cyclopentenone compared an unheated sample.

In order to facilitate the identification of propenylketenes in the pyrolysis of 2-cyclopenetenone, a comprehensive computational investigation of substituted ketenes was undertaken. Optimization and frequency calculations at the B3LYP/6-311++G(d,p) level of theory have been performed on the propenylketenes, as well as ketenes with existing matrix-isolation FTIR benchmarks: ketene, methylketene, and ethylketene. A comparison of calculated frequencies for the C=C=O asymmetric stretch and the known experimental frequencies for matrix-isolated ketene, methylketene, and ethylketene produced a scaling factor (0.9656) that could be used to predict the vibrational bands of unassigned substituted ketenes, in a 4 K argon matrix, in these and future experiments. The predicted, scaled values show that the experimentally observed band at 2129 cm^{-1} is most likely prop-2-enylketene. In order to experimentally confirm this assignment, prop-2-enylketene was isolated in an argon matrix via the pyrolysis of 4-pentenoic anhydride, 0.22% in argon, at 800 K and yielded bands at 2132, 2128, and 2123 cm^{-1}, in agreement with the three computationally predicted conformers of prop-2-enylketene. (Figure 4) Pyrolysis of 3-pentenoic anhydride (0.1% in argon at 800 K) was used to isolate prop-1-enylketene and identify vibrational bands at 2128, 2124 and 2110 cm^{-1}, in agreement with calculated, scaled frequencies for four conformers of prop-2-enylketene. The relative intensities of the bands for the propenylketenes suggest that both prop-2-enylketene and prop-1-enylketene are produced in the pyrolysis of 2-cyclopentenone.

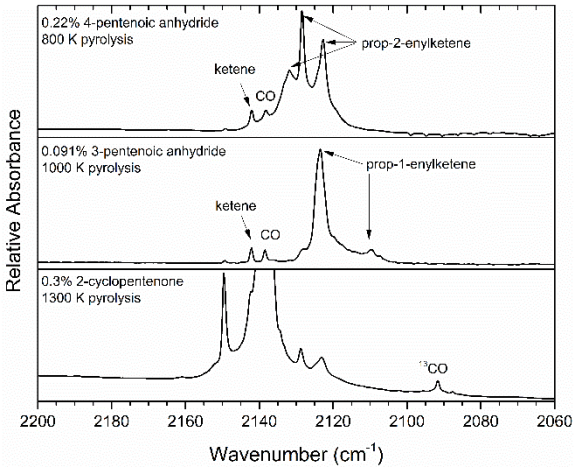

Figure 4. Ar-matrix FTIR spectra of pyrolysis (1300 K) products of 2-cyclopentenone compared to propenylketene precursors 4-pentenoic anhydride and 3-pentenoic anhydride.

The products of pyrolysis of 3-cyclopentenone are: carbon monoxide, ketene, acetylene, ethylene, propyne, allene, vinylacetylene, propargyl, and ethynol. While there are many products

in common with 2-cyclopentenone, the appearance of propyne, allene, and ethynol should lead to interesting revelations about the influence of chemical structure on the pyrolysis mechanism. Work has begun to probe the energetics of the unimolecular dissociation pathways of 3-cyclopentenone. Optimization and frequency calculations at the B3LYP/6-31G(d,p) level of theory have determined energies of the transition states and products for initial reactions in the pyrolysis of 3-cyclopentenone. Initial results show that hydrogen migrations were found to have much lower transition states than ring-opening reactions.

Pyrolysis reactions of pyranones

The products of pyrolysis of 4-pyrone at 1300 K are ketene, carbon monoxide, acrolein, acetylene, vinylacetylene, propyne, methylketene, and formylketene. Preliminary work on electronic structure calculations on 4-pyrone, its unimolecular decomposition products and reaction transition states have been completed. A transition state for the pathway leading to acetylene and *cis*-formylketene has been identified with a barrier of 377 kJ/mol. The assignment of *cis*-formylketene in the FTIR spectrum is consistent with literature reports.

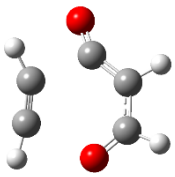

Figure 5. Transition state for formation of formylketene from 4-pyrone.

Pyrolysis experiments with matrix-isolation FTIR on 2-pyrone have been completed recently. Thus far, acetylene, ethylene, propyne, ketene, carbon monoxide, and an aldoketene (HCOCH=CHCH=C=O) have been assigned. The aldoketene is produced by a ring-opening mechanism that has been previously observed via photolysis experiments on matrix-isolated 2-pyrone.

Future Plans

The vacuum chamber, new power supply controller and high Q-head oscillator have been assembled for the new mass spectrometer to be interfaced with the existing pyrolysis source. The final months of the project will see the completion of the instrument with the delivery of the data acquisition software, which has been subject to lengthy delays by the COVID-19 pandemic. Once the software is delivered and the system is validated, pyrolysis experiments will be repeated with mass spectrometry to identify products that could not definitively be assigned in the FTIR spectra for dihydro-2-furanone and 2-cyclopentenone. The mass spectra will also be especially important in confirming the substituted ketenes observed in the matrix-isolation FTIR studies.

The addition of electronic structure calculations mapping the unimolecular reaction pathways has proved fruitful for the study of oxolan-3-one and 2-cyclopentenone. Similar computational studies are underway for 3-cyclopentenone, 4-pyrone, and dihydro-2-furanone. Future work will focus on completing those calculations and employing higher levels of theory to support the understanding of pyrolysis mechanisms for these cyclic, oxygenated hydrocarbons.

Publications During Project Period (2019-present)

1. Brown, G.; Ellis, M.; Martin, T.; McCunn, L. R. Vibrational Bands of the 2-Butyn-1-yl Radical. *J. Phys. Chem. A.* **2020**, *124*, 4081–4086.

Manuscripts Currently Under Review

1. El-Shazly, K.; Sparks, E.; Narkin, K. Legg, H.R., Cardot, J.M.; Hostetler, M.A.; McCunn, L.R. Parish, C.A. The signature C=C=O stretch of propenylketenes and ketene clusters. In *Physical Chemistry Research at Undergraduate Institutions*, ACS Book Series. **In review.**
2. Legg, H.R., Narkin, K., McCunn, L.R., Parish, C.A., Song, X. Experimental and Theoretical Study of Oxolan-3-one Thermal Decomposition. *J. Phys. Chem. A.* **In review.**

Electronic Structure, Spectroscopy, and Bond Dissociation Energies of Small Actinide Molecules

Michael D. Morse (morse@chem.utah.edu)
Department of Chemistry, University of Utah
315 S. 1400 East, Salt Lake City, UT 84112

Program Scope

In this experimental program, we seek to obtain detailed, precise information concerning the electronic structure, spectroscopy, and bond dissociation energies of small thorium and uranium molecules and ions that can be used to assess computational approaches for these systems. The work is focused on advancing our understanding of the role of the 6*d* and 5*f* electrons in the electronic structure of these species. Computational chemistry finds these molecules to be quite challenging, due to the high electronic state density and the highly correlated electronic motions in the partially filled 6*d* and 5*f* subshells. In addition, relativistic effects, including spin-orbit interactions, are of great importance in the actinides. Accurate benchmark data is critically needed to assess method developments in this field.

The major focus is the precise measurement of bond dissociation energies (BDEs) by the observation of a sharp predissociation threshold in a resonant two-photon ionization (R2PI) spectrum. The Morse group has successfully applied this technique to about 30 transition metal dimers and trimers and to more than 90 transition metal-main group diatomics, with error limits generally below 0.01 eV. In this work we plan to measure the BDEs of Th_2, ThB, ThSi, ThP, ThSe, U_2, UB, UC, UN, USi, UP, US, and USe, among others. This method can reduce the error limits on the currently accepted BDE values by factors of 10 to 100, thereby building up a compendium of precise values for testing computational models of the 5f and 6d electrons. Measurements of the BDEs of the actinide cations will also be conducted in a cryo-cooled ion photodissociation spectrometer. BDEs of the more strongly bound Th^+-O, Th^+-N, U^+-O, OU^+-O, *etc.* molecules will be measured by the observation of a sharp predissociation threshold at the two-photon level, using a resonant two-photon dissociation (R2PD) method. Combining the BDEs of the neutral and cationic molecules with precisely known ionization energies from PFI-ZEKE work will close the thermochemical cycle, allowing tests for self-consistency. When the BDE of the neutral cannot be measured due to its high BDE and low IE (ThF, ThO, UF, and UO), the thermochemical cycle will be used to determine the neutral BDE from the three other values. The resulting wealth of highly precise data will enable in-depth probes of computational methods and basis sets, allowing effective computational methods to be identified.

R2PI spectroscopy of actinide neutrals and R2PD spectroscopy of actinide cations will be used to learn about the electronic structure of these species. Rotationally resolved spectroscopy will be used to improve our understanding of electron deficient species such as the ThB, ThC, UB, and UC molecules. These are unlikely to be described by the ligand field methods that have proven to be so useful for actinide metals bonded to more electronegative ligands. We anticipate these species to be bonded by more covalent interactions, with likely 5f bonding contributions in the cases of UB and UC. The spectrum of UO_2 will be investigated in the near-IR, where the density of electronic states is expected to be low enough that meaningful spectra may be obtained. Likewise, spectroscopic work on ThO_2 will be pursued to investigate the extent to which this molecule resembles its TiO_2 and ZrO_2 congeners, for which spectra are known. The existence of empty 5f orbitals may make ThO_2 electronically quite distinct. Among the cations, UB^+ and UN^+ will be investigated. These species are relevant to high-melting reactor substrates (uranium nitrides and borides) that are under consideration for their high heat conductivity and high melting points. In addition, vibronic and rotationally resolved studies of the important UO_2^+ and ThO_2^+ ions are also planned. This work will be the first to probe the electronic structure of these species experimentally.

Recent Progress

Measurements of Bond Dissociation Energies: UC, USe, and US

Using pulsed laser ablation of a uranium sample in a flow of 4% CH_4 in helium, diatomic UC was readily produced and investigated using a scheme in which one photon from an OPO laser excited the molecule and a second photon from the same laser ionized it. A sharp predissociation threshold was observed, allowing a precise bond dissociation energy to be measured, giving $D_0(UC) = 4.304(3)$ eV.

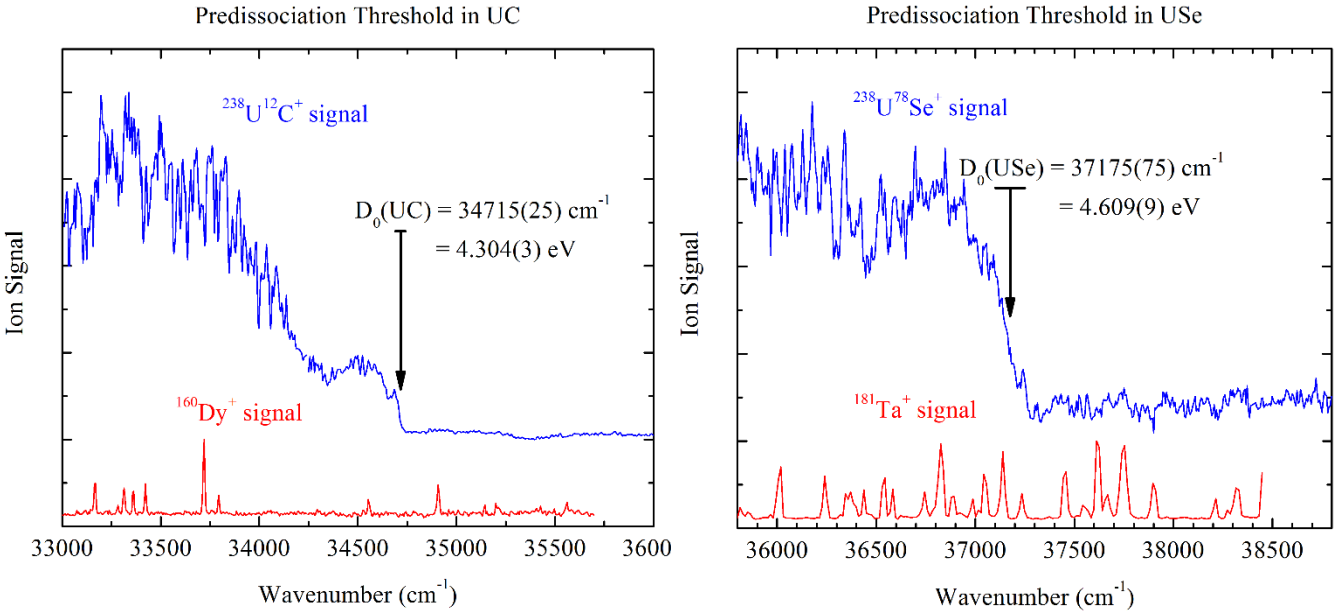

Figures 1 and 2. Predissociation measurements of the bond dissociation energies of UC and USe.

Immediately after the UC scan, a spectrum of atomic Dy was recorded and used to calibrate the wavenumber axis using the atomic energy levels tabulated by NIST.[1] Similarly, USe was produced by laser ablation of uranium in a flow of 0.1% H_2Se in helium and calibrated using Ta atomic transitions, giving $D_0(USe) = 4.609(9)$ eV. The BDE of UC compares to values measured by Knudsen effusion mass spectrometry of 4.81(30) and 4.72(16) eV,[2, 3] lowering the accepted value by 0.4 to 0.5 eV and reducing the error limit by a factor of 50 to 100. Our value exceeds that calculated by CASPT2 theory (4.108 eV) by about 0.2 eV or 19 kJ/mol.[4] This is a significant difference, showing that there is room for improvement in the computational chemistry methodology of the actinides. In the case of USe, ours is the first measurement reported. To our knowledge, no computations have ever been performed on USe.

In other BDE studies, we have measured the BDE of ThSe for the first time, obtaining $D_0(ThSe) = 5.484(12)$ eV, a value that is 0.33 eV greater than that of its congener, HfSe, which is 5.154(4) eV.[5] Our previous measurement of $D_0(ThC) = 5.060(3)$ eV[6] is likewise 0.634 eV greater than that of HfC, 4.426(3) eV.[6] These results demonstrate that the 6d orbitals of Th are more readily accessible for bonding than the 5d orbitals of Hf. Finally, in preliminary data, we have found that the BDE of US lies in the range 42,000 – 42,700 cm^{-1} (5.25 ± 0.05 eV) (see Figure 4). Here we see a sharp drop in signal near 42,000 cm^{-1} followed by weak signal that drops to baseline at about 42,700 cm^{-1}. At this point, we are unsure whether the weak feature between 42,000 and 42,700 cm^{-1} could be an artifact, and are working to reduce the presence of larger clusters in the molecular beam. We have often found that larger clusters can fragment into the mass channel of a smaller species, leading to false signal that could be incorrectly attributed to the smaller molecule. Another possibility is that the weak feature could be due to states excited above the bond dissociation energy that fail to dissociate on a nanosecond time

scale. This experiment was performed using excitation and ionization occurring within the same 5 ns laser pulse. We intend to set up a second laser pulse for the ionization step, so that a delay between excitation and ionization can be introduced. This scheme would allow the initially excited state more time to dissociate and should provide a more precise BDE for the US molecule. Our current value, 5.25(5) eV, is slightly lower than the Knudsen effusion value of 5.38(10) eV.[7, 8] It is substantially lower than the DFT values previously calculated, 5.64 eV (B3LYP) and 5.92 eV (MPW1PW91).[9] It is also noteworthy that our previous studies of 27 MS and MSe molecules demonstrated an exceptional correlation in the BDE of the corresponding MS and MSe molecules, with the MS molecule being 15.6% more strongly bound than the MSe species.[10] Given our value for USe, this would predict a value of D_0(US) of 5.33 eV, reasonably close to our measured 5.25(5) eV.

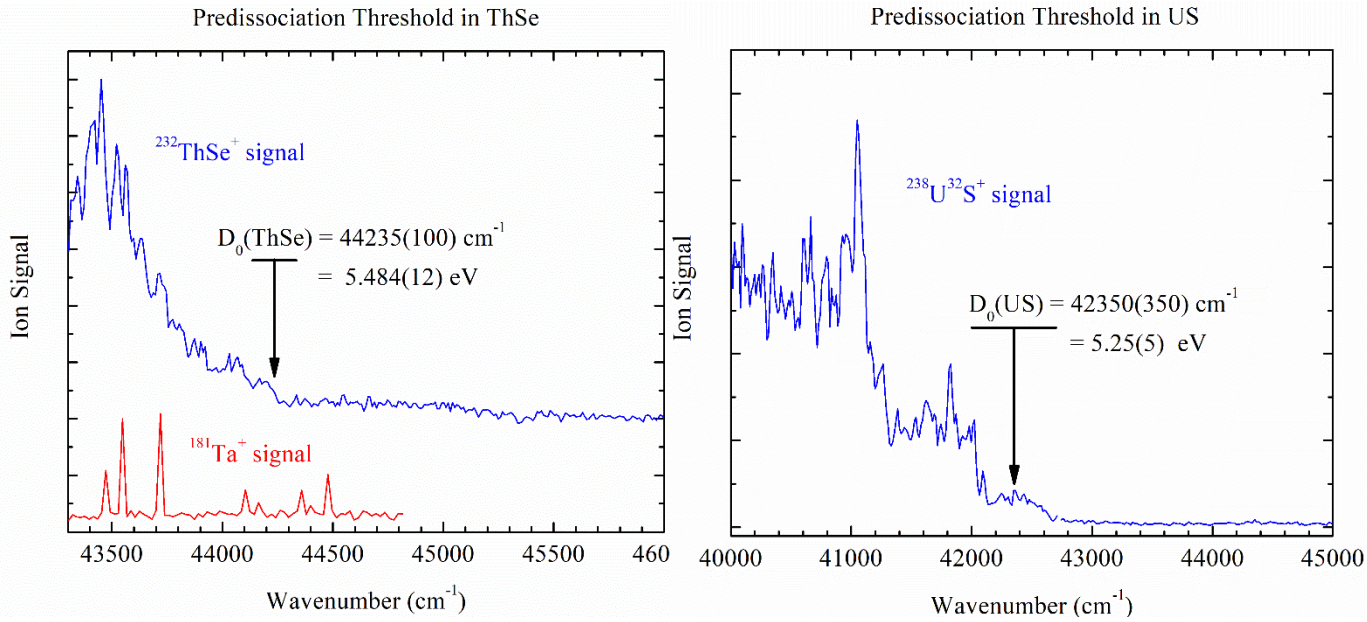

Figures 3 and 4. Predissociation measurements of the bond dissociation energies of ThSe and US.

Construction and Testing of the Cryo-Cooled Ion Photodissociation Spectrometer

During this initial grant period, we have devoted a great deal of effort to completing the construction of our cryo-cooled ion photodissociation spectrometer. The instrument consists of a laser ablation ion source, an ion funnel to collect the ablated ions, and a hexapole trap to collect the initial ions (with the possibility of reacting the thermally equilibrated ions with ligands of interest). From there, the ions are transmitted to a quadrupole mass filter (QMF#1) that selects the ion of interest for further study. The ion then enters a turning quadrupole that transmits it into a cryo-cooled linear quadrupole trap that is attached to a cryostat that can reach temperatures below 5K. One or two lasers can then be fired along the axis of the trap, possibly causing photofragmentation. Ions are released and transmitted into a second quadrupole mass filter tuned to transmit the expected fragment ions. After exiting QMF#2, an octupole ion guide carries the ions to a conversion dynode assembly where the photofragment ion signal is counted. With this instrument, we expect to be able to measure ionic bond dissociation energies to high precision and to conduct spectroscopic studies using one- or two-color resonant photodissociation studies.

During this initial grant period, we have designed and built the laser ablation source, the ion funnel and hexapole trap, the ion optics and octupole that carry the ions to QMF#1, and the octupole that carries the fragment ions to the detector. All of these parts are now mounted in the instrument. We have

also added another large turbomolecular pump to the ion detection chamber in order to prevent discharges. Currently, we are working on building the radio frequency power supplies needed for the front half of the instrument: the ion funnel, hexapole, and octupole. These are the last items that must be completed before bringing the complete instrument online. Using an electron-impact ion source, we have been able to successfully transmit ions through the first quadrupole mass filter, through the turning quadrupole and into the quadrupole ion trap. We anticipate that the remaining electronics will be completed early this summer and we will be able to conduct our first spectroscopic experiments toward the end of the summer.

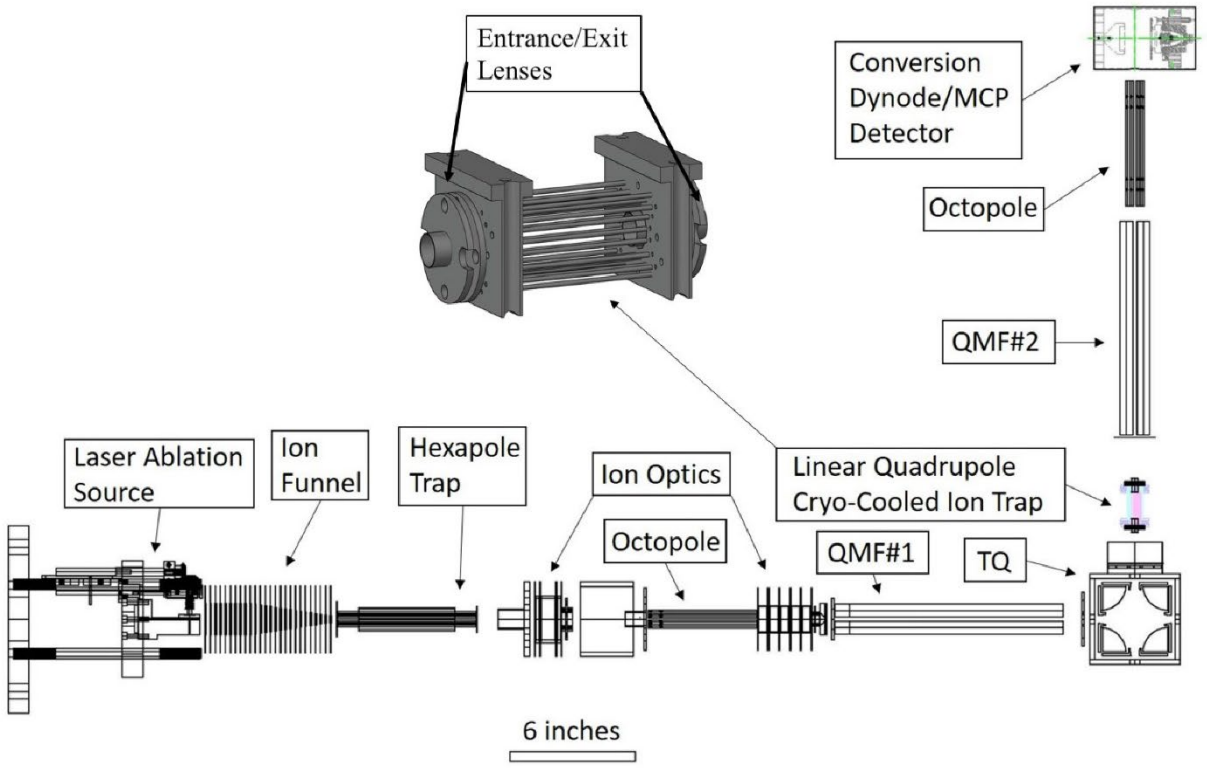

Figure 5. The cryo-cooled ion photodissociation spectrometer.

DOE Supported Publications 2021-

No publications as yet.

References:

[1]A. Kramida, Yu. Ralchenko, J. Reader, and NIST ASD Team, *NIST Atomic Spectra Database (version 5.9)* (National Institute of Standards and Technology, Gaithersburg, MD, 2021).
[2]S. K. Gupta and K. A. Gingerich, J. Chem. Phys. **71,** 3072-3080 (1979).
[3]K. A. Gingerich, J. Chem. Phys. **50,** 2255-2256 (1969).
[4]P. Pogány, A. Kovács, L. Visscher, and R. J. M. Konings, J. Chem. Phys. **145,** 244310 (2016).
[5]J. J. Sorensen, T. D. Persinger, A. Sevy, J. A. Franchina, E. L. Johnson, and M. D. Morse, J. Chem. Phys. **145,** 214308 (2016).
[6]A. Sevy, D. J. Matthew, and M. D. Morse, J. Chem. Phys. **149,** 044306 (2018).
[7]E. D. Cater, E. G. Rauh, and R. J. Thorn, J. Chem. Phys. **44,** 3106-3111 (1966).
[8]E. D. Cater, E. G. Rauh, and R. J. Thorn, J. Chem. Phys. **48,** 538 (1968).
[9]C. C. L. Pereira, C. J. Marsden, J. Marcalo, and J. K. Gibson, Phys. Chem. Chem. Phys. **13,** 12940-12958 (2011).
[10]J. J. Sorensen, E. Tieu, and M. D. Morse, J. Chem. Phys. **154,** 124307 (2021).

Spectroscopy, Kinetics and Dynamics of Radicals and Other Trace Chemical Species

JILA/NIST/Department of Chemistry/Department of Physics
University of Colorado, Boulder 80309
David. J. Nesbitt (djn@jila.colorado.edu)

Our DOE research program involves experimental and theoretical study of transient chemical species relevant to fundamental chemical processes. The work focuses on spectroscopy and unimolecular/bimolecular dynamics of highly reactive radical intermediates, combining i) high-resolution direct IR laser absorption methods with quantum shot noise limited detection, ii) high densities (10^{12}-10^{14} #/cm^3) of jet-cooled hydrocarbon radicals and molecular ions in slit supersonic discharge expansions, accompanied by iii) high-level *ab initio* potential surface and multidimensional quantum mechanics calculations. Over the past few years during COVID, however, our group has branched out considerably and achieved several firsts with ultrasensitive high resolution spectroscopy of transient species in a number of new areas.[1-7] A) For example, for the first time, ultrasensitive direct absorption IR spectroscopy in a slit jet discharge expansion is used to successfully detect and analyze high resolution spectra of cis-formic acid, a highly energetic but metastable rotamer of the normal trans formic acid known to form in copious quantities in the interstellar medium.[3] Furthermore, our studies identify that H atoms from H_2 in the discharge play a crucial role in forming cis from trans-formic acid, which we argue is due to chemical addition of H atoms to the acid carbonyl to form a symmetric dihydroxymethyl radical. B) These slit jet studies have been extended to probe and analyze gas phase C_4 (cyclobutyl) and C_5 (cyclopentyl) cycloalkyl radicals for the first time, which, despite an increasingly large number of atoms (N = 14) continues to exhibit remarkably sharp and high-resolution spectra with little indication of spectral fragmentation due to intramolecular vibrational redistribution (IVR).[5,7] C) We have combined broad band (3-5μm) mid-IR frequency combs with high finesse (Q = 10,000) build up cavities for laser spectroscopy of human breath samples at unprecedented sensitivities, which in combination with machine testing/learning algorithms has allowed us to successfully diagnose COVID positive patients with an accuracy (AUC = 85%) currently limited by the PCR test gold standard.[4] Most importantly, the combination of 20,000 frequency comb "teeth" resonant with a high Q (10,000 meter) absorption cavity yields an upgrade in signal detection over non-frequency comb methods by over $2x10^8$. D) Lastly, we have combined resonant cavity IR laser excitation of buffer gas cooled to probe optical saturation dynamics in buffer gas cooled C_{60}, which represents the first quantum state-to-state rotational and vibrational collisional energy transfer studies in a molecule of this size and complexity.[6] In the interests of space, highlights from only a few of these topics are briefly discussed below, hopefully with opportunities for more detailed discussions at the contractors meeting.

A. Chemical synthesis, cooling, and spectroscopy of highly metastable cis-HCOOH isomers

High-resolution direct absorption infrared spectra of metastable cis-formic acid (HCOOH) trapped in a cis-well resonance behind a 15 kcal/mol barrier are reported for the first time, with the energetically unstable conformer produced in a supersonic slit plasma expansion of trans-formic acid/H_2 mixtures. We present a detailed high-resolution rovibrational analysis for cis-formic acid species in the OH stretch (ν_1) fundamental, providing first precision vibrational band origin, rotational constants, and term values, which in conjunction with a*b initio* calculations at

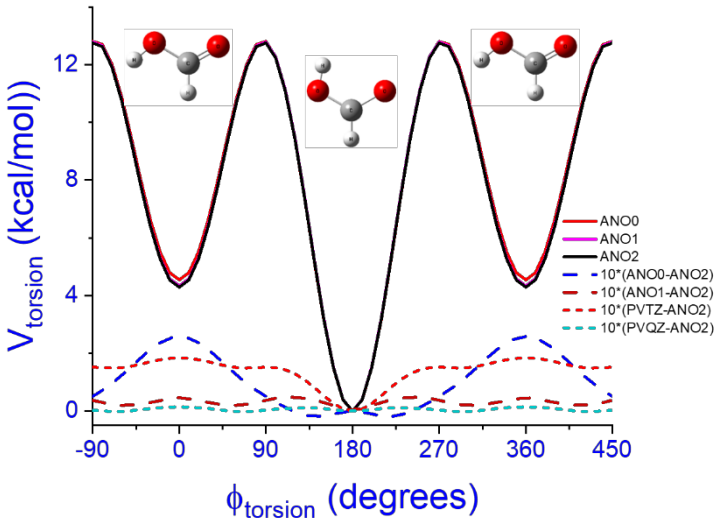

the CCSD(T)/ANOn (n=0,1,2) level support the experimental assignments and establish critical points on the potential energy surface for internal rotor trans-to-cis isomerization. Relative intensities for a- and b-type transitions observed in the spectra permit the transition dipole moment components to be determined in the body fixed frame and prove to be in good agreement with *ab initio* CCSD(T) theoretical estimates but rather poor agreement with simple bond-dipole predictions. The observed signal dependence on H_2 in the discharge suggests the presence of a novel H atom radical chemical mechanism for strongly endothermic "up-hill" internal rotor isomerization between trans- and cis-formic acid conformers.

B. High-resolution CH Stretch Spectroscopy of Jet-Cooled Cyclopentyl Radical: Insights into Structure, Out of Plane Puckering, and IVR Dynamics

First high-resolution sub-Doppler infrared spectroscopic results for cyclopentyl radical (C_5H_9) are reported on the α-C-H stretch fundamental with suppression of spectral congestion achieved by adiabatic cooling to $T_{rot} \approx 19(4)$ K in a slit jet expansion. Surprisingly, cyclopentyl radical exhibits a rotationally assignable infrared spectrum, despite 3N-6 = 36 vibrational modes and an upper vibrational state density ($\rho \approx 40\text{-}90$ #/cm^{-1}) in the critical regime ($\rho \approx 100$ #/cm^{-1}) necessary for onset of intramolecular vibrational relaxation (IVR) dynamics. Such high-resolution data for cyclopentyl radical permit detailed fits to a rigid-rotor asymmetric top Hamiltonian, initial structural information for ground and vibrationally excited states, and opportunities for detailed comparison with theoretical predictions. Specifically, high level *ab initio* calculations at the CCSD(T)/ANOn (n=0,1) levels are used to calculate an out-of-plane bending potential, which reveal a C_2 symmetry double minimum 1D energy surface over a C_{2v} planar transition state. The inversion barrier ($V_{barrier} \approx 3.7(1)$ kcal/mol) is much larger than the effective moment of inertia for out-of-plane bending, resulting in localization of the cyclopentyl

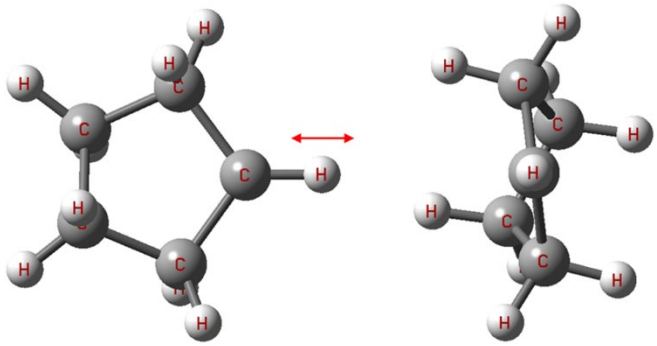

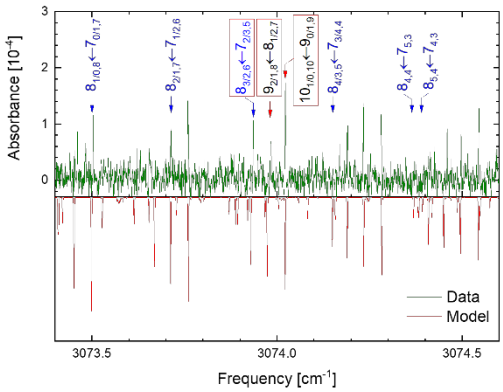

wavefunction near its C_2 symmetry equilibrium geometry and tunneling splittings for the ground state too small (< 1 MHz) to be resolved under sub-Doppler slit jet conditions. The persistence of fully resolved high resolution infrared spectroscopy for such large cyclic polyatomic radicals at high vibrational state densities suggests a "*deceleration*" of IVR for a cycloalkane ring topology, much as low frequency torsion/methyl rotation degrees of freedom have demonstrated a corresponding "*acceleration*" of IVR processes in linear hydrocarbons. The results continue to suggest successful applications of high resolution infrared spectroscopy for even larger terpenyl, purinyl, pyradinyl, and polyaromatic ring radical systems.

C. Frequency comb and machine learning-based breath analysis for COVID-19 classification

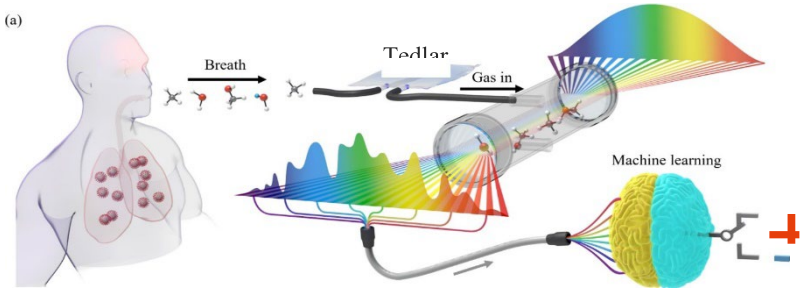

In a fundamentally new direction, the Nesbitt and Ye groups at JILA have joined forces to exploit laser spectroscopy in the ongoing battle for human health.[4] Human breath contains hundreds of volatile molecules that can provide powerful, non-intrusive spectral diagnosis of a diverse set of diseases and physiological/ metabolic states. To unleash the underlying tremendous potential for medical science, we have developed robust analytical methods that simultaneously measures tens of thousands of spectral features in each breath sample, followed by efficient and detail-specific multivariate data analysis for unambiguous binary medical response classification. We combine mid-infrared cavity-enhanced direct frequency comb spectroscopy (CE-DFCS), capable of real-time collection of tens of thousands of distinct molecular features at parts-per-trillion sensitivity, with supervised machine learning, capable of analysis and verification of extremely high-dimensional input data channels. Specifically, we present first applications of this method to the breath detection of Coronavirus Disease 2019 (COVID-19). Based on training and testing with170 individual breath samples from students and faculty at the University of Colorado, we report a cross-validated area under the Receiver-Operating-Characteristics curve of AUC = 0.849(4), indicating excellent prediction performance close to (and therefore starting to be limited by) that currently achieved by PCR methods. Further, this method detected a significant difference between male and female breath as well as other variables such as smoking and abdominal pain. Together, these highlight the utility of CE-DFCS for rapid, non-invasive detection of diverse biological conditions and disease states. The unique properties of frequency comb spectroscopy thus can help establish precise digital spectral fingerprints for building accurate databases and provide means for simultaneous multi-response classifications. Finally, the predictive powers of these methods can and are currently being greatly enhanced with readily scalable comb spectral coverage into the 5-10 μm region.

D. Collision-induced C_{60} rovibrational relaxation probed by quantum state-resolved nonlinear spectroscopy

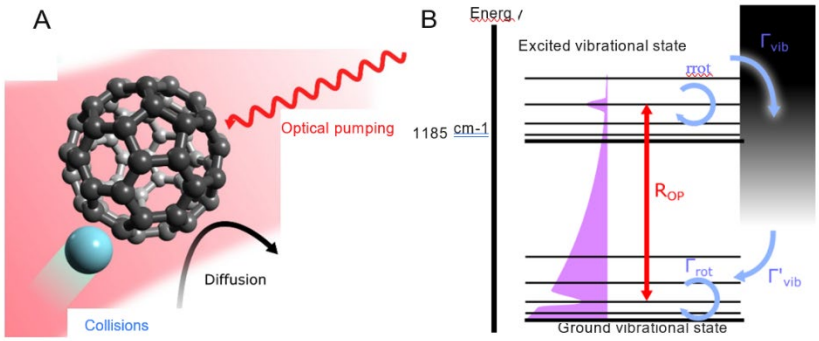

Large buckminsterfullerene molecules with 5 dozen identical ^{12}C atoms offer completely novel opportunities for long lived quantum control in many body spin systems, establishing a gas-phase molecular platform in principle capable of representing a 60-qubit entangled state with potential applications in quantum computation. As a necessary step in this direction, quantum state-resolved spectroscopy has been recently achieved in a Nesbitt/Ye group collaboration for gas phase C_{60} molecules when cooled by buffer gas collisions and probed with a mid-infrared frequency comb.[6] This rovibrational quantum state resolution for the largest molecule on record is facilitated due the remarkable symmetry and rigidity of C_{60}, which also present fundamentally new opportunities and challenges with which to explore energy transfer between quantum states in this many-atom system. By way of first demonstration of these capabilities, we have combined state-specific optical pumping, buffer gas collisions, and ultrasensitive intracavity nonlinear laser spectroscopy to initiate and probe the rotation- vibration energy transfer and relaxation. This approach provides the first detailed characterization of C_{60} collisional energy transfer for a variety of collision partners and determines the rotational and vibrational inelastic and elastic collision cross sections. These results establish a novel route towards quantum state control for creating quantum entanglement in a new class of unprecedentedly large gas phase molecules.

1 D. J. Nesbitt, Y. C. Chan, and A. Kortyna, "High resolution infrared spectroscopy of highly reactive chemical intermediates: Berkeley inspiration and a C.B. Moore retrospective", ACS Books (2021).

2 Y. C. Chan, A. Kortyna, and D. J. Nesbitt, "High-resolution infrared spectroscopy of supersonically cooled singlet carbenes: Bromomethylene (HCBr) in the CH stretch region", J. Chem. Phys. (2021).

3 K. D. Doney, A. Kortyna, Y. C. Chan, and D. J. Nesbitt, "Formation and detection of metastable formic acid in a supersonic expansion: High resolution infrared spectroscopy of the jet-cooled cis-HCOOH conformer", J. Chem. Phys. (in press, 2022).

4 Q. Liang, Y.-C. Chan, J. Toscano *et al.*, "Frequency comb and machine learning-based breath analysis for COVID-19 classification", Optica. (under review, 2022).

5 A. Kortyna, M. A. R. Reber, and D. J. Nesbitt, "High-resolution CH stretch spectroscopy of jet-cooled cyclopentyl radical: First insights into equilibrium structure, out of plane puckering, and IVR dynamics", J. Chem. Phys. (under review, 2022).

6 L. Liu, P. B. Changala, M. Weichman *et al.*, "Collision-induced C_{60} rovibrational relaxation probed by state-resolved nonlinear spectroscopy", (submitted, 2022).

7 Y. C. Chan and D. J. Nesbitt, "Spectroscopy and puckering dynamics of jet-cooled cyclobutyl radical", J. Chem. Phys. (in preparation).

State-to-State Molecular Reactions in the Ultracold Regime

Kang-Kuen Ni
Department of Chemistry and Chemical Biology, Harvard University
12 Oxford St., Cambridge, MA 02138
ni@chemistry.harvard.edu

Research Scope:
We aim to experimentally probe the AB + CD and AB + C types of reactions with state-to-state resolution, which can be compared to advanced theoretical calculations to help elucidate the role of quantum mechanics in the processes of bond breakage and formation. Our approach is to conduct experiments with reactants that are prepared at ultracold temperatures ($< 1\mu K$) such that the quantum effects of translational motion are an important factor. Specific example reactions, including the potassium-rubidium metathesis reaction $KRb + KRb \rightarrow K_2 + Rb_2$ as well as the atom exchange reactions $K + KRb \rightarrow K_2 + Rb$ and $Rb + KRb \rightarrow Rb_2 + K$, are chosen because the technology of quantum internal and motional state control of these types of molecules is particularly advanced. For the majority part of this grant, we have constructed a quantum degenerate gas apparatus that integrates ion detection and velocity map imaging capabilities, allowing us to explore the $KRb + KRb \rightarrow K_2 + Rb_2$ bimolecular reaction in detail. In this work, we mapped out the complete product state distribution, which was compared to a state-counting model based on statistical theory. Our results show an overall agreement with the statistical state counting model, but also reveal several deviating state-pairs. An exact quantum calculation for molecule-molecule collisions, that is needed to understanding the deviations, is however beyond the current state-of-the-art. In the remaining grant period, we focus on atom-molecule collisions, which are theoretically more tractable and will further advance our intuition about chemistry at ultracold temperatures, as well as our ability to control chemistry at the most basic quantum level.

Recent Progress:
For the last funding period, our efforts in ultracold chemical reactions focused on the endothermic Rb + KRb atom-molecule collision. The key result is the observation of exceedingly long-lived KRb_2^* collisional complexes, which is not yet understood. Our experimentally measured complex lifetime deviates from conventional theoretical calculations by five orders of magnitude and has motivated a exploration of the possible physics by theorists to address this discrepancy.

Fundamentally, chemical reactions are defined by the transformation of molecular reactants into products through intermediate complexes. Chemists have long dreamed of being able to trace chemical reaction paths by determining the properties of these intermediate complexes, though this has been made challenging as these complexes are typically short-lived at typical reaction conditions. At sub-microkelvin temperatures, however, their lifetimes can be extended dramatically, greatly impacting the stability of the ultracold molecular clouds from which they originate. As discussed above, compared to the KRb + KRb reaction, the reaction of Rb + KRb is in principle

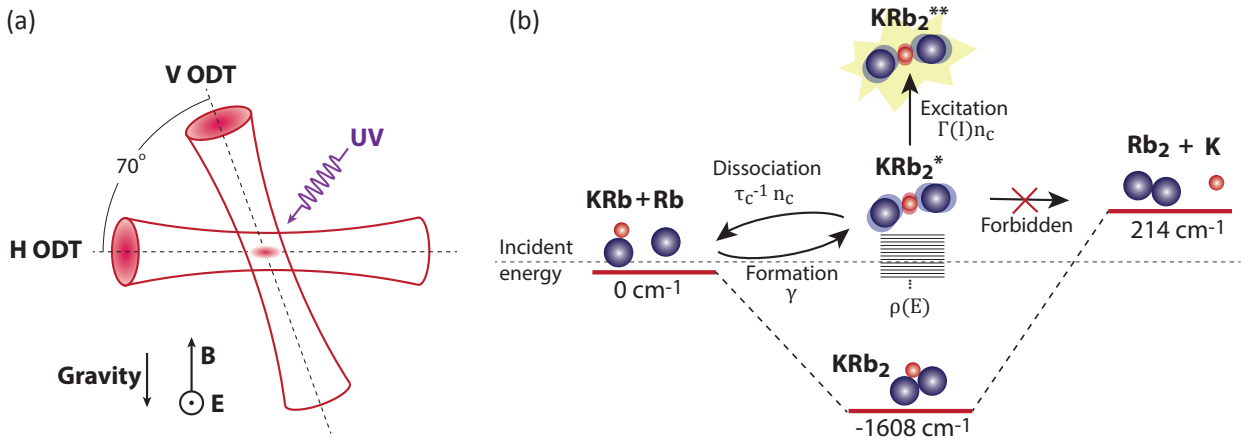

Figure 1: **KRb + Rb collision dynamics in an optical dipole trap (ODT).** (**a**) A diagram of the ODT configuration used to confine the mixture of KRb molecules and Rb atoms. The purple arrow represents the UV ionization laser pulse, used for photoionization detection of KRb_2^* complexes. (**b**) Illustration of the KRb + Rb collision dynamics. The incident energy of one free electronic ground state Rb atom and one free KRb molecule in its rovibronic ground state is defined as the zero of energy.

more tractable theoretically and thus a good candidate for such a study. A thorough understanding of the dynamics in this regime could enable a more refined understanding and control over interactions and losses in ultracold molecular gases, a potential platform for quantum information science.

At sub-microkelvin temperatures, the chemical reaction between Rb and KRb is energetically forbidden, though the loss-rate of molecules is increased dramatically when atoms are introduced. Here we investigate the origin of this loss by directly observing the collisional complex dynamics. As shown in Figure. 1(a), the atoms and molecules are held in a crossed optical dipole trap (ODT) at a wavelength of 1064 nm, which serves not only to confine the atoms and molecules but also affects the dynamics of the complexes formed by their collisions. In the course of these studies, we have found that the ODT light can effectively deplete the intermediate complexes, which we exploit to set a time zero for complex formation, allowing us to monitor the dynamics of this process. This is done by modulating the intensity of the ODT light, followed by a pulse of ionizing UV radiation to allow for the probing of the formed complexes, outlined in Figure. 2(a) and was developed in the previous funding cycles.In this system, loss of the intermediate complex, KRb_2^*, can be from either dissociation into KRb and Rb or be photoexcition by the trapping light, as depicted in Figure. 1(b). This loss rate is in competition with the formation of KRb_2^*, which eventually form an equilibrium, with the complex lifetime as well as the photoexcitation rate determining the time scale of the dynamics.

To precisely estimate the complex lifetime, we must decouple the loss from dissociation and photoexcitation. This is done by varying the ODT light intensity and measure the time constants, resulting in the lifetime measurements at different ODT intensities I depicted in Figure. 2(b). Here, we ensure that when the intensity is changed, the average ODT intensity is kept constant to prevent

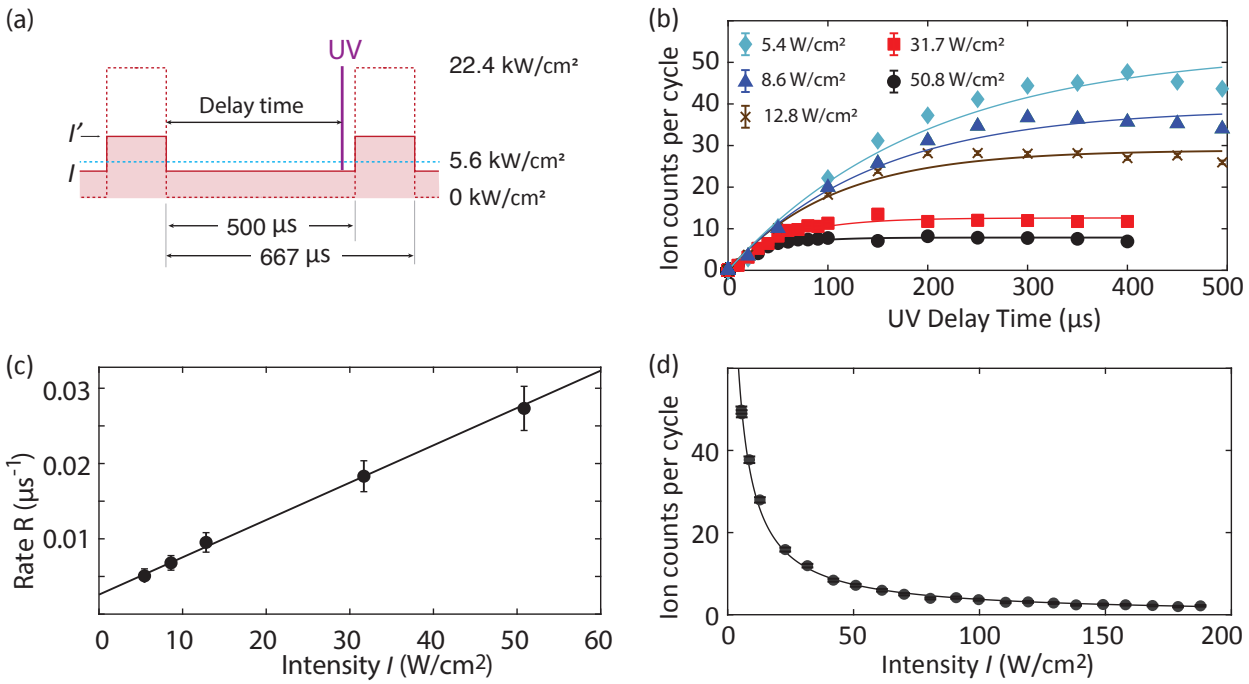

Figure 2: **Lifetime measurements of the KRb_2^* collision complex**. **(a)** The experiment timing diagram, with the red curve showing the ODT intensity. We vary the ODT modulation depth while keeping the time-averaged intensity fixed at the continuously operated level (blue dashed line). The red dashed line is the intensity profile at full modulation depth. **(b)** Time evolution of the KRb_2^* population (measured via the KRb_2^+ ion signal) after a rapid drop in the 1064 nm ODT intensity, for different intensity values. The solid lines are fits a exponential curve. **(c)** Characteristic growth rate of the complex population, as obtained from the fits in (a), versus the corresponding total ODT intensity. **(d)** Steady-state KRb_2^+ ion counts measured at different total ODT intensities.

molecule loss caused by change of trap depth. The complex lifetime is then extrapolated to zero ODT intensity, which we find to be 0.39(6)ms. From this data, we can also extract the photoexcitation rate from the steady-state KRb_2^+ ion counts measurements at different ODT intensities [see Figure.2(d)], which we find to be similar to our previously findings for the $K_2Rb_2^*$ complex. The exceptionally long lifetime renders the complex very sensitive to the ODT light, leading to rapid loss of the atom-molecule mixture under normal trapping conditions.

Previous theoretical calculations of the KRb_2^* lifetime using statistical theories, which assume that the angular momenta and spins are conserved, have determined a value of $\sim$1 ns for the lifetime, off by a factor of 10^5 from our measured value. This discrepancy has spurred many theoretical studies into the physics of atom-molecule collisions and will require further experimental work to guide our understanding.

Future Plans:
Observing such long-lived intermediate complexes in Rb + KRb collisions is equal parts surprising and exciting. Many of the theories proposed to explain the long complex lifetime do not agree with each other, and we have the unique capability to provide experimental insight into the under-

lying physics for these collisions. These capabilities take the form of two distinct experimental directions.

First, we have many handles to alter the conditions of the reactive collisions, including varying the internal state of the molecules and atoms, external electric fields, and external magnetic fields. Altering these parameters may help elucidate their impact on the underlying physics in these collisions.

Second, we aim to detect the quantum states of the collision products directly. Spin and other angular momentum conservation is assumed in many of the theoretical calculations of the complex lifetime, though if this conservation is violated, the predicted lifetime should increase. To validate this assumption, we plan to upgrade our optical setup to allow for the direct probing of the hyperfine spin states of Rb after collision by using Rydberg excitations. In an atom-molecule collision where Rb undergoes a hyperfine state-changing interaction from F = 2 to F = 1, there will be an energy release of ~ 7 GHz that will be imparted into the molecule in the form of recoil energy that can be distinguished using our ion imaging apparatus. Implementing a resonance enhanced multiphoton ionization (REMPI) scheme for state-selective detection of RKb should allow for this study to be performed.

References to publications of DOE sponsored research:

(1) M.-G. Hu*, Y. Liu*, D. D. Grimes, Y.-W. Lin, A. H. Gheorghe, R. Vexiau, N. Bouloufa-Maafa, O. Dulieu, T. Rosenband, and K.-K. Ni. Direct Observation of Bimolecular Reactions of Ultracold KRb Molecules, Science 366, 1111 (2019)
(2) Y. Liu*, D. D. Grimes*, M.-G. Hu*, K.-K. Ni Probing Ultracold Chemistry using Ion Spectrometry, Phys. Chem. Chem. Phys. 22, 4861-4874 (2020)
(3) Y. Liu*, M.-G. Hu*, M. A. Nichols, D. D. Grimes, Tijs Karman, Hua Guo, K.-K. Ni. Steering ultracold reactions through long-lived transient intermediates, Nature Physics 16, 1132-1136 (2020)
(4) M.-G. Hu*, Y. Liu*, M. A. Nichols, L. Zhu, G. Quemener, O. Dulieu, and K.-K. Ni. Nuclear spin conservation enables state-to-state control of ultracold molecular reactions, Nature Chemistry (2020) (5) Y. Liu*, M.-G. Hu*, M. A. Nichols, D. Yang, D. Xie, H. Guo, K.-K. Ni. Precision test of statistical dynamics with state-to-state ultracold chemistry, arXiv:2012.15842 (2020)
(6) G. Quemener, M.-G. Hu, Y. Liu, M. A. Nichols, L. Zhu, and K.-K. Ni. Model for nuclear spin product-state distrubitions of ultracold chemical reactions in magnetic fields, Phys. Rev. A 104, 052817 (2021)
(7) M. A. Nichols, Y.-X. Liu, L. Zhu, M.-G. Hu, Y. Liu, K.-K. Ni. Detection of Long-Lived Complexes in Ultracold Atom-Molecule Collisions, Phys. Rev. X 12, 011049 (2022)

Ultrafast Transient Absorption Spectroscopy of Hydrocarbon Radicals

Melanie Reber
Department of Chemistry, University of Georgia, Athens, GA 30602
mreber@uga.edu

Project Scope

We aim to i) complete an ultrafast cavity-enhanced transient absorption spectrometer and incorporate two sources of radicals in molecular beams and ii) study the excited state dynamics of vinyl radical and allyl radical. The spectrometer consists of a home-built Ytterbium fiber laser frequency comb and Ytterbium fiber chirped-pulse amplification system that generates ultrafast (about 100 fs pulse duration) pulses across much of the visible region. This light is split into pump and probe beams and coupled into enhancement cavities housed in a vacuum chamber. Lock-in detection and noise subtraction techniques are used for noise suppression. With the increase in signal-to-noise with these techniques, it will be possible to perform ultrafast transient absorption spectroscopy in the visible and near-IR spectral regions of radical intermediates in molecular beams. The first goal is to demonstrate the ability to take ultrafast transient absorption spectroscopy of the electronically excited states of radical intermediates.

The second goal is to study the excited state dynamics of vinyl, C_2H_3, and allyl, C_3H_5, radicals. The first excited state of allyl radical exhibits a broad absorption and is thought to connect to the ground state through several conical intersections. The upper state lifetime is less than 5 ps and excitation of this state results in the release of a hydrogen atom. Direct, time-resolved absorption spectroscopy could elucidate this mechanism. Similarly, the first excited state of vinyl radical has picosecond lifetimes, with a decrease in lifetimes with higher vibrational excitation. The frequency-resolved spectroscopy has the signature of ultrafast predissociation from the ground state. We hope to gain insight into these processes in vinyl radical with ultrafast transient absorption spectroscopy. This work will advance our knowledge of excited state processes in combustion intermediates and reactive species.

Recent Progress

The cavity-enhanced transient absorption spectrometer was under construction in Fall 2019 when this project started. We have since completed building the laser system, carried out transient absorption measurements, and are now completing assembly of the vacuum and molecular beam system and photolysis source. Two key results are discussed below, first is a method to decrease our laser pulse duration and the second is the final design of the differential pumping system.

The Ytterbium fiber laser system and chirped-pulse amplification system is operational. While this design was based upon a previously published laser system, we have made some improvements. To shorten the pulse duration, we added a spectral filter to the laser cavity. The filter broadened the laser spectra, which enabled shorter pulses after pulse compression[1]. Figure 1 shows how the inclusion of a 1040 nm longpass filter (panel A) and a 1050 nm shortpass filter (panel B) inside the laser cavity can broaden the laser spectra. The cutoff wavelength of the filter tunes slightly with incidence angle, as shown in the figure. For comparison, the filters were also placed outside the laser cavity and tuned by the same angle (panels C and D). With the additional

[1] N. D. Cooper and M. A. R. Reber, Provisional Patent No. 63/225,263 (2021).

spectral bandwidth, we were able to shorten the laser pulse from 110 fs to around 80 fs, with the bandwidth to go to even shorter pulse durations. This is a potential avenue to sub-30 fs fiber lasers.

Figure 1: Comparison of Yb:fiber laser with intracavity filter (A and B) and the same filter placed outside the cavity (C and D). Rotation of the incident angle on the filter, as labeled, tunes the cutoff frequency.

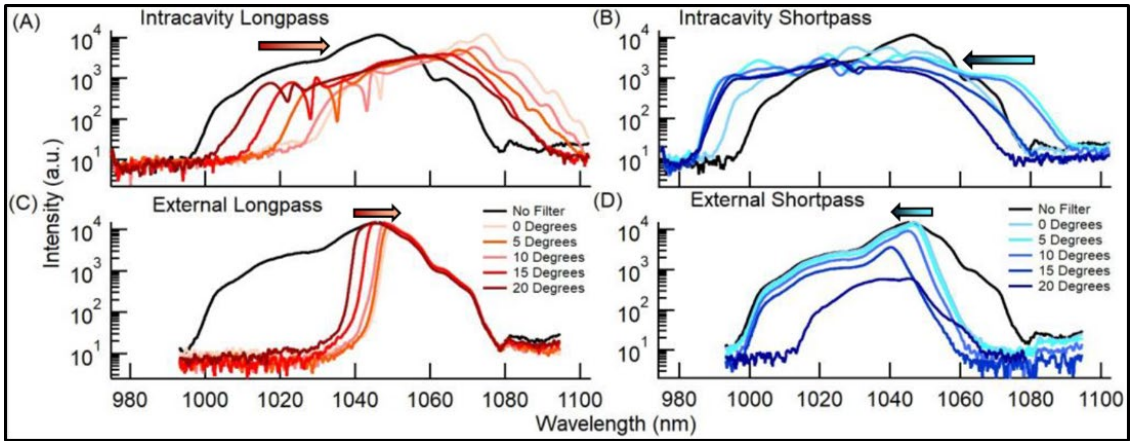

Using both gas kinetic equations and COMSOL Multiphysics software, we explored designs for the new differential pumping system. Supply chain issues have delayed acquisition of the components; however, it is now nearly assembled and ready to test. The molecular beam is on a 3-axis stage to allow for overlap with the two optical cavity beams while the chamber is under vacuum. The molecular beam region is pumped by a Roots blower and rotary vane pump. Small slits in the side walls of the molecular beam region allow the optical cavity beams to enter and exit the molecular beam region, including the photolysis beam (not pictured). Then enhancement cavity beams must enter the molecular beam interaction region through small holes, rather than windows, to maintain the high-finesse of the optical cavity and minimize dispersion. The slits are designed to maintain microTorr level pressures in the optical cavity region while gas is flowing in the molecular beam. The optical cavity region is pumped by a turbomolecular pump. Figure 2 shows the SolidWorks rendering of the chamber. The sides and lid are partially removed in the drawing so the slits into the molecular beam region can be seen. Currently, the molecular beam source is a continuous pinhole nozzle.

Figure 2: Cutaway view of differential pumping and vacuum setup

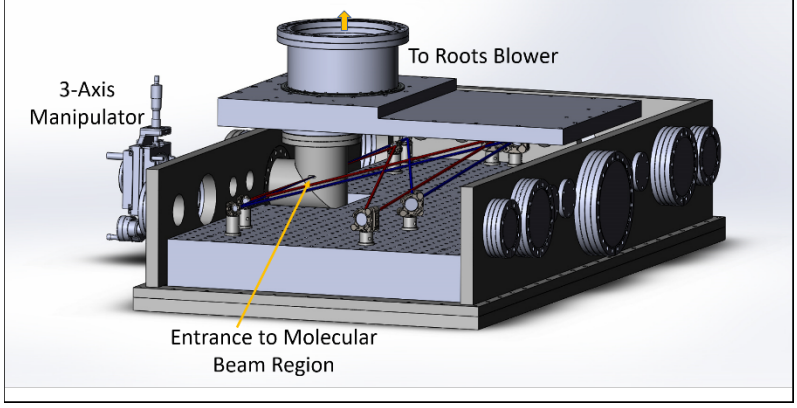

Future Plans:

Once the final vacuum chamber components arrive, we will be ready to test the molecular beam and optical enhancement cavities. We will then start with studying the time-resolved excited state spectroscopy of vinyl and allyl radical. Experiments with a wide range of combustion radicals are planned for the future as well as increasing the spectral range of the spectrometer to include the infrared and mid-infrared region.

Photoinitiated Reactions of Molecules and Radicals in Molecular Beams

Hanna Reisler
Department of Chemistry, University of Southern California
Los Angeles, CA 90089-0482
reisler@usc.edu

Program Scope

The UV photochemistry of organic molecules is a fundamental process that governs reactions in the atmosphere, synthetic chemistry, organic aerosols, and biological damage in living tissues. The ensuing dynamics usually involve pathways that are in competition, such as direct dissociation on excited states, couplings to lower potential energy surfaces, isomerization, and secondary dissociation of products. The current project is focused on the photochemistry of alpha-keto carboxylic acids, a group of acids implicated in aerosol formation and biological processes, which can also be a source of hydroxycarbenes. Another important molecule is pyrazine, a benchmark for vibronic and spin-orbit coupling. Some of these molecules provide pathways to producing transient species important in combustion and atmospheric chemistry. Understanding their complex photochemical behavior requires multiple experimental approaches and close cooperation between experiment and theory.

Recent Progress

The experimental work on pyruvic acid was done in collaboration with Dr. David Osborn, Sandia Combustion Research Facility, and was carried out at the Advanced Light Source (ALS) facility. The experiments exploited multiplexed photoionization mass spectrometry (MPIMS) and tunable VUV. Our goal was to characterize the electronic properties of the three lowest excited singlet electronic states of pyruvic acid and understand how they control dissociation pathways and dynamics, including product branching ratios and secondary reactions. The experimental studies of the photophysics of pyrazine are carried out at USC in molecular beams and benefit from theoretical calculations.

Chemical reactions of methylhydroxycarbene (MHC)

In our experiments, we have observed for the first time MHC, the primary product of the 351 nm photodissociation of pyruvic acid. We have concluded that about half the nascent MHC generated via the S_1 state has internal energy lower than its isomerization barrier to the two other C_2H_4O isomers (acetaldehyde and vinyl alcohol), and it survives long enough to participate in chemical reactions. Indeed, in these experiments we were able to identify the gas phase chemical reaction of MHC with pyruvic acid, giving rise to a product with a molecular formula of $C_4H_8O_2$, or twice the molecular mass of MHC. The only bimolecular reaction consistent with the kinetic observations is the MHC + pyruvic acid reaction forming a $C_4H_8O_2$ product (Species M, m/z =88) whose structure we cannot yet assign. When using d_1- pyruvic acid (having OD rather than OH), we observe the same reaction product at m/z = 90 (see Figure 1).

Even though my group was not allowed to visit the ALS facility due to the pandemic, Dr. Osborn was able to carry out experiments on the reaction of MHC with its acetaldehyde tautomer. He photolyzed pyruvic acid at 351 nm in the presence of excess deuterated acetaldehyde and observed a stable bimolecular product at m/z = 92, which can be either 3-hydroxy-butanal or its ketonic form, acetoin (3-hydroxy-2-butanone). Comparison of the observed photoionization spectrum of the m/z = 92 product with those of the two possible products of the same molecular

formula shows no evidence of 3-hydroxy-butanal, and thus we assign the product to acetoin. Significantly, we were able to stabilize the reaction product in the presence of only 4 Torr of He. This reaction is an analog of the formose reaction, where two formaldehyde molecules react to produce an aldol.[1] It is implicated in the formation of sugars in space but has not been observed before in the gas phase. Here we use the second member of the aldehyde group, acetaldehyde, and demonstrate that its MHC tautomer is the reactant that enables this gas-phase reaction. This intriguing result paves the way to additional studies of the formose reaction and its analogs.

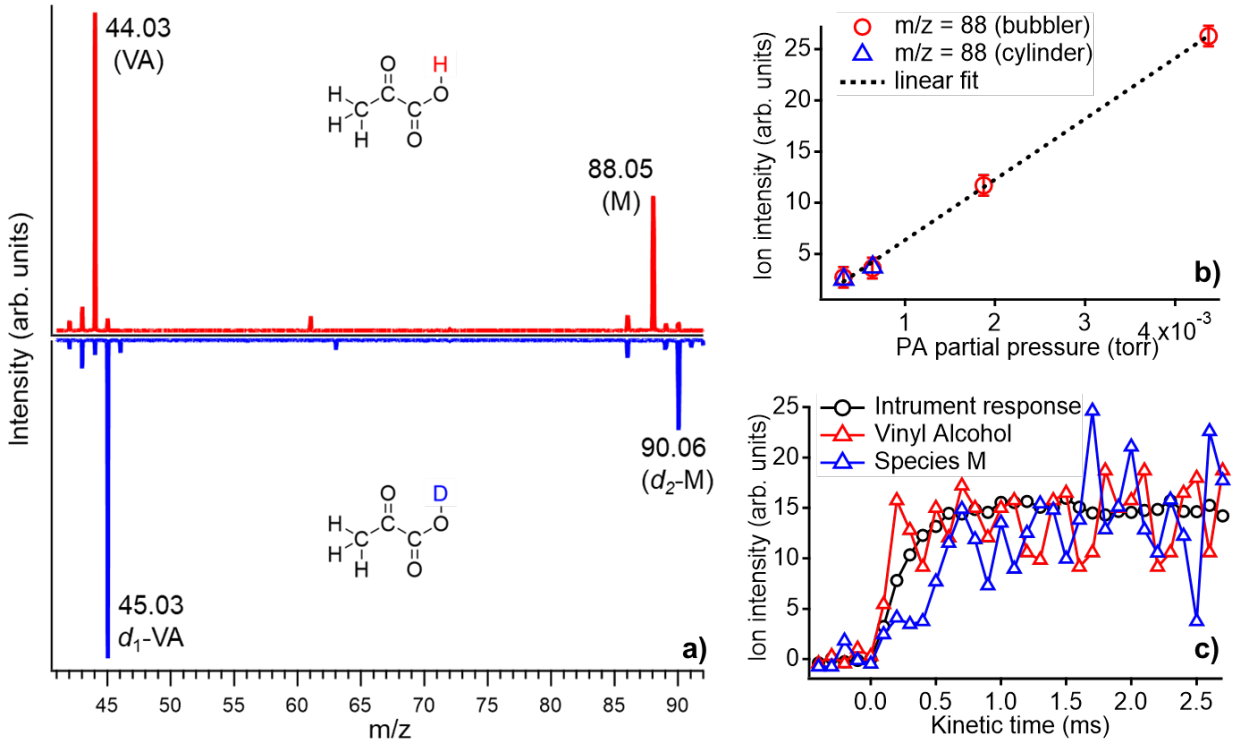

Figure 1: (a) TOF spectra (integrated over 5 – 40 ms) of pyruvic acid (PA, red trace) and d_1-PA (blue trace, inverted for clarity) showing the observed change in mass peaks due to deuteration. (b) Species M signal changes linearly upon change in PA concentration and is independent of the mode of PA sample preparation demonstrated by two different methods: (i) He bubbled through a glass bulb containing PA (red circles) and (ii) sample mixture delivered via a cylinder (blue triangles). (c) At low PA partial pressure (0.3 mTorr) species M shows a slower rise time, whereas vinyl alcohol, formed by rapid isomerization of vibrationally excited primary photoproduct MHC, shows a rise time limited by the instrument response time. The data in this figure are all obtained at a photon energy of 9.65 eV (see publication no. 3 for details).

Our studies demonstrate that pyruvic acid and related alpha-keto carboxylic acids can provide ways to create alkylhydroxycarbenes in the laboratory, enabling exploration of their kinetics and reactivity, which may be relevant to chemical models of complex reaction systems in the atmosphere. MHC should be present in the troposphere from photolysis of pyruvic acid by sunlight, and will be stabilized and further react at 1 atm.

The photophysics of pyrazine on multiple potential energy surfaces

The shutdown of the ALS during the pandemic prevented my group from continuing the experiments on pyruvic acid and its MHC product. Instead, we shifted focus to pyrazine, a molecule that we could study solely at USC. Specifically, we seek to understand how the interactions among the excited states of pyrazine affect its spectroscopy and photophysics following S_2 excitation. For decades, pyrazine has served as a benchmark for both experiment and theory for exploring photophysical decay mechanisms on coupled electronic surfaces. The unimolecular dynamics following excitation of pyrazine to the $^1B_{3u}$ (S_1) excited state, while complicated, is fairly well understood today. This is not the case for the photophysics and photochemistry following excitation to the higher lying $^1B_{2u}$ state, commonly known as S_2. While it is established that the S_2 state decays in about 20 fs to S_1 via a conical intersection,[2,3] how subsequent surface couplings affect its absorption spectrum and photodissociation dynamics is not yet understood. In fact, even the possible involvement of the lower ^1A_u state has only recently been studied by experiment and theory.[3,4]

The 300 K $S_2 \leftarrow S_0$ absorption spectrum of pyrazine (230-280 nm) has only a few broad features, but the jet-cooled spectrum has yet to be reported. Using ultrafast (20-130 fs) time-resolved photoelectron spectroscopy, it has been observed that the S_1 state is reached from S_2 in about 20 fs via a conical intersection located near the Frank-Condon region. The S_1 state lives longer, for about 20 ps near the band origin, and then decays by spin-orbit coupling to lower triplet states, and subsequently to the ground electronic state. Femtosecond laser experiments have shown changes in the photoelectron spectra as a function of time delay following excitation, indicating that several electronic states are involved.[2,3] Pyrazine is known to belong to the so-called intermediate coupling case with respect to vibronic density of states, and its number of coupled states should depend on symmetry, rotational state, and other selection rules. While many calculations of the $S_2 \leftarrow S_0$ vibronic spectrum have been published, the results depend on the model used, and no jet-cooled absorption spectra are available for comparison.

In separate experiments aimed at studying the vibrational predissociation of hydrogen-bonded complexes of pyrazine, carried out in molecular beams with nanosecond lasers, we noted that the one-color REMPI spectrum of the pyrazine monomer that we observed following S_2 excitation had sharp lines, extending to the long-wavelength tail of the 300 K absorption spectrum. This observation was intriguing, and we decided to examine it more closely. The spectrum was reproducible, but the signal was low, which might be explained by the short lifetime of the S_2 state.

Further examination of the time-of-flight mass and REMPI spectra obtained under our experimental conditions showed, however, that the one-color REMPI spectrum we observed for the pyrazine monomer (m/z =80) was identical to the one observed for m/z=107, i.e., pyrazine + 27 amu. After puzzling over these results, we have concluded that the source of our observed signals is a pyrazine cluster. We hypothesize that the signals at m/z= 80 and 107 are both daughter ions deriving from larger ionic clusters of pyrazine. We note that m/z = 27 has the molecular formula of HCN. It is thus possible that further photochemistry in pyrazine cluster ions during the MPI process leads to in-cluster dissociation of the pyrazine moiety generating HCN products. Azabenzene cations are known to lose HCN upon dissociation, and pyrimidine cations, for example, readily form cluster ions with HCN.[5] An ionic cluster of HCN with pyrazine would explain the observed m/z = 107. It is well known that pyrazine, like other N-heterocyclic aromatics, is prone to clustering.

Pyrazine clusters may have many isomers, as even the dimer has at least two isomers. It is still perplexing, however, that an isomer deriving from $(pyrazine)_n$ clusters exhibits a REMPI spectrum with narrow and sparse lines near the origin such as those that we observed. Once we eliminate clustering, we will be able to observe the REMPI spectrum of the isolated pyrazine monomer and compare it both to the 300 K spectrum, and the spectrum at m/z = 107.

Future work

We are setting up experiments to perform 1+1' two color REMPI spectroscopy of the pyrazine monomer, focusing on the $S_2 \leftarrow S_0$ band origin region. By analyzing the spectra and comparing them to theoretical calculations, we will learn about the strength of couplings and the number of states that couple strongly to the S_2 excited state. We also wish to learn about possible tier structure in the coupled states, the roles of symmetry and rotations, and the influence of clustering on the relevant conical intersections and REMPI spectra.

References

1. M. Boutlerow, C. R. Acad. Sci. **53**, 145–147 (1861).
2. V. Stert, P. Farmanara, and W. Radloff, J. Chem. Phys. **112**, 4460 (2000).
3. T. Horio, R. Spesyvtsev, K. Nagashima, R.A. Ingle, Y. Suzuki, and T. Suzuki, J. Chem. Phys. **145**, 044306 (2016).
4. V. Scutelnic, S. Tsuru, M. Pápai, Z. Yang, M. Epshtein, T. Xue, E. Haugen, Y. Kobayashi, A.I. Krylov, K.B. Møller, S. Coriani, and S.R. Leone. Nat. Commun. **12**, 5003 (2021).
5. A.M. Hamid, M.S. El-Shall, R. Hilal, S. Elroby, and S.G. Aziz, J. Chem. Phys. **141**, 054305 (2014).

Publications 2019-2021

1. S. Sutradhar, B.R. Samanta, R. Fernando, and H. Reisler, "Spectroscopy and two-photon dissociation of jet-cooled pyruvic acid", J. Phys. Chem. A **123**, 5906-5917(2019).
2. B.R. Samanta, R. Fernando, D. Rösch, H. Reisler, and D.L. Osborn, "Looking at the bigger picture: Identifying the photoproducts of pyruvic acid at 193 nm", J. Chem. Phys. **153**, 074307 (2020).
3. B. R. Samanta, R. Fernando, D. Rösch, H. Reisler, and D.L. Osborn, "Primary photodissociation mechanisms of pyruvic acid on S_1: observation of methylhydroxycarbene and its chemical reaction in the gas phase", Phys. Chem. Chem. Phys. **23**, 4107-4119 (2021).

FUNCTIONAL GROUP EFFECTS ON UNIMOLECULAR QOOH REACTIONS AT HIGH PRESSURE USING HIGH-RESOLUTION ELECTRONIC ABSORPTION SPECTROSCOPY

Brandon Rotavera
College of Engineering | Department of Chemistry
University of Georgia
Athens, GA 30602

rotavera@uga.edu | (rotavera.uga.edu)

Program Scope

The primary goal of this research program is to produce new fundamental knowledge on connections between molecular structure of hydroperoxy-substituted carbon-centered radicals (ȮOOH) and selectivity towards specific unimolecular reaction pathways (**Figure 1**). This knowledge is derived in part from combustion experiments using a jet-stirred reactor that is employed to measure isomer-resolved species concentration profiles of multi-functional intermediates derived from ȮOOH formed via oxidation of the C4 species in **Figure 2**. As a primary outcome, this research program expands gas-phase chemical kinetics knowledge on the effects of functional groups on chemical reactivity that is necessary to refine computational combustion models that support ongoing efforts to incorporate biofuels in current and future combustion systems. Additionally, owing to the complex combustion behavior of functionalized molecules, this program focuses on identifying new reaction pathways that are studied in greater detail using theoretical chemical kinetics computations, including potential energy surfaces and rate calculations. In addition, a primary focus of the program is to utilize experiments and chemical kinetics modeling to understand the effect of oxygen concentration on competing reactions of ȮOOH radicals formed from the species in **Figure 2**. In particular, experiments are conducted to specifically examine product formation from unimolecular reactions versus from the second-O_2-addition step. The red-highlighted text in Figure 1 indicates the classes of species produced via the former reaction type, which involve both constitutional isomers as well as stereoisomers and are important due to the connection to specific ȮOOH radicals that govern reactivity.

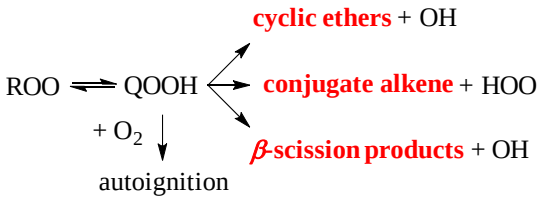

Figure 1. *Reaction mechanisms of ȮOOH radicals are central to understanding and developing modeling capabilities for hydrocarbon and biofuel oxidation. Accurately quantifying product formation from ȮOOH reflects the balance of chain-branching reactions (downward-pointing arrow) to chain-propagation and chain-inhibiting reactions (arrows pointing towards the right), each of which can produce an abundance of isomers.*

Direct measurements of such isomers, e.g. cyclic ethers, provide stringent benchmarks of ȮOOH chemistry and are therefore central to the development of robust chemical kinetics mechanisms. This program bridges knowledge gaps between molecular structure and ȮOOH reactivity for C4 molecules, namely the balance of unimolecular decomposition vs. bimolecular reaction with O_2.

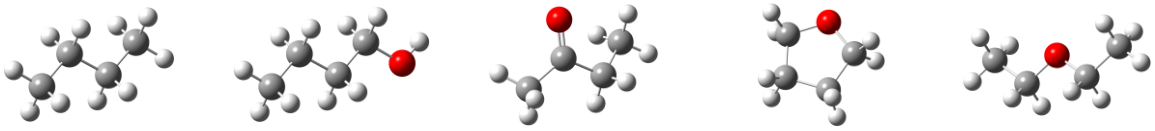

Figure 2. *Molecular structure of C4 species studied in this program (left to right): n-butane, 1-butanol, butanone, tetrahydrofuran, and diethyl ether*.

Recent Progress

Speciation experiments in a jet-stirred reactor: The jet-stirred reactor (JSR) at the University of Georgia is capable of experiments at pressures up to 50 atm and operates with a well-characterized temperature profile. Particular attention is paid to quantifying spatial temperature uncertainty in the sampling region as well as in species quantification. Complete temperature characterization was accomplished using a systematic series of experiments conducted at residence times up to 4000 ms over a range of temperatures controlled independently in two distinct heating regions of the JSR, the reactor region and the pre-heating region. In all cases, owing to a custom-built, woven Inconel and ceramic insulation heating system, 1σ deviations in temperature are <1% of the reaction temperature (up to 1200 K) over a 3-cm sampling distance. Species quantification is accomplished with an uncertainty of ~10% in all cases and is achieved via tandem gas chromatography measurements via two independent detection methods (Figure 3). The first uses electron-impact (EI) mass spectrometry (Figure 3a). The second uses vacuum ultraviolet absorption spectroscopy (Figure 3b). The unique aspect of the tandem approach is that for each retention time, two molecular signatures are produced, an EI mass spectrum and an absorption spectrum measured from 5.167 – 9.920 eV, which enables resolution of both constitutional isomers and stereoisomers. An example of the latter is shown in **Figure 3** and is important due to stereochemical-dependent reaction chemistry [1-3].

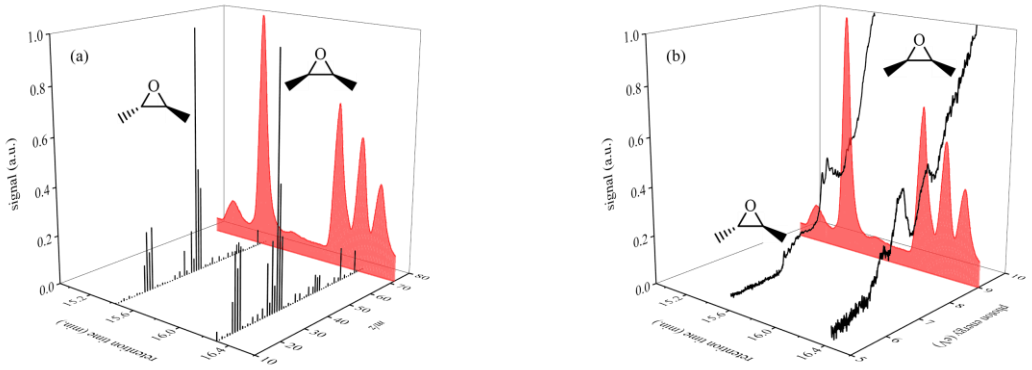

Figure 3. *EI mass spectra (a) and VUV absorption spectra (b) of 2,3-dimethyloxirane isomers.*

To examine the influence of temperature and oxygen concentration on intermediates from *n*-butane [4] and tetrahydrofuran [5], isomer-resolved speciation measurements were conducted at 810 Torr in a jet-stirred reactor (JSR) from 500 – 1000 K. **Figure 4** shows representative experimental data and modeling from *n*-butane oxidation (Figure 4a and Figure 4b) and tetrahydrofuran oxidation (Figure 4c and Figure 4d). The main objective of these experiments is to provide quantitative targets for modeling ȮOOH-mediated chemistry over a range of oxygen concentration to probe the chemistry depicted in Figure 1, particularly species that are uniquely formed via the unimolecular step, including cyclic ethers and HOO-elimination products. Similar experiments were conducted for diethyl ether and butanone. The dependence on $[O_2]$ of 2,3-dimethyloxirane stereoisomer concentrations at 650 K is depicted in Figure 4b. Comparison with the measurements indicate a maximum cyclic ether concentration occurring near $[O_2] \sim 3 \cdot 10^{18}$ molecules $\cdot$ cm^{-3}, corresponding to an equivalence ratio of ~1.1. The model overpredicts the sum of the isomers at both temperatures compared to the experimental sum. For both temperatures, as $[O_2]$ approaches the extrema, the steady state concentration of both 2,3-dimethyloxirane isomers approaches zero. For tetrahydrofuran, and resulting from negative-temperature coefficient behavior, species concentrations peaked at two temperatures, 600 K and 800 K, which were then selected for separate experiments to quantify O_2-dependence using concentrations of $0.37 \cdot 10^{18} – 7.40 \cdot 10^{18}$ molecules cm^{-3}. The disparities observed in Figure 4 indicate an incomplete understanding on the influence of O_2 on the balance of reactions in Figure 1, the correction of which is a primary objective of this program.

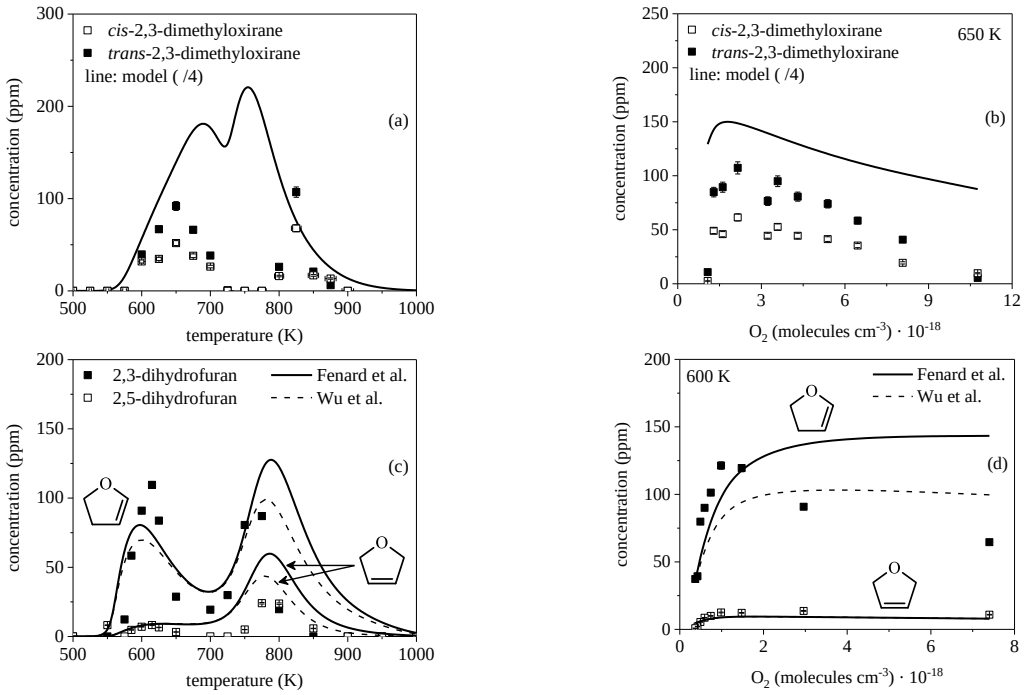

Figure 4. *(a) Temperature dependence of cyclic ethers measured under stoichiometric conditions compared with model predictions using NUIGMech 1.1, which neglects stereochemistry and is therefore a summation of cis- and trans- isomers. The model is divided by a factor of four to delineate qualitative comparisons. (b) O_2-dependence of cis-2,3-dimethyloxirane and trans-2,3-dimethyloxirane concentrations measured at 650 K. (c) Temperature dependence of dihydrofuran isomers measured under stoichiometric conditions: $[O_2] = 0.74 \cdot 10^{18}$ molecules $\cdot$ cm^{-3}. Model predictions produced using the Fenard et al. [6] mechanism. The NTC region is observed from ~625 – 700 K. (d) O_2 dependence of 2,3-dihydrofuran and 2,5-dihydrofuran at 600 K and comparison to Fenard et al. [6] and Wu et al. [7].*

Future Work

High-pressure jet-stirred reactor experiments: A high-pressure control system is currently being implemented into the JSR for operation up to 50 atm. Temperature profile measurements are also being conducted to quantify temperature gradients and uncertainty as a function of reaction pressure in the combustion experiments, which is important due to changes in diffusion rates with pressure. Quantification of measurement uncertainties will be completed over the full range of experimental variables, namely temperature, pressure, and residence time.

Targeting unimolecular reactions of intermediates: Several key intermediates are proposed as unique sources of species detected in tetrahydrofuran oxidation, including (i) oxirane formation from 3,4-epoxytetrahydrofuran and (ii) 2-butenal formation from cyclopropane carboxaldehyde and 2,3-dihydrofuran. To provide clarity to such questions, ongoing experiments in this project are focused on refining understanding of reactions of such intermediates in an effort to narrow the reaction pathways included in chemical kinetics models.

Machine learning and isomer-resolved absorption spectroscopy for species identification: In order to identify spectra for which no reference data are available, machine learning techniques are under development (Doner et al. *Anal. Chem.*, submitted). In such cases, machine learning is employed to identify spectral features that correspond to functional group type, number of π bonds, etc. by relying on a robust training set of spectra that contains varying combinations of these motifs. Future work is aimed at enhancing the predictive capability of the machine learning methods by, among other efforts, increasing the number and diversity of spectra in the training set.

Rate computations: Species for which new reaction pathways are identified, such as those proposed in Hartness et al. [4] and Koritzke et al. [5], will require rate computations and, in some cases, thermochemistry to include in chemical kinetics mechanisms to assess the impact on combustion model predictions. This will be accomplished using KinBot software and the PAPR code in collaboration with both Sandia National Laboratories and Argonne National Laboratory.

Refining chemical kinetics mechanisms: The efforts above combine to achieve one of the primary goals of the program, which is increasing the quantitative prediction capabilities of chemical kinetics mechanisms by (i) providing new, benchmark experimental data, (ii) identifying new reaction pathways that may hold relevance to increasing the accuracy of modeling combustion, and (iii) computing theoretical rates. Future work on this topic will involve using existing mechanisms from the literature on the five species in **Figure 1** and refining via a combination of the efforts above.

Publications/Presentations Acknowledging Support from the Gas-Phase Chemical Physics Program, 2020-Present:

1. (*invited seminar*, March 2022) 7th Irvin Glassman Young Investigator Award Lecture, **The Importance of Reaction Mechanisms in Combustion**, *Spring Meeting of the Eastern States Section of the Combustion Institute*, Orlando, Florida.
2. **Probing O_2-Dependence of Hydroperoxy-Butyl Reactions via Isomer-Resolved Speciation**, S. W. Hartness, N. S. Dewey, M. G. Christianson, A. L. Koritzke, A. C. Doner, A. R. Webb, B. Rotavera, *Proceedings of the Combustion Institute*, Vol. 39, accepted.
3. **Predicting Molecular Structure from Vacuum Ultraviolet Absorption Spectra using Machine Learning**, A. C. Doner, H. A. Moran, A. R. Webb, M. G. Christianson, A. L. Koritzke, G. D. Smith, B. Rotavera, *Analytical Chemistry*, submitted.
4. **Probing O_2-Dependence of Tetrahydrofuranyl Reactions via Isomer-Resolved Speciation**, A. L. Koritzke, M. G. Christianson, S. W. Hartness, N. S. Dewey, A. C. Doner, A. R. Webb, B. Rotavera, *Combustion and Flame (Invited for Special Issue in Honor of Jim Miller)*, submitted.
5. **Vacuum-Ultraviolet Absorption Cross-Sections of Functionalized Four-Carbon Species,** A. C. Doner, M. G. Christianson, A. L. Koritzke, A. Larsson, K. Frandsen, B. Rotavera, *J. Quant. Spec. Rad. Trans.*, submitted.
6. **Influence of Functional Groups on Low-Temperature Combustion Chemistry of Biofuels,** B. Rotavera and C. A. Taatjes, *Prog. Energy Combust. Sci.*, 86, 1-96 (2021); https://doi.org/10.1016/j.pecs.2021.100925.
7. **Vacuum-Ultraviolet Absorption Cross-Sections of Functionalized Cyclic Hydrocarbons: Five-Membered Rings,** M. G. Christianson, A. C. Doner, A. L. Koritzke, K. Frandsen, B. Rotavera, *J. Quant. Spec. Rad. Trans.* **258**, 1-8 (2020); https://doi.org/10.1016/j.jqsrt.2020.107274
8. (*invited seminar*, March 2021) "Influence of Functional Groups on Low-Temperature Combustion Chemistry of Biofuels", Brandon Rotavera, *Princeton/Georgia Tech Combustion Seminar Series* (**link**).

References

[1] A.C. Doner, M.M. Davis, A.L. Koritzke, M.G. Christianson, J.M. Turney, H.F. Schaefer, L. Sheps, D.L. Osborn, C.A. Taatjes, B. Rotavera, *Int. J. Chem. Kin.*, 53 (2021) 127-145.
[2] A.D. Danilack, C.R. Mulvihill, S.J. Klippenstein, C.F. Goldsmith, *J. Phys. Chem. A*, 125 (2021) 8064-8073.
[3] A. Doner, J. Zádor, B. Rotavera, *Faraday Discussions*, (2022).
[4] S.W. Hartness, N.S. Dewey, M.G. Christianson, A.L. Koritzke, A.C. Doner, A.R. Webb, B. Rotavera, *Proc. Combust. Inst.*, 39 (2022) accepted.
[5] A.L. Koritzke, M.G. Christianson, S.W. Hartness, N.S. Dewey, A.C. Doner, A.R. Webb, B. Rotavera, *Combust. Flame*, (2022) submitted.
[6] Y. Fenard, A. Gil, G. Vanhove, H.H. Carstensen, K.M. Van Geem, P.R. Westmoreland, O. Herbinet, F. Battin-Leclerc, *Combust. Flame*, 191 (2018) 252-269.
[7] Y.T. Wu, N. Xu, M. Yang, Y. Liu, C.L. Tang, Z.H. Huang, *Combust. Flame*, 213 (2020) 226-236.

Coordinated Interrogation and Modeling in Ammonia Oxidation Catalysis

William F. Schneider and Jason C. Hicks
Department of Chemical and Biomolecular Engineering, 250 Nieuwland Science Hall, Notre Dame, Indiana, 46556
wschneider@nd.edu, jhicks@nd.edu

Program Scope

The overarching goal of this project, joint between GPCP and Catalysis Science, is to establish the potential for plasma stimulation to modify the behavior of a catalytic system, through application of plasma stimulation to well-defined and well-characterized thermal catalytic systems, chosen for reaction features that are amenable to careful experimental and computational interrogation. While the theory and practice of thermal heterogeneous catalysis is well established and design rules well understood, the same cannot be said of catalysis in the presence of external stimulus. Electrocatalysis and photocatalysis are two familiar examples of stimulated catalysis, but plasma-promoted catalysis is emerging as a third, high potential alternative. Plasmas are easy to generate and have the distinctive feature of creating non-equilibrium energy distributions within the plasma phase. By appropriately coupling this non-equilibrium behavior with a catalytic surface, we hypothesize that it is possible to carry out otherwise difficult or impossible chemical transformations, to do so at high efficiency, to take advantage of renewable electricity to drive chemistry, and to do so at smaller scales than those possible thermally.

This project combines careful synthesis and interrogation of catalytic materials and chemistry under plasma stimulation with first-principles-based microkinetic modeling to both elucidate and guide experiment. Its primary output will be fundamental insights transferable across this space. The project focuses on the catalytic chemistry of nitrogen. Nitrogen reductions and oxidations are of great economic value and critical to environmental protection, thermal catalytic chemistry is well understood, and relevant reactions are simple enough to be readily probed but complex enough to provide non-trivial insights. In particular, we focus on the reduction of N_2 (ammonia synthesis) and oxidation of N_2 (an alternative to the Ostwald process).

Recent Progress

Ammonia synthesis: Ample literature evidence from our group and others indicates that ammonia can be formed at or near ambient conditions in a dielectric barrier discharge (non-thermal) plasma integrated with a catalytic surface. Our prior work (*Nature Catal.* **2018**, doi:10.1038/s41929-018-0045-1; *ACS Catal.* **2020**, doi:10.1021/acscatal.0c00684) reveals that at least one mode of action of the plasma is to decrease the demands on the catalytic surface to dissociate nitrogen. Recently published work (*ACS Sus. Chem. Eng.* **2021**, doi:10.1021/acssuschemeng.1c02713) highlights the potential for competing contributions of radical and vibrational excitations to influence ammonia production.

To provide more clarity into the influence of plasma on mechanisms of NH_3 synthesis on a catalytic material, we performed experiments at the Spallation Neutron Source at Oak Ridge National Laboratory and density functional perturbation theory to probe the relationship between exposure of a catalytic Ni surface to N_2 and/or H_2 plasma and the formed surface species. Both experiments and models highlight the appearance of chemisorbed hydrogen and of partially to fully hydrogenated nitrogen in the N_2/H_2 plasma, in contrast to a plasma-free control. Further, we

find that a sequential exposure to N_2 plasma and to H_2 without plasma leads to the same surface intermediates, highlighting the role of N_2 excitations specifically on ammonia synthesis. This work was published last year (*ACS Energy Lett.* **2021**, doi:10.1021/acsenergylett.1c00643).

The INS experiments provide compelling evidence that plasma activation of N_2 allows it to adsorb and dissociate on an otherwise unreactive catalytic surface. These findings motivated a series of sequential dosing experiments to decouple the plasma phase reactions from surface catalyzed pathways. Recently, we performed systematic plasma-assisted temperature programmed ammonia synthesis reactions (plasma-TPRxn) using this sequential N_2 plasma-catalyst stimulation followed by thermal hydrogen treatment. During the hydrogen treatment, the temperature was ramped to facilitate surface hydrogenation reactions. This approach avoids the influence of plasma-phase reactions and allows for the direct evaluation of the plasma activated nitrogen and the active surface of supported transition metal catalysts. These experiments confirm INS results that show plasma generated surface nitrogen can be converted to NH_3 through surface catalyzed pathways. Peak ammonia desorption temperatures vary with transition metal catalysts (Fe, Co, Ni, and Pt), reflecting differences in the hydrogenation ability of the catalysts as opposed to the ability to adsorb N_2, with Pt desorbing NH_3 at the lowest temperature. Unsteady state microkinetic models that incorporate nitrogen surface coverage dependency were developed and verified ammonia desorption trends across the metal catalysts. This work is in preparation for submission to *ACS Sustainable Chemistry & Engineering*.

Nitrogen oxidation: Nitrogen oxidation to NO is an alternative route to nitrogen fixation that, because it is endothermic, is particularly well suited to plasma promotion. Nitrogen oxidation in thermal plasmas has a long history, and recent evidence indicates that the same is possible in non-thermal plasmas. We have developed a modeling framework to assess the potential for plasma-catalyst combinations to promote nitrogen oxidation over a metal catalyst, based on a reduced model for plasma-phase chemistry and DFT-predicted results for surface catalytic chemistry. The models highlight the sensitivity of NO productivity to plasma conditions (radical density, vibrational temperature, and mixing ratio) and reveal plasma regimes well suited to catalytic promotion of NO production (*J. Phys. D: Appl. Phys*. **2021**, doi:10.1088/1361-6463/ac1bd1). Experiments performed by collaborators at the Dutch Institute for Fundamental Energy Research (DIFFER) agree well with model predictions. The work is particularly significant in that it demonstrates quantitatively a plasma-catalytic coupling at conditions at which intrinsic plasma and catalytic contributions alone are negligible and which produces NO at concentrations that exceed thermal equilibrium (*Nat. Comm.* **2022**, doi:10.1038/s41467-021-27912-2).

Plasma-assisted catalysis has seen a significant growth in research activity over the past decade, primarily motivated by the ability to activate stable molecules (e.g., CH_4, CO_2, and N_2) at relatively low temperature through electrical energy input. However, plasma phase reactions and plasma-surface interactions are highly complex, which has resulted in many empirical studies on the performance of different catalytic materials. Although these studies are extremely important and provide guidance for advancement, they often provide very limited information on the fundamental elementary processes occurring at the plasma-catalyst interface. Therefore, the development of in situ/operando characterization approaches in combination with theory/simulations are needed to advance the field. We realize that a need exists for simple and inexpensive plasma systems that can interface directly with existing and commonly utilized in

situ/operando techniques. We developed an alternative design for a plasma-transmission IR cell capable of surface-sensitive, in situ/operando measurements under a wide range of plasma conditions. The design and function of the cell are comparable to commonly used dielectric barrier discharge (DBD) plasma-catalytic reactors, and can easily be adopted as a widespread tool for rapidly obtaining large volumes of in situ plasma-catalysis data. The effectiveness of the cell was demonstrated using (1) plasma-oxidation of amine-functionalized SBA-15 to establish plasma-surface contact and (2) low-temperature nitrogen oxidation over a Pt/SiO_2 catalyst to provide an example of plasma-catalyst interactions. This work is in preparation for submission to *ACS Engineering Au*.

Microkinetic modeling: Microkinetic models are the bridge between experimental observations and atomistic models. The treatment of adsorbate coverage continues to be a gap in current modeling approaches. We recently published a set of kinetic Monte Carlo simulations probing the consequences of adsorbate interactions on observed rates, which appeared in the Michel Boudart special issue of Journal of Catalysis (*J. Catal.* **2022**, doi:10.1016/j.jcat.2021.12.005).

Future Plans

Work to-date is refining our understanding of how plasma properties, reactor configuration, and material selection interplay to determine the productivity of plasma-catalyst combinations. Further progress depends on improved understanding of the mechanisms of reaction at the catalyst surface. We plan to continue to exploit in situ spectroscopy and transient product analysis to provide these mechanistic insights across a range of metal catalysts, using ammonia synthesis and nitrogen oxidation as our two model reactions. Computational models will be extended to encompass this wider material range. Our modeling strategy will follow two streams, one aimed at capturing trends with variation in material and ambient pressure plasma and the other aimed at quantitative predictions for precisely defined and low pressure plasmas.

Publications Acknowledging DE-SC0021107

Ma, H.; Sharma, R. K.; Welzel, S.; van de Sanden, M. C. M.; Tsampas, M. N.; Schneider, W. F. Observation and Rationalization of Nitrogen Oxidation Enabled Only by Coupled Plasma and Catalyst. *Nat Commun.* **2022**, *13*, 402. https://doi.org/10.1038/s41467-021-27912-2.

Goswami, A.; Ma, H.; Schneider, W. F. Consequences of Adsorbate-Adsorbate Interactions for Apparent Kinetics of Surface Catalytic Reactions. *Journal of Catalysis* **2022**, *405*, 410–418. https://doi.org/10.1016/j.jcat.2021.12.005.

Waitt, C.; Miles, A. R.; Schneider, W. F. Adsorbate Free Energies from DFT-Derived Translational Energy Landscapes. *J. Phys. Chem. C* **2021**, *125*, 20331–20342. https://doi.org/10.1021/acs.jpcc.1c05917.

Nematollahi, P.; Ma, H.; Schneider, W. F.; Neyts, E. C. DFT and Microkinetic Comparison of Ru-Doped Porphyrin-like Graphene and Nanotubes toward Catalytic Formic Acid Decomposition and Formation. *J. Phys. Chem. C* **2021**, *125*, 18673–18683. https://doi.org/10.1021/acs.jpcc.1c03914.

Ma, H.; Schneider, W. F. Plasma-Catalyst Modeling for Materials Selection: Challenges and Opportunities in Nitrogen Oxidation. *Journal of Physics D: Applied Physics* **2021**, *54*, 454004. https://doi.org/10.1088/1361-6463/ac1bd1.

Engelmann, Y.; van ’t Veer, K.; Gorbanev, Y.; Neyts, E. C.; Schneider, W. F.; Bogaerts, A. Plasma Catalysis for Ammonia Synthesis: A Microkinetic Modeling Study on the Contributions of Eley–Rideal Reactions. *ACS Sustainable Chem. Eng.* **2021**, *9*, 13151–13163. https://doi.org/10.1021/acssuschemeng.1c02713.

Barboun, P.; Daemon L., Waitt, C.; Wu, Z.; Schneider, W.F.; and Hicks, J.C., “Inelastic Neutron Scattering Observation of Plasma-Promoted Nitrogen Reduction Intermediates on Ni/g-Al_2O_3”, *ACS Energy Letters,* **2021**, *6*, 2048–2053. https://doi.org/10.1021/acsenergylett.1c00643

Bogaerts, A.; Tu, X.; Whitehead, J. C.; Centi, G.; Lefferts, L.; Guaitella, O.; Azzolina-Jury, F.; Kim, H.-H.; Murphy, A. B.; Schneider, W. F.; Nozaki, T.; Hicks, J. C.; Rousseau, A.; Thevenet, F.; Khacef, A.; Carreon, M. The 2020 Plasma Catalysis Roadmap. *J. Phys. D: Appl. Phys.* **2020**, 53, 443001. https://doi.org/10.1088/1361-6463/ab9048

ADVANCED DIAGNOSTICS

David W. Chandler, Jonathan H. Frank, Nils Hansen, Christopher J. Kliewer, Habib N. Najm, David L. Osborn, Krupa Ramasesha, Leonid Sheps, Craig A. Taatjes, Timothy S. Zwier
Combustion Research Facility, Sandia National Laboratories, MS 9055, Livermore, CA 94551-0969
chand@sandia.gov, jhfrank@sandia.gov, nhansen@sandia.gov, cjkliew@sandia.gov, hnnajm@sandia.gov, dlosbor@sandia.gov, kramase@sandia.gov, lsheps@sandia.gov, cataatj@sandia.gov, tszwier@sandia.gov

PROGRAM SCOPE

A unifying theme throughout the experimental work in this task is the need for incisive advanced diagnostics that illuminate the hidden world of molecules. Over the years, our program has made many innovations that support chemical physics research in areas such as non-linear spectroscopy, ion imaging, 3-dimensional laser-induced fluorescence, multiplexed photionization / photoelectron spectroscopy, and x-ray absorption and scattering. These approaches include *in situ* laser and light source-based techniques that directly probe reacting environments, and *ex situ* techniques that extract species from reactive environments before implementing diagnostics that would be impossible under the native conditions of the chemical reaction. We leverage these experimental innovations with theoretical advances that predict dynamics and kinetics to compare with experiment, and to inform the improvement of diagnostics. Our recent work in optimal experimental design adds a new dimension to the coupling between experiment and theory, providing a feedback loop to optimize an experiment, thereby maximizing extracted information and quantifying uncertainty. Our proposed research includes new developments in areas where we are well established, and additional ideas that broaden our work on both ends of the electromagnetic spectrum. Ultrafast non-linear spectroscopy in the soft and hard x-ray region is a new area of emphasis, as well as combining broadband microwave spectroscopy with specialized molecular sources to enable new spectroscopy of reactive intermediates. As these advanced diagnostics mature, they will provide new tools that enable deeper exploration in Gas Phase Chemical Physics

RECENT PROGRESS

Bayesian Optimal Experimental Design, Application to Time-of-Flight Mass Spectrometry We worked on further development of a Bayesian optimal experimental design (BOED) construction targeting Sandia's high-pressure photoionization mass spectrometry apparatus (HP-PIMS). HP-PIMS samples reacting gas mixtures from a high-pressure laser photolysis reactor and analyzes the chemical composition of the gas in real-time using a 40 kHz pulsed reflectron time of flight (TOF) mass spectrometer with tunable synchrotron VUV photoionization. A proper representation of the instrument sensitivity, and uncertainties associated with the initial reaction conditions, as well as the sampling and detection process, is critical to the interpretation of HP-PIMS data. Over the past year, we finalized our Bayesian calibration of the pre-photolysis model of the experiment, arriving at a calibrated model framework (including a physical model of the experiment and a statistical model-error correction) that fits the pre-photolysis baseline data with quantified uncertainty. These results have been documented in a journal publication currently in press.[1] Aside from this, the bulk of our work has been focused on the post-photolysis model Bayesian evidence estimation and early demonstrations of BOED. We developed the formulation, numerical implementation, and associated computational tools, for the application of BOED in the HP-PIMS system. We executed a first preliminary demonstration where we focused on optimizing the temperature and pressure conditions of the experiment, using 3 predicted peaks in the TOF spectrum, with the object of learning 4 reaction rates in the C_3H_8 mechanism. This preliminary study considers a limited subset of the targeted set of design conditions, reaction rates, and quantities of interest in the spectrum, and is intended to exercise and guide the optimization of the algorithm and code constructions. Our BOED construction optimizes the expected information gain (EIG) relying on a Bayesian optimization (BayesOpt) procedure that employs a combination of exploration and exploitation to provide optimal utilization of computational samples in the design space. The evaluation of the EIG for any proposed design involves a costly Monte Carlo estimation

of a double integral on synthetic data and parameter samples. The demonstration highlighted the capability of the construction for rapid identification of the optimal (T, P) design conditions, as well as the reduction of uncertainty in estimated parameters at the optimal versus sub-optimal design conditions.

Characterizing the Time-Resolved Photoelectron Photoion Coincidence Spectrometer In the past year we commissioned our PEPICO spectrometer at both Sandia and at the Chemical Dynamics Beamline of the Advanced Light Source Synchrotron of Lawrence Berkeley National Laboratory, where tunable vacuum ultraviolet photons maximize the power of the instrument. Our first publication on this instrument, using only fixed-frequency VUV radiation, demonstrated both pulsed- and cw-supersonic jet and chemical reactor tube sources. These initial results show an electron kinetic energy range of 0 – 6 eV with energy resolution of $\Delta E/E$ ~ 4%, excellent mass resolution $m/\Delta m$ = 6700 and mass accuracy of 3 ppm, and the ability to measure kinetic energy release from dissociative photoionization via velocity map imaging of daughter ions. In addition we have tested the time-resolved capability of this spectrometer using the photodissociation of SO_2 at 193 nm as a test case, demonstrating time resolution of ~ 1 ms (although we expect better time resolution in the future). Although there are still challenges to be worked through, the system is performing mostly as expected as a new, highly multiplexed tool for the study of gas phase chemical physics.

Photoionization Cross-Sections In our ongoing need for well-documented photoionization cross sections, used in quantitative analysis of branching ratios in chemical reactions, we have published two articles on important transient species: the formyl radical (HCO) and vinyl alcohol (H_2C=CHOH), a metastable isomer of acetaldehyde.

Broadband Microwave Spectroscopy for Isomer-specific Detection of Transient Intermediates
Over the past year, we have made further improvements to our multiplexed broadband microwave spectrometer. We have incorporated into the instrument a 20 GHz analog/128 GSa/s digitizer that enables us to directly record broadband microwave spectra over the 2-18 GHz range without the need for mixers. We have also improved our flash pyrolysis source for making transient intermediates for study of their microwave spectra. Finally, the BES-funded post-doctoral research associate on the project has begun his work and is perfecting the design of a cryo-cooled buffer gas cell that we hope will provide significantly improved sensitivity towards transient intermediates.

High harmonic generation of extreme ultraviolet pulses
Core-to-valence transient absorption spectroscopy combines the element-specificity of core orbitals with the sensitivity of valence orbitals to bonding environment, making this technique a powerful, site-specific probe of non-adiabatic dynamics. To study ultrafast excited state dynamics in gas phase systems using this technique, we have constructed an apparatus for high harmonic generation (HHG) of extreme ultraviolet (XUV) pulses and transient absorption spectroscopy. This apparatus produces XUV pulses spanning ~30 eV to 100 eV via two-color 800 nm + 400 nm-driven HHG to generate odd and even harmonics for use in transient absorption spectroscopy. These XUV photon energies allow access to core-to-valence transitions in many elements such as first-row transition metals and some halogens. We are currently using this apparatus to monitor excited state dynamics and bond dissociation in gas-phase transition metal carbonyls and acetyl halides as part of the Ultrafast Chemistry subtask in our program.

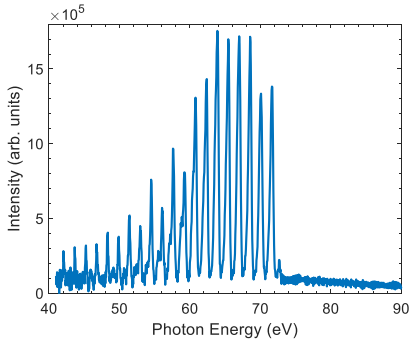

Figure 1: Extreme ultraviolet spectrum from 800 nm-driven high harmonic generation in Ne. The abrupt cut-off at ~72 eV represents the $L_{2,3}$-edge of Al due to an Al filter present in the beam path for blocking residual 800 nm.

Spatial Imaging Microscope of Laser Ionized Species for Near Interface Science The ability to interrogate where chemical transformations occur on a surface by observing the chemical products in the gas phase directly above the surface is an idea we are investigating. As a thought experiment, imagine that products of a catalytic surface reaction only moved perpendicular to the surface upon desorption. In this case the product distribution in the gas phase could uniquely be assigned to spatial features on the surface. However, molecules leave a surface with a broad distribution of velocities, which blurs the spatial image and degrades the ability to make this correlation. We have built an imaging microscope that addresses this problem. We laser ionize the products of a catalytic reaction and velocity map image that distribution, utilizing an electrostatic lens, onto a plate containing a pinhole. The "one" velocity group to transmitted by the pinhole expands as it travels toward an imaging detector, providing spatial resolution on the order of 10 μm. A schematic of the apparatus is given in Figure 2. The ratio of the distance from the laser focus to the velocity imaging plane (containing the pinhole) to the distance from the pinhole to the imaging detector provides a magnification of the laser-produced ions of approximately 15 in our apparatus. Because our imaging detector has a resolution of approximately 300 pixels elements across the line image, this design provides a resolution of ~300 along the approximately 3 mm length of ions formed at the focus of the laser, resulting in ~10 μm resolution along the laser propagation direction. This calculation assumes a single velocity group emerges from the pinhole but our pinhole of 100 μm does not allow us to reach this expected resolution. Future versions will have smaller pinholes that can be translated to provide higher resolution and information about the velocity distribution of the species from the surface.

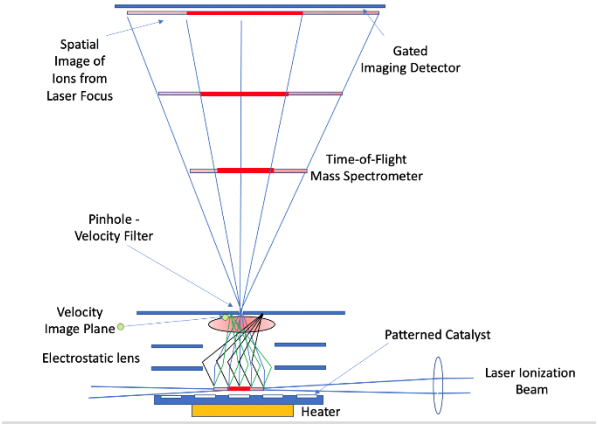

Figure 2: The Spatial Imaging Microscopy for Near Interface Science

PROPOSED WORK

Bayesian Optimal Experimental Design, Application to Time-of-Flight Mass Spectrometry We will extend our BOED demonstration to the full problem setup for the laser photolysis reactor and HP-PIMS system. Significant challenges need to be overcome to extend our current demonstration to the full set of rate constants in the C_3H_8 mechanism, and the 5.1×10^8 quantities of interest (QoIs) in the HP-PIMS spectrum. The extension to the full 5-dimensional design space is less problematic, and well within the expected capabilities of BayesOpt. Our C_3H_8 mechanism involves 1143 reactions, most of which will not be important for resulting uncertainty in the QoIs. Preliminary results using global sensitivity analysis suggest that only about 40 rate parameters are important, which can be a more manageable dimensionality, depending on the requisite order in the polynomial surrogate for the forward model, as necessary for target accuracy in the BOED implementation. The large number of QoIs is a key challenge, which we will address using principal component analysis (PCA) to map the QoIs to a much lower dimensional latent space, where forward model surrogates and Bayesian marginal likelihood estimation will be employed. Our preliminary results in this regard are encouraging, indicating a feasible data model construction in the latent space, along with drastic reduction to a relatively small number of degrees of freedom. With these elements in place, we plan to demonstrate BOED capabilities on the full problem, with close coupling to HP-PIMS experimental measurements, to provide necessary validation, and iterate towards optimal design conditions. This proposed demonstration of BOED with HP-PIMS is synergistic with activities under the joint Argonne-Sandia High-Pressure Combustion Chemistry program, which depend critically on continuous feedback between experiments and theory-based chemical modeling. Our BOED work strengthens the HPCC modeling-experiments link by enabling targeted, impactful experiments to maximally inform the chemical models.

Characterizing the new Photoelectron Photoion Coincidence Spectrometer Now that we have access to the Chemical Dynamics Beamline, providing tunable VUV radiation, we will finalize commissioning and demonstrate mass-resolved Threshold Photoelectron Spectroscopy (ms-TPES) and Slow PhotoElectron Spectroscopy (SPES), which is a powerful extension of threshold photoelectron spectroscopy. After characterization using Ar, Kr, and Xe ionization from supersonic expansions, we will proceed to measure the molecular beam velocity distribution produced by a slow-flow quartz chemical reactor that we've been utilizing for years with Multiplexed Photoionization Mass Spectrometry. Although we initially assumed the expansion from this ~ 2 - 10 Torr source would be nearly effusive, our initial results at Sandia indicate it is a harder expansion than we expected. We will then proceed to study photolytically initiated chemically reacting systems, beginning with known reactions such as $CH_2OO + SO_2$, and progressing to reactions where the improved spectral fingerprints offered by photoelectron spectroscopy will enable new scientific understanding, such as highly unsaturated reactions important in molecular weight growth chemistry, and conformer-specific reactions of *syn*- and *anti*-CH_3CHOO.

Ultrafast soft X-ray transient absorption spectroscopy of chemical dynamics
Over the coming year, we will modify the current HHG/XUV apparatus to generate soft X-ray pulses spanning ~150-350 eV for use in core-to-valence transient absorption spectroscopy at the sulfur L- and the carbon K-edges of gas phase molecules. Pushing the photon energies into the soft X-ray regime requires driving HHG using near-infrared pulses because the high harmonic cut-off photon energy is proportional to the square of the wavelength of the HHG driver pulses. However, the efficiency of HHG drops precipitously with increasing wavelength of the HHG driver pulses, to the inverse sixth power of the wavelength of the driver pulses. This fact necessitates the use of a high-power source of near-infrared pulses to produce sufficient soft X-ray flux for use in pump-probe experiments. To this end, a high-energy commercial OPA (HE-TOPAS-Prime Plus, Light Conversion) has been installed with our ultrafast laser system, generating near-infrared pulses ranging in wavelength from 1100 nm to 2600 nm with few-mJ pulse energies. For soft X-ray generation, near-infrared pulses with ~1400 nm wavelength will be used for driving HHG in helium gas maintained at near-atmosphere pressure in a semi-infinite gas cell. The rest of the apparatus will be largely unchanged from XUV operation, except for modifications to the X-ray spectrometer to allow for detection of higher photon energies.

Broadband Microwave Spectroscopy for Isomer-specific Detection of Transient Intermediates
In collaboration with Kyle Crabtree at UC-Davis, we are presently studying the broadband microwave spectroscopy of a series of methylated phenoxy radicals, *o*-, *m*-, and *p*-methyl phenoxy. These radicals have both methyl internal rotation and electron spin as angular momentum sources, offering a spectroscopic puzzle that has not yet been solved. We also plan to pursue the spectroscopy of *o*-, *m*-, *and p*-pyridoxy radicals in order to probe how the nitrogen heteroatom changes the delocalization of the unpaired electron relative to that in phenoxy radical. When ZrO_2 rather than SiC is used as the pyrolysis tube material, O_2 can be added to the heated mixture, offering many opportunities for detecting oxygen-rich intermediates. Using a ZrO_2 flash pyrolysis source, we will target initially a series of reactions of the resonance-stabilized radicals propargyl (C_3H_3), cyclopentadienyl (C_5H_5), and benzyl (C_7H_7) with O_2. Finally, we are collaborating with Lenny Sheps to incorporate his high-P, high-T source onto the CP-FTMW instrument, providing an alternative means to produce oxygen-rich reactive intermediates.

We are also presently constructing a cryo-cooled buffer gas cell to complement the supersonic expansion as a cooling mechanism for transient intermediates or for making ephemeral complexes. Compared to a pulsed supersonic expansion, the buffer gas cell cools the molecules to a well-defined rotational temperature (making quantitative measurements more accurate) and holds them in the cell for much longer interrogation times (>10 ms) before removal on the cold walls. This latter feature makes it possible to interrogate at up to 50 kHz repetition rate, with the same molecules contributing to the signal throughout their residence time in the cell.

Tandem Mass Spectrometry for Molecular-Weight Growth Reactions To complement and extend photoionization spectroscopy, PEPICO, and rotational spectroscopy, we are working towards adding tandem mass spectrometry to our array of diagnostic techniques. This technique is uniquely suited to identify complex chemical structures. Our mass spectrometer consists of an atmospheric pressure photoionization (APPI) or nanospray ionization source, a quadrupole mass filter, a collision cell filled with Ar for the collision-induced dissociation (CID) process, and a reflectron time-of-flight spectrometer to mass analyze the ions. We have modified the interface to the APPI source (as shown in the figure) to allow for sampling from flash pyrolysis sources for the investigation of radical-radical and radical-molecule reactions in high-temperature hydrocarbon rich environments (see Sandia's Multi-Phase Subtask). The emphasis of this work will be on the detection of aliphatically bridged multi-core PAHs, and on the identification of cross-linked PAHs, which are the centerpieces in the proposed radical-radical chain reaction sequence for soot formation. The first target will be the reaction of phenyl + propargyl, that leads to phenyl-substituted allene and propyne structures in the intermediate temperature range and eventually to indene at higher temperatures (see Sandia's Chemical Kinetics Subtask).

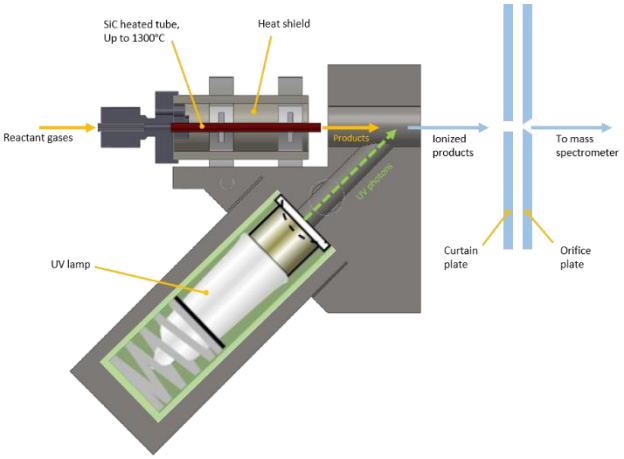

BES-sponsored publications, 2019 – present

1. J. Oreluk, L. Sheps, and H. Najm, Bayesian model calibration for vacuum-ultraviolet photoionization mass spectrometry. *Combustion Theory and Modelling* **2022**. In press. https://doi.org/10.1080/13647830.2022.2030495
2. D. Rösch, R. Almeida, B. Sztaray, and D. L. Osborn, High-Resolution Double Velocity Map Imaging Photoelectron Photoion Coincidence Spectrometer for Gas-Phase Reaction Kinetics, *J. Phys. Chem. A* **2022**, 126, 1761.
3. D. Rösch, R. L. Caravan, C. A. Taatjes, K. Au, R. Almeida, and D. L. Osborn, Absolute Photoionization Cross Section of the Simplest Enol, Vinyl Alcohol, *J. Phys. Chem. A* **2021**, 125, 7920.
4. J. H. Frank, Advances in imaging of chemically reacting flows, *J. Chem. Phys.* **2021**, 154 (4), 040901.
5. S. M. Fritz, P. Mishra, J. Wullenkord, P. G. Fugazzi, K. Kohse-Höinghaus, T. S. Zwier, N. Hansen, Detecting Combustion Intermediates Via Broadband Chirped-Pulse Microwave Spectroscopy, *Proceedings of the Combustion Institute* **2021,** 38, 1761.
6. P. Mishra, S.M. Fritz, S. Herbers, A.M. Mebel, T.S. Zwier, Gas-phase pyrolysis of *trans* 3-pentenenitrile: Competition between Direct and Isomerization-directed Dissociation, *Phys. Chem. Chem. Phys.* **2021**, 23, 6462.
7. B. Zhou, T. Li, J. H. Frank, A. Dreizler, B. Bohm, Simultaneous 10 kHz three-dimensional CH2O and tomographic PIV measurements in a lifted partially-premixed jet flame, *Proceedings of the Combustion Institute* **2021,** 38, 1675.
8. B. Zhou, J. H. Frank, Experimental study of vorticity-strain interactions in turbulent premixed counterflow flames, *Proceedings of the Combustion Institute* **2021,** 38, 2909.
9. T. Li, B. Zhou, J. H. Frank, A. Dreizler, B. Böhm, High-speed volumetric imaging of formaldehyde in a lifted turbulent jet flame using an acousto-optic deflector, *Exp. Fluids* **2020**, 61 (4), 112.

10. N. Hansen, R. S. Tranter, J. B. Randazzo, J. P. A. Lockhart, and A. L. Kastengren, Investigation of sampling-probe distorted temperature fields with X-ray fluorescence spectroscopy, *Proc. Combust. Inst.*, **2019,** 37, 1401-1408.
11. B. Zhou, A. J. Ruggles, E. Huang, J. H. Frank, Wavelet-based algorithm for correction of beam-steering artefacts in turbulent flow imaging at elevated pressures. *Exp. Fluids* **2019**, 60 (8), 136.
12. T. C. W. Lau, J. H. Frank, G. J. Nathan, Resolving the three-dimensional structure of particles that are aerodynamically clustered by a turbulent flow. *Phys. Fluids* **2019**, 31 (7), 071702.

CHEMICAL DYNAMICS METHODS AND APPLICATIONS

David W. Chandler, Laura M. McCaslin, David L. Osborn, Judit Zador, Timothy S. Zwier
Sandia National Laboratories, MS 9051, Livermore, CA 94551-0969
chand@sandia.gov, lmmccas@sandia.gov, dlosbor@sandia.gov,
jzador@sandia.gov, tszwier@sandia.gov

PROGRAM SCOPE

This program focuses on studies of dynamical processes in molecular systems with emphasis on unraveling the mechanisms and timescales of molecular reactions and interactions. Multiplexed experimental and theoretical techniques are used to perform detailed studies of vibrational and electronic dynamics in molecular systems. The studies reported here are closely related to the Ultrafast Physics, Ultrafast Chemistry, and Advanced Diagnostics tasks, which encompass the study of energy flow within molecules, correlations between nuclear and electronic motion, and development of advanced optical techniques, respectively.

Highlights from our program include photoelectron photoion coincidence studies of the unimolecular isomerization of 1,5-hexadiyne to benzene, broadband microwave spectroscopy of tunneling dynamics, IR-induced conformational isomerization in a model synthetic foldamer, studies of electronic energy transfer between remote, near-degenerate chromophores, and the development of *ab initio* molecular dynamics (AIMD) methods to study the infrared spectroscopy of complex systems. AIMD is used to theoretically calculate mechanisms and timescales of dynamical processes in gas phase molecular systems. IR spectra are computed from the dynamics calculations, enabling predictions of the spectral signatures of large amplitude motion and complex dynamics. Spectral decomposition methods have been developed to correlate spectral features with molecular motion.

RECENT PROGRESS

Unimolecular Isomerization of 1,5-Hexadiyne: Fulvene Forms First

One way to reduce complexity in the study of the key molecular weight growth reaction propargyl + propargyl (H_2CCCH) is to begin the reaction not from the radicals, but from 1,5-hexadiyne (1,5-HD), which is the "head-to-head" recombination product of two propargyl radicals. Building on the ground-breaking experiments of Stein and Fahr, we used threshold photoelectron photoion coincidence spectroscopy to probe the unimolecular isomerization of 1,5-HD as a function of temperature. The photoelectron spectra show conclusive evidence for formation of fulvene and benzene via the 3,4-dimethylenecyclobut-1-ene intermediate. Our comparison to the master equations simulations of Klippenstein and Miller adapted to our experimental condition are consistent with parallel (as opposed to sequential) pathways to fulvene and benzene, but unlike the work of Stein and Fahr, show that the onset of fulvene is at a lower temperature than the onset of benzene, consistent with theory.

Photoionization and Autoionization of the Formyl Radical

We studied the photoionization dynamics of the formyl radical (HCO and DCO, X ^{2}A') from 8 – 11.5 eV. We produced HCO/DCO from 308-nm photodissociation of acetaldehyde (CH_3CHO / CD_3CDO), which creates a 1:1 ratio of CH_3 : HCO. We obtained the absolute photoionization cross section of formyl by referencing its signal to that of the CH_3 radical, whose photoionization cross section is known. Turning to autoionization dynamics, the end of the Franck-Condon envelope for ionization to the linear X($^1\Sigma^+$) ground state of HCO^+ is at ~10.1 eV, based on the photoelectron spectrum obtained by John Dyke. However, the photoionization spectrum rises significantly from 10.1 – 11.5 eV, and the spectrum is structured for both HCO and DCO. We assign the observed peaks in this region to excitation into neutral 3sσ and 3p Rydberg states, which converge to the first triplet excited state of HCO^+ a(^{3}A'), followed by autoionization. Each series shows a vibrational progression in the ν_3 (C-O stretch) mode, with quantum defects of $\delta_{3s\sigma} = 1.06 \pm 0.02$ and $\delta_{3p} = 0.821 \pm 0.019$. The fact that we observe both *s* and *p* Rydberg series implies that the HOMO

of HCO, from which the electron is excited, is not well approximated as an atomic orbital. Finally, we examined the semi-empirical model proposed by Xu and Pratt for estimation of free radical photoionization cross sections and conclude that this model is more accurate when applied with a reference species (in this case H_2CO) containing the same atoms as the free radical, rather than using the isoelectronic NO radical as the reference species. We propose that the reason for the better agreement when H_2CO is the reference species is due to the significant charge density that the proton(s) in HCO/H_2CO provide at small distance from the C atom, therefore perturbing the ionic core of the Rydberg molecule. The isoelectronic NO radical lacks these perturbations and behaves more like an atomic system.

Tunneling dynamics in a polar, near-oblate symmetric top

We are presently writing up our work on OH torsional tunneling in perfluorophenol, C_6F_5OH. We have recorded broadband microwave spectra of PFP over the 7.5-17.5 GHz range and have fit the rotational transitions ascribed to PFP. Since the OH group differs little in mass from ^{19}F, this fascinating molecule is a polar, near-oblate symmetric top in which the tunneling hydrogen is the major source of asymmetry. The molecule is so nearly a planar symmetric top that the asymmetry splitting is just resolvable in the spectrum. The tunneling splitting due to the OH group is 24.875 MHz, lower by about a factor of three than anticipated based on other substituted phenols. This splitting is equivalent to a timescale for OH tunneling of about 40 ns, and so is an example of slow H-atom tunneling dynamics. This leads to the unusual circumstance that 'a'-type transitions are split equally on either side of unsplit 'b'-type transitions, producing triplets in the spectrum. The inertial axes also rotate by almost 20^o during the tunneling process.

Selective Conformational Isomerization using IR-population transfer spectroscopy

Conformational isomerization is a ubiquitous process in large, flexible molecules. In order to probe this process under well-controlled conditions, we have studied the process under jet-cooled conditions where isomerization is initiated by selective IR excitation of a single conformer. During the past year, we have written up and published a study of the single-conformation IR and UV spectroscopy of the prototypical capped γ-peptide Ac-γ^4-Phe-NHMe (γ^4F), a model synthetic foldamer. We also used IR population transfer (IR-PT) spectroscopy to study the isomerization dynamics and obtain fractional abundances of the γ^4F conformers in the expansion.

Electronic Energy Transfer along peptide scaffolds

Electronic energy transfer is at the heart of tools used by chemists to explore the time-dependent distance between these chromophores. Much of this work employs Fluorescence Resonance Energy Transfer (FRET) that is based on a model for through-space electronic energy transfer in which donor and acceptor have clear wavelength-resolved fluorescence that reports on the location of electronic excitation. In other contexts, such as photosynthetic light harvesting, an array of chemically identical chromophores in well-defined spatial arrangements absorb photons and direct the electronic energy through the array to a specific reaction center where electron transfer occurs. We are presently conducting experiments designed to study electronic energy transfer on a state-to-state level between two or more nearly identical chromophores.

In particular, we are in the midst of a study of a series of protonated peptide ions in which two nearly identical UV chromophores take up well-defined 3D spatial positions along the same peptide backbone scaffold. We are using UV photofragment spectroscopy of the cryo-cooled ions to record vibronically-resolved spectra involving initial excitation of either chromophore, with the excited state origin transitions separated by no more than a few hundred wavenumbers out of 35,000 cm^{-1}. The location of electronic excitation is then being probed by analyzing the peptide fragmentation that ensues and correlating this with changes in the IR spectrum of the ions in the excited state. Working in collaboration with Prof. Matt Kubasik at Fairfield University, we have prepared members of the peptide series with the two chromophores present either alone or as pairs in either position.

Beyond-Harmonic Approaches to Calculating IR Spectra from Ab Initio Molecular Dynamics

Theoretical prediction of infrared spectra for "floppy" molecules and molecular clusters with large amplitude motion requires approaches that go beyond the harmonic approximation. In particular, systems with conformational changes such as molecules with free rotors or clusters exhibiting proton transfer have complex dynamics that are not sufficiently captured with harmonic-based approaches, including those with perturbative corrections (e.g. VPT2). One approach to capture these complex dynamics in a theoretical IR spectrum is to calculate IR intensities by taking the Fourier transform of the autocorrelation function of the dipole moment in an ab initio molecular dynamics (AIMD) trajectory. Similarly, the vibrational density of states can be computed by taking the Fourier transform of the autocorrelation function of the nuclear velocities. This powerful approach has many benefits; however, the analysis of the intensities is far more difficult than in harmonic-based approaches. Furthermore, the dependence of the intensities on temperature can be computed via changing the nuclear velocities to reflect larger kinetic energy in the molecular motion, though this is a computationally expensive approach.

In light of the challenges to correlating molecular motion to peak intensities as well as the computational expense of understanding temperature dependence, we have developed a computational analysis code that works to improve analysis of IR spectra from AIMD. Understanding the correlation between molecular motion and spectral features requires different coordinate systems for different molecular systems. The recently developed code offers the choices of normal, internal, and generalized normal coordinates for determining the "weight" of a coordinate's displacement within a spectral feature. This spectral decomposition allows for an intuitive understanding of the correlation of complex spectral features and molecular motion. As for the computational expense of computing temperature dependence through explicitly performing additional AIMD trajectories at a higher temperature, we have implemented new theoretical insights from statistical mechanics that allow for calculation of temperature dependence of IR intensities in the linear response regime without additional AIMD trajectory calculations. Our new analysis code thus aids in the development of a more intuitive understanding of complex spectral features from underlying dynamics as well as their temperature dependence. These techniques have been recently used in the Multiphase Subtask to predict the temperature dependence of the OH stretching region of clusters of propanol + $6H_2O$ and propionic acid + $10H_2O$. Future studies will use these methods to predict the ultrafast transient absorption spectra of metal carbonyls in the Ultrafast Chemistry Subtask.

FUTURE WORK

In order to develop our program's study of non-equilibrium systems, experiments involving highly rotationally excited molecules as well as collisions of vibrationally excited ephemeral species will be performed. While the effects of highly excited translational and vibrational states on chemical reactions are well-characterized, the effects of highly rotationally excited molecules are not as well understood. As described in the Ultrafast Physics task, an optical centrifuge is being developed, which will allow for highly rotationally excited N_2O to be formed. Photodissociation of these "super-rotors" will be performed at ~200 nm and N_2 and $O(^1D)$ products will be detected via velocity mapped imaging (VMI). To better understand the reactions of super-rotors and atoms, reactions of rotationally excited N_2O and $O(^1D)$ to form NO will be monitored by VMI. We have recently succeeded in exciting rotors to very high rotational levels in the Ultrafast Physics subtask—please see that abstract for details. On the ephemeral complexes front, studies of collisionally-stabilized association reactions of non-equilibrium vibrationally excited species and atoms will be carried out. Vibronically-excited NO_2 at ~400 nm will be optically generated in a molecular beam within 10 kcal/mol of the NO + O dissociation energy. These excited NO_2 molecules will collide with CO to gauge production of NO via VMI.

In the course of commissioning our new photoelectron photoion coincidence spectrometer, we obtained preliminary evidence of a new photodissociation channel in the 193-nm dissociation of SO_2. The quantum yield for dissociation at this wavelength is nearly 100%, and although the main product channel is $O(^3P)$ +

$SO(^3\Sigma^-)$, our work showed evidence of $S(^3P)$ production. Assuming this process results from the absorption of only one 193-nm photon, the only possible co-product is $O_2(^3\Sigma_g^-)$. However, we could not observe the O_2 co-product. In future work we will examine this system more completely, including a laser power dependence study to confirm or refute the 1-photon hypothesis. In addition, we will attempt to observe the O_2 co-product. We are simultaneously pursuing electron structure calculations to examine the possible mechanisms for this product channel, which could impact mechanisms of sulfur mass-independent fractionation in the atmosphere of early Earth.

In our cryo-cooled ion spectroscopy/dynamics experiments, we will extend our studies of electronic energy transfer between UV chromophores to include model protonated α
In the past there has been much success in testing the potential energy surfaces associated with bimolecular reaction of diatomic molecules with rare gas atoms. Velocity Mapped Ion Imaging enabled measurements of the differential cross section of a single quantum state of the scattered molecule. The image so obtained was of a single Newton sphere, as the rare gas had no internal quantum states that could be populated by the collision energy. Attempts at performing molecule-molecule scattering such that one can investigate ever more complex potential energy surfaces has been hampered by two issues: (i) even in a molecular beam several quantum states of the molecules are often populated, and (ii) the velocity spreads in the molecular beam can obscure/blur the Newton spheres for individual rotational product states of the collision partner. Recently the Meerakker group in the Netherlands has implemented a creative solution by utilizing a Stark decelerator to pick a single quantum state from a molecular beam and then selectively slow a narrow velocity distribution of that selected molecule to use as a scattering partner. However, the ability to Stark decelerate the collision partner(s) limits which molecules can be studied, and the technique, while a tour de force, is expensive. We propose to investigate an alternative technique that is simpler and more universal. With the advent of extremely high-resolution infrared quantum cascade lasers we intend to demonstrate that we can selectively excite a narrow velocity group in a molecular beam to the first vibrational level (as the resolution of the laser is much smaller than the Doppler profile of the molecular beam) and scatter this single quantum state from a molecular partner and thus resolve the correlated scattering differential cross sections for all energetically possible product channels. We will begin with the scattering of NO(v=1 J=1.5) from O_2.

BES-SPONSORED PUBLICATIONS (SINCE 2019)

1) J. D. Savee, B. Sztaray, P. Hemberger, J. Zador, A. Bodi, and D. L. Osborn, Unimolecular Isomerization of 1,5-Hexadiyne Observed by Threshold Photoelectron Photoion Coincidence Spectroscopy, Faraday Discussions, 2022, DOI: 10.1039/D2FD00028H
2) J. D. Savee, B. Sztaray, O. Welz, C.A. Taatjes, D. L. Osborn, Valence Photoionization and Autoionization of the Formyl Radical, *J. Phys. Chem. A* **2021**, 125, 3874. DOI:10.1021/acs.jpca. 1c01775
3) J.L. Fischer, K.M. Blodgett, C.P. Harrilal, P.S. Walsh, S.H. Choi, and T.S. Zwier, Conformer-specific Spectroscopy and IR-induced Isomerization of a Model γ-peptide: Ac-γ^4-Phe-NHMe, J. Phys. Chem. A **126**, 1837 (2022). DOI: 10.1021/acs.jpca.2c00112
4) John T. Lawler, Christopher P. Harrilal, Andrew F. DeBlase, Edwin L. Sibert III, Scott A. McLuckey, and Timothy S. Zwier, "Single-conformation Spectroscopy of Cold, Protonated ^{D}PG-containing peptides: Switching β-turn types and Formation of a Sequential Type II/II' Double β-turn", Phys. Chem. Chem. Phys. **24**, 2095-2109 (2022). DOI: 10.1039/D1CP04852J

5) Edwin L. Sibert III, Karl N. Blodgett, and Timothy S. Zwier, Spectroscopic Manifestations of Indirect Vibrational State Mixing: Novel Anharmonic effects on a pre-reactive H-atom transfer surface, J. Phys. Chem. A **125** 7313 (2021). DOI: 10.1021/acs.jpca.1c04264

6) Christopher Harrilal, Andrew DeBlase, Scott McLuckey, and Timothy S. Zwier, 2-Color IRMPD Applied to Conformationally Complex Ions: Probing Cold Ion Structure and Hot Ion Unfolding", J. Phys. Chem. A **125**, 9394 (2021). DOI: 10.1021/acs.jpca.1c08388

7) A.O. Hernandez-Castillo, Camilla Calabrese, Sean M. Fritz, Iciar Uriarte, Emilio J. Cocinero, and Timothy S. Zwier, "Bond Length Alternation and Internal Dynamics in Model Aromatic Substituents of Lignin", ChemPhysChem **23** (in press). DOI: 10.1002/cphc.202100808

8) Alignment and Dissociation of Electronically-Excited Molecular Hydrogen With Intense Laser Fields, M. Fournier, G.V. Lopez, A.K. Spiliotis, T.A. Casey, T.P. Rakitzis, D.W. Chandler, Mol. Phys. **119**, 1 (2020). DOI: 10.1080/00268976.2020.1778200

9) To Boldly Look Where No One Has Looked Before: Identifying the Primary Photoproducts of Acetylacetone, I. Antonov, K. Voronova, M. W. Chen, B. Sztaray, P. Hemberger, A. Bodi, D. L. Osborn, and L. Sheps, J. Phys. Chem. A **123**, 5472 (2019).

Chemical Kinetics for Complex Systems

Jacqueline H. Chen, Nils Hansen, Habib N. Najm, David L. Osborn, Krupa Ramasesha, Leonid Sheps, Craig A. Taatjes, and Judit Zádor
Sandia National Laboratories, MS 9055, Livermore, CA 94551-0969
jhchen@sandia.gov, nhansen@sandia.gov, hnnajm@sandia.gov, dlosbor@sandia.gov, kramase@sandia.gov, lsheps@sandia.gov, cataatj@sandia.gov, jzador@sandia.gov

Program Scope

We employ experiment and theory to elucidate mechanisms of elementary chemical reactions, which impacts the research theme of Reaction Pathways in Diverse Environments. This task extends the high-resolution view of the "Chemical Dynamics" task to encompass complex interactions in collisional environments, and it provides a basis for the interface studies in the "Gas Phase Interactions with Other Phases" task. Methods developed under the "Advanced Diagnostics" task and analytical tools that use tunable vacuum ultraviolet light from the Advanced Light Source synchrotron at Lawrence Berkeley National Laboratory enable sensitive and sometimes even isomer-specific ionization of reactant and product molecules sampled from chemical reactions. These individual reaction studies are linked to controlled measurements of more complex reaction systems as found in well-defined laboratory scale zero- and one-dimensional reactors. Alongside, we use master equation frameworks based on automated potential energy surface (PES) exploration tools, and approaches to study stochastic and nonthermal effects at the mesoscale.

Recent Progress

Stochastic Chemical Systems[1] We developed fast time integration for the chemical Langevin equation (CLE), a typically stiff stochastic differential equation. The CLE for a homogeneous mixture of reacting species includes both drift and diffusion terms. Previously, we focused on the drift term, where we had used computational singular perturbation analysis to enable large time-step explicit time integration of the stiff drift term. Our latest work addressed stiffness of the diffusion term, relying on a suitable linearization of this term over short time horizons. The combination of both approaches can be used to provide requisite improved performance in time-integration of the stiff CLE.

Uncertainty Quantification in Chemical Models with missing data[2] We extended our "data free inference" (DFI) method to encompass the fusion of information from different experiments. The method addresses a typical situation in chemical kinetic models with parameters estimated from experimentals, where nominal values and marginal bounds are reported, but associated original data is missing. We had previously demonstrated the method to estimate uncertain Arrhenius parameters. Our latest development focused on handling summary-statistics reported from multiple experiments under different conditions. We demonstrated the construction to estimate rate constants in the thermal decomposition of H_2O_2, employing reported summaries from two experiments at different pressures. Our results highlight the utility of using the DFI-generated joint density on uncertain Arrhenius parameters and multiple experimental datasets in providing more accurate lower predictive uncertainties in combustion model outputs.

Direct Simulation Monte Carlo[3] We have confirmed the validity of direct simulation Monte Carlo (DSMC) to simulate the evolution of a turbulent shear in the transonic flow regime. We investigated the possibility of using physics informed neural network (PINN) by inferring the equation of state from shock tube data with DSMC. Lastly, we confirmed that DSMC can capture thermal nonequilibrium induced by local shocks and reveal the interactions between shear layer growth, shock structures, and thermal nonequilibrium.

Non-Thermal Reaction Systems In the past year, we focused on identifying and quantifying the effects of chemically termolecular reactions facilitated by the $H+CH_3$ and H+OH radical-radical recombination and the $H+O_2$ radical-molecule association reactions on the evolution of an initial deflagration front to a developing detonation in H_2/CH_4-air mixtures at high pressure. Compared to the baseline case, the onset of spontaneous ignition in the end-gas region is delayed in the presence of non-thermal termolecular reactions. Concurrently, the developing detonation was significantly stronger. In contrast, applying corrections to the recombination/association rate constants resulted in detonation that occurred due to self-acceleration of the primary flame in the absence of spontaneous ignition in the end-gas region. Ignition delay time, the duration

of major heat release rate and the flame speed were found to be significantly more sensitive to the $H+O_2$ radical-molecule association reaction compared to the two radical-radical recombination reactions. This work is currently under review for publication in *"Combustion and Flame".*

O(^{3}P)+Cyclopentene[4] We investigated the reaction of O(^3P) with cyclopentene at 4 Torr, 298 K using multiplexed photoionization mass spectrometery (MPIMS) and automated theoretical kinetics using KinBot. We found that (i) propylketene is the dominant product (41%) and is initially formed on the triplet surface; (ii) Significant intersystem crossing to the lower singlet surface can occur not only around the geometry of the initial triplet adduct, but also from the triplet propylketene; (iii) The reactivity of O(^{3}P) with cyclic alkenes compared to acylic alkenes is influenced by the greater effective degree of unsaturation in the former, which creates deeper wells on the triplet surface that lead to additional pathways for ISC.

Low-Temperature Oxidation of Cyclopentane[5] We explored and characterized five reactive PESs in the cyclopentyl + O_2 + O_2 reaction system using KinBot to uncover the major pathways under low-temperature oxidation conditions. We compared our theoretical results to high- and low-pressure MPIMS experimental results done under the HPCC project. We have shown that the dominant pathway is ROO (+ O_2) $\rightarrow$ γ-QOOH + O_2 $\rightarrow$ γ-OOQOOH $\rightarrow$ products. Photoionization dynamics calculations, also enhanced by KinBot, enabled the reliable quantification of the time-resolved concentrations of elusive species.[30]

Stereoisomer-Dependent Unimolecular Kinetics of 2,4-Dimethyloxetane (DMO) Peroxy Radicals[6] We determined the kinetics of seven cyclic ether peroxy radicals, which stem from DMO, an important cyclic ether intermediate, using KinBot in a stereochemically resolved manner. We found that (i) diastereomeric cyclic ether peroxy radicals show significantly different reactivities, (ii) stereochemistry of the peroxy radical determines which QOOH isomerization steps are possible, (iii) conventional QOOH decomposition pathways, such as cyclic ether formation and HO_2 elimination, compete with ring-opening reactions, which primarily produce OH radicals, the outcome of which is sensitive to stereochemistry. Some predicted products may complicate the interpretation of experimental results from combustion of *n*-pentane.

CH($X^2\Pi$) + cyc-C_5H_6: A Novel Route to Benzene[7] The methylidyne radical (CH) is highly reactive and can attack unsaturated hydrocarbons, such as cyclopentadiene both via addition and insertion mechanisms. MPIMS experiments at 4 Torr and 373 K show that the dominant product channel is C_6H_6 + H, where 90±5% of C_6H_6 is benzene, and 8±5% is fulvene. With the aid of master equation calculations, we conclude that benzene is the sole cyclic product from CH cycloaddition to a C=C bond, whereas fulvene is the dominant product from two of three pathways for CH insertion into the C-H bonds of cyclopentadiene, consistent with previous work on CH reactions. Isomer-resolved detection combined with theory provides evidence for the less-common insertion pathway.

Identification of the Acetaldehyde Oxide Criegee Intermediate (CI) Reaction Network[8] In collaboration with Prof. Popolan-Vaida (UCF) and Ahren Jasper (ANL), we studied the reaction network of the second simplest CI, acetaldehyde oxide (CH_3CHOO) in an atmospheric pressure JSR during ozonolysis of trans-2-butene using MPIMS. A network of CI reactions was identified below 600 K, characterized by CI addition to trans-2-butene, water, formaldehyde, formic acid, and methanol. Experimental photoionization efficiency scans and ab initio threshold energy calculation lead to identification and quantification of previously elusive intermediates, such as ketohydroperoxide (KHP) and hydroperoxide species. Specifically, the $C_4H_8+O_3$ adduct is identified as a 3-hydroperoxybutan-2-one KHP, while hydroxyacetaldehyde formation is attributed to unimolecular isomerization of the CIs. Our study helps bridging the gap between atmospheric, flame chemistry, and plasma-assisted combustion studies.

Two-Stage Low-Temperature Oxidation of di-n-propyl ether (DPE) In collaboration with Profs. Pitsch (RWTH Aachen) and Yang (Tsinghua) we studied the oxidation of DPE in a JSR at near-atmospheric pressure. Abundant species information including KHPs and hydroperoxide species were obtained using MPIMS. The oxidation of DPE exhibits high low-temperature reactivity and a special two-stage NTC behavior. The first low-temperature reactivity zone is caused by the chain branching reactions of the fuel. With the temperature rising, the oxidation of *n*-C_3H_7 and C_2H_5CHO, crucial intermediates mainly formed through the decomposition of the R and QOOH radicals, can produce a considerable amount of OH and cause the second reactivity zone. Finally, the dissociation of *n*-C_3H_7 and C_2H_5CHO results in a decrease in

the reactivity again and the second NTC. The general cause for the two-stage NTC behavior is the separation of temperature windows of fuel- and intermediates-related low-temperature chain branching reactions.

o-Methylphenyl + C_3H_4: formation of 5- and 6-member rings[9] PAHs containing only 6-member rings are flat, whereas inclusion of one or more 5-member rings induces curvature. We examined the reaction of ortho-methylphenyl radicals with the C_3H_4 isomers allene ($H_2C=C=CH_2$) and propyne ($HC\equiv C-CH_3$). For both isomers, the product channel corresponding to loss of CH_3 radicals yields indene (C_9H_8), a compound with one 5- and one 6-membered ring. However, for the other product channel where an H atom is the co-product to the newly-formed PAH, the isomeric nature of the reactant makes a critical difference. In the case of propyne, methylindene is the product, continuing the trend for 5- and 6-membered rings. However, with allene we observe formation of 1,2-dihydronaphthalene, containing two 6-membered rings. This work provides insight into the transfer of reactant isomeric nature to the introduction of curvature in PAHs.

The Importance of the Reactions of Phenyl and Benzyl with Propargyl for Molecular-Weight Growth[10] In collaboration with Prof. Yang (Tsinghua) and Kukkadapu (LLNL), we unraveled the importance of the reactions of phenyl and benzyl with propargyl for molecular-growth. For benzene and toluene flames doped with propyne, the reaction path analyses revealed that molecular growth was driven by radical-radical recombination, ring-closure, and ring-enlargement reactions with little contribution from the classical HACA mechanism. Indene is formed through the reactions of the phenyl and propargyl radicals, and the benzyl radical plays only a minor role. Reactions of the propargyl radical with fulvenallenyl and to a smaller extent with benzyl contribute to naphthalene formation. Ring-enlargement reactions also produce small amounts of naphthalene. Fulvenallenyl radicals also contribute substantially to phenanthrene formation.

Criegee + HCl/DCl[11] We have continued to measure reaction kinetics of CIs, concentrating recently on resonance-stabilized carbonyl oxides from isoprene ozonolysis in collaboration with Rebecca Caravan (ANL) and Prof. Lester (U Penn) as detailed in their abstracts. We have also characterized the products of formaldehyde oxide, CH_2OO with HCl, which occurs via a 1,2-insertion in the H–Cl bond. Both HCl and DCl isotopologues yield product signal at the mass of the insertion product chloro(hydroperoxy)methane and a dissociative ionisation peak at the mass of the protonated (or deuteronated) CI. The isotopic composition of the insertion product has been measured for reaction mixtures where both HCl isotopologues are present, and the H/D ratio of the product is consistently higher (by a factor of 1.6±0.3) than that of the reactants. Our experiments suggest a normal, $k_H > k_D$ kinetic isotope effect.

Proposed Work

Product Branching in Peroxy Radical – Radical Reactions Peroxy radical self-reactions proceed on singlet and triplet PESs and involve competing product channels, mediated by ISC at the RO−O_2−OR' adduct: H-transfer to form closed-shell carbonyl + alcohol, dissociation to alkoxy radicals, and ^{1}ROOR' stabilization. Kurten and co-workers showed that adduct formation is energetically accessible and is most likely the overall rate-limiting step. However, theoretical branching fractions are highly debated. Similarly, ROO+OH reactions occur on both PESs and may form ^{1}ROOOH adducts at atmospheric pressures. Over the past two years, we have performed experiments on ROO+ROO and ROO+OH reactions (R = CH_3, CH_3CH_2, CH_3CO) between 4 and 760 Torr using MPIMS to probe the chemistry. We obtained preliminary of ROOR and ROOOH formation. We will analyze this rich experimental dataset with a special emphasis on quantifying the product branching on the triplet vs. singlet PES.

Low-Temperature Oxidation of Cyclopentane We continue working on this system to gain more quantitative insight into its kinetics. We are using the automatically generated and characterized stationary points amended by VRC-TST calculations to assemble a full master equation description for the first and second O_2 addition reaction sets involving five PESs and compare the predicted kinetic traces to experimental profiles enhanced by uncertainty-based statistical methods.

Unimolecular kinetics of 2,4-dimethyloxetane radical decomposition In order to complete the description of cyclic ether chemistry, we also initiated work on the decomposition kinetics of 2,4-dimethyloxetane radicals. These calculations are also carried out using KinBot.

Theoretical Investigation of ROO + HO_2 Reactions ROO and HO_2 radicals can react both on the singlet and triplet surface, most likely producing alkyl hydroperoxides (ROOH)+O_2 via a barrierless entrance and

a submerged barrier. We will characterize the ROO+HO_2 reactions in more detail using multireference electronic structure methods, an effective two-transition state for the accurate determination of the capture rate coefficients and using nonadiabatic TST for calculating the branching between the surfaces.

Molecular-Weight Growth in Hydrocarbon Rich Environments We will continue to focus our attention on the formation chemistry and kinetics of aromatic species. Following our work on the formation of indene and naphthalene, we will explore a) the reaction network of the resonance-stabilized cyclopentadienyl radical in more detail. Cyclopentadienyl's contributions to molecular-weight growth are very interesting, as it can undergo ring-opening (and potentially followed by dissociation) forming aliphatically substituted PAHs and it can also undergo ring-enlargement reactions with other radicals to form six-membered ring structures. To investigate these complex reactions at high temperatures, we will use our resistively heated plug-flow reactor that is coupled it to our existing mass-spectrometric analysis tools. Very recently, we have interfaced this reactor with our uniquely powerful measurement tools of MS-MS (see the abstract on Advanced Diagnostics).

Chemically Termolecular Reactions We plan to include both chemically termolecular reactions as well as corrected recombination rate constants as a function of pressure in macroscopic kinetic models. We will also quantify the effects of radical-radical recombination and radical-molecule association induced termolecular chemistry over a broader range of thermodynamic conditions relevant to oblique shocks and rotating detonation engines. The key parameters of interest include detonation induction length, detonation velocity and detonation cell size.

Thermal Nonequilibrium Chemistry We will extend the thermal equilibrium DNS code, S3D, to predict thermal nonequilibrium in air induced by shocks (and validate against DSMC results which solve the Boltzmann equation) which is computationally more expedient than DSMC for low Knudsen number flows. We plan to perform DSMC simulations of H_2-Air reactive flows with strong thermal nonequilibrium including multiple interacting shocks. These DSMC simulations will require detailed molecular level simulations (i.e. QCT) to provide accurate collision cross sections between species. Finally, we will use the DSMC results to build simplified chemical reaction mechanisms that account for thermal nonequilibrium.

Reactions of Methylhydroxycarbene Our publication last year on the 351 nm photodissociation of pyruvic acid (PA, $CH_3C(O)C(O)OH$) showed that methylhydroxycarbene (MHC, CH_3-C-OH) is a primary photodissociation product. That work provided evidence for the first known observation of a bimolecular reaction of MHC, namely MHC+PA → $C_4H_8O_2$+CO_2. Although we could not assign the molecular structure of the $C_4H_8O_2$ product, this work opened the door to the study of reactions of MHC with other molecules. As a first step, we will study the reaction of MHC with aldehydes, specifically acetaldehyde and formaldehyde. These reactions are relevant to the gas phase formose reaction that could provide a route to abotic synthesis of sugars in the early universe.

BES-sponsored publications, 2019 – present

1. Han, X.; Najm, H. N. Modeling fast diffusion processes in time integration of stiff stochastic differential equations. *Communications on Applied Mathematics and Computation* **2022,** *in press*.
2. Casey, T. A.; Khalil, M.; Najm, H. N. Inference and combination of missing data sets for the determination of H2O2 thermal decomposition rate uncertainty. *Combustion and Flame* **2021,** *232*, 111507.
3. Patel, R.; Manickam, I.; Trask, N.; Wood, M.; Lee, M.; Tomas, I.; Cyr, E. Thermodynamically consistent physics-informed neural networks for hyperbolic systems. *Journal of Computational Physics* **2022,** *449*, 110754.
4. Ramasesha, K.; Savee, J. D.; Zádor, J.; Osborn, D. L. A New Pathway for Intersystem Crossing: Unexpected Products in the O(P-3) + Cyclopentene Reaction. *Journal of Physical Chemistry A* **2021,** *125*, 9785-9801.
5. Sheps, L.; Dewyer, A. L.; Demireva, M.; Zádor, J. Quantitative Detection of Products and Radical Intermediates in Low-Temperature Oxidation of Cyclopentane. *Journal of Physical Chemistry A* **2021,** *125*, 4467-4479.
6. Doner, A. C.; Davis, M. M.; Koritzke, A. L.; Christianson, M. G.; Turney, J. M.; Schaefer, H. F.; Sheps, L.; Osborn, D. L.; Taatjes, C. A.; Rotavera, B. Isomer-dependent reaction mechanisms of cyclic ether intermediates:cis-2,3-dimethyloxirane andtrans-2,3-dimethyloxirane. *International Journal of Chemical Kinetics* **2021,** *53*, 127-145.
7. Caster, K. L.; Selby, T. M.; Osborn, D. L.; Le Picard, S. D.; Goulay, F. Product Detection of the CH((XII)-I-2) Radical Reaction with Cyclopentadiene: A Novel Route to Benzene. *Journal of Physical Chemistry A* **2021,** *125*, 6927-6939.
8. Conrad, A. R.; Hansen, N.; Jasper, A. W.; Thomason, N. K.; Hidaldo-Rodrigues, L.; Treshock, S. P.; Popolan-Vaida, D. M. Identification of the acetaldehyde oxide Criegee intermediate reaction network in the ozone-assisted low-temperature oxidation of trans-2-butene. *Physical Chemistry Chemical Physics* **2021,** *23*, 23554-23566.

9. Shiels, O. J.; Prendergast, M. B.; Savee, J. D.; Osborn, D. L.; Taatjes, C. A.; Blanksby, S. J.; da Silva, G.; Trevitt, A. J. Five vs. six membered-ring PAH products from reaction of o-methylphenyl radical and two C3H4 isomers. *Physical Chemistry Chemical Physics* **2021,** *23*, 14913-14924.
10. Hansen, N.; Yang, B.; Braun-Unkhoff, M.; Ramirez, A.; Kukkadapu, G. Molecular-growth pathways in premixed flames of benzene and toluene doped with propyne. *Combustion and Flame* **2022**, 112075.
11. Taatjes, C. A.; Caravan, R. L.; Winiberg, F. A. F.; Zuraski, K.; Au, K.; Sheps, L.; Osborn, D. L.; Vereecken, L.; Percival, C. J. Insertion products in the reaction of carbonyl oxide Criegee intermediates with acids: Chloro(hydroperoxy)methane formation from reaction of CH2OO with HCl and DCl. *Molecular Physics* **2021,** *119*, e1975199.
12. Baroncelli, M.; Felsmann, D.; Hansen, N.; Pitsch, H. Investigating the effect of oxy-fuel combustion and light coal volatiles interaction: A mass spectrometric study. *Combustion and Flame* **2019,** *204*, 320-330.
13. Baroncelli, M.; Mao, Q.; Pitsch, H.; Hansen, N. Effects of C1-C3 hydrocarbon blending on aromatics formation in 1-butene counterflow flames. *Combustion and Flame* **2021,** *230*, 111427.
14. Bierkandt, T.; Hoener, M.; Gaiser, N.; Hansen, N.; Köhler, M.; Kasper, T. Experimental flat flame study of monoterpenes: Insights into the combustion kinetics of alpha-pinene, beta-pinene, and myrcene. *Proceedings of the Combustion Institute* **2021,** *38*, 2431-2440.
15. Bourgalais, J.; Caster, K. L.; Durif, O.; Osborn, D. L.; Le Picard, S. D.; Goulay, F. Product detection of the CH radical reactions with ammonia and methyl-substituted amines. *The Journal of Physical Chemistry A* **2019,** *123*, 2178-2193.
16. Braun-Unkhoff, M.; Hansen, N.; Dietrich, M.; Methling, T.; Moshammer, K.; Yang, B. Entanglement of n-heptane and iso-butanol chemistries in flames fueled by their mixtures. *Proceedings of the Combustion Institute* **2021,** *38*, 2387-2395.
17. Chhantyal-Pun, R.; Shannon, R. J.; Tew, D. P.; Caravan, R. L.; Duchi, M.; Wong, C.; Ingham, A.; Feldman, C.; McGillen, M. R.; Khan, M. A. H. Experimental and computational studies of Criegee intermediate reactions with NH3 and CH3NH2. *Physical Chemistry Chemical Physics* **2019,** *21*, 14042-14052.
18. Chen, B.; Wang, H.; Wang, Z.; Han, J.; Alquaity, A. B. S.; Wang, H.; Hansen, N.; Sarathy, S. M. Ion chemistry in premixed rich methane flames. *Combustion and Flame* **2019,** *202*, 208-218.
19. Chen, B. J.; Ilies, D. B.; Hansen, N.; Pitsch, H.; Sarathy, S. M. Simultaneous production of ketohydroperoxides from low temperature oxidation of a gasoline primary reference fuel mixture. *Fuel* **2021,** *288*, 119737.
20. Chen, B. J.; Kruse, S.; Schmid, R.; Cai, L. M.; Hansen, N.; Pitsch, H. Oxygenated PAH Formation Chemistry Investigation in Anisole Jet Stirred Reactor Oxidation by a Thermodynamic Approach. *Energy & Fuels* **2021,** *35*, 1535-1545.
21. Chen, B. J.; Liu, P.; Li, Z. P.; Hansen, N.; Roberts, W. L.; Pitsch, H. Furan formation pathways exploration in low temperature oxidation of 1,3-butadiene, trans-2-butene, and cis-2-butene. *Combustion and Flame* **2021,** *232*, 111519.
22. Christianson, M. G.; Doner, A. C.; Davis, M. M.; Koritzke, A. L.; Turney, J. M.; Schaefer, H. F.; Sheps, L.; Osborn, D. L.; Taatjes, C. A.; Rotavera, B. Reaction mechanisms of a cyclic ether intermediate: Ethyloxirane. *International Journal of Chemical Kinetics* **2021,** *53*, 43-59.
23. Davis, J. C.; Koritzke, A. L.; Caravan, R. L.; Antonov, I. O.; Christianson, M. G.; Doner, A. C.; Osborn, D. L.; Sheps, L.; Taatjes, C. A.; Rotavera, B. Influence of the Ether Functional Group on Ketohydroperoxide Formation in Cyclic Hydrocarbons: Tetrahydropyran and Cyclohexane. *The Journal of Physical Chemistry A* **2019,** *123*, 3634-3646.
24. Fan, X. F.; Sun, W. Y.; Gao, Y.; Hansen, N.; Chen, B. J.; Pitsch, H.; Yang, B. Chemical insights into the multi-regime low-temperature oxidation of di-n-propyl ether: Jet-stirred reactor experiments and kinetic modeling. *Combustion and Flame* **2021,** *233*, 111592.
25. Han, X.; Valorani, M.; Najm, H. N. Explicit time integration of the stiff chemical Langevin equations using computational singular perturbation. *The Journal of Chemical Physics* **2019,** *150*, 194101.
26. Han, X.; Najm, H. N. Effective construction of eigenvectors for a class of singular sparse matrices. *Journal of Applied Mathematics Letters* **2019,** *97*, 121-126.
27. Hansen, N.; He, X.; Griggs, R.; Moshammer, K. Knowledge generation through data research: New validation targets for the refinement of kinetic mechanisms. *Proceedings of the Combustion Institute* **2019,** *37*, 743-750.
28. Hansen, N.; Moshammer, K.; Jasper, A. W. Isomer-Selective Detection of Keto-Hydroperoxides in the Low-Temperature Oxidation of Tetrahydrofuran. *The Journal of Physical Chemistry A* **2019,** *123*, 8274-8284.
29. Hansen, N.; Kukkadapu, G.; Chen, B.; Dong, S.; Curran, H. J.; Taatjes, C. A.; Eskola, A. J.; Osborn, D. L.; Sheps, L.; Pitz, W. J., *et al.* The impact of the third O2 addition reaction network on ignition delay times of neo-pentane. *Proceedings of the Combustion Institute* **2021,** *38*, 299-307.
30. Huang, C.; Zhou, Z. J.; Li, S.; Tao, T.; Zhang, F.; Hansen, N.; Law, C. K.; Yang, B. From inherent correlation to constrained measurement: Model-assisted calibration in MBMS experiments. *Proceedings of the Combustion Institute* **2021,** *38*, 1071-1079.
31. Kaiser, R. I.; Hansen, N. An Aromatic Universe-A Physical Chemistry Perspective. *Journal of Physical Chemistry A* **2021,** *125*, 3826-3840.
32. Kalvakala, K. C.; Pal, P.; Gonzalez, J. P.; Kolodziej, C. P.; Seong, H. J.; Kukkadapu, G.; McNenly, M.; Wagnon, S.; Whitesides, R.; Hansen, N., *et al.* Numerical analysis of soot emissions from gasoline-ethanol and gasoline-butanol blends under gasoline compression ignition conditions. *Fuel* **2022,** *319*, 123740.
33. Kohse-Höinghaus, K.; Ferris, A. M.; Zetterberg, J.; Lacoste, D. A.; Fjodorow, P.; Wagner, S.; Cai, L.; Rudolph, C.; Zádor, J.; Li, Y., *et al.* Chemistry Diagnostics for Monitoring. In *Combustion Chemistry and the Carbon Neutral Future*, Brezinsky, K., Ed. 2022.

34. Koritzke, A. L.; Davis, J. C.; Caravan, R. L.; Christianson, M. G.; Osborn, D. L.; Taatjes, C. A.; Rotavera, B. QOOH-mediated reactions in cyclohexene oxidation. *Proceedings of the Combustion Institute* **2019,** *37*, 323-335.
35. Kukkadapu, G.; Wagnon, S. W.; Pitz, W. J.; Hansen, N. Identification of the molecular-weight growth reaction network in counterflow flames of the C3H4 isomers allene and propyne. *Proceedings of the Combustion Institute* **2021,** *38*, 1477-1485.
36. Leon, L.; Ruwe, L.; Moshammer, K.; Seidel, L.; Shrestha, K.; Wang, X.; Mauss, F.; Kohse-Höinghaus, K.; Hansen, N. Chemical insights into the larger sooting tendency of 2-methyl-2-butene compared to n-pentane. *Combustion and Flame* **2019,** *208*, 182-197.
37. Liao, H.; Tao, T.; Sun, W.; Hansen, N.; Law, C. K.; Yang, B. Investigation of the low-temperature oxidation of n-butanal in a jet-stirred reactor. *Proceedings of the Combustion Institute* **2019,** *37*, 453-460.
38. Liao, H. D.; Tao, T.; Sun, W. Y.; Hansen, N.; Yang, B. Isomer-specific speciation behaviors probed from premixed flames fueled by acetone and propanal. *Proceedings of the Combustion Institute* **2021,** *38*, 2441-2448.
39. Miller, J. A.; Sivaramakrishnan, R.; Tao, Y. J.; Goldsmith, C. F.; Burke, M. P.; Jasper, A. W.; Hansen, N.; Labbe, N. J.; Glarborg, P.; Zádor, J. Combustion chemistry in the twenty-first century: Developing theory-informed chemical kinetics models. *Progress in Energy and Combustion Science* **2021,** *83*, 100886.
40. Oreluk, J.; Sheps, L.; Najm, H. Bayesian model calibration for vacuum-ultraviolet photoionisation mass spectrometry. *Combustion Theory and Modelling* **2022**, 1-28.
41. Prendergast, M. B.; Kirk, B. B.; Savee, J. D.; Osborn, D. L.; Taatjes, C. A.; Hemberger, P.; Blanksby, S. J.; da Silva, G.; Trevitt, A. J. Product detection study of the gas-phase oxidation of methylphenyl radicals using synchrotron photoionisation mass spectrometry. *Physical Chemistry Chemical Physics* **2019,** *21*, 17939-17949.
42. Pieper, J.; Hemken, C.; Büttgen, R.; Graf, I.; Hansen, N.; Heufer, K. A.; Kohse-Höinghaus, K. A high-temperature study of 2-pentanone oxidation: experiment and kinetic modeling. *Proceedings of the Combustion Institute* **2019,** *37*, 1683-1690.
43. Rieth, M.; Gruber, A.; Williams, F.; Chen, J. H. Enhanced burning rates in hydrogen-enriched turbulent premixed flames by diffusion of molecular and atomic hydrogen. *Combustion and Flame*, **2022,** in press, https://doi.org/10.1016/j.combustflame.2021.111740.
44. Rieth, M.; Gruber, A.; Chen, J. H. A direct numerical simulation study on NO and N2O formation in turbulent premixed ammonia/hydrogen/nitrogen-air flames, *Proceedings of the Combustion Institute*, **2022,** accepted for presentation.
45. Rotavera, B.; Taatjes, C. A. Influence of functional groups on low-temperature combustion chemistry of biofuels. *Progress in Energy and Combustion Science* **2021,** *86*, 100925.
46. Rousso, A.; Hansen, N.; Jasper, A.; Ju, Y. Identification of the Criegee intermediate reaction network in ethylene ozonolysis: Impact on energy conversion strategies and atmospheric chemistry. *Physical Chemistry Chemical Physics* **2019,** *21*, 7341-7357.
47. Ruwe, L.; Cai, L.; Moshammer, K.; Hansen, N.; Pitsch, H.; Kohse–Höinghaus, K. The C5 chemistry preceding the formation of polycyclic aromatic hydrocarbons in a premixed 1-pentene flame. *Physical Chemistry Chemical Physics* **2019,** *206*, 411-423.
48. Ruwe, L.; Cai, L. M.; Wullenkord, J.; Schmitt, S. C.; Felsmann, D.; Baroncelli, M.; Chen, B. J.; Moshammer, K.; Hansen, N.; Pitsch, H., *et al.* Low- and high-temperature study of n-heptane combustion chemistry. *Proceedings of the Combustion Institute* **2021,** *38*, 405-413.
49. Sun, W.; Wang, J.; Huang, C.; Hansen, N.; Yang, B. Providing effective constraints for developing ketene combustion mechanisms: A detailed kinetic investigation of diacetyl flames. *Combustion and Flame* **2019,** *205*, 11-21.
50. Sun, W.; Tao, T.; Liao, H.; Hansen, N.; Yang, B. Probing fuel-specific reaction intermediates from laminar premixed flames fueled by two C 5 ketones and model interpretations. *Proceedings of the Combustion Institute* **2019,** *37*, 1699-1707.
51. Sun, W.; Lailliau, M.; Serinyel, Z.; Dayma, G.; Moshammer, K.; Hansen, N.; Yang, B.; Dagaut, P. Insights into the oxidation kinetics of a cetane improver–1,2-dimethoxyethane (1,2-DME) with experimental and modeling methods. *Proceedings of the Combustion Institute* **2019,** *37*, 555-564.
52. van de Vijver, R.; Zádor, J. KinBot: Automated stationary point search on potential energy surfaces. *Computer Physics Communication* **2020,** *248*, 106947.
53. Vansco, M. F.; Zuraski, K.; Winiberg, F. A. F.; Au, K.; Trongsiriwat, N.; Walsh, P. J.; Osborn, D. L.; Percival, C. J.; Klippenstein, S. J.; Taatjes, C. A., *et al.* Functionalized Hydroperoxide Formation from the Reaction of Methacrolein-Oxide, an Isoprene-Derived Criegee Intermediate, with Formic Acid: Experiment and Theory. *Molecules* **2021,** *26*, 3058.
54. Vansco, M. F.; Zou, M. J.; Antonov, I. O.; Ramasesha, K.; Rotavera, B.; Osborn, D. L.; Georgievskii, Y.; Percival, C. J.; Klippenstein, S. J.; Taatjes, C. A., *et al.* Dramatic Conformer-Dependent Reactivity of the Acetaldehyde Oxide Criegee Intermediate with Dimethylamine Via a 1,2-Insertion Mechanism. *Journal of Physical Chemistry A* **2022,** *126*, 710-719.
55. Wang, Z.; Herbinet, O.; Hansen, N.; Battin-Leclerc, F. Exploring hydroperoxides in combustion: History, recent advances and perspectives. *Progress in Energy and Combustion Science* **2019,** *73*, 132-181.
56. Yang, B.; Sun, W. Y.; Moshammer, K.; Hansen, N. Review of the Influence of Oxygenated Additives on the Combustion Chemistry of Hydrocarbons. *Energy & Fuels* **2021,** *35*, 13550-13568.
57. Zádor, J.; Miller, J. A. Comment on "Influence of Multiple Conformations and Paths on Rate Constants and Product Branching Ratios. Thermal Decomposition of 1-Propanol Radicals". *The Journal of Physical Chemistry A* **2019,** *123*, 1129-1130.
58. Zádor, J.; Hansen, N.; Glarborg, P.; Klippenstein, S. J. In Memoriam: Jim Miller (1946-2021). *Combustion and Flame* **2022,** *235*, 111853.

Machine Learning for Understanding Heavy Hydrocarbon Clustering

Habib Najm[*1], *Judit Zádor*[1], *Michael Eldred*[2], *Hope Michelsen*[3]
[1]*Sandia National Laboratories, Livermore, CA*
[2]*Sandia National Laboratories, Albuquerque, NM*
[3]*University of Colorado, Boulder, CO*

Program Scope

The goal of this program is to use machine learning (ML) to advance the state of the art in our understanding of reaction mechanisms in heavy hydrocarbon clustering, leading to incipient soot formation. We target this by building neural network (NN) potential energy surface (PES) representations for a class of hydrocarbon molecules; using these to explore reactions among a set of initial C_mH_n molecules at concentrations typical in flames; and using stochastic sampling to estimate reaction probabilities and simulate growth leading to production of heavier hydrocarbons. Our objective is to identify reactions that dominate molecular weight growth, and explore the role of resonantly stabilized radicals (RSRs) in this process. Our NN training data comes from quantum chemistry computations at a range of levels of theory, and we use the information thus gained from models of different fidelities in a multilevel-multifidelity (ML/MF) formalism to efficiently attain requisite NNPES test accuracy. We also rely on active learning to identify conditions for which additional *ab initio* computations provide maximal expected information gain. We rely on KinBot [https://github.com/zadorlab/KinBot] for exploration of the PES for generating geometries for training, and for exploring the trained NNPES to estimate reaction rate coefficients and expand the initial pool of molecules.

Recent Progress

We have made progress on several fronts this year, as outlined in the following.

Generation and curation of training data using automated kinetics:

We used *KinBot*, our open-source tool, to discover and characterize stationary points on the reactive C_5H_5 PES at the wB97XD/6-311++G** level of theory. This is a model RSR system, with rich chemistry, including many newly discovered pathways not published in the literature. We continued to generate and curate training points with our *sampler* code for the NN at the B3LYP/6-31+G* level, an affordable choice within the ML/MF context where we will eventually apply higher-order corrections to achieve chemical accuracy in important regions. Our data includes over 100k labeled points stored in an SQLite database. To facilitate expansion of the database on DOE supercomputers, we recently added *FireWorks* workflow management and *Q-Chem* compatibility to *sampler* and ran calculations on NERSC that way. We also enabled *KinBot* with *FireWorks* and *Q-Chem* capabilities, thus allowing it to run on DOE clusters as well.

Machine Learning Capability Development and Demonstration:

Continuing development of our NNPES construction, we enhanced our atomic environment vector (AEV) C++/Python pybind11 capability to include both first and second analytical derivatives of the AEV feature vector with respect to Cartesian atom coordinates. We relied on automatic differentiation using SACADO (https://docs.trilinos.org/dev/packages/sacado/doc/html/index.html) to provide the 2nd derivatives, thus the AEV Hessian, which is necessary for force training and for KinBot exploration of the NNPES. We released this "aevmod" capability as an open-source software utility (https://github.com/sandialabs/aevmod).

We also pursued targeted demonstrations of our NNPES construction in systems of increasing complexity. We trained the NNPES on GPU hardware resources on NERSC, relying on our above developed databases. To optimize data usage, we relied on query-by-committee active learning to propose geometries for which DFT computations are targeted, thereby providing maximal reduction in training error among the available pool of unlabeled structures. This approach relies on training an ensemble of NN PES models, using

[*] Principal Investigator. Address: P.O. Box 969, MS 9051, Livermore, CA 94551; Email: hnnajm@sandia.gov

randomized subsets of the data, and relying on the resultant scatter in predictions at unlabeled points to estimate predictive uncertainty as a surrogate for the error in predictions. The method also provides for robust predictions, employing ensemble averaging among the trained models, thereby improving predictive accuracy, and reducing the detrimental consequences of overfitting. For training and test data generation, we used randomized normal mode sampling, extending over approximately 40 kcal/mol energies around wells, saddle, and IRC points, providing a very broad description of the reactive PES.

We demonstrated the utility of the construction in representing the important portion of the reactive PES for the C_5H_5 system, a two-basin region describing a 1,3 internal H-transfer reaction of cyclopentadienyl. We used this fitted NNPES to predict high-pressure-limit rate coefficients for the reaction over a wide temperature range, and compared them to rate coefficients computed using DFT molecular properties. The results, shown below in Figure 1, highlight the efficacy of the construction. We observe agreement within a factor of 2.5 in the computed rate coefficients over temperatures ranging from 400 to 2000K.

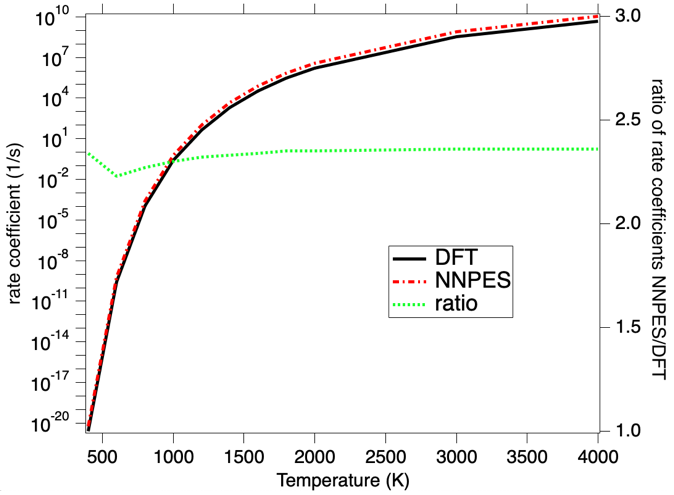

Figure 1. 1,3 H-atom shift isomerization reaction rate coefficient for cyclopentadienyl on the C_5H_5 PES. The NNPES rate coefficients agree with the DFT-based ones within a factor of 2.5.

Using active learning, we extended our demonstrations to span the full PES of C_5H_5, spanning ~100 stationary points and their corresponding IRC paths. Achieving accurate training in this context required enhanced complexity in the NN. The two-basin demonstration in Figure 1 used two NNs, one for each element (C,H), with each employing 3 hidden layers with (128, 64, 64) neurons. Fitting the full PES with sufficiently low (<1kcal/mol) error required enhanced layer widths of (512, 256, 128) neurons. This architecture achieved RMS training errors of about 0.2kcal/mol on ~10^5 data-points/structures. We are currently in the process of assessing/reducing test errors.

We are also working towards direct high-level calculations on some of the key reactions for molecular weight growth models. We equipped *KinBot*'s heuristics and chemical interpretation modules to handle several rings or very rigid structures, and cut down on unrealistic saddle point searches for these kinds of structures. We have reexplored the C_6H_6 PES, and are currently analyzing the data to understand the implications for molecular weight growth.

Derivative-enhanced Training of the NNPES Construction:

We demonstrated the utility of derivative-enhanced NNPES training, which we refer to as force-training, on the above two-basin C_5H_5 subsystem. Results highlighted the utility of inclusion of forces as part of the

training-loss computation, beyond the existing energy misfit loss term. Specifically, as illustrated in Figure 2, we showed that we achieve same test-error performance with 25x less DFT-computational data points.

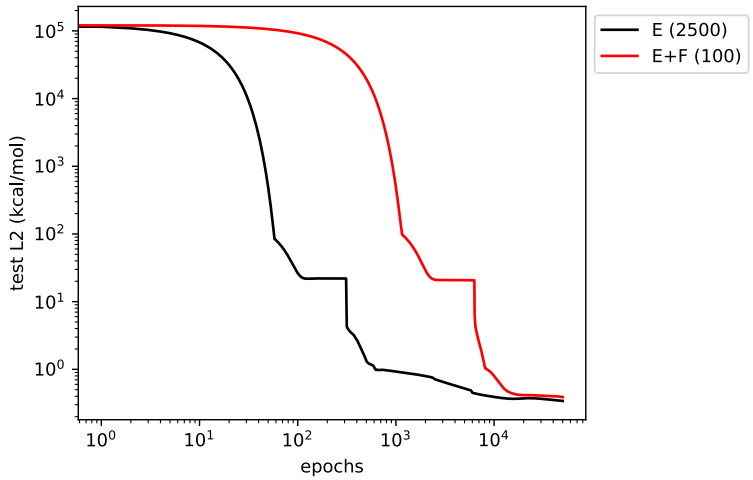

Figure 2. Decay of test-error in C_5H_5 potential energy for NN training using energy only or energy+force. The same test error is achieved with 100 vs 2500 DFT simulations given force training.

***Multilevel / Multifidelity (ML/MF) Methods*:**
We are extending existing ML/MF concepts to the case of NN surrogates so that we can achieve accurate NNPES models at a reduced total cost by incorporating data from *ab-initio* quantum chemistry (QC) computations at different levels of theory. We seek an accurate and affordable mapping from AEV inputs to high-level theory PES outputs by decomposing this mapping across multiple modeling levels. Starting from a NNPES for the lowest level of theory, we add NN constructions for each additional level of theory until we can collectively emulate the highest-level theory. A critical component of this approach is the allocation of varying amounts of training data commensurate with the relative cost of the QC simulations at each level of theory. We explored multiple composite NN topologies, notably *discrepancy-based* (each downstream NN models the difference in model predictions as a function of the AEV inputs), *sequential* (each downstream NN takes the upstream level predictions as its inputs to predict the next level of theory), and *hybrid* formulations (each downstream NN takes both the AEV inputs and the upstream level predictions as its inputs to predict the next level of theory, where these upstream/downstream predictions can be either sequential or discrepancy-based). Moreover, training processes for the composed NN components can either be fully *independent*, to reduce training scale, or *all-at-once*, for which upstream network parameters can be optimized for both local and downstream accuracy.

Following earlier explorations with model problems, we have focused on the two-basin NNPES for C_5H_5 using two levels of theory. In this context, we pursued model selection (based on estimator variance in multifidelity Monte Carlo sampling) to evaluate the correlation versus cost trade-off among QC models with a range of complexity, including B2PLYPD3/6-311++G(d,p), WB97XD/6-311++G(d,p), B3LYP/6-31+G(d), B3LYP/6-31G, and HF/6-31G. The top performing case involved the most extreme pair, B2PLYPD3/6-311++G(d,p) and HF/6-31G, with a cost factor of 84x between the two models. We have selected these as our high- and low-fidelity models going forward. To date, we have observed the best performance in QC formulations using a *hybrid discrepancy-based* architecture with *all-at-once* training. Comparing the single-fidelity with multi-fidelity two-basin NNPES, we have successfully demonstrated an order of magnitude reduction in median prediction RMS test error for the same equivalent cost, or roughly two orders of magnitude reduction in cost for similar accuracy. These savings were even more pronounced for median prediction L-infinity test errors.

Validation Data:

Our goal is to identify and test particle-inception mechanisms. We target the chemistry that leads to a transition from gas-phase species to condensed-phase particles. Such a transition can be identified when the properties (e.g., density, specific heat, and absorption and scattering cross sections) of the particle or cluster depart from those of the gas-phase species from which it is composed and begin to exhibit properties of a bulk material. We performed an analysis of measurements of particles formed pyrolytically in a heated flow reactor. Particle composition and precursor characterization were inferred from vacuum ultraviolet photoionization aerosol mass spectrometry (VUV-AMS) measurements performed at the Advanced Light Source, and particle size distributions were derived from scanning mobility particle sizing. Our results showed that indene, a direct precursor to the resonance-stabilized radical (RSR) indenyl, formed particles at lower temperatures than ethylene and that adding a small amount of indene to ethylene lowered the temperature of particle formation to that of indene. At particle onset temperatures, no sign of acetylene or involvement of the hydrogen abstraction acetylene addition (HACA) mechanism was observed to contribute to particle formation. RSRs, on the other hand, were prominent in VUV-AMS data and demonstrated masses expected during hydrocarbon clustering at particle onset temperatures. These results support the hypothesis of particle inception driven by the clustering of hydrocarbons via RSR-driven chain reactions [3]. To facilitate studies of incipient particles *in situ* in reactive non-equilibrium environments, we have developed a new method to distinguish between gas-phase and nanoparticle scattering in small-angle X-ray scattering measurements [4]. We have employed this new method for studies of particle formation in a sooting flame [4, 5]. We have also developed a new model for extracting information about the nanostructure of particles growing and evolving in an aerosol reactor and demonstrated its use on a sooting flame [5].

Proposed Work

Going forward, there are numerous lines of development/inquiry that we are actively working on.

Automated kinetics on NNPES:

Our immediate goal is to demonstrate the ML framework, focusing on the C_5H_5 PES, to test if we can explore the same chemistry using the NNPES. We will assess the differences between the *ab initio*- and NN-calculation-based rate coefficients the same way as shown in Figure 1, both in terms of accuracy and timing. To accomplish this, beyond a good quality NNPES, we will need to modify KinBot to enable interfacing with our NNPES through the Atomic Simulation Environment (ASE), and, in order to use the NNPES, we need to have robust and flexible geometry optimizers that are not attached to an electronic structure code. To this end, we will enhance KinBot with ASE's optimizer and with our own, ASE-based optimizer called Sella (https://github.com/zadorlab/sella), which we developed in a different DOE-supported grant. This will also allow us to have better control over geometry optimizations in the workflow.

We will also continue our work on the C_5H_5 and C_6H_6 systems and give updated and detailed kinetics description for them. In tandem with the NNPES work, we will also explore larger PESs, such as C_7H_7, to provide richer training data.

Machine Learning Capability Development and Demonstration:

We will continue our work on qualification of the trained NN representation of the full C_5H_5 PES. Preliminary data suggests that the current NNPES, while well-trained on ~10^5 data points/structures, exhibits large errors on test structures not used in training. We will work on multiple fronts to address this.

First, we will conduct training/testing studies on smaller regions of the PES encompassing successively larger numbers of connected basins to assess the scaling of data needs with PES complexity. This will provide both improved understanding of the complexity of the machine learning problem at the full-PES scale, and a reliable estimate of the data sizes needed for the full problem. It will also provide an opportunity for refinement of the strategy for test-data selection, in a direction that is more goal-oriented as informed by the NNPES intended usage, and therefore hopefully more efficient. Second, we will make use of our

force-training capabilities to provide improved regularization of the trained NNPES, thereby improving its test-error with significant reduction in data needs. We have hitherto not activated force-training in the full PES demonstration, relying on training with energies only as a baseline reference case. If our above two-basin system 25x requisite data-size savings extend to the full system, that would be quite significant. Third, we will evolve the NNPES training code towards making simultaneous use of multiple GPUs. This will be necessary to avoid memory constraints with current GPU hardware, and is required whether we move forward with larger data sizes and energy-only training, or with smaller data sizes and force-training, as memory needs grow excessively in both cases. With this bottleneck resolved, we plan to work on qualification of the full NNPES for C_5H_5 for KinBot use for exploration and rate computations.

***Multilevel-Multifidelity (ML/MF) Methods*:**
There are several potential future directions of enhancement for MF NNPES, including force training, multifidelity active learning, alternative underlying NN architectures (ResNet, recurrent NN), extended model ensembles (beyond bi-fidelity incorporating general non-hierarchical graphs), extended accuracy (beyond B2PLYPD3/6-311++G(d,p) towards coupled-cluster level accuracy), and extended PES contexts (full C_5H_5 PES prediction, and extensions to C_6H_6, C_7H_7 and beyond.)

The primary priority at this time is migrating from *a priori* determination of multifidelity data allocations to multifidelity active learning approaches, where the most effective training dataset increments are determined adaptively based on an integrated competition across data refinement candidates that span multiple levels of theory. This capability is critical to move us forward from MF NNPES concept demonstration to the effective automation of efficient and accurate MF NNPES constructions.

Validation Data:
We will continue to analyze previously recorded measurements of particles generated during pyrolysis in order to gain more insight into the role of RSRs on particle formation. We will study the impact of propyne, a direct precursor to propargyl, on clustering propensity using VUV-AMS measurements of particle formation as a function of temperature of our flow reactor. We will incorporate new results from KinBot into a chemical kinetic model to address our understanding of clustering mechanisms.

Publications supported by this project 2019-2022

1. H. A. Michelsen, Effects of Maturity and Temperature on Soot Density and Specific Heat, *Proc. Combust. Inst*., **38** (2020) DOI: 10.1016/j.proci.2020.06.383. Distinguished Paper Award.
2. H. A. Michelsen, M. B. Colket, P.-E. Bengtsson, A. D'Anna, P. Desgroux, B. S. Haynes, J. H. Miller, G. J. Nathan, H. Pitsch, H. Wang, A Review of Terminology Used to Describe Soot Formation and Evolution Under Combustion and Pyrolytic Conditions, *ACS Nano*, **14** 12470-12490 (2020). DOI: 10.1021/acsnano.0c06226.
3. J. A. Rundel, C. M. Thomas, P. E. Schrader, K. R. Wilson, K. O. Johansson, R. P. Bambha, and H. A. Michelsen, "Promotion of Particle Formation by Resonance-Stabilized Radicals During Hydrocarbon Pyrolysis", *Combust. Flame*, in press (2021) DOI:10.1016/j.combustflame.2021.111942.
4. H. A. Michelsen, M. F. Campbell, I. C. Tran, K. O. Johansson, P. E. Schrader, R. P. Bambha, J. A. Hammons, E. Schaible, C. Zhu, and A. van Buuren", Distinguishing Gas-Phase and Nanoparticle Contributions to Small-Angle X-ray Scattering in Reacting Aerosol Flows", *J. Phys. Chem. A*, in press (2022) DOI:10.1021/acs.jpca.2c00454.
5. H. A. Michelsen, M. F. Campbell, K. O. Johansson, I. C. Tran, P. E. Schrader, R. P. Bambha, E. Cenker, J. A. Hammons, E. Schaible, C. Zhu, J. Silberstein, and A. van Buuren "Soot Particle Core-Shell and Fractal Structures from Small-Angle X-ray Scattering Measurements in a Flame", *Carbon*, in press (2022).

ELECTRON-DRIVEN CHEMISTRY

David W. Chandler, Jonathan H. Frank, Laura M. McCaslin, Krupa Ramasesha, Leonid Sheps
Sandia National Laboratories, MS 9051, Livermore, CA 94551-0969
chand@sandia.gov, jhfrank@sandia.gov, lmmccas@sandia.gov, kramase@sandia.gov, lsheps@sandia.gov

PROGRAM SCOPE

Electron-driven chemistry, which we define as chemical transformations driven by long-range motion of electrons or charges, underpins many areas of interest to the DOE. The goal of this program is to deepen understanding of reactivity that is driven by motion of charges. We will apply a combination of sophisticated experimental and theoretical methodologies to provide detailed time- and state-resolved views of complex charge-transfer processes. These investigations will illuminate phenomena that defy the common simplifying assumptions of the Hartree-Fock and Born-Oppenheimer approximations and will aid in developing more sophisticated descriptions of coupled electron and nuclear motion. This work extends the research we have done on neutral processes, using quantum state-resolved experiments that provide detailed information about molecular potential energy landscapes and the dynamics involving coupled potential energy surfaces. We pursue experiments that include: 1) induced charge separation in an isolated molecule, 2) dynamics following attachment of a free electron to a neutral molecule or cluster, and 3) coupled chemical and physical evolution of a laser-induced plasma. In each area, we apply advanced techniques, including techniques presently being developed, to provide a new and deeper understanding of chemical physics processes. This effort complements research being performed in the Solar Photochemistry and Condensed-Phase and Interfacial Molecular Sciences programs and addresses BES Grand Challenges associated with the study of the nature of excited electronic states and the breakdown of the Born-Oppenheimer approximation. This research is closely tied to other work in our program. The study of ultrafast intramolecular charge transfer dynamics of large conjugated systems has strong connections to the ultrafast non-adiabatic dynamics studied in the "Ultrafast Chemistry" task and uses X-ray techniques from the "Advanced Diagnostics" task. Research described in this subtask extends the work performed under the "Chemical Dynamics" task to investigate inelastic collisions of electrons with molecules, and links to studies of neutral reacting systems in the "Chemical Kinetics" task.

RECENT PROGRESS

Coupled chemical and physical evolution of a laser-induced plasma

Our recently developed VMI apparatus for high-resolution electron scattering and excited-state dissociative electron attachment (DEA) has also enabled studies of the dynamics of laser-initiated plasmas and plasma-induced chemistry in well-controlled, field-free conditions. A tunable laser initiates the plasma by generating electrons and cations via resonance-enhanced multiphoton ionization (REMPI) in an atomic or molecular beam produced by a pulsed supersonic expansion. This produces electrons with tunable energy and a narrow energy distribution that can then interact with species in the atomic/molecular beam. Our experiments are the first to exploit velocity map imaging to study the dynamics of plasma formation on a nanosecond timescale. Crucial to this effort is the use of high-voltage pulses with sub-nanosecond duration in the VMI ion optics to disrupt and accelerate plasma electrons with high-time resolution while maintaining good detection sensitivity and imaging capability (see Fig. 1).

We have shown that plasmas initiated by very low kinetic energy electrons (2 meV) produced by two-color 1+1' REMPI of NO seeded in He reproducibly eject a plume of electrons from the main plasma volume. Velocity mapping and spatial imaging of the electrons reveals the detailed ejection dynamics, although the dynamics of the NO^+ cations during this event have not yet been determined. The evaporation of plasma electrons from comparable systems is an important cooling mechanism, but the role of discrete electron emission events has to our knowledge not been reported in the literature. Velocity map imaging shows that the electrons in the main plasma are mapped to a single circular distribution consistent with an isotropic

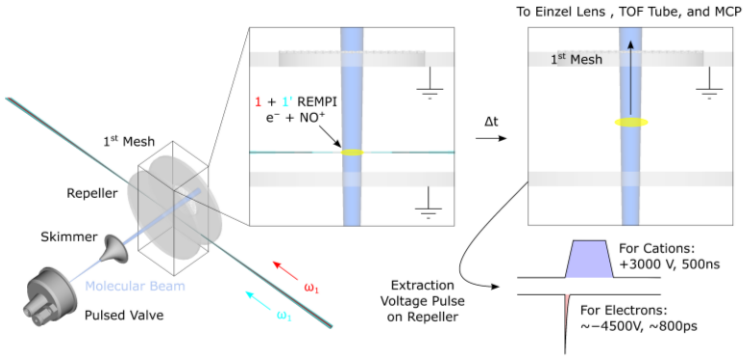

Fig. 1: Velocity map imaging apparatus for studying laser-initiated plasma.

Maxwell-Boltzmann velocity distribution near 50 K. However, at a delay time of 20 ns, the main plasma increases in brightness and size corresponding to a sudden increase in the electron number and temperature. These increases are correlated with the development of a plume, as shown in Fig. 2. At early times, the plume distribution is smaller (colder) and less intense (smaller number) than the electron distribution in the main plasma. Additionally, the first moment of the plume distribution radially separates from the stationary first moment of the main plasma distribution as the delay time increases, indicating that the center of mass of the plume is accelerating away from the main plasma. At extraction times for which the main and plume distributions are cylindrically symmetric, the distributions are separated, and Abel inversion is used to extract precise information on the internal energy distribution of each.

The spatial and velocity distributions of NO^+ ions in the plasma can be measured using the same apparatus by changing the voltages applied to the ion optics. The initial spatial distribution of the cations has a large aspect ratio with the longer axis aligned in the direction of laser beam propagation ($\vec{k}$). Upon extraction, space charge effects accelerate the NO^+ ions in a direction orthogonal to $\vec{k}$. The result is a broad spatial distribution and a highly asymmetric velocity distribution that is narrow along the $\vec{k}$ direction and broadly distributed in the orthogonal direction (see Fig. 3).

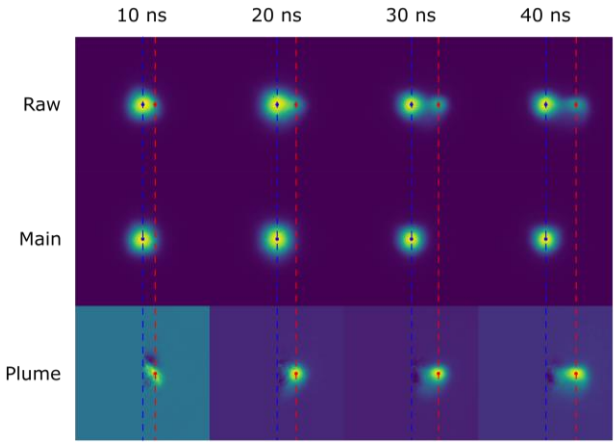

Fig. 2: Time-resolved velocity mapped images of electrons in a 1+1' NO REMPI plasma during the initial stages of plume formation. Images of main peak are obtained by mirroring the left half of the raw images. Images for the plume peak are obtained by subtracting the main image from the raw image. Blue and red dots indicate the center of the main plasma and plume, respectively.

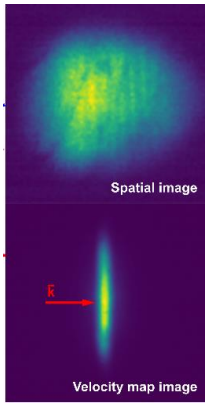

Fig. 3: Spatial (top) and velocity (bottom) distributions of NO^+ ions produced in a plasma initiated by 1+1' REMPI of NO. Grid lines in spatial image result from mesh with 215 μm wire spacing and provide a length scale reference. Velocity map shows rapid acceleration of cations in direction orthogonal to the laser beam propagation direction ($\vec{k}$) following extraction of electrons from the plasma.

Dynamics following attachment of a free electron to a neutral molecule or cluster

Our VMI apparatus enables studies of electron attachment to weakly bound molecular clusters. Electron reactions with clusters serve as a link between gas phase and condensed phase reactions. As an initial demonstration of this capability, we detected the formation of O_2^- ions produced by electron attachment to clusters in a molecular beam of O_2 and Ar. For these experiments, our electron apparatus is equipped with an electron gun that produces a tunable electron beam that interacts with the molecular beam. The electron gun provides access to higher electron energies than are obtainable by laser REMPI generation with a broader energy spread (0.5 eV). Measurements of the electron energy dependence of the O_2^- ion signal in Fig. 4 are consistent with previously detected resonances except for the increasing cross-sections above 15 eV.[1, 2] Our observation is consistent with production of very small clusters as the cross section rise at 10 eV in the previous data (red line) is associated with electron capture by Ar in $O_2(Ar)_n$ clusters. Our experiments were performed at expansion conditions where clusters only begin to contribute.

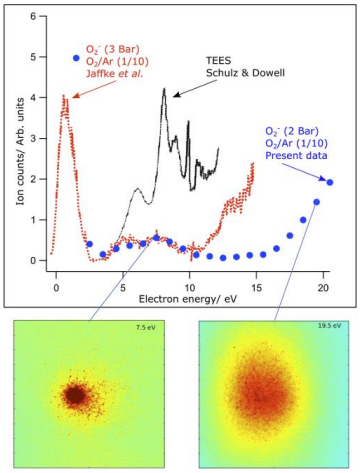

Fig. 4: Comparison of ion yields of O_2^- from O_2/Ar clusters with previous ion yield measurements[1] and threshold electron excitation spectrum (TEES)[2] of the O_2 molecule. Velocity mapped images show the increased kinetic energy of O_2^- from DEA of 7.5 and 19.5 eV electrons.

FUTURE WORK

Coupled chemical and physical evolution of a laser-induced plasma

The combination of VMI with well-controlled laser-generated plasmas opens many opportunities for detailed studies of chemical reactions of molecules in plasmas with tunable electron energy distributions. Our initial plasma-chemistry studies will focus on nitric oxide (NO), which can be used both to generate the plasma and to study plasma chemistry. Preliminary results show enhanced production of vibrationally excited NO(v=1) as a result of interactions with the plasma. After intiating a plasma with 1.2 eV electrons by 1+1 REMPI of ground state NO(v=0) at 226 nm, the remaining neutral NO(v=0) molecules in the beam interact with the plasma to produce vibrationally excited NO(v=1). A second tunable pulsed laser at 236 nm is used for state-specific REMPI probing of the NO(v=1) molecules at a time delay of a few hundred nanoseconds. A comparison of the resulting REMPI spectra of NO(v=1) with and without the plasma is used to identify the specific rotational states that experience enhanced population as a result of plasma interactions (see residual signal in Fig. 5). Planned experiments will investigate the temporal evolution of the plasma excitation of NO and provide better understanding of the excitation process as well as the origins of the background NO(v=1) signal.

Another feature of our laser-initiated plasma experiments is that we can study dissociative recombination that results in the temporal decay of electron and cation signals after initiating plasma formation. In particular, dissociative recombination of plasma electrons with NO^+ cations is expected to produce neutral atomic O^3P and N^4S. Simulations predict that dissociative recombination is very rapid consuming half of

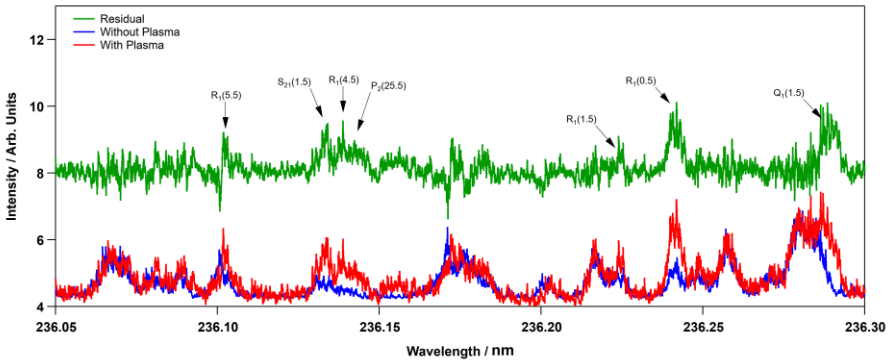

Fig. 5: REMPI excitation spectra showing signal intensity from 1+1 REMPI of NO(v=1) with and without a plasma. Residual is the difference between the spectra with and without a plasma and is offset in the vertical axis for clarity. Peaks in residual show enhancement in the presence of a plasma environment.

the plasma ions in ~100 ns. Simulations also predict interesting spatial dynamics where formation of neutral O and N is initially localized in the plasma core but migrates to the wings at later times. Under certain conditions, indirect evidence from experiments suggests that anomalous dissociative recombination may occur when the ions in the plasma are strongly coupled. To date, no experimental verification of this plasma dynamics has been made. We intend to use 2+1 REMPI to interrogate these kinetics and image the dynamics of neutral O and N formation in laser-generated plasmas.

Dynamics following attachment of a free electron to a neutral molecule: Experimental studies

Detailed insights into the fundamental chemical interactions that occur in charge distributions such as plasmas can be obtained by investigating the dynamics following attachment of free electrons to isolated molecules or clusters. For these studies, our electron scattering apparatus has two characteristics that we are taking advantage of. One is the high energy resolution of the electrons dictated by the frequency spread of the laser beam. This allows us to scan the frequency of the laser and thereby scan the energy of the electrons with approximately 0.5 cm^{-1} (0.06 meV) resolution. This feature is essential for resolving narrow low energy resonances. In the next year, these studies will focus on DEA of nitric oxide and sulfur dioxide.

To better understand dynamics of electron attachment to ground state NO followed by detachment, we will scan the energy of the electrons through low energy resonances of NO. We will then use 1+1 REMPI to detect the formation of vibrationally excited NO. In this manner, we will measure the natural linewidth of the resonances associated with production of vibrationally excited ground state transient ions and therefore determine the lifetime of the transient anions. The other characteristic that we will take advantage of is the time resolution of using pulsed lasers to produce the electrons. The electrons traverse the molecular beam in a time that is shorter than the laser pulse duration. Therefore, all transient anions will be formed during the 5-ns laser pulse as the electrons encounter molecules in the molecular beam. As we have control over the time of the electron generation, we can excite a molecule in the molecular beam prior to the electron production. In this manner, we will study the production of transient anions from electronically excited states of NO and SO_2.

The motivation for studying DEA to nitric oxide is that it exhibits significant changes in dissociative electron attachment to the ground and electronically excited states that require a more detailed understanding. Dissociative electron attachment to ground state NO requires a minimum electron energy of approximately 7.5eV. In contrast, DEA to electronically excited NO in the $A^2\Sigma^+$ state (5.48 eV) is exothermic by 0.45eV, and the DEA cross sections are three orders of magnitude larger for the electronically excited state.[3] This extraordinary enhancement in the cross section is associated with a Feshbach resonance. The dissociation channel in the excited state also differs from that of ground state NO. DEA to ground state NO primarily produces $N(^2D) + O^-(^2P)$, and DEA to electronically excited NO(A) produces $N(^4S) + O^-(^2P)$.[4] The sensitivity of the DEA enhancement and branching of dissociation channels to varying levels of vibronic excitation are not well established. We plan to investigate the enhancement

and branching ratios of DEA to excited-state NO by selective laser excitation to different vibronic states prior to electron attachment.

Electronic excitation of sulfur dioxide, SO_2, has profound effects on the dissociation channels following electron attachment, resulting in nearly complete suppression in the production of some ionic fragments. For DEA to SO_2 in the excited electronic state ($\tilde{B}^1B_1$), the cross sections for formation of products O^- and SO^- are enhanced by factors of 6 and 1.5, respectively, while the formation of S^- is almost entirely suppressed.[5] Previous studies of these effects of DEA to excited state SO_2 primarily focused on using time-of-flight mass spectrometry (TOFMS) and included limited investigation into the sensitivity of cross sections and product channels to different levels of excitation. We will conduct a series of detailed studies of DEA to SO_2 using velocity mapped imaging to provide mass selective detection of the kinetic energy and angular distribution of the DEA fragments following laser excitation of the parent molecule.

Dynamics following attachment of a free electron to a neutral molecule: Theoretical studies

We will pair experimental studies with theoretical investigations of the DEA processes in excited-state molecules. In order to probe the underlying dynamics and electronic structure involved in the vibrational- and electronic-state dependence of reactions such as $SO_2 + e^-$, non-adiabatic mixed quantum-classical (NA-MQC) dynamics calculations will be performed. Though these are relatively small systems, the electronic structure is quite difficult to describe due to the multiconfigurational nature of the wavefunctions. Electronic structure methods such as equation-of-motion coupled cluster in its electron-attachment variant (EOM-EA-CCSD) will be benchmarked against methods that incorporate treatments of both static and dynamic electron correlation such as CASPT2 in order to identify methods with an appropriate balance of accuracy and computational efficiency for employment in dynamics calculations.

Intramolecular charge transfer dynamics in gas phase donor-bridge-acceptor systems

We will begin a series of studies focusing on excited-state dynamics in large, conjugated molecules with extended π-orbitals. These dynamics are governed by the molecular structure, the nature of participating valence orbitals, the interactions among electronic states, and the surrounding environment. Donor-bridge-acceptor (DBA) molecules are a class of π-conjugated systems, where large amplitude changes to molecular structure are coupled to intramolecular charge transfer (ICT). Given the known sensitivity of ICT to external electric fields and solvent interactions, we propose to first study the *baseline* charge transfer dynamics in isolated gas phase DBA molecules in cold molecular beams, free from interaction with the environment. The system we will first study is *p*-nitroaniline (PNA), which has an electron-acceptor $–NO_2$ group and an electron-donor $–NH_2$ group. Following electronic excitation to the locally excited singlet state, excited state evolution to the twisted ICT state and to triplet states via intersystem crossing are expected to compete. Our experiments will study excited state dynamics in jet-cooled PNA using ultrafast core-level X-ray absorption and X-ray photoelectron spectroscopies following electronic excitation to the locally excited state. Core-

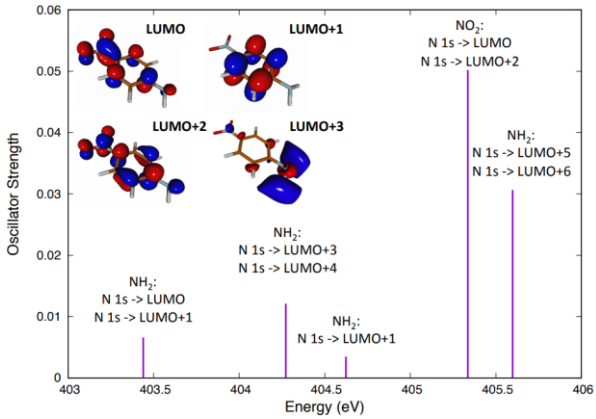

Fig. 6: The calculated lowest-energy core nitrogen K-edge transitions in ground state PNA, originating from the nitrogen atoms in the NH_2 and NO_2 moieties.

level spectroscopy near the O and N K-edges will serve as site-specific probes of ICT dynamics, and to this end, we will be writing a user proposal for beam time at the LCLS. In order to guide interpretation of results from these experiments, we calculated the nitrogen and oxygen K-edge transitions at the core-valence separation ADC(2) level of theory with a 6-31G* basis. The nitrogen 1s core-to-valence transition energies of ground state PNA, shown in Fig. 6, demonstrates that transitions from the NH_2 and NO_2 moieties of PNA are sufficiently separated in energy to be experimentally distinguished. In the planned experiments, we will detect valence excitation and charge transfer-induced changes in the electronic structure in the vicinity of the NH_2 and NO_2 groups, reflected in shifts of these core-to-valence transition energies and intensities, which will be compared with theoretical predictions of electronically excited PNA. The effects of valence excitation on oxygen 1s core-level spectra will also be computed for comparison.

Long-range electron transfer in rare gas/large molecule clusters

In the next year, we plan to initiate studies of charge transfer dynamics in rare gas-molecule van der Waals clusters (Rg·M). The excitation of meta-stable electronic states of Rg in these clusters is expected to lead to Penning ionization, in which an electron ejected from Rg* is replaced by another from M (PI, $Rg^*{\cdot}M \rightarrow Rg + M^+ + e^-$), or to charge-transferred ion-pair formation (CT, $Rg^*{\cdot}M \rightarrow Rg^+{\cdot}M^-$). Both processes are long-range electron transfers that depend sensitively on the interaction of the Rg and M. We seek to understand which atomic and molecular orbitals are involved in the electron transfer and how this charge motion couples to the vibrational modes of M or Rg·M.

Our first experiments will produce Kr·NO clusters in a pulsed supersonic expansion, excite them with continuous VUV radiation at the Advanced Light Source synchrotron, and detect the charged fragments formed via PI by a new double-imaging PEPICO apparatus, built by D. Osborn. NO has a well resolved photoelectron spectrum, and we hypothesize that coincidence detection of NO^+ and e^- will enable vibrationally state-resolved measurements with full fragment momentum matching (since Kr has no internal degrees of freedom). This will shed light on the coupling of long-range electron transfer to specific molecular motions in the cluster and provide new detailed benchmarks for theory.

If the initial studies are successful, we will progress to more complex molecular partners (M), such as toluene and *p*-nitroaniline. The purpose of these studies will be to probe which frontier orbitals of M (e.g., those localized on the benzene ring or those partially extended onto the substituent groups) most strongly couple to Rg and participate in the PI process. We will also introduce pulsed laser excitation of Rg·M (Rg = Kr or Xe) via allowed UV 2-photon transitions into the 5p or 6p state manifold, respectively, using tunable (212 – 256 nm) ~5-ns laser pulses. These experiments will enable a wider choice of Rg excitation energies and metastable states. Furthermore, pulsed laser excitation will enable the photodetachment of electrons from charge-transferred $Rg^+{\cdot}M^-$ ion pairs by a second, time-delayed laser pulse, providing time-resolved measurements of the CT process.

References

1. Jaffke, T.; Hashemi, R.; Christophorou, L. G.; Illenberger, E., Mechanisms of anion formation in O2, O2/Ar and O2/Ne clusters; the role of inelastic electron scattering. *Zeitschrift für Physik D Atoms, Molecules and Clusters* **1992,** *25* (1), 77-85.
2. Schulz, G. J.; Dowell, J. T., Excitation of Vibrational and Electronic Levels in O_2 by Electron Impact. *Physical Review* **1962,** *128* (1), 174-177.
3. Kuo, C. T.; Hardwick, J. L.; Moseley, J. T., Low-energy-electron attachment to excited nitric oxide. *J. Chem. Phys.* **1994,** *101* (12), 11084-11085.
4. Kuo, C. T.; Ono, Y.; Hardwick, J. L.; Moseley, J. T., Dissociative attachment of electrons to the A $^2\Sigma^+$ state of nitric oxide. *J. Phys. Chem.* **1988,** *92* (18), 5072-5074.
5. Krishnakumar, E.; Kumar, S. V. K.; Rangwala, S. A.; Mitra, S. K., Dissociative-attachment cross sections for excited and ground electronic states of SO_2. *Phys. Rev. A* **1997,** *56* (3), 1945-1953.

IMAGING THE NEAR-SURFACE GAS PHASE: A NEW APPROACH TO COUPLED GAS-SURFACE CHEMISTRY

Jonathan H. Frank, Farid El Gabaly, Nils Hansen, Christopher J. Kliewer, David L. Osborn
Sandia National Laboratories, Livermore, CA
jhfrank@sandia.gov, felgaba@sandia.gov, nhansen@sandia.gov, cjkliew@sandia.gov, dlosbor@sandia.gov
Coleman Kronawitter and Ambarish Kulkarni
Department of Chemical Engineering, University of California, Davis
ckrona@ucdavis.edu, arkulkarni@ucdavis.edu

PROGRAM SCOPE

The chemical reactivity of gases with solid surfaces is ubiquitous in natural and industrial energy transformation. Cooperative effects that couple gas phase chemistry with surface chemistry are critical for foundational understanding but challenging to probe experimentally and theoretically. Heterogeneous catalysis is an ideal field to expose and isolate the fundamental chemical physics of these cooperative effects. Our program seeks to characterize gas-surface coupling through chemically specific, temporally and spatially resolved probes of both reacting surfaces and the near-surface gas phase. The program combines optical spectroscopy with mass spectrometry and photoelectron spectroscopy of both gas phase and surface species. The long-term goal is to elucidate the fundamental mechanisms of cooperative gas-surface chemistry, influencing DOE mission research in catalysis, synthesis, and energy transformation.

This program comprises two interrelated thrusts that are distinguished by the physical mechanism of gas-surface coupling – transport or reaction – and employ differing degrees of chemical complexity and control over the model catalyst surface. The first thrust explores how molecular transport in the gas phase may mediate coupling between different domains on a surface without gas-phase chemical reactions. It employs well-controlled reactions on atomically cleaned crystalline and polycrystalline surfaces prepared under ultra-high vacuum (UHV) conditions, with reactivity studied under pressures of 10^{-6} to 760 Torr. The second thrust adds the complexity of reactive coupling, with bond breaking and formation among intermediates occurring in the gas phase as well as on the surface. Thrust 2 utilizes both polycrystalline films and more complex surfaces (e.g., doped metal oxides, and bifunctional supported catalysts), with reactivity studied at elevated temperatures (400 - 1250 K) and pressures of 1 – 1500 Torr.

RECENT PROGRESS

Near-Surface Measurement of H-atom During Catalytic and Noncatalytic Dehydrogenation of Ethane One fundamental hypothesis of this program has been that the emission of reactive intermediates into the gas phase during catalytic reactions is likely for more prevalent than had previously been thought. At ambient or higher pressures, the constant barrage of gas phase molecules at every surface site increases this possibility. Catalytic dehydrogenation reactions over platinum catalysts have long been modeled as a purely surface related chemistry. Hydrocarbon molecules adsorb, undergo dissociative dehydrogenation at the surface, yielding a surface-bound H. Desorption of the parent molecule then proceeds often through the formation of an intramolecular double or triple bond, and the surface H migrate until desorbed as molecular H_2. H-atom however is a highly reactive intermediate in the gas phase, and could itself induce further reactions in the near-surface gas-phase if present in significant concentrations. To directly probe this possibility, we employed femtosecond three-photon laser-induced fluorescence experiments in the near-surface region of platinum-based catalysts as well as SiO_2 substrates. As shown in Figure 1, significant gas-phase H-atom concentration was found in the near-surface gas phase over these catalysts. In fact, it was found that most Pt-based catalysts started the dehydrogenation reaction with strong emission of H-atom into the gas phase, but as the catalyst deactivated through surface coking, the emission of H-atom into

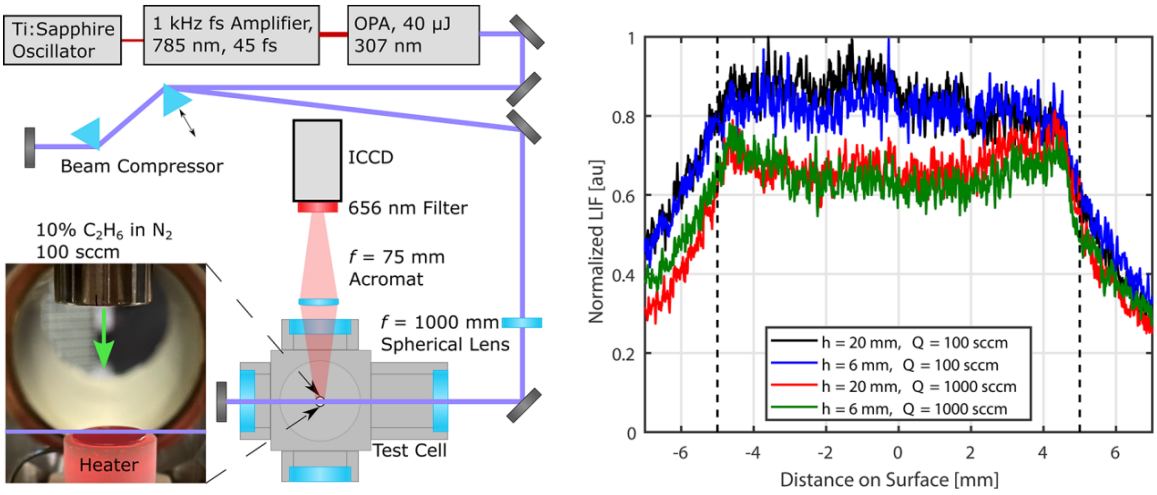

Figure 1. (left) Laser setup for femtosecond three-photon laser-induced fluorescence of H-atom in the near surface region over either Pt-based catalyst or SiO_2. (right) 1D-TPLIF signal from H-atom over a heated SiO_2 surface. Significant H-atom concentration is detected over the substrate during dehydrogenation. Black dashed lines indicate the edge of the sample. This is the first known near-surface measurement of H-atom during dehydrogenation reactions known to these authors.

the gas phase decreased concomitantly with the dehydrogenation rate. In contrast, dehydrogenation carried out over bare SiO_2 exhibited both strong H-atom emission and dehydrogenation rates, as well as negligible deactivation, presumably because of a lack of coke formation at the surface. These finding have been summarized in a recent publication (1) referenced below.

Commissioning of the Optically Accessible Ambient Pressure Imaging X-Ray Photoelectron Spectrometer In the previous fiscal year, we designed a novel experimental system that simultaneously allows for optical spectroscopy techniques, including 2D coherent anti-Stokes Raman scattering (2D-CARS), femtosecond sum-frequency generation (SFG) and planar laser-induced fluorescence (PLIF), to be performed alongside 2D imaging ambient pressure X-ray photoelectron spectroscopy (AP-XPS). The system also includes a flexible gas handling system and a variety of surface science techniques such as LEED, Auger, and sputtering. Imaging AP-XPS delivers the power of x-ray photoelectron spectroscopy to measure, via core-level transitions, spatially resolved (~10 µm) oxidation states of surface species. AP-XPS is successful even with gas pressures of 1 – 20 Torr above a surface.

In late calendar year 2021, this system was installed at Sandia-CA. Initial experiments have begun on the instrument. In first experiments the practical spatial resolution of the instrument has been tested, as this is important for understanding the types of spatial domains that can be imaged in real time for correlated AP_XPS and near-surface spectroscopic imaging experiments. For these experiments a TEM grid with copper wires was used and a spatial resolution in both x and y of ~25 µm was established for the instrument, as seen in Figure 2. As described below in the Future Work section, the first system we are studying for correlated gas-surface measurements is the $H_2 + O_2 \rightarrow H_2O$ system over Pt and Rh catalysts.

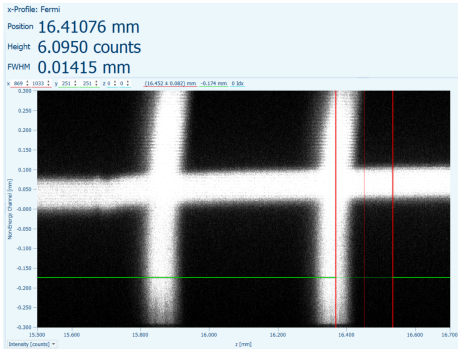

Figure 2. AP-XPS image of a copper TEM grid, demonstrating x and y imaging resolution of ~25 µm.

Imaging of Gas-Phase Species in Catalytic Oxidation of Methanol A great deal of catalysis research has focused on investigating surface chemistry in UHV. However, most catalysts are operated at pressures that are orders of magnitude above UHV conditions. Elevated pressures involve a different operating regime with higher surface coverage of reactants and a greater probability of gas-phase chemical reactions. Therefore, *operando* experiments are needed to provide mechanistic understanding at realistic conditions. We have continued refining methods for imaging the near-surface gas phase using combinations of 1D Raman scattering, 2D PLIF, and near-surface molecular beam mass spectrometry of minor species. Our initial studies were focused on metallic film catalysts, but detailed studies of powder catalysts are required to address a broader range of catalysis chemistry. In recent work, we extended our diagnostics approaches to imaging the near-surface gas phase above powder catalysts such as Li/MgO and Pd/MgO.

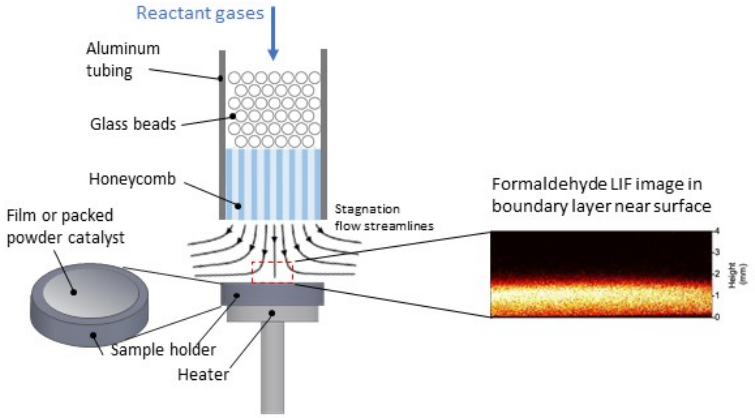

Figure 3: Stagnation Flow Reactor

We have also updated the experimental configuration of our optically accessible flow reactor to include a stagnation flow geometry, as shown in Fig. 3. The reactor consists of a 1-inch diameter nozzle with flow conditioning providing a uniform flow of reactants that impinge on the surface of a 1-inch diameter catalyst. The catalyst is mounted in a machinable ceramic sample holder, which is positioned on top of a button heater. The sample holder can be used for either film catalysts coated on a substrate or a powder catalyst that is packed into a circular wafer. The stagnation flow geometry produces a boundary layer with uniform thickness and facilitates comparisons with modeling because the centerline species and temperature profiles can be compared to computationally tractable 1D simulations. For facilitating direct comparison of the imaging experiments with the near-surface mass spectrometry results, the same flow geometry has been adapted for the complementary mass spectrometry experiments.

Methoxymethanol is a Common Intermediate in Methanol Catalytic Oxidation In a collaboration led by our UC Davis colleagues Coleman Kronawitter and Ambarish Kulkarni we recently studied partial oxidation of methanol over Pd and Au_xPd_y catalysts. We observed clear evidence of the intermediate species methoxymethanol (CH_3OCH_2OH) in the near-surface gas phase. This species has been previously proposed as an intermediate in the coupling reaction for catalytic synthesis of methyl formate (CH_3OCHO) from methanol, and was also observed in our previous work over silver catalysts. The direct observation of this species provides strong evidence that surface coupling of methoxy radicals (CH_3O) with formaldehyde (CH_2O) represents a key mechanistic step on the path to methyl formate. In addition, we observe desorption of dimethoxymethane (DMM, $CH_3OCH_2OCH_3$). Informed by density functional theory calculations of Gibbs free energies of surface-bound species, reactive saddle points, and surface/gas-phase products, this work provides new information on the detailed reaction mechanism. We propose that methoxymethanol is an intermediate leading to DMM formation in competition with the oxidative pathway that leads to methyl formate. The experiments using alloys of gold and palladium showed that $AuPd_2$ has a higher activity for production of both methoxymethanol and methyl formate compared to Pd and AuPd. Because our methoxymethanol signals are not on an absolute basis, we can't yet quantify how the catalyst alloy stoichiometry affects the competition between methoxymethanol and methyl formate, but our work demonstrates that higher local conversion of methanol favors the pathway to DMM (via methoxymethanol) at the expense of methyl formate production.

FUTURE WORK

Transport-Mediated Gas-Surface Coupling and Domain-Specific Chemistry

Resolving the local reaction kinetics and mechanism during surface catalyzed reactions as they vary from one crystallographic domain to the next, under ambient pressure conditions, is a foundational but elusive measurement for understanding gas-surface catalytic reactions. We aim to accomplish this task by directly monitoring local gas-surface reactive exchange rates across the many crystallographic domains of a typical polycrystalline catalyst. These measurements will show the effects that the local crystallographic termination, structure, and oxidation state, or the local average concentration of steps and defects within a domain, have on the product formation rate for polycrystalline (nonuniform) catalysts. Gas-phase composition measurements will also determine which key species are transported via the gas-phase to other crystallographic domains.

As described in the Recent Progress section, we recently demonstrated the first near-surface measurement of H-atom emission during catalytic dehydrogenation. In the coming year, we aim to begin the first correlated near-surface spectroscopic and AP-XPS measurements to solve an age old debate in one of the simplest catalytic reactions, $H_2 + O_2 \rightarrow H_2O$. The simple Langmuir-Hinshelwood type mechanism that has been used to describe this reaction fails to reproduce the rate of formation of H_2O directly observed in experiments. Additionally, evidence that the H* + O* → *OH surface step barrier height is incorrectly understood has been reported. It is currently questioned whether there is a new, previously unconsidered reaction intermediate formed on the surface, or whether a specific surface site contributes to enhanced formation rate of *OH. We will carry out AP-XPS experiments during $H_2 + O_2 \rightarrow H_2O$ over Pt single crystals of varying step densities. Simultaneously, we will incorporate the near-surface LIF imaging of H atom, O atom, and OH radicals. Careful variation of surface step densities (i.e. such as moving from Pt(111) to Pt(557)) will allow monitoring for evidence of enhanced reaction or oxidation rates induced by step edges. Gas phase observation of O and OH will be first of their kind experiments and we hypothesize will reveal detail on local catalytic turnover rate. We will search for the possible surface intermediate hydronium (H_3O^+) in the AP-XPS spectra under various conditions. By correlating these data, the rate of production of O, H, and OH with respect to local surface oxidation and speciation will reveal whether a special set of surface sites or possible new intermediates need to be included in this mechanism. AP-XPS/LIF measurements will be complemented with eventual LEEM work function mapping. Local work function changes as O, H, H_2O, OH, H_3O^+, and other molecules adsorb/desorb on different Pt surface features (terraces, steps, surface orientations). We will map the work function at varying T and P with 20nm resolution using LEEM. Measured work function changes by surface catalytic intermediates can be compared with ab-initio calculations. These LEEM measurements will be used as a quick screening method that narrows the most relevant gas/surface conditions to be studied with greater detail using AP-XPS/LIF.

Next, we will study the oxidation of H_2 over polycrystalline Rh. It is known that this reaction proceeds with time-varying, even oscillatory reactions kinetics. The unproven mechanism is believed to be a feedback between surface oxidation states, which in turn alters the dissociative adsorption rate of gas phase O_2. As the sub-surface oxide is consumed, the adsorption rate of O_2 increases. Once a high enough surface concentration of O is achieved, sub-surface O begins to form, and the sticking coefficient for O_2 again decreases allowing dissociative adsorption of H_2 to again compete. However, there is little direct proof of this proposed mechanism. By combining gas-phase imaging of the reactants and products with surface specific AP-XPS and SFG, we will directly measure whether this is the true feedback mechanism which creates oscillating kinetics for hydrogen oxidation over Rh.

Mechanistic Studies of Oxidative Coupling of Methane In the coming year, we will study a more complex reaction – the oxidative coupling of methane (OCM) – that involves dynamic exchange of intermediates between the surface and gas phase. Although much is known about the reaction mechanism, fundamental details about the feedback between gas-phase and surface reactions remain elusive. It is generally accepted that the first C-H activation step is surface-mediated and is related to the activity of the catalyst. The overall OCM reaction on a metal-doped oxide surface involves (1) activation of the C-H bond

in methane and desorption of •CH_3, (2) coupling of •CH_3 in the gas phase to form C_2 products, and (3) creation of surface oxygen vacancies by water desorption, which are replenished by O_2 dissociation. Although direct evidence is lacking, a wide variety of catalysts are believed to follow this mechanism. In collaboration with UC Davis, we will directly probe the near-surface reactive species and provide fundamental insights into the reaction mechanism. Specifically, we plan to begin our studies with Li-doped MgO powder, owing to the considerable available literature for Li-doped MgO catalysts. We are currently validating a photofragment laser-induced fluorescence method (PF-LIF) for 2-D imaging of CH_3, which does not itself fluoresce. Our goal is fundamental mechanistic understanding, derived from 1) experimental probes of gas-phase species using PLIF and near-surface mass spectrometry, and 2) theoretical investigations of how the modified surface (*i.e.* the active site) controls the nature of the interaction with methane and of the subsequent binding/release of radicals. As described above, we have implemented a new experimental geometry to provide a flow field with well-defined boundary conditions, facilitating easy comparison of our observations with numerical simulations using detailed chemical models (microkinetic modeling). Following these preliminary experiments, studies on OCM are planned in collaboration with UC Davis, using CO_2 and N_2O as oxidizers and ZnO-based catalysts.

CH_3 detection by PF-LIF To better capture the thermochemical state of the gas phase above different catalytic systems, particularly OCM, we propose to expand our diagnostics suite to include *in situ* 2D imaging of the methyl radical, CH_3. Imaging of methyl is challenging since methyl cannot be directly detected by LIF due to strong pre-dissociation of electronically excited states. We are developing the use of a PF-LIF technique that was previously used as a combustion diagnostic in methane flames. Recently, we demonstrated the PF-LIF technique for near-surface methyl imaging in plasmas, as shown in Fig. 4. This is a pump-probe technique in which the pump laser (e.g. 5th harmonic of a Nd:YAG laser at λ=212.8nm) photo-dissociates methyl to form ground state CH($X^2\Pi$) fragments. The probe laser excites laser-induced fluorescence of CH, such as excitation of the B←X(v'=0,v"=0) band near 390 nm, and fluorescence emission from the A→X and B→X(0,1) bands is detected at 420-440 nm. This technique has possible interferences from other photo-induced fragments, and quantitative interpretation of the LIF signal must account for temperature-dependent variations in the CH_3 absorption cross-section, Boltzmann population fractions of the CH(X) fragments, and collisional quenching of the laser excited CH(A). We have developed a calibration method using photodissociation of acetone to produce a known concentration of methyl within the flow reactor. As a verification/calibration of the PF-LIF technique, we can also use our MBMS apparatus to perform complementary measurements of CH_3 concentrations at individual locations in the gases above the catalyst surface under the same experimental conditions. This ability to perform complementary measurements is one of the key advantages of the synergistic diagnostic expertise and capabilities within our team.

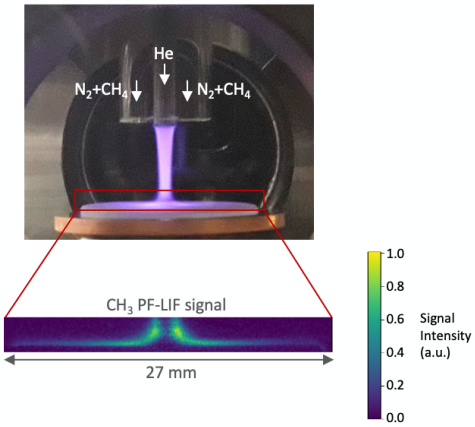

Figure 4: in a nanosecond pulsed plasma jet impinging on a fused silica surface.

Perturbing Catalytic Systems with laser-generated OH radicals We are adding diagnostic capabilities and methods for investigating the response of coupled gas-surface reactions to well-controlled perturbations of the chemistry, such as *in situ* measurements of the temporal response of an *operando* catalyst to a transient perturbation of the gas composition. We use highly repeatable laser photolysis of a precursor molecule in the reactant flow to generate a pulse of reactive species, such as radicals, at a prescribed distance from the catalytic surface.

For the partial oxidation of methanol over a silver catalyst, we perturb the flow by creating a transient pulse of excess OH radicals by photodissociation of H_2O_2 precursor that is seeded into the gas above the catalyst. We then investigate the relative enhancement of formaldehyde production via pure gas-phase reactions and combined gas-surface reactions. To increase the probability of these OH molecules interacting with the catalyst surface before being depleted by gas-phase reactions, we operate the reactor at a total pressure of only a few Torr. The addition of OH sufficiently close to the surface could increase the adsorbed OH and enhance the reaction $CH_3O_{ads} + OH_{ads} \rightarrow CH_2O_g + H_2O$, where the subscripts "$ads$" and "$g$" indicate adsorbed and gas-phase species, respectively. After introduction of additional OH, we will monitor the temporal response of the gas-phase formaldehyde using PLIF imaging.

The interpretation of the results could be complicated by purely gas-phase reactions with OH that also produce formaldehyde. To distinguish between surface-mediated reactions and gas-phase reactions, we will investigate the response to additional OH in an axisymmetric stagnation flow using an inert circular substrate of fused silica that that is coated with a thin film of silver catalyst only on one half. Above the silver-coated portion of the surface, both pathways could contribute to formaldehyde production, but over the fused silica, the response to the OH impulse will be entirely due to gas-phase reactions. The OH-LIF images in Fig. 5 demonstrate the production of a sheet of OH radicals by photodissociation of H_2O_2 using the 5th harmonic of a Nd:YAG laser (λ=212.8 nm). The dissociation laser beam is formed into a horizontal sheet that is parallel to the catalyst surface and can be positioned at different heights above the catalyst. We follow the temporal evolution of the OH as it diffuses and reacts using a probe laser (λ=282 nm) that excites laser-induced fluorescence of OH in the A←X(1,0) band at different time delays relative to the photodissociation laser. The probe laser is formed into a vertical sheet that is parallel to the nozzle axis and perpendicular to the catalyst surface. This pump-probe approach will be used to study the transient production of species such as formaldehyde that are enhanced by interactions of laser-generated OH with the catalyst surface.

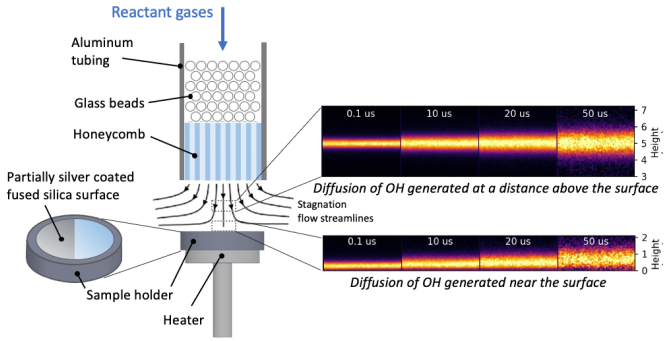

Figure 5: Time series of OH-LIF images shows the diffusion of a sheet of OH radicals following their production by photodissocation of H_2O_2 that is seeded into the reactant mixture. A reactor pressure of 7 Torr was used to increase the width of the OH diffusion layer. The OH can be "written" into the gas flow at different heights above the catalyst surface, as demonstrated by the two sets of LIF images. The OH-LIF signal intensity is normalized by the peak value within each frame. The raw LIF signals decrease with increasing time delay as the OH diffuses and reacts.

BES-sponsored publications, 2019 – present

1) S. A. Steinmetz, A. T. DeLaRiva, C. Riley, P. Schrader, A. Datye, E. D. Spoerke, and C. J. Kliewer, Gas-Phase Hydrogen-Atom Measurement above Catalytic and Noncatalytic Materials during Ethane Dehydrogenation, *J. Phys. Chem. C* **126**, 3054 (2022).
2) S. M. Gurses, T. Price, A. Zhang, J. H. Frank, N. Hansen, D. L. Osborn, A. Kulkarni, and C. X. Kronawitter, Near-Surface Gas-Phase Methoxymethanol is Generated by Methanol Oxidation over Pd-Based Catalysts, *J. Phys. Chem. Lett.*, **12**, 11252 (2021).
3) B. Zhou, E. Huang, R. Almeida, S. Gurses, A. Ungar, J. Zetterberg, A. Kulkarni, C. X. Kronawitter, D. L. Osborn, N. Hansen, and J. H. Frank, Near-Surface Imaging of the Multicomponent Gas Phase above a Silver Catalyst during Partial Oxidation of Methanol, *ACS Catalysis* **11**, 155 (2021).

Citations to Literature

1. Li, B.; Zhang, D.; Yao, M.; Li, Z., Strategy for single-shot CH_3 imaging in premixed methane/air flames using photofragmentation laser-induced fluorescence. *Proc. Combust. Inst.* **2017,** *36* (3), 4487-4495.

GAS PHASE INTERACTIONS WITH OTHER PHASES

David W. Chandler, Farid El Gabaly, Nils Hansen, Christopher J. Kliewer, Laura M. McCaslin, Habib N. Najm, David L. Osborn, Leonid Sheps and Craig A. Taatjes
Combustion Research Facility, Sandia National Labs, Livermore, CA 94550

chand@sandia.gov, felgaba@sandia.gov, nhansen@sandia.gov, cjkliew@sandia.gov, lmmccas@sandia.gov, hnnajm@sandia.gov, dlosbor@sandia.gov, lsheps@sandia.gov, cataatj@sandia.gov

PROGRAM SCOPE

This research program encompasses experimental and computational investigations of a wide range of multiphase phenomena, investigating the formation of particulates in gas-phase reaction systems, measuring and modeling the gas-phase processes at reactive interfaces and probing the physical and chemical interactions between phases. Understanding reactions that lead to particle formation and calculating surface reactions draw on work in the Sandia "Chemical Kinetics for Complex Systems" task, and experiments employ innovations from the "Ultrafast Physics: Nonlinear Optical Spectroscopy and Diagnostics" and "Advanced Mass Spectrometry and X-Ray Diagnostics" tasks. Recent emphasis is on chemically controlled gas-to-particle conversion; proposed new directions will extend work into understanding the interactions of gas-phase molecules with liquid and solid surfaces. These initiatives complement the catalytic surface investigations in Sandia's "Imaging the Near-Surface Gas Phase" program.

RECENT PROGRESS

Ion imaging above reactive surfaces We continue to investigate the possibility to use the near-surface gas-phase as a local reporter of surface chemical activity. In a unique approach, we are using resonance enhanced multiphoton ionization to detect catalytic products during gas-surface reactions and spatially imaging the location of where the ions are formed to learn about the catalytic activity of the sample just below the laser focus. In a first experiment, two pulsed valves are used to adsorb H_2 and D_2 onto a surface heated to 400 K with 1 mm wide strips of platinum 3 mm apart. The sample had been prepared by vapor deposition of the Pt onto a gold surface through a mask with a Pt thickness of ~100 nm. We then use 202-nm light to perform 2 +1 resonantly enhanced multiphoton ionization (REMPI) of HD (in J=4) directly above the surface. The apparatus has been described in the Advanced Diagnostic abstract to this meeting. In the left panel of figure 1, the image of the focused laser-line as it passes across the surface is observed. This image results from ions generated in the laser focus that are accelerated through the velocity-selecting pinhole at the VMI plane, and then detected at the MCP/phosphor screen at the spatial image plane of the ion optics. The local concentration of the HD products is imprinted on the profile observed on the detector. There is however some background impurity HD gas introduced with the D_2 gas so this must be subtracted from the signal, as shown in the right panel of the figure. In order to do this, we tune the laser to a REMPI transition of the D_2 molecule and record a profile of background D_2 gas (the amount of D_2 gas injected into the apparatus swamps any D_2 that is formed on the surface). Since this concentration profile is, in principle, uniform throughout the probed region, this serves as a background measurement of the image transmission efficiency through the velocity-selecting pinhole and differences in laser intensity through the focal region. By subtracting the normalized signal of D_2 from the normalized signal obtained on the HD line, the difference spectrum shows dramatically enhanced HD production localized over the Pt strip, with an apparent hot spot of catalytic turnover in this polycrystalline sample. Each image was averaged for 15 minutes at 30 Hz laser repetition rate. By moving the laser focus horizontally, we are able to obtain profiles on different parts of the sample. Moving the laser focus horizontally by a known distance and watching the

image movement on the CCD enables us to experimentally obtain the magnification for the microscope. Our present apparatus has ~10-micron resolution, as determined by the line-spread function of the focused laser beam image. While only a preliminary demonstration of this idea, this compelling evidence for the ability to image local catalytic activity through velocity selected REMPI ion spatial imaging demonstrates a critical step forward.

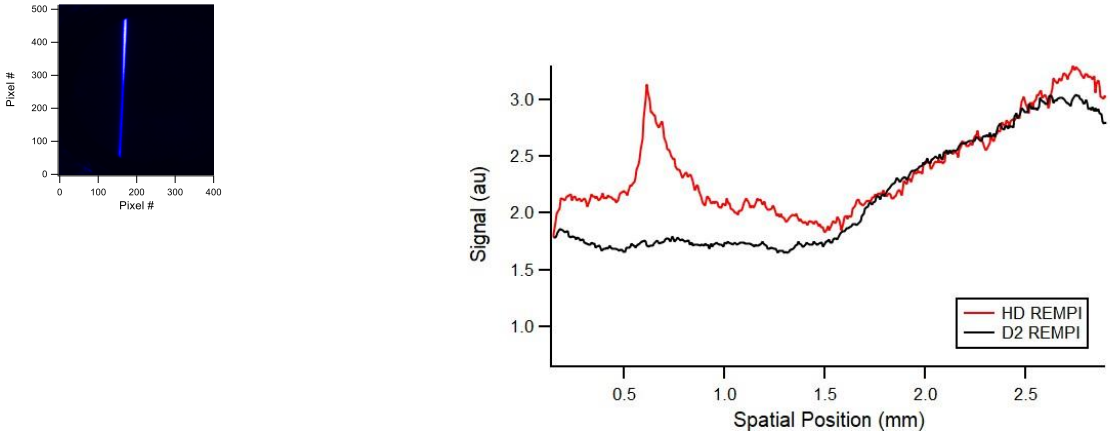

Figure 1. (Left Panel) Image collected on the intensified CCD camera of spatially imaged and velocity selected ions generated by focusing a ~202 nm (2+1) REMPI laser beam over a patterned Pt surface bombarded by H_2 and D_2 molecular beams. Both time gating of the MCP/Phosphor screen and tuning of the resonance wavelength, the instrument readily discriminates between arrival of D_2, H_2, and HD cations. (Right) Difference in normalized REMPI intensity along the laser line by simply tuning the laser from D_2 (J=4) to HD (J=4) reveals enhanced HD production over a Pt strip situated near the 1 mm position of the image.

Soot Nucleation Soot nucleation in flames is extremely challenging to model on a fundamental basis, and chain reactions may contribute to the formation of nucleation initiators. It was proposed that radical-radical chain reactions provide a route to rapid hydrocarbon growth in both low- and high-temperature environments in a mechanism termed CHRCR (clustering of hydrocarbons by radical chain reactions). We used a silicon carbide tubular reactor that at low pressures of a few Torr was resistively heated up to 1600 K at its hottest point and an electron ionization time-of-flight mass spectrometer to probe the products of the phenyl + benzyl reaction as a function of temperature. This reaction is a good candidate for a chain reaction because the closed-shell adduct, diphenylmethane (Ph_2CH_2), has a sp^3-hybridized carbon that prevents full conjugation. We experimentally observed the radical-radical chain reaction of phenyl and benzyl radicals to form the Ph_2CH radical by prompt, well-skipping H-atom loss. The chain reaction continues when Ph_2CH associates with phenyl radicals to form Ph_3CH and Ph_3C. This direct observation of a radical chain reaction supports the CHRCR mechanism where radical-radical recombination is followed by rapid H loss to produce larger aliphatically bridged RSRs without decreasing the radical pool.

In subsequent work, we used controlled pyrolysis in the same microreactor to isolate and examine the role of well-skipping channels in the phenyl+propargyl radical-radical reaction at temperatures of 800-1600 K and pressures near 25 Torr. The temperature and concentration dependence of the closed-shell (C_9H_8) and radical (C_9H_7) products agree well with a simulation of the reactor employing a skeleton chemical mechanism based on recent rate coefficient calculations (done in collaboration with Kukkadapu at LLNL). In contrast, eliminating the well-skipping reactions from the chemistry mechanism causes a substantial discrepancy in the temperature dependence of the radical concentration, revealing that the well-skipping pathways, especially to form indenyl radical, are significant at temperatures of 1200 K and higher. An additional simulation of the present reaction near atmospheric pressure shows that the well-skipping

channel only contributes around 3% of the C_9H_7 yield at atmospheric pressure, while being the dominant source of C_9H_7 at 25 Torr, thus indicating a negligible role of the well-skipping pathways at atmospheric and higher pressures.

Developing Tools to Detect the Vibrational Signatures of Ice Nucleation at the Surface of Sea Spray Aerosols Techniques for analyzing IR spectra, described in the Chemical Dynamics task, have been applied to studies of the spectral signatures of ice nucleation at aerosol interfaces. Atmospheric ice nucleation greatly impacts precipitation, radiative forcing, and climate, especially in colder regions of the atmosphere. Over remote oceans in the Southern atmosphere, sea spray aerosol (SSA) particles play a large role in ice nucleation, though these are not correctly accounted for in global climate models. Investigation into the role of monolayer composition at the surface of SSA's has shown that long-chain alcohol monolayers efficiently nucleate ice, though long-chain fatty acids, short-chain fatty acids, and polysaccharides are also active in ice nucleation. Infrared Reflection-Absorption Spectroscopy (IRRAS) was performed in the group of Heather Allen (Ohio State) on water surfaces covered in a monolayer of long chain alcohols and carboxylic acids at 21 ℃ and 1 ℃. Corresponding theoretical studies of the vibrational structure of the first solvation shell around carboxylic acid and alcohol model systems were performed using *ab initio* molecular dynamics (AIMD). Propanol + $6H_2O$ and propionic acid + $10H_2O$ are investigated in detail at the temperatures studied experimentally. These model studies successfully predicted the energetic and intensity shifts in the OH stretching regions corresponding to the first solvation shell surrounding the carboxylic acid and alcohol.

Competition between Cl^- Substitution and Hydrolysis of N_2O_5 at the Surface of Sea Spray Aerosols Recent studies in collaboration with R. Benny Gerber's group (Hebrew University, UC Irvine) and Mark Johnson's group (Yale) indicate that nitrogen oxide species in the atmosphere, including N_2O_5 and $ONONO_2$, undergo a new class of S_N2-type substitution reactions when in contact with seawater and sea spray aerosols. The competition between halide substitution and hydrolysis reactions of nitrogen oxides has major implications for the levels of molecules such as O_3, OH, Cl, and CH_4, thus directly affecting radiative forcing and global climate. In order to study the competition between halide substitution and hydrolysis of nitrogen oxides, we've developed theoretical model systems of the type $N_2O_5 + Cl^- + nH_2O$ (n=1-5) and studied the barriers to reaction using high-level electronic structure methods (FNO-DF-CCSD(T)/cc-pVDZ). We have additionally performed *ab initio* molecular dynamics (AIMD) calculations to unravel the mechanisms and timescales of the competing reactions. In model studies of the cluster $N_2O_5 + Cl^- + nH_2O$, we determine that when Cl^- is close to N_2O_5, Cl^- substitution is a fast reaction. However, $ClNO_2$ is unstable on longer timescales, reacting with H_2O to form HNO_3. For clusters n=2-5, mechanisms for the formation of HNO_3 from the direct attack of H_2O on N_2O_5 were identified, but found to be inhibited by the presence of a nearby Cl^-. Formation of HNO_3 from N_2O_5 is more likely to occur in a two-step mechanism through a $ClNO_2$ intermediate when Cl^- is within a few Å of N_2O_5.

Kinetic Monte Carlo for surface kinetics We have worked on development of an improved time integration strategy for kinetic Monte Carlo (KMC) computations of stiff surface kinetics. Our target has been to enable efficient modeling of fast processes in a manner that accounts for the dynamical character of the system. Our framework extends the "tau-leaping" strategy whereby processes faster than some given time scale τ are approximated, while the rest are resolved accurately. We formulated an approach that determines τ adaptively in time and are in the process of empirically evaluating its performance. We are doing this using a CO oxidation surface catalysis model, where we are empirically comparing the performance of different tau-leaping strategies versus the standard stochastic simulation algorithm (SSA) for KMC.

Assessment and physicochemical properties of gasified electrocatalytical radicals We performed preliminary experiments to study phenomena of electrocatalytic intermediates (electro-radicals) in the gas phase. The production of these out-of-equilibrium, efficient radicals, which have never before been

observed in the gas phase, have the potential to become useful for methane and CO_2 capture and chemical conversion, directly in the gas phase.

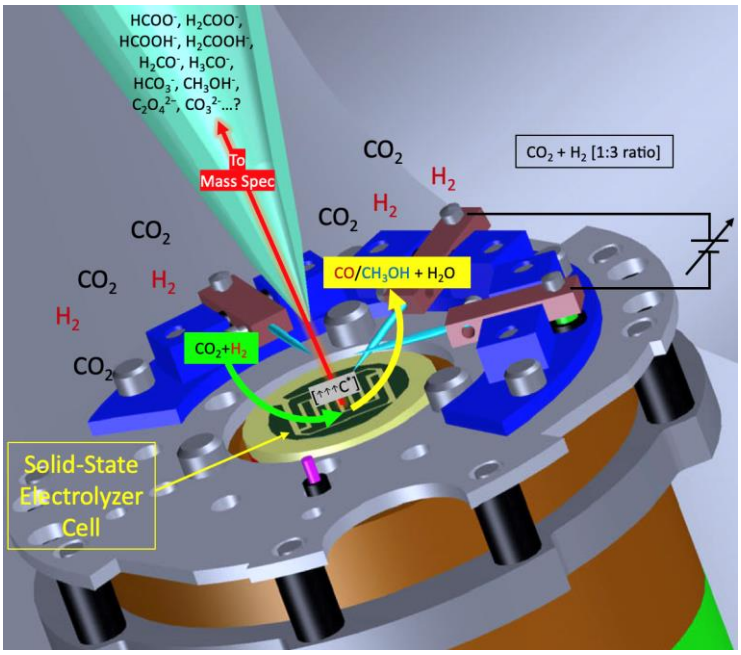

Figure 2: Experimental setup for the characterization of volatilized surface intermediates using mass spectrometry. As an example, the schematic represents the sampling of intermediates in the electrochemical CO_2 hydrogenation by a solid-state electrolyzer cell.

In our experiments, we used a custom-designed solid-state electrolyzer cell at overvoltage conditions in an electrochemical holder we have created for high-temperature electrocatalysis (Fig. 2). The experiment creates a supersaturation condition at the electrode/electrolyte interface, leading to excess electro-radicals on the surface. After desorption from the surface, they were detected with mass spectrometry. We have also fabricated the special thin-film solid-state electrolyzer cells. We are currently finalizing the assembly of all the experimental parts. As a model reaction, we used gas mixtures combining CO_2 and H_2 over symmetric M/YSZ/M (M = Ni, Pt, Ce) solid oxide electrolyzers to identify the key electro-radicals that can be volatilized and isolated for CO_2 capture and clean H_2 production. We have completed exploratory measurements and the data is awaiting detailed analysis.

PROPOSED WORK

Kinetic Monte Carlo for surface kinetics We will finalize testing and evaluation of our adaptive tau-leaping strategy for KMC computations of stiff surface kinetics. The key figure of merit is accurate estimation of the dominant features of the mean system response, particularly as regards the surface dynamics of species dominated by slow time scales. We will also evaluate the retrieval of salient features of the fast dynamics when the system is reverted to detailed SSA time integration at any point in time. We also plan to examine the dynamical strategy for adaptive τ estimation in terms of its relevance in general ordinary differential equation systems and compare results with those available from computational singular perturbation of the system response.

Femtosecond nonresonant ionization spatial ion microscopy As described above, in the previous year we have developed and demonstrated a unique approach for the direct imaging of the spatial distribution of catalytic desorption of products into the gas phase through velocity selecting a subgroup of products at the VMI plane prior to expansion of the spatial image onto the MCP/phosphor screen detector. Time-gating of the MCP allows for isolation of individual products based upon the ion time of flight to the detector, which is of course highly mass specific. We first demonstrated this in a simple cell with two crossed molecular beams of H_2 and D_2 monitoring for increased production of HD. In the coming year, we will move to more exciting chemical reactions. One specific reaction, which is the focus of increased effort under our core Gas-Surface FWP, is the reaction of H_2 and O_2 to form H_2O over Platinum catalysts. Recent work has revealed that, while this is the oldest studied catalytic reaction, much remains unknown about the detailed

mechanism. One key question includes whether a special surface site exists at step edges that promotes the H* + O* -> *OH elementary step, as DFT calculations predict an energy barrier far higher than what is apparent from experiments. By implementing a curved crystal of Pt, where step densities are continuously varied across the surface, we can image the production of H_2O locally with this new approach. We will use this to obtain a map of local reaction rate as a function of step density. Two crossed molecular beams will provide the H_2 and O_2 surface coverage. If successful, not only will this begin to yield answers to age-old questions in gas-surface chemistry through direct probing of the gas phase speciation but will further develop our approach. Femtosecond nonresonant ionization is a ubiquitous ionization approach, while mass selective time-gating of the signal allows for the time- and spatially- resolved probing of specific products. Key to the success of this approach will be gaining an understanding of dissociation rates of the parent ion following "soft" femtosecond ionization.

Gas-liquid scattering In collaboration with the group of Prof. Ken McKendrick of Heriot Watt University in Scotland we will study the scattering of OH radicals from liquid surfaces that contain highly oxygenated species as these are surrogate molecules for those believed to populate the outside surface of aerosol particles. Highly oxygenated species have been a focus of the ignition chemistry studied in this program and are also important in atmospheric nucleation and growth of aerosols. In collaboration with the McKendrick group we will select species that have highly oxygenated groups but low vapor pressure to be studied in vacuum with reactive molecular beam scattering. The quantitative scattering measurements allow one to correlate the sticking/reaction cross section of the OH radical with the molecular constituents of the surface molecules. As OH radicals are the major radical in the atmosphere, their chemistry with the surface of aerosols is expected to effect aerosol growth and properties. Prof. McKendrick has built a second-generation apparatus to form a molecular beam of OH radicals and scatter them from a rotating pinwheel whose surface is covered with a low-vapor-pressure liquid. His apparatus uses laser induced fluorescence of the OH radical to image the scattering. We will explore ways to include quantitative Velocity Mapped Imaging to Prof. McKendrick's apparatus in order to enhance the number of species that can be detected.

Molecular weight growth and particle inception Particle formation in extreme environments remains an intriguing phenomenon that covers a broad range of physical-chemistry aspects. In a simplified scheme, chemical reactions in the gas phase lead to polycyclic aromatic hydrocarbons (PAHs) and, following the transition from gas-phase species to solid particles, the so-called particle inception, multi-phase surface growth reactions and physical coagulation become important. The recently proposed CHRCR mechanism (clustering of hydrocarbons through radical chain reactions) inspired new efforts to measure kinetic rate coefficients and branching fractions for radical chain propagation reactions (see above). We will continue to investigate the role resonance stabilized radical-radical reactions in molecular-weight growth processes leading to particle inception in high-temperature conditions.

Both, phenyl and cyclopentadienyl radicals have received some attention in the kinetics community, however, recombination reactions of these radicals have not been studied. Rather than simply forming a stable adduct, the $C_6H_5 + C_5H_5$ reaction can lead to non-Boltzmann "well-skipping" H-loss to form the phenylcyclopentadienyl delocalized radical (C_6H_5-C_5H_4). We will collaborate with Kukkadapu (modeling, LLNL) and Jasper (theoretical kinetics, ANL) to test this reaction using dilute flash pyrolysis at 30 Torr. Of particular interest are the three competing decay pathways of the C_6H_5-C_5H_4 product following ring-opening: H-loss, C_3H_3-loss, and C_2H_2-loss. The latter pathway is of particular interest as it ultimately leads to indene. Insights into the formation chemistry of cyclopenta-fused PAHs (such as indene) might be important for understanding the formation of non-planar bowl-shaped PAHs.

While a set of important reactions evolves for molecular-weight growth processes, a detailed understanding has not been achieved for the chemistry and physics of the particle inception step and several hypotheses are awaiting experimental validation and are still discussed controversially. Aliphatically bridged aromatic molecules and cross-linked PAHs have received considerable attention and we plan to extend our work on the high-temperature molecular weight growth that approaches inception of soot particles by studying the chemistry of propyl- and butyl-substituted aromatic species with an emphasis on the competition between

decomposition and growth of the side-chain and cyclization followed by dehydrogenation reactions. We plan to implement the tandem mass spectrometric detection with the newly designed atmospheric pressure photoionization source (see Advanced Diagnostics abstract). This capability will allow inference of structural information for larger molecules and will allow visualization of the growth processes as a function of the temperature. For unraveling the importance of various species in the particle nucleation and growth processes, a rigorous comparison between gas-phase and particle phase will be necessary. To this end, we propose to combine our experimental set-up with an aerosol mass spectrometer, to sample small particles and to determine their average chemical composition.

Publications acknowledging support from this project 2019 – 2022

1. David E. Couch, Goutham Kukkadapu, Angie J. Zhang, Ahren W. Jasper, Craig A. Taatjes, Nils Hansen, "The role of radical-radical chain-propagating pathways in the phenyl + propargyl reaction," *Proc. Combust. Inst.*, accepted for presentation (2022).
2. Hope Michelsen, Emeric Boigné, Paul E. Schrader, K. Olof Johansson, Matthew F. Campbell, Ray P. Bambha, and Matthias Ihme, "Jet-entrainment sampling: A new method for extracting particles from flames," *Proc. Combust. Inst.*, accepted for presentation (2022).
3. James A. Rundel, Charlotte M. Thomas, Paul E. Schrader, Kevin R. Wilson, K. Olof Johansson, Ray P. Bambha, and Hope A. Michelsen, "Promotion of particle formation by resonance-stabilized radicals during hydrocarbon pyrolysis," *Combust Flame*, https://doi.org/10.1016/j.combustflame.2021.111942 (2022)
4. M.G. Vazquez de Vasquez, K.A. Carter-Fenk, L.M. McCaslin, E.E. Beasley, J.B. Clark, and H.C. Allen, "Hydration and Hydrogen Bond Order of Octadecanoic Acid and Octadecanol Films on Water at 21 and 1°C", *J. Phys. Chem. A*, 125, 10065 (2021).
5. David E. Couch, Angie J. Zhang, Craig A. Taatjes, and Nils Hansen, "Experimental Observation of Hydrocarbon Growth by Resonance Stabilized Radical-Radical Chain Reaction", *Angew. Chem. Int. Ed.* **60**, 27230-27235 (2021).
6. S. Mitra, N. Yang, L.M. McCaslin, R.B. Gerber, and M.A. Johnson, "Size-Dependent Onset of Nitric Acid Dissociation in $Cs^+(HNO_3)(H_2O)_{n=0-11}$ Clusters at 20K", *J. Phys. Chem. Lett.*, 12, 3335 (2021).
7. N. Hansen, B. D. Adamson, S. A. Skeen, and M. Ahmed, "Nucleation of Soot: Experimental Assessment of the Role of Polycyclic Aromatic Hydrocarbon (PAH) Dimers," *Z. Phys. Chem.* **234**, 1295-1310 (2020).
8. Q. Wang, P. Elvati, D. Kim, K. O. Johansson, P. E. Schrader, H. A. Michelsen, and A. Violi, "Spatial dependence of polycyclic aromatic compound growth in counterflow flames", *Carbon* **149**, 328-335. (2019).

ULTRAFAST CHEMISTRY: PROBES OF NON-ADIABATIC DYNAMICS

Krupa Ramasesha, Laura M. McCaslin, Christopher J. Kliewer, Nils Hansen
Combustion Research Facility, Mail Stop 9055; Sandia National Laboratories, Livermore, CA 94550
kramase@sandia.gov, lmmcas@sandia.gov, cjkliew@sandia.gov, nhansen@sandia.gov

I. Program Scope

This program aims to apply ultrafast spectroscopy and theoretical calculations to investigate fundamental gas-phase chemical dynamics. Our research uses diverse experimental probing techniques to follow coupled electronic and nuclear motion on femtosecond to picosecond timescales in gas-phase molecules, as well as advanced quantum chemical calculations to investigate these dynamics and predict experimental observables. The coupling of electronic and nuclear degrees of freedom, representing a breakdown of the Born-Oppenheimer approximation, gives rise to complex pathways for non-radiative energy dissipation in electronically excited molecules, often involving participation of multiple electronic states. Identifying the motions that couple electronic states, the timescales and dynamics of excited state population relaxation, and the role of coupled vibrational modes of a molecule in guiding energy flow is crucial to our understanding of non-equilibrium dynamics, and it forms the mainstay of this program. The work in this task has strong connections to the laser spectroscopy investigated under the "Ultrafast Physics: Nonlinear Optical Spectroscopy and Diagnostics" task, and the high photon-energy techniques developed in the "Advanced Diagnostics" task. This task extends the "Chemical Dynamics Methods and Applications" work down to the fundamental timescales of vibrational and electronic motion. *Ultrafast Chemistry* is one of the synergistic research themes of CSGB and this work addresses two key aspects of the Grand Challenges for Basic Energy Sciences: (1) investigating the nature of electronic excited states, and (2) exploring the breakdown of the Born-Oppenheimer approximation.

II. Recent Progress

Photodissociation dynamics of nickel tetracarbonyl at 261 nm and 197 nm: Like other first-row transition metal carbonyls, UV irradiation of nickel tetracarbonyl [$Ni(CO)_4$, NT] results in the excitation of the metal-to-ligand charge transfer (MLCT) state, leading to the rapid elimination of multiple CO groups from NT. However, owing to a full *d* orbital and, consequently, the lack of metal-centered d→d ligand-field transitions, the valence electronic structure and excited state dynamics of NT are distinct from other first-row transition metal carbonyls. To understand the mechanism for CO elimination in NT, we performed ultrafast UV pump—IR probe spectroscopy, probing the evolution of the C≡O stretching frequency in nickel carbonyls following 261 nm excitation. These experiments were performed in conjunction with high-level electronic structure theory to unravel photodissociation mechanisms and assign spectral features. Previous time-resolved studies using non-resonant multiphoton ionization probing following 266 nm excitation suggested purely sequential dissociation within the singlet manifold to ultimately form $Ni(CO)_2$, with the first CO loss happening on a 600 fs timescale and the second CO loss occurring

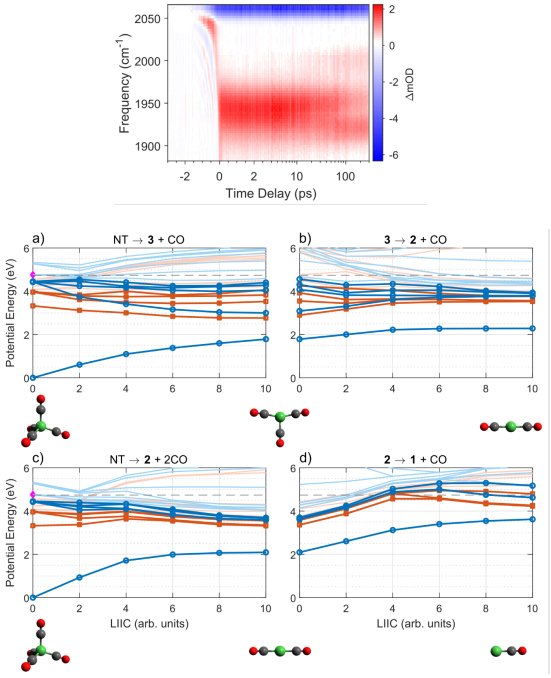

Figure 1: (top) Transient infrared spectra of gas phase NT following 261 nm excitation. (bottom a-d) Potential energy cuts along different dissociation coordinates; singlet surfaces are shown in blue and triplet surfaces are shown in orange. Dashed horizontal line is the 261 nm photon energy.

on a 55 ps timescale.[1] Our transient infrared spectra obtained after 261 nm excitation (Figure 1) reveal dynamics occurring on <160 fs, 600 fs, 15 ps and 90 ps timescales; we attribute the 600 fs and 90 ps time constants to the primary and secondary CO loss during sequential dissociation, and the <160 fs and 15 ps time constants to concerted dissociation involving intersystem crossing (ISC) to ultimately form Ni(CO). These interpretations were informed by potential energy cuts (Figure 1) along dissociation coordinates as well as calculations of ISC rates using EOM-CCSD, which reveal (a) energetically favorable concerted dissociation, (b) high density of electronic states, and (c) several singlet-triplet crossings with large spin orbit coupling constants. Comparison of experimental and calculated excited state vibrational frequencies using TD-DFT allowed qualitative assignment of spectral features. Our work thus shows that the photodynamics in NT are far more complicated than the relatively simple frameworks used previously.

There has been no prior work on NT photodissociation dynamics following excitation near 200 nm. Our ultrafast infrared spectra after 197 nm excitation of NT exhibit broad, featureless transient spectra at early time delays suggesting fast dynamics and probably several competing dissociation pathways. A feature at 2000 cm^{-1}, which likely corresponds to the C≡O stretching vibration of Ni(CO), appears at time delays as early as 200 fs, suggesting that excitation at this higher photon energy can lead to ultrafast, possibly concerted, elimination of at least three CO groups from NT. Quantum chemical calculations including *ab initio* molecular dynamics simulations, currently underway, promise to shed light on the sub-picosecond excited state dynamics that initiate the pathway towards forming Ni(CO).

Ultrafast photodissociation of dimethyl disulfide: Dimethyl disulfide (DMDS, CH_3SSCH_3) is a model system for the disulfide (S–S) bond, an important moiety in protein structure. Despite its central role in maintaining the structural integrity of proteins, the disulfide bond is photolabile with several electronic excited states proposed to be dissociative along the S–S and C–S bonds. Photodissociation studies on the first excited state, $S_1(n\sigma^*_{S\text{-}S})$, of DMDS have found exclusive S–S bond fission.[2] However, relatively little work has been done on the photochemistry of the higher lying electronic excited states near the DMDS absorption maximum at 195 nm, where early nanosecond experiments suggested cleavage of C-S and S-S bonds.[3] We performed ultrafast electron diffraction (UED) at the SLAC MeV-UED facility to probe the competing pathways in the ultrafast photodissociation of DMDS following 200 nm excitation. Results show prompt appearance of negative signal at 2 Å and 3 Å interatomic distances (Figure 2), corresponding to the loss of C-S/S-S distances and the second-nearest neighbor C---S distances, respectively. This prompt response is followed by subtle evolution on a 1 ps timescale at interatomic distances of ~2.6 Å. These photochemical pathways are being analyzed using genetic algorithm fitting. The S-S and C-S dissociation pathways have been characterized via one-dimensional cuts through the ground and excited state potential energy surfaces using EOM-CC methods, with TD-DFT *ab initio* molecular dynamics simulations currently underway to understand the origins of the 1 ps timescale. We are also collaborating with Vasilios Stavros for performing ultrafast photofragment velocity-mapped imaging of the CH_3 fragment to spectroscopically characterize this dissociation. Future studies will use electronic state-sensitive ultrafast soft X-ray transient absorption spectroscopy near the S L-edge and C K-edge following 200 nm excitation, in order to monitor excited state electronic dynamics.

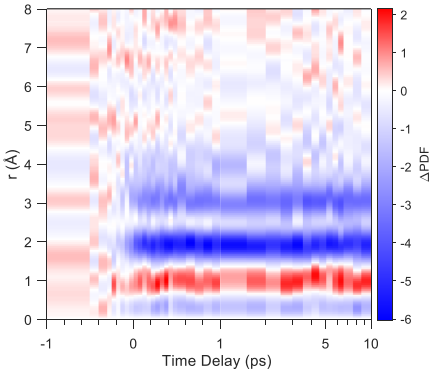

Figure 2: Evolution of the pair distribution function with respect to pump-probe time delay and interatomic distance following 200 nm excitation of dimethyl disulfide.

Excited state dynamics of iron pentacarbonyl: It is well known that UV excitation of gas phase iron pentacarbonyl [IP, $Fe(CO)_5$], a prototypical organometallic system, causes rapid elimination of CO groups. The sequential mechanism of CO elimination following 266 nm excitation has been studied previously, including our own work using ultrafast UV pump—IR probe spectroscopy. However, the evolution of the electronic structure on sub-100 fs or even sub-picosecond timescales after excitation is unknown, as there have been no experimental studies that spectroscopically monitor electronic dynamics on these short time scales. A 266 nm photon excites the 1^1A_2" MLCT state; rapid internal conversion from the initially excited MLCT state to lower lying metal-centered ligand-field states is said to play a role in the dissociation of the Fe-C bonds. We have performed ultrafast core-to-valence transient absorption spectroscopy near the Fe $M_{2,3}$ edge (3p-to-valence transitions) to study these excited state dynamics in IP. Transient XUV spectra (Figure 3) show a bleach signal at 61 eV due to depletion of ground state IP, and induced absorption features at 65 eV, 59 eV and 54 eV. Whereas the 59 eV feature appears immediately following excitation, the 54 eV feature grows in on a few-picosecond timescale; these features are likely associated with excited states of smaller iron carbonyls formed after CO loss. The 65 eV feature, on the other hand, has a short ~100 fs decay component, which may be attributable to electronic excited states involving distorted IP prior to bond dissociation. Current efforts are dedicated to theoretically predicting core-level transitions to aid in interpreting experimental results, with particular emphasis on the short time dynamics.

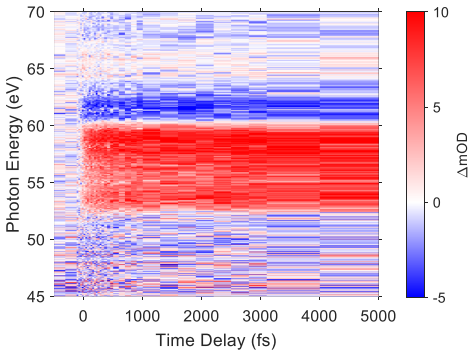

Figure 3: Transient XUV absorption spectra of IP following 266 nm excitation.

Photodissociation dynamics of acetyl iodide: Ketones and aldehydes typically display Norrish Type-I cleavage of the α C-C bond following electronic excitation to the $^1n\pi^*$ state. This bond dissociation is said to happen following intersystem crossing to a nearby $^3n\pi^*$ state. In acetyl halides [CH_3-C(O)-X; X=halogen atom], however, despite the C-X and C-C bonds having comparable strengths, the C-X bond is known to break first. Furthermore, in acetyl iodide [CH_3-C(O)-I, AcI] specifically, photofragment translational spectroscopy studies have suggested that both the primary C-I bond dissociation in AcI and the secondary C-C bond cleavage of the acetyl radical happen on ultrafast timescales.[4] To understand the excited state electronic dynamics for both the primary and secondary dissociation processes, we are performing ultrafast core-to-valence transient absorption spectroscopy via the I 4d-to-valence transitions (for the primary dissociation) and the C 1s-to-valence transitions (for the secondary dissociation), in conjunction with electronic structure theory and *ab initio* molecular dynamics simulations. Our experimental results (Figure 4) show fast formation of both ground state and spin-orbit excited I atoms following 266 nm excitation. In addition, we see transient spectral features that evolve with a <100 fs time constant, likely corresponding to excited state wavepacket evolution in AcI prior to C-I bond dissociation. Theoretical work to compute excited state potential energy surfaces, perform *ab initio* molecular dynamics simulation for understanding the <100 fs wavepacket evolution, and calculate core-level spectra for interpreting the experimental results, is currently underway.

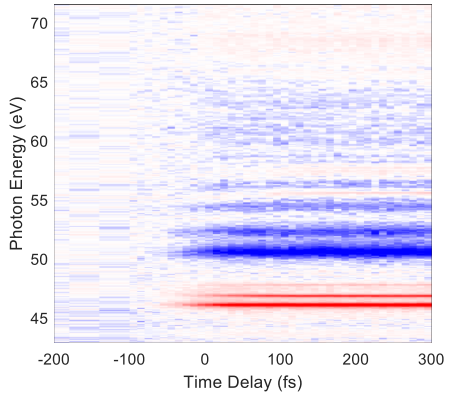

Figure 4: Transient XUV absorption spectra of AcI following 266 nm excitation.

III. Future Work

Photoisomerization and ring-opening in 1,3,5-triazine: Knowledge of the photochemistry of aromatic heterocycles, such as pyridine and pyrimidine, is crucial to a bottom-up understanding of the photostability of these fundamental building blocks of life. In particular, the role of conical intersections (CIs) in the non-adiabatic dynamics of these heterocyclic rings has been the subject of intense study for several decades. While the photochemistry of pyridine and pyrimidine has been well studied, the related system 1,3,5-triazine (*c*-$C_3H_3N_3$, *sym*-triazine, ST) has received less attention. ST is both an important model biochromophore and is a prototypical example of three-body dissociation dynamics. Photodissociation of ST only occurs following internal conversion (IC) to the ground electronic state, with conflicting evidence for synchronous *vs*. asynchronous concerted three-body dissociation mechanisms. Also, there is limited information on the ST structural changes that accompany IC. The only time-resolved study of ST used mass spectrometry to follow the evolution of ST^+ yield after photoexcitation at 277 nm.[5] This study reported decay time constants of <200 fs and ~100 ps, implying rapid excited state isomerization, with no experimental evidence for the structural evolution presented. Subsequent computational work on ST has instead suggested a ring-open pathway to return to the ground electronic state.[6] Conversely, recent MeV-UED work[7] on the related system pyridine has suggested a ring-pucker CI, which facilitates excited state population transfer back to the ground electronic state—such ring-puckering dynamics play an important role in the excited state relaxation of biologically relevant aromatic heterocycles. To understand the excited state structural dynamics and the role of photoisomerization versus ring-open intermediates in ST, we have been awarded beam time at SLAC's MeV-UED facility to perform ultrafast electron diffraction following 266 nm excitation in June 2022. Our predicted differential scattering intensities and pair distribution functions suggest that the ring-closed intermediates (Hückel, Dewar and ring-puckered structures) can be clearly distinguished from the ring-open intermediate and the three-body dissociation products.

***Treatment of Non-Adiabatic Effects in Systems with a High Density of Electronic States*:** Accurately treating non-adiabatic effects in molecular dynamics involving a dense manifold of electronic states is a well-known problem in chemical theory. The Born-Oppenheimer (BO), or adiabatic, approximation breaks down at molecular configurations such that two or more potential energy surfaces are close in energy. In mixed quantum-classical (MQC) dynamics, a molecular system's energy and nuclear forces are calculated on ground and excited state BO surfaces using quantum chemistry methods, allowing for the time propagation of the nuclear coordinates using Newton's equations of motion. Two of the most common methods for treating non-adiabatic effects in MQC dynamics are fewest-switches surface hopping (FSSH)[8] and Ehrenfest dynamics.[9] FSSH methods are stochastic in nature and "hop" between surfaces over the course of a trajectory, causing significant inefficiencies in systems with a high density of electronic states, including those with many quasi-degenerate states. Ehrenfest dynamics, on the other hand, allows for trajectories to propagate on a weighted average of potential energy surfaces, which can result in unphysical chemical behavior if the surfaces diverge in character. In order to balance accuracy and computational efficiency, we are interested in combining these approaches to create a hybrid scheme that treats quasi-degenerate states as one weighted average potential (Ehrenfest) and allows for the system to "hop" (FSSH) between these weighted average potentials. We will compare our techniques with high-accuracy quantum dynamics simulations to test the limits of this hybrid approach, including how to combine surfaces and their weighting schemes.

Probing cyclic azide formation: The azide radical (N_3) is the smallest polynitrogen compound and its $^2\Pi_g$ ground state has been quite extensively studied experimentally and theoretically. Other stationary points also exist on the ground doublet surface of N_3, the most remarkable being a *cyclic*-N_3 ($^2B_1$) minimum, 30.3 kcal mol^{-1} above the $X\,^2\Pi_g$ state. *cyclic*-N_3 is an interesting molecule: It is a stable isomer needing 33.1 kcal mol^{-1} of energy to dissociate into $N(^2D)$ + N_2 ($X\,^1\Sigma_g^+$) and 31.9 kcal mol^{-1} to overcome the barrier for isomerization to *linear*-N_3. There is accumulating experimental evidence concerning the formation of the

cyclic-N_3 by photolysis of a suitable precursor.[10] Wodtke and coworkers observed the formation of N_3 products from ClN_3 photodissociation using velocity map ion imaging and photofragment translational spectroscopy. Synchrotron-based experiments revealed an ionization energy of the high-energy form of N_3 0.4-0.5 eV below the ionization of 11.06(±0.01) eV of the *linear*-N_3,[11] in agreement with *ab initio* calculations of 10.595 eV for the *cyclic*-N_3.[12] We are interested in applying ultrafast electron diffraction for probing the structural evolution to *cyclic*-N_3 following UV photolysis of ClN_3, from the initial photodissociation to the isomerization of the N_3 radical to the cyclic conformation.

Three-body photodissociation of thionyl chloride: Since its observation in acetone, photo-induced three-body dissociation has been discovered in several small gas phase molecules. One example is thionyl chloride (TC, $SOCl_2$), which serves as an ideal testbed for investigating non-adiabatic processes in three-body dissociation using soft X-ray transient absorption. TC's ultraviolet absorption spectrum shows two discernable features: a strong absorption that peaks at wavelengths less than 200 nm, and a shoulder centered at 250 nm. These features are assigned to partially overlapping electronic transitions, $n_s \rightarrow \sigma^*_{SCl}$ and $n_s \rightarrow \pi^*_{SO}$ at longer wavelengths and similar transitions originating from the lone pair on the Cl atoms at shorter wavelengths. Three dissociation schemes (two-body molecular, two-body radical and three-body radical channels) have been identified for this molecule.[13-15] However, several open questions remain about this system. Particularly, is the three-body dissociation channel asynchronously concerted or sequential? How do the fragmentation mechanisms and timescales vary with excitation energy? What are the non-adiabatic pathways of the excited TC in each of these three excitation regimes? To address these questions, we will apply high-harmonic generation based soft X-ray transient absorption spectroscopy near the sulfur L-edge at ~165 eV, following valence electronic excitation at different excitation wavelengths. The sulfur 2p-to-valence transitions are expected to be particularly sensitive to the orbital occupancies and electronic energies of molecular orbitals associated with the sulfur atom (e.g. n_s, σ^*_{SCl}, π^*_{SO}), and in turn, will report effectively on the local bonding environment and electronic structure in the vicinity of the sulfur atom.

Photoinduced ring-opening in oxazole: Organic heterocycles serve as building blocks in a variety of biological systems. Ultraviolet excitation to a ππ* state in these systems is typically followed either by a deformation of the ring structure (ring puckering) as the molecule relaxes back to the ground electronic state, or ring-opening via bond cleavage following non-adiabatic passage to an nσ* state. Ultrafast photoelectron spectroscopy and accompanying theory[16] on oxazole (*c*-C_3H_3NO) suggested <100 fs ring opening and several picosecond timescale ring puckering; however, this experiment could not detect photoproducts, and unambiguous assignment of experimental spectra to specific non-adiabatic processes was not achieved. In collaboration with Anja Roeder and Sonia Coriani, we propose to study the excited state dynamics of oxazole using near-edge X-ray absorption spectroscopy that allows site-specific probing at the N and O K-edges following 200 nm photoexcitation at SLAC/LCLS.

IV. BES-sponsored publications (2019-present)

1. Cole-Filipiak, N. C.; Tross, J.; Schrader, P. E.; McCaslin, L. M.; Ramasesha, K., Ultraviolet Photodissociation of Gas-Phase Iron Pentacarbonyl Probed with Ultrafast Infrared Spectroscopy, *The Journal of Chemical Physics*, **2021**, *154* (13), 134308
2. Cole-Filipiak, N. C.; Tross, J.; Schrader, P. E.; McCaslin, L. M.; Ramasesha, K., Ultrafast infrared transient absorption spectroscopy of gas-phase $Ni(CO)_4$ photodissociation at 261 nm, *The Journal of Chemical Physics*, **2022** (in press)

V. References

1. Fuss, W.; Schmid, W.; Trushin, S., Ultrafast photodissociation dynamics of Ni (CO) 4. *The Journal of Physical Chemistry A* **2001,** *105* (2), 333-339.

2. Schnorr, K.; Bhattacherjee, A.; Oosterbaan, K. J.; Delcey, M. G.; Yang, Z.; Xue, T.; Attar, A. R.; Chatterley, A. S.; Head-Gordon, M.; Leone, S. R., Tracing the 267 nm-induced radical formation in dimethyl disulfide using time-resolved x-ray absorption spectroscopy. *The journal of physical chemistry letters* **2019,** *10* (6), 1382-1387.

3. Nourbakhsh, S.; Liao, C. L.; Ng, C., A 193 nm laser photofragmentation time-of-flight mass spectrometric study of CH3SSCH3, SSCH3, and SCH3. *The Journal of chemical physics* **1990,** *92* (11), 6587-6593.
4. Kroger, P. M.; Riley, S. J., Dynamics of three-body half collisions. I. Secondary product decomposition in the photodissociation of acetyl iodide. *The Journal of Chemical Physics* **1977,** *67* (10), 4483-4490.
5. Zhong, D.; Diau, E. W.-G.; Bernhardt, T. M.; De Feyter, S.; Roberts, J. D.; Zewail, A. H., Femtosecond dynamics of valence-bond isomers of azines: transition states and conical intersections. *Chemical physics letters* **1998,** *298* (1-3), 129-140.
6. Dyakov, Y.; Mebel, A.; Lin, S.; Lee, Y.; Ni, C.-K., Photodissociation of 1, 3, 5-triazine: An ab initio and RRKM study. *The Journal of Physical Chemistry A* **2007,** *111* (38), 9591-9599.
7. Yang, J.; Zhu, X.; F. Nunes, J. P.; Yu, J. K.; Parrish, R. M.; Wolf, T. J.; Centurion, M.; Gühr, M.; Li, R.; Liu, Y., Simultaneous observation of nuclear and electronic dynamics by ultrafast electron diffraction. *Science* **2020,** *368* (6493), 885-889.
8. Tully, J. C., Molecular dynamics with electronic transitions. *The Journal of Chemical Physics* **1990,** *93* (2), 1061-1071.
9. Li, X.; Tully, J. C.; Schlegel, H. B.; Frisch, M. J., Ab initio Ehrenfest dynamics. *The Journal of chemical physics* **2005,** *123* (8), 084106.
10. Hansen, N.; Wodtke, A. M.; Goncher, S. J.; Robinson, J. C.; Sveum, N. E.; Neumark, D. M., Photofragment translation spectroscopy of ClN3 at 248 nm: Determination of the primary and secondary dissociation pathways. *Journal of Chemical Physics* **2005,** *123* (10).
11. Samartzis, P. C.; Lin, J. J. M.; Ching, T. T.; Chaudhuri, C.; Lee, Y. T.; Lee, S. H.; Wodtke, A. M., Two photoionization thresholds of N-3 produced by ClN3 photodissociation at 248 nm: Further evidence for cyclic N-3. *Journal of Chemical Physics* **2005,** *123* (5).
12. Mozhayskiy, V. A.; Babikov, D.; Krylov, A. I., Conical and glancing Jahn-Teller intersections in the cyclic trinitrogen cation. *Journal of Chemical Physics* **2006,** *124* (22).
13. Baum, G.; Effenhauser, C.; Felder, P.; Huber, J. R., Photofragmentation of thionyl chloride: competition between radical, molecular, and three-body dissociations. *The Journal of Physical Chemistry* **1992,** *96* (2), 756-764.
14. Chichinin, A.; Einfeld, T. S.; Gericke, K.-H.; Grunenberg, J.; Maul, C.; Schäfer, L. V., Photodissociation dynamics of SOCl 2. *Physical Chemistry Chemical Physics* **2005,** *7* (2), 301-309.
15. Abulimiti, B.; Hao, Q.-l.; Qin, C.; Xiang, M.; Zhang, B., Three-Body photodissociation of thionyl chloride. *Chinese Journal of Chemical Physics* **2018,** *31* (3), 257-262.
16. Geng, T.; Ehrmaier, J.; Schalk, O.; Richings, G. W.; Hansson, T.; Worth, G.; Thomas, R. D., Time-Resolved Photoelectron Spectroscopy Studies of Isoxazole and Oxazole. *The Journal of Physical Chemistry A* **2020,** *124* (20), 3984-3992.

ULTRAFAST PHYSICS: NONLINEAR OPTICAL SPECTROSCOPY AND DIAGNOSTICS

Christopher J. Kliewer, David L. Osborn, Krupa Ramasesha, David W. Chandler
Sandia National Laboratories, MS 9051, Livermore, CA 94551-0969
cjkliew@sandia.gov, chand@sandia.gov, kramase@sandia.gov, jhfrank@sandia.gov

Program Scope

The interaction of intense pulsed laser fields with atoms, molecules, and surfaces induces a coherent response in the material. At especially high intensities, the material response becomes nonlinear and gives rise to a wealth of approaches to both *control* and to *probe* molecular processes in gas-phase and interfacial chemical physics, even processes very far from chemical equilibrium. In this program, our goal is to develop ultrafast optical methods to both measure and control matter at the molecular level and on molecular timescales. On the measurement side, ultrafast nonlinear approaches are advanced for the detection of transient reactive molecular species. In addition, broadband approaches enable the sampling of many spectroscopic transitions at once, allowing for the assessment of instantaneous molecular energy partitioning and energy transfer. A critical aspect of our research includes the study of fundamental spectroscopy, energy transfer, molecular dynamics, and photochemical processes. This aspect of the research is essential to the development of accurate models and quantitative application of techniques to complex environments. We are uniquely positioned to study molecular systems driven far from equilibrium, as well as relaxation rates and pathways. Time-resolved collisional dephasing measurements provide insight into the local chemical environment as well as inform spectroscopic models for quantitative interpretation.

Recent Progress

Development of the Ultrafast Molecular Centrifuge The selective control of population in the various degrees of freedom in molecules has opened the possibility for unprecedented understanding of reactive potential energy surfaces in gas phase chemical physics. While significant work has been dedicated to understanding, and controlling, the vibrational and translational degrees of molecular freedom, far less attention has been paid to the direct molecular control of rotational energy. In part, this is due to the quantum mechanical selection rules that govern rotational excitation. Only small changes in angular momentum are allowed during an optical absorption or Raman process. In recent years, however, pioneering work has established a method for spinning molecules into very high angular momentum states. Like adiabatic passage methods for vibrational ladder climbing, passage up the rotational ladder has now been demonstrated on several molecules. The first experimental demonstration of the optical centrifuge technique, by Corkum and coworkers [1], was performed on Cl_2. Rotationally induced dissociation was observed through mass spectrometry for Cl_2 molecules driven to $J \sim 420$. Later work demonstrated theoretically the possibility of breaking the stronger chemical bond in HCN through tailoring of the chirp rate in an optical centrifuge [2]. Mullin and co-workers coupled a transient IR absorption spectrometer to an optical centrifuge to follow the rotational relaxation dynamics of CO_2[3], N_2O[4], and CO[5]. These works provided a wealth of new information on the collisional dynamics and energy transfer mechanisms for molecules driven to very high rotational energies. During this past year, we have built a high-power femtosecond amplifier and two-arm optical molecular centrifuge. We began by constructing a 20 Hz high-power 7-pass bow-tie amplifier to generate the high-powered pulses required to trap and centrifuge molecules. Next, the pulse was separated into two arms, left- and right- circularly polarized, and chirped such that the difference frequency between the two arms increases at a given time increases from 0 cm^{-1} to 500 cm^{-1}. The two arms are combined at the experiment, creating a linear polarization of high intensity. This polarization rotates with an accelerating frequency throughout the pulse, trapping and driving molecules into higher rotational states. Because the optical centrifuge follows a series of sequential impulsive Raman transitions, the resulting molecular ensemble is highly aligned along the laser polarization

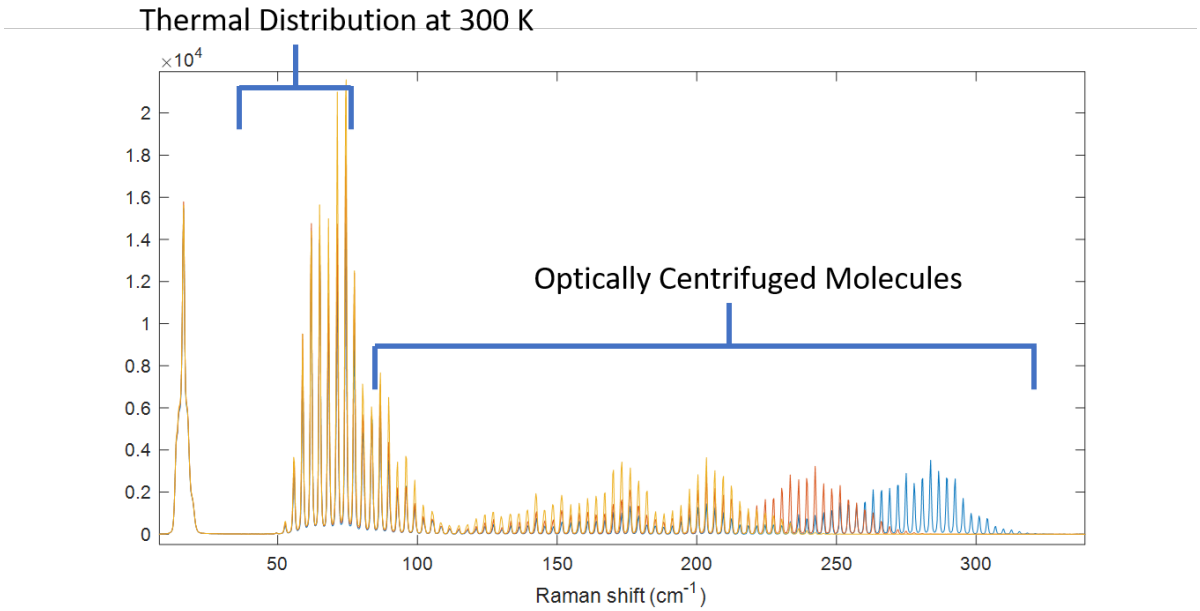

Figure 1. First demonstration of the optical molecular centrifuge at Sandia. CO_2 has been centrifuged to J~220 super-rotor state. The molecules are detected through coherent Raman scattering of a picosecond probe pulse from the centrifuged molecules, which are evolving in a coherent rotational wave-packet. Tailoring of the frequency content of the centrifuge

axis as $J \approx M_J$. The rotational wavepacket created through the excitation process will evolve coherently, and thus the distribution of rotational states created from the optical centrifuge may be probed using nonlinear scattering of a time-delayed picosecond probe pulse. This approach is analogous to the innovative hybrid femtosecond/picosecond CARS approaches we have developed in the Ultrafast Diagnostics laboratory in recent years. Figure 1shows initial results from our home-built optical centrifuge. Molecular CO_2 was driven from its thermal population at 300 K climbing the rotational ladder to $J > 220$. The probing of these molecules through simple scattering of a picosecond probe pulse allows for the multiplex detection of all populated states from the centrifuge simultaneously. One of the hypotheses of this work has been that the final state distribution can be tailored through appropriate pulse-shaping approaches prior to the recombination of the centrifuge arms. Indeed, as can be observed in the yellow, red, and blue traces of Fig. 1., selectively blocking frequency content in the stretcher portion of the centrifuge arms significantly modifies the obtained rotational distribution of the centrifuged molecules.

Rotational coherence beating for assessment of rovibrational nonequilibrium Molecular systems far from equilibrium are a grand challenge in chemical physics research and pose a unique test for our understanding of reaction kinetics and dynamic quantum simulations. Rotation-vibration non-equilibrium and energy transfer is a key area of study for low temperature plasmas that enhances chemical reactivity in applications such as carbon nanotube synthesis[6], plasma catalysis[7], CO_2 dissociation[8], and methane reforming[9]. Therefore, it is of great interest to be able to conduct spatially resolved measurements of rotation-vibration non-equilibrium in these systems. Furthermore, as described in the previous section, we have very recently demonstrated the development of a tailored optical centrifuge for extreme rotational excitation of molecules for use in chemical dynamics studies. Here once again, the ability to follow the vibrational and rotational distributions (and transition frequencies) is of critical importance to understand the energy transfer channels and state distribution following the centrifuge pulse and prior to chemical dynamics studies using the generated super-rotors. During this previous year, we have extended the ability to probe rotation-vibration nonequilibrium using time-domain coherence beating. Because rotational constants are slightly perturbed by vibrational excitation of a molecule, the transition frequency for rotational transitions for molecules in

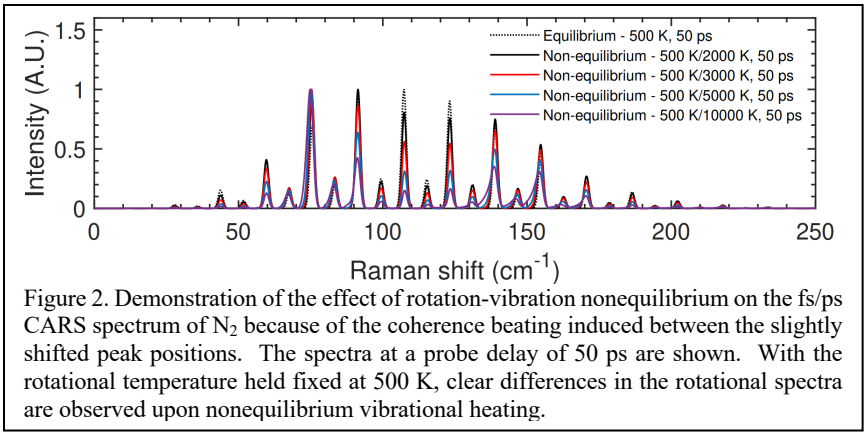

Figure 2. Demonstration of the effect of rotation-vibration nonequilibrium on the fs/ps CARS spectrum of N_2 because of the coherence beating induced between the slightly shifted peak positions. The spectra at a probe delay of 50 ps are shown. With the rotational temperature held fixed at 500 K, clear differences in the rotational spectra are observed upon nonequilibrium vibrational heating.

v=1 or v=2 are shifted from the v=0 bandhead. Thus, if the probe pulse of the fs/ps CARS sequence is broader than the separation between these peaks (as is typically the case for ps probe pulses), this will result in a J-dependent frequency beating within the generated spectrum. Thus, a suitable probe delay can be determined to maximize the interference from this beating pattern. This allows for a highly sensitive probe of rotation-vibration nonequilibrium in a single shot.

Ultimate detection sensitivity for time-domain coherent Raman approaches In recent years, both in our lab as well as others, many advances have been made in ultrafast coherent Raman approaches for chemical physics studies. The excitation of Raman coherences with ultrafast pulses is far more efficient than traditional nanosecond or picosecond based spectroscopies. In many applications of chemical physics, such as in heterogeneous catalysis, molecular dynamics studies in cross molecular beams, and plasma chemistry, the time-resolved detection of transient, minor, chemical speciation is needed. Thus one question which commonly arises is whether or not ultrafast Raman approaches can be employed for minor chemical speciation, and what the minimum detection sensitivity enables. Thus, we recently reported a careful assessment of the detection sensitivity for ultrafast Raman approaches for a series of gas-phase molecules. Additionally, for studies at low number densities, coherence lifetimes are quite long. In this case, a long nanosecond probe pulse can be utilized to improve detection limits following impulsive femtosecond excitation. We demonstrated this effect, and have shown that fs/ns approaches can yield decreased lower detection limit for trace species determination. Figure 3 shows the signal to noise ratio for a range of gas concentrations down to the 100's of ppm. Using fs/ns excitation, the fundamental detection sensitivity for several gasses important to gas-surface catalysis (such as H_2, O_2, and CO) was shown to be 10^{14}-10^{15} /cm^3. This detection limit applies to a spatial resolution of ~50 µm x 1 mm and sets a baseline for planning new experiments in gas-surface chemistry using coherent Raman imaging as a local probe of reaction rates.

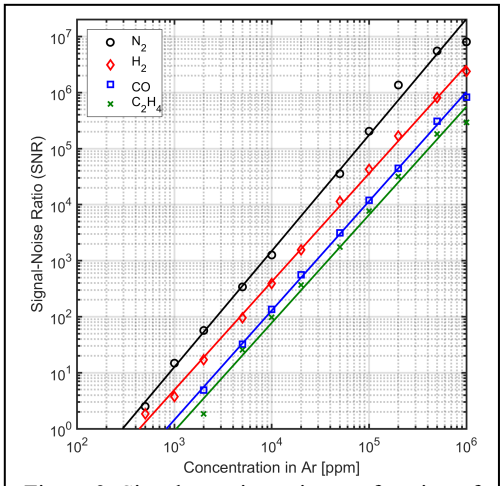

Figure 3. Signal to noise ratio as a function of concentration for fs/ps CARS of several gas-phase species.

Future Work

Assessing energy transfer in optically centrifuged molecules Building on our recent success in constructing and demonstrating the ultrafast optical molecular centrifuge, we plan to begin chemical dynamics investigations with this exciting new approach. One interesting topic involves the flow of energy from rotation to vibration in highly rotationally excited molecules. Further building upon our recent developments for determining vibration-rotation nonequilibrium state distributions from the pure-rotational spectrum, using both time- and frequency- domain approaches, we plan to deduce the rotation-to-vibration excitation rates within the optical centrifuge. As shown in Fig. 4, initial results from centrifuge experiments on CO_2 indicate that excess population in up to two quanta of the v_2=1 and v_2=2 bending mode of CO_2

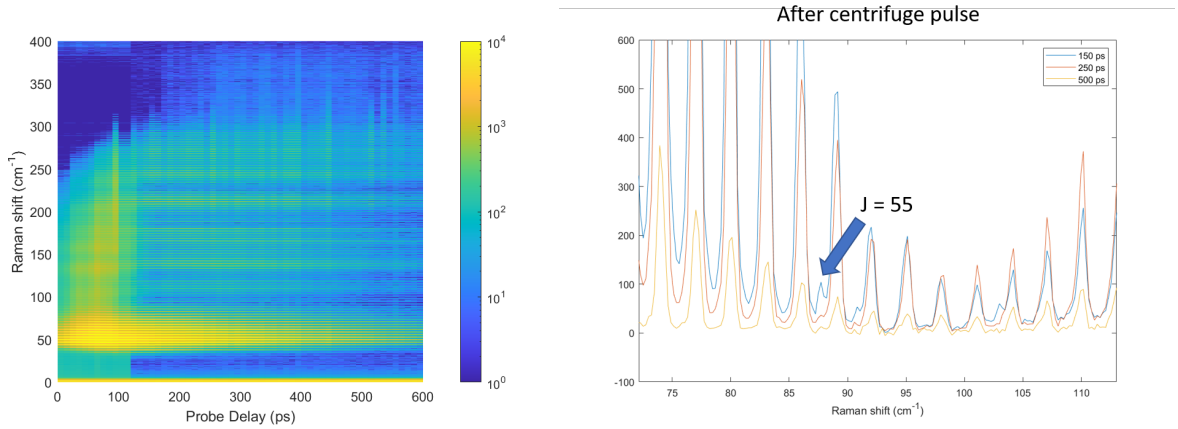

Figure 4. (left) Coherent scattering signal from the output of the optical centrifuge as a function of probe delay. The highly excited "super-rotor" states exhibit long-lived lifetimes. (right) The highlighted peak corresponds to population in the v_2=1 bending mode of CO_2.

appears to be excited and evolves following the centrifuge pulse. A very rudimentary amplitude ratio assessment shows an apparent vibrational population in this bending mode of as much as 1500 K (if one were to view the ratio from a Boltzmann analysis). Thus, it is very clear that although there is some population expected in the bending mode at 300 K, significant excess population is driven into this mode in the centrifuged molecules. Previous work by the group of Amy Mullin had also observed excess vibrational population induced by the rotational centrifuge [3] but the origin of the excess population remained unclear, whether excited through a collisional process or by the centrifuge pulse itself. Because our approach to resolving the population of the centrifuged molecules allows for both time resolution on the ps timescale and the multiplexed detection of all states, we plan to investigate the origin of population in the vibrational levels of CO_2 by following the time evolution following a probe delay. In addition, we have begun higher-order nonlinear optical experiments using a pump-probe scheme where the "pump" is the centrifuge pulses and the "probe" is a full CARS sequence. This allows for an extra delay axis to follow the evolution the ensemble T_1 times separately from the dephasing process.

Optical centrifuge of N_2O for photodissociation dynamics studies In the coming year, planned work at Sandia involves the study of the photodissociation of N_2O super-rotors. This work is described in the "Chemical Dynamics" abstract of the Sandia Gas-Phase Chemical Physics program. To enable these studies, we need to tailor our optical centrifuge for efficient centrifuging of the N_2O molecule. In order to efficiently trap target molecules, the optical centrifuge must be tailored to the molecular system such that $8\pi\delta/E^2 < \Delta\alpha/I$, where δ is the rate of optical acceleration, E^2 is the laser intensity, $\Delta\alpha$ is the molecular polarizability anisotropy, and I is the molecular moment of inertia. Thus, for each new molecule studied, the pulse shaper must be once again optimized. An important aspect of the design is the effective turn-on time for the optical centrifuge pulse. Prior to interaction with the laser pulse, the gas-phase ensemble of molecules will be isotropically oriented about the laboratory coordinate. As the optical centrifuge turns on, it will begin exerting an aligning force on these molecules. If the turn-on time is too fast, the molecule will not have time to respond and become adiabatically trapped within the potential well created by the laser. In angular coordinates, the laser must cover π radians during the turn-on period to effectively trap all orientations. If the turn-on is too slow, the angular frequency will be too fast by the time the pulse is at full intensity and will not be able to retain the molecules, i.e. the kinetic energy of the molecules gained during centrifuge turn-on must be always less than the current potential well depth induced by the laser pulse. Spanner and Ivanov [10] have proposed a method to derive these upper and lower limits, and have found

that $(2\pi/\delta)^{\wedge}.5 < t_{on} < (U_0/[I\delta^2])$ allows for molecules to be effectively coupled into the centrifuge. Here, again, δ is the angular acceleration rate of the trap, t_{on} is the pulse turn-on time, U_0 is the potential well depth felt by the molecule from the laser, and I is the molecular moment of inertia. This year we will demonstrate efficient driving of N_2O to $J > 150$.

Direct visualization of $O_2(a^1\Delta_g)$ using nonlinear optical methods and virtually imaged phase array spectrometer The direct time-resolved and spatially-resolved detection and visualization of the concentration $O_2(a^1\Delta_g)$ has been a difficult goal for many years. A weak absorption cross-section for excitation to the next lowest-lying electronic state thus requires a cavity ring-down or cavity-enhanced type setup for detection. Such methods have very long effective path lengths and are line-of-sight limited and are thus not applicable to many areas of gas phase chemical physics (such as combustion and plasma assisted chemistry) where $O_2(a^1\Delta_g)$ is known or suspected to play a major kinetic role. In collaboration with Prof. Christopher Limbach (Texas A&M) we have recently incorporated a virtually imaged phase array spectrometer [11] for high resolution coherent Raman scattering studies. With this approach, we are able to resolve spectral lines with spectral resolution of better than 200 MHz. We have recently developed a fs/ns coherent Raman technique to directly visualize $O_2(a^1\Delta_g)$. In the coming months we will demonstrate this technique by measuring fs/ns CARS of $O_2(a^1\Delta_g)$ through the VIPA spectrometer, quantifying the detection limits, and then applying the method in measurements of plasma generated $O_2(a^1\Delta_g)$.

Coherence Lifetime Imaging through Structured Illumination
Coherence dephasing times are often governed by intermolecular interactions. In gas-phase systems, collisional energy transfer is the dominant source of rotational and vibrational coherence dephasing. Thus measuring the coherence decay rate allows for the in-situ mapping of collisional energy transfer rates, which are highly dependent on collision partner, number density, and collision energy. In condensed phase samples, the coherence lifetime gives an indication of the coupling of individual vibrational states to the surrounding environment. In microscopy applications, coherence lifetime would provide a novel imaging contrast mechanism sensitive subtle changes in local chemical environment. In previous work, we demonstrated the ability to measure coherence lifetimes within a single laser shot in the gas phase by separating the probe pulse into four separate weak probe pulses, each with a different phase matching angle. We propose here to develop a 2D coherence lifetime imaging approach which can have impact in both gas-phase chemistry applications as well as in condensed phase fields. Similarly to fluorescence lifetime imaging, the coherence lifetime image will provide information on the chemical coupling and energy transfer to the local environment.

In order to realize single-shot coherence lifetime imaging, we will combine our recently developed 2D-CARS approach, with the structured illumination approach developed by our colleagues at Lund University. More specifically, the probed molecules will be excited with a pump/Stokes femtosecond laser sheet. The probe beam, however, will be separated via beam-splitters into four separate beams. Each of these beams will propagate through a time-of-flight optical delay stage and then be passed through a transmission grating. These gratings will be designed to optimize the +/- 1 orders. The position of the grating will be relay imaged to the experiment. In this way, each of the four probe beams gets imprinted with a fringe pattern at a controllable angle. The CARS beams will then be recombined into a single beam and scattered from the sample. The resulting image will contain four separate probe delays, with independent spatial frequencies, which can be extracted through spatial Fourier transform. In gas phase chemistry applications such as combustion, or coupled gas-surface chemistry, such an approach would enable simultaneous speciation, measurement of energy distributions, as well as provide an assessment of the degree of coupling to other molecules or the surface.

Journal publications supported solely by this BES project (2019-2022)

1. T.Y. Chen, B.M. Goldberg, B.D. Patterson, E. Kolemen, Y. Ju, and C.J. Kliewer*, "1-D imaging of rotation-vibration non-equilibrium from pure rotational ultrafast coherent anti-Stokes Raman scattering" Opt. Lett. **45**, 15, 4252-4255 (2020)
2. T.Y. Chen, C.J. Kliewer*, B.M. Goldberg, E Kolemen, and Y Ju, "Time-domain modelling and thermometry of the CH_4 Q-branch using hybrid femtosecond/picosecond coherent anti-Stokes Raman scattering" Combustion and Flame **224**, 183-195 (2021)
3. M. Linne, N.T. Mecker, C.J. Kliewer, D. Escofet-Martin, B. Peterson, "Revisiting N_2-N_2 collisional linewidth models for S-branch rotational Raman scattering" Combustion and Flame https://doi.org/10.1016/j.combustflame.2021.111928, (2021)
4. S.A. Steinmetz, C.J. Kliewer*, "Gas detection sensitivity of hybrid fs/ps and fs/ns CARS" Opt. Lett. **47**, 1470-1473 (2022)
5. T.Y. Chen, N. Liu, C.J. Kliewer, A. Dogariu, E. Kolemen, Y Ju, "Simultaneous single-shot rotation-vibration non-equilibrium thermomemtry using pure rotational fs/ps CARS coherence beating" Opt. Lett. **47**, 1351-1354 (2022) *Highlighted as an "Editor's Pick" article

***corresponding author**

References

1. D. M. Villeneuve, S. A. Aseyev, P. Dietrich, M. Spanner, M. Y. Ivanov, and P. B. Corkum, Phys. Rev. Lett. **85**, 542-545 (2000).
2. R. Hasbani, B. Ostojic, P. R. Bunker, and M. Y. Ivanov, Journal of Chemical Physics **116**, 10636-10640 (2002).
3. L. W. Yuan, S. W. Teitelbaum, A. Robinson, and A. S. Mullin, Proc. Natl. Acad. Sci. U. S. A. **108**, 6872-6877 (2011).
4. L. W. Yuan, C. Toro, M. Bell, and A. S. Mullin, Faraday Discuss. **150**, 101-111 (2011).
5. M. J. Murray, H. M. Ogden, C. Toro, Q. N. Liu, and A. S. Mullin, ChemPhysChem **17**, 3692-3700 (2016).
6. E. Plonjes, P. Palm, G. B. Viswanathan, V. V. Subramaniam, I. V. Adamovich, W. R. Lempert, H. L. Fraser, and J. W. Rich, Chem. Phys. Lett. **352**, 342-347 (2002).
7. T. Nozaki, and K. Okazaki, Catal. Today **211**, 29-38 (2013).
8. T. Kozak, and A. Bogaerts, Plasma Sources Sci. Technol. **23**, 17 (2014).
9. J. T. Sun, and Q. Chen, J. Energy Chem. **39**, 188-197 (2019).
10. M. Spanner, and M. Y. Ivanov, J. Chem. Phys. **114**, 3456-3464 (2001).
11. C. M. Limbach, Opt. Lett. **44**, 3821-3824 (2019).

Quantum Chemistry of Radicals and Reactive Intermediates

John F. Stanton
Quantum Theory Project
Departments of Chemistry and Physics
University of Florida
Gainesville, FL 32611
johnstanton@ufl.edu

Scope of Research

My research group works in the area of theoretical chemical physics, especially on the properties and chemistry of organic radicals and other reactive intermediates. This research follows a number of paths, including first-principles calculation of bond energies and other thermochemical information (as well as development of methodology needed for such calculations), methods for the simulation and analysis of molecular spectra (especially those relevant to experiments that can be used to glean thermochemical information), the development of *ab initio* quantum chemical methods needed for the accurate treatment of fundamental aspects of electronic structure and potential energy surfaces, and computational kinetics including semiclassical transition state theory and master equation modeling of chemical reactions.

Summary of Selected Recent Accomplishments and Future Plans

• At present, the group is very actively engaged in extremely high-level thermochemical calculations, a project that was initiated by a question posed by one of my graduate students. Specifically, they asked "Just how accurately can we calculate a bond energy?". Initial results of this research were presented at the 2021 contractors' meeting, but a much larger quantity of data has been generated since that time. This research leverages developments in coupled-cluster theory and program development by my group, which is available to any academic or government researchers *via* the CFOUR program system. Aided by the development of new basis sets by Feller, our work has led to the most elaborate conventional calculations yet performed for several very small molecules (CO, N_2 and H_2O, listed in publications below), and others (most of those found in the standard HEAT database[1]) which have not yet been written up for publication. In the end, it appears that bond energies can be calculated by this new method with an accuracy of no worse than *ca.* 10-20 cm^{-1} (0.02 kJ mol^{-1}). This does, of course, come at great cost: basis sets of up to *octuple*-zeta are used, and electron correlation effects are assessed with calculations extending to coupled-cluster singles, doubles and triples

[1] A. Tajti *et al. J. Chem. Phys.* 121, 11599 (2004).

with a perburbative treatment of quadruple excitations (CCSDT(Q)$_\Lambda$) with a quintuple zeta basis[2].

Having established "what it takes" for this level of accuracy, ongoing efforts are underway to identify some simplifications to this most elaborate protocol that nevertheless enable calculations to be done for larger molecules with a level of accuracy which still exceeds that of existing methods. Some such strategies are under development and in the benchmarking stage, and initial results are encouraging. For example, the table below[3] shows the results obtained for the full method (here designated as S-HEAT) and a few approximations to it. That this level of absolute accuracy can be attained for a molecule as difficult (in the sense of being a challenging case for electron correlation treatments) as ozone is remarkable, and we are very much encouraged by this progress. Two papers will be forthcoming: one on the application of the method designated here as S-HEAT to some standard and well-known problems (water dimerization energy, singlet-triplet splitting of methylene, ammonia inversion barrier), and another will present comparisons for all of the molecules in the HEAT dataset.

Table 1: Total atomization energies (in cm^{-1}) for H_2O and O_3.

	H_2O	O_3
S-HEAT	76722	a
S-HEAT*	76721	49812
S-HEAT**	76727	49811
ATcT	76726(2)	49833(3)

[a]Computational demands exceed capabilities.

Finally, we have recently completed calculations on the enthalpy of formation of HONO – a case where standard high-level thermochemical methods (W4[4] and previous HEAT variants) give poor results but for which S-HEAT performs remarkably well – and the chlorine oxides ClO, ClOO, OClO, ClOOCl, Cl-ClO_2 as well as their cations. Work is also progressing on the sulfur-containing species SO, S_2 and SO_2. These latter studies that target atoms in the third row of the periodic table (Z=11-18) have revealed some systematic issues with blindly applying the most logical extension of the HEAT protocol to these systems. In particular, double-zeta basis sets do not suffice to treat higher-level (beyond triples) correlation effects, and certain details associated with core correlation require more care in their treatment.

All of the work described above is associated with the Active Thermochemical Tables (ATcT) project[5] of Ruscic at ANL. Much of the direction of our research in this area is informed through regular (Zoom) meetings with Ruscic and other members of the task force with which we are affiliated (comprising Ellison at Colorado, Baraban at Ben Gurion University, Changala at Harvard, together with Ruscic's group).

[2]Calculations at the CCSDTQ(P) level are also done, but with a minimal basis set.

[3]The costs of the approximations to S-HEAT are, roughly, S-HEAT*/S-HEAT 0.2-0.5; S-HEAT**/S-HEAT 0.05-0.1. It must be emphasized here that the full S-HEAT approach is very expensive.

[4]A. Karton, E. Rabinovich, J.M.L. Martin and B. Ruscic *J. Chem. Phys.* 125, 144108 (2006).

[5]B. Ruscic *et al. J. Phys. Chem. A* 108, 9979 (2004).

In another project largely associated with thermochemistry, the stabilities of species related to carbonic acid (H_2CO_3) are being investigated. This project was given to an undergraduate in the belief that it was "easy", but it has turned out to be anything but. In particular, the $HOCO_2$ radical provides a demanding and interesting challenge to theory. It is related to the parent formyloxyl radical, which has been widely studied in our group and that of others (Neumark, UC-Berkeley) for more than twenty years, but it is an even greater challenge. This challenge arises from the fact that the "symmetry-breaking" electronic structure effect in symmetric formyloxyl radicals (HCO_2, FCO_2, $HCCCO_2$, *etc.*) is present in this species, as well. However, the molecular symmetry of the radical is lowered from C_{2v} to C_s, and the competing SCF solutions (that comprise localized and delocalized unpaired spin) now belong to the same irreducible representation $^2A'$. Hence, it is not possible to conveniently "avoid" the symmetry broken solution and all of the trouble it presents. The electronic structure of this species is very rich, and a report on it is currently in preparation.

• Motivated by recent spectroscopic work by the groups of R.C. Woods and R.J. McMahon (UW-Madison), we have been working on the development of methods suitable for very accurate calculation of parameters associated with rotational spectroscopy. This field, which has undergone a renaissance since the development of the chirped-pulse approach[6], plays an important role in our understanding of the chemistry of the universe, and is seeing continually growing use as an analytical technique. The Woods-McMahon collaboration centers on high-precision measurement of a sufficiently large number of lines (*ca.* 10^3) to fit relatively high-order effective Hamiltonians (with meaningful fits of centrifugal distortion through hexic terms), often for multiple vibrational states. The means for calculating parameters needed for this sort of work (*e.g.* vibrational dependent quartic centrifugal distortion constants, quadratic terms (in n+$\frac{1}{2}$) involved in the expansion of rotational constants in terms of those that are directly proportional the reciprocal inertia tensor of the equilibrium structure) are largely unavailable. My outstanding postdoc, Peter Franke (a graduate of the Douberly group at Georgia) has been working on all of these problems, and has made considerable progress. This work has already been useful in explaining certain oddities obtained through fits of data to the molecules 1,2,3- and 1,2,4-triazole, and is playing a role in an ongoing study of the equilbrium structure of benzene. A number of papers related to this work are forthcoming.

• In the area of vibronic coupling, we continue to pursue a number of projects. At present, work continues on the excited $^2E''$ state of the nitrate radical (NO_3), the spectroscopy of which began long ago[7] but has been greatly developed in the last twenty years[8]. Another is the seemingly simple cation C_2H^+, which has a triplet ground state but possesses an infrared spectrum that is largely unassignable. Brunken (at Radhout University in the Netherlands) presented this problem to us in 2016, and we are just beginning to make progress during the last six months. Both of these projects are being done in collaboration with Changala (Harvard), whose NITROGEN program is needed since neither of these systems can be adequately treated by means of a Hamiltonian based on polynomial expansions in a

[6]G.G. Brown *et al. Rev. Sci Instru.* 79, 053103 (2008).

[7]A. Weaver *et al. J. Chem. Phys.* 94, 1740 (1991); E. Hirota *J. Chem. Phys.* 107, 2829 (1997).

[8]A. Deev, J. Sommer and M. Okumura *J. Chem. Phys.* 122, 224305 (2005); T. Codd *et al. J. Chem. Phys.* 142, 184305 (2015).

set of normal coordinates. Quite interesting in the C_2H cation is the CC stretching mode, which appears prominently in the laboratory spectrum apparently some 200 cm^{-1} below its harmonic frequency. Such a large anharmonicity for a "heavy atom" stretching mode is unusual, and it is not immediately apparent why this is so. It is noteworthy that a another anomalous anharmonic shift of similar magnitude is seen in the corresponding neutral species. Notably, the vibronic coupling in C_2H only involves the π bending mode in lowest order, but the symmetry of the CC stretch is such that it does not mix the ground $^2\Sigma$ and low-lying (*ca.* 3600 cm^{-1}) $^2\Pi$ states. This led to an investigation of this curious puzzle (see below for reference), which is in fact attributable to vibronic coupling; it also provides an important example of the distinction between equation-of-motion (EOM-CC) and normal coupled-cluster (CC) methods.

• Additional information about our DOE-supported research can be found in the publications listed at the end of this document.

Students and Postdoctoral Supported:
J.T. Thorpe (student)
M.B. Bentley (student)
P.R. Franke (postdoc)

References from 3/2020-3/2021 citing BES-GPCP grant

D. Feller, J.F. Stanton and E.R. Davidson Atomic Isotropic Hyperfine Properties for First Row Elements (B - F) Revisited J. Chem. Phys. 156, 034304 (2022).

L.T. Nguyen and J.F. Stanton Thermal Decomposition of CH_3O: A Curious Case of Pressure-Dependent Tunneling Effects J. Phys. Chem. A, 125, 6761 (2021).

J.T. Thorpe, J.L. Kilburn, D. Feller, P.B. Changala, D.H. Bross, B. Ruscic and J.F. Stanton Elaborated Thermochemical Treatment of HF, CO, N_2 and H_2O: Insight into HEAT and its Extensions J. Chem. Phys. 155, 184109 (2021).

J.F. Stanton Why the CC Stretch in CCH is so Anharmonic J. Phys. Chem. A 125, 7694 (2021).

Y. Benitez, T.L. Nguyen, A.J. Parsons, J.F. Stanton and R.E. Continetti Probing the Exit Channel of the OH + CH_3OH H_2O + CH_3O Reaction by Photodetachment of CH_3O-(H_2O) J. Phys. Chem. Lett. 13, 142 (2021).

J. Borsovszky, K. Nauta, J. Jiang, C.S. Hansen, L.K. McKemmish, R.W. Field, J.F. Stanton, S.H. Kable and T.W. Schmidt Photodissociation of Dicarbon: How Nature Breaks an Unusual Multiple Bond Proc. Natl. Acad. Sci. 118, e2113315118 (2021).

Universal and State-Resolved Imaging Studies of Chemical Dynamics

Arthur G. Suits
Department of Chemistry, University of Missouri, Columbia MO 65211
suitsa@missouri.edu

1. Program Scope

The focus of this program is on combining universal ion imaging probes providing global insight with high-resolution state-resolved probes providing quantum mechanical detail, to develop a molecular-level understanding of chemical phenomena. Particular emphasis is placed upon elementary reactions involving transient species and in revealing new aspects of reaction mechanisms and the dynamical behavior of molecules. Much of the current effort here is in generalizing the lessons from simple systems as we investigate the behavior of larger polyatomic molecules and radical-molecule reactions. This research is conducted using state-of-the-art molecular beam machines, photodissociation, reactive scattering, and vacuum ultraviolet lasers in conjunction with velocity map ion imaging and other techniques we develop. One focus of our effort remains crossed-beam reactive scattering of polyatomic molecules. In addition, new directions in ultrafast time-resolved studies of photochemical processes are also underway.

2. Recent Progress

2.1 Crossed Beam Scattering

We continue our ongoing studies of bimolecular reaction dynamics using crossed-beam velocity map imaging with a universal 157nm probe. We are wrapping up OH studies now before moving on to hot H atom reactions with polyatomic molecules.

OH Radical Reactions

A new student has just joined the crossed-beam effort following the departure of the post-doc. As mentioned last year, we have studied reaction of both propanol isomers with OH in crossed beams, to our knowledge the first experimental dynamics investigation of these reactions. We have nice results at higher collision energy (around 8 kcal/mol) but, as is almost always the case for our VUV probe, we have interference from photochemistry that becomes problematic at lower collision energies. We are currently optimizing the experiment for better signal-to-noise at lower collision energies for improved data for publication while we train the new student on the instrument.

2.2 Ultrafast Experiments

Our ultrafast effort is pursued along two directions: Laboratory studies involving Coulomb Explosion Imaging (CEI), and experiment at the ultrafast electron diffraction beamline at LCLS. We have made good progress in both pursuits as described in the following.

Coulomb Explosion Imaging

In favorable cases, molecular structure and dissociation dynamics can be inferred from the ionic fragments' momentum images recorded in a Coulomb Explosion experiment when multiple electrons are rapidly driven from a molecule. The ability of CEI to directly probe the structure of a molecule following multiple ionization by ultrafast methods has led to significant interest in both the technique itself and its application in time-resolved experiments. In order to acquire the full picture of the dynamics, it is necessary to determine the correlation between various fragments' momenta. This can be done using multi-mass imaging techniques along with correlation-based analysis methods. We have now had considerable success using Wen Li's 3D (time and position) coincidence detection approach to perform CEI experiments, exploring its capabilities for reliable structure determination and suitability future pump-probe real-time dynamics studies. Our initial target systems are two carbonyl sulfenyl chlorides for which synchrotron studies have

examined ionic decomposition products following core ionization: chlorocarbonylsulfenyl chloride (ClC(O)SCl; hereafter CCSC) and methoxycarbonylsulfenyl chloride ($CH_3OC(O)SCl$; MCSC). We reported the CCSC results last year and present the MCSC results here. Our results on these systems have been published in two papers and a PhD thesis that was just successfully defended.

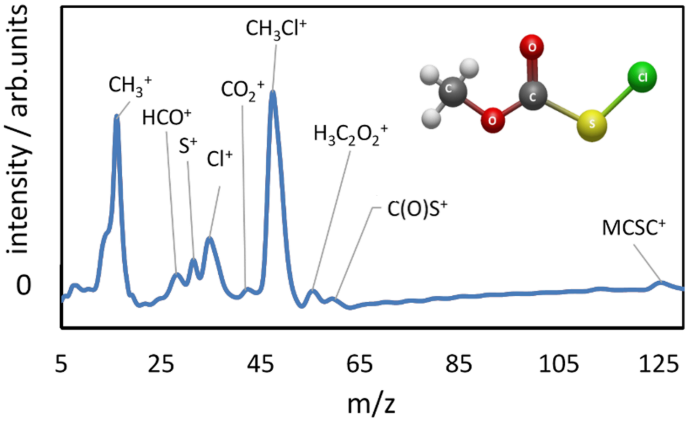

Figure 1. Time of flight mass spectrum following CEI of MCSC.

The TOF mass spectrum resulting from Coulomb explosion of MCSC with an intensity of ~ 2×10^{14} W/cm^2 at 800 nm is shown in Figure 1. Here the velocity map ion images of multiple fragments were then recorded by defining a delay time window for the MCP such that it includes the TOF of all our fragments of interest. We combined this multi-mass imaging technique with covariance map analysis to find correlations between pairs of photoproducts which were produced from the same ionization events. Covariance images of the CH_3^+/Cl^+ pair exhibited a very sharp feature at 180° indicates that these two fragments are likely produced from a two-body-like channel (process 1).

$$CH_3Cl^{2+} \rightarrow CH_3^+ + Cl^+ \quad (1)$$

Erben et al.[34] assigned this correlation to a three or four body dissociation channel with a deferred charge separation mechanism (DCS) where an intermediate $CH_3\text{-}SCl^{2+}$ or $CH_3\text{-}Cl^{2+}$ is formed along with an ejected neutral co-fragment. On the other hand Vallance et al. showed that the covariance images for a three-body DCS mechanism has an oval shaped distribution which is in contrast with the sharp features see in the covariance analysis. Therefore, we suspected that the correlation between this pair of ions is a result of pure two-body dissociation of methyl chloride formed as an impurity in the gas line or the source chamber before MCSC goes through dissociation. Direct analysis of CEI of CH_3Cl showed nearly identical distributions, confirming this as the origin of the correlation. We also observed a correlation between HCO^+ and $C(O)S^+$ fragments' momenta as shown in Fig. 2. This correlation was not observed in synchrotron studies. The covariance images of $HCO^+/C(O)S^+$ show a broader distribution of signal intensity peaking at about 180°. This broadening of the intensity is indicative of an initial or deferred charge separation mechanism in which the non-negligible momenta of the neutral fragments results in less sharp signals compared to what is observed for two-body fragmentation. The correlation found between HCO^+ and $C(O)S^+$ is assigned to a 4-body dissociation giving neutral Cl and H_2 as coproducts, possibly via excited electronic states of the doubly charged parent ion. These results further demonstrate the promise of multimass

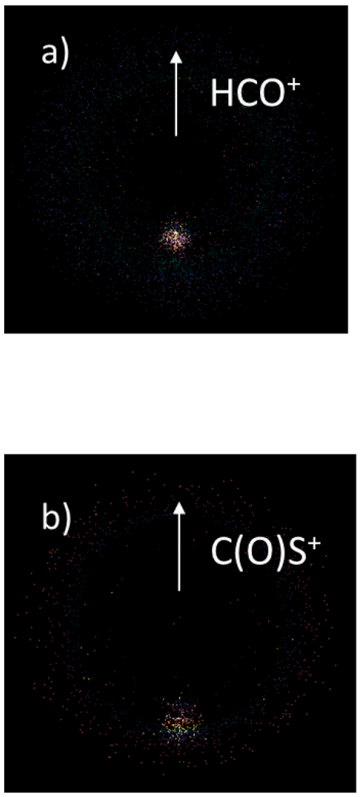

Figure 2. Covariance images of $C(O)S^+/HCO^+$ pair.

imaging using tabletop lasers for time-resolved dynamics monitored using CEI.

Time-Resolved Photodissociation Dynamics at the MeV UED Facility at LCLS

Last year we described preliminary results after our first experiment at the MeV-UED instrument of the LCLS User Facility. Our objective here is to examine the photodissociation dynamics of oxalyl chloride, $(ClCO)_2$ an unusual system in which UV dissociation gives rise to four fragments. The UV

photodissociation of this molecule has been studied at a range of UV wavelengths with some attendant controversy. In these experiments, a femtosecond pump beam at 200 nm was used to excite the system and then its time-dependent structural evolution was probed using an ultrafast relativistic electron beam. The electron diffraction patterns acquired at different pump-probe time delays is used to extract the pair distribution functions (PDF) which include the structural information. The key question was whether any bound COCl remains following photoexcitation, and what the time scales are for the associated dynamics. The structure of the two conformers of oxalyl chloride and the ΔPDF are shown in Fig. 3. Our own TD-

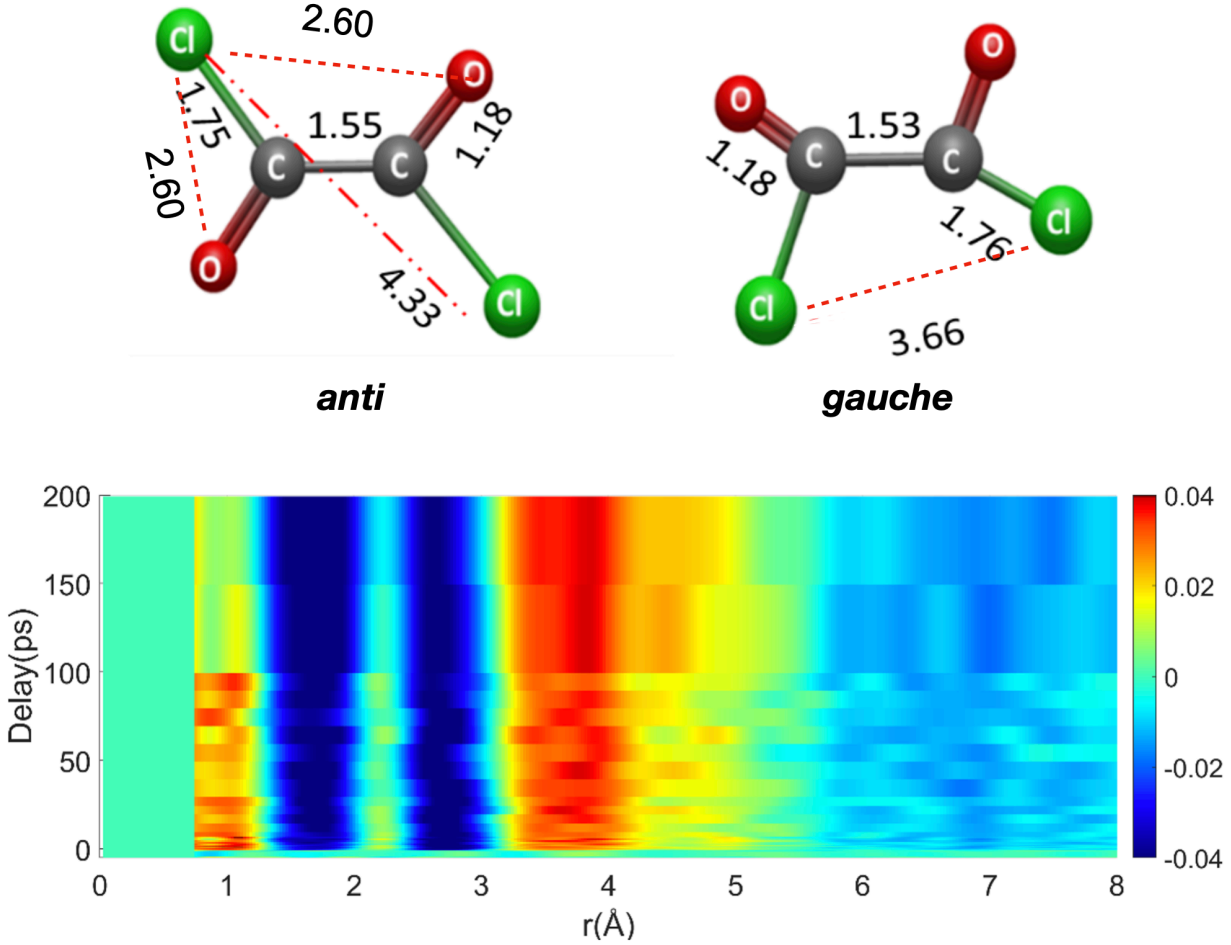

Figure 3. Conformer structures with bond distances in Å (top). Time-dependent ΔPDF obtained from analysis of diffraction signals (bottom).

DFT calculations suggest the *gauche* conformer is optically inactive at 200 nm, while the *anti* form has a strong transition. The ΔPDF shows very rapid onset dynamics, with bleaches around 1.7 and 2.8 Å corresponding to loss of C-C and C-Cl bonding distances and Cl-O nonbonding distances in the *anti* conformer. Positive signals are seen near 1 Å and 3.8 Å. The former corresponds to the CO distance in the carbon monoxide product, while 3.8 Å is ascribed to the Cl-Cl nonbonding distance in the *gauche* conformer

that is undissociated and appears as the *anti* conformer is depleted. No sign of any signals associated to ClCO were found.

3. Future Directions

Crossed-beam H atom reactions. In the next year we plan hot H atom reactions with polyatomic molecules using our universal VUV probe. This is a good opportunity to bring the power of our single-photon ionization detection to bear to probe the reaction dynamics, including abstraction site specificity, for an important class of polyatomic reactions. We intend to expand the range

Time-resolved CEI

To perform time-resolved coulomb explosion measurements we first need to shorten the 140 fs pulse that the laser now produces. To do this we have constructed a set-up to place a hollow fiber in the beamline. The fiber has an inner diameter of 500 μm which guides the laser beam over a length of around 70 cm. This keeps the intensity high over a long distance meaning non-linear effects can lead to significant spectral broadening allowing for shorter laser pulses. We are now trying to compress the pulse down to shorter temporal lengths using chirp mirrors. The pulse lengths are measured with a commercial FROG.

Argon is the most commonly used gas to fill hollow core fibers, however, a recent paper showed that for longer initial pulse lengths, greater broadening will occur in molecular gases. We have explored and confirmed significant broadening with different gases. Currently CO_2 is being used as it produces the largest broadening (up to 200 nm) as well as being a relatively inexpensive. We are now currently working to compress these pulses.

MeV UED Experiments

We also have upcoming beamtime in July at the SLAC LCLS facility to perform an ultrafast electron diffraction experiment on isoxazole photodissociation. Isoxazole is a five-membered heterocycle with a weak N-O bond. Previous work as shown two dissociation pathways with an intermediate near a conical intersection governing both. The goal of this experiment is to study the slower dissociation pathway which spends a more extended period of time on the ground state.

4. DOE Publications 2019-present

H. Li and A. G. Suits, "Universal Crossed Beam Imaging Studies of Polyatomic Reaction Dynamics," *Phys Chem Chem Phys.* (2020) **22**, 11126-11138 DOI: 10.1039/D0CP00522C.

H. Li, D. Troya and A. G. Suits, "Multichannel dynamics in the OH + n-butane reaction revealed by crossed-beam slice imaging and quasiclassical trajectory calculations," *J. Chem. Phys.* (2020) 153, 104302. DOI: 10.1063/5.0013585.

G. A. Cooper, S. T. Alavi, W. Li, S.-K. Lee, and A. G. Suits, "Coulomb Explosion Dynamics of Chlorocarbonylsulfenyl Chloride," *J. Phys. Chem. A.* (2021) **125**, 5481-5489. DOI: 10.1021/acs.jpca.1c02332.

S. Tahereh Alavi, Graham A. Cooper and Arthur G. Suits "Coulomb Explosion Dynamics of Methoxycarbonylsulfenyl Chloride by 3D Multimass Imaging," Mol. Phys. (2021) **120**, e1988170, DOI: 10.1080/00268976.2021.1988170.

Curvature Formation During TCD for Activity Regeneration by Partial Oxidation for Maintaining Autocatalytic Activity

Randy Vander Wal[1,2], Adri van Duin[2] and Margaret Kowalik[2]
[1]The EMS Energy Institute and [2]The Dept. of Mechanical Engineering
Penn State University
University Park, PA 16802
ruv12@psu.edu, acv13@psu.edu

I. Program Scope

Motivation for Thermo-catalytic Decomposition

Hydrogen is envisioned as the energy carrier (fuel) of the future and is a crucial feedstock for various manufacturing industries. Thermo-catalytic decomposition (TCD) of methane can produce CO_X-free hydrogen for PEM fuel cells, oil refineries, ammonia and methanol production [1]. Recent research has focused on enhancing the production of hydrogen by the direct thermo-catalytic decomposition of methane to form elemental carbon and hydrogen as an attractive alternative to the conventional steam reforming process [2].

Carbon as a catalyst has many advantages compared to other catalytic materials: a) fuel flexibility, b) insensitivity to sulfur poisoning and c) high temperature resistance. TCD offers 100% carbon capture with the solid, high purity carbon useful as electrode material for energy storage [3]. Despite these advantages, carbon as a catalyst also problematically deactivates. Ideally the deposited carbon would be autocatalytic but all studies with methane find that *the deposited carbon is not as active a catalyst as the original carbon.*

Addressing TCD and Regeneration Research Needs

High fidelity parallels exist between TCD and soot processes. The TCD rate may be viewed as equivalent to a soot particle growth rate. Both reactions add mass via heterogenous radical-driven reactions. In a flame environment, variables affecting growth are highly coupled. In TCD these factors may be disentangled, and their contributions resolved. Of particular interest are the relationships between nanostructure, active sites and growth rate. These same connections apply to TCD. Nanostructure governs active site number. In turn, active sites determine kinetic rates. Additionally, deposition conditions determine nanostructure and thus kinetic rates.

The proposed TCD measurements provide direct measures of each of these parameters, resolved by species, parametric with temperature and differentiated by nanostructure of nascent carbon. As detailed objectives,

1. Quantified nanostructure, time-resolved and correlated with TCD rate tests the dependence of rate on initial nanostructure and its time-variation.
2. Similarly, the TCD dependence on active sites tests the correlation between active sites and kinetic rates.
3. Correlation between nanostructure and active sites throughout TCD tests continuity of dependence.
4. Ties between experiments and atomistic- plus continuum-scale simulations include a) capturing the evolving nanostructure of the carbon deposit under TCD and soot relevant conditions, b) resolving nanostructure impact on regeneration and connecting to (renewed) activity in TCD and c) active site identification.

Active sites are related to nanostructure by comparison of simulations to experimental chemical kinetic rates and nanostructure metrics. Sequential rate measurements are made along the course of TCD and regeneration reactions. At the same corresponding points nanostructure are observed and quantified by

HRTEM and image analyses, enabling development of the hypothesized correlations. The overall project goal is to connect active sites, nanostructure and deposition rates in concert with ReaxFF-based modeling.

II. Recent Progress

Approach

A hot-wall CVD reactor is used for carbon deposition with quartz substrates using natural gas mixtures as feed. Reaction kinetics are evaluated based upon deposited carbon. Carbon deposition is determined by measuring film thickness via SEM image analysis. The test matrix consists of reaction duration (0.5 – 3 hrs.) and temperature (700 – 1,100 °C) for each gas mixture. Active sites are determined by a two-step procedure consisting of activated O_2 chemisorption at 300 °C followed by XPS analysis for surface oxygen concentration and resolution by bonding type. Nanostructure is characterized by HRTEM and fringe image analysis applied to deposited carbon films, extracted and deposited upon TEM grids.

Results

Shown in Fig. 1 is a SEM image of the TCD carbon deposit formed under TCD. Carbon deposition rate is measured by film thickness and can be translated into mass. The uniformity and 2D aspect of these TCD films is beneficial for XPS analysis of active sites. Such would not be possible using a packed bed configuration wherein such uniformity would not exist.

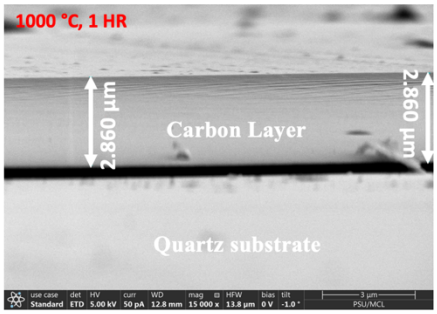

Fig. 1 – SEM image of carbon deposit upon a quartz substrate.

XPS has three key advantages for active site determination when coupled with chemisorption, compared to temperature programmed desorption – the more commonly used technique. First, it is quantitative for oxygen content, at.(%), and second, it has better sensitivity (~0.1%). Third, XPS directly measures chemisorbed oxygen rather than derivative reaction products (CO and CO_2) as in temperature programmed desorption. Therein it also differentiates oxygen groups, which otherwise can be scrambled by interconversion during the high temperature ramp used in TPD.

Given the often-observed declining rates in TCD, regeneration by partial oxidation is a solution. Before applying chemisorption – XPS analysis to measure active sites in TCD, we are testing the methodology against partially oxidized carbons – for which active sites are known to increase upon partial oxidation [4,5]. Here carbon blacks with well characterized nanostructure and oxidation behaviors are used as model materials and surrogates for TCD carbon deposits.

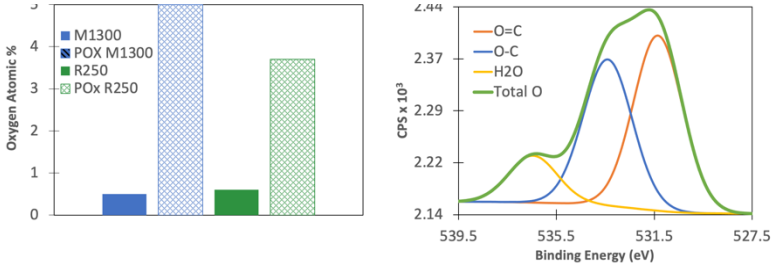

Fig. 2 – Surface atomic oxygen for nascent and partially oxidized carbons and a representative high-resolution O1s scan identifying the different oxygen groups.

Shown in Fig. 2 is the comparative increase in active sites upon partial oxidation as measured by O_2 chemisorption followed by XPS analysis. The high-resolution scan about the O1s region and deconvolution distinguishes the different oxygen functional groups formed during the activated chemisorption process. R250 and M1300 are two carbon blacks with different nanostructure. Partial oxidation creates active sites – quantified by the increased chemisorbed O_2.

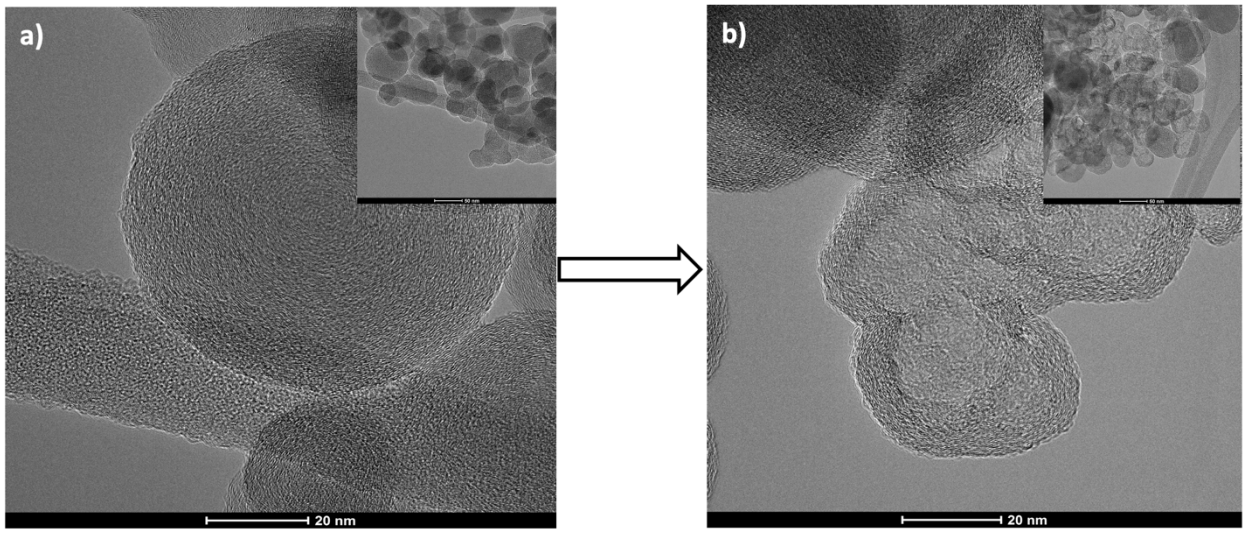

Fig. 3 – HRTEM images showing a) nascent carbon structure, and b) its change upon partial oxidation. The coarser structure observed along the particle perimeter is "visual" evidence of nanostructure breakup due to oxidation and corresponding increase in active (edge) sites (as per XPS) as lamellae regress in size.

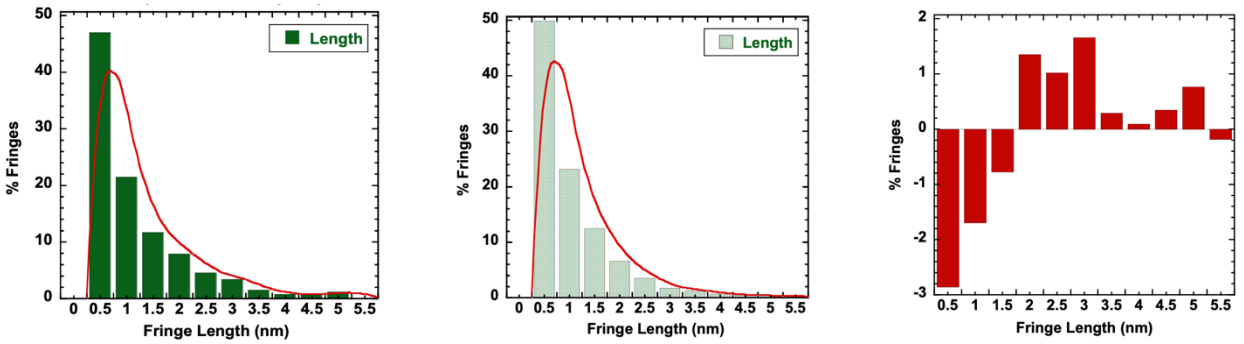

Fig. 4 – Fringe analyses for fringe length of the nascent carbon, partially oxidized form and difference plot (nascent – partially oxidized).

The fringe length distributions correspond to the nascent and partially oxidized carbon. The difference plot highlights the effect of partial oxidation upon the lamellae length distribution – where the positive values correspond to a larger fraction of longer lamellae in the nascent carbon compared to negative values – representing the larger content of shorter lamellae in the partially oxidized carbon. Alternatively stated, partial oxidation breaks up longer lamellae, thereby creating a larger content of shorter lamellae. These analyses support the visual inference from the HRTEM images and are consistent with XPS results. Comparative differences in these distributions upon partial oxidation will be correlated to active sites as measured by XPS to test their correspondence with nanostructure.

III. Future Plans

Carbon deposition occurs at actives sites in TCD with loss of activity presumably due to loss of active sites. Regeneration creates new active sites – with a rate dependent upon the increase in active sites with reaction extent. The premise is that the sites formed during regeneration (i.e., gasification) are sites active for TCD. Therein the rate of TCD immediately following regeneration ought to strongly correlate with the final

regeneration/oxidation rate. Experiments will test the equivalency of active sites by comparative rates versus active sites at systematic intervals during TCD and regeneration, coupled with nanostructure quantification. Notably the ReaxFF method can identify such sites and track their evolution as carbon deposits during TCD.

Additionally, TCD conditions producing lamellae curvature coupled with oxidative regeneration present a synergistic pairing of reaction processes sufficient to maintain and/or increase TCD rate in cycling TCD and regeneration. Formation of an initial basal plane vacancy results in a geometrical progression in the number of new interior edge sites – via internal edge recession. This magnification of reactive edge sites is manifested as an increasing rate as oxidation proceeds, i.e., as the interior "hole" becomes larger. Moreover, the next underlying (curved) lamella is now exposed for initial basal attack (not shown). By such nanostructure directed gasification, only partial regeneration would be required thereby largely preserving the CO_2 advantages of TCD. Moreover, the CO generated by the regeneration (gasification) reaction could be combined with TCD produced H_2 for Fischer-Tropsch synthesis of liquid fuels.

Project Outcomes

If nanostructure can be correlated to active sites, a surrogate metric will be established by which to gauge carbon structure for reactivity under TCD and regeneration conditions. Nanostructure provides a more straightforward method of assessing carbon reactivity based on structure than active site measurement – the latter being very dependent upon sample preparation and chemisorption procedure. In concert a significant outcome of the reactive force field-based atomistic-scale simulations will be a) identification of the active sites under TCD and regeneration, b) elucidation of deposit nanostructure in relation to reaction parameters, and c) atomistic scale interpretation of kinetic parameters.

IV. Publications acknowledging DOE_BES support (2021-2022)

Nkiawete, M., and Vander Wal, R., Thermo-catalytic decomposition of methane: Focus on nanostructure Session/Paper 2A15: 149NEC-0118. 2022 Spring Technical Meeting, Eastern States Sections of The Combustion Institute, University of Central Florida Orlando, Florida March 6-9, 2022.

V. References

1. Muradov N. (2002). Thermo-catalytic CO_2-free production of hydrogen from hydrocarbon fuels. U.S. DOE Hydrogen Program Review. U.S.: Department of Energy (DOE); NREL/CP-610-32405.

2. Ahmed, S., Aitani, A., Rahman, F., Al-Dawood, A., and Al-Muhaish, F. (2009). Decomposition of hydrocarbons to hydrogen and carbon. *Applied Catalysis A: General*, *359*(1), 1-24.

3. De Falco, M., Basile, A. (Eds.). (2015). *Enriched Methane: The First Step Towards the Hydrogen Economy*. Springer.

4. Singh, M., Srilomsak, M., Wang, Y., Hanamura, K., & Vander Wal, R. (2019). Nanostructure changes in diesel soot during NO2–O2 oxidation under diesel particulate filter-like conditions toward filter regeneration. *International Journal of Engine Research*, *20*(8-9), 953-966.

5. Gaddam, C. K., Vander Wal, R. L., Chen, X., Yezerets, A., & Kamasamudram, K. (2016). Reconciliation of carbon oxidation rates and activation energies based on changing nanostructure. *Carbon*, *98*, 545-556.

Probing Nonvalence Excited States of Anions Using Photodetachment and Photoelectron Spectroscopy

Lai-Sheng Wang
Department of Chemistry, Brown University, Providence, RI 02912
Email: lai-sheng_wang@brown.edu

Program Scope

This program is aimed at obtaining energetic, electronic, and vibrational information of molecules and radicals important in combustion or the atmosphere, such as polycyclic aromatic hydrocarbons (PAHs), using new anion spectroscopic techniques. Negative ions do not possess Rydberg states, but highly-diffuse nonvalence states can exist in anions as a result of long-range forces between the extra electron and the neutral molecular cores. Valence-bound anions may possess diffuse nonvalence excited states just below the detachment threshold. The objective of this program is to probe the nonvalence excited states that exist in anions of PAH or functionalized PAH species and to utilize the nonvalence excited states as a new window to obtain energetic and spectroscopic information of the underlying neutral PAH radicals and molecules. The PI's lab has built a high-resolution electrospray photoelectron imaging apparatus equipped with a cryogenically-cooled ion trap, which is ideal to probe this class of nonvalence anionic excited states. Photodetachment spectroscopy will be used to search for the nonvalence excited states of PAH anions via resonant two-photon detachment or vibrational autodetachment. The autodetachment process is investigated by resonantly-enhanced photoelectron spectroscopy. The combination of photodetachment spectroscopy and resonant photoelectron spectroscopy can yield rich energetic, electronic, and vibrational information about the underlying neutral species, as well as information about vibronic coupling leading to autodetachment.

Recent Progress

Probing the Dipole-Bound State in the 9-Phenanthrolate Anion by Photodetachment Spectroscopy, Resonant Two-Photon Photoelectron Imaging, and Resonant Photoelectron Spectroscopy.[12] Valence-bound anions with a dipolar core can support dipole-bound states (DBSs) below the electron detachment threshold. The highly diffuse DBS observed is usually of σ symmetry with an *s*-like orbital. A π-type DBS was observed previously in the 9-anthrolate anion ($9AT^-$) and it was shown to be stabilized due to the large anisotropic polarizability of the 9AT core. To confirm the general existence of π-DBS and its structural dependence, we investigated the 9-phenanthrolate anion ($9PT^-$), which has a different structure and lower symmetry than $9AT^-$. Photodetachment spectroscopy revealed a DBS 257 cm^{-1} below the detachment threshold of $9PT^-$ at 19,627 cm^{-1} (2.4334 eV). Resonant two-photon photoelectron imaging indeed showed a π symmetry for the DBS. Similar to that observed in $9AT^-$, the π-DBS in $9PT^-$ is also stabilized by the anisotropic polarizability of the 9PT core and accessed via non-adiabatic population transfer (NAPT) from the initially populated σ-DBS (Fig. 1). Photodetachment spectroscopy unveiled nine above-threshold vibrational resonances of the DBS, resulting in nine highly non-Franck-Condon resonant photoelectron spectra by tuning the detachment laser to the vibrational

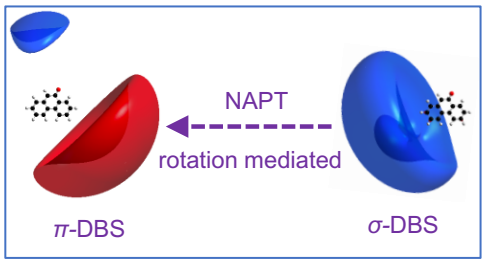

Fig. 1. Non-adiabatic population transfer from the σ- to the π-DBS.

resonances. The combination of photodetachment spectroscopy and resonant photoelectron spectroscopy allowed frequencies for nine vibrational modes of the 9-phenathroxy radical to be measured, including the six lowest frequency bending modes.

Observation of A Dipole-Bound Excited State in 4-Ethynylphenoxide and Comparison with the Quadrupole-Bound Excited State in the Isoelectronic 4-Cyanophenoxide.[13] Negative ions do not possess Rydberg states, but can have Rydberg-like nonvalence excited states near the electron detachment threshold, including DBSs and quadrupole-bound states (QBSs). While DBSs have been studied extensively, quadrupole-bound excited states have been more rarely observed. 4-cyanophenoxide ($4CP^-$) was the first anion observed to possess a quadrupole-bound exited state 20 cm^{-1} below its detachment threshold. We observed a DBS in the isoelectronic 4-ethynylphenoxide anion ($4EP^-$), providing a rare opportunity to compare the behaviors of a dipole-bound and a quadrupole-bound excited state in a pair of very similar anions. Photodetachment spectroscopy (PDS) of cryogenically-cooled $4EP^-$ reveals a DBS 76 cm^{-1} below its detachment threshold. Photoelectron spectroscopy (PES) at 266 nm shows that the electronic structure of $4EP^-$ and $4CP^-$ are nearly identical. The observed vibrational features in both the PDS and PES, as well as autodetachment from the nonvalence excited states, are also found to be similar for both anions. However, resonant two-photon detachment (R2PD) from the bound vibrational ground state is observed to be very different for the DBS in $4EP^-$ and the QBS in $4CP^-$. The R2PD spectra reveal that decays take place from both the DBS and QBS to the respective anion ground electronic states within the 5 ns detachment laser pulse due to internal conversion followed by intramolecular vibrational redistribution (IVR) and relaxation, but the decay mechanisms appear to be very different. In the R2PD spectrum of $4EP^-$, we observe strong threshold electron signals, which are due to detachment, by the second photon, of highly rotationally excited anions resulted from the decay of the DBS. On the other hand, in the R2PD spectrum of $4CP^-$ we observe well-resolved vibrational peaks due to the three lowest-frequency vibrational modes of $4CP^-$, which are populated from the decay of the QBS. The different behaviors of the R2PD spectra suggest unexpected differences between the relaxation mechanisms of the dipole-bound and quadrupole-bound excited states.

Resonant Two-Photon Photoelectron Imaging and Adiabatic Detachment Processes from Bound Vibrational Levels of Dipole-Bound States.[14] The binding energies of DBSs are usually small, ranging from a few to few hundred wavenumbers and generally cannot support bound vibrational levels below the detachment threshold. Thus, vibrational excitations in the DBS are usually above the electron detachment threshold and they have been used to conduct resonant photoelectron spectroscopy, which is dominated by state-specific autodetachment. We investigated a cryogenically-cooled complex anion, the enantiopure (*R*)-(-)-1-(9-anthryl)-2,2,2-trifluoroethanolate (*R*-$TFAE^-$). The neutral *R*-TFAE radical is relatively complex and highly polar with a non-planar structure (C_1 symmetry). Photodetachment spectroscopy reveals a DBS 209 cm^{-1} below the detachment threshold of *R*-$TFAE^-$ and seven bound and eight above-threshold vibrational levels of the DBS. Resonant two-photon detachment (R2PD) via the bound vibrational levels of the DBS exhibits strictly adiabatic photodetachment behaviors by the second photon, in which the vibrational energies in the DBS are carried to the neutral final states, because of the parallel potential energy surfaces of the DBS and the corresponding neutral ground electronic state. Relaxation processes from the bound DBS levels to the ground and low-lying electronic excited states of *R*-$TFAE^-$ are also observed in the R2PD photoelectron spectra. The combination of photodetachment and resonant photoelectron spectroscopy yields frequencies for eight vibrational modes of the *R*-TFAE radical.

Observation of Core-Excited Dipole-Bound States.[15] Polar molecules can bind an electron in a diffuse orbital due to the charge-dipole interaction. Electronic excited states of polar molecules can also bind an electron to form core-excited dipole-bound states (DBSs), analogous to core-excited Rydberg states. However, core-excited DBSs have not been observed because of the complicated electronic structure of molecular systems. Here we report the observation of a core-excited DBS in the pyrazolide anion as a result of the favorable electronic structure of the neutral pyrazolyl core, which has a low-lying excited state ($\tilde{A}^2B_1$) only 266 cm^{-1} above its ground state ($\tilde{X}^2A_2$). The binding energy of the DBS associated with the ground state is measured to be 221 cm^{-1}, while that of the core-excited DBS is 276 cm^{-1}, which is still a bound state relative to the detachment threshold. Vibrational Feshbach resonances are observed for both DBSs and their autodetachment behaviors are studied by resonant photoelectron imaging.

Probing the Electronic Structure and Spectroscopy of the Pyrrolyl and Imidazolyl Radicals using High Resolution Photoelectron Imaging of Cryogenically-Cooled Anions.[16] High-resolution photoelectron imaging and photodetachment spectroscopy of cryogenically-cooled pyrrolide and imidazolide anions are used to probe the electronic structure and spectroscopy of the pyrrolyl and imidazolyl radicals. The high-resolution data allow the ground state vibronic structures of the two radicals to be completely resolved, yielding accurate electron affinities of 2.1433 ± 0.0008 eV and 2.6046 ± 0.0006 eV for pyrrolyl and imidazolyl, respectively. Fundamental frequencies for eight vibrational modes of pyrrolyl and ten vibrational modes of imidazolyl are measured, including numerous nonsymmetric Franck-Condon-forbidden modes. Two electronic excited states are also observed for the two radicals, displaying diffuse spectral features in both systems. The observations of nonsymmetric vibrational modes in the ground states and the diffuse excited state features provide strong evidence of vibronic couplings between the ground state and the two close-by excited states. The 2-pyrrolide isomer is also observed as a minor species from the electrospray ionization source and the electron affinity of 2-pyrrolyl is measured to be 1.6690 ± 0.0030 eV along with five vibrational frequencies. Even though the HOMOs of both pyrrolide and imidazolide are p orbitals, photodetachment spectroscopy reveals completely different threshold behaviors for the two anions: a *d*-wave-dominated spectrum for pyrrolide and an *s*-wave-dominated spectrum for imidazolide. The current study provides a wealth of electronic and spectroscopic information, which is ideal to compare with more accurate vibronic coupling calculations for these two important radicals, as well as interesting information about the photodetachment dynamics of the two anions.

Future Plans

Experiments on dipole-bound excited states will be continued on O- and N-containing PAH anions. We have found recently that N-containing 5-memebered ring systems have rich spectroscopy and complicated vibronic couplings, which can be effectively interrogated using our cryogenic ion trap and high-resolution photoelectron imaging.[15,16] We will continue this effort and also extend to O-containing 5-membered ring systems, before we move to larger PAH species.

Publications resulted from the BES-GPCP sponsored research (2019-2022)

1. G. Z. Zhu, C. H. Qian, and L. S. Wang. Tautomer-Specific Resonant Photoelectron Imaging of Deprotonated Cytosine Anions. *Angew. Chem. Int. Ed*. **58**, 7856-7860 (2019). (DOI: 10.1002/anie.201903444)

2. J. Czekner, L. F. Cheung, G. S. Kocheril, and L. S. Wang. Probing the Coupling of A Dipole-Bound Electron with the Molecular Core. *Chem. Sci*. **10**, 1386-1391 (2019). (DOI: 10.1039/c8sc04771e)
3. G. Z. Zhu, L. F. Cheung, Y. Liu, C. H. Qian, and L. S. Wang. Resonant Two-Photon Photoelectron Imaging and Intersystem Crossing from Excited Dipole-Bound States of Cold Anions. *J. Phys. Chem. Lett*. **10**, 4339-4344 (2019). (DOI: 10.1021/acs.jpclett.9b01743)
4. C. H. Qian, G. Z. Zhu, and L. S. Wang. Probing the Critical Dipole Moment to Support Excited Dipole-Bound States in Valence-Bound Anions. *J. Phys. Chem. Lett*. **10**, 6472-6477 (2019). (DOI: 10.1021/acs.jpclett.9b02679)
5. G. Z. Zhu and L. S. Wang. High-Resolution Photoelectron Imaging and Resonant Photoelectron Spectroscopy via Noncovalent-Bound Excited States of Cryogenically-Cooled Anions. *Chem. Sci.* **10**, 9409-9423 (2019) (Invited article). (DOI: 10.1039/C9SC03861B)
6. D. F. Yuan, Y. Liu, C. H. Qian, Y. R. Zhang, B. M. Rubenstein, and L. S. Wang. Observation of a π-Type Dipole-Bound State in Molecular Anions. *Phys. Rev. Lett*. **125**, 073003 (2020). DOI: 10.1103/PhysRevLett.125.073003.
7. C. H. Qian, G. Z. Zhu, and L. S. Wang. Photodetachment Spectroscopy and Resonant Photoelectron Imaging of the 2-Naphthoxide Anion via Dipole-Bound Excited States. *J. Chem. Phys*. **152**, 214307 (13 pages) (2020). DOI: 10.1063/5.0011234.
8. Y. T. Wang, C. G. Ning, H. T. Liu, and L. S. Wang. High-Resolution Photoelectron Imaging and Photodetachment Spectroscopy of Cryogenically-Cooled IO^-. *J. Phys. Chem. A* **124**, 5720-5726 (2020). DOI: 10.1021/acs.jpca.0c04080.
9. D. F. Yuan, Y. Liu, C. H. Qian, G. S. Kocheril, Y. R. Zhang, B. M. Rubenstein, and L. S. Wang. Polarization of Valence Orbitals by the Intramolecular Electric Field from a Diffuse Dipole-Bound Electron. *J. Phys. Chem. Lett*. **11**, 7914-7919 (2020). DOI: 10.1021/acs.jpclett.0c02514
10. Y. Liu, G. Z. Zhu, D. F. Yuan, C. H. Qian, Y. R. Zhang, B. M. Rubenstein, and L. S. Wang. Observation of a Symmetry-Forbidden Excited Quadrupole-Bound State. *J. Am. Chem. Soc*. **142**, 20240-20246 (2020). DOI: 10.1021/jacs.0c10552
11. C. H. Qian, Y. R. Zhang, D. F. Yuan, and L. S. Wang. Photodetachment Spectroscopy and Resonant Photoelectron Imaging of Cryogenically-Cooled 1-Pyrenolate. *J. Chem. Phys*. **154**, 094308 (2021). DOI: 10.1063/5.0043932
12. D. F. Yuan, Y. R. Zhang, C. H. Qian, Y. Liu, and L. S. Wang. Probing the Dipole-Bound State in the 9-Phenanthrolate Anion by Photodetachment Spectroscopy, Resonant Two-Photon Photoelectron Imaging, and Resonant Photoelectron Spectroscopy. *J. Phys. Chem. A* **125**, 2967-2976 (2021). DOI: 10.1021/acs.jpca.1c01563
13. "Observation of A Dipole-Bound Excited State in 4-Ethynylphenoxide and Comparison with the Quadrupole-Bound Excited State in the Isoelectronic 4-Cyanophenoxide" (Y. R. Zhang, D. F. Yuan, C. H. Qian, and L. S. Wang), *J. Chem. Phys*. **155**, 124305 (2021). doi:10.1063/5.0065510
14. "Resonant Two-Photon Photoelectron Imaging and Adiabatic Detachment Processes from Bound Vibrational Levels of Dipole-Bound States" (D. F. Yuan, Y. R. Zhang, C. H. Qian, and L. S. Wang), *Phys. Chem. Chem. Phys*. **24**, 1380-1389 (2022). DOI: 10.1039/D1CP05219E
15. "Observation of Core-Excited Dipole-Bound States" (Y. R. Zhang, D. F. Yuan, and L. S. Wang), *J. Phys. Chem. Lett*. **13**, 2124-2129 (2022). DOI: 10.1021/acs.jpclett.2c00275
16. "Probing the Electronic Structure and Spectroscopy of the Pyrrolyl and Imidazolyl Radicals using High Resolution Photoelectron Imaging of Cryogenically-Cooled Anions" (Y. R. Zhang, D. F. Yuan, and L. S. Wang), *Phys. Chem. Chem. Phys*. **24**, 6505–6514 (2022).
    DOI: 10.1039/D2CP00189F

Experimental and Computational Study of Quantum Nuclear and Many-Body Effects in Water Network Formation and Water-Surface Interaction in PAH-Water Cluster Ions

J. Mathias Weber[1,2] (weberjm@jila.colorado.edu, PI)
Joel D. Eaves[2] (joel.eaves@colorado.edu, Co-PI)

[1]JILA, 440 UCB, University of Colorado Boulder, Boulder, CO 80309-0440
[2]Department of Chemistry, 215 UCB, University of Colorado Boulder, Boulder, CO 80309-0215

Program Scope

In this combined experimental and theoretical program, we aim to quantify interactions between water molecules and aromatic hydrocarbons (PAHs) at an unprecedented level of detail. Molecular clusters are excellent systems for theoretical and computational work, since they are sufficiently small for high-accuracy electronic structure calculations, and their spectroscopy can unveil important information about details of molecular interactions that remain obscured in the condensed phase. The precise control over experimental conditions in cryogenic cluster ion experiments, both through mass selection and cooling, dramatically reduces systematic uncertainties compared to analogous condensed phase work. Crucially, quantum nuclear effects that arise from non-classical, quantum behavior of protons in water often display modest effects in bulk liquid at room temperature. These effects are expected to be more pronounced in small water-PAH clusters, particularly at low temperatures. Thus, the proposed systems will allow us to explore several different treatments for including quantum nuclear and many-body effects in the computational description of water-PAH interactions.

PAHs are valuable model systems for both neutral and charged graphene and their chemical derivatives. The water-graphene interaction is of paramount importance in materials chemistry. Theoretical predictions and careful experiments have shown that the graphene wetting characteristics are highly sensitive to small changes in the chemistry on the graphene surface. For example, the application of small voltages applied to nanoporous graphene is predicted to increase water throughput in desalination applications, and the predicted water transport through such systems strongly depends on the details of the model for water-carbon interaction used. This implies that applications ranging from battery technology to electrocatalysis depend on interfacial phenomena that contemporary theoretical models only poorly describe. Experimentally probing the molecular level details of the interaction of single-layer graphene with water is also rather challenging, due to pitfalls in the preparation of clean single-layer graphene films and the size and shape heterogeneity of graphenic nanostructures synthesized in typical chemical preparations.

We will study the interaction of water molecules with charged PAHs in mass-selected cluster ions of the form $PAH^{+/-}\cdot(H_2O)_n$, using infrared photodissociation spectroscopy, and compare the experimental results with theoretical predictions. From an experimental point of view, using mass-selected PAH ions allows us to precisely control the size and shape of the graphenic system, as well as the number of water molecules interacting with it. This strategy leads to exquisitely well-controlled experimental conditions because it removes fluctuations in the solvent environment and lets us study solvent interactions one molecule at a time.

In the theoretical/computational component of this project, we will parameterize the many-body intermolecular potential, and test both centroid and ring-polymer molecular dynamics approximations to relevant quantum time correlation functions associated with transitions between stable structures of the clusters and IR spectroscopy. Fully predictive molecular models for aqueous chemistry must account for complexities in both the nuclear potential energy surface and the dynamics on those surfaces. The potential energies have received the lion's share of attention. We pursue a complementary approach that focuses on the dynamics.

Recent Progress

In the experimental component of the program, we have explored different avenues for generating $PAH^{-}\cdot(H_2O)_n$ cluster ions. We first investigated routes to prepare $PAH^{-}\cdot(H_2O)_n$ cluster ions by electrospray ionization. Using an organic electron donor, tetrakis(diethylamino)ethylene (TDAE), with solutions of PAHs (pyrene, tetracene), and analyzing the product ions ultimately showed that this strategy mainly yields their deprotonation products, $[PAH\text{-}H]^{-}$, with relatively low yields. The generation of ions generated from PAHs with acidic protons, such as indole and pyrene carboxylic acid is more facile. While up to three water molecules could be attached to pyrene carboxylic acid, we judged that this target would not be relevant to the project, since exploratory DFT calculations showed that the water adducts would not interact with the π system of the molecule, and would therefore not contribute to the main thrust of the project. Other PAH anions (such as deprotonated indole) did not attach water molecules in the cryogenic trap. This finding has surprised us. We hypothesize that the density of vibrational states in the PAH ion is insufficient to allow efficient collisional cooling in the ion trap, preventing the formation of water adducts. We have changed our ion formation strategy, building a heated pulsed valve and setting up a laser vaporization

We therefore used our expertise in ion sources to set up other ion sources for generating PAH radical anions by electron attachment in discharge plasmas and in laser vaporization plumes. We assembled and tested a supersonic entrainment source based on thermal evaporation of PAHs, and we are in the process of setting up a laser vaporization source as well.

The theoretical side of the project has developed time-correlation function methods to compute the absorption spectra, directly, from molecular dynamics trajectories, without reference to a harmonic reference system. By introducing anharmonic vibrations into an existing potential, parameterized to reproduce gas phase vibrational spectra, we now have a molecular potential for water suitable both for gas phase spectra and solution phase thermodynamics. Further theoretical investigation has found several basins on the potential energy surface of two to three water molecules with a naphthalene anion that are structurally similar, but that do not interconvert with one another—kinetic traps—a subtlety that is very difficult to see using conventional computational methods for small molecule gas phase spectra. To sample efficiently, we employed parallel-tempering, a mixed Monte-Carlo/molecular dynamics method that can allow systems to cross energy barriers in frustrated systems, like solvated proteins.

With both the potential and sampling method in place, the time-correlation function calculation of the IR spectrum does indeed reproduce many of the observed spectral features, but with transitions systematically shifted to the blue. The potential we created does indeed reproduce the absorption spectrum of liquid water, from THz to IR, particularly in the hydrogen bonding window near 3600 cm^{-1}. We therefore suspect that the differences between observation and prediction lie in the fact that the potential does not allow the electron from the naphthalene anion to enter the antibonding σ^* orbital on oxygen, which would weaken the bond and lead to a red shift. While we currently do not account for this feature, we plan to include it systematically in the next phase of the project.

Future Plans

The next steps in the experimental program are to generate hydrated PAH cluster anions, $PAH^{-}\cdot(H_2O)_n$. For smaller PAHs such as anthracene and pyrene, we will try to use thermal evaporation of the PAH, while laser vaporization will be necessary for the larger species such as corannulene and coronene. Once these hydrated cluster anions are prepared, we plan to acquire their infrared spectra. If possible, we will use Ar tagging, i.e., the preparation of target ions of the form $PAH^{-}\cdot(H_2O)_n\cdot Ar_m$, looking for the loss of Ar atoms upon infrared absorption. This strategy ensures that the target clusters have low temperatures (in the range of 50-100 K). We also plan to use the loss of water molecules from clusters without Ar tagging to obtain data at higher temperatures.

In the computational part of the program, we plan to explore how completely classical calculations of the IR spectra, using the time correlation function formalism, compare to those which include quantum nuclear effects, and we will compare how these different methodologies perform for the dynamics. Our early

data on naphthalene-water clusters make the case that we may need a more sophisticated treatment of the electron in the anionic cluster as a quantum object, and so we may need to develop a pseudopotential for it. Many believe that quantum nuclear effects are absorbed into the parameterization of the potential, but that has not been easy to show rigorously. These studies aim to find which parts of the potential are hiding the effects of quantum nuclear motion in purely classical dynamical simulations. We will test both water-naphthalene anion clusters and water-pyrene carboxylate clusters and benchmark both potentials and dynamics methods against experimental results.

Fundamental chemical kinetics of siloxane and silicon compounds

DOE BES Grant #18SC503179

Margaret S. Wooldridge (PI)
University of Michigan, Department of Mechanical Engineering, 2350 Hayward St., Ann Arbor, MI, 48109-2125, mswool@umich.edu
Andrew B. Mansfield
Eastern Michigan University Mechanical, Engineering, College of Technology, Ypsilanti, MI, 48197, amansfi3@emich.edu,
Robert S. Tranter
Chemical Sciences and Engineering Division, Argonne National Laboratory, Argonne, IL, 60439, tranter@anl.gov

Program Scope

Siloxanes and other silicon compounds play significant roles as impurities in land-fill gas and as primary feedstock materials for high-value and large-volume products, yet the fundamental reaction chemistry of gas-phase silicon compounds remains largely unexplored. This research program integrates two complementary experimental efforts to significantly advance the science of gas-phase silicon reaction chemistry. The primary research focus is on the elementary thermal reactions of siloxanes and their decomposition products with a progression in the chemical structure of the compounds studied to elucidate the effects of bond structure. An additional area of interest is the interaction of gas-phase species with silica nanoparticles that are formed naturally as products of the thermal reactions of siloxanes and during oxidation.

Recent Progress

Experimental Approach: The experimental approach leverages the strengths of the University of Michigan (UM) rapid compression facility (RCF) and atmospheric burner and the diaphragmless shock tube (DFST) and the high-repetition rate shock tube (HRRST) at Argonne National Laboratory for advancing understanding of siloxane chemistry. The combination of experimental approaches allows a broad and complementary range of state conditions to be studied with temperatures in the range of 700-2000 K and pressures of 0.1-50 bar. Previous work on this project (reported in the 2021 meeting) included high-fidelity RCF and HRRST measurements of ignition times of trimethylsilanol (TMSO) and hexamethyldisiloxane (HMDSO) and intermediate species measurements during decomposition of TMSO, HMDSO and hexamethylcyclotrisiloxane. With the RCF studies, the past year focused on narrow-line laser absorption measurements to measure the formation of the OH radical during ignition of H_2 and CO with and without the addition of trace amounts of TMSO. OH is the radical chain carrier in these ignition systems and the impact of trimethylsilanol on OH provides insight into the reaction pathways active during siloxane oxidation. The RCF experiments were complemented by atmospheric pressure burner studies that were used to develop calibration strategies for gas-chromatography and other experimental diagnostics (that will be applied in future RCF and Argonne experiments) and to characterize the composition of the nanoparticles created during siloxane oxidation (that will also be applied in future RCF experiments).

RCF OH Absorption studies: **Figure 1** shows recent measurements of OH radical concentrations obtained during ignition studies using narrow-line laser absorption during RCF experiments with H_2 and CO mixtures with and without the addition of 100 ppm of TMSO. The addition of 100 ppm

TMSO accelerates ignition from τ_{ign} = 6.7 ms to τ_{ign} = 4.8 ms and the OH time history is significantly affected by the TMSO. The OH time-history of the baseline case (with no TMSO), shows two distinct OH peaks at approximately 4 ms and the time of ignition, 6.7 ms. Two peaks of OH are expected based on model simulations of H_2 and CO with no siloxane. However, as seen in the OH data from the experiment with TMSO, the presence of the siloxane suppresses the formation of the earlier OH peak; only one OH maximum is observed at the time of ignition. Results of sensitivity and rate of production analyses of the baseline H_2+CO system (not shown here) indicate $H_2O_2(+M) = OH+OH(+M)$ dominates the formation of OH during the first step of the ignition process. Once the H_2 supply is consumed at the end of the first step of the ignition, the dominant formation reactions then change to primarily $H+O_2 = OH + O$ and $O+H_2O = OH + OH$. At the conditions studied, $H+O_2 = OH + O$ is in direct competition with $H+O_2(+M) = HO_2(+M)$ The suppression of the first OH peak with the addition of TMSO indicates that TMSO disrupts the H_2O_2/HO_2 kinetics, e.g., increasing the formation of H_2O_2, resulting in faster/earlier formation of OH. While the data are quite preliminary, the results clearly show significant sensitivity to the siloxane chemistry. Additional OH studies at broader state conditions and for additional siloxane mixtures will help clarify the specific effects on the reaction pathways. More broadly, the OH RCF data will directly complement the planned STF OH studies as well as the planned measurements of stable intermediate species in the RCF studies.

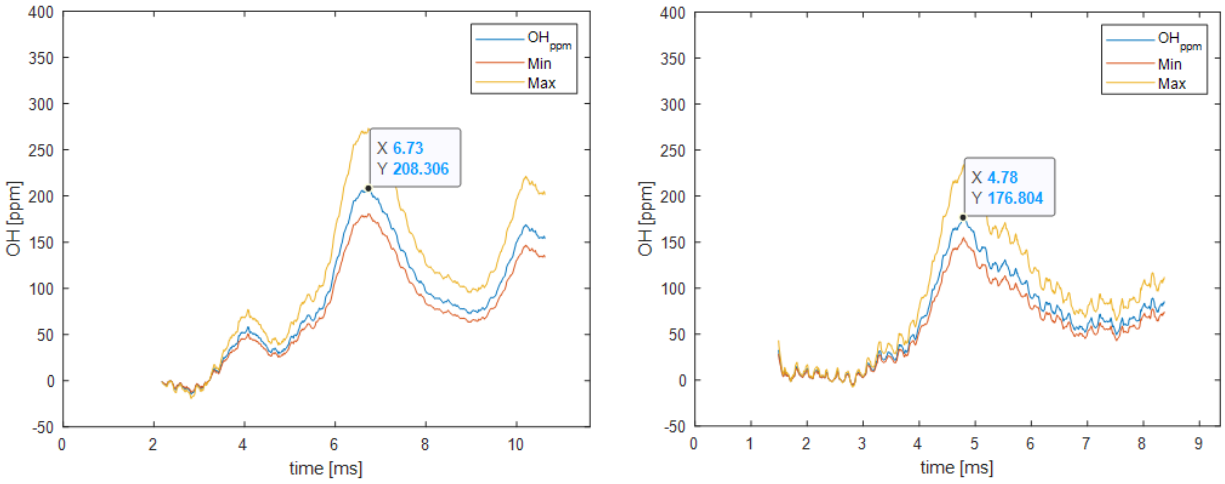

Figure 1. Comparison of measured OH time-histories obtained during RCF $H_2$and CO oxidation experiments at T = 1050 K, P = 5.1 atm without TMSO (left panel, τ_{ign} = 6.7 ms) and with 100 ppm TMSO (right panel, τ_{ign} = 4.8 ms). The lines represent the nominal OH values and the upper and lower bound of the uncertainty limits.

X-ray fluorescence imaging of flames for nanoparticle formation: We have employed the x-ray fluorescence (XRF) technique (see also GPCD-Kinetics abstract) at the Advanced Photon Source (APS) at Argonne [1,2,3] to establish reference measurements for siloxane flame studies. For this portion of the project, an atmospheric pressure multi-element diffusion burner (MEDB), which has been previously well documented for silane studies at UM [4], was delivered to Argonne and the reaction environment was characterized for baseline methane (CH_4) oxidation conditions. The MEDB is a valuable tool for developing reaction chemistry due to the nearly one-dimensional

behavior of the burner. In the Fall 2021 APS experiments, krypton XRF was used to map temperature fields for two burner configurations shown in **Figure 2**. The fuel gas was doped with krypton which was excited by a focused (5x6 μm cross section) 15 keV x-ray beam. The resulting Kr-Kα photons were collected orthogonal to the x-ray beam. The fluorescence signal yielded the number density of Kr atoms at each measurement location which was converted to a local temperature through the ideal gas law [2]. In one mode of operation, CH_4 was delivered to the entire 2.54 cm x 2.54 cm array of the burner, but not to central tube through which particle precursors can be delivered (the right panel of **Figure 2)**. In the other mode, methane was delivered to the square array as well as a central tube (the left panel of **Figure 2**). The steady operation of the burner allowed highly spatially resolved (5×6×200 μm volumes) x-ray measurements to be made from within 0.1 mm of the burner surface to above the flame. **Figure 3** shows images in the x-y plane (i.e., top-view of the burner) at 0.1 mm and 0.5 mm above the surface of the burner. The results show the rapid mixing that occurs between the fuel and oxidizers tubes to create the nearly one-dimensional flame sheet seen in the right panel of **Figure 2**. These results form a solid foundation for studies where particle formation will be investigated by introducing methylsilanes or methylsiloxanes to the fuel flow.

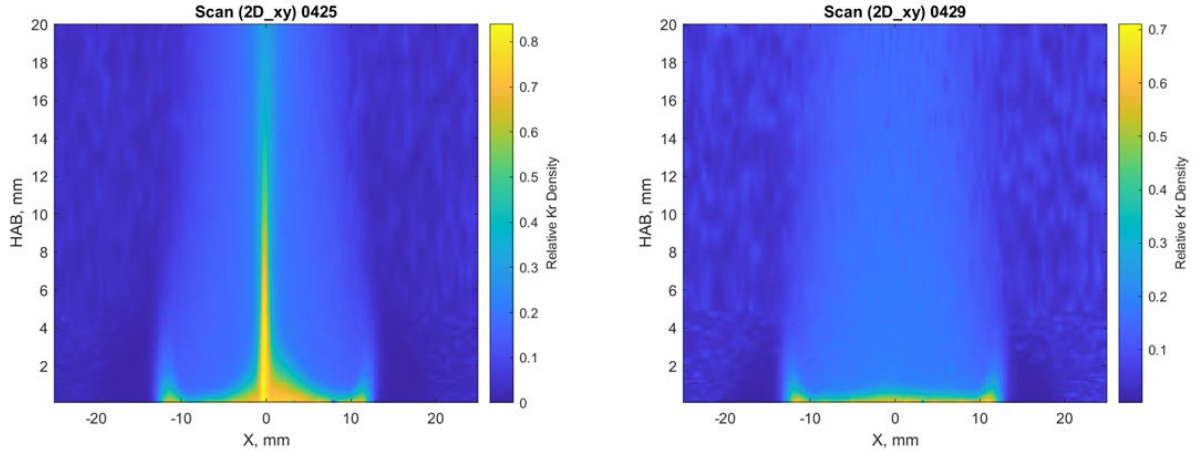

Figure 2. Comparison of Kr concentrations (x-z plane/side view imaging) during methane combustion with methane flow in the central tube in addition to the main flow (left panel) and methane flow in the main burner region only (right panel).

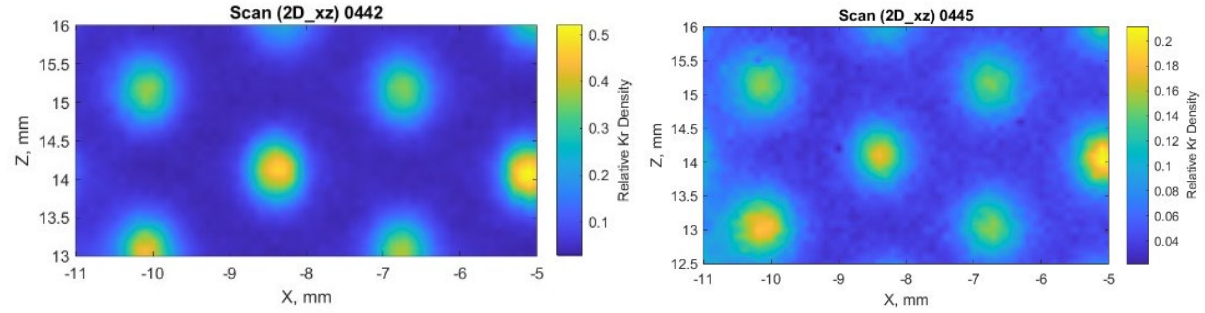

Figure 3. Kr concentrations at 0.1 mm (left panel) and 0.5 mm (right panel) above the surface of the burner during methane combustion with Kr in the main fuel tubes.

Future Plans

We continue to expand our ignition and thermal decomposition studies to additional siloxane species with canonical molecular structures using the facilities and diagnostics of the UM and Argonne. Our plans include UM graduate students collaborating with Tranter on shock tube studies leveraging the ALS. Just recently (5/22) UM doctoral student John Kim was selected to receive a DOE SCGSR award to conduct siloxane chemistry studies at ANL. Future plans include advancing the reaction theory of siloxanes using the results of the experimental efforts. More details are provided here.

High-temperature oxidation kinetics and mechanisms: We have previously studied oxidation kinetics of TMSO and HMDSO using ignition delay time and heat release rates as the primary metrics of characterizing reaction pathways, and the OH data reported here. We will continue the OH studies and expand our measurements to include rapid gas sampling of intermediate species during ignition. Similarly, we are using gas sampling to characterize the products of MEDB studies of methane and siloxane flames. The stable and radical species measurements are the primary focus of the RCF studies for the next year.

High-temperature dissociation kinetics and mechanisms: We previously conducted broad investigations of the pyrolysis of HMDSO and TMSO with the aim of developing chemical kinetic models that support the RCF studies. The data include shock tube facility (STF) electron impact ionization and photoionization (Advanced Light Source) time-of-flight mass spectrometry and STF laser schlieren densitometry (LS) experiments. Interpretation of the data is ongoing and has been hampered in part by a lack of reliable thermochemical data for Si containing species. This is being remedied through collaboration with Sivaramakrishnan (Argonne) and Ruscic (Argonne). The experimental results suggest that existing literature mechanisms [5,6] for dissociation of HMDSO cannot reproduce either the mass spectral or LS information. This may be due in-part to differences in reaction conditions and the types of studies performed. However, the mass spectral data indicate that at the temperatures of the shock tube work HMDSO and TMSO rapidly form SiO and SiO_2 species rather than participating in molecular growth reactions that would be analogous to PAH formation from hydrocarbons. Additionally, the LS experiments indicate exothermic (e.g., radical recombination reactions) are of minor importance, consistent with the mass spectra. Developing a mechanism that reproduces the LS experiments is a principle focus of effort for the next year.

In addition to the STF experiments, complementary thermal decomposition studies will be conducted using the UM RCF. We have recently demonstrated the capability to use rapid gas-sampling during pyrolysis to identify stable intermediate species and quantify reaction pathways with n-propanol studies [7]. We will extend the methods to TMSO and HMDSO pyrolysis studies that complement the temperature and pressure conditions studied by Tranter at Argonne.

Trimethylsilyl radical reactions: Trimethylsilyl (TMS), $(CH_3)_3Si$, is a key species in the gas phase chemistry of methylated silanes. For example, two TMS radicals are formed from scission of the Si-Si bond in hexamethyldisilane These can abstract an H-atom from HMDSO and the resulting carbon centered radical rearranges to a silicon centered radical, but with a Si-C-Si linkage instead of a Si-Si bond as in the following scheme proposed by Davidson and Howard [8].

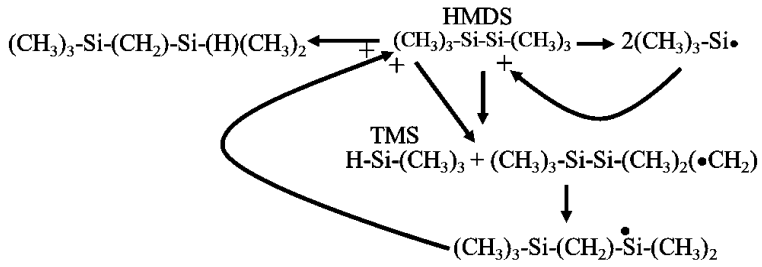

The abstraction reaction competes with recombination and disproportionation of TMS radicals. There are relatively few studies of TMS recombination (R1) to HMDS and apparently no studies of the disproportionation reaction (R2) apart from ones that yield branching ratios for disproportionation/recombination at or close to room temperature.

$$2\ (CH_3)_3Si \rightarrow (CH_3)_3SiSi(CH_3)_3 \qquad (R1)$$
$$2\ (CH_3)_3Si \rightarrow (CH_3)_3SiH + (CH_3)Si{=}CH_2 \qquad (R2)$$

Literature recombination rates span 10^{13} – 10^{14} $cm^3/mol/s$ and branching ratios from 0.1 to 0.5. We intend to use $(CH_3)_3SiI$ as a source of TMS by thermally cleaving the Si-I bond behind shock waves. We will apply the techniques we have developed for studying alkyl radicals to TMS with the goal of determining branching ratios at elevated temperatures and pressures. ST/LS studies will allow the rate of dissociation of $(CH_3)_3SiI$ to be precisely determined from the density gradient at the start of reaction and simulation of the remainder of the LS profile will allow the rates and branching ratio between R2 and R4 to be estimated. The LS studies will be facilitated by collaboration with Ruscic for thermochemistry of the ioidide and TMS. The relative concentrations of the disproportionation products will be measured in HRRST/SVUV-TOF-MS studies at the ALS. These studies will confirm the identities of the species, allow photoionization mass spectra to be obtained and most importantly allow direct determination of the branching between R2 and R4 which will inform the modeling of the LS profiles. Finally, it may also be possible to observe the silicon centered radicals or products therefore formed from attack of TMS on HDMS.

DOE publications supported by this project

Kim, J. H., Mansfield, A. B., Burnett, M. A., Wooldridge, M. S. (2022), "A Study of OH Measurements during Auto-ignition of Syngas and Siloxane Mixtures," 2022 Spring Technical Meeting of The Central States Section of the Combustion Institute, May 15–17, 2021, Detroit, Michigan.

Kim, J. H., Mansfield, A. B., Burnett, M. A., Wooldridge, M. S., (2021) "An Experimental Study of OH During Auto-Ignition of Syngas with Trace Trimethylsilanol," 12th National Meeting of the U.S. Sections of the Combustion Institute.

Mansfield, A.B. Wooldridge, M.S. The effect of impurities on syngas combustion, Combust. Flame 162 (2015) 2286-2295.

Meng, Q., Banyon, C., Kastengren, A. L., Wooldridge, M. S., Tranter, R. S., (2022) "Experimental Measurement of the Rapid Mixing of Fuel and Air in a Multi-Element Diffusion (Hencken) Burner," 2022 Spring Technical Meeting of The Central States Section of the Combustion Institute, May 15–17, 2021, Detroit, Michigan

Schwind, R. A., 2019, *Understanding the Combustion Chemistry of Siloxanes: Reaction Kinetics and Fuel Interactions*, Ph.D. Thesis, University of Michigan, Ann Arbor.

Schwind, R., Wooldridge, M. S., (2019) "Effects of Organic Silicon Compounds on Syngas Auto-ignition Behavior," *Combustion and Flame*, 212 pp. 234-241.
Schwind, R. A., Wooldridge, M. S., Sivaramakrishnan, R., (2019) "Understanding Siloxane Combustion Chemistry: Computational and Experimental Studies of Hexamethyldisiloxane (HMDSO)," 11th National Meeting of the U.S. Sections of the Combustion Institute, Paper No. 1A18, Pasadena, CA.

References

1. Hansen, N., Tranter, R. S., Moshammer, K., Randazzo, J. B., Lockhart, J. P. A., Fugazzi, P. G., Tao, T., Kastengren, A. L. (2017) "2D-imaging of sampling-probe perturbations in laminar premixed flames using Kr x-ray fluorescence," *Combust. Flame* 181:214-224.
2. Hansen, N., Tranter, R. S., Randazzo, J. B., Lockhart, J. P. A., Kastengren, A. L. (2019) "Investigation of sampling-probe distorted temperature fields with x-ray fluorescence spectroscopy," *Proc. Combust. Inst.* 37:1401-1408.
3. Tranter, R. S., Kastengren, A. L., Porterfield, J. P., Randazzo, J. B., Lockhart, J. P. A., Baraban, J. H., Ellison, G. B. (2017) "Measuring flow profiles in heated miniature reactors with x-ray fluorescence spectroscopy," *Proc. Combust. Inst.* 36:4603-4610.
4. Donovan, M. T., Hall, D. L., Torek, P. V., Schrock, C. R., Wooldridge, M. S. (2003) "OH absorption measurements in $SiH_4/H_2/O_2$/Ar flames," *Proc. Combust. Inst.* 29:2635-2643.
5. Chernyshev, E. A., Krasnova, T. L., Sergeev, A. P., Abramova, E. S. (1997) "Siloxanes as sources of silanones," *Russian Chem. Bull.* 46:1586-1589.
6. Almond, M. J., Becerra, R., Bowes, S. J., Cannady, J. P, Ogeden, J. S., Young, N. A., Walsh, R. (2009) "A mechanistic study of the low pressure pyrolysis of linear siloxanes," *Phys. Chem. Chem. Phys.* 11:9259–9267.
7. Miles Burnett, (2022) "Alternative Fuels and Combustion Strategies for Emissions Reductions: Experimental Studies of C3 Fuel Kinetics," Doctoral Thesis, University of Michigan.
8. Davidson, I. M. T., Howard, A. V. (1975) "Mechanism of thermolysis of hexamethyldisilane and the silicon-silicon bond dissociation energy," *J. Chem. Soc. Faraday Trans.* 1 71:69-77.

Spectroscopic and Computational Studies of Spin-Orbit Coupling of Lanthanide Oxides

Dong-Sheng Yang, University of Kentucky (Principal Investigator)
Mark S. Gordon, Iowa State University and Ames Laboratory (Co-Principal Investigator)
dyang0@uky.edu, mark@si.msg.chem.iastate.edu

Program Scope

Spin-orbit (SO) coupling makes it possible for spin forbidden transitions or reactions within non-relativistic quantum theory feasible. Thus, quantification of such interactions has important implications in photophysics and chemical catalysis. This work aims to quantify SO interactions using lanthanide (Ln) oxides as target molecular systems. Through these systems, we examine the impact on the SO coupling by electron configurations and 4f orbital occupancies of Ln elements and sizes of the metal oxides. By examining these factors, we explore how SO coupling is affected by the number of Ln 4f electrons for a given size of molecules and if the Ln 4f orbitals remain atomic in nature in these small clusters. Ln oxides are produced in laser ablation molecular beams, identified with time-of-fight mass spectrometry, and characterized with laser spectroscopy and relativistic quantum chemical computations. Spectroscopic measurements include mass-analyzed threshold ionization (MATI), zero electron kinetic energy, and slow electron velocity-map imaging spectroscopies. Relativistic computations treat scalar relativistic corrections, electron correlations, and SO interactions. The main results are SO terms and energies of the neutral molecules and singly charged cations, ionization energies of the neutral species, metal-metal and metal-oxygen vibrational frequencies of the ions and, in some cases, neutrals as well, and charge effects on the bonding and structures.

Recent Progress

We have focused on the spectroscopy and computations of LnO and their singly charged positive ions (Ln = La, Ce, Pr, and Lu),[1-3] where the Ln elements are in a single or predominantly single isotope and have fewer 4f electrons or holes (La, $5d^16s^2$; Ce, $4f^15d^16s^2$; Pr, $4f^36s^2$; and Lu, $4f^{14}5d^26s^1$) than those in the middle of the Ln series. The single or predominantly single isotope simplifies the separation of the ions produced by laser ionization from those generated by delayed-field ionization in the MATI experiments. The Ln elements with fewer 4f electrons or holes were thought to facilitate the theoretical treatment, though Lu was found to be an unexpected exception. The measured adiabatic ionization energies (IEs) are two-fold improvements over previously reported values where the comparison is available. The IE of the neutral molecule and vibrational frequencies in the neutral and ionized states quantify the charge effects on the metal-oxygen bonding, and the vibrational frequencies of these molecules in the gas phase also reveal the effects of low-temperature inert-gas matrices when compared with previous matrix-isolation infrared spectroscopic measurements. The SO terms and energies quantify the extent and strength of electron spin and spatial orbital mixing. In comparing with the measured spectroscopic constants, computations yield reasonable agreements for the ground states of the neutral and ionized molecules.

Lanthanum oxide and its singly charged cation.[1] The spectrum of LaO (Figure 1A) displays a single vibronic band system with a strong origin band, two vibrational intervals of the

ion, and four intervals of the neutral molecule. The single band system arises from the transition of the ground state ($X^2\Sigma^+$) of the neutral molecule with the La($6s^1$)O($2p^6$) major valence configuration to the ground state ($X^1\Sigma^+$) of the singly charged ion with the La($6s^0$)O($2p^6$) configuration. The measured adiabatic IE from the $X^2\Sigma^+$ neutral state to the $X^1\Sigma^+$ ion state is 42300 (5) cm^{-1} or 5.2445(6) eV. This represents a two-fold improvement over the literature value with the smallest reported uncertainty, 4.9(1) eV. From the four vibrational intervals observed for the neutral molecule, a quadratic polynomial fit yields ω_e = 814.23 ± 1.25 cm^{-1} and $x_e\omega_e$= 1.86 ± 0.30 cm^{-1}. The neutral frequency from the MATI spectrum is ~18 cm^{-1} higher than the value (796.7 cm^{-1}) of LaO deposited in a low-temperature Ar matrix. For the LaO^+ ion, the two vibrational intervals of the ion are measured to be 877 and 883 cm^{-1}, with the average of 880 cm^{-1}. The gaseous ion frequency is ~ 42 cm^{-1} higher than that (838.2 cm^{-1}) measured in the Ar matrix. The lower stretching frequencies of LaO and LaO^+ deposited in the low-temperature Ar matrix suggest that Ar is likely bound with the metal oxide via the metal atom or ion and that such bonding reduces the strength of the La-O bond, and the reduction is more pronounced for the ion. The spectral intensity is not governed by the Franck-Condon (FC) principle. For example, the intensity of the first-quantum vibronic band relative to that of the origin band is measured to be ~ 7%, while the corresponding FC intensity is estimated to be ~ 37%. The coupled cluster CCSD(T) calculated vibrational frequencies of the neutral (808 cm^{-1}) and ion (871 cm^{-1}) and IE of the neutral molecule (5.32 eV) are satisfactory.

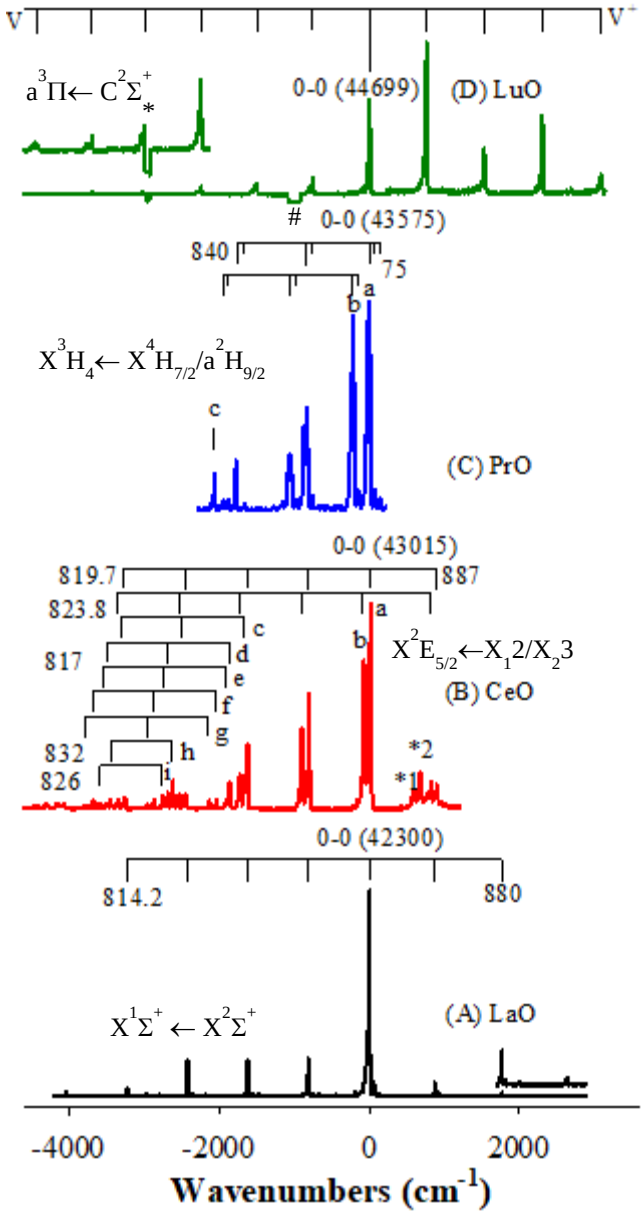

Figure 1. MATI spectra of LnO (Ln = La, Ce, Pr and Lu.

Cerium oxide and its singly charged cation.[1] The MATI spectrum of CeO (Figure 1B) is much more complex than that of LaO. It consists of eleven vibronic band systems (a-i) from transitions of low-energy SO levels of the neutral molecule to the lowest SO level of the ion and two band systems (a and b) from transitions of the two lowest SO levels of the neutral molecule to the first excited SO level of the ion (*1 and *2). The eleven SO terms of the neutral molecules are identified in the order of 1Δ (X_12) (0) < 1Φ (X_23) (88 cm^{-1}) < 1Π (W_11) (819 cm^{-1}) < 2Δ (W_22) (912 cm^{-1}) < $2^3\Pi$ (V_1O^-) (1675 cm^{-1}) < 3Π (V_21) (1873 cm^{-1}) < $1\Sigma^+$(U_1O^+) (1920 cm^{-1}) < $2^3\Phi$ (X_34) (2048 cm^{-1}) < 3Φ (X_43) (2144

cm^{-1}) < 4Φ ($W_3$3)(2626 cm^{-1}) <3Δ ($W_4$2) (2771 cm^{-1}), and the two lowest SO term of the ion are $X^2\Sigma_{5/2}$ (43015 cm^{-1}) and $A^2\Sigma_{3/2}$ (43680 cm^{-1}). The electronic energies (T_0) of 1Π and 2Δ overlap with the first vibrational quanta of 1Δ and 1Φ, respectively. The SO terms are predicted by the SO multiconfiguration quasi-degenerate second-order perturbation theory (SO-MCQDPT2), where the terms without electron multiplicities are mixtures of Russell-Saunders (RS) singlet and triplet states. The main valence electron configurations are Ce($4f^16s^1$)O($2p^6$) for the neutral molecule and Ce($4f^1$)O($2p^6$) for the ion. The SO-MCQDPT2 predicted SO term energies agree with the measured values. The adiabatic IE value of $X^2\Sigma_{5/2} \leftarrow 1\Delta$ from the measurements is 43015 (5) cm^{-1} or 5.3332 (6) eV, which again is a two-fold improvement over the literature value with the smallest reported uncertainty. The IE of CeO is slightly higher than that of LaO, even though the IE of Ce (5.5387 eV) is a little lower than that of La (5.5769 eV). This observation suggests that the bond-energy difference between the ion and neutral molecule is slightly smaller for the Ce oxide (0.2055 eV) than for the La oxide (0.3323 eV). For the 1Δ and 1Φ terms of the neutral molecule, the harmonic frequency and anharmonicity are fitted as ω_e= 819.72 ± 0.27 cm^{-1} and $x_e\omega_e$ = 0.36 ± 0.06 cm^{-1} for the 1Δ level and ω_e= 823.81 ± 0.80 cm^{-1} and $x_e\omega_e$ = 0.93 ± 0.19 cm^{-1} for the 1Φ level. The vibrational intervals of the $2^3\Pi$, 3Π, $1\Sigma^+$, $2^3\Phi$, and 3Φ terms are averaged as 817 ± 2 cm^{-1}, while those of 4Φ and 3Δ are measured to be 832 and 826 cm^{-1}, respectively. For the ion, the vibrational frequency is 887 cm^{-1} for the $X^2E_{5/2}$ level. Like LaO, the vibrational frequencies of CeO and CeO^+ in the gas phase are higher than those (808.4 and 849.5 cm^{-1}) of the neutral and ionized molecules deposited in an Ar matrix.

Praseodymium oxide and its singly charged cation.[2] The MATI spectrum of PrO (Figure 1C) consists of the origin band at 43575 (5) cm^{-1} or 5.4026 (6) eV, two vibronic band systems (a and b) separated by 215 cm^{-1} and an additional band (c) at 2071 cm^{-1} below the 0-0 transition. Each band system consists of two vibrational intervals of ~ 840 cm^{-1} and at least one satellite band at 75 cm^{-1} from each member of the band systems. The 840 cm^{-1} interval is the vibrational frequency of the neutral states, while the 75 cm^{-1} satellite bands are sequence bands, which yield the vibrational frequency of 915 cm^{-1} [(840 + 75) cm^{-1}] for the ion. To understand the spectrum and electronic structures of the neutral and ionized molecules, we have conducted extensive SO-MCQDPT2 calculations, and the results are presented in Figure 2. The ground state of the neutral molecules is predicted to be $X^4H_{7/2}$, followed by an $a^2H_{9/2}$ state at 1263 cm^{-1}. Both states have a

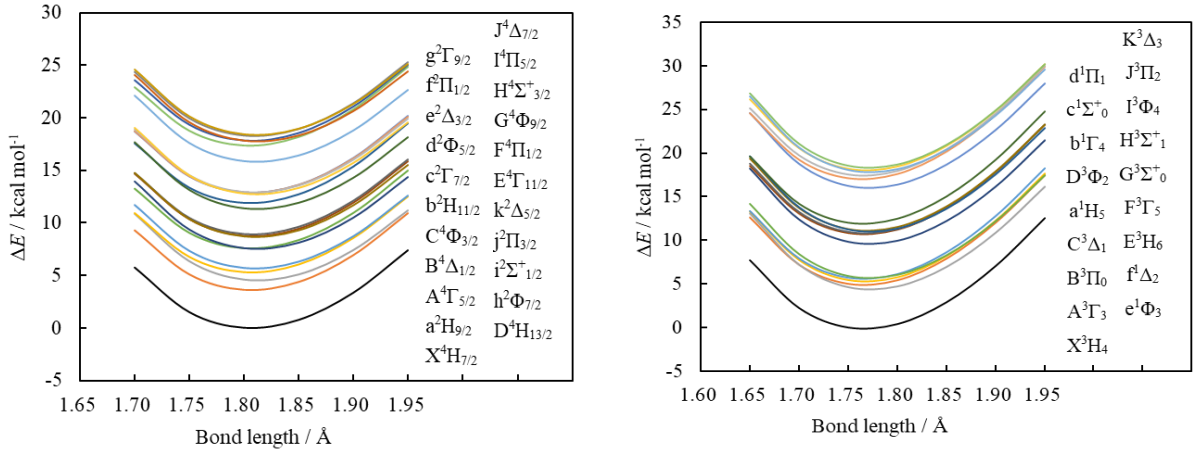

Figure 2. Potential energy curves of PrO (left) and PrO^+ (right) at the state-averaged SO-MCQDPT2 level. The active space are (3,8) for PrO and (2, 7) for PrO^+. The term symbols are listed in the order of increasing bond length beginning from the PrO ground state $X^4H_{7/2}$ or the PrO^+ ground state X^3H_4.

predominant electron configuration of $Pr(4f^26s^1)O(2p^6)$. The ground state of the ion is predicted to be X^3H_4, which is generated by removing the Pr $6s^1$ electron. The calculated IE for the $X^3H_4 \leftarrow X^4H_{7/2}$ is 43613 cm^{-1}, in excellent agreement with the measured value of 43575 cm^{-1}. The observed 215 cm^{-1} separation could be assigned to the energy difference between the $X^3H_4 \leftarrow X^4H_{7/2}$ and $X^3H_4 \leftarrow a^2H_{9/2}$ transitions with a computed value of 1263 cm^{-1}. To improve the theoretical prediction, we then consider the state mixing of the quartet and doublet states of the neutral molecule. The state-mixing calculations show that the ground SO level is still essentially $X^4H_{7/2}$ (95%), but the second SO level is a mixture of $a^2H_{9/2}$ (55%) with a quartet state. Such state mixing reduces the separation from 1263 to 179 cm^{-1}, which is now much closer to the measured value of 215 cm^{-1}. The calculated vibrational frequencies at the level of density functional theory (B3LYP) are 828 cm^{-1} for the neutral molecule and 913 cm^{-1} for the ion, in reasonable agreements with the experimental values of 840 and 915 cm^{-1}, respectively. The 2071 cm^{-1} band below the 0-0 band does not belong to either of the vibronic band systems. This band may be attributed to a transition from a spin-mixed SO level calculated at 2116 cm^{-1} to the ground SO level of the ion.

Lutetium and its singly charged cation.[3] Figure 1D presents a partial MATI spectrum of LuO, with the full spectrum spanning an energy range of ~ 10,000 cm^{-1}. The spectrum displays the origin band at 44699 (5) cm^{-1} [5.5420 (6) eV]. On the higher energy side of the origin band are four stronger vibronic bands with intervals ≥ 766 cm^{-1}, while on the lower energy side are nine weaker bands (six bands are shown in the figure) with intervals ≤ 750 cm^{-1}. The 44699 cm^{-1} band is considered to be the origin band because the vibrational intervals are distinctively different on the two sides of this band. The energy intervals above the origin band (766, 767, 769, and 782 cm^{-1} for v^+ = 1-4) are associated with the cation, while those (750, 746, 747, 730, 730, 725, 719, 660, and 705 cm^{-1} for v = 1-9) below the origin band arise from vibrational levels of the neutral molecule. The two intervals (730* cm^{-1}) labeled between v = 3 and v = 5 are the average rather than individual intervals. This is because the head of the v = 4 band marked with "*" is interfered by a strong Lu atomic transition $^1S_0$ (Lu^+) ← $^2D_{5/2}$ (Lu), which makes it difficult to determine its exact position. There is another Lu atomic transition marked with "#" in the spectrum, which corresponds to the $^1S_0$ (Lu^+) ← $^2D_{3/2}$ (Lu) atomic transition but does not interfere with any vibronic transition of LuO. Most vibronic bands have an asymmetric shape and are degraded toward the red. Although rotational transitions are not resolved in the spectra, the red degradation of the vibronic bands suggests an increase of the metal-oxygen bond length from the initial neutral state to the final ion state.

It is unlikely that the MATI spectrum is associated with the ionization of the neutral ground state because early measurements indicated the ground state IE to be much higher (6.5-7.8 eV) than the energy of the origin band. Table 2 lists allowed ionization processes and energies calculated with MCQDPT2. Among the predicted neutral and ion states, all ionization transitions are allowed, except for $X^1\Sigma^+ \leftarrow B^2\Delta$ and $b^3\Sigma^+ \leftarrow b^2\Delta$, which are forbidden by the $\Delta\Lambda = 0, \pm1$ selection rule. Among the allowed transitions, only the energies of $a^3\Pi \leftarrow C^2\Sigma^+$ (47430 cm^{-1}) and $A^1\Pi \leftarrow C^2\Sigma^+$ (47916 cm^{-1}) are close to the energy of the 0-0 band (44699 cm^{-1}) of the MATI spectrum. Because the intensity profile of $a^3\Pi \leftarrow C^2\Sigma^+$ matches with the experimental spectral profile, the MATI spectrum is assigned to the triplet ← doublet transition. Although the intensity profiles of the LaO and CeO MATI spectra that involve transitions between the ground states of the neutral and ionic molecules are not governed by the FC principle, the FC intensity involving the excited states of LuO and LuO^+ appears to be consistent with the measured intensity of the cold bands. The predicted harmonic frequencies are 770 and 654 cm^{-1} for the $C^2\Sigma^+$ neutral state and the $a^3\Pi$ ion state, while the measured fundamentals for these states are 750 and 766 cm^{-1},

respectively. The computed vibrational frequency of the neutral excited state is in excellent agreement with the experimental value, though the calculations yield a lower fundamental frequency for the excite ion state. The MATI spectrum shows abnormal vibrational intervals in both the neutral and cation states. The abnormality is likely due to vibrational perturbations caused by nearby electronic states. In the future, we will also attempt to measure resonant two photon MATI spectra via the $A^2\Pi$ or $C^2\Sigma^+$ excited states.

Table 2. Ionization processes and energies (cm^{-1}) predicted by MCQDPT2 calculations and probed by MATI spectroscopy. $^aX^1\Sigma^+ \leftarrow B^2\Delta$ and $b^3\Sigma^+ \leftarrow b^2\Delta$ transitions are forbidden as dictated by the $\Delta\Lambda = 0 \pm 1$ selection rule.

MCQDPT2	$X^1\Sigma^+$	$a^3\Pi$	$A^1\Pi$	$b^3\Sigma^+$
$X^2\Sigma^+$	55680	75055	75542	80397
$A^2\Pi$	35952	55327	55813	60668
$B^2\Delta$	NA[a]	52382	52960	NA[a]
$C^2\Sigma^+$	28054	47430	47916	52771
$D^2\Sigma^+$	7597	26972	27458	32313
$E^2\Pi$	7175	26550	27036	31891
MATI		$a^3\Pi$	$A^1\Pi$	
$C^2\Sigma^+$		44699		

Software development. To meet the need of this project, we have implemented several new features in the GAMESS code originally developed in our group. These new developments include, but are not limited to, (1) support for relativistic integrals involving h and i functions for spin-orbit calculations. This is in addition to the support for scalar relativistic methods that was previously implemented. (2) a special case for diatomic molecules in the numerical Hessian code that reduces the number of energy evaluations from 108 to 4. This approach rotates the coordinates to realign the molecule along the principal axes after each displacement, thus preserving symmetry. This has the two-fold advantage of reducing the number of energy evaluations needed based on symmetry constraints while simultaneously allowing for the use of symmetry to aid in the optimization of excited state. (3) a special case for diatomic molecules that allows for the use of symmetry when computing excited states with the vibrational self-consistent field method. (4) parallelization of the computation of the transition density matrix in the spin-orbit code. (5) expanding support for the density-based bonding analysis to allow for the use of the graphical unitary group approach-based multireference methods. Previously, this functionality was limited to use of the occupation restricted multiple active space method. (6) support for effective core potentials (ECPs) that use a h-ul potential with a coefficient of zero. This allows for the use of the Stuttgart-Dresden ECPs and by extension the correlation consistent pseudopotential-based basis sets. The h-ul potential provides an upper limit (ul) for the angular momentum as well as a reference point for difference potentials that are computed based on the s, p, d, f, and g potentials

provided in the input file. (7) support for the generation of valence virtual orbitals when using model core potentials.

Future Plans

We will investigate Ln oxide clusters containing two or three Ln atoms and various numbers of oxygen atoms. Experimental measurements will be focused on the search of vibronic spectra of the clusters of interest, and theoretical computations will be performed in coordination with the experiments. It is expected that the theoretical treatment of Ln cluster oxides will be more challenging due to the larger size of the systems and the possible coupling of the 4f electrons on separated Ln atoms. We thus will implement new functionalities in the GAMESS code to accomplish the task as specific needs become apparent in the course of this work.

Publications supported by the BES-GPCP program (8/2020-present)

1. W. J. Cao, Y. C. Zhang, L. Wu, and D. -S. Yang, "Threshold Ionization Spectroscopy and Theoretical Calculations of LnO (Ln = La and Ce)," J. Phys. Chem. A **125**, 1941-1948 (2021). DOI: 10.1021/acs.jpca.1c00533.

2. Y. C. Zhang, T. Nakamura, W. J. Cao, L. Wu, M. Roudjane, M. S. Gordon, and D. -S. Yang, "Spectroscopy and Electronic States of Praseodymium Oxide and its Singly charged Cation," J. Chem. Phys. (to be submitted).

3. L. Wu, G. Schoendorff, Y. Zhang, M. Roudjane, M. S. Gordon, and D. -S. Yang, "Excited States of Lutetium Oxide and its Singly Charged Cation," *J. Chem. Phys.* **156**, 084303 (2022). DOI: 10.1063/5.0084483.